Kinematic Plate Models of the Neoproterozoic

Andrew S. Merdith
2017

This thesis is submitted in fulfilment of the requirements for the degree of Doctor
of Philosophy

School of Geosciences
The University of Sydney, New South Wales
Australia

Declaration

I declare that this thesis is less than 80,000 words in length and that the work contained in this thesis has not been submitted for a higher degree at any other university or institution.

Andrew S. Merdith
August, 2017

Preface

This Ph.D thesis consists of two articles that have been published in international, peer-reviewed journals, and one article submitted to an international, peer-reviewed journal. A fourth article completed during this Ph.D and that has been published in an international, peer-reviewed journal is included in the Appendix. The thesis also contains a an introductory chapter that provides an overview of the concepts and topics discussed in the subsequent chapters, and a discussion chapter that ties together the themes of each article.

Acknowledgements

Authorship Attribution

Chapter Two of this thesis is published as:

Merdith, A.S., Williams, S.E., Müller, R.D. and Collins, A.S., 2017. Kinematic constraints on the Rodinia-Gondwana transition. Precambrian Research, in press.

I designed the study, analysed and interpreted the data and wrote the drafts of the manuscript.

Chapter Three of this thesis is published as:

Merdith, A.S., Collins, A.S., Williams, S.E., Pisarevsky, S., Foden, J.F., Archibald, D., Blades, M.L., Alessio, B.L., Armistead, S., Plavsa, D.,Clark, C., and Müller, R.D., 2017. A full-plate global reconstruction of the Neoproterozoic. Gondwana Research, 50

I co-designed the study, constructed the model, extracted the data and wrote the majority of the draft of the manuscript
----

Chapter Four of this thesis is prepared for submission as:

Merdith, A.S., Williams, S.E., Brune, S., Collins, A.S., Riggs, R. and Müller, R.D., Manuscript prepared for submission. Quantifying the link between subduction and continental rifting across two supercontinent cycles. Global and Planetary Change.

I designed the study with the co-authors. I constructed the model, extracted the data; and interpreted the analysis with co-authors. I wrote the drafts of the manuscript.

The Appendix of this thesis is published as:

Merdith, A.S., Landgrebe, T.C. and Müller, R.D., 2015. Prospectivity of Western Australian iron ore from geophysical data using a reject option classifier. Ore Geology Reviews, 71, pp.761-776.

I extracted and interpreted the data and wrote the drafts of the manuscript.

Andrew Merdith   10/08/17
Student Name   Signature   Date

As supervisor for the candidature upon which this thesis is based, I can confirm that the authorship attribution statements above are correct.

Dietmar Müller   10/08/17
Supervisor Name   Signature   Date

Abstract

Plate tectonic reconstructions traditionally use a combination of palaeomagnetic and geological data to model the changing positions of continents (cratons, terranes or blocks) throughout Earth history. Plate reconstructions are particularly useful because they provide a framework for testing a range of hypotheses pertaining to climate, seawater chemistry, evolutionary patterns and the relationship between mantle and surface through supercontinent cycles. During the Mesozoic and Cenozoic these are underpinned by data from the ocean basins that preserve relative plate motions, and data from hotspot chains and tomographic imaging of subducted slabs within the mantle to constrain absolute plate motions. For the Palaeozoic and earlier times, neither ocean basins nor subducted slabs are preserved to assist with constructing plate models. Previously published plate models are usually built around times that have high quality palaeomagnetic data and between these times, the motion of continental crust is usually interpolated. Alternatively, regional tectonic models are developed predominantly from using geological data but without integrating the model into a global context. Additionally, until now all global plate models for the Neoproterozoic model only describe the configurations of continental blocks and do not explicitly consider the spatial and temporal evolution of plate boundaries. In this thesis, I present the first topological plate model of the Neoproterozoic that traces the dynamic evolution and interaction of tectonic plates, which encompass the entire earth. This model synthesises new geological and palaeomagnetic data, along with conclusions drawn from kinematic data to help discriminate competing continental configurations of the western area of the Neoproterozoic supercontinent, Rodinia. In this western area of Rodinia, the eastern margin of Australia and the Mawson craton (East Antarctica) are paired with the western margin of Laurentia. Due to difficulties in dating some of the sedimentary sequences preserved on the Australian margin, geological and palaeomagnetic data cannot be used alone to discriminate between four alternative configurations, the time of rifting, and the rift-drift transition. I design an experiment to use kinematic data (e.g. rates of motion and angular rotation) to examine which configuration and rifting time are more kinematically feasible, assuming that plate tectonics in the Neoproterozoic operated on similar principles as is evident today. The results suggest that the AUStralia-Western United States (AUSWUS) configuration with rifting time at 800 Ma is the kinematically most feasible, though both the AUStralia-MEXico (AUSMEX) and South West United States, East-AnTarctica (SWEAT) configurations are realistic, with average rates of motions for all three configurations ranging from 60 mm/a to 85 mm/a (present day average is 30 mm/a ± 40). For younger times, rates of motion become unrealisitcally high, with rifting at 725 Ma for all configurations necessitating plate motions of up to 150 mm/a. Understanding the kinematic controls on plate motions are useful for pre-Pangea plate reconstructions as they provide a mechanism by which we can build confidence in plate motions during times where there is little palaeomagnetic or geological data. The model of Rodinia being proposed here adopts the AUSWUS configuration with early rifting at 800 Ma. In addition to this, India and South China are removed from Rodinia completely and move as a separate, congruent portion of continental lithosphere through the Neoproterozoic until they amalgamate with Gondwana at ca. 550 Ma. I also introduce a rotation of Congo-Saõ Francisco (including Azania, the proto-Arabian Nubian Shield and the Sahara Metacraton) from polar to equatorial latitudes, relative to Rodinia during the Tonian to account for new palaeomagnetic data. This model catalogues the preservation of subduction zones through the Neoproterozoic in order to help constrain relative plate motions and to build a network of continuously closing plate topologies that evolve through time. A key value of these models is that the boundaries, especially convergent boundaries, act as the interface between the kinematic evolution of plate tectonics on the surface, and the geodynamic evolution of the underlying mantle. I extend the proposed Neoproterozoic model forward in time through the Early Palaeozoic to meet other published topological models for Phanerozoic. Using a plate model from 1 Ga to present I extract the length of rifting episodes, continent-margin arcs, and the perimeter-to-area ratio of continents to examine the relationship between these and the supercontinent cycle. While broadly the supercontinent cycle is described by the amalgamation and dispersal of all continental lithosphere, I find that it is difficult to elucidate a clear interpretation of the supercontinent cycle from any of the three measures

individually. Rather each measure quantitatively reveals a part of the cycle, with times of supercontinent existence revealed in the perimeter-to-area ratio, the amalgamation of Gondwana from changes in continental arc lengths, and the breakup of Rodinia and Pangea from rift lengths. In particular, I find that the assembly of Pangea is not clearly revealed through changes in continent-margin arc length, and in the perimeter-to-area ratio. Rather, Pangea assembly is evident as the culmination of a global decrease in the perimeter-to-area ratio that begins with the the assembly of Gondwana, suggesting that they form part of the same period of supercontinent existence. The length of continental arcs increase slowly as Gondwana amalgamates, but does not appear to correspond with continual 'unzipping' of the supercontinent, rather I speculate that it plays a more prominent role in the initial fragmentation of a supercontinent. Given problems with palaeo-geographic definitions of what a supercontinent is, as well as the important role that supercontinents are hypothesised to play for mantle dynamics, a geodynamic definition based on my quantitative reconstructions of plate boundary evolution could help with forming a concrete understanding of a supercontinent. In this case, a supercontinent forms when a global peak of continental arc forms and then abruptly drops to a lower minima than it was prior to the peak. Under this definition the amalgamation of Gondwana would mark the existence of a Phanerozoic supercontinent cycle that finished with the breakup of Pangea.

This thesis is based on the following articles:

Article One

Merdith, A.S., Williams, S.E., Müller, R.D. and Collins, A.S., 2017. Kinematic constraints on the Rodinia-Gondwana transition. *Precambrian Research, in press*.

Article Two

Merdith, A.S., Collins, A.S., Williams, S.E., Pisarevsky, S., Foden, J.F., Archibald, D., Blades, M.L., Alessio, B.L., Armistead, S., Plavsa, D.,Clark, C., and Müller, R.D., 2017. A full-plate global reconstruction of the Neoproterozoic. *Gondwana Research*, 50

Article Three

Merdith, A.S., Williams, S.E., Brune, S., Collins, A.S., Riggs, R. and Müller, R.D., Manuscript prepared for submission. Quantifying the link between subduction and continental rifting across two supercontinent cycles. *Global and Planetary Change*.

A first author publication completed during this study is included in the Appendix:

Article Four

Merdith, A.S., Landgrebe, T.C. and Müller, R.D., 2015. Prospectivity of Western Australian iron ore from geophysical data using a reject option classifier. *Ore Geology Reviews*, 71, pp.761-776.

Table of Contents

Introduction

1-1 Background information

Plate tectonics is the surface expression of cooling processes occurring in the Earth's interior, and provides a potential window in mantle dynamics. Plate tectonics and mantle dynamics are two components of the Earth system that drive the physical evolution of our planet. Understanding the long-term evolution of either of these components can provide important information about the other (e.g. Anderson, 2001; Dal Zilio et al., 2017; Gurnis and Zhong, 1991; Mallard et al., 2016; Murphy et al., 2009; Rolf et al., 2017; Tackley, 2000; Zhong et al., 2007). Models depicting the motion of cratonic lithosphere have been constructed for discrete time periods back unto the Palaeoproterozoic (e.g. Li et al., 2008; Pehrsson et al., 2016; Pisarevsky et al., 2014). Most plate models (especially for Precambrian times) depict the motion of only continental lithosphere, and do not specifically model complete tectonic plates (referred to as topological plate models). Plate models typically contain data constraining relative plate motions (how one plate or portion of lithosphere moves relative to another) and absolute plate motions (how one plate or portion of lithosphere moves relative to a fixed reference point, e.g. the spin-axis or the mantle) expressed as a stage rotation (a rotation around an Euler Pole between two discrete time intervals). Relative plate motions are constrained by crustal geological information giving clues to direction and rate of plate motions (e.g. fracture zones, subduction zones), and absolute plate motions are constrained by mantle- or core-induced geological or geophysical information (e.g. palaeomagnetic data, hotspot trails, tomographic imaging of slabs). However, as we look further back in earth history, preserved evidence of relative plate motions is typically lost due to subduction - essentially limiting our insights past the last supercontinent amalgamation. By combining a series of stage rotations within a hybrid reference frame (e.g. relative plate motions coupled with absolute plate motions when possible) we can build plate models that depict the motion of tectonic plates through supercontinent cycles.

The supercontinent cycle is the theory that continental crust periodically aggregates together into a 'supercontinent', which exists for some period of time, before dispersing and re-aggregating at a later time (e.g. Worsley et al., 1984). This cycle was first proposed based the periodic occurrences of times dominated by orogens (representing amalgamation) and large igneous provinces (representing dispersion). Three supercontinents are readily accepted, Pangea (ca. 340 to 180 Ma), Rodinia (ca. 1000 to 800 Ma) and Nuna (also called Columbia, ca. 1600 to 1400 Ma), with earlier supercontinents (sometimes referred to as super cratons, cf. Evans, 2013) from the Palaeoproterozoic and Neoarchaean also proposed. The supercontinent cycle is thought to directly impact the long term evolution of the mantle through (at least) two key mechanisms. Firstly, it insulates and prevents heat dispersal from the underlying mantle. This leads to a build of heat at the base of the continental lithosphere, resulting in extension and crustal thinning, often interpreted as a 'superplume'. Other geological evidence of extension (and a superplume) are large igneous provinces (LIPs) and large-scale dyke swarms. Secondly, the cycle creates degree-2 mantle convection, since supercontinents are ringed by subduction zones (e.g. Cawood and Buchan, 2007; Cawood et al., 2016; Collins, 2003). In order to more fully understand the geological and tectonic reasons, and to determine if there is geological evidence for these ideas, plate reconstructions can be used to temporally and spatially map the evolution of the continental lithosphere.

Plate boundaries, where two or more tectonic plates interact, act as the physical interface between the mantle and the surface as they allow a glimpse at lithosphere/mantle interactions. Convergent boundaries are marked by subduction zones whereby cold, dense oceanic lithosphere is consumed and recycled into the mantle underneath the overriding lithosphere. Subduction typically (but not always) eventuates in a continental orogen, where two portions of continental lithosphere collide and form a mountain range, in which case subduction ceases. Subduction zones are typically preserved in the geological record either as ophiolites or rocks with arc-like geochemical and petrological features. Most plate divergence occurs at mid-ocean ridges (MORs), which are recorded by oceanic crust preserved either in situ (for last 200 Myr) or as ophiolites, though evidence of divergence between plates is also preserved within rift

basins (representing early stages of divergence) and as passive margins (indicative of breakup and generation of oceanic lithosphere). Transform boundaries are also preserved in ocean basins, offsetting sections of mid-ocean ridges, and within continental lithosphere they are preserved as lineaments juxtaposing allochthonous portions of crust. As ocean basins preserve a large amount of the data available to constrain plate boundaries, plate tectonic models of the Mesozoic and Cenozoic have already been completed (e.g. Müller et al., 2016; Seton et al., 2012; Stampfli and Borel, 2002) using fracture zones (e.g. Matthews et al., 2011) and extinct ridges as a key constraint on relative plate motions and a combination of absolute reference frames providing a constraint on absolute position (e.g. Doubrovine et al., 2012; O'Neill et al., 2005). In the Palaeozoic, prior to the breakup of Pangea, the absence of preserved ocean basins, hotspot trails and subducted slabs (which have a maximum lifespan in the mantle of ca. 300 Ma, e.g. Van der Meer et al., 2010) within the mantle makes constraining both relative and absolute position of plates more difficult. It also creates problems with constraining the position of divergent and transform boundaries, as they are principally preserved in ocean basins, especially for large Pacific-style oceans (e.g. the Panthalassa and Mirovoi oceans during the Palaeozoic and Neoproterozoic respectively). Consequently, plate boundaries for pre-Pangean times are best known where evidence of their existence are preserved on continents, typically as passive margin sequences (proxy for divergent margins) and as arc rocks (proxy for convergent margins). Global tectonic models of the Palaeozoic that include the evolution of plate boundaries have been constructed (e.g. Domeier, 2016; Domeier and Torsvik, 2014) using palaeomagnetic data and the assumption of fixed large low shear velocity provinces (LLSVPs) to provide absolute constraints on palaeolatitude and palaeolongitude. Consequently, the Neoproterozoic is at the frontier for plate reconstructions, both in respect to modelling plate tectonics and also for better constraining the long-term evolution of the mantle and understanding how plate tectonics relates to the mantle over a supercontinent cycle.

The Neoproterozoic is dominated by two tectonic phenomena, the supercontinent Rodinia (existing from ca. 1000 to 800 Ma) and the amalgamation of Gondwana (ca. 650 to 520 Ma). The existence of a pre-Pangean supercontinent was first alluded to by Valentine and Moores (1970) and Piper (1976), although McMenamin and McMenamin (1989) were the first to propose the name 'Rodinia' (Russian for 'to beget') for the supercontinent. Three studies, Dalziel (1991), Hoffman (1991) and Moores (1991) all proposed similar configurations of this supercontinent based on palaeomagnetic and geological data, and since then numerous studies have shed further light on the configuration, timing of amalgamation and timing of breakup events of the supercontinent (e.g. Dalziel, 1992; 1997; Pisarevsky et al., 2003; Powell et al., 1993; Torsvik, 2003; Torsvik et al., 1996). In particular, Li et al. (2008) summarised nearly two decades of work and constructed a plate model from 1100 to 550 Ma that encompassed Rodinia's amalgamation and breakup, and the amalgamation of Gondwana. Throughout all plate models of Rodinia and the Neoproterozoic there are broad similarities in the configuration (except for a series of studies by Piper, 2000; 2007; 2010 and a purely palaeomagnetically constrained model by Evans, 2009). Laurentia remains at the core of Rodinia due to it being surrounded by Neoproterozoic passive margins, Australia and Antarctica are attached to the western margin of Laurentia, Siberia is off the northern margin, Baltica and Amazonia (± West African Craton) are on Laurentia's eastern margin and Kalahari is attached to the southern margin. The other two main cratonic components, the Congo-Saõ Francisco craton (along with the enigmatic Sahara Metacraton) and India have been excluded from Rodinia in some models due to conflicting palaeomagnetic and geological data (e.g. Pisarevsky et al., 2003). However, all these models outline only the motion of cratonic crust, and while they are built using geological information pertinent to plate boundaries (see also Li et al., 2013) they do not contain dynamically evolving plates.

A significant hurdle in constructing pre-Pangean topological models is how to build confidence that plates are moving with 'geodynamic plausibility'. Geodynamic plausibility is constructed to mean that the motion and evolution of lithospheric plates should be in accordance with the physics of the lithosphere and mantle (e.g. Gurnis et al., 2012). The simplest interpretation of 'geodynamic plausibility' sug-

gests that where two portions of lithosphere collide, an orogen (or an arc) should have formed, and where two portions of lithosphere separate, an ocean basin should have formed. More complex, and oft-repeated rules pertain to maximum velocities of plates (e.g. Gordon and Jurdy, 1986; Gurnis and Torsvik, 1994; Meert et al., 1993; Stoddard and Abbott, 1996; Zahirovic et al., 2015) and the motion of subduction zones (e.g. Funiciello et al., 2008; Lallemand et al., 2008). However, there is subjectivity and uncertainty as to the importance of 'geodynamic plausibility' for deeper time reconstructions, especially pertaining as to whether it should overrule reliable palaeomagnetic or geological data in constraining plate motions, and if so, to what extent? And for how far back in time should we (or can we) use this approach? This uncertainty is due, in part, to the absence of ocean basins that preserve relative plate motions through fracture zones and mid-ocean ridges, and also because it is uncertain whether the tectonic regime observed today is applicable to deep time (i.e. uniformitarianism). If we do assume a uniformitarianism approach to plate tectonics (at least to the Palaeozoic and the Neoproterozoic), then the present-day evolution of ocean basins (e.g. Matthews et al., 2011) provides a mechanism by which we can expect tectonic plates could move around in the Neoproterozoic.

Evidence for plate boundaries for deep time reconstructions are best constrained close to the margins of cratons and are typically convergence-related, as continental arcs often remain stable for long periods of time until a continent-continent collision (e.g. the Andes at the present day). Divergent margins are best constrained at the onset of spreading, when a mid-ocean ridge is still close to the plates that it separates. As the system evolves it becomes more difficult to determine both the position and orientation of the mid-ocean ridge. A key idea to help build deep time reconstructions is that changes in plate motions are not random, but always linked to further afield, regional or global events. In particular subduction cessation (such as following a continent-continent collision) or subduction initiation (amongst other events) are major drivers in plate re-organisations (e.g. Austermann et al., 2011; Patriat and Achache, 1984). Importantly, evidence of these two drivers can be preserved in the geological record, meaning that events triggering changes in plate motions (sug-

gested by palaeomagnetic data for example) can be accounted for, in part, by analysing the subduction history within a global framework.

In this thesis I undertake to build upon the work of earlier plate models of the Neoproterozoic to construct a topological plate model of the Neoproterozoic that specifically models complete tectonic plates, by mapping the evolution of plate boundaries between 1000 and 520 Ma. The consequences of building a topological model for this time, and being able to link it to topological models of the Phanerozoic, are that we can extract and analyse key mechanisms on the plate tectonics side of the plate tectonics-mantle relationship. In particular, being able to isolate and analyse subduction length, and the amount of continental lithosphere present will have implications for, and could potentially help further extend our understanding of the supercontinent cycle and couple of surface-mantle processes.

1-2 Thesis Overview

This thesis contains three articles on plate tectonics in the Neoproterozoic, and the implications of subduction and rifting to the supercontinent cycle. The thesis begins with the exposition of a novel method to assist with constructing deep-time plate reconstructions (Article One) and is followed by a topological plate model of the Neoproterozoic that ties together geological, palaeomagnetic and kinematic data to produce a new model that encompasses the existence and breakup of Rodinia, and the amalgamation of Gondwana (Article Two). The final article explores the implications arising from analysing spatio-temporal data extracted from a (semi-) continuous 1000 to 0 Ma topological plate model in order to better understand the supercontinent cycle and long-term relationship between tectonic plates and the mantle. A brief discussion is offered at the end of the three articles that ties together some common themes from the body of work, and also provides some ideas for potential future areas of investigation. A fourth article that investigates the coupling of machine learning techniques with mineral prospectivity and that was completed during this degree is included in the Appendix, but does not form part of the main body of work.

1-2-1 Article One

Article One explores four different proposed Australia-Laurentia configurations and rifting time during the Neoproterozoic, of which the geological and palaeomagnetic data can not discriminate between. The article outlines a methodology using kinematic data to help provide insight into which is the most kinematically optimal configuration and rifting time, given that the end position of Australia is well constrained at 650 Ma, both palaeomagnetically and geologically. I find that the AUSWUS and AUSMEX are the most kinematically preferred configurations, though rifting time provides a stronger constraint on reasonable kinematic motions, with early rifting at 800 Ma being the only time that results in spreading rates consistent with what we observe at present day. This article traces Australia's story between Rodinia and Gondwana, and concludes with looking at the amalgamation of India and Australia into Gondwana, against the Congo and Kalahari cratons and provides a rudimentary model integrating kinematic constraints of this transition.

1-2-2 Article Two

Article Two builds upon the methodology of Article One and presents a kinematic, topological plate model of the Neoproterozoic (1000 to 520 Ma). It integrates the conclusions presented in Article One, and additionally, diverges slightly from previous models of this time by omitting South China and India from Rodinia, and by introducing a rotation of the Congo-Saõ Francisco cratons against Rodinia between 850 and 750 Ma to better fit palaeomagnetic data. This model traces the dynamic evolution of plate boundaries through time in accordance with plate tectonic theory — where each rigid plate is bounded by either a transform, divergent or convergent boundary and the boundaries are fully interconnected. This model used the rotations of the Li et al. (2008) study, in addition to some amendments from Li et al. (2013).

1-2-3 Article Three

In this article I link the model proposed in Article two with younger models of the Phanerozoic to have semi-continuous topological model from 1000 to 0 Ma in order to explore how the supercontinent cycle changes over the past 1 Ga. The purpose of the continuous model is to facilitate the extraction of length of continental arcs through this time. To supplement this I compile a series of rifting events from the Neoproterozoic, and use previously published lengths of rifting events from the Phanerozoic to complete a database of rifting length from 1 to 0 Ga. The variations length and duration of rifting events and continental arcs suggest that subduction is a key driver of supercontinent breakup, rather than superplume arrival. We also find that a traditional understanding of the supercontinent cycle (short periods of supercontinent existence with longer intermittent times of dispersal and assembly) difficult to observe in the data we extract from models, and we suggest that, at least for the last 1 Ga, supercontinent existence is a dominant force in global tectonics, punctuated by shorter periods of assembly and dispersal.

1-3 Data and Methodologies

The relevant data and methodology for the thesis are explained in detail in each chapter. I present here a brief overview of the main approaches used for each study. The majority of the work completed in this thesis was based in the interactive plate reconstruction software, GPlates (www.gplates.org), and the python library pyGPlates.

1-3-1 Article One

Published palaeomagnetic and geological data are used to constrain possible Australia-Laurentia configurations during Rodinia. Kinematic data, including velocity and angular rotation, based on different rifting times and the alternative configurations are extracted from the models. Published geological and palaeomagnetic information is also used to build a kinematically constrained model of the amalgamation of eastern Gondwana (Australia-India-Congo). The global framework within which this work is grounded is provided by Li et al. (2008) and Li and Evans (2011). Terranes, polygons were used or modified from Li et al. (2008).

1-3-2 Article Two

This study, involving the construction of a topological plate model for the Neoproterozoic, used the

reconstructions of Li et al. (2008; 2013) and Li and Evans (2011) as a base. Published geological and palaeomagnetic data in addition to an extensive literature review of Neoproterozoic tectonics were used to supplement, update and alter the reconstruction, and to constrain the (possible) positions of plate boundaries. Data presented within the discussion of this article were extracted by the author from either the model being presented, or from the Matthews et al. (2016) model for younger times.

1-3-3 Article Three

The extension of the Neoproterozoic model (Article Two) into the Early Palaeozoic was achieved by linking it to the model of Domeier (2016), who created a topological plate model for the Iapetus and Rheic realms (Laurentia, Baltica, Gondwana and Avalonia). Palaeomagnetic and geological data from the literature were used to help constrain the position of the other cratonic components (Siberia and the Chinese cratons). A literature review was undertaken to determine the ages, length and duration of rifting events. The length of continental arcs were extracted from the Domeier (2016), Matthews et al. (2016) and a slightly modified version of the Merdith et al. (2017) (Chapter Two) models. Other data presented in this article were taken from their appropriate studies.

Chapter Two

Kinematic constraints on the Rodinia-Gondwana transition

Kinematic constraints on the Rodinia to Gondwana transition

CrossMark

Andrew S. Merdith [a,b,*], Simon E. Williams [a], R. Dietmar Müller [a], Alan S. Collins [c]

[a] EarthByte Group, School of Geosciences, The University of Sydney, Madsen Building F09, Australia
[b] Data61, Australian Technology Park, Australia
[c] Tectonics, Resources and Exploration (TRaX), Department of Earth Science, The University of Adelaide, SA 5005, Australia

A B S T R A C T

Earth's plate tectonic history during the breakup of the supercontinent Pangea is well constrained from the seafloor spreading record, but evolving plate configurations during older supercontinent cycles are much less well understood. A relative paucity of available palaeomagnetic and geological data for deep time reconstructions necessitates innovative approaches to help discriminate between competing plate configurations. More difficult is tracing the journeys of individual continents during the amalgamation and breakup of supercontinents. Typically, deep-time reconstructions are built using absolute motions defined by palaeomagnetic data, and do not consider the kinematics of relative motions between plates, even for occasions where they are thought to be 'plate-pairs', either rifting apart leading to the formation of conjugate passive margins separated by a new ocean basin, or brought together by collision and orogenesis. Here, we use open-source software tools (GPlates/pyGPlates) to assess quantitative plate kinematics inherent within alternative reconstructions, such as rates of relative plate motion. We analyse the Rodinia-Gondwana transition during the Neoproterozoic, investigating the proposed Australia-Laurentia configurations during Rodinia, and the motion of India colliding with Gondwana. We find that earlier rifting times provide more optimal kinematic results. The AUSWUS and AUSMEX configurations with rifting at 800 Ma are the most kinematically supported configurations for Australia and Laurentia (average rates of 57 and 64 mm/a respectively), and angular rotation of ∼1.4°/Ma, compared to a SWEAT configuration (average spreading rate ∼76 mm/a) and Missing-Link configuration (∼90 mm/a). Later rifting, at, or after, 725 Ma necessitates unreasonably high spreading rates of >130 mm/a for AUSWUS and AUSMEX and ∼150 mm/a for SWEAT and Missing-Link. Using motion paths and convergence rates, we create a kinematically reasonable (convergence below 70 mm/a) tectonic model that is built upon a front-on collision of India with Gondwana, while also incorporating sinistral strike-slip motion against Australia and East Antarctica. We use this simple tectonic model to refine a global model for the breakup of western Rodinia and the transition to eastern Gondwana.

© 2017 Elsevier B.V. All rights reserved.

1. Introduction

Our knowledge of plate tectonic configurations through Earth history is limited by the availability of data through time and space. Geological, geophysical, palaeomagnetic, geochemical, structural and tectonic (e.g. large scale orogenies, passive margins) information helps to constrain both the motions of plates, and the relative configurations of continents within past supercontinents. The fabric and geophysical signatures preserved within the ocean basins, in particular, magnetic anomalies and fracture zones (Matthews et al., 2011; Wessel and Müller, 2015), allow the construction of detailed, global relative plate models for the Mesozoic and Cenozoic (e.g. Müller et al., 2016; Seton et al., 2012 – models of the Palaeozoic tend to rely more heavily on palaeomagnetic data (e.g. Domeier and Torsvik, 2014; Torsvik et al., 2012). These features indicate the extent to which relative plate motions are stable or change over timescales of millions to tens-of-millions years. For example, spreading rates globally are typically in the range 10–70 mm/a (Müller et al., 2008). In the Atlantic basins, spreading rates have remained within 20 and 40 mm/a over the last ∼200 Ma. An analysis of global kinematic motions of the last 200 Ma by Zahirovic et al. (2015) indicated that the median of global root-mean squared (RMS) velocities is ∼40 mm/a, in broad agreement with the earlier results of Schult and Gordon (1984).

Zahirovic et al. (2015) demonstrated that as the portion of cratonic crust increases on a single tectonic plate the RMS velocity decreases, with plates consisting of 25% cratonic crust moving at only ~28 mm/a. In addition to spreading rates, the present-day ocean basins reveal abrupt changes in direction of relative plate motion at spreading centres, witnessed by sharp fracture zone bends (Matthews et al., 2011, 2012). Mechanisms to explain major changes in relative plate motion rate and direction are either grouped into 'top-down' tectonic mechanisms or 'bottom-up' mantle flow mechanisms. These localised plate reorganisation events are typically linked to regional and global changes in plate boundary forces including subduction initiation (e.g. Cawood and Buchan, 2007; Whittaker et al., 2007), cessation (Austermann et al., 2011; Patriat and Achache, 1984), or changes in the subduction regime through subduction of ridges (Seton et al., 2015), thick oceanic plateaus (Knesel et al., 2008) or young, buoyant oceanic crust (Matthews et al., 2012). Proposed mantle flow mechanisms include influence of plume heads arriving at the base of the lithosphere (Cande and Stegman, 2011; van Hinsbergen et al., 2011), decoupling due to lubrication from plume arrival (Ratcliff et al., 1998) and heat buildup around subducted slabs leading to a reduction of negative buoyancy (King et al., 2002; Lowman et al., 2003). Recognising plausible motions and spreading rates of present-day plates, and understanding mechanisms behind the reasons why changes in their regime occur are important for pre-Pangea plate reconstructions because they provide a possible constraint on what plate motions could resemble, especially between the periods of supercontinent existence.

The supercontinent cycle theory implies that over time continents disperse forming ocean basins, before re-amalgamating into a new supercontinent (e.g. Cawood and Hawkesworth, 2014; Nance and Murphy, 2013; Worsley et al., 1984). Evidence for this cyclicity is provided by palaeomagnetic data that permit long-lived tight fits between plate pairs (e.g. Li et al., 2008; Pisarevsky et al., 2014a,b; Rogers and Santosh, 2002), periodic peaks in continental-continental orogenies related to amalgamation (e.g. Condie, 2002), and peaks in rifting, passive margins and large igneous provinces, related to dispersal (e.g. Bradley, 2008, 2011; Condie, 2002). The theory suggests that the formation and breakup of supercontinents are intricately linked to both deeper earth processes, as well as surface, ocean and atmospheric processes (Bradley, 2011; Nance et al., 2014). While Pangea, the most recent supercontinent, is well known, Proterozoic supercontinents are less well established due to the absence of preserved ocean basins and the paucity of fossil evidence. Rodinia is the hypothesised late Mesoproterozoic to early Neoproterozoic supercontinent, originally envisioned on the basis of global orogenies (the Grenvillian orogeny of Laurentia and coeval Stenian-Tonian orogenies worldwide) at ca.1.2–0.9 Ga (Dalziel, 1991; Hoffman, 1991; Moores, 1991). However, not all Proterozoic cratons clearly exhibit orogenies of these ages; if they do, the orogenies are not synchronous (Fitzsimons, 2000), and, as more data have become available, a proliferation of plate configurations for the Neoproterozoic have been developed, including models with a large, long-lived Rodinia (Johansson, 2014; Li et al., 2008), palaeomagnetically defined models (Evans, 2009; Powell et al., 1993), and models that have a partially complete supercontinent, with one-two cratons separate (usually Congo-São Francisco and/or India, e.g. Collins and Pisarevsky, 2005; Pisarevsky et al., 2014a,b; Meert, 2003; Merdith et al., 2017). Generally, most models of Rodinia tend to have Laurentia as the heart of the supercontinent due to the presence of rifted margins on the perimeter of the continent. Australia–East-Antarctica are typically matched to the western coast of Laurentia; Siberia-North China off the northern margin; Amazonia, Baltica and West Africa on the eastern margin; and the Kalahari craton on the south-

ern margin (e.g. Dalziel, 1991; Hoffman, 1991; Johansson, 2014; Li et al., 2008, 2013; Meert and Torsvik, 2003; Moores, 1991), though some variations exist (e.g. Sears and Price, 2000).

For pre-Pangea times, where ocean basins are not preserved, it becomes more important to use other approaches to help discriminate between competing plate motions and continental configurations. Typically either geological or palaeomagnetic data (or a combination of both) are used to build deep-time plate models. For example, Goodge et al. (2008) used isotopic data from granites to tie East-Antarctica and Laurentia together at ca. 1.4 Ga; Ganade et al. (2016) dated zircons to constrain the timing of western Gondwana collision; geochemical signatures of large igneous provinces were used to determine pre-rift matches of cratons for Kenor, Nuna and Rodinia (e.g. Ernst et al., 2008, 2013; Ernst and Bleeker, 2010); and, detrital zircon analyses have been used to link provenances together (e.g. Li et al., 2015; Mulder et al., 2015; Wang and Zhou, 2012; Archibald et al., 2015) and, allowing for the incompleteness of the geological record, provide an indirect measure of secular changes in the volume of continental crust (e.g. Condie et al., 2009; Condie, 2003). Evans (2009) constructed a (completely) palaeomagnetically derived model of Rodinia, and Meert (2002) built a palaeomagnetically constrained model of Nuna. Recent models that integrate both geological and palaeomagnetic data for the globe have also been developed for Nuna (Pisarevsky et al., 2014a,b) and Rodinia (Li et al., 2008, 2013). These models anchor relative plate configurations and motions suggested by geology with absolute position as determined through palaeomagnetic data, as approaches to determining absolute plate motions for recent times for example, hot spot chains (Morgan, 1971; Müller et al., 1993; Steinberger et al., 2004) and tomographic imaging of slabs (Butterworth et al., 2014; van der Meer et al., 2010) are not applicable to deep time reconstructions.

Absolute plate motion models constructed for the Palaeozoic (Domeier, 2016; Domeier and Torsvik, 2014) use a combination of palaeomagnetic data and the assumption of fixed large low-shear-velocity provinces (LLSVPs) to constrain palaeolatitude and palaeolongitude (Torsvik et al., 2008). These models are also supplemented with geological and palaeontological data (e.g. Cocks and Torsvik, 2002; Torsvik and Cocks, 2013) to help with constraining the timing of events, palaeolatitude and plate configurations. For reconstructions of all but the latest Neoproterozoic (e.g. Meert and Lieberman, 2008), palaeontological data are unavailable as complex life had not yet evolved; therefore, the focus shifts to either palaeomagnetic and/or geological information to reconstruct plate motions. During supercontinent assembly times, palaeomagnetic data are especially useful, as a small number of reliable poles from different blocks can be pooled together to constrain the motion of a large number of cratons, leading to models that are built upon absolute plate motions; however, during times of supercontinent dispersal and amalgamation it becomes more difficult to infer absolute plate motions due to fragmented apparent polar wander paths (APWPs) and an absence of data from some cratons. Two consequences of this are the development of tectonic models that cluster around palaeomagnetic 'pierce points' (i.e. times at which high quality palaeomagnetic data exist) such that these models simply consist of a series of snapshots of the positions of continents at specified times without incorporating relative motions suggested by geology. Another consequence is the construction of tectonic models that do not allow us to distinguish between competing configurations or motions due to missing or poor quality data.

The Neoproterozoic, in particular the transition to Gondwana from Rodinia, is a key stage in global plate reconstructions due to the (near-)global glaciation events that occurred at that time (e.g. Gernon et al., 2016; Hoffman and Li, 2009; Schmidt and

Williams, 1995; Cox et al., 2016). Gondwana, consisting primarily of Africa, South America, Australia, India and Antarctica, was the precursor to Pangea, and the major landmass of the southern hemisphere for much of the Phanerozoic. It occupies a particularly important position for both geological and biological purposes, as it is the oldest proposed supercontinental amalgamation for which a variety of geological data are readily available (Cawood and Buchan, 2007; Collins and Pisarevsky, 2005; Li et al., 2008; Meert, 2003), as well being integral to the evolution and dispersion of complex life (e.g. Brasier and Lindsay, 2001; Halverson et al., 2009; Maruyama and Santosh, 2008; Meert and Lieberman, 2008; Santosh, 2010; Squire et al., 2006). However the configuration of Rodinia is much less certain, with disagreement about whether specific continents were part of Rodinia (e.g. Congo-Saõ Francisco, Pisarevsky et al., 2003a), and also about the exact configuration and fit between two cratons (e.g. 'tight-fit' Siberia vs. 'loose-fit' Siberia, cf. Ernst et al., 2016; Pisarevsky and Natapov, 2003). While it is widely accepted that Australia-East Antarctica were attached to the western margin of Laurentia in Rodinia, there is yet to be a definitive answer as to the exact configuration. There are currently four proposed models; **S**outh-**W**est United States – **E**ast **A**ntarctica (SWEAT - Dalziel, 1991; Moores, 1991); **Aus**tralia-**W**estern **U**nited **S**tates (AUSWUS – Brookfield, 1993; Karlstrom et al., 1999); **Aus**tralia-**Mex**ico (AUSMEX – Wingate et al., 2002), and; Missing-Link (Australia-South China-Laurentia – Li et al., 1995, 2008, or Australia-Tarim-Laurentia, Wen et al., 2017). All four models pair Australia-Antarctica with Laurentia, though they differ in how far north Australia-East Antarctica sit relative to Laurentia (Fig. 1). Additionally, though sedimentation occurs from ca. 830 Ma (e.g. Preiss, 2000), the time of rifting and transition to drift are poorly constrained due to difficulties dating the sequences. This is exacerbated by sedimentary sequences suggesting a passive margin didn't develop until sometime in the late Cryogenian (Li and Evans, 2011), yet palaeomagnetic data suggests breakup prior to 750 Ma (Wingate and Giddings, 2000) unless an intraplate rotation of the North Australian Craton relative to the South Australian Craton is applied (Li and Evans, 2011). Consequently, rifting has been interpreted to be Ediacaran aged (ca. 540 Ma, e.g. Veevers et al., 1997), mid-Cryogenian age (ca. 700 Ma – Preiss, 2000; Li et al., 2008) or early Cryogenian in age (prior to 750 Ma, e.g. Wingate and Giddings, 2000).

Here we focus on an alternative approach to discriminate between competing Proterozoic reconstructions, using kinematic data extracted from a continent-focussed plate reconstruction model (adapted from Li et al., 2008, 2013). We use modern relative plate motion kinematics derived from the late Phanerozoic evolution of ocean basins to help make informed decisions for plate reconstructions during times of supercontinent dispersal and amalgamation, when large gaps in the coverage of palaeomagnetic data limit our ability to constrain plate motions. From this, we generate a simple tectonic reconstruction of the breakup of western Rodinia (i.e. western Laurentia, Australia and Antarctica) and amalgamation of eastern Gondwana. We demonstrate this during dispersal times by comparing the four competing Neoproterozoic configurations of Laurentia and Australia–East-Antarctica, reconstructing them from a common end point (650 Ma) back to the possible rifting times permitted by both palaeomagnetic and geological data, and then in times of amalgamation, by tracing and constraining the relative motions of India with respect to Australia, and with respect to the Congo-São Francisco continent.

2. Australia-Laurentia configurations

Four configurations of the Australia–East-Antarctica – Laurentia connection have been proposed in the last twenty years based on

geological and palaeomagnetic grounds, though both sets of data are insufficient to fully discriminate between them. SWEAT, juxtaposing the south-west USA with eastern Antarctica (Australia lies further north, near Wyoming and the Canadian border) (Dalziel, 1991; Hoffman, 1991; Moores, 1991) (Fig. 1a); AUSWUS, which matches the east coast of Australia with the west coast of the USA (Karlstrom et al., 1999) (Fig. 1b); AUSMEX, which pushes Australia–East-Antarctica further south, such that Queensland is against Mexico (Wingate et al., 2002) (Fig. 1c); and the Missing-Link model, which fits South China as a continental slither between Laurentia and Australia (Li et al., 1995) (Fig. 1d). Variations on the Missing-Link model include swapping out South China and instead replacing it with the Tarim continent (Wen et al., 2017). Here we stay with the traditional South China version; many of the arguments pertaining to South China as the missing-link are just as relevant for Tarim.

Generally, the conjugate margins of both corresponding continents have thick sedimentary sequences intruded by magmatic dykes (e.g. Davidson, 2008; Preiss, 2000; Rainbird et al., 1996; Walter et al., 1994; Yonkee et al., 2014; Young et al., 1979) that suggest rifting somewhere between 825 and 700 Ma, though the transition from rift to drift is unconstrained partly due to difficulties in precisely dating many of the formations of the Adelaidean Rift Complex. Li and Evans (2011), suggested a passive margin developed by 680 Ma based on global correlations of glacial units preserved in the Adelaidean Rift Complex, though more recent work on the Laurentian margin suggests a series of rifting events at ca. 700 and 600 Ma (e.g. Colpron et al., 2002; Prave, 1999; Yonkee et al., 2014).

2.1. SWEAT

The original Rodinian connection proposed between Laurentia and Australia by Dalziel (1991), Hoffman (1991) and Moores (1991) was based on a number of similarities including the inferred extension of the Grenvillian Orogen into Antarctica (and India) (Moores, 1991) and similar tectonic histories and tectonostratigraphy of their margins (e.g. Bell and Jefferson, 1987; Dalziel, 1991; Eisbacher, 1985). Both the west coast of Laurentia and the east coast of Australia are characterised by thick, broadly correlatable, sedimentary successions (e.g. Rainbird et al., 1996; Young et al., 1979; Young, 1981) that are cut by dyke swarms (e.g. Ernst et al., 2008). These reconstructions placed the margin of eastern Antarctica against the southwest United States margin (hence the acronym SWEAT), with the east coast of Australia aligning with the Wopmay Belt of north-eastern Canada (Moores, 1991) (Fig. 1a).

2.2. AUSWUS

The AUSWUS (Australia-Western United States, Fig.1b) connection was originally proposed based on the structural relationship of the offsets from three transform faults between Laurentia and Australia, and then using them to more accurately align the margins (Brookfield, 1993). Karlstrom et al. (1999, 2001) refined this connection (terming it 'AUSWUS') by connecting the Grenvillian Orogen in Laurentia with the Albany-Fraser and Musgrave Orogens in Australia and Burrett and Berry (2000, 2002) expanded on it further, matching the Broken Hill and Mt Isa Terranes in Australia with the Mojavia Province and San Gabriel Terrane in the western United States, suggesting a stronger affinity between eastern Australia and Western US, than Australia and Canada.

2.3. AUSMEX

AUSMEX (Australia-Mexico) was proposed by Wingate et al. (2002) in response to perceived poor reliability in palaeomagnetic
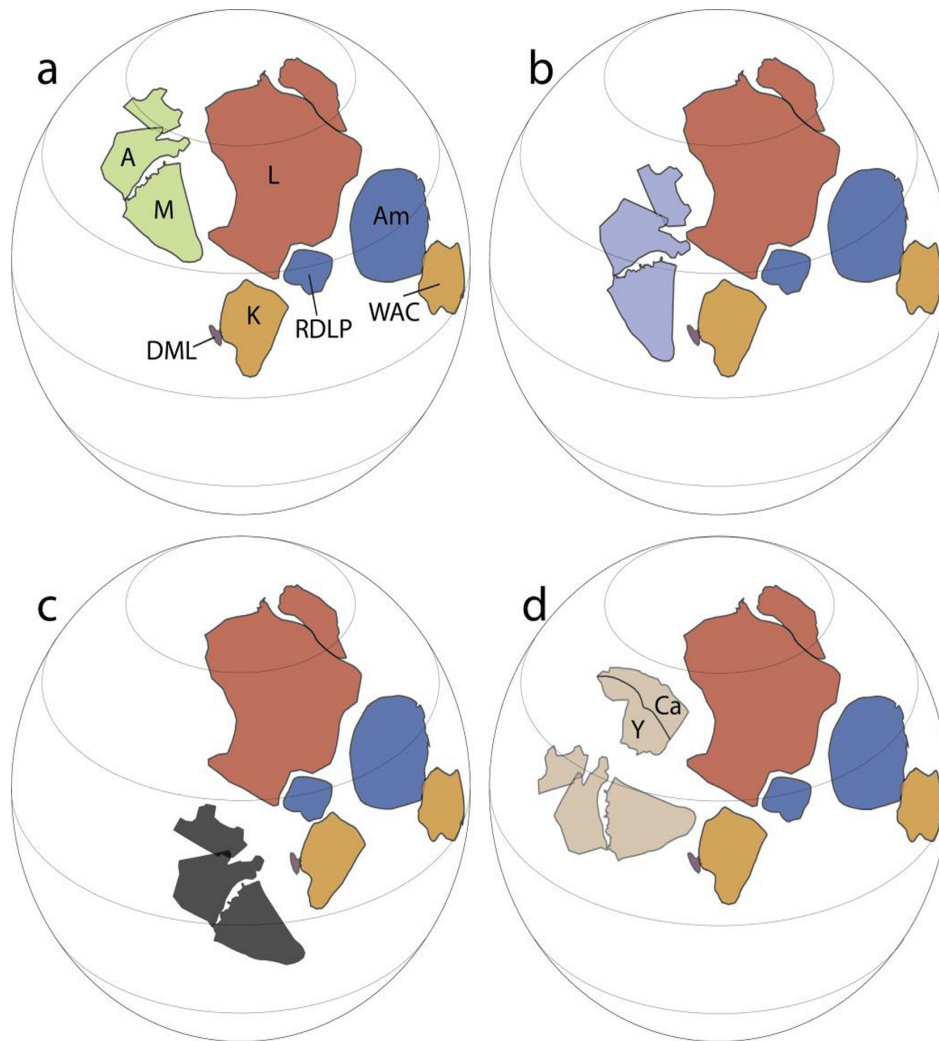
Fig. 1. The different configurations of Laurentia with Australia-Eastern Antarctica and South China with pre-Neoproterozoic geology overlain. Laurentia is fixed in its present-day position with all other blocks rotated relative to it at 800 Ma (after Li et al., 2008, 2013). (a) SWEAT fit (green), eastern Antarctica is pushed against the southwest US, while Australia lies further north near the US-Canadian border (Dalziel, 1991; Hoffman, 1991; Moores, 1991); (b) AUSWUS fit (blue), eastern Australia is matched against the southwest United States of America (Karlstrom et al., 1999); (c) AUSMEX (black), Australia has only a small connection with Laurentia, where the north tip of Queensland fits against Mexico (Wingate et al., 2002), Kalahari Craton is shifted further south to accommodate Mawson; (d) Missing-Link model (tan), which fits South China as a continental slither between Australia and Laurentia (Li et al., 1995). A, Australia; Am, Amazonia; Ca, Cathaysia (part of South China); DML, Dronning Maud Land; K, Kalahari; L, Laurentia; M, Mawson (East Antarctica); RDLP, Rio de la Plata; WAC, West Africa Craton; Y, Yangtze (part of South China). The colour of the other blocks represents their present-day geographical position. South America – dark blue; Africa – orange; Antarctica – purple; North America – red; China – yellow. For all the following figures where it is pertinent to depict different configurations, the above colours of Australia and East Antarctica are used (typically 800–650 Ma). Where the different configurations are not used (650–500 Ma) Australia is magenta (e.g. Fig. 4). (For interpretation of the references to colour in this figure legend, the reader is referred to the web version of this article.)

data during the latest Mesoproterozoic that made both SWEAT and AUSWUS models untenable (though this was later resolved by Schmidt et al. (2006)). They proposed that if Australia–East-Antarctica was connected to Laurentia at all in the late Mesoproterozoic, then it could only be a marginal connection with northern Queensland with Mexico. This reconstruction uses a new palaeomagnetic pole from WA to constrain Australia's location at 1050 Ma (Fig. 1c). A palaeomagnetic pole from the Officer Basin at 780 Ma provides a stronger argument for an AUSMEX-type configuration than either SWEAT or AUSWUS when compared to similar-aged Laurentian poles (Pisarevsky et al., 2007), though it doesn't completely disqualify the other configurations. A notable problem with the AUSMEX configuration is the absence of geological evidence that supports this configuration. Greene (2010) argued for an AUSMEX configuration (or Missing Link configuration) based on mismatches in strike of rift basins within Australia and Laurentia.

2.4. Missing-Link

The Missing-Link model was originally proposed by Li et al. (1995) with the South China Craton acting as a continental slither caught between the amalgamation of Australia–East-Antarctica and Laurentia in an otherwise typical SWEAT configuration (Fig. 1d). While the broad stratigraphy across eastern Australia-Laurentia is congruent, there are a number of mismatches such as geochemical discontinuities (Borg and DePaolo, 1994) and the inferred mantle plume record during the Neoproterozoic. Other issues exist such as mismatched stratigraphy (Li et al., 2008), but are either difficult to disprove or prove concisely due to ice cover in Antarctica, or they disallow a SWEAT connection for a late Mesoproterozoic but not necessarily the Neoproterozoic.

The Missing-Link model neatly accounts for these, as South China shares a similar stratigraphy with both Australia and Laurentia and has been used to explain the magmatic dyke record across

all three cratons (Li et al., 1999). The offset provided by positioning this block between Australia and Laurentia also alleviated some of the problems fitting the timing of rifting within palaeomagnetic constraints of Australia, though the 40° intraplate rotation suggested by Li and Evans (2011) offered a neat solution supporting SWEAT-like configurations. A controversial component of the Missing-Link model is the presence of extensive magmatism in South China in the early Neoproterozoic (e.g. Du et al., 2014; Zhao et al., 2011). Li et al. (1999, 2008) ascribed these to rifting and intra-continental intrusions, though recent geochemistry suggests that they are from active subduction zones, suggesting that South China needs to face an open ocean and not occupy a central position of Rodinia (Cawood et al., 2013, in press; Du et al., 2014). Additionally, analysis of the sedimentary basins in South China inferred to be congruent with sedimentation on the Laurentian and Australian margins are not orientated correctly in their reconstructed positions (Jiang et al., 2003). A recent suggestion put Tarim in this Missing-Link position, which fits new palaeomagnetic data (Wen et al., 2017). However, the Neoproterozoic geology of Tarim appears to preclude this; especially hard to resolve are the inferred subduction-zone metamorphism and related arc-magmatism along present northwest Tarim, in the Aksu area (Yong et al., 2013). These require ocean subduction in the Tarim just when it would need to be rifting from Australia in the Missing-Link model.

3. Palaeomagnetic constraints of Rodinia breakup

3.1. Australian constraints

Palaeomagnetic data from the Albany-Fraser Orogen and the Gnowangerup–Fraser Dyke Suite during the Late Mesoproterozoic (ca. 1.2 Ga) require Australia to be situated at polar latitudes (Pisarevsky et al., 2003b, 2014a,b), whereas comparable data from Laurentia place it closer to the equator (Palmer et al., 1977). From 1070 Ma palaeomagnetic data permit a connection between Australia and Laurentia (e.g. Schmidt et al., 2006; Wingate et al., 2002) in an AUSMEX type fit; with SWEAT, AUSWUS and Missing-Link type fits being permissible from 1050 Ma (Powell et al., 1993). There are little reliable Australian palaeomagnetic data from the early Neoproterozoic (Table 1 – which includes both the nominal and possible age range of poles), which makes it difficult to discriminate between both the differing configurations and rifting time, though poorly dated results from the 830 to 720 Ma

Buldya Group, constrain its position to low-latitudes (Pisarevsky et al., 2007) (Figs. 2–4). In particular, an 830–730 Ma pole from the Browne Formation and an 800–730 Ma pole from the Hussar Formation suggests low latitudes, with the latter pole favouring an AUSMEX configuration *if* Australia-Laurentia had not separated yet (Fig. 2a, b) (Pisarevsky et al., 2007; Schmidt, 2014).

Two palaeomagnetic 'grand-poles' (mean of two or more key-poles from separate laboratories) from Precambrian Australia were determined for the late Neoproterozoic by Schmidt (2014). The first, from the Mundine Dyke Swarms (MDS), combines a 755 Ma pole (Wingate and Giddings, 2000) with a 748 Ma pole (Embleton and Schmidt, 1985), and the second encompasses the Elatina Formation (EF), and is dated at ca. 635 Ma (Schmidt et al., 2009; Schmidt and Williams, 1995; Sohl et al., 1999). The former pole places Australia at low latitudes and was interpreted to constrain rifting to ca. 750 Ma at the latest (Wingate and Giddings, 2000) (Fig. 3b); however, the 40° intraplate rotation of Li and Evans (2011) permits rifting to continue later (until ca. 700 Ma), by reconciling the MDS with the ca. 770–750 Ma Walsh Tillite Cap pole (Li, 2000). A 780–660 Ma pole from the Johnny's Creek Member of the Bitter Springs in central Australia by Swanson-Hysell et al. (2012) also supports this intraplate rotation, as the rotation reconciles this pole with the MDS pole (Schmidt, 2014) (Fig. 3a).

Palaeomagnetic data are available for the Ediacaran in Australia, with a series of poles from 650 to 580 Ma, including the EF grand pole (Schmidt et al., 2009; Schmidt, 2014) that constrain its position from equatorial to sub-equatorial (Schmidt et al., 2009; Schmidt and Williams, 1996; Schmidt and Williams, 2010; Sohl et al., 1999), but having rotated counterclockwise relative to Laurentia, such that it is aligned NW-SE as opposed to NE/E-SW/W (depending on starting configuration) within Rodinia (Fig. 4a, b). The Yaltipena Formation (Sohl et al., 1999) (Fig. 4a), taken here as 650 Ma after Li et al. (2013), and on the basis that it must be older than the Elatina glaciation which has a maximum age of 640 Ma (Schmidt, 2014; Williams et al., 2008) (Fig. 4b) is the start of the Australian Ediacaran polar wander path, which indicates that Australia drifted in low latitudes (Schmidt and Williams, 2010). At some time in the Neoproterozoic prior to 650 Ma, Australia (together with East-Antarctica) must rift from Laurentia to reach this position, and we use this position as our common end point for all configurations.

We note that SWEAT, AUSWUS and AUSMEX configurations are all problematic with younger rifting times (younger than ca.

Table 1
Summary of palaeomagnetic data discussed above. * indicate poles used to constrain position, nominal age is provided for these poles only.

| Location	Age (Ma)		Pole		A95	Reference
	Range	Nominal	°N	°E		
Australia						
Browne Formation	830–730 Ma		44.5	141.7	7.9	Pisarevsky et al. (2007)
Hussar Formation	800–730 Ma		62	86	14.6	Pisarevsky et al. (2007)
*Johnny's Creek Member	780–660	770	15.8	83	13.5	Swanson-Hysell et al. (2012)
*Mundine Dyke Swarms ('Grand Pole')	758–752	755	45.3	135.4	5	Embleton and Schmidt (1985), Schmidt (2014), Wingate et al. (2002)
*Yaltipena Formation	650–635	650	−44.2	352.7	11	Sohl et al. (1999)
*Elatina Formation ("Grand Pole")	645–635	640	−43.7	359.3	4.2	Schmidt (2014), Schmidt and Williams (2010)
Laurentia						
Galeros Formation,	800–748		−2	163	6	Weil et al. (2004)
*Wyoming Dykes	785 ± 8	780	13	131	4	Harlan et al. (1997)
*Tsezotene Sills,	779 ± 2	780	2	138	5	Park et al. (1989)
Kwagunt Fomration	748–736		18	166	8.4	Weil et al. (2004)
Franklin-Natkusiak Magmatic Event	727–712		8	164	2.8	Denyszyn et al. (2009)
India						
*Malani Igneous Suite	770	770	68	73	9	Gregory et al. (2009)
*Bhander and Rewa Series	550	550	47	213	6	McElhinny et al. (1978)
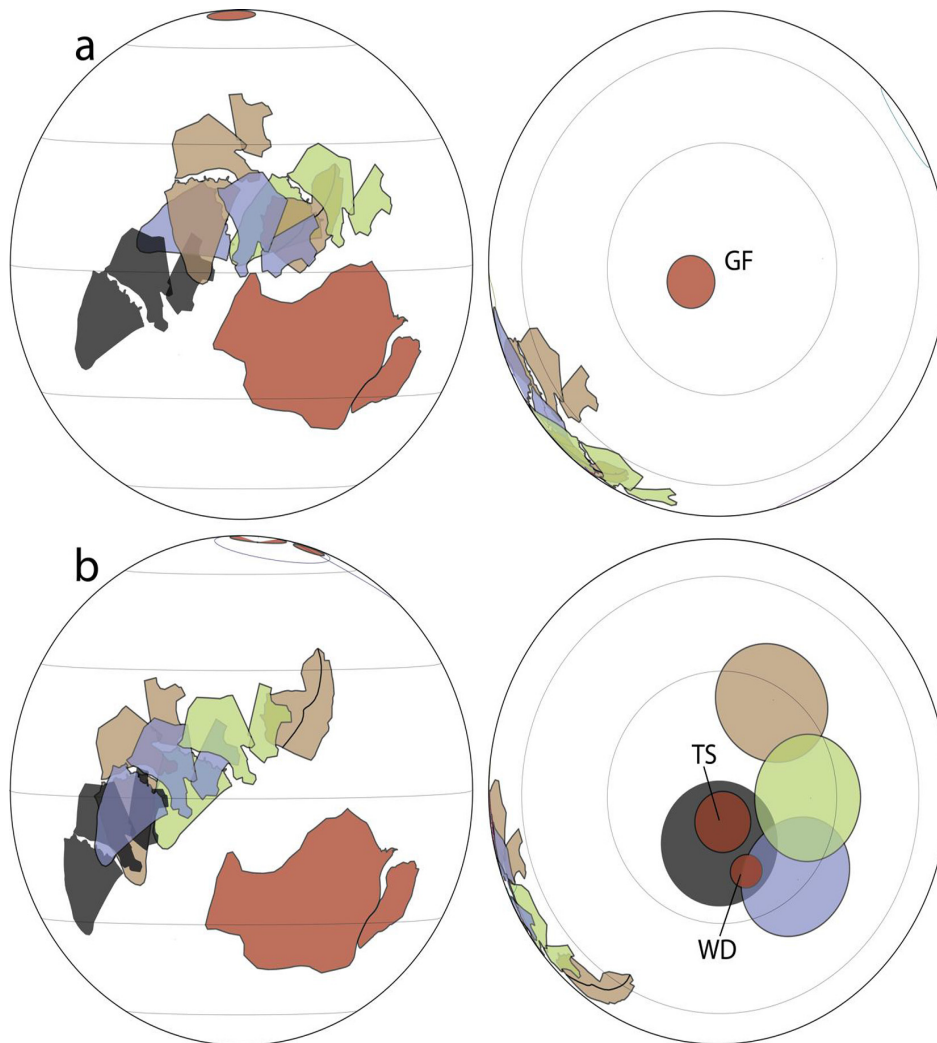
Fig. 2. Palaeomagnetic data for Australia and Laurentia at (a) 800 Ma, and (b) 780 Ma. Alternate Australia configurations are colour-coded; SWEAT – green; AUSWUS – blue; AUSMEX – black; Missing-Link – tan. Laurentia is in red. GF, Galeros Formation, TS, Tsezotene Sills, WD, Wyoming Dykes. Australian pole in (b) is the Hussar Formation. (For interpretation of the references to colour in this figure legend, the reader is referred to the web version of this article.)

770 Ma) on palaeomagnetic grounds due to the mismatch between the MDS pole and equatorial position of Laurentia, which, given these fits, would have to sit N-S (similar to present day) rather than E-W (Wingate and Giddings, 2000). Importantly, the position of Australia in the Missing-Link model helps minimise the offset of the MDS pole (as it is situated more 'upright' relative to Laurentia).

3.2. Laurentia

Only a few poles constrain Laurentia's position between 830 and 650 Ma. Two higher quality poles, the 782 Ma Wyoming Dykes (Harlan et al., 1997) and the 779 Ma Tsezotene sills and dykes (Park et al., 1989), both indicate Laurentia lay at low latitudes (Fig. 2b). A ca. 720 Ma pole from the Franklin Dykes limits Laurentia to a low latitude (Denyszyn et al., 2009). Finally, two poorly-dated poles from the Galeros and Kwagunt formations (800–740 Ma) (Fig. 2a) also suggest a low latitude Laurentia during this time (Weil et al., 2004), though the lack of a reliable age makes them difficult to use in reconstructions. No palaeomagnetic data exist for Laurentia (or Baltica and Amazonia) at 650 Ma with the closest reliable pole on the younger side from the Long Range Dykes (Murthy et al., 1992) placing Laurentia equatorially at

615 Ma. We follow Li et al. (2008, 2013) in assuming a simple interpolation between the two poles, leaving Laurentia at equatorial latitudes during this time.

4. Assembly of eastern Gondwana

4.1. Palaeomagnetic data

Palaeomagnetic data from India are incredibly sparse, hence the uncertainty attached to its position by nearly all global tectonic models of the Neoproterozoic (Table 1). Positions include having it attached to northwestern Australia (e.g. Li et al., 2008) attached to western Australia–East-Antarctica (similar to its Gondwana position) (e.g. Dalziel, 1991; Hoffman, 1991; Moores, 1991), or not part of Rodinia at all (Powell and Pisarevsky, 2002; Torsvik et al., 2001a,b; Merdith et al., 2017). Generally, it's relative position is always to the north-west/west of Australia, such that by 650 Ma subduction of the ocean separating it from Australia and the Congo Craton leads towards Gondwana amalgamation. A 770 Ma pole from the Malani Igneous Suite (Gregory et al., 2009; Torsvik et al., 2001b) indicates a mid-latitude position for Neoproterozoic India at this time (Fig.5a), and is supported by a 750 Ma pole from
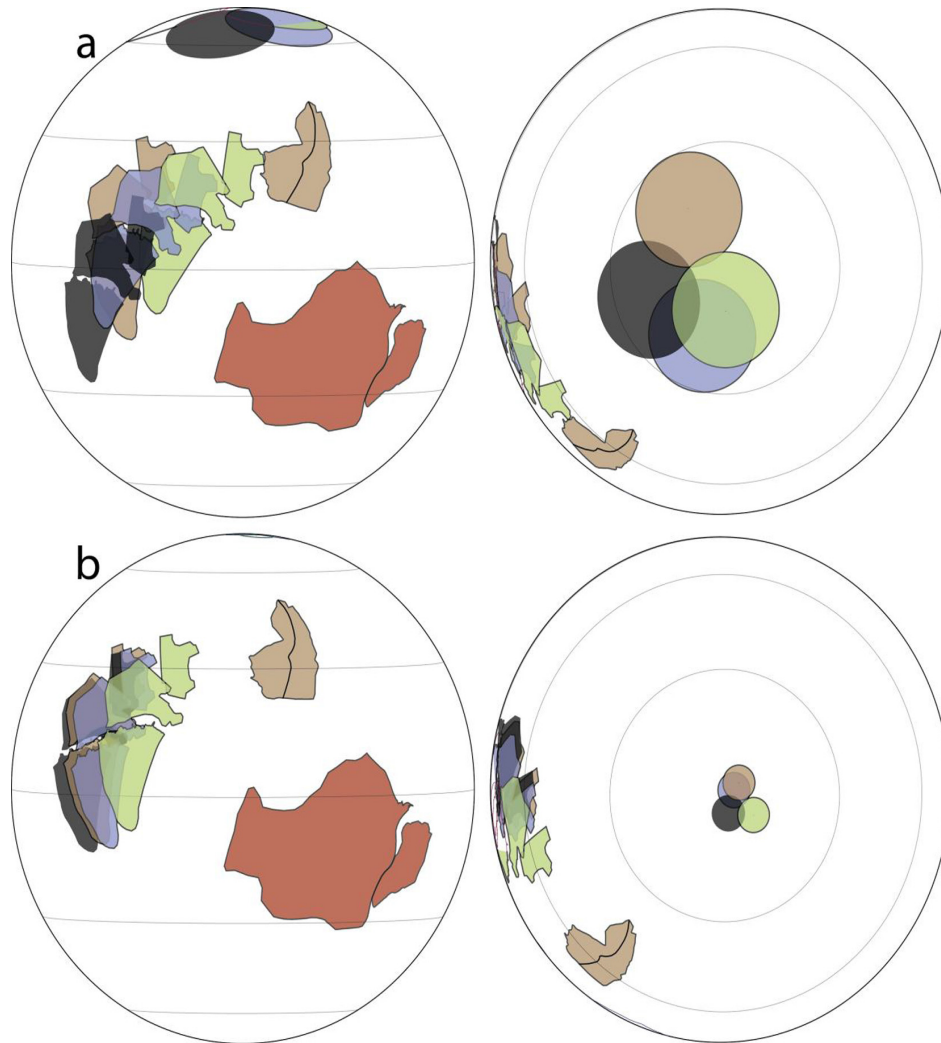
Fig. 3. Palaeomagnetic data for Australia and Laurentia at (a) 770 Ma (Johnny Creek Pole), and (b) 750 Ma (Mundine Dyke Swarms). Alternate Australia configurations are colour-coded; SWEAT – green; AUSWUS – blue; AUSMEX – black; Missing-Link – tan. Laurentia is in red. (For interpretation of the references to colour in this figure legend, the reader is referred to the web version of this article.)

the Seychelles that indicates a similar position (Torsvik et al., 2001a). Chronologically, the next Indian pole is that from the Bhander and Rewa Series at ca. 550 Ma, which constrains it to a sub-equatorial position, and is coeval with the final collision of India-Congo (Fig. 5b) (McElhinny et al., 1978). India's motion between these two poles is generally interpreted to be drifting south, which suggests that it wasn't part of a Rodinia through this time.

4.2. Geological data

The assembly of eastern Gondwana was driven primarily by the subduction of the Mozambique Ocean recorded in the formation of two major orogens, the East African Orogen between India and Congo (Collins and Pisarevsky, 2005), and the Kuungan (or Pinjarra in Australia) Orogen between India and Australia–East-Antarctica (Meert, 2003). Detailed geological synopsis of this collision have been undertaken previously (e.g. Boger et al., 2015; Collins et al., 2014; Johnson et al., 2005), and we summarise below the pertinent geological observations available to constrain relative plate motion between India-Australia and India-Gondwana that links absolute positions constrained by palaeomagnetic data.

Southward movement of India during the Cryogenian suggested by palaeomagnetic data is broadly compatible with the geological record, where preserved ophiolites in the Manumedu Complex suggest not only supra-subduction zone setting between 800 and 700 Ma, but also that this formed the southern extent of Neoproterozoic Greater India (e.g. Collins et al., 2014; Yellappa et al., 2010). Southern India consists of a core of cratonised Archaean-aged crust, the Dharwar Craton, and the Southern Granulite terrane, which constitutes a series of Neoarchaean and Proterozoic-aged terranes broadly younging southwards; the Northern Madurai Block and Southern Madurai Block, which are separated from the Palaeoproterozoic Trivandrum Block and Nagercoil Blocks by the Achankovil Shear Zone (Collins et al., 2014). Collins et al. (2014) and Plavsa et al. (2014) show that these southern blocks of present-day India were likely to be part of Azania and the Malagasy arc (Archibald et al., 2015), outboard of the Congo craton, on the basis of detrital zircon signatures and similarities in meta-igneous rocks, so that by the mid-Neoproterozoic a backarc basin (termed Neomozambique Ocean by Plavsa et al., 2014, 2015) separated Congo from Azania (and the southern Indian blocks), and the larger Mozambique ocean separated Azania from India. Greater India entered a period of tectonic quiescence from
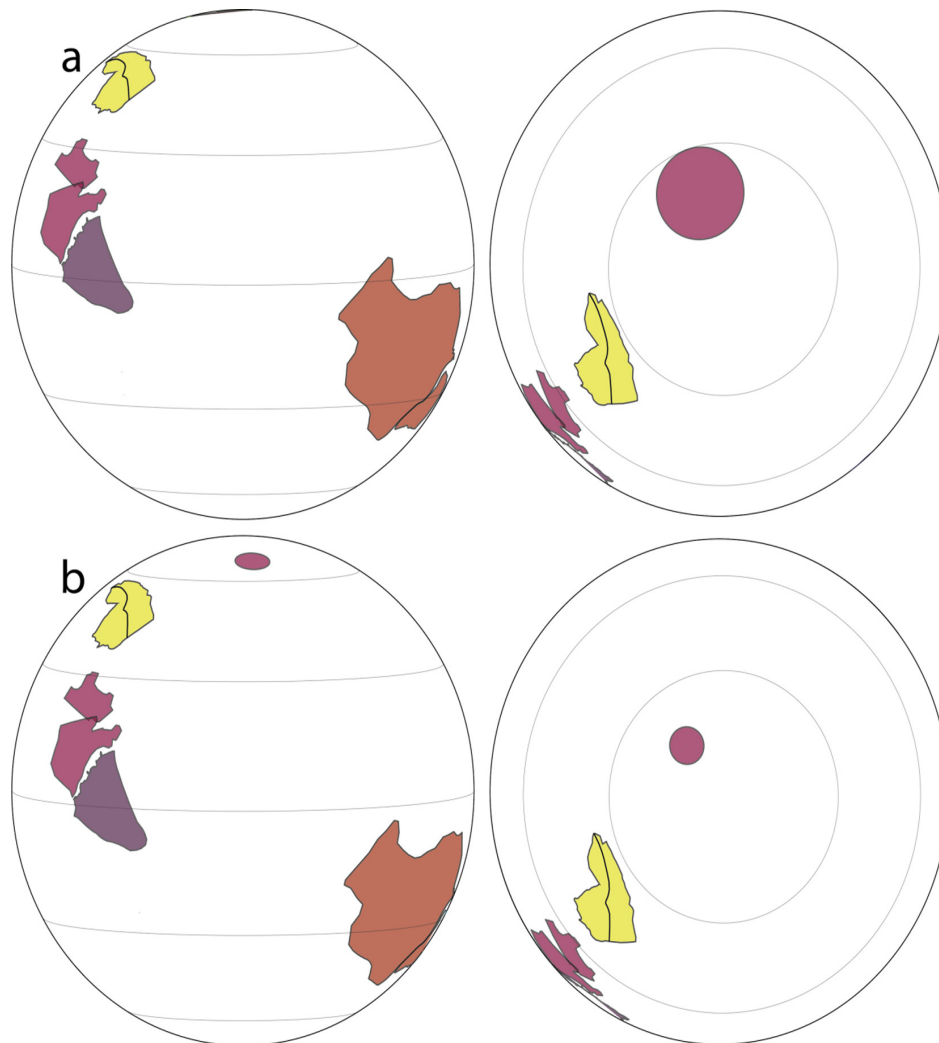
21

Fig. 4. Palaeomagnetic data for Australia and Laurentia at (a) 650 Ma, and (b) 640 Ma. The alternate Rodinian configurations for Australia are now identical. Australia is now magenta, Antarctica is purple, South China is yellow and Laurentia is in red. Australian poles are the Yaltipena Formation (a) and the 'grand-pole' of the Elatina Formation (b). (For interpretation of the references to colour in this figure legend, the reader is referred to the web version of this article.)

700 to 625 Ma, though on the other side of the Mozambique ocean, Azania records convergence-related deformation and metamorphism from 675 to 500 Ma (Ashwal et al., 1998; Buchwaldt et al., 2003; Collins, 2006; Collins et al., 2014; Wit et al., 2001). The Malagasy orogeny is recorded in Azania (and the southern India blocks) from 625 to 500 Ma (Collins et al., 2014; Vijaya Kumar et al., 2017), with an inferred collision between it and Greater India at ca. 550 Ma (e.g. Boger, 2011; Collins and Pisarevsky, 2005; Meert, 2003).

The synthesis of palaeomagnetic and geological data suggests a continuous southerly drift of India during the Cryogenian, with a subduction reversal, at ca. 700 Ma onto the southern margin of the Mozambique Ocean (i.e. north side of Azania), resulting in destruction of this ocean basin. Synchronously, subduction of the Neomozambique Ocean under Congo occurred, resulting in the closure of the basin between Congo-Azania. This created double-dipping subduction (Plavsa et al., 2014) and resulted in a perpendicular, 'head on' collision between India and the rest of Gondwana (Collins et al., 2014), the evidence for which, in part, is shown by the granulite facies metamorphism recorded in the Mozambique suture and the development of a major orogenic plateau in this region of Gondwana (e.g. Collins et al., 2007; Fitzsimons, 2016).

The motion of India relative to Australia during the mid-late Neoproterozoic (i.e. 750–550 Ma) was originally envisioned as

relatively minor and intra-continental (Harris and Beeson, 1993). This was largely due to an interpretation of the metamorphism and magmatism in the intervening region as being due to crustal thinning and strike-slip deformation rather than crustal thickening and plate convergence. This interpretation was revised during the 2000's with studies of the metamorphism, deformation and geochronology of SW Australia (Collins, 2003), the Prydz Bay area of Antarctica (Kelsey et al., 2007), and NE India (Yin et al., 2010) concluding that the Neoproterozoic orogen between India and Australia in Gondwana represented periodic ocean subduction and crustal thickening, and can therefore be considered a true oceanic suture. To explain the (now necessary) relative motion of India to Australia during Gondwana assembly times, a sinistral strike-slip motion along the Darling Fault in Western Australia is used (e.g. Collins, 2003; Fitzsimons, 2003; Harris, 1994; Powell and Pisarevsky, 2002), suggesting that India was dragged south, past Australia, into a collision with the rest of Gondwana.

5. Methodology

We investigate the relative motion for two specific geological episodes: firstly, rifting between Australia—East-Antarctica and Laurentia during Rodinia breakup and subsequent continued
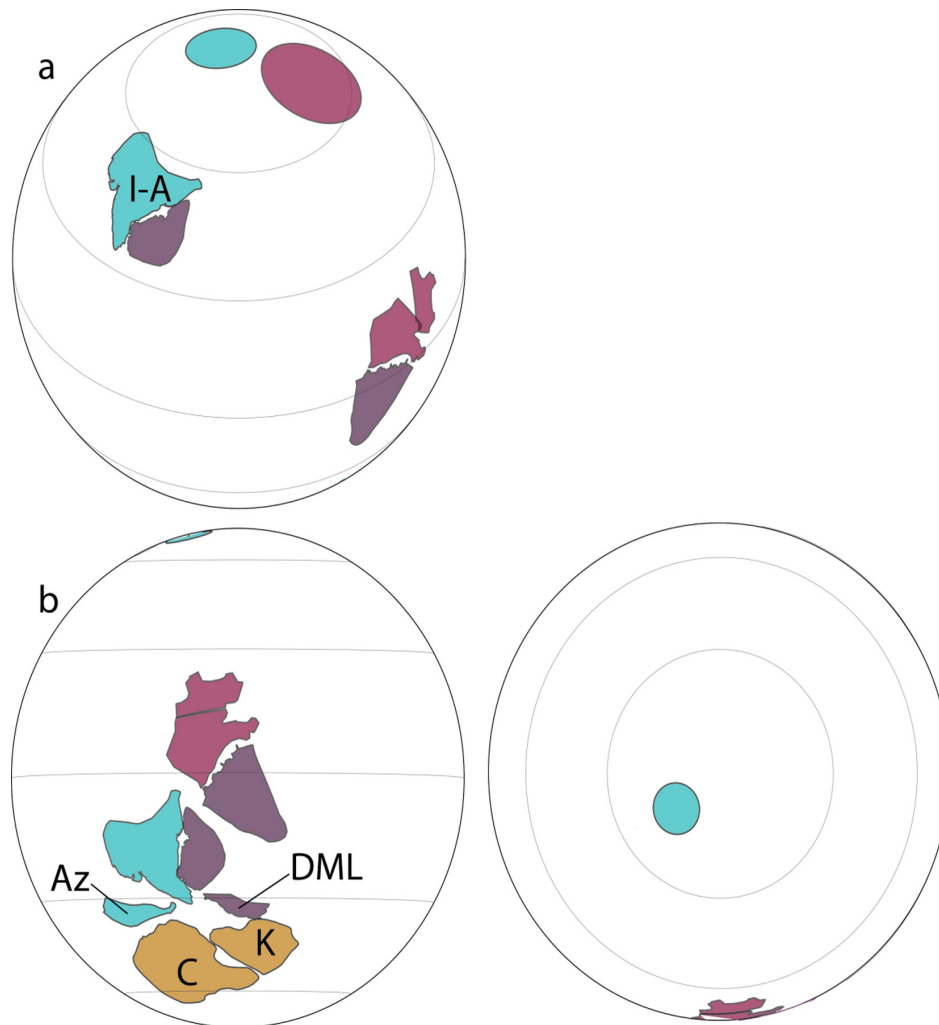
Fig. 5. Palaeomagnetic data for India at (a) 770 Ma (Malani Igneous Suite), and (b) 550 Ma (Bhander and Rewa Series). Az, Azania; C, Congo Craton; DML, Dronning Maud Land; I-A, India-Antarctica (J. Halpin, pers. com. 2017); K, Kalahari. The colour of the blocks represent their present day location. Africa, orange; Antarctica, purple; Australia, magenta; India and the Middle East, light blue. The Australian pole is the (a) Johnny Creek Member pole. (For interpretation of the references to colour in this figure legend, the reader is referred to the web version of this article.)

divergence; and secondly, convergence between India and Australia, and India and Congo, during Gondwana amalgamation. The rifting time and alternative configurations of Australia—East-Antarctica and Laurentia were analysed to determine which timings and configurations are more kinematically feasible (i.e. compared to present-day kinematics) as well as to determine the possible range of relative palaeolongitudinal distance between Australia—East-Antarctica and Laurentia for times postdating their interpreted connection. We implement the intraplate rotation of Li and Evans (2011) of the North Australian Craton (NAC) to the South Australian Craton (SAC) for each configuration, leaving the SAC fixed in the published Euler pole rotation for each configuration, and rotating the NAC. For the amalgamation of eastern Gondwana, known geological and palaeomagnetic constraints of India, Congo and Australia were used to build a kinematically feasible, relative plate convergence model.

5.1. Formulation of analysis

For Australia—East-Antarctica and Laurentia rifting, we generated alternative scenarios as follows:

- Alternative starting configurations were based on published poles of rotation (Fig. 1).
- The Euler Pole describing Australia's position at 650 Ma is the same for all configurations, and defined by the beginning of the magnetostratigraphy of the South Australian sedimentary sequences (e.g. the Yaltipena, Elatina, Nuccaleena, Bunyeroo Formations).
- Variations of rifting time between Australia–East-Antarctica and Laurentia were generated in 25 Ma time steps from 800 to 725 Ma to examine how spreading rates change, with earlier rifting times adjusted by the insertion of a new Euler pole rotation at 750 Ma in order to satisfy the latitudinal constraint of the MDS pole

Though SWEAT, AUSWUS, AUSMEX configurations are palaeomagnetically problematic with later rifting times (post 770 Ma), we include their analyses to further highlight whether late rifting is likely or not. Consequently, this creates a 30° mismatch the MDS pole and the reconstructions for rifting at 750 and 725 Ma for these configurations.

Absolute constraints on palaeolongitude have been explored for the Palaeozoic (e.g. Torsvik et al., 2008), though the only method

for constraining longitude in the Precambrian preserves the position of a supercontinent, and not individual plates (Mitchell et al., 2012). We constrain plate positions using the following criteria:

- Geological data, specifically regarding major blocks colliding, sharing a connection, or separating from one another.
- Kinematic criteria supported by observations from present-day ocean basins – reconstructions may be considered more likely where the spreading rates within oceans forming after continental rifting are reasonable.
- Latitudinal positions as described by palaeomagnetic data (i.e. we assume simple, continuous paths between the palaeomagnetic end points).

To deal with uncertainties in relative palaeolongitudinal positions of continents we calculate a range of possible widths for the Palaeo-Pacific Ocean (between Australia–East-Antarctica, Kalahari and Laurentia) at 650 Ma based on slow (20 mm/a) and fast (120 mm/a) spreading, while constraining the latitudinal position of each continent to remain consistent with palaeomagnetic data.

For the Gondwana amalgamation we reconstructed India-Australia and India-Congo motions we used the following criteria:

- Start position of Australia–East Antarctica is from 650 Ma and follows the Australian Ediacaran APWP (Schmidt and Williams, 2013; Schmidt, 2014).
- Congo at 550 Ma is situated mid-latitudes using a mean Gondwana pole (Torsvik et al., 2012).
- India is interpreted to have a southward motion based on the closure of the Neomozambique and Mozambique oceans under Congo and Azania respectively.
- India collided head-on with Congo.
- A sinistral transform fault separated Australia–East Antarctica from India between 650 and 550 Ma this time.

To assess the relative plate motions implied by Neoproterozoic plate models, we consider the post-Pangea evolution of the ocean basins. Fig. 6a shows the fracture zones of the present-day ocean basins (Matthews et al., 2011; Wessel et al., 2015) and indicates that rapid changes in the orientation and rate of seafloor spreading can occur *when* they coincide with changes in the global plate regime. For example, the change in the Indian Ocean is due to the onset of rifting between Australia and Antarctica at 40 Ma. Fig. 6b shows the most recent compilation of seafloor spreading rates since Pangea breakup (Müller et al., 2016). The global mean spreading rates of currently preserved ocean crust is 37 mm/a, with a standard deviation of 27 mm/a (Fig. 6b). We take the optimal range of spreading rate to be 10–70 mm/a, though we note that faster rates of spreading can be acceptable in certain circumstances, such as plates without cratonic lithospheric roots or plates comprised predominantly of oceanic crust (Zahirovic et al., 2015). We also note that as continental-continental collision occurs, the convergence rate of the moving plate slows, as suggested by India's collision with Eurasia (Cande and Patriat, 2015; van Hinsbergen et al., 2011). Finally, based on Bird (2003) and Argus et al. (2010, 2011) the angular rotation for cratonic landmasses in the present day is <5 °/Ma though smaller plates without cratonic crust can exhibit faster (up to 20 °/Ma) rates of angular rotation.

Six sets of kinematic data were extracted; flowlines, position and angular rotation of Euler poles that describe the motion, relative spreading rates, and, mid-ocean ridge orientation, were extracted from the relative motions of Australia-Laurentia rifting and Kalahari-Laurentia rifting, and motion paths and convergence rates were extracted from the relative motion of India to Congo and
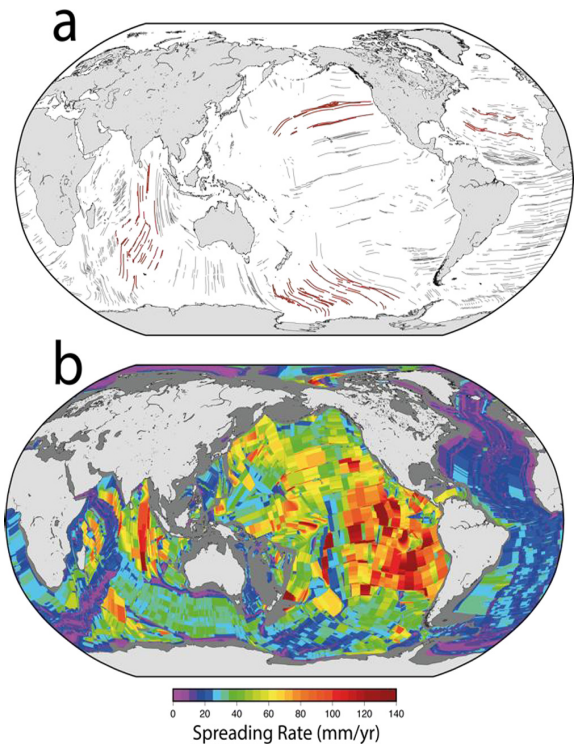

Fig. 6. (a) Present-day seafloor fabric map after Matthews et al. (2011) showing the geometry of present-day fracture zones. In particular, we highlight the rapid changes of spreading direction that occur regularly in the modern day ocean basins (visible along fracture zones highlighted red). (b) Global seafloor spreading rates based on Müller et al. (2016). The mean global spreading rate in ocean floor preserved today is ∼37 mm/a, with a standard deviation of 27 mm/a. (For interpretation of the references to colour in this figure legend, the reader is referred to the web version of this article.)

Australia. Kinematic data were analysed at a regular time interval of 5 Ma, although, provided a full reconstruction is supplied, this can be altered to be of any temporal resolution. For the assembly of Gondwana, motion paths and convergence rates were extracted from the relative motion of India-Australia and India-Congo. The rotations of other continental plates, while not used for the analysis, were plotted to help with visual reference by placing Australia, India, Congo and Laurentia within a global context. The rotations of these continents were adapted from Li et al. (2008, 2013).

6. Results

Results are presented below in Figs. 7 and 8 and Table 1. SWEAT, AUSWUS and AUSMEX all have comparably simple rifting patterns and flowlines, while the Missing-Link model has a more convoluted spreading history. The present-day range of spreading rates is plotted in black for each configuration for comparison. Average rates of motion refer to the average across all synthetic flowlines, while the maximum rate of motion refers to the single instance of maximum motion on any flowline for the specific configuration and rifting time.

6.1. Rodinia breakup

In SWEAT configurations the flowlines are simple, and the degrees of angular rotation are low for an 800 Ma rifting time, (∼1 °/Ma), but higher for 750 Ma and 725 Ma rifting times (1.3 °/Ma and 1.7 °/Ma respectively), and divergence rates increase
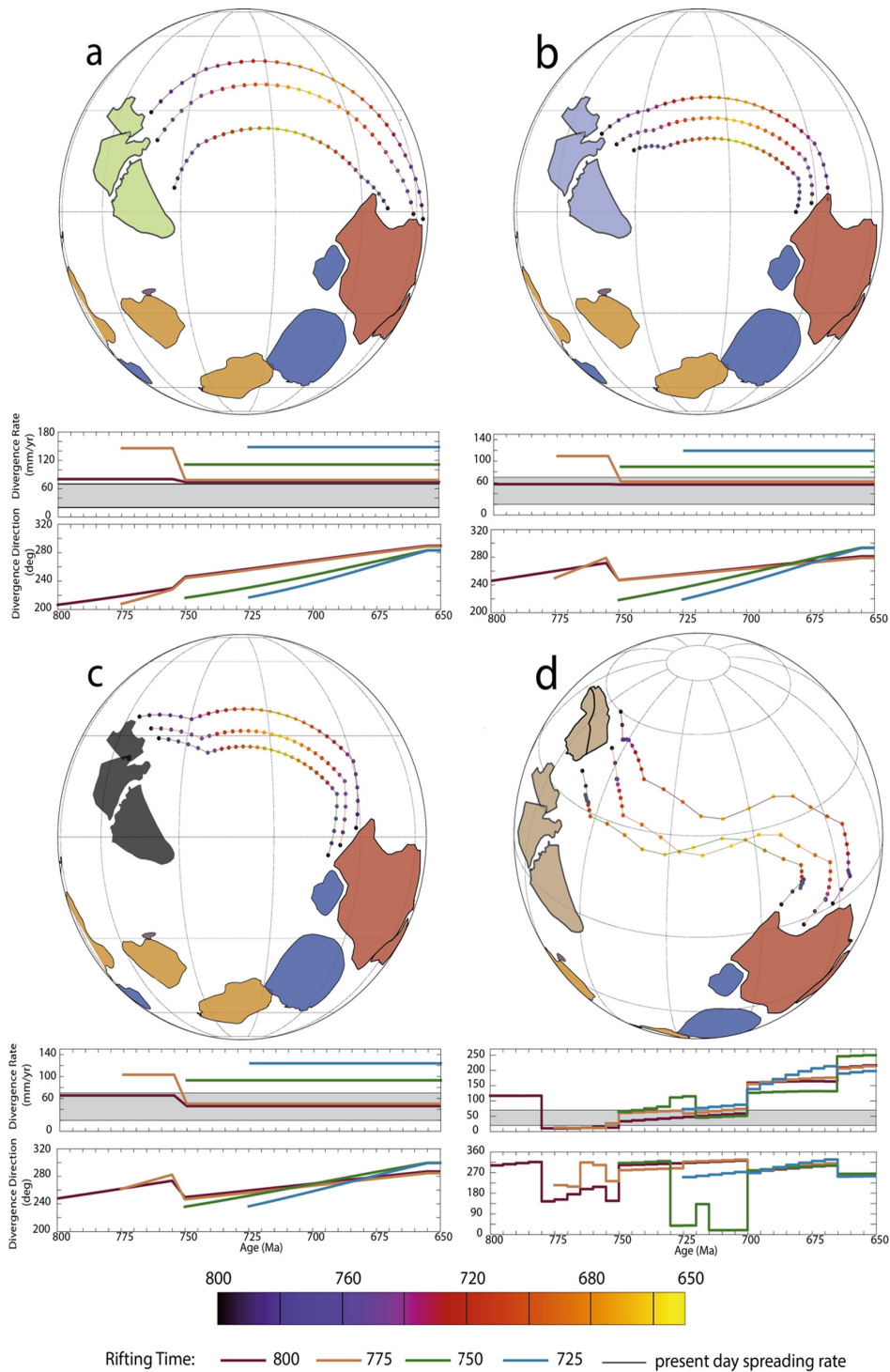
Fig. 7. Kinematic results from Neoproterozoic Australia-Laurentia configurations, (a) SWEAT (green), (b) AUSWUS (blue), (c) AUSMEX (black), (d) Missing-Link (tan). Flowlines depicted are of rifting at 800 Ma, results for spreading rates and orientation of spreading are colour coded by rifting ages. Africa, orange; Antarctica, purple; Laurentia, red; South American cratons are dark blue; and, South China, yellow. (For interpretation of the references to colour in this figure legend, the reader is referred to the web version of this article.)

with later rifting times (average/maximum 76/94 mm/a at 800 Ma and 149/170 mm/year at 725 Ma). Divergence direction changes from 210° at rifting time towards 290° at 650 Ma (Fig. 7a).

AUSWUS configurations show simple flowlines with the degrees of angular rotation increasing as the timing of rifting gets younger (from 1.5 °/Ma at 800 Ma to 1.8 °/Ma at 725 Ma) (Fig. 7b).

The relative spreading of the plates away from each other is much lower with earlier rifting (average/maximum rates 56/73 mm/year for 800 Ma) and increases as rifting time decreases (average/maximum, 120/147 mm/year for 725 Ma) (Fig. 7b). For all rifting times the orientation of spreading changes from 220°, at rifting time, to 290° at 650 Ma (Fig. 7b).
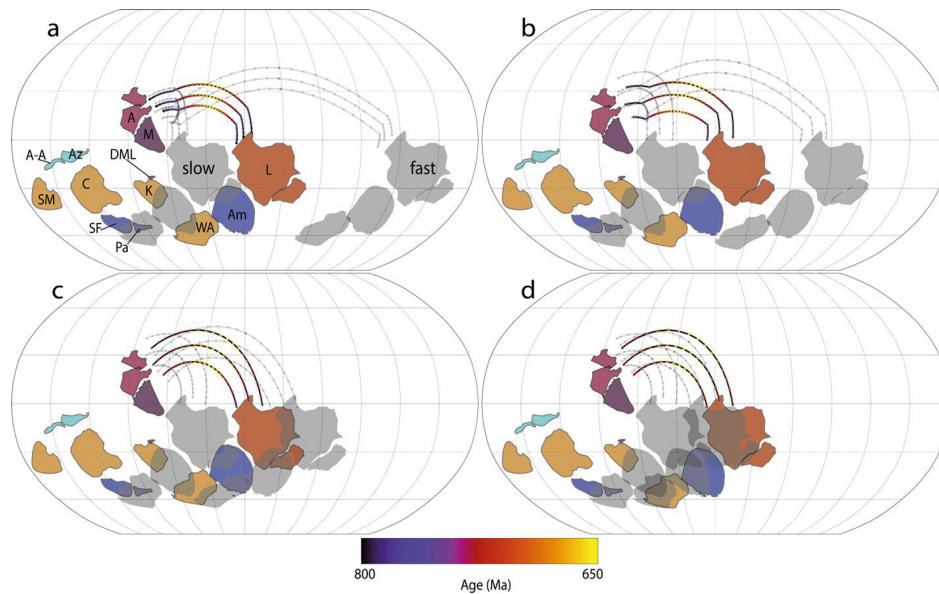
Fig. 8. Laurentia and Gondwana constituents at 650 Ma with rifting at (a) 800 Ma, (b) 775 Ma, (c) 750 Ma, and (d) 725 Ma. Original configuration of Australia–East-Antarctica and Laurentia was the AUSWUS configuration, though all configurations have the same final position of Australia and Laurentia. Grey outlines are the position of Laurentia and the two major Gondwana cratons that remained attached to it, Amazonia and West Africa, but positioned if spreading rates were slow or fast (120 mm/a). The rate of slow spreading is determined by the minimum spreading distance between Laurentia and Australia (~6000 km) required to satisfy their latitudinal position (see text). Colours of blocks and as per Figs. 1 and 5. A-A, Afif-Abas; SF, São Francisco; SM, Sahara Metacraton, and; Pa, Parana. For other labels and colours of cratons see Figs. 1 and 5.

The kinematics for AUSMEX configurations have similar results to AUSWUS configurations. Angular rotation is highest at 725 Ma where it reaches 1.6 °/Ma. The divergence rates follow the same pattern as AUSWUS, increasing as rifting time decreases (average-/maximum, 64/87 mm/a with rifting at 800 Ma and 113/135 mm/a at 725 Ma rifting, Fig. 7c) and rifting orientation increases stepwise from 220° at rifting time to 300° at 650 Ma (Fig. 7c).

The Missing Link configurations have the most complex flowlines of all configurations, depicting a series of reorganisations between rifting time and 650 Ma (Fig.7d). All rifting times have periods of angular rotation at ~2 °/Ma), and the orientation of seafloor spreading changes more regularly than other configurations, with five different adjustments occurring between rifting time and 650 Ma for 800 and 775 Ma, four for 750 Ma, and three for 725 Ma. Average spreading rates mimic that of the other configurations, being slowest at earlier rifting times (90 mm/a at 800 Ma) and higher at younger rifting times (150 mm/a at 725 Ma), though all rifting times have similar maximum spreading rates of ~210 mm (Fig. 7d). In all cases the orientation of the spreading ridge varies between 60° and 270 °/Ma (Fig. 7d).

6.2. Longitudinal separation of Australia and Laurentia at 650 Ma

The two criteria governing the paleolongitude of Laurentia (and West Africa and Amazonia that were attached to Laurentia) are ensuring a reasonable rate of divergence from Australia, and ensuring that it drifts far enough to avoid early (i.e. before 580 Ma) collision between the eastern and western Gondwanan constituents. Fig. 8 shows a range of possible positions of Laurentia relative to Australia (with palaeolatitudes consistent between all cases) given specific spreading rates at the different rifting times. To satisfy the palaeolatitude constraints, at least ~3000 km of crust must be generated on both sides of the rift at a minimum (a total of 6000 km, Fig. 8, position of 'slow' Laurentia), this creates variations in the required minimum spreading rates depending on rifting time, with 800 Ma rifting able to satisfy this with a rate of 40 mm/a, 775 Ma

rifting at 48 mm/a, 750 Ma rifting at 60 mm/a and 725 Ma rifting at 80 mm/a. Comparably, fast spreading rates, especially for the earlier rifting times (775 and 800 Ma) would place Laurentia 15,000–18,000 km away respectively. Importantly, only these earlier rifting times can satisfy the constraints of modern day spreading rates, and for the later rifting times (750 and 725 Ma) the faster spreading rates (greater than 70 mm/a) are required for moving Laurentia (with Amazonia and West Africa) far enough away to avoid collision with the Kalahari (Fig. 8c, d).

6.3. Eastern Gondwana amalgamation

The motion of India relative to Congo shows a front on collision of the southern tip of India with Congo, through to the north-west margin colliding with Azania and northern Madagascar. The rate of motion decreases from 60 to 75 mm/year between 700 and 650 Ma to 20 and 30 mm/year between 650 and 550 Ma (Fig. 9a). Comparably, the movement of India relative to Australia (Fig. 9b) depicts a sinistral motion from 650 to 550 Ma between the two continents. From 550 to 520 Ma the motion becomes convergent as Australia–East-Antarctica collide with India during the Kuungan orogeny. The rate of motion of India relative to Australia is 60 mm/year during the transform motion, before slowing to 20–30 mm/year at 550 Ma for convergence.

As India's position between 650 and 550 Ma is unconstrained, we determined possible positions of India relative to Congo (indicated by an arc, Fig. 10) assuming motion towards the Gondwana nucleus (as suggested by continuous southerly subduction) with alternative, uniform convergence rates. Slow convergence (~20 mm/a) places India more southerly than Australia at 650 Ma, whereas convergence at 70 mm/a places it slightly further north if the strike-slip boundary with Australia is preserved. A more westerly India that follows a similar convergence rate would remove this component. Fast convergence (140 mm/a) places India ~14,000 km away from the Gondwana nucleus and implies a vast area of ocean being subducted (See Fig. 10).
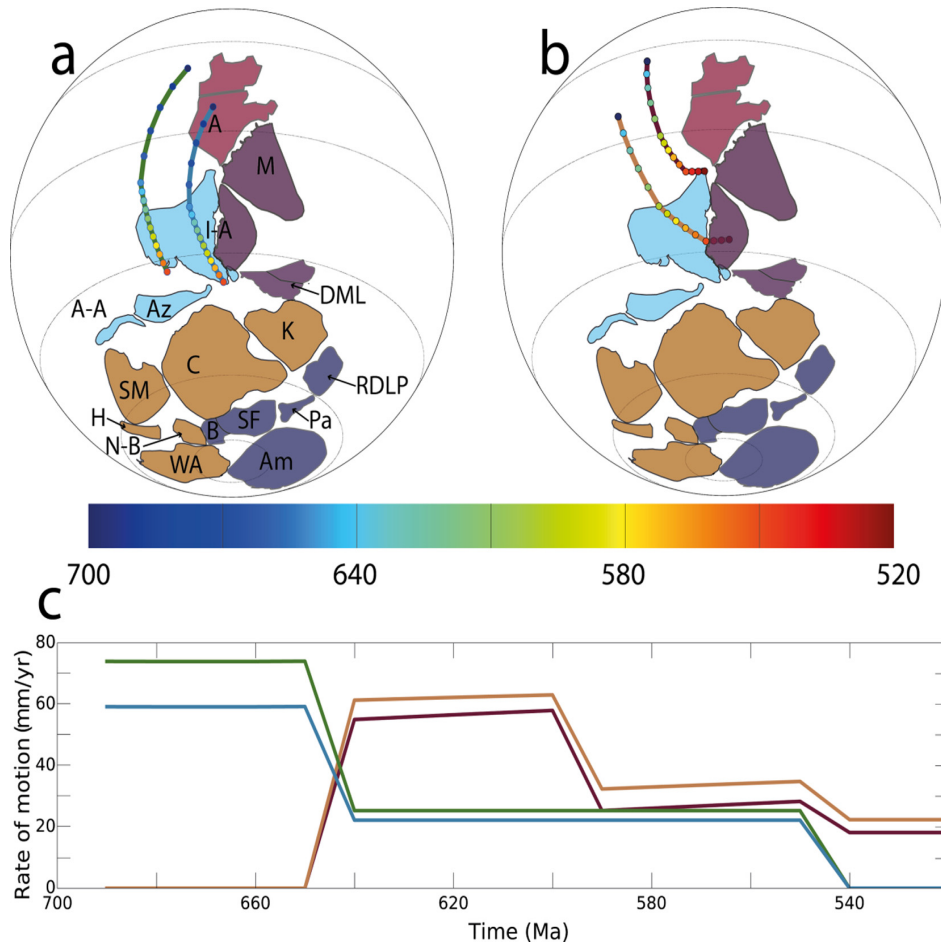
Fig. 9. Kinematic results for India's motion relative to (a) Australia and (b) Congo. (c) Depicts the convergence rates of India. Green and blue lines in (c) represent India-Congo relative convergence, orange and red lines represent India-Australia relative convergence. H, Hoggar; N-B, Nigeria-Benin Block, see Figs. 1, 5 and 8 for other labels and colours of cratons and blocks. (For interpretation of the references to colour in this figure legend, the reader is referred to the web version of this article.)
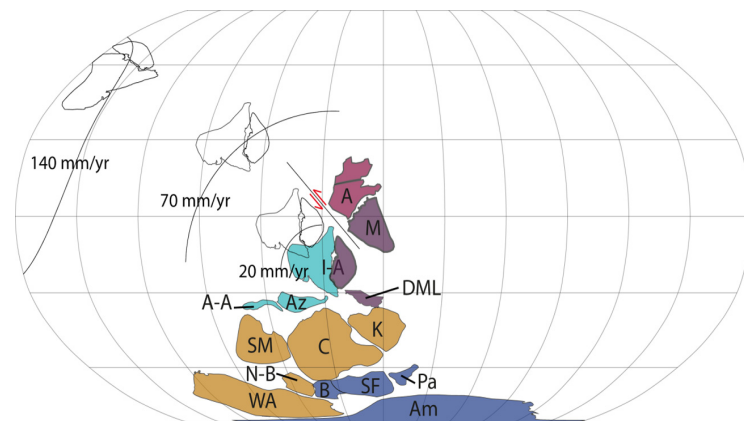
Fig. 10. Possible positions of India relative to Gondwana constituents. Coloured polygons depict their positions at 550 Ma (time of India-Congo collision) (see Figs. 1, 5 and 9 for labels and colours). Three potential positions of India are shown based on convergence rates, they are depicted by the black arcs at 650 Ma (i.e. India could sit anywhere along the arc and its convergence rate would be 20/70/140 mm/a). The black line is where India would be considered moving relative to Australia along a transform boundary.

7. Discussion

7.1. Spreading and convergence rates

As the final position of Australia at 650 Ma is the same for all configurations (defined latitudinally by palaeomagnetic data), Australia *must* move a similar distance for each rifting time. Consequently, its angular rotation varies only by how the orientation of each configuration (i.e.~040° for AUSMEX, 050° for AUSWUS, 080° for SWEAT and 010° for Missing Link) differs, and by how far north along the Laurentian coast Australia is attached. We find that maximum spreading rates for all configurations occur at 725 Ma, with spreading rate increasing as rifting time decreases due to Australia having to move the same distance, in a shorter time (i.e. 3500 km of spreading in 150 Ma, or 75 Ma). Similarly, the angular rotation rate is higher because of the shorter time between rifting and 650 Ma. Coupled with changes in rifting times, we can see that the reconstruction with the highest angular rotation is SWEAT at 725 Ma, while the reconstruction with the lowest angular rotation is AUSMEX at 800 Ma. Given modern day limits on spreading rates and angular rotation (e.g. Bird, 2003; Zahirovic et al., 2015), either an AUSWUS or AUSMEX configuration with rifting at 800 Ma is, kinematically, the most optimal configuration, though SWEAT at 800 Ma could be permissible, though the spreading rate would be just over the upper limit of modern day acceptability. Later rifting times for all configurations must account for the higher spreading rate, and rifting at either 750 Ma or 725 Ma must also account for high rates of angular rotation. Later rifting times also create a limit on the size of the Palaeo-Pacific Ocean, even permitting faster spreading rates (120–140 mm/a), the maximum basin width is limited to ~3500 km (between Mawson and Laurentia, equivalent to 10,000 km of seafloor spreading). A global reconstruction would necessitate having a wide enough ocean basin to allow for both Amazonia and West Africa to slip past southern Gondwana (along the trans-Brasiliano lineament?). Earlier rifting times between Australia and Laurentia can accommodate larger basin sizes while maintaining reasonable rifting rates.

Convergence rates for India's motion towards Gondwana are also within present-day limits and bear similarity with the present-day convergence rates of India and Eurasia. The slow down at 650 Ma of India relative to Congo is likely related to the tectonic configuration between it and Congo during this time, when a series of terranes (e.g. Azania) were being accreted to the Congo margin prior to India's arrival. Closure of a backarc basin between Azania and Congo between 650 and 580 Ma (Collins and Pisarevsky, 2005), or double dipping subduction of the Mozambique ocean under Azania, along with subduction under Congo closing the back-arc basin (Plavsa et al., 2014, 2015), are similar to tectonic models of India-Eurasia convergence today (Jagoutz et al., 2015; Van der Voo et al., 1999). Importantly, inferences for India's kinematic history between the times where its position is known from palaeomagnetic data (the Malani Igneous Suite and Bhander and Rewa Series at 770 Ma and ca. 550 Ma respectively) are reasonable. Assuming a direct interpolation between both poles requires a convergence rate of ~50–70 mm/year. We have followed the idea that India slipped past Australia along a transform boundary, though a range of positions of India at 650 Ma are shown in Fig. 9 that satisfy the geological data of its collision with Congo but not necessarily this transform boundary with Australia. If India converges too slowly it is further south than Australia, while high convergence rates create an incredibly large ocean basin that is consumed.

7.2. Relative plate motion stability

The orientation of spreading systems for AUSMEX, AUSWUS and SWEAT configurations is perhaps unrealistic, especially for the

older times. Since Pangea breakup, every major ocean basin (Atlantic, Indian, Pacific) has experienced reorganisation events of varying magnitudes (Matthews et al., 2011; Müller et al., 2016). Changes in plate kinematics are obviously not captured in the simpler reconstruction cases, which exhibit a first order pattern similar to an Atlantic-type basin opening. We would expect that post Australia-Laurentia rifting, other constituents of western Rodinia also begin to separate (e.g. Congo-São Francisco at ca. 750 Ma, Kalahari at ca. 700 Ma; Jacobs et al., 2008; Li et al., 2008) leading to new MOR complexes and the potential for reorganisation events that would impact the Australia-Laurentia MOR. Ideally, complete plate models (i.e. continents and plate boundaries) for the Neoproterozoic can be used to help constrain possible motions and configurations (e.g. Merdith et al., 2017).

The more complex flowlines and series of Euler Poles for the Missing-Link Model, compared with the relatively smooth flowlines of the other three models, are a function for the motions of Australia and South China relative to Laurentia implemented in this model. They explain the motion of South China northwards from the Australia-Laurentia nexus, and then westwards over Australia, and then southwards down the west coast of Australia for Gondwana amalgamation, while Australia is also rifting westwards from Laurentia (Li et al., 2008, 2013). This more complex motion necessitates several major changes in angular rotation, mid-ocean ridge orientations and spreading rates. The movement of Australia relative to Laurentia is similar to that of SWEAT, as Australia is located in a similar position relative to the Laurentian coastline, though it is more upright (N-S orientated), which has the effect of reducing both its spreading rate and angular rotation (when compared to SWEAT), and would create an even more kinematically conservative rifting pattern than AUSWUS or AUSMEX.

A potential solution to account for the motion of South China in the Missing Link Model could be one where the Yangtze Block of South China represents an earlier accretionary complex that grew on the north side of the Cathaysia craton. This is similar to the process (not palaeogeography) suggested by Cawood et al. (2013, in press). This would suggest that South China was yet to be fully cratonised and potentially lack a deep cratonic root, allowing for more rapid and diverse motions than what we would expect using cratonic crust in the present day. Additionally, following the reasoning behind the Missing-Link model, the presence of a plume head (Li et al., 1999) could help facilitate more rapid and diverse motions as well through decoupling from the underlying mantle (e.g. Ratcliff et al., 1998). A similar exposition of plate motions could be found in the tectonic evolution of the Southeast Asia over the last ~150 Ma, where periodic rifting of small terranes and continental slithers during the Mesozoic from the northern Gondwanan margin to the southern Eurasian margin, has, in part, resulted in a complex melangé of terranes, seafloor spreading complexes, extinct ridges, subduction zones and changes in plate motion (e.g. Metcalfe, 1996; Metcalfe, 2011; Zahirovic et al., 2014).

7.3. Integration of kinematic observations

By integrating both sets of kinematic observations, along with the motion of two (poorly constrained) cratons, Congo-São Francisco (C-SF) and Kalahari, we can build a quantitative relative plate model bounded by absolute plate positions and constrained by geology. Following Li et al. (2008), but acknowledging the wide array of ideas about the Neoproterozoic journeys of C-SF and Kalahari (e.g. Evans, 2009; Frimmel et al., 2011; Johnson et al., 2005; McGee et al., 2012; Wingate et al., 2010), we take the AUSWUS fit with rifting at 800 Ma (Fig. 11a), C-SF-Laurentia rifting at 750 Ma (McGee et al., 2012) (Fig. 11b) and Kalahari-Laurentia rifting at 700 Ma (Fig. 11c,d). Based on the maximum expected spreading rate of Australia rifting from Laurentia at 800 Ma, we

see a configuration with Australia and Kalahari with ~15° of latitude and longitude separation, but otherwise in a position favourable with what we expect for Gondwana amalgamation. Following the present-day development of ocean basins (e.g. East Gondwana breakup), we interpret that the new spreading system between Laurentia-Kalahari at 700 Ma is most likely to be an extension of the existing one between Australia-Laurentia, either rifting in the same direction as Australia, or causing a reorganisation and altering the divergence direction such that while there is some minor relative motion between Australia-Kalahari (to accommodate the 650 Ma Yaltipena pole), they are otherwise moving on the same longitude. Given the lack of palaeomagnetic data from the Kalahari Craton, it is impossible to constrain its position until 550 Ma when it collides with Congo forming the Damara–Lufilian–Zambezi Orogen (Johnson et al., 2005), at which point it 'palaeomagnetically reappears', using the Gondwana APWP, at mid-latitudes (Torsvik et al., 2012). This is more southerly than it's (inferred) rifting position from Laurentia, suggesting that it's relative motion can't be aligned with orientation of Australia-Laurentia spreading system (Fig. 11c), rather there is a reorganisation, changing the orientation of Australia-Laurentia rifting (Fig. 11d). We express this relative motion by a stage rotation of Australia relative to Congo around the Euler Pole −5°S −98°W 57°.

By 650 Ma, India is starting its (plotted) southward descent into Gondwana around the Euler Pole 11°N 59°E −72° (Fig. 11e,f). The position of Australia can be constrained well now, due to palaeomagnetic data, and we see that the conjunction of the absolute latitudinal position of Australia, along with geological data, fit well with the relative motions of the Indian plate to both Australia and Congo, with India moving past Australia along a transform fault (Fig. 11f). The rotation of Australia into Gondwana is more uncertain, primarily because of the lack of data from Antarctica, which forms the nucleus of eastern Gondwana amalgamation (e.g. An et al., 2015; Boger, 2011). Both the Coats Land Block (colliding with Dronning Maud Land in Kalahari at 560 Ma after

Boger (2011)), and the enigmatic 'South Pole Terrane (Ferraccioli et al., 2011) perhaps act as an extension of the Mawson Craton and are the precursor to Australia–East-Antarctica's collision, which is likely to have occurred along a suture represented by the East-Antarctica Mountain Ranges (EAMOR) (An et al., 2015). The high quality poles from the Lower Arumbera and Upper Pertatataka Formations at ca. 540 Ma (Kirschvink, 1978) and the ca. 570 Ma Wonoka pole (Schmidt and Williams, 2010) constrain Australia to a position where its movement into Gondwana is head on into India along the Kuungan orogeny (Meert, 2003; Meert and Van der Voo, 1997), with a strike-slip motion along the Coats Land Block (Fig. 11g,h). This is perhaps somewhat supported by the granulite facies along the Kuungan orogeny suggesting a major collisional event (e.g. Kelsey et al., 2007; Grantham et al., 2013), though we note that future data from Antarctica may cause this to be revised. The motion of Australia–East-Antarctica relative to Congo is defined by the Euler Pole −38°S −75°W 40°.

7.4. Non-uniqueness of solutions

The (rudimentary) model described above is a non-unique solution of the Rodinia-Gondwana transition. Variations in Australia-Laurentia configurations can change interpretations about spreading systems in late-stage Rodinia breakup, particularly with respect to the position of South China. Changes in rifting time of this configuration will also strongly alter both the kinematics (if one desires Australia to be in the position described above) and development of spreading systems during late-stage Rodinia rifting when considering the other cratonic components (e.g. Kalahari, C-SF, Rio de la Plata). We also sidestep the problem of India's position (and inclusion) in Rodinia, noting that its 700 Ma position would be similar for models with India separate from Rodinia or as a product of early rifting, and that its final position in Gondwana is well established (e.g. Collins and Pisarevsky, 2005; Meert, 2003). Rather, the emphasis here is on how kinematic tools and data
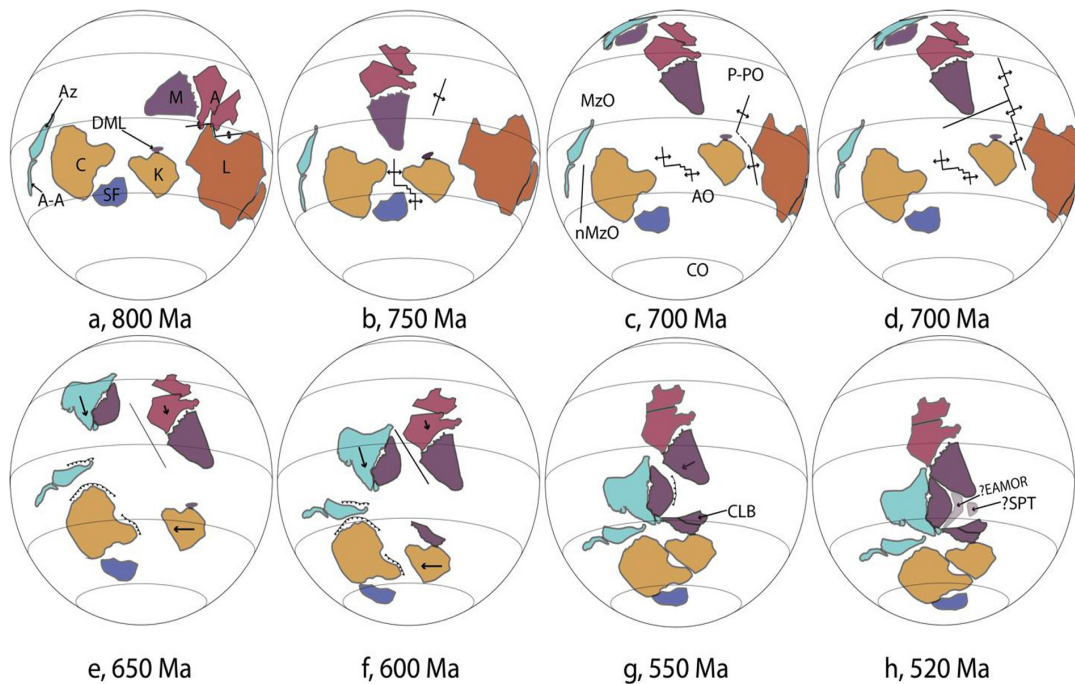
Fig. 11. Reconstruction incorporating breakup of western Rodinia and amalgamation of Eastern Gondwana. Two possible options of spreading ridges at 700 Ma (when Kalahari rifts from Laurentia) either having divergence between Australia-Kalahari (c), or both moving along the same longitude (d). AO, Adamastor Ocean; CO, Clymene Ocean; EAMOR, East Antarctic Mountain Range (An et al., 2015); MzO, Mozambique Ocean; nMzO, Neomozambique Ocean; P-PO, Palaeo-Pacific Ocean; ?SPT, South Pole Terrane (Ferraccioli et al., 2011). See Fig. 9 for other label details.

can help users make educated, quantitative decisions about relative plate motions in deep time, especially when there is limited palaeomagnetic data (e.g. either a begin or end position/time is well constrained, but the other is not). We also stress that decisions about the distances that plates move in a given model carry implications for mantle processes and geodynamics. For example, the maximum convergence rate of India-Congo from 700 to 550 Ma necessitates the closure of a ~14,000 km wide ocean basin. The implication of a large slab burial ground (as compared to a slower convergence model, which results in less subducted oceanic crust) is a strong drawdown effect of any overlaying portions of continental crust, potentially preserving a dynamic topography signature within sedimentary basins (e.g. Flowers et al., 2012).

8. Conclusions

Kinematic data suggest that a tectonic model where Rodinia splits up before 750 Ma is more consistent with Phanerozoic plate tectonics than competing models, in that an early split-up minimises both the speed and angular rotation of the Australian Plate, with rifting at ca. 800 Ma producing the only models that are within Phanerozoic spreading rate limits. SWEAT, AUSWUS and AUSMEX all have similar maximum rates of angular rotation (~1.9 °/Ma at 725 Ma), though the SWEAT configuration has the highest average spreading rate for all rifting times (149 mm/a at 725 Ma rifting). AUSWUS has the lowest average spreading rates (56 mm/a at 800 Ma rifting), though AUSMEX is only slightly faster at 64 mm/a. Kinematically, AUSWUS and AUSMEX at 800 Ma are the two preferred rifting configurations/times, though SWEAT at 800 Ma could be justifiable (76 mm/a maximum spreading rate). As the onset of rifting becomes younger, the viability of configurations decreases due to the corresponding increase in subsequent spreading rates. For a rifting time of 725 Ma for any configuration, viable reasons for spreading rates of greater than 130 mm/a would have to be provided. Similarly, for the Missing-Link Model, rifting at 800 Ma presents the most optimal spreading rates, though the flowlines and spikes in spreading rate and angular rotation for South China require a more complex explanation than that of the other configurations. We also demonstrate how kinematic tools can help constrain relative plate motions by creating a simple model that explicitly links together palaeomagnetic, geological and kinematic data to explain the relative motions of India to Congo and Australia during its collision with Gondwana.

Acknowledgements

Appendix A. Supplementary data

Supplementary data associated with this article can be found, in the online version, at http://dx.doi.org/10.1016/j.precamres.2017.07.013.

References

An, M., Wiens, D.A., Zhao, Y., Feng, M., Nyblade, A.A., Kanao, M., Li, Y., Maggi, A., Lévêque, J.J., 2015. S-velocity model and inferred Moho topography beneath the Antarctic Plate from Rayleigh waves. J. Geophys. Res. 120 (1), 359–383.

Archibald, D.B., Collins, A.S., Foden, J.D., Payne, J.L., Taylor, R., Holden, P., Razakamanana, T., Clark, C., 2015. Towards unravelling the Mozambique Ocean conundrum using a triumvirate of zircon isotopic proxies on the Ambatolampy Group, central Madagascar. Tectonophysics 662, 167–182.

Argus, D.F., Gordon, R.G., Heflin, M.B., Ma, C., Eanes, R.J., Willis, P., Peltier, W.R., Owen, S.E., 2010. The angular velocities of the plates and the velocity of Earth's centre from space geodesy. Geophys. J. Int. 180 (3), 913–960.

Argus, D.F., Gordon, R.G., DeMets, C., 2011. Geologically current motion of 56 plates relative to the no-net-rotation reference frame. Geochem. Geophys. Geosyst. 12 (11).

Ashwal, L.D., Hamilton, M.A., Morel, V.P., Rambeloson, R.A., 1998. Geology, petrology and isotope geochemistry of massif-type anorthosites from southwest Madagascar. Contrib. Miner. Petrol. 133 (4), 389–401.

Austermann, J., Ben-Avraham, Z., Bird, P., Heidbach, O., Schubert, G., Stock, J.M., 2011. Quantifying the forces needed for the rapid change of Pacific plate motion at 6 Ma. Earth Planet. Sci. Lett. 307 (3), 289–297.

Bell, R.T. and Jefferson, C.W., 1987. An hypothesis for an Australian-Canadian connection in the Late Proterozoic and the birth of the Pacific Ocean, vol. 87. In: Proceedings, Pacific Rim Congress. pp. 39–50.

Bird, P., 2003. An updated digital model of plate boundaries. Geochem. Geophys. Geosyst. 4 (3).

Boger, S.D., 2011. Antarctica—before and after Gondwana. Gondwana Res. 19 (2), 335–371.

Boger, S.D., Hirdes, W., Ferreira, C.A.M., Jenett, T., Dallwig, R., Fanning, C.M., 2015. The 580–520 Ma Gondwana suture of Madagascar and its continuation into Antarctica and Africa. Gondwana Res. 28 (3), 1048–1060.

Borg, S.G., DePaolo, D.J., 1994. Laurentia, Australia, and Antarctica as a Late Proterozoic supercontinent: constraints from isotopic mapping. Geology 22 (4), 307–310.

Bradley, D.C., 2008. Passive margins through earth history. Earth Sci. Rev. 91 (1), 1–26.

Bradley, D.C., 2011. Secular trends in the geologic record and the supercontinent cycle. Earth Sci. Rev. 108 (1), 16–33.

Brasier, M.D., Lindsay, J.F., 2001. Did Supercontinental Amalgamation Trigger the "Cambrian Explosion". The Ecology of the Cambrian Radiation. Columbia University Press, New York, pp. 69–89.

Brookfield, M.E., 1993. Neoproterozoic Laurentia-Australia fit. Geology 21 (8), 683–686.

Buchwaldt, R., Tucker, R.D., Dymek, R.F., 2003. Geothermobarometry and U-Pb Geochronology of metapelitic granulites and pelitic migmatites from the Lokoho region, Northern Madagascar. Am. Mineral. 88 (11–12), 1753–1768.

Burrett, C., Berry, R., 2000. Proterozoic Australia-Western United States (AUSWUS) fit between Laurentia and Australia. Geology 28 (2), 103–106.

Burrett, C., Berry, R., 2002. A statistical approach to defining proterozoic crustal provinces and testing continental reconstructions of Australia and Laurentia-SWEAT or AUSWUS? Gondwana Res. 5 (1), 109–122.

Butterworth, N.P., Talsma, A.S., Müller, R.D., Seton, M., Bunge, H.P., Schuberth, B.S.A., Shephard, G.E., Heine, C., 2014. Geological, tomographic, kinematic and geodynamic constraints on the dynamics of sinking slabs. J. Geodyn. 73, 1–13.

Cande, S.C., Patriat, P., 2015. The anticorrelated velocities of Africa and India in the Late Cretaceous and early Cenozoic. Geophys. J. Int. 200 (1), 227–243.

Cande, S.C., Stegman, D.R., 2011. Indian and African plate motions driven by the push force of the Reunion plume head. Nature 475 (7354), 47–52.

Cawood, P.A., Buchan, C., 2007. Linking accretionary orogenesis with supercontinent assembly. Earth Sci. Rev. 82 (3), 217–256.

Cawood, P.A., Hawkesworth, C.J., 2014. Earth's middle age. Geology 42 (6), 503–506.

Cawood, P.A., Wang, Y., Xu, Y., Zhao, G., 2013. Locating South China in Rodinia and Gondwana: a fragment of greater India lithosphere? Geology 41 (8), 903–906.

Cawood, P.A., Zhao, G., Yao, Wang, W., Xu, Y. and Wang, Y. in press. Reconstructing South China in Phanerozoic and Precambrian supercontinents. Earth Sci. Rev.

Cocks, L.R.M., Torsvik, T.H., 2002. Earth geography from 500 to 400 million years ago: a faunal and palaeomagnetic review. J. Geol. Soc. 159 (6), 631–644.

Collins, A.S., 2003. Structure and age of the northern Leeuwin Complex, Western Australia: constraints from field mapping and U-Pb isotopic analysis. Aust. J. Earth Sci. 50 (4), 585–599.

Collins, A.S., 2006. Madagascar and the amalgamation of Central Gondwana. Gondwana Res. 9 (1), 3–16.

Collins, A.S., Pisarevsky, S.A., 2005. Amalgamating eastern Gondwana: the evolution of the Circum-Indian Orogens. Earth Sci. Rev. 71 (3), 229–270.

Collins, A.S., Clark, C., Sajeev, K., Santosh, M., Kelsey, D.E., Hand, M., 2007. Passage through India: the Mozambique Ocean suture, high-pressure granulites and the Palghat-Cauvery shear zone system. Terra Nova 19 (2), 141–147.

Collins, A.S., Clark, C., Plavsa, D., 2014. Peninsular India in Gondwana: the tectonothermal evolution of the Southern Granulite Terrain and its Gondwanan counterparts. Gondwana Res. 25 (1), 190–203.

Colpron, M., Logan, J.M., Mortensen, J.K., 2002. U-Pb zircon age constraint for late Neoproterozoic rifting and initiation of the lower Paleozoic passive margin of Western Laurentia. Can. J. Earth Sci. 39 (2), 133–143.

Condie, K.C., 2002. The supercontinent cycle: are there two patterns of cyclicity? J. Afr. Earth Sci. 35 (2), 179–183.

Condie, K.C., 2003. Supercontinents, superplumes and continental growth: the Neoproterozoic record. Geol. Soc. 206 (1), 1–21. London, Special Publications.

Condie, K.C., Belousova, E., Griffin, W.L., Sircombe, K.N., 2009. Granitoid events in space and time: constraints from igneous and detrital zircon age spectra. Gondwana Res. 15 (3), 228–242.

Cox, G.M., Halverson, G.P., Stevenson, R.K., Vokaty, M., Poirier, A., Kunzmann, M., Li, Z.-X., Denyszyn, S.W., Strauss, J.V., Macdonald, F.A., 2016. Continental flood basalt weathering as a trigger for Neoproterozoic Snowball Earth. Earth Planet. Sci. Lett. 446, 89–99.

Dalziel, I.W., 1991. Pacific margins of Laurentia and East Antarctica-Australia as a conjugate rift pair: evidence and implications for an Eocambrian supercontinent. Geology 19 (6), 598–601.

Davidson, A., 2008. Late Paleoproterozoic to mid-Neoproterozoic history of northern Laurentia: an overview of central Rodinia. Precambr. Res. 160 (1), 5–22.

Denyszyn, S.W., Halls, H.C., Davis, D.W., Evans, D.A., 2009. Paleomagnetism and U-Pb geochronology of Franklin dykes in High Arctic Canada and Greenland: a revised age and paleomagnetic pole constraining block rotations in the Nares Strait region. Can. J. Earth Sci. 46 (9), 689–705.

Domeier, M., 2016. A plate tectonic scenario for the Iapetus and Rheic oceans. Gondwana Res. 36, 275–295.

Domeier, M., Torsvik, T.H., 2014. Plate tectonics in the late Paleozoic. Geosci. Front. 5 (3), 303–350.

Du, L., Guo, J., Nutman, A.P., Wyman, D., Geng, Y., Yang, C., Liu, F., Ren, L., Zhou, X., 2014. Implications for Rodinia reconstructions for the initiation of Neoproterozoic subduction at ~860 Ma on the western margin of the Yangtze Block: evidence from the Guandaoshan Pluton. Lithos 196, 67–82.

Eisbacher, G.H., 1985. Late Proterozoic rifting, glacial sedimentation, and sedimentary cycles in the light of Windermere deposition, western Canada. Palaeogeogr. Palaeoclimatol. Palaeoecol. 51 (1–4), 231–254.

Embleton, B.J.J., Schmidt, P.W., 1985. Age and significance of magnetizations in dolerite dykes from the Northampton Block, Western Australia. Aust. J. Earth Sci. 32 (3), 279–286.

Ernst, R., Bleeker, W., 2010. Large igneous provinces (LIPs), giant dyke swarms, and mantle plumes: significance for breakup events within Canada and adjacent regions from 2.5 Ga to the Present. Can. J. Earth Sci. 47 (5), 695–739.

Ernst, R.E., Wingate, M.T.D., Buchan, K.L., Li, Z.X., 2008. Global record of 1600–700 Ma Large Igneous Provinces (LIPs): implications for the reconstruction of the proposed Nuna (Columbia) and Rodinia supercontinents. Precambr. Res. 160 (1), 159–178.

Ernst, R.E., Bleeker, W., Söderlund, U., Kerr, A.C., 2013. Large igneous provinces and supercontinents: toward completing the plate tectonic revolution. Lithos 174, 1–14.

Ernst, R.E., Hamilton, M.A., Söderlund, U., Hanes, J.A., Gladkochub, D.P., Okrugin, A. V., Kolotilina, T., Mekhonoshin, A.S., Bleeker, W., LeCheminant, A.N., Buchan, K. L., 2016. Long-lived connection between southern Siberia and northern Laurentia in the Proterozoic. Nat. Geosci. 9 (6), 464–469.

Evans, D.A., 2009. The palaeomagnetically viable, long-lived and all-inclusive Rodinia supercontinent reconstruction. Geol. Soc. 327 (1), 371–404. London, Special Publications.

Ferraccioli, F., Finn, C.A., Jordan, T.A., Bell, R.E., Anderson, L.M., Damaske, D., 2011. East Antarctic rifting triggers uplift of the Gamburtsev Mountains. Nature 479 (7373), 388–392.

Fitzsimons, I.C.W., 2000. Grenville-age basement provinces in East Antarctica: evidence for three separate collisional orogens. Geology 28 (10), 879–882.

Fitzsimons, I.C.W., 2003. Proterozoic basement provinces of southern and southwestern Australia, and their correlation with Antarctica. Geol. Soc. 206 (1), 93–130. London, Special Publications.

Fitzsimons, I.C., 2016. Pan-African granulites of Madagascar and southern India: Gondwana assembly and parallels with modern Tibet. J. Mineral. Petrol. Sci. 111 (2), 73–88.

Flowers, R.M., Ault, A.K., Kelley, S.A., Zhang, N., Zhong, S., 2012. Epeirogeny or eustasy? Paleozoic-Mesozoic vertical motion of the North American continental interior from thermochronometry and implications for mantle dynamics. Earth Planet. Sci. Lett. 317, 436–445.

Frimmel, H.E., Basei, M.S., Gaucher, C., 2011. Neoproterozoic geodynamic evolution of SW-Gondwana: a southern African perspective. Int. J. Earth Sci. 100 (2–3), 323–354.

Ganade, C.E., Cordani, U.G., Agbossoumounde, Y., Caby, R., Basei, M.A., Weinberg, R. F., Sato, K., 2016. Tightening-up NE Brazil and NW Africa connections: New U-Pb/Lu–Hf zircon data of a complete plate tectonic cycle in the Dahomey belt of the West Gondwana Orogen in Togo and Benin. Precambr. Res. 276, 24–42.

Gernon, T.M., Hincks, T.K., Tarell, T., Rohling, E.J., Palmer, M.R., 2016. Snowball Earth ocean chemistry driven by extensive ridge volcanism during Rodinia breakup. Nat. Geosci. 9 (3), 242–248.

Goodge, J.W., Vervoort, J.D., Fanning, C.M., Brecke, D.M., Farmer, G.L., Williams, I.S., Maow, P.M., DePaolo, D.J., 2008. A positive test of East Antarctica-Laurentia juxtaposition within the Rodinia supercontinent. Science 321 (5886), 235–240.

Grantham, G.H., Macey, P.H., Horie, K., Kawakami, T., Ishikawa, M., Satish-Kumar, M., Tsuchiya, N., Graser, P., Azevedo, S., 2013. Comparison of the metamorphic history of the Monapo Complex, northern Mozambique and Balchenfjella and Austhameren areas, Sør Rondane, Antarctica: implications for the Kuunga Orogeny and the amalgamation of N and S. Gondwana. Precambrian Res. 234, 85–135.

Greene, D.C., 2010. Neoproterozoic rifting in the southern Georgina Basin, central Australia: implications for reconstructing Australia in Rodinia. Tectonics 29 (5).

Gregory, L.C., Meert, J.G., Bingen, B., Pandit, M.K., Torsvik, T.H., 2009. Paleomagnetism and geochronology of the Malani Igneous Suite, Northwest India: implications for the configuration of Rodinia and the assembly of Gondwana. Precambr. Res. 170 (1), 13–26.

Halverson, G.P., Hurtgen, M.T., Porter, S.M., Collins, A.S., 2009. Neoproterozoic-Cambrian Biogeochemical Evolution. In: C. Gaucher, A.N. Sial, G.P. Halverson, H. E. Frimmel (Eds.), Neoproterozoic-Cambrian Tectonics, Global Change and Evolution: A Focus on Southwestern Gondwana. Developments in Precambrian Geology, Vol. 16, Elsevier. pp. 351–365.

Harlan, S.S., Geissman, J.W., Snee, L.W., 1997. Paleomagnetic and 40Ar/39Ar geochronologic data from late Proterozoic mafic dikes and sills, Montana and Wyoming. US Government Printing Office. p. 1580.

Harris, L.B., 1994. Neoproterozoic sinistral displacement along the Darling mobile belt, Western Australia, during Gondwanaland assembly. J. Geol. Soc. 151 (6), 901–904.

Harris, L.B., Beeson, J., 1993. Gondwanaland significance of Lower Palaeozoic deformation in central India and SW Western Australia. J. Geol. Soc. 150 (5), 811–814.

Hoffman, P.F., 1991. Did the breakout of Laurentia turn Gondwanaland inside-out. Science 252 (5011), 1409–1412.

Hoffman, P.F., Li, Z.X., 2009. A palaeogeographic context for Neoproterozoic glaciation. Palaeogeogr. Palaeoclimatol. Palaeoecol. 277 (3), 158–172.

Jacobs, J., Pisarevsky, S., Thomas, R.J., Becker, T., 2008. The Kalahari Craton during the assembly and dispersal of Rodinia. Precambr. Res. 160 (1), 142–158.

Jagoutz, O., Royden, L., Holt, A.F., Becker, T.W., 2015. Anomalously fast convergence of India and Eurasia caused by double subduction. Nat. Geosci. 8 (6), 475–478.

Jiang, G., Sohl, L.E., Christie-Blick, N., 2003. Neoproterozoic stratigraphic comparison of the Lesser Himalaya (India) and Yangtze block (south China): Paleogeographic implications. Geology 31 (10), 917–920.

Johansson, Å., 2014. From Rodinia to Gondwana with the 'SAMBA' model—a distant view from Baltica towards Amazonia and beyond. Precambr. Res. 244, 226–235.

Johnson, S.P., Rivers, T., De Waele, B., 2005. A review of the Mesoproterozoic to early Palaeozoic magmatic and tectonothermal history of south–central Africa: implications for Rodinia and Gondwana. J. Geol. Soc. 162 (3), 433–450.

Karlstrom, K.E., Williams, M.L., McLelland, J., Geissman, J.W., Ahall, K., 1999. Refining Rodinia: geologic evidence for the Australia-Western US connection in the Proterozoic. GSA Today 9 (10), 2–6.

Karlstrom, K.E., Åhäll, K.I., Harlan, S.S., Williams, M.L., McLelland, J., Geissman, J.W., 2001. Long-lived (1.8–1.0 Ga) convergent orogen in southern Laurentia, its extensions to Australia and Baltica, and implications for refining Rodinia. Precambr. Res. 111 (1), 5–30.

Kelsey, D.E., Hand, M., Clark, C., Wilson, C.J.L., 2007. On the application of in situ monazite chemical geochronology to constraining P-T–t histories in high-temperature (>850 °C) polymetamorphic granulites from Prydz Bay, East Antarctica. J. Geol. Soc. 164 (3), 667–683.

King, S.D., Lowman, J.P., Gable, C.W., 2002. Episodic tectonic plate reorganizations driven by mantle convection. Earth Planet. Sci. Lett. 203 (1), 83–91.

Kirschvink, J.L., 1978. The Precambrian-Cambrian boundary problem: paleomagnetic directions from the Amadeus basin, central Australia. Earth Planet. Sci. Lett. 40 (1), 91–100.

Knesel, K.M., Cohen, B.E., Vasconcelos, P.M., Thiede, D.S., 2008. Rapid change in drift of the Australian plate records collision with Ontong Java plateau. Nature 454 (7205), 754–757.

Li, Z.X., 2000. New palaeomagnetic results from the 'cap dolomite'of the Neoproterozoic Walsh Tillite, northwestern Australia. Precambr. Res. 100 (1), 359–370.

Li, Z.X., Evans, D.A., 2011. Late Neoproterozoic 40° intraplate rotation within Australia allows for a tighter-fitting and longer-lasting Rodinia. Geology 39 (1), 39–42.

Li, Z.X., Zhang, L., Powell, C.M., 1995. South China in Rodinia: part of the missing link between Australia-East Antarctica and Laurentia? Geology 23 (5), 407–410.

Li, Z.X., Li, X.H., Kinny, P.D., Wang, J., 1999. The breakup of Rodinia: did it start with a mantle plume beneath South China? Earth Planet. Sci. Lett. 173 (3), 171–181.

Li, Z.X., Bogdanova, S.V., Collins, A.S., Davidson, A., De Waele, B., Ernst, R.E., Fitzsimons, I.C.W., Fuck, R.A., Gladkochub, D.P., Jacobs, J., Karlstrom, K.E., Lu, S., Natapov, L.M., Pease, V., Pisarevsky, S.A., Thrane, K., Vernikovsky, V., 2008. Assembly, configuration, and break-up history of Rodinia: a synthesis. Precambr. Res. 160 (1), 179–210.

Li, Z.X., Evans, D.A., Halverson, G.P., 2013. Neoproterozoic glaciations in a revised global palaeogeography from the breakup of Rodinia to the assembly of Gondwanaland. Sed. Geol. 294, 219–232.

Li, Z., Qiu, N., Chang, J., Yang, X., 2015. Precambrian evolution of the Tarim Block and its tectonic affinity to other major continental blocks in China: new clues from U-Pb geochronology and Lu–Hf isotopes of detrital zircons. Precambr. Res. 270, 1–21.

Lowman, J.P., King, S.D., Gable, C.W., 2003. The role of the heating mode of the mantle in intermittent reorganization of the plate velocity field. Geophys. J. Int. 152 (2), 455–467.

Maruyama, S., Santosh, M., 2008. Models on Snowball Earth and Cambrian explosion: a synopsis. Gondwana Res. 14 (1), 22–32.

Matthews, K.J., Müller, R.D., Wessel, P., Whittaker, J.M., 2011. The tectonic fabric of the ocean basins. J. Geophys. Res. 116 (B12).

Matthews, K.J., Seton, M., Müller, R.D., 2012. A global-scale plate reorganization event at 105–100 Ma. Earth Planet. Sci. Lett. 355, 283–298.

McElhinny, M.W., Cowley, J.A., Edwards, D.J., 1978. Palaeomagnetism of some rocks from Peninsular India and Kashmir. Tectonophysics 50 (1), 41–54.

McGee, B., Halverson, G.P., Collins, A.S., 2012. Cryogenian rift-related magmatism and sedimentation: South-western Congo Craton, Namibia. J. Afr. Earth Sc. 76, 34–49.

Meert, J.G., 2002. Paleomagnetic evidence for a Paleo-Mesoproterozoic supercontinent Columbia. Gondwana Res. 5 (1), 207–215.

Meert, J.G., 2003. A synopsis of events related to the assembly of eastern Gondwana. Tectonophysics 362 (1), 1–40.

Meert, J.G., Lieberman, B.S., 2008. The Neoproterozoic assembly of Gondwana and its relationship to the Ediacaran-Cambrian radiation. Gondwana Res. 14 (1), 5–21.

Meert, J.G., Torsvik, T.H., 2003. The making and unmaking of a supercontinent: Rodinia revisited. Tectonophysics 375 (1), 261–288.

Meert, J.G., Van Der Voo, R., 1997. The assembly of Gondwana 800–550 Ma. J. Geodyn. 23 (3), 223–235.

Merdith, A.S., Collins, A.S., Williams, S.E., Pisarevsky, S., Foden, J.F., Archibald, D.A., Blades, M.L., Alessio, B.L., Armistead, S., Plavsa, D., Clark, C., Müller, R.D., 2017. A full-plate global reconstruction of the Neoproterozoic. Gondwana Res., 50.

Metcalfe, I., 1996. Pre-Cretaceous evolution of SE Asian terranes. Geol. Soc. 106 (1), 97–122. London, Special Publications.

Metcalfe, I., 2011. Tectonic framework and Phanerozoic evolution of Sundaland. Gondwana Res. 19 (1), 3–21.

Mitchell, R.N., Kilian, T.M., Evans, D.A., 2012. Supercontinent cycles and the calculation of absolute palaeolongitude in deep time. Nature 482 (7384), 208–211.

Moores, E.M., 1991. Southwest US-East Antarctic (SWEAT) connection: a hypothesis. Geology 19 (5), 425–428.

Morgan, W.J., 1971. Convection plumes in the lower mantle. Nature 230, 42–43.

Mulder, J.A., Halpin, J.A., Daczko, N.R., 2015. Mesoproterozoic Tasmania: witness to the East Antarctica-Laurentia connection within Nuna. Geology 43 (9), 759–762.

Müller, R.D., Royer, J.Y., Lawver, L.A., 1993. Revised plate motions relative to the hotspots from combined Atlantic and Indian Ocean hotspot tracks. Geology 21 (3), 275–278.

Müller, R.D., Sdrolias, M., Gaina, C., Roest, W.R., 2008. Age, spreading rates, and spreading asymmetry of the world;s ocean crust. Geochem. Geophys. Geosyst. 9 (4).

Müller, R.D., Seton, M., Zahirovic, S., Williams, S.E., Matthews, K.J., Wright, N.M., Shephard, G.E., Maloney, K., Barnett-Moore, N., Hosseinpour, M., Bower, D.J., 2016. Ocean basin evolution and global-scale plate reorganization events since Pangea breakup. Annu. Rev. Earth Planet. Sci. 44 (1), 107–138.

Murthy, G., Gower, C., Tubrett, M., Pätzold, R., 1992. Paleomagnetism of Eocambrian Long Range dykes and Double Mer Formation from Labrador, Canada. Can. J. Earth Sci. 29 (6), 1224–1234.

Nance, R.D., Murphy, J.B., 2013. Origins of the supercontinent cycle. Geosci. Front. 4 (4), 439–448.

Nance, R.D., Murphy, J.B., Santosh, M., 2014. The supercontinent cycle: a retrospective essay. Gondwana Res. 25 (1), 4–29.

Palmer, H.C., Merz, B.A., Hayatsu, A., 1977. The Sudbury dikes of the Grenville Front region: paleomagnetism, petrochemistry, and K-Ar age studies. Can. J. Earth Sci. 14 (8), 1867–1887.

Park, J.K., Norris, D.K., Larochelle, A., 1989. Paleomagnetism and the origin of the Mackenzie Arc of northwestern Canada. Can. J. Earth Sci. 26 (11), 2194–2203.

Patriat, P. and Achache, J., 1984. India-Eurasia collision chronology has implications for crustal shortening and driving mechanism of plates.

Pisarevsky, S.A., Natapov, L.M., 2003. Siberia and Rodinia. Tectonophysics 375 (1), 221–245.

Pisarevsky, S.A., Wingate, M.T., Powell, C.M., Johnson, S., Evans, D.A., 2003a. Models of Rodinia assembly and fragmentation. Geol. Soc. 206 (1), 35–55. London, Special Publications.

Pisarevsky, S.A., Wingate, M.T.D., Harris, L.B., 2003b. Late Mesoproterozoic (ca 1.2 Ga) palaeomagnetism of the Albany-Fraser orogen: no pre-Rodinia Australia-Laurentia connection. Geophys. J. Int. 155 (1), F6–F11.

Pisarevsky, S.A., Wingate, M.T.D., Stevens, M.K., Haines, P.W., 2007. Palaeomagnetic results from the Lancer 1 stratigraphic drillhole, Officer Basin, Western Australia, and implications for Rodinia reconstructions. Aust. J. Earth Sci. 54 (4), 561–572.

Pisarevsky, S.A., Elming, S.Å., Pesonen, L.J., Li, Z.X., 2014a. Mesoproterozoic paleogeography: supercontinent and beyond. Precambr. Res. 244, 207–225.

Pisarevsky, S.A., Wingate, M.T., Li, Z.X., Wang, X.C., Tohver, E., Kirkland, C.L., 2014b. Age and paleomagnetism of the 1210 Ma Gnowangerup-Fraser dyke swarm, Western Australia, and implications for late Mesoproterozoic paleogeography. Precambrian Res. 246, 1–15.

Plavsa, D., Collins, A.S., Payne, J.L., Foden, J.D., Clark, C., Santosh, M., 2014. Detrital zircons in basement metasedimentary protoliths unveil the origins of southern India. Geol. Soc. Am. Bull. 126 (5–6), 791–811.

Plavsa, D., Collins, A.S., Foden, J.D., Clark, C., 2015. The evolution of a Gondwanan Collisional Orogen: a structural and geochronological appraisal from the Southern Granulite Terrane, South India. Tectonics 34, 820–857.

Powell, C.M., Pisarevsky, S.A., 2002. Late Neoproterozoic assembly of east Gondwana. Geology 30 (1), 3–6.

Powell, C.M., Li, Z.X., McElhinny, M.W., Meert, J.G., Park, J.K., 1993. Paleomagnetic constraints on timing of the Neoproterozoic breakup of Rodinia and the Cambrian formation of Gondwana. Geology 21 (10), 889–892.

Prave, A.R., 1999. Two diamictites, two cap carbonates, two δ13C excursions, two rifts: the Neoproterozoic Kingston Peak Formation, Death Valley. Calif. Geol. 27 (4), 339–342.

Preiss, W.V., 2000. The Adelaide Geosyncline of South Australia and its significance in Neoproterozoic continental reconstruction. Precambrian Res. 100 (1), 21–63.

Rainbird, R.H., Jefferson, C.W., Young, G.M., 1996. The early Neoproterozoic sedimentary Succession B of northwestern Laurentia: correlations and paleogeographic significance. Geol. Soc. Am. Bull. 108 (4), 454–470.

Ratcliff, J.T., Bercovici, D., Schubert, G., Kroenke, L.W., 1998. Mantle plume heads and the initiation of plate tectonic reorganizations. Earth Planet. Sci. Lett. 156 (3), 195–207.

Rogers, J.J., Santosh, M., 2002. Configuration of Columbia, a Mesoproterozoic supercontinent. Gondwana Res. 5 (1), 5–22.

Santosh, M., 2010. Supercontinent tectonics and biogeochemical cycle: a matter of 'life and death'. Geosci. Front. 1 (1), 21–30.

Schmidt, P.W., 2014. A review of Precambrian palaeomagnetism of Australia: Palaeogeography, supercontinents, glaciations and true polar wander. Gondwana Res. 25 (1), 1164–1185.

Schmidt, P.W., Williams, G.E., 1995. The Neoproterozoic climatic paradox: equatorial palaeolatitude for Marinoan glaciation near sea level in South Australia. Earth Planet. Sci. Lett. 134 (1), 107–124.

Schmidt, P.W., Williams, G.E., 1996. Palaeomagnetism of the ejecta-bearing Bunyeroo formation, late Neoproterozoic, Adelaide fold belt, and the age of the Acraman impact. Earth Planet. Sci. Lett. 144 (3), 347–357.

Schmidt, P.W., Williams, G.E., 2010. Ediacaran palaeomagnetism and apparent polar wander path for Australia: no large true polar wander. Geophys. J. Int. 182 (2), 711–726.

Schmidt, P.W., Williams, G.E., 2013. Anisotropy of thermoremanent magnetisation of Cryogenian glaciogenic and Ediacaran red beds, South Australia: Neoproterozoic apparent or true polar wander? Global Planet. Change 110, 289–301.

Schmidt, P.W., Williams, G.E., Camacho, A., Lee, J.K., 2006. Assembly of Proterozoic Australia: implications of a revised pole for the ~1070 Ma Alcurra Dyke Swarm, central Australia. Geophys. J. Int. 167 (2), 626–634.

Schmidt, P.W., Williams, G.E., McWilliams, M.O., 2009. Palaeomagnetism and magnetic anisotropy of late Neoproterozoic strata, South Australia: implications for the palaeolatitude of late Cryogenian glaciation, cap carbonate and the Ediacaran System. Precambrian Res. 174 (1), 35–52.

Schult, F.R., Gordon, R.G., 1984. Root mean square velocities of the continents with respect to the hot spots since the Early Jurassic. J. Geophys. Res. 89 (B3), 1789–1800.

Sears, J.W., Price, R.A., 2000. New look at the Siberian connection: no SWEAT. Geology 28 (5), 423–426.

Seton, M., Müller, R.D., Zahirovic, S., Gaina, C., Torsvik, T., Shephard, G., Talsma, A., Gurnis, M., Turner, M., Maus, S., Chandler, M., 2012. Global continental and ocean basin reconstructions since 200 Ma. Earth Sci. Rev. 113 (3), 212–270.

Seton, M., Flament, N., Whittaker, J., Müller, R.D., Gurnis, M., Bower, D.J., 2015. Ridge subduction sparked reorganization of the Pacific plate-mantle system 60–50 million years ago. Geophys. Res. Lett. 42 (6), 1732–1740.

Sohl, L.E., Christie-Blick, N., Kent, D.V., 1999. Paleomagnetic polarity reversals in Marinoan (ca. 600 Ma) glacial deposits of Australia: implications for the duration of low-latitude glaciation in Neoproterozoic time. Geol. Soc. Am. Bull. 111 (8), 1120–1139.

Squire, R.J., Campbell, I.H., Allen, C.M., Wilson, C.J., 2006. Did the Transgondwanan Supermountain trigger the explosive radiation of animals on Earth? Earth Planet. Sci. Lett. 250 (1), 116–133.

Steinberger, B., Sutherland, R., O'connell, R.J., 2004. Prediction of Emperor-Hawaii seamount locations from a revised model of global plate motion and mantle flow. Nature 430 (6996), 167–173.

Swanson-Hysell, N.L., Maloof, A.C., Kirschvink, J.L., Evans, D.A., Halverson, G.P., Hurtgen, M.T., 2012. Constraints on Neoproterozoic palaeogeography and Paleozoic orogenesis from paleomagnetic records of the Bitter Springs Formation, Amadeus Basin, central Australia. Am. J. Sci. 312 (8), 817–884.

Torsvik, T.H., Cocks, L.R.M., 2013. New global palaeogeographical reconstructions for the Early Palaeozoic and their generation. Geol. Soc. 38 (1), 5–24. London, Memoirs.

Torsvik, T.H., Ashwal, L.D., Tucker, R.D., Eide, E.A., 2001a. Neoproterozoic geochronology and palaeogeography of the Seychelles microcontinent: the India link. Precambrian Res. 110 (1), 47–59.

Torsvik, T.H., Carter, L.M., Ashwal, L.D., Bhushan, S.K., Pandit, M.K., Jamtveit, B., 2001b. Rodinia refined or obscured: palaeomagnetism of the Malani igneous suite (NW India). Precambrian Res. 108 (3), 319–333.

Torsvik, T.H., Steinberger, B., Cocks, L.R.M., Burke, K., 2008. Longitude: linking Earth's ancient surface to its deep interior. Earth Planet. Sci. Lett. 276 (3), 273–282.

Torsvik, T.H., Van der Voo, R., Preeden, U., Mac Niocaill, C., Steinberger, B., Doubrovine, P.V., van Hinsbergen, D.J., Domeier, M., Gaina, C., Tohver, E., Meert, J.G., 2012. Phanerozoic polar wander, palaeogeography and dynamics. Earth Sci. Rev. 114 (3), 325–368.

Van der Meer, D.G., Spakman, W., Van Hinsbergen, D.J., Amaru, M.L., Torsvik, T.H., 2010. Towards absolute plate motions constrained by lower-mantle slab remnants. Nat. Geosci. 3 (1), 36–40.

Van der Voo, R., Spakman, W., Bijwaard, H., 1999. Tethyan subducted slabs under India. Earth Planet. Sci. Lett. 171 (1), 7–20.

van Hinsbergen, D.J., Steinberger, B., Doubrovine, P.V., Gassmöller, R., 2011. Acceleration and deceleration of India-Asia convergence since the Cretaceous: roles of mantle plumes and continental collision. J. Geophys. Res. 116 (B6).

Veevers, J.J., Walter, M.R., Scheibner, E., 1997. Neoproterozoic tectonics of Australia-Antarctica and Laurentia and the 560 Ma birth of the Pacific Ocean reflect the 400 my Pangean supercycle. J. Geol. 105 (2), 225–242.

Vijaya Kumar, T., Bhaskar Rao, Y.J., Plavsa, D., Collins, A.S., Tomson, J.K., Vijaya Gopal, B., Babu, E.V.S.S.K., 2017. Zircon U-Pb ages and Hf isotopic systematics of charnockite gneisses from the Ediacaran-Cambrian high-grade metamorphic terrains, southern India: constraints on crust formation, recycling and Gondwana correlations. Geol. Soc. Am. Bull. 129, 625–648.

Walter, M.R., Grey, K., Williams, I.R., Calver, C.R., 1994. Stratigraphy of the Neoproterozoic to early Palaeozoic Savory basin, western Australia, and correlation with the Amadeus and Officer basins. Aust. J. Earth Sci. 41 (6), 533–546.

Wang, W., Zhou, M.F., 2012. Sedimentary records of the Yangtze Block (South China) and their correlation with equivalent Neoproterozoic sequences on adjacent continents. Sediment. Geol. 265, 126–142.

Weil, A.B., Geissman, J.W., Van der Voo, R., 2004. Paleomagnetism of the Neoproterozoic Chuar Group, Grand Canyon Supergroup, Arizona: implications for Laurentia's Neoproterozoic APWP and Rodinia break-up. Precambrian Res. 129 (1), 71–92.

Wen, B., Evans, D.A.D., Li, Y.-X., 2017. Neoproterozoic paleogeography of the Tarim Block: an extended or alternative "missing-link" model for Rodinia? Earth Planet. Sci. Lett. 458, 92–106.

Wessel, P., Müller, R.D., 2015. 6.02 – plate tectonics. In: Schubert, G. (Ed.), Treatise on Geophysics (Second ed.). Elsevier, Oxford, pp. 45–93.

Wessel, P., Matthews, K.J., Müller, R.D., Mazzoni, A., Whittaker, J.M., Myhill, R., Chandler, M.T., 2015. Semiautomatic fracture zone tracking. Geochem. Geophys. Geosyst. 16 (7), 2462–2472.

Whittaker, J.M., Müller, R.D., Leitchenkov, G., Stagg, H., Sdrolias, M., Gaina, C., Goncharov, A., 2007. Major Australian-Antarctic plate reorganization at Hawaiian-Emperor bend time. Science 318 (5847), 83–86.

Williams, G.E., Gostin, V.A., McKirdy, D.M., Preiss, W.V., 2008. The Elatina glaciation, late Cryogenian (Marinoan Epoch), South Australia: sedimentary facies and palaeoenvironments. Precambrian Res. 163 (3), 307–331.

Wingate, M.T., Giddings, J.W., 2000. Age and palaeomagnetism of the Mundine Well dyke swarm, Western Australia: implications for an Australia-Laurentia connection at 755 Ma. Precambrian Res. 100 (1), 335–357.

Wingate, M.T., Pisarevsky, S.A., Evans, D.A., 2002. Rodinia connections between Australia and Laurentia: no SWEAT, no AUSWUS? Terra Nova 14 (2), 121–128.

Wingate, M.T., Pisarevsky, S.A., De Waele, B., 2010. Paleomagnetism of the 765 Ma Luakela volcanics in Northwest Zambia and implications for Neoproterozoic positions of the Congo Craton. Am. J. Sci. 310 (10), 1333–1344.

Wit, M.J., Bowring, S.A., Ashwal, L.D., Randrianasolo, L.G., Morel, V.P., Rambeloson, R. A., 2001. Age and tectonic evolution of Neoproterozoic ductile shear zones in southwestern Madagascar, with implications for Gondwana studies. Tectonics 20 (1), 1–45.

Worsley, T.R., Nance, D., Moody, J.B., 1984. Global tectonics and eustasy for the past 2 billion years. Mar. Geol. 58 (3–4), 373–400.

Yellappa, T., Chetty, T.R.K., Tsunogae, T., Santosh, M., 2010. The Manamedu complex: geochemical constraints on Neoproterozoic suprasubduction zone ophiolite formation within the Gondwana suture in southern India. J. Geodyn. 50 (3), 268–285.

Yin, A., Dubey, C.S., Webb, A.A.G., Kelty, T.K., Grove, M., Gehrels, G.E., Burgess, W.P., 2010. Geologic correlation of the Himalayan orogen and Indian craton: Part 1. Structural geology, U-Pb zircon geochronology, and tectonic evolution of the Shillong Plateau and its neighboring regions in NE India. Geol. Soc. Am. Bull. 122 (3–4), 336–359.

Yong, W., Zhang, L., Hall, C.M., Mukasa, S.B., Essene, E.J., 2013. The 40Ar/39Ar and Rb-Sr chronology of the Precambrian Aksu blueschists in western China. J. Asian Earth Sci. 63, 197–205.

Yonkee, W.A., Dehler, C.D., Link, P.K., Balgord, E.A., Keeley, J.A., Hayes, D.S., Wells, M. L., Fanning, C.M., Johnston, S.M., 2014. Tectono-stratigraphic framework of Neoproterozoic to Cambrian strata, west-central US: Protracted rifting, glaciation, and evolution of the North American Cordilleran margin. Earth Sci. Rev. 136, 59–95.

Young, G.M., 1981. Upper Proterozoic supracrustal rocks of North America: a brief review. Precambrian Res. 15 (3), 305–330.

Young, G.M., Jefferson, C.W., Delaney, G.D., Yeo, G.M., 1979. Middle and late Proterozoic evolution of the northern Canadian Cordillera and Shield. Geology 7 (3), 125–128.

Zahirovic, S., Seton, M., Müller, R.D., 2014. The Cretaceous and Cenozoic tectonic evolution of Southeast Asia. Solid Earth 5 (1), 227.

Zahirovic, S., Müller, R.D., Seton, M., Flament, N., 2015. Tectonic speed limits from plate kinematic reconstructions. Earth Planet. Sci. Lett. 418, 40–52.

Zhao, J.H., Zhou, M.F., Yan, D.P., Zheng, J.P., Li, J.W., 2011. Reappraisal of the ages of Neoproterozoic strata in South China: no connection with the Grenvillian orogeny. Geology 39 (4), 299–302.

Chapter Three

A full-plate global reconstruction of the Neoproterozoic

GR focus review

A full-plate global reconstruction of the Neoproterozoic

Andrew S. Merdith [a,b,*], Alan S. Collins [c], Simon E. Williams [a], Sergei Pisarevsky [d,e], John D. Foden [c], Donnelly B. Archibald [c,f], Morgan L. Blades [c], Brandon L. Alessio [c], Sheree Armistead [c], Diana Plavsa [c], Chris Clark [g], R. Dietmar Müller [a]

[a] EarthByte Group, School of Geosciences, The University of Sydney, Madsen Building F09, Camperdown, NSW 2006, Australia
[b] Data61, CSIRO, Australian Technology Park, Eveleigh, NSW 2015, Australia
[c] Centre for Tectonics, Resources and Exploration (TRaX), Department of Earth Sciences, The University of Adelaide, Adelaide, SA 5005, Australia
[d] The Institute for Geoscience Research (TIGeR), Department of Applied Geology, Curtin University, GPO Box U1987, WA 6845, Australia
[e] Earth Dynamics Research Group, ARC Centre of Excellence for Core to Crust Fluid Systems (CCFS), Australia
[f] Department of Earth Sciences, St. Francis Xavier University, Antigonish, Nova Scotia, B2G 2W5, Canada
[g] Department of Applied Geology, Curtin University, Perth WA 6845, Australia

ARTICLE INFO

ABSTRACT

Neoproterozoic tectonic geography was dominated by the formation of the supercontinent Rodinia, its break-up and the subsequent amalgamation of Gondwana. The Neoproterozoic was a tumultuous time of Earth history, with large climatic variations, the emergence of complex life and a series of continent-building orogenies of a scale not repeated until the Cenozoic. Here we synthesise available geological and palaeomagnetic data and build the first full-plate, topological model of the Neoproterozoic that maps the evolution of the tectonic plate configurations during this time. Topological models trace evolving plate boundaries and facilitate the evaluation of "plate tectonic rules" such as subduction zone migration through time when building plate models. There is a rich history of subduction zone proxies preserved in the Neoproterozoic geological record, providing good evidence for the existence of continent-margin and intra-oceanic subduction zones through time. These are preserved either as volcanic arc protoliths accreted in continent-continent, or continent-arc collisions, or as the detritus of these volcanic arcs preserved in successor basins. Despite this, we find that the model presented here still predicts less subduction (ca. 90%) than on the modern earth, suggesting that we have produced a conservative model and are likely underestimating the amount of subduction, either due to a simplification of tectonically complex areas, or because of the absence of preservation in the geological record (e.g. ocean-ocean convergence). Furthermore, the reconstruction of plate boundary geometries provides constraints for global-scale earth system parameters, such as the role of volcanism or ridge production on the planet's icehouse climatic excursion during the Cryogenian. Besides modelling plate boundaries, our model presents some notable departures from previous Rodinia models. We omit India and South China from Rodinia completely, due to long-lived subduction preserved on margins of India and conflicting palaeomagnetic data for the Cryogenian, such that these two cratons act as 'lonely wanderers' for much of the Neoproterozoic. We also introduce a Tonian-Cryogenian aged rotation of the Congo-São Francisco Craton relative to Rodinia to better fit palaeomagnetic data and account for thick passive margin sediments along its southern margin during the Tonian. The GPlates files of the model are released to the public and it is our expectation that this model can act as a foundation for future model refinements, the testing of alternative models, as well as providing constraints for both geodynamic and palaeoclimate models.

© 2017 International Association for Gondwana Research. Published by Elsevier B.V. All rights reserved.

Contents

* Corresponding author at: EarthByte Group, School of Geosciences, The University of Sydney, Madsen Building F09, Camperdown, NSW 2006, Australia.
E-mail address: Andrew.merdith@sydney.edu.au (A.S. Merdith).

1. Introduction

Since its conception during last century, the theory of plate tectonics is intricately linked to advancements in geology. The theory provides a global framework, within which the microscopic textures and fabric of rocks can be reconciled through space and time with both the broad scale expression of geological features evident on the surface of our planet, and the dynamic evolution of the mantle underneath. Following Wegener's theory of continental drift (Wegener, 1912) and the adoption of plate tectonics during the 1960's by geoscientists, continents have been 'stitched' back together in order to understand long term trends and variations in mantle dynamics (e.g. Tackley, 2000), faunal diversity and evolutionary patterns (e.g. Cocks and Torsvik, 2002; Halverson et al., 2009; Meert and Lieberman, 2004; Valentine and Moores, 1972), distribution of ore deposits (e.g. Barley and Groves, 1992; Bierlein et al., 2009; Butterworth et al., 2016; Meyer, 1988; Pehrsson et al., 2016), seawater chemistry (Halverson et al., 2007; Hardie, 1996), palaeogeography and climate (Hoffman et al., 1998a; Kirschvink, 1992).

Reconstructing the interaction of plates along their boundaries – as opposed to reconstructing positions of continental blocks only – allows for testing and optimising reconstructions using plate tectonic and geodynamic principles, and assimilating the geological evidence preserved, especially along ancient subduction boundaries. Just as the predecessor of plate tectonic theory was continental drift, plate tectonic reconstructions are evolving from the relative (and absolute) motions of continental blocks to 'topological' plate models with closed plate boundaries that dynamically evolve through time (Gurnis et al., 2012). The importance of this paradigm shift of plate models is attributed to the significance that plate boundaries play in creating and destroying key geological environments, such as passive margins, island arcs and orogenic mountain belts, in better understanding hazards facing human society (e.g. volcanoes and earthquakes), and as an interface between mantle and crustal processes. Additionally, complete plate models create a foundation within which a broad range of hypotheses pertaining to topics such as magmatism, spreading rates, ocean basin size, mantle evolution and long-term palaeoclimatic variation can be tested more thoroughly than is possible through a model depicting only continental motions.

Plate models for the Cenozoic and Mesozoic (Müller et al., 2016; Seton et al., 2012), the late Palaeozoic (Domeier and Torsvik, 2014) and a bridging model between the two (Matthews et al., 2016) are available and global models for the Early Palaeozoic are partially complete (Domeier, 2016). However, as the amount of palaeomagnetic and, particularly, geological data that are available to constrain plate motions and boundaries increases, and software better able to compute topological plate models is developed (e.g. GPlates2.0 – gplates.org), the opportunity has arisen to construct such models further back in time in the Neoproterozoic. This is important as the transition from the Neoproterozoic to Phanerozoic is marked by the Ediacaran biotic revolution (Droser and Gehling, 2015), followed by the Cambrian explosion and the evolution of most present-day phyla and complex life (Meert and Lieberman, 2008). The Neoproterozoic was also a time of extreme climatic variation with (near?) global ice coverage over possibly as much as 60 million years at a time (Rooney et al., 2015). Many suggestions of how the planet descended into this ice-house world involve questions that can be addressed using a global topological plate model. For example, it has long been suggested that distributing continents around the tropics increases global albedo assisting with cooling the planet (Hoffman et al., 1998a; Kirschvink, 1992; Worsley and Kidder, 1991). However, more recently, volcanism has been identified as a possible cause, either by sulphuric acid aerosol production (Stern et al., 2008), weathering of terrestrial basalts (Goddéris et al., 2003; Cox et al., 2016) or by submarine hydration of volcanic glass produced along extensive ridge systems (Gernon et al., 2016). These suggested causal mechanisms, which relate to the tectonic geography of the times, and, in particular, the possible contribution of changing mid-ocean ridge lengths, can only be evaluated using a global topological plate model.

We present the first topological plate model for the Neoproterozoic, encompassing the evolution and breakup of Rodinia and subsequent amalgamation of Gondwana. The approach here is similar to that of both Domeier and Torsvik (2014) and Domeier (2016), with the model constrained by palaeomagnetic and geological data, as well as basic principles of plate kinematics (e.g. rates of movement). We stress that, considering the relative sparsity and uncertainty of data available to constrain plate kinematics and plate boundary configurations in the period covered by our study, there are likely to be many disagreements about the positions and movements of plates during this time. Furthermore, the configuration of boundaries within the oceanic domains of our model is almost entirely unconstrained by observations away from the continents. In such areas, we use simple plate tectonic rules to construct plausible plate boundary configurations that are consistent with our model for continental kinematics. To facilitate improvements and development of alternative models we make our plate model and all related files available to the public.

1.1. Previous models of Neoproterozoic supercontinents

Although the existence of a late Palaeozoic-Mesozoic supercontinent had been proposed in the early twentieth century, the possibility of earlier, Precambrian, supercontinents, is a much more recent suggestion. Piper et al. (1976) proposed a long-lived Pangaea ('Palaeopangaea') existing through the entire Proterozoic. This was based exclusively on palaeomagnetic data, and as data accumulated through the 1970's and 1980's, McMenamin and McMenamin (1990) suggested that a more plausible reconstruction involved two Neoproterozoic continents (East Gondwana and West Gondwana) that were derived from the breakup of a late Mesoproterozoic/early Neoproterozoic supercontinent, which they called Rodinia (from the Russian 'rodit', meaning 'to beget' or 'give birth'). Studies published by Dalziel (1991), Hoffman (1991) and Moores (1991) were the first papers to put forward a model for a Precambrian supercontinent, by integrating geological evidence with palaeomagnetic data. Principally, these reconstructions matched the east coast of Australia-Antarctica with the west coast of Laurentia (the

cratonic part of North America) in the so-called SWEAT fit – **S**outh**w**est U.S. – **E**ast **A**ntarctica, and attached Amazonia to the east coast of Laurentia, whereas previously the only well-established connection was between Laurentia and Baltica (the cratonic part of Europe). The Laurentia-Australia connection was based on the similarly aged, and broadly congruent, sedimentary successions of eastern Australia-Antarctica and the Laurentian Cordillera, and an extension of the Grenville Orogen into the Shackleton Ranges of Antarctica (Dalziel, 1991; Moores, 1991). Hoffman (1991) also suggested a mechanism for the transition from Rodinia to Gondwana, with a 'fan-like' collapse of continents on the east and west side of Laurentia (India-Australia-Antarctica and Amazonia-West Africa respectively), around the Gondwanan nucleus of the Congo-São Francisco (C-SF) Craton (which rifted from the southern Laurentian margin) (Fig. 1a). Dalziel (1992) proposed a reconstructed Neoproterozoic supercontinent (Fig. 1b) that Torsvik et al. (1996) altered into a fit where Rodinia was more strongly constrained by the palaeomagnetic data available at the time, with a new configuration for Laurentia-Baltica-Amazonia (Fig. 3c). Both models followed Hoffman's (1991) suggestion of a 'fan-like' transition to Gondwana. These models were broadly supported by available palaeomagnetic data of McMenamin and McMenamin's East Gondwana, consisting of Australia, India and East Antarctica, which, at this time, was thought to act congruently, supported by the geological correlation of late Mesoproterozoic to early Neoproterozoic orogenies across India, Australia and Antarctica (e.g. Katz, 1989), and Laurentia proposed by Powell et al. (1993). Powell et al. (1993) suggested that Rodinia breakup occurred at ca. 700 Ma and final Gondwana amalgamation was at ca. 520 Ma, with East Gondwana remaining in low latitudes and Laurentia (including Baltica, Amazonia and West Africa) moving to polar latitudes. Finally, Dalziel (1997) capped nearly a decade of study since the proposal of Rodinia with a model spanning 725 to 422 Ma that summarised the consensus of previously published geological, palaeomagnetic and palaeontological data (Fig. 1c). Australia-Antarctica was placed against Laurentia in a SWEAT configuration, Baltica was placed against northern Greenland, with Amazonia placed slightly further down the northeast coast of Laurentia, connecting the Grenville Orogen in Laurentia with the Sunsas Orogen in Amazonia (Dalziel, 1992). The main deviation from the earlier, Dalziel (1992), model was that C-SF was tucked in closer to Amazonia along the eastern margin of Laurentia, rather than outboard of Kalahari, off the southern margin of Laurentia. This suggested that the western Gondwanan cratons were only separated by small ocean basins between Rodinia and Gondwana, and that they followed similar motion paths during the amalgamation of Gondwana. The model also considered the existence of Pannotia (e.g. Powell et al., 1995), a hypothesized, transient supercontinent occurring ca. 600 Ma, after amalgamation of Gondwana, but before the opening of the Iapetus Ocean (i.e. Laurentia, Baltica and Gondwana).

The suggestion that East Gondwana did not act congruently through the Neoproterozoic was originally proposed by Meert et al. (1995) based on geochronological data that suggested discrete phases of orogeny, between ca. 800 and 650 Ma and at ca. 550 Ma (Stern, 1994). They proposed that this represented a two-stage collision, between the Arabian-Nubian Shield, India, Madagascar, Kalahari and a small slither of Antarctica (a terrane they called IMSLEK), with Congo, as the earlier stage, and then the collision between this amalgamated continent with Australia-Antarctica as the later stage (Meert et al., 1995). Meert and Van der Voo (1997) extended this idea, describing the amalgamation of Gondwana as a series of three orogenic events. The Brasiliano Orogeny (between Congo and Amazonia-West Africa-Rio de la Plata), the East African Orogeny (between Congo and India-Madagascar) and the Kunngan Orogeny (between the rest of Gondwana and Australia-Antarctica). A key implication arising from their multi-stage amalgamation model was that irrespective of their positions in the early Neoproterozoic, India and Australia-Antarctica moved independently from one another during the transition from Rodinia to Gondwana. This was further supported by geochronological data from Antarctica,
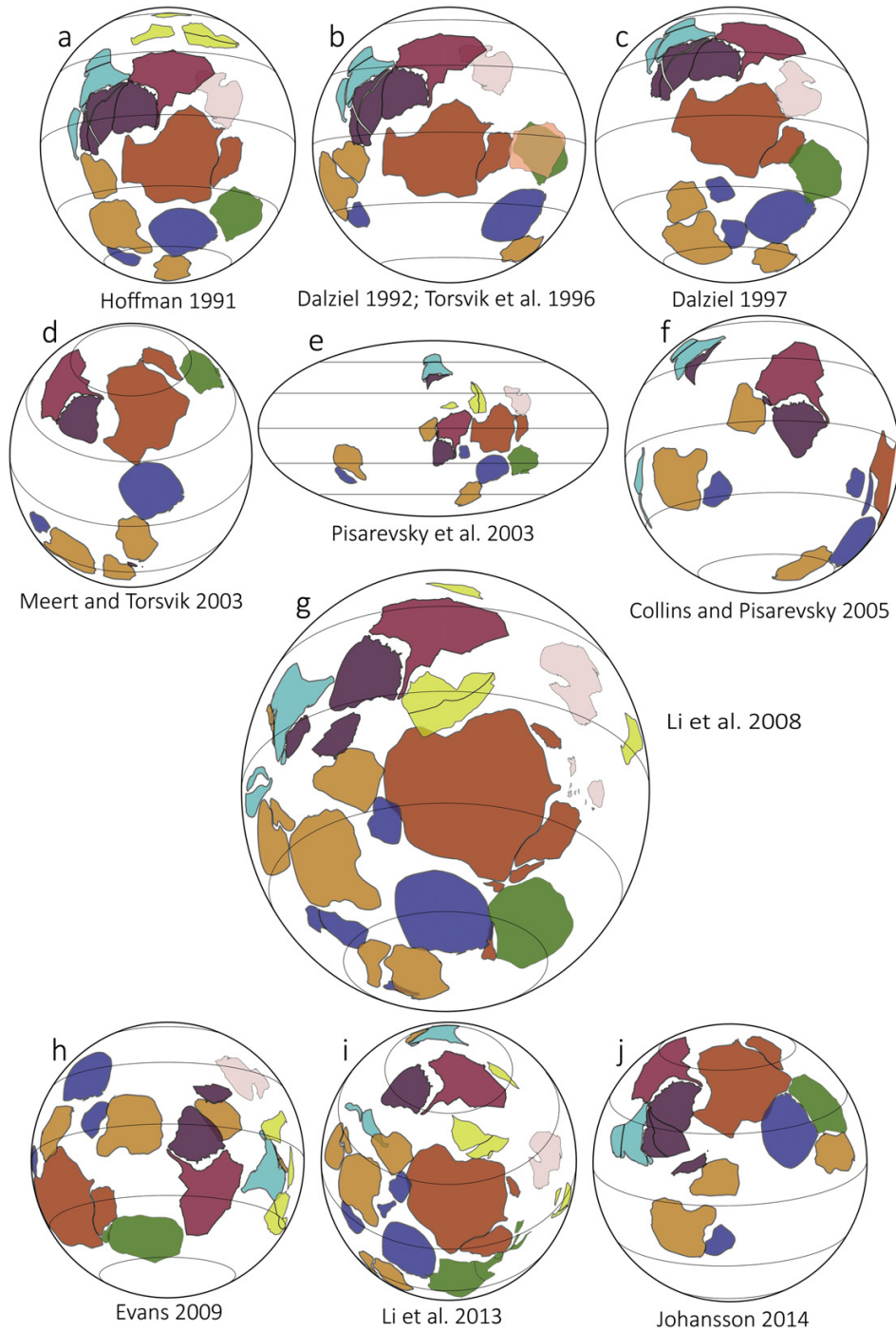
Fig. 1. Previous models of Rodinia reconstructed in *Gplates* using published Euler Pole rotations or reverse-engineered, if poles were not available. (a) Hoffman (1991) at 800 Ma; (b) Dalziel (1992) and Torsvik et al. (1996) at 750 Ma. The green Baltica belongs to Torsvik et al. (1996), and the pink belongs to Dalziel (1992). (c) Dalziel (1997) at 725 Ma; (d) Meert and Torsvik (2003) at 800 Ma; (e) Pisarevsky et al. (2003) at 800 Ma; (f) Collins and Pisarevsky (2005) at 750 Ma; (g) Li et al. (2008) at 900 Ma; (h) Evans (2009) at 900 Ma; (i) Li et al. (2013) at 800 Ma, and; (j) Johansson (2014) at 900 Ma. Cratonic blocks are colour coded by present day geography; North America, red; South America, dark blue; Baltica, green; Siberia, grey; India and the Middle East, light blue; China, yellow; Africa, orange; Australia, crimson; Antarctica, purple. (a)–(c), (e)–(i) in absolute framework; (d), (j) in Laurentian co-ordinates.

which indicated that the late Mesoproterozoic to early Neoproterozoic orogenies that were originally thought to tie East Gondwana together were separate events (Boger et al., 2001; Fitzsimons, 2000a,b), and by new high quality palaeomagnetic data from India and Australia at ca. 750 Ma that indicated at least a 30° latitudinal separation between them (Torsvik et al., 2001a,b; Wingate and Giddings, 2000). This led to a re-interpretation of the Darling Fault and the Leeuwin Block of south-west Western Australia (Collins, 2003), from being interpreted as a product of intracratonic deformation (e.g. Harris and Beeson, 1993) to representing a sinistral strike-slip tectonic boundary between two cratons moving independently (e.g. Fitzsimons, 2003), and suggested a staggered amalgamation of eastern Gondwana.

Palaeomagnetically constrained models of Rodinia without a unified East Gondwana were proposed by Meert and Torsvik (2003) (Fig. 1d) and Pisarevsky et al. (2003) (Fig. 1e). In addition to separating the constituents of East Gondwana during Rodinia breakup, both studies moved C-SF, Kalahari and India significantly from the 'traditional' model of Dalziel (1992, 1997). Meert and Torsvik (2003) analysed the possible positions of the major Precambrian cratons using palaeomagnetic data and moved C-SF, along with the Kalahari craton, to a distal position, outboard of Amazonia and West Africa. They also removed India completely from Rodinia. Comparably, Pisarevsky et al. (2003) removed both C-SF and India from Rodinia, and attached the Kalahari craton to the 'traditional' position of India, along the west coast of Australia-Antarctica, while leaving the other cratons in similar positions to Dalziel (1997). In their model, a ~7000 km ocean basin separated C-SF (and presumably the Saharan Metacraton (SM) and Hoggar) from Rodinia. Collins and Pisarevsky (2005) modelled the breakup of Rodinia to the amalgamation of Gondwana, with particular focus on the eastern Gondwana cratons (Fig. 1f). They adopted similar cratonic positions at 750 Ma as Pisarevsky et al. (2003) but focussed more closely on the closure of the Mozambique Ocean, and the suture between India and Congo. They drew attention to portions of Archaean-Palaeoproterozoic crust (Collins and Windley, 2002) preserved in modern day Madagascar, suggesting the existence of a small continent between Congo and India. They referred to this intra-East African Orogen continent as 'Azania' and proposed a two-stage collision of India-Azania-Congo, with initial closure of an ocean separating Azania and Congo (termed the Neomozambique ocean by Fitzsimons and Hulscher, 2005), followed by the collision of India with the then combined Congo and Azania, and the closure of the Mozambique Ocean sensu stricto (Collins and Pisarevsky, 2005).

The most holistic model of Neoproterozoic plate motions was by Li et al. (2008) as a contribution to IGCP 440, and that work underpins large parts of the model presented here (Fig. 1g). Using intersecting lines of evidence (e.g. palaeomagnetic data, geology, plate kinematics) a full reconstruction from 1100 to 520 Ma was built that depicted the assembly and breakup of Rodinia, and the transition from Rodinia to the amalgamation of Gondwana. Their interpretation of the temporal and spatial constraints of subduction zones, coupled with locations of dyke swarms, lead to the inferred presence of a large plume underneath Rodinia (e.g. Li et al., 2004). This model (re-) attached both India and C-SF to Rodinia on geological grounds. Coeval bimodal magmatism in India, South China and Australia was interpreted to indicate proximity between these cratons above a mantle plume (Li et al., 2003). Subsequently, India was placed in its 'traditional' configuration outside eastern Antarctica, with the accretion to Rodinia occurring between the early Neoproterozoic Eastern Ghats Belt of India with the Rayner Province of Antarctica. C-SF was attached to Rodinia based on U-Pb geochronological data indicating tectonism and magmatism between ca. 1050 and 950 Ma in the Irumide belt (de Waele et al., 2003), which was interpreted as an extension of the Grenvillian Orogeny. Inertial Interchange True Polar Wander (IITPW, Evans, 1998) was incorporated into the model between 820 and 750 Ma in order to account for a spread of palaeomagnetic data across South China (e.g. Li et al., 2004). The possible driver for IITPW was the hypothesized presence of the large mantle plume underneath Rodinia

while it lay at a high latitude (a position suggested palaeomagnetically by the ca. 802 Ma Xiaofeng Dykes, Li et al., 2004). While acknowledging the variety of Australia-Laurentia configurations that are viable, they adopted the 'Missing-Link' configuration of Li et al. (1995), positioning South China in between Australia and Laurentia. Due to the large collaborative effort, as well as the broad range of evidence used, this model of Rodinia acts as a foundation for other global reconstructions, and also regional studies that seek to fit geological data into a larger Neoproterozoic picture.

In a marked departure from the 'traditional' configurations of Rodinia, Evans (2009) built an alternate model ('Radical Rodinia'), adhering strictly to palaeomagnetic data to define cratonic configurations (Fig. 1h). Laurentia still occupied a central position and Baltica was attached in a similar location to its 'traditional' position. Australia-Antarctica and India were placed outside of Baltica away from Laurentia, with Siberia and the three Chinese cratons placed outside of India, further away. C-SF was fitted against the northern coast of Laurentia and West Africa attached to the west coast of Laurentia, with Amazonia acting as a (large) promontory of Rodinia. A small intracontinental sea lay between Australia-Congo-Greenland. Although more recent palaeomagnetic data have disallowed parts of this configuration (e.g. Evans et al., 2016a, and references therein), a salient point of Evans (2009) is that any model presented will be a non-unique solution of the data available to constrain it and habitual familiarity with previous models can hinder us from approaching a 'true' reconstruction.

A new iteration of the Li et al. (2008) model that focussed predominantly on the analysis of sedimentary rocks deposited during the Cryogenian and Ediacaran and their relationship with both global glaciations and broad-scale geodynamics of supercontinent breakup was proposed by Li et al. (2013) (Fig. 1i). They updated palaeogeographic maps for the transition between Rodinia and Gondwana and included recent developments in Neoproterozoic tectonics, such as the intraplate rotation of Australia (Li and Evans, 2011), and tightened palaeomagnetic constraints. In order to account for the prevalent, late Tonian global evaporite deposits, a second, earlier pulse of IITPW was suggested to occur just prior to the IITPW event described in Li et al. (2008). This IITPW event would have dragged Rodinia from low-latitudes (where the evaporates were deposited) to higher latitudes at ca. 825 Ma, before the later event related to a high-latitude superplume in the mantle pulled Rodinia back to lower latitudes between 800 and 780 Ma (Li et al., 2013).

A derivative of the model proposed by Li et al. (2008) is the SAMBA (South AMerica-BAltica) model of Johansson (2009, 2014), which is based upon a long-lived Proterozoic connection between Baltica and Amazonia that is preserved through both Nuna (the Mesoproterozoic supercontinent, e.g. Pisarevsky et al., 2014a and references therein) and Rodinia until the opening of the Iapetus Ocean from ca. 615 Ma (Johansson, 2009). This model of Rodinia depicts the positions of Australia, Siberia and Kalahari in similar positions to Li et al. (2008); Australia-Antarctica is depicted in a SWEAT configuration, although Johansson (2014) outlines that a Missing-Link configuration would also be compatible (Fig. 1j). Amazonia is rotated anti-clockwise from its position in Li et al. (2008), and is fitted into the (present day) southern margin of Baltica so that similar aged orogenic belts are aligned across the two cratons (from an Archaean core in the east, younging towards the west, and terminating with the ca. 1.1–1.0 Ga Sveconorwegian and Sunsas Orogens, which are linked to the Grenville Orogeny and Rodinia's amalgamation). West Africa is rotated 80° clockwise from its present-day position, and is placed outboard against both Amazonia and Baltica, in a tight fit that closes most of south and south-eastern Baltica off from an open ocean. However, the direction of tectonic growth of Palaeoproterozoic Baltica indicated by Bogdanova et al. (2015) would be perpendicular to the direction of coeval growth in Amazonia (in the Ventauri-Tapajos province), if they were in the SAMBA position, suggesting that this configuration may not be reliable for parts of the Proterozoic. The transition described by Johansson

(2014) from Rodinia to Gondwana would fit an 'orthoversion' type model of the supercontinent cycle (Mitchell et al., 2012), whereby the transition to the next supercontinent (i.e. Gondwana) occurs through ocean closure along the great circle of the girdle of subduction around the recently rifted apart supercontinent (i.e. Rodinia), similar in concept to the 'fan-like' collapse of Hoffman (1991).

An underlying assumption of previous models, and the model we present here, is that plate tectonics in the Neoproterozoic operated as they did in the Phanerozoic, and a key objective of this work is to provide the foundation for a geodynamic study that fully encompasses the transition from one supercontinent to another. The supercontinent cycle (e.g. Nance and Murphy, 2013; Worsley et al., 1984) presupposes cyclicity through plate divergence and convergence, necessitating, in some capacity, a mechanism for the motion of plates. Whether this motion during Precambrian times was through the coupling of the mantle with the crust similar to today, or through a different mechanism, such as 'lid tectonics' is uncertain (e.g. Roberts, 2013). The similarity between key cratonic configurations in Nuna and Rodinia (e.g. Meert, 2014a), despite both palaeomagnetic and geological data indicating relative significant motions of cratons between the two supercontinents (e.g. Pisarevsky et al., 2014) is suggested as by some workers evidence for a variation of plate tectonics, as the motions were either minor re-adjustments (e.g. Cawood et al., 2010, Baltica's rotation into Laurentia) or failed rifting events that reclosed along similar suture lines (e.g. Payne et al., 2009, Proto-SWEAT in Nuna). Nonetheless, Bradley (2011) outlined that most secular trends in the geological record were established either by or during the Neoproterozoic implying that modern day plate tectonics was probably recognisable during the Rodinia-Gondwana transition (Nance et al., 2014). An interesting note is that for all the new data collected since the original propositions of Rodinia (e.g. Dalziel, 1992; Hoffman, 1991), spatially, very little has changed in the overarching positions of most of the major Precambrian cratons; Laurentia still sits at the heart of Rodinia, Baltica and Amazonia on the east coast, Australia-East Antarctica on the west coast, C-SF and Kalahari on the south coast and Siberia off the north coast (Fig. 1).

2. Methodology

2.1. Foundations and starting points

The foundation of the plate tectonic model presented here is the Neoproterozoic reconstruction proposed by Li et al. (2008), which was principally based on geological observation and palaeomagnetic data from the late Mesoproterozoic to the Cambrian (ca. 1100–500 Ma). We supplement this with additional recent palaeomagnetic and geological data, and tectonic amendments (e.g. Evans et al., 2016b; Li and Evans, 2011; Pisarevsky et al., 2013) to create a new, topological plate model for the Neoproterozoic that encompasses the breakup of Rodinia and amalgamation of Gondwana. A description of both geological and palaeomagnetic data used to constrain cratonic configurations, positions and motions is provided in Sections 3, 4 and 5. We use cratonised blocks and terranes whose evolution can be tightly linked to the motions of larger cratons to create the model (Fig. 2a and b), with the expectation that other smaller, more poorly constrained terranes can be included in future iterations. The rationale for using the cratonised blocks is because during the late Neoproterozoic there was a major episode of continental crust building, involving the formation and accretion of many terranes to Gondwana along long-lived subduction zones (e.g. Arabian-Nubian Shield, Central Asian Terranes and Avalonian Terranes), and, due to the limited data available from the time, it is difficult to properly constrain both their absolute and relative positions.

Reliable palaeomagnetic data are the most useful data for deep time reconstructions, as they constrain continental palaeolatitudes at a specific time. However, major uncertainties include determining the age of magnetisation and accounting for any post-magnetisation deformation events. Consequently, palaeomagnetic data are often sparse for long periods of time, to the extent that all terranes and some cratons lack any reliable Neoproterozoic poles (e.g. Kalahari, West Africa, Azania, Amazonia, North China), while other blocks have no reliable poles for large time intervals (e.g. Australia between 1000 and 800 Ma, India between 1000 and 770 Ma and 750–550 Ma). Geological evidence is used to complement palaeomagnetic data, where age-dated tectonic geographic phenomena such as arc and rift magmatism, orogenic belt development, ophiolite formation and obduction, stratigraphic columns, metamorphism and shear zones help constrain both the motion of plates relative to one another, and the timing of key events (i.e. rifting and collision). In some cases, where there are no palaeomagnetic data available, the relative motions of a given craton are determined through geological observation and inference. An additional line of evidence used (in part as a 'sanity check' on plate motions) are plate kinematic rules, relating to how, geometrically, rigid plates move over a semi-rigid mantle. Using the evolution of the modern-day ocean basins as a guide, there are limits on the rates of motion and angular rotation that we expect plates to achieve. Such limits can help constrain a range of possible motions or help test competing plate configurations. As the majority of this reconstruction is before the evolution of complex life forms, palaeontological data is only useful for modelling the youngest time intervals (e.g. Meert and Lieberman, 2008).

2.2. Constructing the model

The plate reconstruction was built using the *GPlates* software (www.gplates.org). Gurnis et al. (2012) developed a topological functionality for *GPlates*, whereby plates can be defined by a finite list of boundaries (each boundary possessing its own Euler Pole) that dynamically evolve through time allowing for a 'continuously closed plate' (e.g. Fig. 2a). Plate boundaries in the Neoproterozoic are most tightly constrained around the margins of continents and/or continental crust; (i) where geological evidence for a subduction zone is preserved (e.g. ophiolites, subduction related magmatism, high pressure metamorphic rocks etc.), (ii) where there is evidence for continental rifting and breakup, so that two continents break apart and a spreading ridge forms (e.g. sedimentation, half grabens etc.), and, (iii) where there is transform motion between continental blocks preserved in the rock record (e.g. shearing, wrench tectonics). Away from continental crust, plate boundaries are more difficult to determine, so they must be inferred, either from connecting more tightly constrained boundaries, or from observing the motion of continental crust (such as from palaeomagnetic data) and interpreting the appropriate boundary requirement. Changes in the regional arrangement of plate boundary configurations (i.e. plate reorganisations) are linked, where possible, to broader global tectonic changes, such as initiation of rifting or subduction, since we have analogous evidence for plate reorganisation occurring as a consequence of these events in the Mesozoic-Cenozoic. For example, subduction cessation due to arc or terrane collision can cause reorganisations (e.g. Austermann et al., 2011; Patriat and Achache, 1984), as can subduction initiation (e.g. Faccenna et al., 2012; Whittaker et al., 2007), subduction of ridges or young buoyant oceanic crust (e.g. Matthews et al., 2012; Seton et al., 2015), and subduction of thickened crust (Knesel et al., 2008). Similarly, the arrival of plumes and superplumes is also thought to contribute to plate reorganisations (e.g. Cande and Stegman, 2011; van Hinsbergen et al., 2011), making times of supercontinent breakup critical for understanding and modelling plate motions and plate boundary changes. The process of constructing the model was completed iteratively to ensure that each boundary is both self-consistent with the paradigm of motion (i.e. convergence leads to subduction) as well as consistent with other boundaries forwards and backwards in time to ensure continuity.

The motions of the plates are described using a plate hierarchy similar to that of Seton et al. (2012) and Müller et al. (2016), such that a series of Euler poles describes each plate moving relative to another
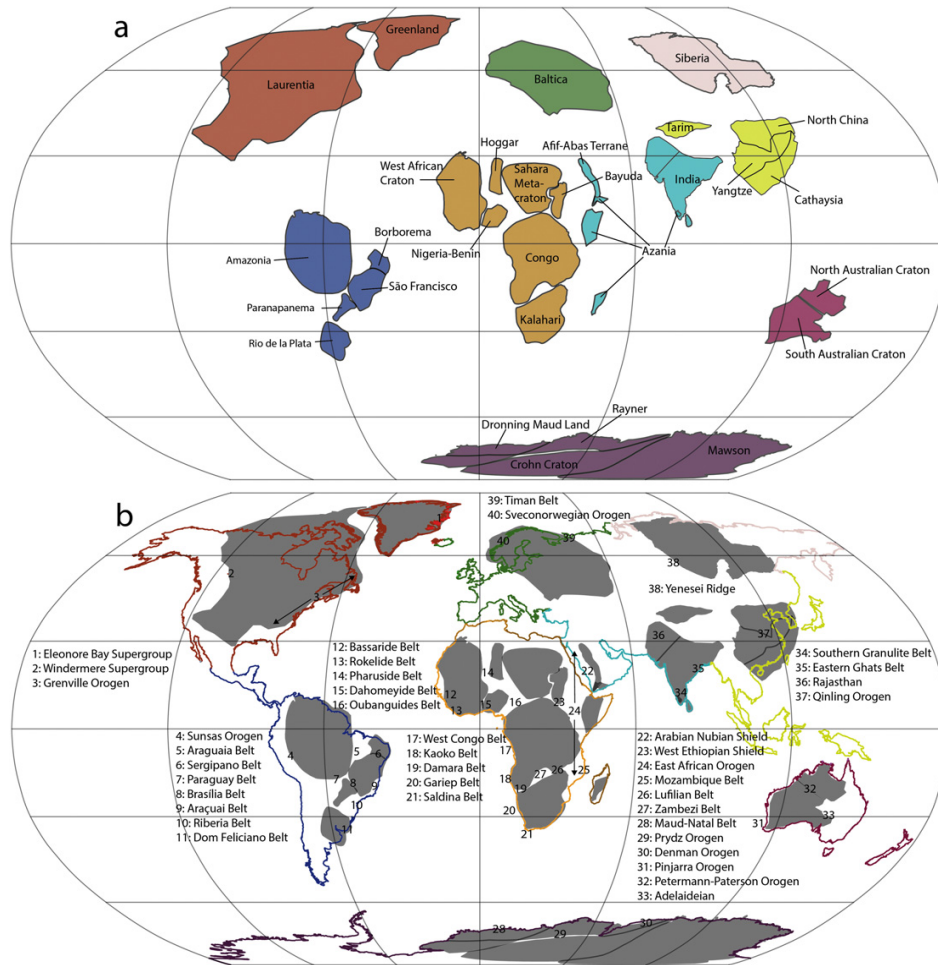
Fig. 2. (a) Map of Precambrian cratonic crust used in the reconstruction in their present-day locations. (b) Present day geographical map of the world with Precambrian cratonic crust used in the reconstruction in grey. Some key geological areas referred to sections 3, 4 and 5 are highlighted in (b). In both (a) and (b) cratonic crust and modern day continents are colour coded by their present-day position (consistent for all reconstruction figures).

(Fig. 3b). For the early part of the model (ca. 1000–700 Ma) the motions of plates are described relative to Laurentia, as it occupied the central position in Rodinia. From ca. 700 to 520 Ma, the motions of all plates except Laurentia, Baltica and Siberia are described relative to the Congo Craton, due to its central position in Gondwana. As there are no preserved ocean basins from this time, in some cases oceanic plates without a terrane or craton are constructed as a necessary requirement of plate tectonic theory. These plates have an arbitrary plateID and an artificial rotation to demonstrate that oceanic plates are implied to be present with new crust forming at spreading ridges, but there are no geological or palaeomagnetic constraints available to quantify the extent or velocity of these plates, rather their existence is inferred from the preservation of ocean-continent subduction zones in the geological record. The motion of synthetic oceanic plates is modelled to follow the general rule that slab pull dominates plate motions (Conrad and Lithgow-Bertelloni, 2002). By definition, convergence of oceanic plates towards active margins necessitates the modelling of divergent plate boundaries within the ocean basins. In these divergent settings, the precise geometry of these ridge and transform segments is synthetic and is drawn such that the orientation of the spreading segments follow great circles passing through the Euler Pole that describes the relative movement of one of the two plates, while transform segments offsetting this
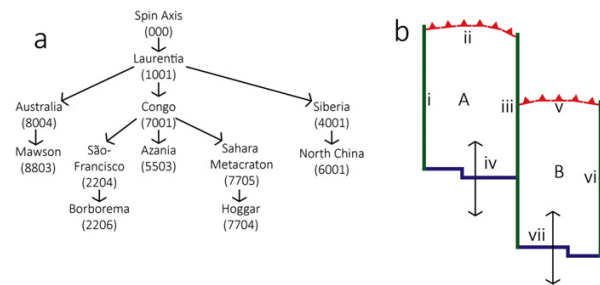
Fig. 3. Schematic depiction of (a) plate hierarchy (with some continents and their plateIDs), and (b) topological boundaries. In the plate hierarchy, all plates move relative to the plate above it (i.e. Hoggar moves relative to the Sahara Metacraton, which moves relative to Congo, which moves relative to Laurentia, which moves relative to the spin axis. The advantage of this is that it preserves relative plate motion between portions of crust that may not have any palaeomagnetic data. For example, the relative motion between Azania and Congo might involve some form of convergence inferred from geological data; there are no palaeomagnetic data to constrain Azania, but there are data to constrain Congo. Using a hierarchy, moving Congo into a palaeomagnetically defined position will preserve the relative rotations built on the geological basis between Azania and Congo, while allowing Congo to now better fit a pole. In (b), Plate A is defined by the boundaries consisting of (i), (ii), (iii) and (iv), Plate B is defined by the boundaries consisting of (iii), (v), (vi) and (vii).

spreading system follow small circles drawn around the same Euler Pole. We specifically point out that the large number and length of transform boundaries in the model are due to this simplification of boundaries and not an inherent indication that transform motions dominated Neoproterozoic tectonics.

3. Tonian evolution of Rodinia (1000–750 Ma)

3.1. 'North' Rodinia (Laurentia-Siberia ± North China)

Although a geological and palaeomagnetic connection between Siberia and Laurentia is generally accepted for the Mesoproterozoic and early Neoproterozoic (Ernst et al., 2016; Gladkochub et al., 2010a,b; Pisarevsky et al., 2014) there are large variations in possible configurations for Siberia as part of Rodinia (see Pisarevsky et al., 2008a for a review, e.g. Condie and Rosen, 1994; Frost et al., 1998; Hoffman, 1991; Rainbird et al., 1998, along the northern margin of Laurentia, or Sears and Price, 2000, along the western margin of Laurentia). We have attached Siberia to northern Laurentia following Pisarevsky and Natapov (2003), as it was adopted by Pisarevsky et al. (2008a, 2013) and Li et al. (2008). This configuration leaves a 30° gap between the northern margin of Laurentia and the southern margin of Siberia (possibly to be filled by minor North American terranes, e.g. 'Arctida' of Zonenshain et al., 1993). In the early Neoproterozoic Siberia was bordered by passive margins on its eastern, northern, western and maybe southern margins (Metelkin et al., 2012; Pisarevsky and Natapov, 2003). A subduction zone lay outboard of western margin of Siberia by ca. 880–860 Ma, which is represented by the Central Angara Terrane (Vernikovsky et al., 2016) that migrated to the continental margin by ca. 750 Ma (Vernikovsky et al., 2004; Metelkin et al., 2012). This subduction system has been proposed to be a continuation of the Valhalla Orogeny of Cawood et al. (2010) (e.g. Likhanov et al., 2014, 2015). Five terranes are identified, divided by the ENE sinistral Angara Fault. The oldest terrane (the Angara-Kan Terrane) is located on the southern side of the fault, and consists of Palaeoproterozoic, upper amphibolite-granulite metamorphosed volcanic and sedimentary rocks that overthrust the younger, Neoproterozoic aged island-arc assemblages of the Predivinsk Terrane (Nozhkin et al., 1999; Popov, 2001; Vernikovsky et al., 2004). The other three terranes are located on the northern side of the fault, and are Mesoproterozoic-Neoproterozoic aged marine sedimentary successions, consisting of carbonates, siliciclastics and ophiolites, which are generally metamorphosed to greenschist facies. The northern margin of Siberia transformed from a passive to active regime by ca. 750 Ma (Vernikovsky et al., 2004), with the accretion of the Central Taimyr terrane, which consists of volcanic and sedimentary units, during the late Neoproterozoic, at ca. 600 Ma. Here we match the east north-eastern margin of Siberia with the southern margin of North China, creating a nearly closed sea accounting for the thick sedimentation on the eastern margin of the Siberian Craton (Vernikovsky et al., 2004). The south-western margin of North China is outboard of Rodinia and here interpreted as a further extension of the Valhalla Orogen (and the early subduction outboard of Siberia), allowing for long-lived subduction and the collision of the North Qinling Terrane with the North China Block from ca. 900 Ma (Dong and Santosh, 2016; Wang et al., 2011). Considering the paucity of palaeomagnetic data for North China in the Neoproterozoic (Section 6.2), a position outboard of Australia could be an alternative to its position adjacent to Siberia. This is suggested by the similarity of their Mesoproterozoic positions (e.g. Pisarevsky et al., 2014; Zhang et al., 2012a) and their Palaeozoic positions (e.g. Metcalfe, 2006).

A relative motion of Siberia and North China to Laurentia along a dextral transform fault between ca. 800 and 720 Ma, which closes the gap between the two continents, is adopted here (Pisarevsky et al., 2013). This is based primarily on palaeomagnetic data (see Section 6). However, it does spatially associate the ca. 720 Ma mafic rocks of southern Siberia (e.g. the ca. 725 Ma Irkutsk large-igneous-province (LIP),

Ernst et al., 2013, 2016) with the Franklin magmatic event in Laurentia, and suggests rifting from Rodinia during the mid Cryogenian from a position outboard of Greenland.

3.2. 'East' Rodinia (Laurentia-Baltica-Amazonia ± West Africa)

The formation of Rodinia in the late Mesoproterozoic–early Neoproterozoic necessitates a large (~95°) clockwise rotation of Baltica relative to Laurentia during the late Mesoproterozoic (Cawood et al., 2010), forming the Sveconorwegian Orogeny in Baltica and the Grenvillian Orogeny in Laurentia (Fig. 2b). Bingen et al. (2008) suggested that the primary phase of the Sveconorwegian Orogeny, consisting of granulite facies metamorphism, occurred between ca. 1050 and 980 Ma, and that orogenesis was over by ca. 920 Ma. After the Grenvillian-Sveconorwegian Orogeny, the Valhalla Orogeny initiated on the outboard margin of Greenland (Cawood et al., 2010) and possibly off Siberia and North China (see above). While the early stages of orogenesis here overlap with the final stages of the Grenvillian Orogeny, the two events are tectonically distinct, with the Valhalla Orogeny constituting an exterior rather than an interior orogeny due to the dominance of calc-alkaline magmatism (Cawood et al., 2010). The Valhalla Orogeny consists of two stages, the earlier Renlandian Orogeny, preserved in the Hebridean foreland of Scotland, from ca. 980 to 910 Ma, is characterised by peak metamorphism of upper amphibolite facies between 950 and 930 Ma (Cutts et al., 2009). This was followed by the Knoydartian Orogeny, from 830 to 710 Ma, preserved in the Moine succession in Scotland (Cawood et al., 2010). The Timan margin of Baltica was a passive margin throughout the Tonian and Cryogenian, with thick (>9000 m), predominantly terrigenous, sedimentary successions that were only mildly deformed during the Timan Orogeny (e.g. Cawood et al., 2007, 2016; Olovyanishnikov et al., 2000; Siedlecka et al., 2004). The eastern margin of Greenland and adjacent terranes also record thick sedimentary sequences during this time, preserved in the Krummedal and Eleonore Bay Supergroups in Greenland (e.g. Cawood et al., 2007; Strachan et al., 1995), in the Pearya Terrane of Canada (e.g. Malone et al., 2014) and in the Murchisonfjorden Supergroup of Svalbard (Gee and Teben'kov, 1996; Halverson et al., 2004). Malone et al. (2014) extends the Valhalla orogeny of Cawood et al. (2010) outboard of these passive margin sequences, suggesting that subduction continued (?) ~2000–3000 km offshore.

Similar to the Baltica-Laurentia connection, the Amazonia-Laurentia connection is also well established for the Neoproterozoic. The late Mesoproterozoic Ji-Paraná shear zone suggests a sinistral strike-slip movement of Amazonia from southern Laurentia up towards Baltica and northern Laurentia (e.g. Tohver et al., 2005a,b), and results in the 1300–1000 Ma Sunsas orogenic belt of southwest Amazonia (Litherland and Power, 1989; Santos et al., 2000, 2008a) being paired with the Grenville Orogen on the eastern margin of Laurentia (e.g. Hoffman, 1991; Li et al., 2008; Pisarevsky and Natapov, 2003; Sadowski and Bettencourt, 1996), just south of Baltica (Fig. 2b). Evans (2013) provides an alternative model for the collision, with a clockwise rotation of Amazonia into Laurentia between 1200 and 1000 Ma using new palaeomagnetic data. Evidence for a Baltica-Amazonia Grenvillian-aged collision is lacking, suggesting a small intracratonic sea separated the two, although some models propose paired movement of Baltica and Amazonia, suggested by an extension of the Mesoproterozoic belts from Amazonia into Baltica (e.g. SAMBA model, Johansson, 2009). Other models suggest that smaller late Mesoproterozoic terranes occupy this space (and hence the deformation), such as Oaxaquia (e.g. Cardona et al., 2010; Keppie and Ortega-Gutiérrez, 2010). We follow the 'traditional' configuration, with Amazonia linked to Laurentia along its western margin, matching the Sunsas Belt to the Grenville Orogen, proximal to Baltica after Hoffman (1991) and Li et al. (2008), but leaving space in between Amazonia and Baltica for minor terranes.

The West African Craton (WAC) remains enigmatic throughout the Neoproterozoic, with little information constraining its position for this time. By convention (and for ease of reconstruction) the WAC is attached to Amazonia in a configuration similar to its Gondwanan configuration (e.g. Hoffman, 1991; Li et al., 2008; Meert and Torsvik, 2003). The poorly dated early Neoproterozoic passive-margin sequences on the east and north coast of the WAC (e.g. Álvaro et al., 2014; Bouougri and Saquaque, 2004; Thomas et al., 2002, 2004), the Ougarta Aulacogen (Ennih and Liégeois, 2001) on the north-eastern margin and the Gourma Aulacogen in Mali to the southeast of the craton (e.g.; Ennih and Liégeois, 2001; Gasquet et al., 2005; Moussine-Pouchkine and Bertrand-Sarfati, 1978) suggest rifting between the WAC and an unknown craton by 800–750 Ma at the latest. The northern passive margin is 4–5 km thick and consists predominantly of volcano-sedimentary rocks, that grade from shallow marine facies of carbonates and quartzite, cross-cut by tholeiitic dolerite dykes (Álvaro et al., 2014; Thomas et al., 2002, 2004) to overlying deeper-water turbidites (Ennih and Liégeois, 2001; Fekkak et al., 1999). Ophiolites are also preserved further outboard from the margin (Samson et al., 2004), and the protoliths of tonalitic gneisses and biotitic schists were dated to ca. 750 Ma (Thomas et al., 2002), suggesting that the northern-north eastern extent of the WAC had transitioned to an island arc setting, with the WAC as the downgoing plate. Based on the position of C-SF during the early Neoproterozoic as constrained by palaeomagnetic data (Section 6.5), we infer that this unknown craton is the western margin of C-SF, and that this rifting propelled C-SF northwards along a dextral transform fault against the Rodinian margin towards the Kalahari Craton and Australia-Antarctica. This rifting event also resulted in minor separation between WAC and Amazonia (e.g. Paixão et al., 2008).

The opening of the Iapetus Ocean through the breaking up of Laurentia-Baltica-Amazonia was one of the final events in Rodinia's dispersal. Early extension along the eastern margin of Laurentia is recorded in rhyolitic lava flows in the central Appalachians between ca. 760 and 700 Ma (Aleinikoff et al., 1995) and the subsequent deposition of the Pinelog Formation (Li and Tull, 1998). However, a hiatus in deposition during the late Cryogenian (Li and Tull, 1998) suggests two phases of rifting, and that this earlier rifting was either aborted (e.g. Novak and Rankin, 2004) or related to rifting on the western margin of Laurentia (e.g. Cawood et al., 2001). The later phase of extension consists of a multi-stage rifting event (Cawood et al., 2001; Pisarevsky et al., 2008b) above a mantle plume (Puffer, 2002). The ca. 615 Ma Long Range and Egersund dyke swarms (in Laurentia and Baltica respectively, Bingen et al., 1998) demonstrate the first stage and suggests opening of the northern Iapetus Ocean (Baltica-Laurentia) and the Tornquist Sea (Baltica-Amazonia) (Bingen et al., 1998; Pisarevsky et al., 2008b; Puffer, 2002), although the deposition of deep water carbonates and development of the passive margin in north-eastern Laurentia is thought to have occurred later, in the Early Cambrian, from both stratigraphic controls and faunal distributions (Allen et al., 2010; Cawood et al., 2001; Lavoie et al., 2003). The second stage, the opening of the southern Iapetus Ocean, between Laurentia and Amazonia occurred later and was slightly more prolonged, with rift-related magmatism evident in a series of three pulses; the tholeiitic, ca. 590 Ma Grenville swarm (Kamo et al., 1995; Seymour and Kumarapeli, 1995) and ca. 580 Ma Blair River metagabbro dykes (Miller and Barr, 2004); the 565–560 Ma Sept Isle intrusion and Catoctin volcanics (Aleinikoff et al., 1995; Higgins and van Breemen, 1998); and the ocean island basalt (OIB)-like 550 Ma Skinner Cove volcanics (McCausland et al., 1997; Puffer, 2002), and development of a passive margin by ca. 540 Ma (Cawood et al., 2001). To reconcile robust palaeomagnetic data that indicate a large ocean basin between Laurentia, Baltica and Gondwana by 550 Ma (e.g. Cawood et al., 2001; Lubnina et al., 2014; Pisarevsky et al., 2008b), with a rift-drift transition by 540 Ma along the Laurentian margin, Cawood et al. (2001) proposed a more complex breakup model, whereby a rift-drift transition occurred at 570 Ma, followed by another rifting event at ca. 540 Ma, where a smaller microcontinent was rifted

from the Appalachian margin. This second rifting event led to the development of the thick passive margin preserved today, and the microcontinent is typically thought to be the Argentine Precordillera (Allen et al., 2010; Cawood et al., 2001). However, since coeval dyke swarms or magmatism are yet discovered in Amazonia, a proper temporal constraint on the opening of the southern Iapetus remains enigmatic. Here our model depicts the earlier, 570 Ma, rift-drift transition, and is compatible with later rifting of the Argentine Cordillera.

3.3. 'West' Rodinia (Laurentia-Australia-Antarctica ± Tarim)

The pairing of the west coast of Laurentia with Australia-East Antarctica was one of the original motivators for suggesting Rodinia due to the thick sedimentary sequences (e.g. Rainbird et al., 1996; Young, 1981; Young et al., 1979), dyke swarms (Ernst et al., 2008) and rifted margins on their respective west and east margins. The original pairing of the two continents linked southwest Laurentia with East-Antarctica (SWEAT, Dalziel, 1991; Hoffman, 1991; Moores, 1991). Three other specific configurations were proposed based on palaeomagnetic and geological grounds. **AUS**tralia-**MEX**ico (AUSMEX), which pairs northern Queensland (Australia) with the southwest tip of Mexico, was proposed by Wingate et al. (2002) due to mismatches in the late Mesoproterozoic palaeomagnetic record of Laurentia-Australia. In this configuration, the conjugate margin to Laurentia is usually considered to be South China or Tarim (e.g. Pisarevsky et al., 2003). **AUS**tralia-**W**estern **U**nited **S**tates (AUSWUS), pushes Australia further south down the Laurentian coast so that Australia (and not Antarctica as in SWEAT) matches south west Laurentia. This configuration was originally proposed using Neoproterozoic-aged transform faults (as extensions of transform offsets of the spreading centre) to assist in matching stratigraphy between Australia and Laurentia (Brookfield, 1993). It was extended by Karlstrom et al. (1999, 2001) by suggesting that the Grenville Orogen, which is truncated in southern Laurentia, extended through into Australia and is expressed as the Albany-Fraser and Musgrave Orogens, on the basis of broadly similar tectonic histories and by Burrett and Berry (2000, 2002) who matched key geological provinces (e.g. Broken Hill-Olary block with Mojave terrane) that allowed a tighter fit between Australia and Laurentia. The Missing-Link model, originally proposed by Li et al. (1995), locates Antarctica in a similar position to SWEAT, although Australia is offset further away from northern Laurentia, with the South China craton sitting in between Laurentia and Australia (as the 'Missing-Link'). This model corrects some of the stratigraphic mismatches between Laurentia-Australia as well as connecting the temporally similar Sibao and Gardiner dyke swarms (Li et al., 1999, 2008). It also permits later breakup to occur as it more easily fits the ca. 750 Ma Mundine Dyke Swarm palaeomagnetic pole (Wingate and Giddings, 2000).

Rifting, and the transition from rift-to-drift, between Australia and Laurentia is poorly constrained to between 825 and 700 Ma due to difficulties in dating sedimentary sequences of the Adelaidian complex (e.g. Preiss, 2000). The 827 Ma Gardiner Dyke Swarm and flood basalts in the Adelaidian fold belt are typically seen as the first stage of rifting, although there are no matching swarms in Laurentia until 780 Ma (Park et al., 1995; Wingate et al., 1998) (the Missing Link model has coeval plumes in South China at ca. 827 Ma, Li et al., 1999). Comparatively, sedimentary sequences suggest later rifting, with deep-water sediments being more prevalent after 750 Ma. Palaeomagnetic data, which originally constrained breakup to ca. 750 Ma at the latest (Wingate and Giddings, 2000), now permit rifting until ca. 720–700 Ma with an intraplate rotation of the Northern Australian Craton (NAC) relative to the South Australian Craton (SAC) for some configurations (Li and Evans, 2011). Unfortunately, neither geological or palaeomagnetic data clearly discriminate a rifting time. We adopt here the earlier rifting at ca. 800 Ma with an AUSWUS configuration, to minimise the relative spreading velocity and angular rotation of Australia-Antarctica, but we note that later rifting events before ca. 770 Ma are kinematically

feasible, and that the model here is broadly compatible with an AUSMEX configuration.

Tarim is typically attached to northern or north-western Australia during the Neoproterozoic (e.g. Huang et al., 2005; Li et al., 1996, 2008; Wen et al., 2013), although a tectonic model that fully integrates geological and palaeomagnetic data and its relationship with other blocks has only been recently proposed (Ge et al., 2014). U-Pb dating of zircons from granitic gneisses in the North Qaidam belt of (southern) Tarim and long lived subduction in the Quruqtag region along its northern margin during the Neoproterozoic are generally interpreted as evidence of it being included as part of Rodinia in a peripheral position, with its northern margin facing an open ocean (Ge et al., 2014, 2016; Liu et al., 2015; Shu et al., 2011; Song et al., 2012; Yu et al., 2013). A transition between ca. 830 and 780 Ma to retreating accretion on the northern margin, opening of the South Tianshan Ocean and deposition of the volcanic rock bearing, clastic Beiyixi Formation (Ge et al., 2014; Xu et al., 2005), 820–795 Ma mafic-ultramafic intrusives (Zhang et al., 2007) and a series of ca. 775 to 750 Ma mafic dyke swarms (Zhang et al., 2009) are suggested to be related to the break-up of Rodinia and motion of Australia-Antarctica and Tarim (on a single plate) away from Laurentia. Younger, 650–630 Ma dyke swarms (Zhu et al., 2008), ca. 615 Ma basalts, the geochemistry of which suggest an intracratonic rift environment (Xu et al., 2013), and sediment deposition forming the Sugetbrak Formation are interpreted here as indicators of the rifting away of Tarim from northern Australia during the intraplate rotation of the North Australia Craton into the Southern Australian Craton (Li and Evans, 2011). While we find the geological evidence convincing for having Tarim fixed off the northern margin of Australia in Rodinia, this position does not fit three reasonably reliable Tonian-Cryogenian aged palaeomagnetic poles (815–795 Ma Aksu dykes, Chen et al., 2004; 760–720 Ma Qiaoenbrak Formation, Wen et al., 2013, and; 770–717 Baiyisi Volcanics, Huang et al., 2005), although it does fit a younger three (also reasonably reliable) palaeomagnetic poles (635–550 Ma Sugetbrak Formation, Zhan et al., 2007; ca. 635 Ma Tereeken Cap Carbonate, Zhao et al., 2014; 621–609 Ma Zhamoketi Andesite, Zhao et al., 2014). To fit all poles, Tarim would have to be located in equatorial-low latitudes between ca. 800 and 700 Ma, and then transition and rotate ~180° to be in mid-high latitudes during the Cambrian. Palaeontological data from both the Cambrian and Ordovician suggest it was in close proximity to Australia, South China and North China at that time (e.g. Chen and Rong, 1992; Metcalfe, 2006, 2013; Rong et al., 1995). We find this motion difficult to account for given the global context of other portions of cratonic crust and inferred spreading systems; consequently, we omit Tarim from this model prior to 700 Ma, and expect that future work on palaeomagnetic data can help resolve this problem, although we do note recent proposals where Tarim acts as an extension of South China in a 'Missing-Link' position (Wen et al., 2017).

Reconstructions of Phanerozoic Gondwana and the cyclical opening and closing of the Tethyian oceans place all southeast Asian terranes and cratons outboard and proximal to both Australia and India (e.g. Burrett et al., 2014; Metcalfe, 2006, 2011, 2013). The larger cratons (South China, North China, Tarim) occupy the most distal positions from Gondwana, with the smaller terranes (e.g. Indochina, Lhasa, Qiantang, Sibumasu) located between them and the north Gondwanan margin, suggesting that their formation must predate the Palaeozoic Gondwanan configuration. Detrital zircon and palaeontology are used to infer affinity of these terranes with either Australia or India (or both). Typically, from west (India-affinity) to east (Australia-affinity), Indochina and Qiantang are placed outboard of northwest India, due to a peak of detrital zircon ages at ca. 950 Ma, suggesting input from the subduction outboard of NW or N India (e.g. Usuki et al., 2013). Indochina also contains a peak of zircons between ca. 700 and 500 Ma, likely from the East African Orogen, so it is inferred to be placed further west than Qiantang (Burrett et al., 2014). Comparably, the Lhasa terrane contains slightly older detrital zircon peaks of ca. 1170 Ma, which are

typically associated with the Albany-Fraser Orogen of Australia (e.g. Zhu et al., 2011). The Sibumasu Terrane is inferred to share affinity with Australia due to similar faunal assemblages during the Palaeozoic (e.g. Fortey and Cocks, 1998; Metcalfe, 2011). Sparsely exposed basement in the North Lhasa terrane of southern Tibet consists of Neoproterozoic aged granulites (Zhang et al., 2012b, 2014). U-Pb dating of zircon cores and in-situ zircons from the granulites gives a protolith age of ca. 900 Ma, with metamorphism occurring at ca. 650 Ma (respectively), inferred to have occurred as a response to Gondwana amalgamation. Whole rock geochemistry suggests that the terrane protolith was oceanic crust (Zhang et al., 2012a,b). On the northern border of the Lhasa Terrane, the Amdo basement preserves an orthogneiss with a protolith age of 900–820 Ma, with a similar metamorphic overprint age as in the North Lhasa terrane (Guynn et al., 2006, 2012). Comparatively, the Sibumasu Terrane, placed outboard of Lhasa in Gondwana reconstructions, does not preserve any Neoproterozoic signatures. Younger protolith ages as young as ca. 740 Ma derived from U-Pb dating of inherited zircon cores have also been reported from the Nyainqnetanglha Group in southern Lhasa (Dong et al., 2011). Assuming a close link between western Australia and Lhasa they could be related in some capacity to 750 Ma granitoids of the Leeuwin Complex (Collins, 2003). We (tentatively) propose that subduction outboard of Australia was occurring for most of the Neoproterozoic, during the Tonian as an extension of a circum-Rodinia subduction zone, and during the Cryogenian as a response to Australia-Antarctica rifting from Laurentia, and is preserved in Lhasa and other southeast Asian terranes.

3.4. 'South' Rodinia (Laurentia-Kalahari-Rio de la Plata)

Southern Rodinia is probably the least constrained of all the Rodinian margins. We have followed the convention of previous models in attaching Kalahari to southern Laurentia, and fitting the other sizable South American craton, Rio de la Plata (RDLP), into the gap between the southeast Laurentian margin and Kalahari (e.g. Hoffman, 1991; Jacobs et al., 2008; Li et al., 2008). The Kalahari craton itself consists of an Archaean-Palaeoproterozoic nucleus that underwent substantial growth during the Mesoproterozoic (e.g. Hanson, 2003; Hanson et al., 2006; Jacobs et al., 2008). The Namaqua-Natal-Maud belt on its southern and southeastern margins is associated with the Rodinia amalgamation, and, depending on its orientation, was suggested as an extension of the Grenville Orogen, with the collision of Kalahari with the Coats Land Block (Loewy et al., 2011). Rifting during the breakup of Rodinia is preserved on the northwest-west-southwest-south margins of Kalahari (Jacobs et al., 2008) while any rifting on the eastern margin has been overprinted due to the high grade metamorphic events occurring with the amalgamation of eastern Gondwana. The Kalahari-Laurentia configuration is updated to that of Loewy et al. (2011) where the south and south-west margins have collided with RDLP and Laurentia, allowing the Maud-Natal Belt (Fig. 2b) to act an extension of the Grenville Orogen. This has two additional benefits; firstly, it creates a larger space between Australia-Antarctica and Kalahari, allowing more space for an AUSWUS configuration, or even for an AUSMEX-like configuration if desired. Secondly, it removes the need for the development of a thick passive margin on the eastern margin of Kalahari, as its relationship with Australia post Rodinia breakup is along a transform boundary.

The RDLP craton is more difficult to constrain than the Kalahari craton due to it being almost completely overprinted and reworked during Gondwana amalgamation. There are only minor suggestions of a Mesoproterozoic aged tectono-thermal event based on K-Ar muscovite ages (Basei et al., 2000) and detrital zircon (Gaucher et al., 2008). Previous studies have proposed a central positioning of the RDLP craton to Rodinia (e.g. Fuck et al., 2008; Gaucher et al., 2011), with it being positioned at the locus of Amazonia, Kalahari and Laurentia. This is based on the abundance of late Mesoproterozoic detrital zircons present in Ediacaran-aged sandstones, suggesting that the RDLP was ringed by Mesoproterozoic orogenic belts (Gaucher et al., 2011), although recent

isotope geochemical studies have suggested that the eastern margin faced an open ocean from 800 Ma (e.g. Koester et al., 2016; Lenz et al., 2013).

We adopt a central position of RDLP on the southeastern margin of Laurentia between Kalahari and Amazonia as a small cratonic fragment recording part of the Grenvillian Orogeny (Gaucher et al., 2011). This puts RDLP into a strong position for its preferred model of amalgamation into Gondwana, through a series of dextral transform faults and oblique subduction (Rapela et al., 2007). There are little data to provide an accurate model of rifting, as such we suggest rifting from Laurentia at 590 Ma on the basis that RDLP forms the southern extent of the opening of the Iapetus Ocean, although we note that earlier rifting is permissible (provided it occurs after Kalahari has rifted away from Rodinia).

3.5. 'Extra South' Rodinia (Congo, Azania, Arabian Nubian Shield ± Sahara Metacraton)

The Congo-São Francisco craton (C-SF), a Palaeoproterozoic amalgam of Archaean cratons, has a disputed history during the Neoproterozoic due to the absence of large scale, continental-continental collision and related high pressure metamorphism as is evident in other Rodinian cratons (de Waele et al., 2008). Consequently, there are a number of models wherein C-SF is not part of Rodinia (e.g. Collins and Pisarevsky, 2005; Meert, 2003; Pisarevsky et al., 2003). Comparably, the C-SF forms the nucleus of Gondwana, because the craton is surrounded by a series of Ediacaran-Cambrian orogenies (Section 5), including the Brasiliano Orogen that traces the suture between Amazonia and C-SF, and the East African Orogen, consisting of the Kuungan Orogen (sometimes referred to as Pinjarra, or Pinjarra-Denman-Prydz Orogen) that stitches Antarctica together, the Malagasy Orogen, that connects India with C-SF through Madagascar and Azania, and the Damara Orogen, between the Congo and Kalahari cratons (Collins and Pisarevsky, 2005; Fitzsimons, 2003; Meert, 2003).

The present-day southern margin of the African Congo Craton preserves evidence for quite diverse Tonian tectonic environments along its length. The basement of the central Damara Belt of Namibia preserves evidence for Stenian orogenesis that is correlated with similar-aged volcanic-arc plutonism and volcanism in the Rehoboth inlier (Becker and Schalk, 2008). This reflects collision between the Kalahari craton and the C-SF at the end of the Mesoproterozoic (Becker et al., 2005). Evidence for early and mid-Tonian tectonism exists as rift-basin formation along the southern C-SF margin before ca. 760 Ma (McGee et al., 2012a; Miller, 2013). Extensive rifting along this margin, however, does not occur until ca. 750 Ma as shown by voluminous volcanic rocks and intrusions occur (Hoffman et al., 1996). Further east along this margin, in the Lufilian Arc of Zambia and the Democratic Republic of Congo, deposition of the syn-rift lower Roan Group, the basal group of the Katanga Supergroup, is constrained to after ca. 877 Ma, the age of the nonconformably underlying Nchanga Granite (Armstrong et al., 2005; Miller, 2013). Carbon isotope stratigraphy coupled with a sequence stratigraphy suggests that Tonian rifting ended, but then rejuvenated prior to the deposition of the basal Cryogenian Grand Conglomérat Formation of the Nguba Group, which overlies the Roan Group (Bull et al., 2011). In contrast to Namibia, considerable earlier Tonian magmatism occurs within the basement of the Katanga Supergroup. As well as the aforementioned Nchanga Granite, magmatism in the Lusaka area is dated at 820 ± 15 Ma (Johnson et al., 2007), which terminates rift basin formation in the Lusaka-Zambezi region that began with ca. 880 Ma felsic extrusive rocks (Johnson et al., 2007). We interpret the Tonian extension that these igneous rocks represent, reflects the increasing proximity of the Congo Craton to an active plate margin.

The Southern Irumide Belt lies to the south-east of the Lufilian Arc and the Zambezi supracrustal rocks. Here, latest Mesoproterozoic gneisses are interpreted to represent a Stenian volcanic arc terrane that accreted to the C-SF during the Irumide orogeny (Johnson et al.,

2005, 2006; Karmakar and Schenk, 2016). Further east, in north-east Mozambique, high-grade metamorphism is early Tonian (ca. 950 Ma; Bingen et al., 2009), suggesting progressive accretion on this active margin along the south-east apex of the C-SF craton (Johnson et al., 2005; de Waele et al., 2008). Younger Tonian volcanic arc systems are preserved within the East African Orogen, east of the C-SF in Gondwana, and outboard of the Mozambique Tonian accretionary system. The Dabolava Arc of west Madagascar formed over a similar period to the Southern Irumide and Mozambique arc terranes (Tucker et al., 2007, 2011, 2014). It, however, formed over a west dipping subduction zone before colliding with central Madagascar (Azania) at ca. 950 Ma (D.B. Archibald, unpublished data). These arc-continent collisions preceded the intrusion of ca. 930–900 Ma igneous rocks in the Malagasy Vohibory volcanic arc terrane (Collins et al., 2012; Jöns and Schenk, 2008). This event in Madagascar may correlate with the Galana Arc of south-east Kenya (Hauzenberger et al., 2007) and the so-called TOAST terrane of East Antarctica (Jacobs et al., 2015). Finally, the major ca. 850–750 Ma continental margin arc that resulted in the emplacement of the Imorona-Itsindro Suite (Archibald et al., 2016; Archibald et al., in press; Boger et al., 2014; Handke et al., 1999) developed within Azania. Geochemical data are equivocal for determining subduction polarity (Archibald et al., in press), therefore subduction polarity was either from eastward-directed subduction of the ocean separating Azania from the C-SF continent, or, (as is portrayed here), from continued west-dipping subduction, but with a trench east of Azania subducting the Mozambique Ocean between central Madagascar and India.

The northern margin of C-SF is marked by the poorly known Oubanguides Belt (Fig. 2b) in Africa (Bouyo et al., 2013; de Wit et al., 2008; Poidevin, 1985; Toteu et al., 1994, 2001, 2006; Van Schmus et al., 2008) and the Sergipano Belt in Brazil. The Oubanguides consists of pre-Neoproterozoic and juvenile 1100 to 625 Ma thrust sheets emplaced over the Lindian Supergroup, a Neoproterozoic passive margin succession on the north margin of the C-SF (de Wit and Linol, 2015; Toteu et al., 2006). Deformation and metamorphism of these belts occurred in the Cryogenian to Ediacaran and are discussed below.

The Sahara Metacraton (SM) is typically placed to the north of the C-SF. However, whether it was fixed to the same plate as the C-SF or had some relative movement (and if so, how much?) is unknown, principally because palaeomagnetic data are unavailable. The term 'metacraton' refers to a quasi-stabilised section of crust that was remobilised to some degree and exhibits deformation throughout its entire area, not just its margins, while still maintaining geological coherency (i.e. never fully rifted apart) (Abdelsalam et al., 2002; Liégeois et al., 2013). The SM is referred to as a 'metacraton' by Abdelsalam et al. (2002) because during the Neoproterozoic it neither appears to have acted rigidly and congruently as cratons do, nor does it appear to be dominated by juvenile accreted terranes and be fully tectonically mobile as is the Arabian-Nubian Shield (ANS), for example. The SM is dominated by medium to high grade gneisses, migmatites and the intrusion of post 750 Ma granitoids (Abdelsalam et al., 2002), and is tectonically and geologically distinct from both the other African cratons that are surrounded by thick continental orogenies, and the lower grade, greenschist facies, volcano-sedimentary metamorphic rocks of the ANS (e.g. Johnson et al., 2011). The southern parts of the SM were recently shown to be made of composed late Mesoproterozoic crust (de Wit and Linol, 2015). The western SM boundary has been taken to be the Raghane shear zone, as it juxtaposes the Neoproterozoic aged Assodé-Issalane terrane, which exhibits amphibolite facies metamorphism during Gondwana amalgamation, from the older Aouzegueur terrane that exhibits only greenschist facies metamorphism (Henry et al., 2009; Liégeois et al., 1994). The primary movement of this shear zone is thought to have occurred no later than 590–580 Ma (e.g. Abdallah et al., 2007; Henry et al., 2009) due to the emplacement of undeformed granitoids that exhibit distinct magnetic foliations aligned with the Raghane shear zone (Henry et al., 2009). The eastern margin is typically defined by the sinistral, Keraf Suture, preserved in northern Sudan, which juxtaposed the

younger, juvenile arc terranes of the ANS against Mesoproterozoic-aged rocks of the eastern SM (e.g. Abdelsalam et al., 1998) between 640 and 600 Ma (Johnson et al., 2011; Stern et al., 1989). ^{40}Ar-^{39}Ar dating on biotite and hornblende from a deformed granite suggest that shear zone deformation ended by ca. 580 Ma (Abdelsalam et al., 1998). The Keraf Suture was inferred to be a response to a sinistral, transpressive tectonic regime related to the closing of the Mozambique Ocean and amalgamation of Gondwana (Abdelsalam et al., 1998) (Section 5.1).

Pulses of 920–900 Ma magmatism and amphibolite facies metamorphism are recorded in the Bayuda Block in North Sudan, south of the Keraf Suture (Evuk et al., 2014; Karmakar and Schenk, 2015; Küster et al., 2008), with slightly younger 850–760 Ma oceanic arc magmatism recorded in the Western Ethiopian Shield (WES) (Ayalew et al., 1990; Blades et al., 2015; Johnson et al., 2011), and outboard the Bayuda Block at ca. 805 Ma, where geochemical trends and volcaniclastic sedimentary successions suggest the existence of a back-arc basin (Küster and Liégeois, 2001). Finally, collisions of arc terranes with the Bayuda Block at ca. 700 Ma are used to support the existence of an ocean basin between the ANS and SM during the Tonian (Evuk et al., 2014; Küster and Liégeois, 2001), although the main phase of compression and deformation occurred later during Gondwana amalgamation.

The ANS is a series of juvenile Neoproterozoic island arc terranes that accreted to the Sahara Metacraton during the East African Orogeny. The tectonic history of the ANS is complicated, perhaps similar to the island arcs of present day southeast Asia, where, if they were to be accreted to Asia, would preserve a complex melange of terranes, accreted arcs, extension and back-arc basins, subduction polarity reversals and changes in major stress regimes. Recent syntheses (e.g. Fritz et al., 2013; Johnson et al., 2011) have summarised the geological and tectonic history of the area, but, without palaeomagnetic data, it is difficult to constrain its position, relative to both the SM and C-SF. Early Neoproterozoic subduction follows on from late Mesoproterozoic subduction in west Sudan/Chad (de Wit and Linol, 2015) and the Sinai (Be'eri-Shlevin et al., 2012; Eyal et al., 2014). These are followed by a distinct period of quiescence during the mid Tonian (ca. 930–880 Ma) followed by voluminous volcanic arc development between ca. 870 and 830 Ma (Robinson et al., 2014, 2015a) and accretion of these terranes to the SM during the late Cryogenian to Ediacaran (ca. 650–580 Ma, Johnson et al., 2011, Section 5.1). The Afif terrane contains a small Palaeoproterozoic sub-terrane (the Khida terrane - Stacey and Hedge, 1984; Stoeser et al., 2001; Whitehouse et al., 2001), and potentially Archaean-aged basement rocks based on Nd model ages (Abas terrane - Whitehouse et al., 1998, 2001; Windley et al., 1996), suggesting that they could represent a northern extension of Azania, acting as a semi-continuous palaeogeographic, but not necessarily tectonically congruent, archipelago.

Fritz et al. (2013) identified four distinct, but overlapping stages of accretion. Broadly, the first two stages are pertinent to Rodinia, while the latter two relate to Gondwana amalgamation and are a response to the closure of the Mozambique Ocean and East African Orogeny (Section 5.1). In the first stage, arc age decreases from the Tokar/Barka Terrane in the south (870–840 Ma), towards the Hijaz Terrane in the north (780–710 Ma), with suturing between them occurring from 830 to 710 Ma (Johnson et al., 2011; Johnson and Woldehaimanot, 2003). The second stage involved the formation of the 810–710 Ma Midyan-Eastern Desert terrane further north, against the interior of the older Sa'al Terrane, and its suturing with the earlier, southern terranes between ca. 760 and 730 Ma along the E-W Yanbu-Onib-Sol Hamed-Gerf-Allaqi-Heiani suture, forming the western arc or oceanic terranes of the ANS (Stoeser and Frost, 2006). The older, further east, Afif-Jiddah-Abas terranes amalgamated with the oceanic terranes close to the Cryogenian-Ediacaran boundary (ca. 650 Ma). Subduction is inferred to be east dipping under the Afif-Jiddah-Abas terranes, which conflicts with the slightly earlier, supposed west dipping subduction in the more westerly WES and Bayuda Block, perhaps suggesting a subduction polarity reversal during the late Tonian, or a spreading system with

subduction occurring on each side. The final stages relate specifically to the suturing of the youngest arcs (post ca. 680 Ma) on the eastern margin of the Afif Terrane and the closure of the Mozambique Ocean, and young to the east, away from the ANS (Cox et al., 2012).

The western margin of the Saharan Metacraton consists of a series of (primarily) dextral strike-slip faults and a regime of transpressive tectonics (e.g. Fezaa et al., 2010). The evolution of Hoggar and the west Saharan Metacraton represents a series of accreted arcs, with a transition to a dextral-transpressive tectonic environment during the late Neoproterozoic as the WAC collided with it (Fezaa et al., 2010; Liégeois et al., 2003). The suture of the Hoggar Shield and Saharan Metacraton is the Raghane shear zone (Henry et al., 2009; Liégeois et al., 1994), and was tectonically active from ca. 730 to 580 Ma, at the conclusion of which most of western Gondwana was amalgamated. Early suturing was of the easternmost terrane of the Hoggar shield (the Aïr Massif) was with the Sahara Metacraton between 700 and 670 Ma (Liégeois et al., 1994). Tectonic models for the evolution of the central and western parts of the Hoggar Shield are more convoluted. Proposed tectonic models suggest some separation between the western, central and eastern (which are attached to the Sahara Metacraton) terranes allowing for a complex history of subduction to occur amongst 23 identified terranes (Black et al., 1994; Caby, 2003). The central terranes, principally the LATEA (**L**aouni, **A**zrou-n-Fad, **T**efedest, **E**géré-**A**leksod) terranes (Liégeois et al., 2003), acted as the nucleus for the majority of the Hoggar Shield, as they had a series of smaller terranes accreted onto them between 900 and 580 Ma (Caby and Monié, 2003; Liégeois et al., 2003). Initially, subduction was away from the central terranes, with the Iskel Island Arc accreting onto the western margin of LATEA by ca. 850 Ma (Liégeois et al., 2003). Further subduction to the west resulted in a series of small terranes (such as the ca. 690–650 Ma Pharusian terrane, Caby, 2003) being accreted onto LATEA by 620 Ma (Caby, 2003). Subduction was east dipping under Hoggar for this collision (Berger et al., 2014).

Further south from the Hoggar Shield are the Benin-Nigeria and Borborema provinces of present day Africa and South America respectively. Their congruency during the Neoproterozoic is interpreted from their broadly similar lithologies and tectonic history. These consist of an Archaean nucleus with rift-related magmatism occurring during the Palaeoproterozoic (ca. 1.85–1.73 Ga), similar detrital zircon spectra and a range of metasedimentary and metavolcanic rocks with Sm-Nd model ages between 1.6 and 1.0 Ga (Arthaud et al., 2008; Brito Neves et al., 2000; Kalsbeek et al., 2012). Both provinces sit on the eastern margin of the cryptic Transbrasiliano Lineament (that divides C-SF and the SM from Amazonia and the WAC), suggesting affinity with C-SF and/or the SM prior to Gondwana amalgamation. The Borborema Province, in particular, was strongly deformed and reworked during Gondwana amalgamation, as it was located at the locus of convergence between the Amazonia, West Africa, Congo, São Francisco and Sahara cratons (e.g. Brito Neves et al., 2000; Ganade de Araujo et al., 2014a,b, Section 5.8). An earlier magmatic event, the Cariris Velhos orogeny, is preserved towards the southern margin in the Transversal Zone in the Borborema (e.g. Brito Neves et al., 1995; Santos et al., 2008b). Here, 1000 to 920 Ma gneisses, migmatites and volcanoclastic sequences suggest a continental-arc environment, perhaps with the development of a back-arc basin, but without considerable crustal thickening occurring at its conclusion (Caxito et al., 2014; Santos et al., 2010; Van Schmus et al., 2008). The Tamboril-Santa Quitéria Complex of the Ceará Central Domain in western Borborema records long-lived subduction from the mid-Tonian until Gondwana accretion. U-Pb dating of zircon constrain the timing of earliest subduction to be from ca. 900 Ma, although the development of a juvenile arcs is suggested to be from 880 to 800 Ma due to the emplacement of tonalite and granodiorite with positive $\varepsilon_{Hf}(t)$ and $\varepsilon_{Nd}(t)$ and a low ^{87}Sr/^{86}Sr ratio (Ganade de Araujo et al., 2012, 2014a). Juvenile arc signatures persisted until the late Cryogenian-early Ediacaran (ca. 660–650 Ma), when subduction matured due to the subduction of the approaching WAC (Section 5.9) (Ganade de Araujo et al., 2014b).

Owing to the uncertainty of Borborema's position in Rodinia (e.g. Fuck et al., 2008) and the slightly younger ages of the Cariris Velhos orogeny, it is difficult to determine how Borborema relates to wider Rodinian tectonic geology. We leave Borborema fixed to the SM, and infer this subduction to be part of the closure of an ocean basin between the wider SM Plate and the C-SF Plate, although the (present-day) western margin of Borborema faced an open ocean.

We include C-SF (and by extension, SM) as a distal part of Rodinia, although with some relative movement between it and the Rodinian core of Laurentia-Baltica-Amazonia-Kalahari-Australia. The subduction along the eastern margin (i.e. Azania, ANS etc.) acts as a leading edge of the continent as it moves along a dextral fault, relative to Rodinia, from outboard of WAC to outboard of Kalahari.

4. Tonian evolution of India and South China

Both India and South China are enigmatic continents throughout the Neoproterozoic, as data are available from both cratons without providing a strong discriminatory argument for both their position and motion. Inevitably, this has led to the proposition of a number of positions of both continents. For India, suggestions have included omitting it from Rodinia altogether (e.g. Pisarevsky et al., 2003; Collins and Pisarevsky, 2005); if it was in Rodinia, it has been placed outboard of East Antarctica (e.g. Li et al., 2008), or outboard of Australia (e.g. Meert and Torsvik, 2003). South China has been put as the heart of Rodinia (Li et al., 1995, 2008), or attached to Western Australia (e.g. Cawood et al., 2013; Niu et al., 2016). Generally, the only well established (and agreed) upon positions and motions of India and South China are from the late Neoproterozoic, where their palaeomagnetic (e.g. Zhang et al., 2013) and geological (e.g. Collins et al., 2014) data suggest a southward motion due to subduction of the Mozambique Ocean under the Gondwana nucleus, with South China located north of India such that it can rift off uninhibited during the Palaeozoic (see Section 5.1).

The core of India consists of a series of Archaean-aged cratons overlain by a series of Proterozoic basins, separated by Proterozoic-aged orogenic belts. These cratons make up two main groups that formed separate Mesoproterozoic continents. A northern Bhundelkund craton was separated from a southern cratonic group, consisting of the Dharwar, Bastar and Singhbhum cratons, by the Central Indian Tectonic Zone (see Meert et al., 2010 for a recent synthesis). The timing of amalgamation between these continents has been controversial (Acharyya, 2003; Mishra et al., 2000; Rekha et al., 2011; Roy and Prasad, 2003; Roy et al., 2006; Stein et al., 2006), but recent work on the age of collisional metamorphism in the Sausar Orogeny that sutured the continents, demonstrated that peak orogenesis occurred at ca. 1.06 Ga (Bhowmik et al., 2012). Sedimentological studies of late Mesoproterozoic rocks in the Chhattisgarh Basin where an oceanic connection through the CITZ is inferred from the basin architecture and the documentation of tidal bedforms support this hypothesis (Patranabis-Deb, 2004; Saha et al., 2016). Prior to this latest Mesoproterozoic orogenesis, India was at least two separate continents, with the beginning of the Neoproterozoic marking the amalgamation of the kernel of Peninsular India.

The northwest boundary between this latest Mesoproterozoic core of India and the Stenian-Neoproterozoic crust that extends west from the Delhi-Aravalli Orogen, is a major lithospheric boundary visible on deep seismic reflection surveys where it is interpreted as reflecting an oceanic suture pre-dated by east-dipping subduction beneath the Bhundelkund Craton (Rao and Krishna, 2013) (Fig. 2b). We suggest that this boundary is the ultimate 'east' margin of the northern East African Orogen (see below).

Stenian-Tonian times saw the progressive accretion of volcanic arc rocks to this NW margin of Neoproterozoic India, this accretion extends through the basement of Pakistan; into eastern Arabia, where Tonian-aged arc rocks occur as inliers in Oman (Alessio et al., in press; Allen,

2007; Bowring et al., 2007; Whitehouse et al. 2016). Afghanistan lies between the Indian Subcontinent and Oman in Gondwana reconstructions. Archaean rocks were reported from the Kabul Block (Collett et al., 2015; Faryad et al., 2016) that show ca. 2.8–2.5 Ga protoliths overprinted by a ca. 1.85–1.80 Ga metamorphic event, with a further, lower temperature, tectonothermal event in the Tonian. We suggest that this terrane forms a microcontinent accreted to the active NW Indian margin in the Tonian. Faryad et al. (2016) noted the similarity in tectonothermal events recorded in the Kabul Block to those in South China, but dismissed this possible link due to palaeogeographic considerations. However, we suggest that the accretionary history of western South China (i.e. the Yangtze Block), as a series of terranes assembled to an older eastern continental terrane (Cawood et al., 2013), is remarkably similar to that of NW India as detailed above. Therefore, we support the observation of Faryad et al. (2016) and suggest that the Kabul Block is a similar micro-continental terrane to that proposed for the pre-Neoproterozoic of the Yangtze Block of South China.

The Seychelles microcontinent shares similar geology to west Rajasthan, with granitoids intruded between ca. 810 and 750 Ma (Stephens et al., 1997; Torsvik et al., 2001b; Tucker et al., 2001). Similar-aged (ca. 750–730 Ma) juvenile arc granitoids are also found in the northern Bemarivo Belt in NE Madagascar (Collins, 2006; Collins and Windley, 2002; Thomas et al., 2009; Tucker et al., 1999; Tucker et al., 2014). We propose that these presently disparate regions, which were Gondwana neighbours, also form part of the Tonian-aged accretionary complex northwest of India and west of South China.

The Eastern Ghats Orogen (on the eastern margin of India), and the Krishna Orogen to its south, were active subduction zones for most of the Mesoproterozoic and early Neoproterozoic (Dobmeier and Raith, 2003; Henderson et al., 2014) (Fig. 2b). The orogens are tectonically complex, and were divided into discrete terranes based on lithological differences (Ramakrishnan et al., 1998), isotope provinces (Rickers et al., 2001) or crustal provinces based on distinct geological histories between different areas (Dobmeier and Raith, 2003). Recent geochronological and petrological studies confirmed the distinction between the ca. 1.6 Ga Krishna Orogeny in the southern Eastern Ghats region (Henderson et al., 2014) and the ca. 1.0–0.9 Ga Eastern Ghats Orogeny sensu stricto in the north (Korhonen et al., 2013). The Eastern Ghats Orogen is linked with the similar-aged Rayner province in Antarctica, due to a similar tectonic and metamorphic history, as well as similar Nd model ages for gneisses in both areas, suggesting that the combined Rayner/Eastern Ghats complex grew as a consequence of the long-lived subduction on the eastern margin of India (Dobmeier and Raith, 2003; Mikhalsky et al., 2013; Rickers et al., 2001). The outboard margin of the Rayner/Eastern Ghats complex is marked by the Archaean Ruker terrane, the southernmost rocks exposed in East Antarctica, at ca. 960 Ma, followed by full closure by ca. 900 Ma (Boger et al., 2008; Corvino et al., 2008; Dasgupta et al., 2013; Mezger and Cosca, 1999). This prolonged magmatism/metamorphism during the early Tonian served as evidence of India's amalgamation with Rodinia (e.g. Dasgupta et al., 2013; Li et al., 2008), however, here we follow the suggestion that India was a separate continent and that this subduction represents the final accretion of Indian-Antarctica with India (e.g. Liu et al., 2013). Later Tonian and Cryogenian tectonothermal events rework the Eastern Ghats orogen between 900 and 650 Ma (Dobmeier and Simmat, 2002; Gupta, 2012; Nanda et al., 2008), which, although 'intra-continental', suggests that a plate margin outboard of the exposed Rayner/Eastern Ghats Complex still periodically transmitted compressive stress inland.

We adopt the position of Cawood et al. (2013) for a connection between South China and India in the late Mesoproterozoic, and preserve this for the entire Neoproterozoic (i.e. no relative motion between South China and India). South China is also reduced to its Cathaysian core at the beginning of the Neoproterozoic, with the Yangtze 'craton' here interpreted as a Tonian-aged accretionary complex in a manner following Cawood et al. (2013). The Jiangnan Orogen in central South

China preserves evidence for a Tonian (ca. 870–860 Ma) accretionary complex that post-dates earlier subduction/accretion complexes (Wang et al., 2015) and pre-dates final continent formation in this region (Yao et al., 2016). Subduction polarity was suggested to dip to the west (present-day coordinates), suggesting that the western Archaean-Palaeoproterozoic core of the Yangtze Block may have formed a microcontinental kernel for Tonian arc-accretion that collided with the Cathaysia block at ca. 860 Ma (Yao et al., 2016). As discussed above, we correlate this Yangtze Block core with the Kabul Block and suggest that the accretionary record of South China is coeval with the accretionary history of NW India (Bhowmik et al., 2010, 2012; Cawood et al., 2013; Meert et al., 2013; Roy and Prasad, 2003).

5. Rodinia to Gondwana: geology of the Gondwana-forming orogens

5.1. East African Orogen

Rocks deformed and metamorphosed in the East African Orogen (Stern, 1994) extend, in a reconstructed Gondwana, from the Eastern Mediterranean in the north (e.g. Candan et al., 2016), through Arabia (including NW India/Pakistan/Afghanistan), eastern Africa, Madagascar, southern India, Sri Lanka to East Antarctica where outcrop disappears beneath the ice south of Lützow-Holm Bay and Sør Rondane (Fig. 2b). The orogen is likely to follow the subglacial East Antarctica Mountain Range (An et al., 2015) to the Gambutschev suture (Ferraccioli et al., 2011), where, it meets the Kuunga Orogen (Meert et al., 1995; also known as the Pinjarra-Prydz-Denman Orogen; Fitzsimons, 2003). Together, these orogens delineate the west, south and east margins of Neoproterozoic India.

The northern East African Orogen is commonly called the Arabian-Nubian Shield (Johnson et al., 2011) and is characterised by voluminous juvenile Neoproterozoic crust that formed as a series of volcanic arcs, dominantly younging away from an older continental terrane (Robinson et al., 2014, 2015a,b). Less extensive continental terranes exist in the region, particularly in the Sinai (Be'eri-Shlevin et al., 2012; Eyal et al., 2014), in the Khida and Afif Terranes of Saudi Arabia (Stoeser et al., 2001; Whitehouse et al., 2001) and in Yemen (Whitehouse et al., 1998, 2001; Windley et al., 1996) with corollaries along the southern Gulf of Aden escarpment (Collins and Windley, 2002; Sassi et al., 1993; Whitehouse et al., 2001). The eastern margin of the East African Orogen in Arabia is often left at the margin of the exposed Neoproterozoic in Saudi Arabia, but similar magnetic anomalies to the eastern-most exposed Saudi terrane (the Ar-Rayn terrane, Cox et al., 2012; Doebrich et al., 2007) occur beneath the Ediacaran Rub Al-Khali Basin of Saudi Arabia (Johnson and Stewart, 1995) and where Precambrian basement is exposed in the east of the Arabian Peninsula—in Oman—it is again Neoproterozoic juvenile crust that formed in volcanic arc tectonic environments (Alessio et al., in press; Bowring et al., 2007; Whitehouse et al., 2016). This leads us to extend the East African Orogen to regions of Gondwana east of the Arabian Peninsula—regions that now form the basement of southern Afghanistan, Pakistan and NW India (see also Cozzi et al., 2012, and above).

The Mozambique Belt is the common name for the southern East African Orogen and here the Tonian and pre-Tonian terranes described earlier came together in two main orogenic events. The earlier one occurred at ca. 650–640 Ma and forms the time of peak metamorphism in Uganda, Kenya, Tanzania and in northern Mozambique (Appel and Schenk, 1998; Fritz et al., 2013; Hauzenberger et al., 2004, 2007; Tenczer et al., 2013). This orogenic event was interpreted as being due to intra-arc extension (Appel and Schenk, 1998), based on its anticlockwise path, but on a regional scale, it correlates with the amalgamation of the main Arabian-Nubian Shield along the Keraf Suture to the north, and is focussed along the suture of Azania with the C-SF. This is particularly apparent in Madagascar where ca. 650–640 Ma metamorphic ages occur in the west of the country (Jöns and Schenk, 2008), whereas the east of the country is dominated by younger metamorphic ages of ca.

570–540 Ma (Collins et al., 2003; Jöns and Schenk, 2008; Tucker et al., 1999, 2014). This younger, eastern, orogenesis correlates with the Ediacaran arc accretion recorded in the far east of the Saudi Arabian Shield that separates the exposed Saudi Shield from the basement of Oman. These observations led Collins and Pisarevsky (2005) to propose that the western ca. 650–640 Ma orogenesis was due to late Cryogenian collision of Azania with the C-SF continent (the East African Orogeny sensu stricto; e.g. Meert and Van der Voo, 1997; Stern, 1994), while the younger ca. 570–540 Ma orogenesis was due to the final collision of Neoproterozoic India with the then amalgamated Azania/C-SF continent, closing the Mozambique Ocean (and forming the Malagasy Orogeny; Collins and Pisarevsky, 2005). Studies from southern India support this hypothesis because orogenesis in the Southern Granulite Belt is focussed at 570–520 Ma and forms a part of the Malagasy Orogeny (Clark et al., 2015; Collins et al., 2007a,b, 2014; Johnson et al., 2015; Plavsa et al., 2012, 2014, 2015; Taylor et al., 2015; Kumar et al., 2016).

5.2. Oubanguides-Sergipano Orogen

The Oubanguides and Sergipano belts run roughly E-W across central Africa and South America, separating Congo and the SM in Africa, and between the São-Francisco Craton and the Borborema Block in South America (Fig. 2b). The Oubanguides are interpreted to continue between the two cratons towards Sudan in the east, though they crop out most prominently, and have only been studied, in the west; in Cameroon, Chad and the Central African Republic (e.g. Pin and Poidevin, 1987). Broadly, the Oubanguides consists of Palaeoproterozoic basement thrust over the Congo Craton, with intense metamorphism (granulite facies) following collision (e.g. Toteu et al., 2004). It is divided into three tectonic units separated by shear zones. These are, from south to north, the schistose and gneissic Yaoundé Domain, which contains extensive nappes thrust over the Congo Craton (e.g. Owona et al., 2011), the reworked Palaeoproterozoic Adamawa-Yadé Domain, intruded by numerous syn- to late tectonic ca. 630–570 Ma granitoids, and the volcano-sedimentary schistose and gneissic Western Cameroon Domain, which was intruded by calc-alkaline granites between 660 and 580 Ma (Toteu et al., 2001). Dating of metagabbroic rocks in the northern Yaoundé domain show the earliest intrusions to be 660 ± 22 Ma (Toteu et al., 2006), likely due to slight extension as a response to subduction further south. This facilitated deposition within the Yaoundé Basin (Toteu et al., 2006). Deformation and metamorphism are constrained to ca. 660–600 Ma (Nkoumbou et al., 2014; Owona et al., 2011; Rolin, 1995; Toteu et al., 2006). Dating of granitoids from shear zones within the Western Cameroon belt (northernmost unit) constrain a period of sinistral shear motion to ca. 620 Ma, and a younger, more dominant, period of dextral shear at 580 Ma, likely due to collision of Amazonia and WAC with the Gondwana nucleus (Kwékam et al., 2010).

This correlates with the Sergipano Belt of NE Brazil where metamorphism and deformation is constrained to ca. 630–570 Ma (Neves et al., 2016; Oliveira et al., 2015). A continental margin arc is suggested here at ca. 630 Ma, overprinted by syn- continent-continent collisional granitoids emplaced between 590 and 570 Ma (Oliveira et al., 2015). The Sergipano Belt consists of five domains sutured by shear zones; from south to north these are the Estância, Vaza Barris, Macururé, Poço Redondo-Marancó and Canindé Domains (Davison and Dos Santos, 1989; Oliveira et al., 2010). The three southerly domains consist predominantly of metasedimentary and sedimentary rocks. From south to north, the domains are interpreted to represent the foreland basin (Estância domain), grading towards a fold thrust belt consisting of slightly deformed sedimentary rocks of a shallow platform (Vaza Barris domain) with provenance from the south (i.e. São Francisco), and deformed metasedimentary rocks (Macururé domain) derived from the north (i.e. Borborema) (Oliveira et al., 2010). The only age constraints available for these domains are from the Macururé Domain, where 620–570 Ma granitoids intrude (Bueno et al., 2009; Silva Filho et al., 1997). Here, the ca. 620 Ma granites are inferred to be emplaced in a

continental arc environment (Bueno et al., 2009). The two more northerly domains are more varied in their composition; the Poço Redondo-Marancó contains metasedimentary rocks deformed up to amphibolite facies, with calc-alkaline andesitic-dacitic rocks likely derived from a volcanic or continental arc, and large granitoid intrusions. Ages determined from the volcanic arc rocks (Carvalho et al., 2005), and granitic intrusions (Oliveira et al., 2015) suggest magmatism spanned from ca. 630 to 600 Ma. The Canindé Domain contains a broad range of rock units, leading to multiple interpretations of its tectonic environment, including ophiolitic remnants, island arc accretions and intracontinental magmatism (Jardim de Sá et al., 1986; Oliveira and Tarney, 1990; Silva Filho, 1976). Recent U-Pb dating of some of the igneous bodies give ages ranging from ca. 720 Ma to 620 Ma (Nascimento et al., 2005; Oliveira et al., 2010), and, coupled with geochemical trends, suggest that the Canindé Domain represents a Wilson Cycle of ocean basin formation and then destruction (Oliveira et al., 2010).

Oliveira et al. (2015) dated granitic bodies from the Canindé, Poço Redondo-Marancó and Macururé Domains. They found two distinct age clusters, an early cluster between 630 and 618 Ma, preserved in all three domains, wherein the granitic bodies contain prominent mafic enclaves, and a later cluster emplaced between 590 and 570 Ma, present only on in the metasedimentary successions of the Macururé Domain. The early cluster constrains the latest onset of subduction to ca. 618 Ma and was interpreted to represent magma mingling from the melt of the underthrusted C-SF plate, with slab break off allowing for upwelling in the asthenosphere and partial melting of the slab, generating mafic fluids. The later cluster is thought to represent continent-continent collision between Borborema and São Francisco (Bueno et al., 2009; Oliveira et al., 2015), and is related to strike-slip granites generated further into the Borborema Block away from active margins (Bueno et al., 2009), suggesting that relative motion was finalised by ca. 570 Ma. Brito Neves et al. (2016) focussed on the northern margin of the Sergipano Belt and suggested that in this area between ca. 673 and 647 Ma, extension and basin formation ended with contractional orogenesis by ca. 630–600 Ma.

5.3. Zambezi-Lufilian-Damara Orogen

The Zambezi-Lufilian-Damara orogeny marks the closure of the Khomas Ocean and the collision of the Kalahari craton against C-SF. The Zambezi Belt passes east into the East African Orogen in Malawi and Mozambique (Fig. 2b). To the west, the belt is displaced by the large sinistral ca. 550–530 Ma Mwembeshi Shear Zone (Naydenov et al., 2014). West of this shear zone, the boundary between the C-SF and Kalahari continents is delineated by the broad curve of the Lufilian Arc, snaking through Zambia and the Democratic Republic of Congo, before linking up with the Central Damara Belt in Botswana and Namibia. Here, it meets a triple junction of Neoproterozoic oblique subduction, with the Gariep-Saldania Belt to the south along the coast of Namibia and South Africa, and the Ribeira-Kaoko Belt to the north, marking the coasts of Brazil and Namibia and tracing the RDLP-C-SF suture.

The Zambezi Belt preserves evidence of the formation of a significant ocean between the Kalahari and C-SF continents that was being subducted from at least ca. 670 to 600 Ma (John et al., 2003, 2004a). A gabbro-metagrabbro-eclogite assemblage preserves incompatible elemental patterns similar to that of MORB, and are, therefore, interpreted to represent subduction of oceanic crust (John et al., 2003). John et al. (2003) also calculated a low thermal gradient (~8 °C/km), and, coupled with the subduction depth, concluded that the oceanic crust would have to be at least 30 Myr old, suggesting that the oceanic domain between C-SF and Kalahari was larger than 1000 km. Collision between the Kalahari and the C-SF is constrained to between 545 and 525 Ma (Goscombe et al., 2000; John et al., 2004b) by more regional metamorphism through the Zambezi Belt. This is roughly coeval with the greenschist to lower amphibolite facies metamorphism evident in the Lufilian Belt (e.g. Rainaud et al., 2005), although peak orogeny in the Lufilian Belt is

inferred to be between 560 and 530 Ma based on U-Pb from monazite grains (John et al., 2004b), magmatic intensity (Hanson, 2003) and crustal thickening exhibited by extensive folding, thrusting, and nappe development, peaking with the formation of whiteschists at ca. 520 Ma (John et al., 2004b; Rainaud et al., 2005). The Lufilian Belt hosts the late Tonian-Cryogenian Katanga Supergroup that itself hosts world-class Cu-Co deposits (El Desouky et al., 2010). Evidence for early continental deformation here is constrained to ca. 590 Ma preserved in metamorphic monazite from the Roan and Nguba Groups of the Chambishi Basin (Rainaud et al., 2005). Termination of convergence is estimated to be ca. 530–520 Ma due to successive ages from 510 Ma interpreted to reflect post orogenic cooling (John et al., 2004b; Rainaud et al., 2005). The tectonic evolution of the sinistral Mwembeshi Shear Zone (MSZ), separating the Zambezi and Lufilian Belts, is poorly known. The displacement was explained by variation in shortening between the Zambezi Belt, which is narrower and experienced a higher grade of metamorphism, compared to the Lufilian Belt, which is wider and records predominantly greenschist metamorphism, with the MSZ representing a reactivated fault during Gondwana amalgamation (Porada and Berhorst, 2000). Recent dating of the Hook Batholith by Naydenov et al. (2014), located just north of the MSZ in the Lufilian Belt, shows emplacement occurred between ca. 550 and 530 Ma based on U-Pb dating. The ages are syntectonic with an early (ca. 550 Ma) deformation event that resulted in E-W shortening associated with closure of the Mozambique Ocean. A slightly younger (ca. 520 Ma) N-S shortening event associated with Kalahari-C-SF collision is preserved in the Katanga Supergroup and the Hook Batholith, suggesting that the MSZ responded to accommodate oblique convergence (Naydenov et al., 2014).

Further west, the Damara Belt preserves a similar age range of deformation and convergence, although it is structurally more complex, and, geologically, considerably larger than the Lufilian and Zambezi Belts (see Frimmel et al., 2011; Gray et al., 2008 for overviews). Frimmel et al. (2011) described the sedimentation in the Damara Belt as occurring between the Kalahari Craton and the smaller Angola Craton (present-day southern Congo Craton) that they interpreted to have rifted off Kalahari earlier, but which acted separately from the larger C-SF craton further northwards until Gondwana amalgamation. Thus, in their model, while the Damara Belt records the convergence and closure of the ocean basin between Kalahari and Angola (and, by extension, Kalahari and C-SF), the extension and sedimentation that it preserves is not necessarily a record of C-SF rifting from Kalahari, but records a related, later rifting event. The Damara Belt is divided into zones of distinct tectonostratigraphy that are typically bounded by faults and/or lineaments, and, broadly, preserve the development of a Cryogenian-Ediacaran passive margin and its deformation into a fold belt (e.g. Frimmel et al., 2011; Hoffmann et al., 2004; Miller and Becker, 2008). Fold interference from the Gariep and Kaoko belts is prevalent throughout the northern units of the Damara Belt (e.g. Lehmann et al., 2016), and three main phases of deformation were identified; D1, early (ca. 620 Ma) N-S shortening from closure of the Khomas Ocean; D2, (ca. 580 Ma) E-W shortening due to closure of the Adamastor Ocean; and, D3, late (ca. 530 Ma) N-S shortening due to Kalahari-C-SF collision (Lehmann et al., 2016). Thick (>6000 m), relatively flat-lying strata preserved in grabens in the northern units, are comprised of dominant feldspathic sandstones with minor evaporates and some volcanic detritus. These are overlain by diamictites of the Chuos Formation and followed by thick platform carbonates until ca. 635 Ma, when units of the Ghuab glaciation (Hoffmann et al., 2004) were deposited, suggestive of a failed rift (rifting moved further south) and shallow sea, which preserved little N-S deformation from convergence (e.g. Frimmel et al., 2011). Further to the south, passed the Okahandja Lineament, these older sediments are not preserved, rather basal MORBs are observed (Matchless Amphibolite Group, Schmidt and Wedepohl, 1983) and are inferred to be younger than 635 Ma (no evidence of glaciation). The turbiditic and schistose units of the Kuiseb Formation overlie them,

and the southern zones are interpreted to preserve short-lived sea floor spreading. Closure of the basin occurred from 600 Ma, somewhat synchronous with the Lufilian and Zambezi belts, although the primary phase of collision was between 560 and 530 Ma as demonstrated by prominent magmatism and granitoid emplacement. Higher metamorphic grades of deformation due to N-S convergence are primarily preserved in the central and southern units (as opposed to northern units), with higher metamorphic grades and fold interference more common towards the west (Hartmann et al., 1983; Lehmann et al., 2016). There are few temporal constraints on early convergence related deformation. Miller (1983) proposed that early deformation began just prior to 650 Ma based on Rb-Sr whole rock age dating on granitoids that intruded D1 folds. The southern zones, which are reminiscent of an accretionary wedge, underwent medium pressure-temperature metamorphism (Kasch, 1983), while 580 to 520 Ma magmatism coupled with crustal thickening leading to low-granulite facies metamorphism occurred in the central zones (Jung and Mezger, 2003; Jung et al., 2000; Longridge, 2012; Longridge et al., 2014; Ward et al., 2008). Similar to the Lufilian and Zambezi belts, the Damara Belt was intruded by post-collisional granitoids from 500 to 480 Ma (e.g. Jung et al., 2000).

5.4. Pinjarra-Prydz-Denman (Kuunga) Orogen

The Pinjarra-Prydz-Denman orogeny is the final major amalgamation of continental crust into Gondwana, with the suturing of Australia-East Antarctica against India and Kalahari. The Pinjarra orogeny typically refers to the entire orogen, although here we separate the three to discretely talk about varying tectonic events. The Pinjarra orogeny preserves the suture along the west coast of Australia. Further south, in Antarctica, snow and ice cover limit most exposure, although the suture is preserved in outcrops in the Denman glacier area, and, further south, in the Prince Charles Mountains-Prydz Bay area, where India and the Rayner province collided with the main crustal part of Antarctica (e.g. Boger, 2011) (Fig. 2b).

Exposure of the Pinjarra orogeny in Australia is constrained to small inliers along the western coastline of the continent, such as the Leeuwin, Northampton and Mullingara Complexes. The Leeuwin Complex in the southwest best preserves the orogeny (e.g. Collins, 2003; Collins and Fitzsimons, 2001). Here pink granitic gneisses had their protoliths emplaced at ca. 750 Ma and exhibit upper amphibolite-granulite metamorphism dated to ca. 522 Ma (Collins, 2003). This is broadly coeval with the end of tectonism, as ca. 520 Ma dykes that intrude the Leeuwin Complex exhibit no deformation (e.g. Fitzsimons, 2003). The tectonic environment of emplacement was inferred to be a rift, related to Rodinia breakup (Collins, 2003), since at the time it was postulated that Kalahari was attached to this margin of Australia (e.g. Powell and Pisarevsky, 2002). Sinistral shearing is preserved in the Northampton Complex (Embleton and Schmidt, 1985), and alkali granitoids in the Leeuwin Complex originally inferred to be rift related, are now thought to have been emplaced in a sinistral transpressive environment (e.g. Fitzsimons, 2003; Harris, 1994). Further evidence of this motion is preserved in the Darling Fault along the coastline of Western Australia, where structures from the Albany Fraser Orogen were sinistrally rotated nearly 90° (Beeson et al., 1995; Fitzsimons, 2003). Dating of dykes affected by the shear suggest that the motion was occurring at least between 600 and 550 Ma, although an earlier initiation is inferred by reconstructions (e.g. Fitzsimons, 2003; Powell and Pisarevsky, 2002). Further south, the Denman Glacier area is on the coast of Antarctica fitting tightly with the Leeuwin Complex in a reconstructed Gondwana. Here, U-Pb dating of zircons from syenite give an age of ca. 516 Ma, and orthogneisses with a protolith age of ca. 3 Ga record a metamorphic overprint age between 550 and 520 Ma (e.g. Halpin et al., 2008). Some data show substantial lead loss between 600 and 520 Ma (Black et al., 1992), indicating a similar Ediacaran history to rocks further north in Australia. The suture between India-Antarctica and Australia-Antarctica

is typically traced from this area, south, towards Prydz Bay and the Prince Charles Mountains (e.g. Boger et al., 2001).

The Prydz Bay area is found further south in Antarctica and preserves the primary suture between India-Antarctica and Australia-Antarctica, since it is found slightly further away from a reconstructed India than the late Mesoproterozoic-early Neoproterozoic Rayner Province. Due to the similarity of protoliths, neodymium modelling ages and metamorphic events, the Prydz Bay area is inferred to be part of the Indo-Antarctica plate (e.g. Boger, 2011; Kelsey et al., 2007; Liu et al., 2009; Wang et al., 2008; Zhao et al., 1995). Here too, late Ediacaran-early Cambrian metamorphism up to granulite facies (Liu et al., 2003) is evident, with 540–500 Ma charnockite and granite plutons intruding gneisses (Liu et al., 2006, 2009; Mikhalsky and Sheraton, 2011). Further inland from Prydz Bay (Antarctica), zircons from gneiss within the Grove Mountains suggest magmatic emplacement at ca. 900 Ma, with a high-grade metamorphic overprint between 530 and 520 Ma (Liu et al., 2003; Zhao et al., 2000). Intruding ca. 500 Ma granitic dykes exhibit no metamorphism suggesting deformation had finished by this time (Zhao et al., 2000).

5.5. Gariep-Dom Feliciano-Kaoko Orogen

The Gariep, Dom Feliciano and Kaoko belts preserve the suture between C-SF, RDLP and Kalahari, and form two arms of the triple junction between the cratons, with the Damara Belt, between C-SF and Kalahari, being the third arm (Fig. 2b). The Kaoko belt of the western Congo Craton traces the suture through northwest Namibia towards the junction with the Damara Belt in central Namibia, it is extended further to the south along the southwestern Namibia border and western South Africa as the Gariep Belt. The suture is preserved on the South American side of Gondwana through the Dom Feliciano Belt, which extends from southern Brazil in the north, through Uruguay to the south, along the eastern margin of the RDLP craton, where it is juxtaposed against by the Neoproterozoic-aged, sinistral Sarandí del Yi megashear.

The Kaoko Belt is divided into three distinct tectonostratigraphic units (Miller, 1983); the Eastern Kaoko Zone is a late Tonian(?) to Cryogenian carbonate platform, containing some deeper water argillite sequences (Miller, 2008), and is broadly coeval to the northern zone in the Damara Orogen (e.g. Hoffman et al., 1998b). The Central Kaoko Zone consists of deformed and metamorphosed Archaean and Palaeoproterozoic basement, with metamorphic grade increasing to the west, from greenschist to upper-amphibolite facies. The Western Kaoko Zone (WKZ) was subjected to an even higher grade of metamorphism, up to granulite facies, and consists predominantly of metasedimentary rocks with some Neoproterozoic granitoids. A high temperature metamorphic event from 650 to 630 Ma in the WKZ not preserved elsewhere in the Damara region, suggests that the WKZ contains an exotic terrane (the Coastal Terrane, Goscombe et al., 2003a), linked to arc accretion over an east dipping subduction zone until ca. 600 Ma (Goscombe and Gray, 2008; Goscombe et al., 2003a,b; Gray et al., 2008; Masberg et al., 2005). This is roughly synchronous with the collision of the Oriental Terrane further north in the Brazilian Ribeira belt (e.g. Heilbron and Machado, 2003). Younger metamorphic events, between 580 and 550 Ma, which are preserved in the entire belt and get progressively weaker towards the east, are interpreted to be related to sinistral, transpressional deformation from oblique collision between the South American cratons and the C-SF craton. Peak metamorphism was reached early in the main metamorphic cycle (ca. 580–570 Ma, Goscombe et al., 2003a), with granitoid intrusions and magmatism occurring until ca. 550 Ma. Minor N-S shortening occurred between 530 and 510 Ma, likely related to the arrival of either (or both) RDLP and Kalahari against the C-SF Craton (Goscombe et al., 2003b; Gray et al., 2008).

The Gariep Belt lacks the higher grades of metamorphism prevalent in the African belts further north and, consequently, it better preserves Neoproterozoic sedimentary sequences from the Adamastor Ocean.

Two distinct units are recognised, the folded and thrusted(?) volcano-sedimentary Port Nolloth Group in the east, and the younger, oceanic Marmora Terrane. The Marmora Terrane is comprised of oceanic crust with minor overlaying carbonates with an approximate minimum age of ca. 600 Ma based on U-Pb dating of zircon in a stromatolite (Frimmel and Fölling, 2004; Frimmel et al., 2002). The young age of oceanic crust indicates some seafloor spreading occurred until relatively late in the Adamastor Ocean. High-pressure metamorphism is preserved in the Marmora Terrane at ca. 575 Ma and peak metamorphism inferred to occur between ca. 550 and 540 Ma with continent-continent collision and the thrusting of the Marmora Terrane onto the Port Nolloth Group (Frimmel and Frank, 1998). Ages from muscovite in the Port Nolloth group at ca. 530–525 Ma suggest post-tectonic cooling and exhumation at this time.

The Dom Feliciano Belt (DFB) of Uruguay preserves an older record of subduction than either the Gariep or Kaoko belts and presents a more complicated story that has invited alternate interpretations that have profound implications on Neoproterozoic palaeogeography. The DFB runs from the southeast corner of Brazil to the south of Uruguay, parallel to the Atlantic coastline. Unlike the Gariep and Kaoko belts, which consist predominantly of folded sediments and oceanic terranes from basin inversion, the Dom Feliciano Belt preserves fragments of Palaeoproterozoic continental crust, Neoproterozoic arcs and sedimentary wedges, forced together under a transpressional tectonic regime (Basei et al., 2000). Three distinct domains (or belts) were identified (Basei et al., 2000), the Western Domain consists of ca. 750 Ma juvenile arc rocks, followed by ca. 730 Ma mafic rocks associated with ophiolitic assemblages (serpentine, peridotite) and volcanoclastic sedimentary successions (Leite et al., 1998). The Central Domain in Brazil contains Palaeoproterozoic gneisses overlain by lower grade Neoproterozoic supracrustal rocks, and is represented further south in Uruguay by a schistose volcanosedimentary fold/thrust belt prevalent in the Lavalleja Complex and Nico Perez Terrane (Sanchez Bettucci et al., 2010). Both the Western and Central Domains crop out mostly in the north (southern Brazil); towards the south they narrow between the RDLP craton and the rocks of the Eastern Domain. The Eastern Domain (or Granite belt) comprises a long orogenic belt of syn-post tectonic calc-alkaline granitic batholiths that were emplaced in the south between 650 and 550 Ma (Basei et al., 2000; Hartmann et al., 2002; Oyhantçabal et al., 2007, 2009). Towards the south in Uruguay, the Eastern Domain crops out between the older rocks of the RDLP craton and central/schist belt, with sedimentation here leading to the development of a foreland basin (e.g. Oyhantçabal et al., 2009). The foreland belt (acting as the southerly extent of the Central Domain in the north), is bounded by a reworked Archaean and Palaeoproterozoic terrane (Nico Perez Terrane), and overlying volcano-sedimentary units (Basei et al., 2000; Hartmann et al., 2001). Various terranes within the Eastern Domain are proposed to be linked with both the Gariep Belt (e.g. Basei et al., 2005), and the Kaoko Belt (e.g. Oyhantçabal et al., 2009).

The northern rocks of the DFB preserve older magmatic signatures, with continental arc magmatism preserved from the early Cryogenian (e.g. Koester et al., 2016; Lenz et al., 2013; Saalmann et al., 2006). In the south, magmatic age decreases from ca. 650 to 600 Ma with the emplacement of the granitoid bodies; although recent studies have found small areas of earlier magmatism do exist from 800 to 770 Ma, with a metamorphic overprint at ca. 650 Ma (Lenz et al., 2013). Similar to the Kaoko and Gariep belts, transpressional deformation is prevalent from ca. 580 Ma (e.g. Oyhantçabal et al., 2011). The DFB is thought to have not developed on the RDLP craton; firstly, because of the shear and thrust relationships between them, secondly, because of the allochthonous older terranes in the Central Domain, and, finally, because RDLP's position in Rodinia does not allow long lived subduction on its northern and eastern margins (e.g. Fuck et al., 2008; Gaucher et al., 2011). The model of Rapela et al. (2011) suggests that a ca. 800 Ma rifting event between the Kalahari, Nico Perez Terrane and the Angola Block (part of Congo) was responsible for the opening of the Adamastor Ocean and

building of the DFB, and that sinistral shearing occurred when the RDLP collided with Kalahari, squeezing the fold belts.

5.6. Ribeira-Araçuaí-West Congo Orogen

The Araçuaí belt in South America (and its African equivalent, the West Congo belt) formed from the closure of the intra-cratonic ocean basin between the São Francisco and Congo Cratons, and is connected to the more southerly Damara-Dom Feliciano-Kaoko belts through the Ribeira Belt, which lies along the southern tip of the São Francisco craton (Pedrosa-Soares et al., 2001) (Fig. 2b). The Ribeira Belt contains a number of tectonostratigraphic units (e.g. Heilbron et al., 2008), preserving Archaean-Palaeoproterozoic basement (e.g. Occidental Terrane, Trouw et al., 2000), early Neoproterozoic rift histories (e.g. Andrelândia Basin, Paciullo et al., 2000; Valladares et al., 2004) and Cryogenian to Cambrian subduction and magmatism (e.g. Oriental Terrane, Heilbron and Machado, 2003; Heilbron et al., 2010). MORB-like magmatism in ca. 848 Ma intrusions in these terranes suggests that there was an ocean basin between them and the São Francisco Craton during the Tonian (Heilbron and Machado, 2003). The Oriental Terrane of the southern São Francisco Craton preserves the oldest evidence of subduction, with early arc complexes recording a ca. 790 Ma U-Pb age in zircon and monazite from tonalitic gneiss (Heilbron et al., 2003). The primary phrase of subduction in the Ribeira Belt is inferred to have occurred from 650 to 620 Ma, with the collision of the Rio Negro Arc and the Oriental Terrane (Heilbron and Machado, 2003; Heilbron et al., 2008; Tupinambá et al., 2012). This collision is roughly synchronous with the collision of the Coastal Terrane in the Kaoko Belt further south, suggesting a long-lived semi-continuous arc between São Francisco and the Congo (or Angola?) Craton. Closure of the ocean basin and continental collision occurred after 620 Ma, with collision of the Oriental Terrane and São Francisco Craton occurring between 580 and 550 Ma (Heilbron and Machado, 2003). Heilbron and Machado (2003) inferred a small landlocked sea between Congo and São Francisco in the south that did not close until the earliest Ordovician (Schmitt et al., 2008; Fernandes et al., 2015).

Further north, the Araçuaí Belt preserves the closure of an ocean basin that is surrounded on three margins by cratonic crust, leading to a tectonically complex kinematic evolution (e.g. Maurin, 1993; Pedrosa-Soares et al., 1992), where 'nutcracker' tectonics are inferred as one of the drivers of subduction (rather than slab pull) (Alkmim et al., 2006). Here, the earlier magmatism of the Rio Negro Arc is not preserved, and five generations of granite emplacement are recognised (Pedrosa-Soares and Wiedemann-Leonardos, 2000). The earliest generation of granites are calc-alkaline and dated between 630 and 590 Ma, indicating the start of subduction (da Silva et al., 2005; Pedrosa-Soares et al., 2001; Tupinamba, 1999). Closure and development of a thick orogen occurred between 590 and 570 Ma, demonstrated by a second generation of S-type granitoids, and peak metamorphic conditions and deformation to granulite facies (e.g. da Silva et al., 2003, 2005; Pedrosa-Soares et al., 2001). Post-collisional escape tectonics occurred to the south, towards the Kaoko and Dom Feliciano belts, and is coupled with the third generation of granite emplacement between 560 and 510 Ma (Alkmim et al., 2006). This closure is described as having occurred because the approaching Amazonia-WAC cratons pushed against the São Francisco, forcing convergence between itself and the Congo Craton, which could help explain sinistral displacement further south in the Kaoko and Dom Feliciano Belt between RDLP and Kalahari. The final two generations of granite intrusions relate to orogenic collapse and were emplaced between 510 and 480 Ma (Pedrosa-Soares and Wiedemann-Leonardos, 2000).

5.7. Brasília Orogen

The Brasília Belt forms the eastern part of the primary suture between Amazonia and C-SF, the two largest areas of Precambrian crust

in South America and Africa, and is preserved on the western margin of the São Francisco Craton (Fig. 2b). It forms part of the Brasiliano Orogen, along with the Araguaia, Paraguay, Dahomeyide and Pharuside belts that stitch the WAC and Amazonia to the C-SF and the SM. The Brasília Belt contains a number of distinct zones, from east (SF) to west (Amazonia), including a foreland basin sitting unconformably above the Archaean-Palaeoproterozoic basement of the São Francisco craton and an external zone of metasedimentary rocks deposited in a shelf environment comprising both silicic and carbonate successions (Dardenne, 2000; Paciullo et al., 2000; Pimentel et al., 2011). Further west, an internal zone is preserved, with W-NW verging nappes and pelitic metasedimentary rocks, suggesting deeper shelf sedimentation, although further to the north along the zone, rocks derived from an oceanic environment become more prominent, perhaps suggesting an open ocean to the N-NW (Seer and Dardenne, 2000; Seer et al., 2001; Valeriano et al., 2008). Westerly subduction is inferred to have occurred under the Neoarchean granite-greenstone Goiás Massif between 650 and 610 Ma (e.g. Campos Neto and Caby, 1999; Töpfner, 1996; Valeriano et al., 2004), acting here as a microcontinent (Queiroz et al., 2008; Valeriano et al., 2008) accreted to the Brasília Belt sometime during the Neoproterozoic. The southerly extension of the Goiás Massif is typically inferred to be the Paranapanema Block (e.g. Valeriano et al., 2008). The Goiás magmatic arc is preserved both north and south of the Goiás Massif, and records magmatism from the Tonian, with juvenile magmatism and intrusions of tonalite-granodiorite from 860 to 610 Ma, with the younger rocks becoming more evolved (Matteini et al., 2010; Pimentel et al., 2000, 2004, 2011). Peak metamorphic grade is upper amphibolite to lower granulite facies and is constrained between 650 and 630 Ma (e.g. Moraes et al., 2002; Piuzana et al., 2003; Seer et al., 2005; Valeriano et al., 2004), with post tectonic cooling from 610 to 600 Ma, suggesting collision between the Goiás magmatic arc, Goiás Massif and São Francisco occurred prior to the opening of the Iapetus Ocean.

5.8. Paraguay-Araguaia-Rokelides-Bassarides Orogen

The Paraguay and Araguaia belts, south and north of the Brasília Belt, respectively, preserve the final suture of Amazonia and C-SF, although on the Amazonian side of the margin rather than the São Francisco side (Cordani et al., 2003; Moura et al., 2008) (Fig. 2b). The Rokelide and Bassaride belts lie further north, in present-day Africa, between Amazonia and the WAC in a reconstructed Gondwana.

The Paraguay belt consists of a northern and southern section separated by Phanerozoic cover. Traditionally the belt was interpreted as an inverted rift, as metasedimentary and sedimentary rocks dominate it with the only granitic bodies being from post-collisional tectonism (e.g. Alvarenga et al., 2009; McGee et al., 2012b). Broadly, the lower units in the northern Paraguay Belt are interpreted to represent passive margin sedimentation and are dominated by a thick diamictite layer, overlain by a foreland succession of carbonate and sandstone layers, with a thinner diamictite layer (Alvarenga et al., 2008, 2009; McGee et al., 2013). The lower diamictite has a carbonate cap dated to ca. 630 Ma, suggesting it is part of the Marinoan glacial event (Alvarenga et al., 2004), while the higher, thinner layer, is stratigraphically correlated to the 580 Ma Gaskiers glaciation (Alvarenga et al., 2007; Pu et al., 2016). U-Pb dated detrital zircon provides a maximum depositional age of ca. 706 Ma (Babinski et al., 2013; McGee et al., 2015a,b). Furthermore, Sm-Nd modelling ages of the sediments in the basin, U-Pb detrital zircons and ^{40}Ar-^{39}Ar detrital muscovite ages suggest that older sediments were sourced from the Amazonian Craton due to the predominance of Archaean and Palaeoproterozoic signatures, while the younger, higher sediments have a younger component (Dantas et al., 2009; McGee et al., 2015a,b). Dantas et al. (2009) and McGee et al. (2015a,b) suggested that the Goiás Magmatic Arc in the Brasília Belt was a likely source, with sediment derived from this belt as the intervening Clymene Ocean closed in the late Ediacaran/Cambrian (Tohver

et al., 2010; Bandeira et al., 2012). In the Southern Paraguay Belt the glacial events are more poorly preserved, and the stratigraphy differs broadly, being comprised predominantly of siliciclastic rocks (Alvarenga et al., 2009). A transition from rift to drift is suggested in the Corumbá Group, although age controls are poor, with only one of the drift successions having an age constraint of ca. 540 Ma from zircon in a volcanic ash, suggesting that drifting happened sometime in the late Ediacaran (Alvarenga et al., 2009; Babinski et al., 2008). The connection between the southern and northern Paraguay belts is poorly understood due to overlaying Phanerozoic basins. No evidence of oceanic crust exists in the Paraguay Belt, and deformation is constrained to 550–520 Ma as one of the latest events in the Brasiliano Orogeny, with peak metamorphism only reaching greenschist facies (e.g. Pimentel et al., 1996; Trompette, 1994). A minimum age for deformation and metamorphism is ca. 520 Ma based on undeformed, post tectonic granite emplacement (McGee et al., 2012b).

The Araguaia Belt separates rocks deformed during Gondwana amalgamation to the east with the undeformed rocks of the Amazonian Craton to the west and is interpreted to represent the northerly extension of the Paraguay Belt, although the two have quite a different stratigraphy and geology. Rocks increase in metamorphic grade to the amphibolite facies (Abreu et al., 1994) in the east, and are comprised predominantly of sedimentary successions thrust westwards over Amazonia. Protoliths are mainly siliciclastic rocks, with some minor carbonates and mafic-ultramafic rocks, and are classified into the Baixa Supergroup (Alvarenga et al., 2000). The western portion of the belt is comprised mostly of schists with minor quartzite and phyllite, grading towards phyllite and slate, with minor quartzite (e.g. Alvarenga et al., 2000). Mafic-ultramafic rocks (serpentinised peridotites) are also evident here, and are described as metamorphosed ophiolites dated to ca. 757 Ma (Paixão et al., 2008). Comparably, the eastern portion contains schist, quartzite and meta-conglomerates, without any mafic-ultramafic bodies (Alvarenga et al., 2000). Sm-Nd model ages of zircon taken from quartzite units of the Baxio Supergroup do not support provenance from only Amazonia, as younger signatures are preserved as well as older Archaean-Palaeoproterozoic signatures (Moura et al., 2008). Instead, Moura et al. (2008) proposed that a source of detritus for the Araguaia basin was from the Goiás Magmatic Arc, Goiás Massif and Brasília Belt. Early deformation is possibly slightly older than in the Paraguay Belt, with zircon from granitoids dated at ca. 650 Ma (Moura and Gaudette, 1993), although these zircons may be inherited, as a range of zircon ages are also recorded (Teixeira et al., 2002). A recent age of ca. 550 Ma was found by Alves (2006) and is now thought to be a better representation of the timing of the collision.

The Araguaia Belt is bound to the more easterly Brasília Belt by the cryptic Transbrasiliano Lineament, which separates pre-Neoproterozoic western Gondwana crust into Congo-affinity (e.g. São Francisco, Paraná, Borborema, SM) or Amazonia-affinity (e.g. WAC). The Araguaia Belt is typically extended into northern Africa along the 4°50′ or Kandi fault (e.g. Caby, 1989; Cordani et al., 2013; de Wit et al., 2008; Ganade de Araujo et al., 2016). This lineament is prominent as a sub-continental-scale magnetic discontinuity (e.g. Curto et al., 2014; Fairhead and Maus, 2003), and is interpreted as a dextral transform boundary, active sometime during the Ediacaran and Early Cambrian (e.g. Ganade de Araujo et al., 2014b; Ramos et al., 2010), although due to Palaeozoic basin cover, and the prominence of oblique subduction throughout the Brasiliano belts, it could represent a transpressive regime. Timing of the lineament is also poorly constrained; Ganade de Araujo et al. (2016) suggested ca. 590 Ma activation to match the Borborema-São Francisco collision along the Sergipano Orogen, whereas Ramos et al. (2010) preferred a late Ediacaran-Early Cambrian time to fit a Pampia-RDLP collision.

The Rokelide-Bassaride belts (from south to north) preserve a cryptic Neoproterozoic-Palaeozoic suture on the western and southwestern margin of the WAC, from Morocco in the north towards Liberia in the south (Fig. 2b). The belts are not synchronous with each other, but

rather preserve separate events and indicate that Amazonia and the WAC did not act congruently throughout the Neoproterozoic, with the Bassaride Belt preserving an earlier ca. 650 Ma suture and the Rokelides a ca. 550 Ma suture (e.g. Villeneuve, 2008). The Bassaride Belt consists of two lower groups overlain by sedimentary sequences (Villeneuve, 1984). The basal lower group (Guinguan Group) consists of rocks metamorphosed to greenschist-amphibolite facies including amphibolites, schists, metamorphosed basalts and dolerites, and serpentinites. The second group (Niokolo Koba Group), thrusted over the Guinguan Group, consists of granitoid batholiths and lava flows, including a basaltic-andesitic series and rhyolitic series (Villeneuve, 1984). Rb-Sr dating of the batholiths gave an age of 683–660 Ma (Bassot and Vachette, 1983; Villeneuve, 2008), with metamorphism of the Guinguan group thought to be ca. 660 Ma based on the younger ages of these intrusions. High K_2O content suggests that the collision was continent-continent (Villeneuve et al., 1991). The lavas of the Niokolo Koba Group are inferred to be younger (Villeneuve, 2008), and the volcanosedimentary and sedimentary successions that overlie the Niokolo Koba Group contain some Cambrian microfossils (Culver et al., 1996), although an age date of ca. 600 Ma was suggested by Deynoux et al. (2006) based on stratigraphic correlation. Here alkali basalts that preserve MORB affinity are also present, suggesting that Amazonia and the WAC were not fellow travellers for all the Neoproterozoic (Villeneuve, 1984).

The Rokelide Belt, lying slightly further south than the Bassaride Belt, represents the Amazonia-WAC suture preserved in Gondwana through to the Mesozoic opening of the Atlantic Ocean. It is broadly similar to the Bassaride Belt but exhibits a higher metamorphic grade, with granulitic gneisses and schists prevalent within the thrust belt (Villeneuve, 1984). Three stages of metamorphism were identified, an early peak event at granulite facies, followed by a second amphibolite facies event and later retrogression, with post tectonic granitoids dated at ca. 530 Ma using Rb-Sr and ^{40}Ar-^{39}Ar (Dallmeyer et al., 1987). Further dating on syntectonic granitoids and gneisses suggest an age of 570–550 Ma for peak metamorphism and continent-continent collision (Delor et al., 2002), inferred to be between Amazonia and WAC.

5.9. Dahomeyide-Pharuside Orogen

The Dahomeyide and Pharuside belts are the northerly extension of the Brasiliano Belt and record the suture of the WAC to the Borborema Block in the south (Dahomeyides), the accretion of the westerly terranes and shields (e.g. Hoggar, LATEA, Tuareg Shield etc.) and the WAC to the SM in the north (Pharusides) (Fig. 2b). Few data are available for either belt due to lack of exposure and access. The Dahomeyides expose the suture through central western Africa, predominantly in Togo, Benin, Nigeria, but also in Ghana and Cameroon. Here, the passive margin of the WAC collided with the Nigerian Shield (inferred to act as the northern extension of the Borborema Block), creating a thick fold belt, with subduction to the east, under the Nigerian Shield, away from the WAC (Santos et al., 2008b). The belt consists of a western external zone (foreland of WAC?) consisting of units of undeformed sedimentary successions in the west and quartzite, schist and gneiss towards the east that crop out as nappes (Attoh et al., 1997; Castaing et al., 1993, 1994). The suture zone itself is more heavily metamorphosed, consisting of rocks deformed to granulite and eclogite facies (e.g. Attoh et al., 1997), and zircon from gneiss in the suture zone record a U-Pb age of ca. 610 Ma, interpreted to represent peak metamorphism (Attoh et al., 2013), with later ^{40}Ar-^{39}Ar muscovite data recording an exhumation age of ca. 580 Ma (Attoh et al., 1997).

Further north, the Pharuside Belt has a more extensive record preserved, as ongoing subduction and accretion within the Hoggar Shield, off the western margin of the SM, continued throughout most of the Neoproterozoic (e.g. Caby, 2003). Earlier accretion is attributed to the organising/accretion of the terranes preserved in the Tuareg and Hoggar Shield, with further accretion and more intense deformation more prevalent in the Ediacaran, as a response to the closing of the Pharusian

Ocean and the incipient collision with the approaching WAC (e.g. Caby, 2003; Liégeois et al., 1994). Calc-alkaline granitoids preserve magmatic ages between 700 and 520 Ma (see Caby, 2003 for an overview). The 700 to 650 Ma ages, are typically associated with intrusions into the westernmost terranes of the Hoggar Shield, while the later magmatism (ca. 620 Ma) is associated with HP eclogite formation after rapid (~3 Myr) exhumation (e.g. Caby and Monié, 2003; Berger et al., 2014). A transition to a transpressive tectonic regime is inferred to occur after this event (Berger et al., 2014), and to last until at least 592 Ma, where U-Pb dated dykes were affected by the event (Hadj-Kaddour et al., 1998). Later dextral motion was also suggested to have occurred at ca. 530–520 Ma (Paquette et al., 1998).

5.10. Gondwanides

The Gondwanides (or Terra Australis Orogen after Cawood, 2005) are a series of accreted terranes along the southern margin of Gondwana that formed due to long-lived subduction after Gondwana amalgamated. They initiated in the Cambrian and at their maximum length, stretched from Australia (Delamerian orogeny; Foden et al., 2006) through Antarctica (Ross orogeny), across South Africa (Saldania belt, Cape Fold belt) and into South America (Sierra del Ventana, Pampian orogeny, Patagonia fold belt) (Cawood, 2005) (Fig. 2b). The timing of subduction initiation is thought to have occurred from 540 to 500 Ma based on arc magmatism assemblages preserved in eastern Australia (Johnson et al., 2016; Foden et al., 2006), granitoids preserved in Antarctica (Vogel et al., 2002) and ophiolites in South America (Rapela et al., 1998), with a more mature subduction system developing by the Ordovician. Their initiation is typically interpreted as a consequence of Gondwana amalgamation, with interior subduction zones closing and repositioning to the exterior of the supercontinent, forming a circum-Gondwana subduction system.

5.11. Avalonia and Cadomia

The peri-Gondwanan terranes are a series of oceanic and continental arcs accreted to the north-eastern margin of Gondwana during the Ediacaran and Cambrian that later rifted off, closing the Iapetus Ocean and opening the Rheic Ocean (e.g. Murphy et al., 2004; Nance et al., 1991). These terranes were accreted to Baltica and Laurentia, and are currently preserved in southern and western Europe and eastern North America (e.g. Domeier, 2016; Mallard and Rogers, 1997; Murphy et al., 2004; Nance et al., 1991, 2008). Of particular interest to the Neoproterozoic are the Avalonian terranes of Laurentia and northern Europe, and the Cadomian terranes of southern Europe. Detrital zircon and muscovite data suggest that the Avalonian terranes evolved outboard of Amazonia (e.g. Nance et al., 2008; Gutiérrez-Alonso et al., 2005) (Fig. 2b), although recent studies of hafnium isotopes suggest that Baltica may have also provided some detritus (e.g. Henderson et al., 2016). The Avalonian terranes evolved on juvenile, or Mesoproterozoic recycled crust, with the earliest development of primitive oceanic arcs suggested to be at ca. 1.2–1.0 Ga based on Sm-Nd model ages (Murphy et al., 2000). The oldest preserved basement rocks consist of recycled felsic orthogneiss and variably deformed calc-alkaline plutons, dated between 750 and 675 Ma that formed above an active subduction zone (Murphy et al., 2000). Arc accretion to Amazonia (±West Africa) by ca. 650 Ma is suggested by medium- to high-grade metamorphism preserved throughout the terranes (e.g. Strachan et al., 1996, 2007), and was followed by more mature, 640 to 540 Ma subduction, reflecting the dominant period of Avalonian magmatism (Murphy et al., 2013; Nance et al., 1991). They consist predominantly of magmatic volcanic rocks, volcano-sedimentary turbidites and sedimentary successions attributed to a variety of tectonic environments including back-arc and intra-arc basins, and are inferred to have occurred under a regime of oblique subduction (Murphy et al., 1999; Murphy and Nance, 1989). A transition from a convergent tectonic setting to an intracontinental wrench setting is

suggested to occur during the late Ediacaran (ca. 590–550 Ma), based on the synchronous development of transtensional basins and bimodal magmatism (e.g. Nance et al., 2008). This is inferred to represent the rifting of Avalonia from Gondwana, which is also indicated by faunal distributions (Landing, 2005). Ridge subduction (or ridge-trench interaction) was suggested to have occured during the latest Neoproterozoic due as well to a diachronous termination of subduction along the margin (e.g. Keppie et al., 2000; Nance et al., 2002).

The Cadomian terranes have exposed Palaeoproterozoic (ca. 2.1 Ga) basement, indicating that early magmatism in the Neoproterozoic occurred along a slither of continental crust (e.g. Samson and D'Lemos, 1998). The similarity in age of this basement to the WAC, coupled with detrital zircon data, suggest that the Cadomian terranes developed further east than the Avalonian terranes, outboard of WAC instead of Amazonia or Baltica (Fig. 2b). Their development during the Neoproterozoic is similar to that of the Avalonian terranes, with early magmatism from ca. 750 Ma preserved as the protolith ages of orthogneisses (Egal et al., 1996), and collision indicated by metamorphism and deformation occurring (slightly) later than in Avalonia, at ca. 620 Ma (Inglis et al., 2005; Samson and D'Lemos, 1999). Volcanoclastic sedimentary successions including turbidites (Egal et al., 1996) and detritus input also from the SM (Garfunkel, 2015) during the late Ediacaran, suggest some extension, likely due to the formation of a back-arc basin (Linnemann et al., 2008). Later magmatism in a transpressional tectonic regime due to oblique subduction was suggested to have occurred from ca. 540 Ma (Linnemann et al., 2008; Strachan et al., 1989).

6. Palaeomagnetic constraints

A summary of palaeomagnetic data used in the reconstruction is presented in Table 1. The abbreviations in this table refer to orthogonal reconstructions shown in Figs. 5–14 in Section 7.

6.1. Laurentia and Baltica

Palaeomagnetic data from Laurentia and Baltica are important to defining the motion of Rodinia for much of the early Neoproterozoic due to the central position that Laurentia occupies in the supercontinent. Unfortunately, high quality Early Neoproterozoic palaeomagnetic data from Laurentia are unavailable (Table 1) due to the majority of data coming from rocks that underwent intense metamorphism during the Grenvillian orogeny (e.g. Weil et al., 2006). The Grenvillian loop (the name ascribed to the early Neoproterozoic Apparent Polar Wander Path (APWP) of Laurentia) is based on a collection of poles from three distinct time periods, at 1100–1020 Ma indicating an equatorial position (e.g. Jacobsville Sandstone, Roy and Robertson, 1978), at ca. 980 Ma indicating high latitudes (e.g. Haliburton Intrusions A, Buchan and Dunlop, 1976; although these were re-dated to ca. 1015 Ma, Warnock et al., 2000) and at ca. 800 Ma suggesting a motion back towards the Equator (e.g. Galeros Formation, Weil et al., 2004). However, only the late Mesoproterozoic poles are well dated, leading to uncertainty as to whether the loop is clockwise (Hyodo and Dunlop, 1993) or counter-clockwise (e.g. Weil et al., 1998, 2006). Comparably, the Sveconorwegian APWP from Baltica consists of poorly age-constrained poles during the latest Mesoproterozoic (1100–1000 Ma, e.g. Elming et al., 2014 and references therein), but, the early Neoproterozoic poles (ca. 950–850 Ma, Table 1) are well dated. Using palaeomagnetic data from Baltica to supplement the Laurentian data suggests a clockwise motion, but also suggests a decoupling of the Grenvillian loop from the Sveconorwegian loop due to a ~150 Myr age difference in the poles constraining their highest latitude positions (Elming et al., 2014). This age disparity is based on the suggestion that the high latitude Baltican poles from 920 to 900 Ma were remagnetised (Walderhaug et al., 2007). In spite of this discrepancy in APWPs, a movement from low-to-high latitudes and back again, between ca.

940 Ma and 800 Ma, with the peak occurring at 870 Ma, is implemented following Elming et al. (2014).

There is a converse situation for the time interval between 800 and 700 Ma, where there are several reliable Laurentian poles, but no poles for Baltica. Harlan et al. (2008) combined several palaeomagnetic studies on the ca. 780 Ma Gunbarrel intrusions, and related rocks, into one reliable pole (Table 1). Weil et al. (2004, 2006) reported a well-dated pole from the Kwagunt Formation and the imprecisely dated, but similar pole from the Uinta Formation (Table 1, Fig. 10b, c). There are many palaeomagnetic studies on the Franklin magmatic province, with the most recent, highly reliable pole compiled by Denyszyn et al. (2009) (Table 1). All these poles constrain Laurentia's position to low latitudes during the mid-late Cryogenian. There is a plethora of Laurentian poles for the Ediacaran and Early Cambrian (e.g. Lubnina et al., 2014). Ediacaran poles from Laurentia have a convoluted story, with models proposing either a high and low latitude Laurentia between ca. 620 and 540 Ma based on palaeomagnetic data (e.g. Cawood and Pisarevsky, 2006; Collins and Pisarevsky, 2005; Li et al., 2008, 2013; Pisarevsky et al., 2008b). Well dated ca. 615 Ma (Long Range Dykes, Murthy et al., 1992) and ca. 550 Ma (Skinner Cove Formation, McCausland and Hodych, 1998) poles keep Laurentia at low latitudes, although a series of poles between 600 and 560 Ma place Laurentia at either a high, or low latitude position (e.g. the 575 Ma Callander Complex, McCausland et al., 2011; Symons and Chiasson, 1991). Unreasonably high rates of motion or Inertial Interchange True Polar Wander (IITPW) are some hypotheses used to account for the palaeomagnetic poles, although Hodych et al. (2004) notes that the 600 to 560 Ma poles simply permit Laurentia to be at a high latitude, rather than require a high latitude position. Halls et al. (2015) reported a new detailed study on the Laurentian Ediacaran mafic intrusions. They demonstrated that highly reliable palaeomagnetic data from two coeval well-dated dykes are very different, with one (steep remanence) supporting the high-latitude position of Laurentia, while the other (shallow remanence) supported a low-latitude position. Even IITPW cannot explain such high speeds of apparent plate motion. In addition, Halls et al. (2015) found that 90% of altered dykes carry the steep remanence direction, while 75% of petrographically fresh dykes do not. Halls et al. (2015) suggested that the "duality" in Laurentian Ediacaran poles were caused by a combination of remagnetisation and high reversal frequency at that time. Hence, here we have elected to keep Laurentia at low latitudes, omitting the majority of Ediacaran palaeomagnetic data from Laurentia. A somewhat similar shift from high to low latitudes is also observed in palaeomagnetic poles from Baltica (e.g. Lubnina et al., 2014; Klein et al., 2015), although an absence of 600 to 580 Ma Baltican poles coupled with geological evidence indicating that Baltica and Laurentia had separated by this point (e.g. Cawood et al., 2007), make it difficult to determine whether the same disparity is evident in Baltican poles.

The reliable ca. 615 Ma pole, from the Egersund dykes (Walderhaug et al., 2007, Table 1) constrains Baltica to a mid-latitude position (with Laurentia still equatorial). This pole overlaps with the ca. 615 Ma Long Range Dykes pole from Laurentia (Table 1), supporting a Neoproterozoic connection between the two, and constraining rifting to after 615 Ma. A series of 570 to 550 Ma late Ediacaran Baltic poles (Iglesia Llanos et al., 2005; Levashova et al., 2013; Lubnina et al., 2014; Popov et al., 2002, 2005; Table 1) suggest a mid-high latitude Baltica, rotating approximately ~90° counter-clockwise from its position against Laurentia to be in mid latitudes at 570 Ma and low-mid latitudes by ca. 550 Ma (Lubnina et al., 2014; Meert, 2014b). The large rotation can (perhaps in part) be accounted for by the presence of a triple junction between Amazonia-Baltica-Laurentia coupled with the onset of subduction in the Timan area (creating a 'pulling' force for Baltica), which would explain its movement towards the equator.

In lieu of the absence of reliable Cambrian poles from Baltica, we follow the reconstruction of Lubnina et al. (2014) for Baltica from 600 to 550 Ma, and then fit Baltica at 520 Ma in a position similar to that in the 2009 Atlas of Plate Reconstructions of Lowver et al. (http://www-

Table 1

List of palaeomagnetic data used in the reconstruction. Q-factor after Van der Voo (1990). Key is used for identification of poles in reconstruction Figs. 5–14.

Key	Rock unit	Age	Plat	Plong	A95	Author, year	Q-factor
Laurentia							
L1	Gunbarrel Intrusions combined	780–776	9.2	138.7	9	Harlan et al., 2008	1110111 (6)
L2	Uinta Formation	800–750	0.8	161.3	4.7	Weil et al., 2006	0110111 (5)
L3	Kwagunt Formation	748–736	18.2	166	7	Weil et al., 2004	1111111 (7)
L4	Franklin Dykes	727–712	8.4	163.8	2.8	Denyszyn et al., 2009	1111111 (7)
L5	Long Range Dykes	617–613	−19	175.3	17.4	Murthy et al., 1992; Hodych et al., 2004 Age: Kamo and Gower, 1994	1011111 (6)
L6	Skinner Cove Formation	554–548	15	157	9	McCausland and Hodych, 1998	1111001 (5)
Baltica							
B1	Southern Sweden Dykes	946–935	−0.9	240.7	6.7	Elming et al., 2014; Pisarevsky and Bylund, 2006	1111111 (7)
B2	Brantön-Älgö Anortthosite	927–905	5	249	3.9	Stearn and Piper, 1984; age: Schersten et al., 2000	1110101 (5)
B3	Rogaland Igneous Complex	883–855	−46	238	18.1	Walderhaug et al., 2007	1010101 (4)
B4	Hunnedalen Dykes	875–821	−41	222	10	Walderhaug et al., 1999	1110101 (5)
B5	Egersund Dykes	619–613	−31.4	224.1	15.6	Walderhaug et al., 2007	1111011 (6)
B6	Kurgashlya Formation	570–560	−51	135	4.9	Lubnina et al., 2014	1110111 (6)
B7	Bakeevo Formation	570–560	−42	119	5.3	Lubnina et al., 2014	1111111 (7)
B8	Winter coast sediments	558–552	−25.3	132.5	2.8	Popov et al., 2002; age: Martin et al., 2000	1110111 (6)
B9	Zolotitsa sediments I, Russia	560–550	−31.7	112.9	2.4	Popov et al., 2005	1111111 (7)
B10	Verkhotina sediments	560–550	−32.2	107.1	2	Popov et al., 2005	1110111 (6)
B11	Zolotitsa sediments II	560–550	−28.3	109.9	3.8	Iglesia Llanos et al., 2005	1110111 (6)
B12	Zigan Formation	552–544	−16	138	3.7	Levashova et al., 2013	1110111 (6)
Siberia							
S1	Ust-Kirba Formation	960–930	−8.1	182.6	10.4	Pavlov et al., 2002	0110101 (4)
S2	Kitoi Dykes	762–754	−0.4	201.8	6.1	Pisarevsky et al., 2013	1111101 (6)
S3	Kesyussa Formation	542–535	−37.6	165	5.2	Pisarevsky et al., 1997	1010111 (5)
W. Australia							
WA1	Browne Formation	830–730	44.5	141.7	6.8	Pisarevsky et al., 2007	0010101 (3)
WA2	Hussar Formation	800–730	62.2	85.8	10.3	Pisarevsky et al., 2007	0010111 (4)
WA3	Mundine Dykes	758–752	45.3	135.4	4.1	Wingate and Giddings, 2000	1111101 (6)
N. Australia							
NA1	Johnny's Creek Member	780–660	15.8	83	13.5	Swanson-Hysell et al., 2012	0111101 (5)
S. Australia							
SA1	Angepena Formation	660–640	47.1	176.6	5.3	Williams and Schmidt, 2015	0111111 (6)
SA2	Yaltipena Formation	650–635	44.2	172.7	8.2	Sohl et al., 1999	1111111 (7)
SA3	Elatina Formation, MEAN	645–635	49.9	164.4	13.5	Embleton and Williams, 1986 Schmidt et al., 1991 Schmidt and Williams, 1995 Sohl et al., 1999	1111111 (7)
SA4	Nuccaleena Formation	635–610	32.3	170.8	2.9	Schmidt et al., 2009	1111111 (7)
SA5	Brachina Formation	620–590	46	135.4	3.3	Schmidt and Williams, 2010	0111111 (6)
SA6	Bunyeroo Formation	590–570	18.1	196.3	8.8	Schmidt and Williams, 1996	1111111 (7)
SA7	Wonoka Formation	575–555	5.2	210.5	4.9	Schmidt and Williams, 2010	1011111 (6)
North China							
NC1	Huaibei Sills 890 Ma	913–876	−52.3	149.3	3.5	Fu et al., 2015	1011110 (5)
South China							
SC1	Yanbian Dykes A	830–818	45.1	130.4	19	Niu et al., 2016	1111011 (6)
SC2	Xiaofeng Dykes	812–792	13.5	91	10.9	Li et al., 2004	1110111 (6)
SC3	Yanbian Dykes B	814–798	14.1	32.5	20.4	Niu et al., 2016	1011001 (4)
SC4	Liantuo Formation	735–705	9.9	160.3	4.6	Jing et al., 2015 + Evans et al., 2000 combined	1111111 (7)
SC5	Nantuo Formation	641–631	7.5	161.6	5.9	Zhang et al., 2013; Zhang and Piper, 1997	1111111 (7)
SC6	Doushantuo Formation	614–590	25.9	185.5	6.7	Zhang et al., 2015	1110111 (6)
Congo							
C1	Luakela Volcanics A	770–757	−40.2	122	14.1	Wingate et al., 2010	1110111 (6)
C2	Mbozi Complex	773–713	−46	145	6.7	Meert et al., 1995	1110111 (6)
Sao Francisco							
SF1	Bahia Dykes (N + R)	928–912	7.3	106.4	6.2	Evans et al., 2016b	1111100 (5)
Tarim							
T1	Sugetbrak Formation	635–550	19.1	149.7	9.3	Zhan et al., 2007	0111111 (6)
T2	Tereeken Cap Carbonate	ca. 635	27.6	140.4	9.9	Zhao et al., 2014	0111101 (5)
T3	Zhamoketi Andesite	621–609	−4.9	146.7	3.9	Zhao et al., 2014	0110101 (4)
India							
I1	Malani Igneous Suite grand mean	770–734	69.4	75.7	6.5	Meert et al., 2013	1111111 (7)
I2	Bhander and Rewa formations	650–530	47.3	212.7	5.8	McElhinny et al., 1978	0110111 (5)
I3	Jodphur Group	570–520	1	164	6.7	Davis et al., 2014	0110111 (5)
Seyshelles							
SE1	Mahe Dykes	753–747	54.8	57.6	12.1	Torsvik et al., 2001a,b	1110001 (4)
Rio de La Plata							

Table 1 (*continued*)

Key	Rock unit	Age	Plat	Plong	A95	Author, year	Q-factor
RP1	Sierra de las Ánimas Complex	582–574	12.2	78.9	14.9	Rapalini et al., 2015	1110011 (5)
RP2	Sierra de los Barrientos Redbeds	600–500	15.1	72.6	12.4	Rapalini, 2006	0110111 (5)1

udc.ig.utexas.edu/external/plates/), as a connection on its motion towards the 500 Ma position in Domeier (2016).

6.2. Siberia and North China

A connection between southern Siberia and northern Laurentia during Rodinia with an approximately 30° gap between them, is supported by palaeomagnetic data for the early Neoproterozoic as both share a common APWP from 1050 to 980 Ma (Pisarevsky and Natapov, 2003; Pisarevsky et al., 2003 but see alternative hypothesis – Evans et al., 2016a). An absence of Tonian and early Cryogenian poles from Siberia makes it difficult to test whether this configuration remains constant for the early Neoproterozoic, although a ca. 760 Ma pole from the Kitoi dykes (Table 1) suggests that there had been some relative movement between Siberia and Laurentia since the Mesoproterozoic (Pisarevsky et al., 2013). This pole suggests that Siberia moved closer to Laurentia along a dextral transform boundary, and it is inferred that the beginning of this motion is a response to early stages of Rodinia breakup. Given the spatial proximity of Siberia to Australia in Rodinia, we infer Siberia's motion to be the antithesis of the rifting of Australia off Laurentia, which we depict at ca. 800 Ma (about ~20 Myr earlier than Pisarevsky et al., 2013). Although we note that based on the distance that Siberia moved (~30° of latitude), that this movement beginning anytime between ca. 900 and 800 Ma would produce a spreading rate congruent with present day limits. High quality poles from the late Cryogenian and Ediacaran are also scarce for Siberia. A ca. 540 Ma pole from the Kessyusa Formation (Pisarevsky et al., 1997) necessitates a large (~180°) rotation of the Siberian craton from its 760 Ma position (e.g. Smethurst et al., 1998). Recent palaeomagnetic data from sedimentary successions of Siberia (e.g. Pavlov et al., 2015 and references therein) generally support this rotation, but because of uncertain ages, an unequivocal model for this rotation has yet to be made.

The exact configuration of North China around Laurentia in Rodinia is uncertain due to the disparity in geology between it and other cratons. The reconstruction of North China in Rodinia, close to Siberia (Li et al., 2008), was suggested on the basis of the Precambrian APWP (1300–510 Ma) for North China proposed by Zhang et al. (2006), from a palaeomagnetic study of sedimentary successions in Henan Province. However, recent geochronological data (Su et al., 2012) clearly indicate that the poles of Zhang et al. (2006) are significantly older, and that the proposed 1300 to 510 Ma APWP should be dismissed. On the other hand, the recently published ca. 890 Ma Huaibei Sills pole (Fu et al., 2015) suggests a mid-latitude for North China at this time, consistent with its position relative to Siberia and Laurentia shown in Li et al. (2008). Consequently, we still use this model, although we note that North China's position is very poorly constrained and future palaeomagnetic data may change its position. Palaeomagnetic data from the Dongija Formation dated at ca. 650 Ma (Zhang et al., 2000) and from the Wennan Area (Late Cambrian, Zhao et al., 1992) suggest North China remained in low latitudes between 700 and 520 Ma.

6.3. Australia

The Neoproterozoic palaeomagnetic record from Australia is fragmented; there are no reliable palaeomagnetic poles from the Tonian, although there are a number of poles from the Cryogenian and from Ediacaran-Cambrian sedimentary successions. The sparse record in the early Neoproterozoic is particularly troublesome as it makes it difficult to determine both Australia's fit against Laurentia into Rodinia and

to isolate the time of rifting (Section 3.3). Two poorly dated poles, from the Browne and Hussar formations (Pisarevsky et al., 2007), with regional correlation ages between 830 and 800 Ma and 800 and 760 Ma respectively, and a better dated pole from the Johnny's Creek Member (ca. 770 Ma, Swanson-Hysell et al., 2012) (Table 1) suggest Australia was at low latitudes, with the Hussar formation favouring an AUSMEX configuration (Wingate et al., 2002) if rifting from Laurentia was late (post 775 Ma). However, the Browne and Hussar poles may be younger due to their age uncertainties and the closeness of the Browne pole to the Mundine Well pole. Schmidt (2014) recently reviewed the palaeomagnetic Precambrian record for Australia, and determined two 'Grand Poles' (similar results from a key pole from two independent laboratories), the Mundine Dyke Swarms (MDS) at ca. 750 Ma, and the Elatina Formation (EF) at ca. 635 Ma (Table 1). The MDS pole also suggests a low latitude position, and requires that SWEAT-type (including AUSWUS) configurations had already broken up (Missing-Link, or configurations where Australia is more distal from Laurentia can accommodate the MDS pole without earlier breakup). The 40° intraplate rotation of NAC to SAC proposed by Li and Evans (2011) can allow for later rifting of SWEAT-like configurations, and more importantly, reconciles a triad of pairs of poles from the Mesoproterozoic to Neoproterozoic. Significant to Rodinia reconstructions is the restoration of the Walsh Tillite Cap (WTC) (Li, 2000) and the Johnny's Creek Member to the MDS. The absence of high quality, pre-ca. 825 Ma palaeomagnetic data limit our ability to determine the configuration between Australia and Laurentia, because geological evidence for rifting between the two cratons does not conclusively discriminate rifting time more precisely than between 825 and 700 Ma. This means that the Cryogenian-aged poles discussed above are accommodated by most configurations simply by arguing for earlier rifting (an argument supported on kinematic grounds, see above). The series of Ediacaran poles come from 650 to 555 Ma sedimentary successions in South Australia and allow for the construction of an Ediacaran-Cambrian APWP for Australia (Schmidt, 2014). The poles indicate a low-mid latitude position of Australia, consistent with the Gondwana nucleus (i.e. Congo-Amazonia) being over the South Pole.

6.4. India, Seychelles and South China

Palaeomagnetic data from India are sparse, only three (semi-) reliable poles exist for the Neoproterozoic (Table 1); a 770 to 750 Ma pole from dykes in the Malani Igneous Suite (Torsvik et al., 2001a; Gregory et al., 2009; Meert et al., 2013), a ca. 750 Ma pole from the Seychelles (Torsvik et al., 2001b) and a pole from the Bhander and Rewa Series (McElhinny et al., 1978) that is commonly attributed to ca. 545 Ma, but is of questionable age. An earlier pole, the 815 Ma Harohalli dykes (Miller and Hargraves, 1994), suggests a polar location for India, although it has been redated to ca. 1200 Ma and so is discounted here (Pradhan et al., 2008). These poles suggest a movement from polar to equatorial latitudes during the Cryogenian and Ediacaran. The paucity of early Neoproterozoic data make India's position in Rodinia difficult to determine (or even if it was part of Rodinia at all). Traditionally India was placed against the northwestern margin of Australia (e.g. Boger et al., 2001; Powell and Pisarevsky, 2002) in a similar position to its location in Gondwana, in part due to the assumption that East Gondwana acted congruently since the Mesoproterozoic (e.g. McWilliams, 1981). The large mismatch between the 770–750 Ma poles from Malani and the Seychelles with the MDS pole from Australia necessitated early rifting of India from Rodinia (e.g. Li et al., 2008, 2013),

although some reconstructions favoured removing India completely from Rodinia (e.g. Collins and Pisarevsky, 2005). We have followed this approach and have excluded India from Rodinia in the model presented here.

Palaeomagnetic data from South China are broadly similar to that from India, with early Cryogenian poles (830–790 Ma) in South China indicating a high latitude position (e.g. Xiaofeng Dykes, Li et al., 2004; Yanbian Dykes, Niu et al., 2016) and successive data from the later Cryogenian and Ediacaran suggesting movement towards lower latitudes (e.g. Liantuo Formation, Evans et al., 2000; Jing et al., 2015, and Nantuo Formation, Zhang et al., 2013; Zhang and Piper, 1997). There is a large discrepancy between the poles of the Xiaofeng Dykes (Li et al., 2004) and the Yangbian Dykes A and B (Niu et al., 2016) that is difficult to resolve without resorting to extra-ordinary explanations such as true polar wander (Table 1). We elect to follow the pole from the Yangbian Dykes A, which is more compatible with that of the Xiaofeng Dykes than is the pole of the Yangbian Dykes B. Assuming a fixed geological relationship between South China and India, a ~55° rotation of South China and India is needed to fit the Indian 770–750 Ma poles from the Mahe Dykes and Malani Igneous Suite, with the ca. 720 Ma Liantuo Formation from South China, which constrains South China to a mid-latitude position. Late Cryogenian and Ediacaran poles from South China suggest an equatorial position, consistent with it moving towards its inferred position in Gondwana (Zhang et al., 2013).

6.5. Congo-São Francisco

A São Francisco palaeomagnetic pole, which was previously dated as Late Mesoproterozoic, suggested a low-mid latitude position (D'Agrella-Filho et al., 1990; Renne et al., 1990), necessitating a gap between C-SF and Laurentia in the Late Mesoproterozoic (D'Agrella-Filho et al., 2004). However, the age of this pole has been recently reconsidered as Tonian (Evans et al., 2016b). During the Neoproterozoic, a 928–912 Ma pole from the Bahia Dykes in the São Francisco Craton constrains its position to low latitudes (Evans et al., 2016b). Originally, two poles in the Congo Craton, the ca. 795 Ma Gagwe Lava and 750 Ma Mbozi Complex (Meert et al., 1995) necessitated a rapid 90° counter-clockwise rotation at low latitudes between 800 and 750 Ma. Further work by Wingate et al. (2010) demonstrated that the ca. 795 Ma Gagwe remanence was probably not primary due to its similarity to the secondary reprint of the ca. 765 Ma (maximum age) Luakela volcanics (component B). However, the Mbozi pole coupled with another reliable 770–757 Ma pole (Luakela Volcanics A, Wingate et al., 2010, Table 1) suggests that the C-SF was relatively stable during the late Tonian, and that the 90° clockwise rotation occurred after 765 Ma (Wingate et al., 2010).

6.6. Rio de la Plata

The only well-dated pole from RDLP is from the Sierra de las Ánimas Complex, which is dated to between 582 and 574 Ma, constraining RDLP to a mid-high latitude (Rapalini et al., 2015). The reliable, but poorly dated Sierra de los Barrientos pole (Rapalini, 2006) is very close to the Sierra de las Ánimas pole (Table 1).

6.7. Tarim

Three Ediacaran poles from Tarim (Table 1) are not precisely dated, but are internally consistent and two of them are supported by positive fold tests. These poles suggest a low-mid latitude position, consistent with Tarim being situated as a northern extension of Australia. As discussed previously (Section 3.3) three earlier poles from the Tonian and Cryogenian are not compatible with Tarim in this position, and consequently we only incorporate Tarim from 700 Ma in this model.

7. Plate model

In this section, we present snapshots of the plate model at times pertinent to understanding the tectonic evolution of the Neoproterozoic. Although the plate model is based on the geological and palaeomagnetic constraints described above, we also present a discussion on the integration of these observations with plate tectonic theory at these time steps, comparing the final model with the current understanding of plate tectonics from better-constrained reconstructions of the Phanerozoic. We encourage readers to access either the animation or both the associated plate model files and Gplates (www.gplates.org) in the online version of the publication (Supplementary Material) to further investigate periods of interest. Where possible we have labelled oceans based on previous and standard nomenclature and, except were otherwise outlined, they refer to the entire ocean basin, as opposed to a specific plate. For example, the Adamastor Ocean refers to the non-cratonic portion of plates that were built from the spreading system between Kalahari and RDLP, and consists of both the Kalahari Plate and the RDLP plate. For the descriptions below, all orientations are expressed relative to the reconstructed model except where explicitly stated that they are relative to present day. To help follow the latitudinal movements of the cratons in this time we have plotted palaeolatitude vs. time for each major craton (Fig. 4a–e).

7.1. 1000–950 Ma, Rodinia

The core of Rodinia occupies equatorial-low latitudes for the early Neoproterozoic, with Australia sitting at ~30° N, and Baltica, Amazonia, West Africa sitting at ~30° S (Figs. 4d, e and 5). The opening of the Araçuaí Basin between the Congo and São Francisco cratons initiates at ca. 1000 Ma (Pedrosa-Soares et al., 2001). Based on the active subduction on the other side of the Congo Craton, preserved in the Southern Irumide arc in Zambia (e.g. Johnson et al., 2006) and the Dabolava arc (Tucker et al., 2007) outboard of Congo against Azania (D.B. Archibald, unpublished data), we move Congo northwards, with the Southern Irumide arc acting as the boundary between the Congo Plate and the larger Rodinian plate. This subduction zone is offset by a transform fault to the north, linking it with the Dabolava arc, and the extension of this subduction system away from Rodinia, along the (present day) northern margin of Congo is the early Neoproterozoic subduction between the SM-Borborema Plate and the C-SF Plate preserved in the Cariris Velhos orogeny (e.g. Caxito et al., 2014; Santos et al., 2010). A transform boundary connects the inferred spreading ridge outside of the SM with the subduction zone between the SM-Borborema Plate and C-SF Plate, although given the complexity of the Hoggar Shield area and cover of the Sahara Desert early small-scale subduction could be preserved at this time as well. This subduction zone forms the furthest extent of the circum-Rodinia subduction girdle, and is connected via an inferred subduction zone outboard of São Francisco (based on crustal displacement due to spreading in the Araçuaí Basin) to distal subduction outside West Africa-Amazonia-Baltica (Fig. 5).

The earliest evidence of the Avalonian and Cadomian terranes is late Mesoproterozoic to early Neoproterozoic (see Section 5.11, e.g. Murphy et al., 2000), yet there is no record of subduction or arc collision in Baltica and Amazonia until the late Neoproterozoic. We therefore extend the circum-Rodinian subduction zone outboard of Amazonia-WAC-Baltica, such that the Rodinian plate in this section contains a large portion of oceanic crust allowing for the development of thick sedimentary sequences. It is offset by a transform fault to account for the more proximal Valhalla orogeny against Greenland (Cawood et al., 2010), and then extended into North China and Siberia to account for Tonian subduction preserved in the North Qinling Terrane (Dong and Santosh, 2016) and the Yenesei Ridge (Volobuev, 1993; Vernikovsky et al., 2016) respectively.

There is no record of subduction in Western Australia during the Neoproterozoic, which is somewhat problematic for both leaving

Australia exposed on the margin of Rodinia, and for its rifting during the Cryogenian. Similar to the distal subduction zone of Baltica and Amazonia, we infer subduction at a distance from the margin, and note that alternate configurations of Rodinia that place either South China or Tarim here would be broadly compatible with subduction taking place. We instead propose a hypothesis that this Tonian subduction is preserved in the basement of the southeast Asian terranes, such as Sibumasu, Indochina and Lhasa, which record faint magmatic age and detrital zircon signatures from the late Mesoproterozoic to the Cambrian (e.g. Lan et al., 2003; Nagy et al., 2000; Qi et al., 2014; Zhang et al., 2014; Zhu et al., 2011, see Section 3.3).

Late Mesoproterozoic palaeomagnetic data from the Majhgawan Kimberlite Pipe in India suggest a low latitude position (e.g. Gregory et al., 2006), although this pole represents just one kimberlite pipe without properly averaging the geomagnetic secular variation. However, Pradhan et al. (2010) reported higher palaeomagnetic inclination from the 1027.2 ± 13 Ma Anantapur dyke swarm of the Dharwar craton, which indicates medium palaeolatitude. The (chronologically) next reliable pole being the 770–750 Ma Malani Igneous Suite and Takamaka dyke from the Seychelles, suggesting polar latitudes (Gregory et al., 2009; Torsvik et al., 2001a,b). As such we tentatively assume an equatorial-low latitude position for India and South China,
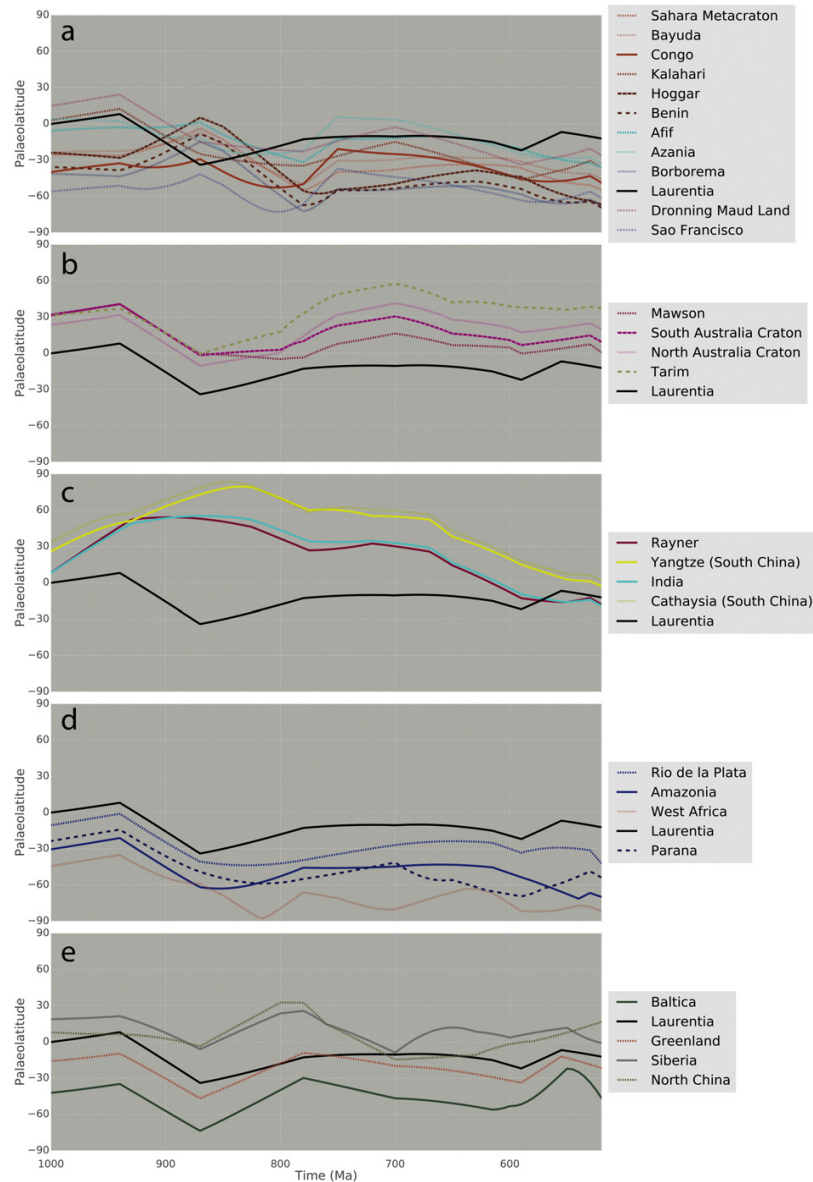
Fig. 4. Palaeolatitude of continental crust fragments in the Neoproterozoic. Each panel broadly reflects a common Neoproterozoic journey; (a) Congo-São Francisco and the Sahara Metacraton (extra south Rodinia); (b) Australia and Mawson (west Rodinia); (c) India and South China; (d) Amazonia (east Rodinia); (e) Laurentia and northern Rodinia. Colour is based on present day geographical position; red – North America; dark blue – South American; green, Europe; grey, Siberia; light blue, India, Madagascar and the Middle East; yellow, China; purple, Australia and Antarctica. Laurentia is plotted in black in each panel as it is considered the heart of Rodinia.

Fig. 5. Tectonic geography at 1000 Ma. A-A, Afif-Abas Terrane; Am, Amazonia; Az, Azania; Ba, Baltica; Bo, Borborema; By, Bayuda; Ca, Cathaysia (South China); C, Congo; Ch, Chortis; G, Greenland; H, Hoggar; I, India; K, Kalahari; L, Laurentia; Ma, Mawson; NAC, North Australian Craton; N-B, Nigeria-Benin; NC, North China; Pp, Paranapanema; Ra, Rayner (Antarctica); RDLP, 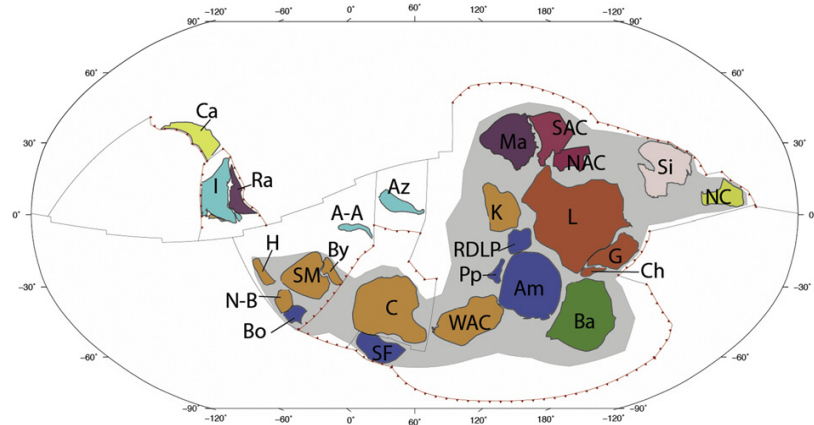Rio de la Plata; SAC, South Australian Craton; SF, São Francisco; Si, Siberia; SM, Sahara Metacraton; WAC, West African Craton. Shaded grey area is inferred extent of Rodinia and is meant as a guide only. The longitude is arbitrary and unconstrained, and used here as a relative reference. Cratonic crust is coloured by present day geography: North America, red; South America, dark blue; Baltica, green; Siberia, grey; India and the Middle East, light blue; China, yellow; Africa, orange; Australia, crimson; Antarctica, purple.

with gradual northwards movement through the Neoproterozoic to fit the two younger, robust 770–750 Ma poles. A large ocean basin encompassing the North Pole separates India-South China and Australia-Antarctica-Tarim, we refer to this as the Mawson Sea after Meert (2003), and its closure beneath Rodinia (outboard of Australia, Antarctica and Tarim) and underneath India-South China through the Eastern Ghats, is in part the driving force of pulling India-South China northwards. The Archaean-aged Ruker Terrane collided with the Eastern Ghats-Rayner Province at ca. 960 Ma, although subduction is inferred to continue outboard of this. The present day northwest margin of India and northern margin of the Cathaysia craton of South China underwent substantial growth during the early Neoproterozoic, and
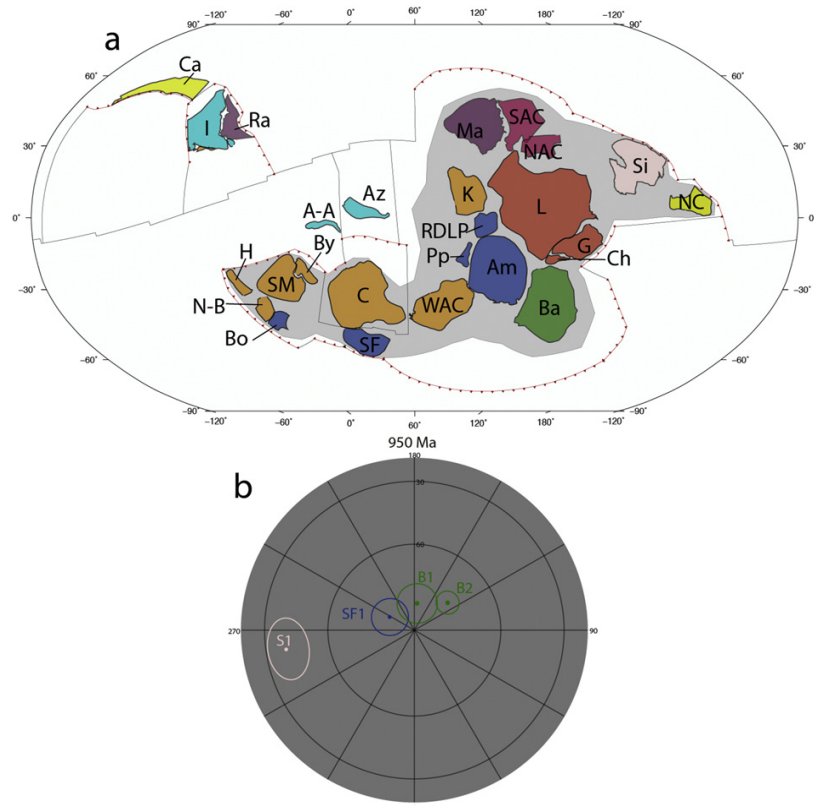

Fig. 6. (a) Tectonic geography at 950 Ma, see Fig. 5 for abbreviations. (b) Palaeomagnetic poles around 950 Ma.

are interpreted here to act as a continuous subduction zone through this time, with accretion occurring for most of the Tonian and including rocks now found in Pakistan and Oman (Alessio et al., in press; Whitehouse et al., 2016).

7.2. 950–850 Ma

At 950 Ma Rodinia remains in a similar latitudinal position to where it was at 1000 Ma (Fig. 4). The plate boundaries are also broadly similar, although we infer a jump in the subduction between Azania and Congo after the collision of the Dabolava Arc with Azania at ca. 950 Ma, with subduction now occurring continuously against the western margin of Azania in the Neomozambique Ocean. This subduction zone is inferred to consist of (from present day south to north) the Antarctic TOAST terrane (Jacobs et al., 2015), the Malagasy Vohibory volcanic arc (Collins et al., 2012) and the Galana Arc (Hauzenberger et al., 2007), and extends northwards towards the SM, through the ANS, correlating it with the early Neoproterozoic (1030–930 Ma) Sa'al Arc (Eyal et al., 2014). This presupposes the legitimacy of extending the Neomozambique Ocean (between Azania and Congo) northwards to between the ANS and SM, as opposed to discrete positions of the ANS and Azania for the early Neoproterozoic. However, it does reconcile mid-Tonian metamorphism and magmatism on the eastern margin of the Bayuda Block (Küster et al., 2008), implying that a long subduction zone was active during the early-mid Tonian along this margin (Fig. 6). The subduction turns off around ca. 900 Ma with the collision of the Malagasy-Vohibory arc with Azania, and this part of the C-SF margin becomes tectonically quiet until ca. 850 Ma. On the present-day western margin of the SM, in the Hoggar Shield, evidence of early sea-floor spreading (pillow basalts), with a transition to a more dominant subduction regime

occurring from ca. 900 Ma with the formation of the Iskel magmatic arc (Caby, 2003). Further south, the existence of this subduction zone is also supported by subduction initiating between 900 and 800 Ma preserved in juvenile arcs on the western margin of the Borborema Province (Ganade de Araujo et al., 2012, 2014a), suggesting that by the mid-Tonian the SM was surrounded by large subduction zones. The subduction zone outboard of Borborema is offset slightly, but otherwise occurs along the same margin as the inferred subduction zone outboard of the São Francisco craton due to spreading in the Araçuai Basin.

As with the spatial uncertainties between the ANS and the SM, it is unknown how close the pre-Neoproterozoic crustal elements (Hoggar, Borborema) were to the SM due to an absence of palaeomagnetic data and significant crustal reworking during Gondwana's amalgamation. We place the subduction zone close to Borborema due to the stronger evidence of earlier subduction preserved here and slightly more distal from Hoggar due to the later evidence of subduction. Palaeomagnetic data from Baltica indicate that it lay in polar regions by ca. 870 Ma. Assuming the congruency of Rodinia at this time and to limit plate velocity, we rotate Rodinia from 940 Ma so that by 870 Ma Baltica sits near the geographic south pole (Figs. 4 and 7a) (Walderhaug et al., 1999, 2007). The implication of this is that both the C-SF and the SM portions of crust now occupy equatorial positions, and, given the geometry of Rodinia, subduction is inferred to have encompassed the SM from 940 Ma to accommodate this motion.

North of the SM and separated by an inferred spreading system, the India-South China plate is continuing to move northwards, with the subduction-accretion forming the Yangtze Block and north-western India through this time. Subduction on the other side of India, outboard of the Eastern Ghats, is still interpreted to be ongoing after collision of the Ruker Terrane against the Rayner Province, with granulite facies
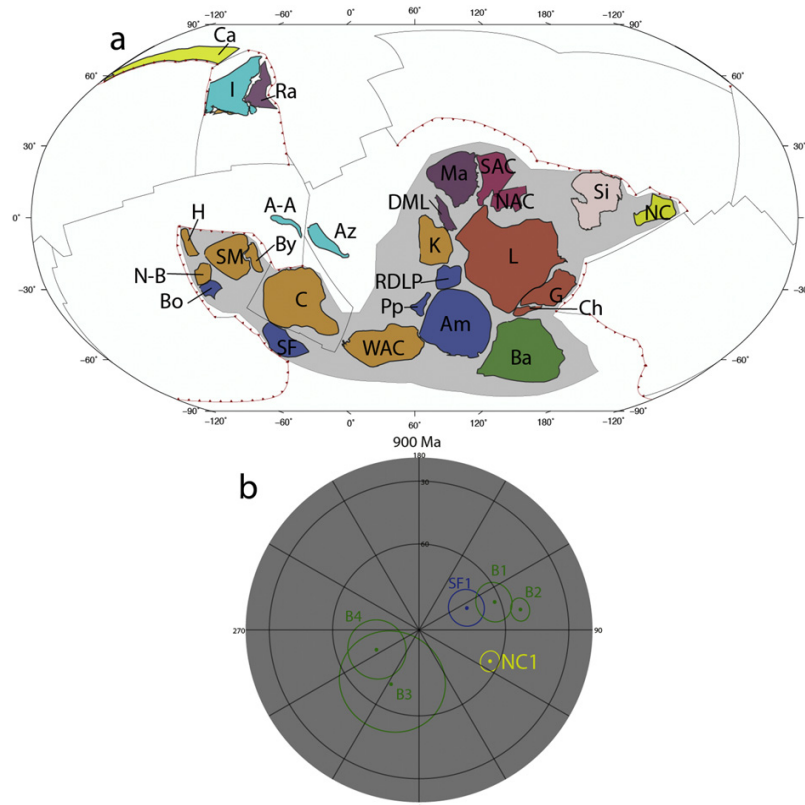

Fig. 7. (a) Tectonic geography at 900 Ma; DML, Dronning Maud Land, for other abbreviations see Fig. 5. (b) Palaeomagnetic poles around 900 Ma.

metamorphism and overprinting preserved (e.g. Gupta, 2012), suggesting that a convergent tectonic regime was still present. This ongoing convergence is a principal reason why we argue that India (and by extension South China) was not part of Rodinia.

7.3. 850–800 Ma, Congo-São Francisco displacement

After the bulk of Rodinia transitioned to higher latitudes, the supercontinent drifted back towards equatorial-mid latitudes by ca. 800 Ma, with Laurentia occupying a low-mid latitude position, and Australia-Antarctica and Siberia lying on the equator (Figs. 4 and 9a). The C-SF plate (along with the SM, ANS and Azania) underwent a relative movement with respect to the rest of Rodinia from a mid to equatorial latitude to fit the reliable ca. 750 Ma Mbozi Complex and Luakela Volcanics A poles (Meert et al., 1995; Wingate et al., 2010). The spreading system associated with this movement forms two passive margins. Firstly, along the (present day) northern, eastern and south-eastern margins of the WAC by 850 Ma, accounting for the ~4 km thick passive margin sequences in the north, and the Gourma Aulacogen towards the south (e.g. Bouougri and Saquaque, 2004; Thomas et al., 2002, 2004). Secondly, the conjugate margin here is preserved on the southern flank of the C-SF Plate with the deposition from ca. 850 Ma of the Katanga Supergroup (Bull et al., 2011). Earlier rifting here minimises the spreading velocity required to move C-SF and the SM from the pole to the equator to fit the palaeomagnetic data (~7 cm/yr vs. ~14 cm/yr for 850 and 800 Ma rifting respectively).

To accommodate spreading on the southern side of C-SF, subduction initiates on the northern margin. There is some evidence of intra-oceanic subduction preserved in the oldest rocks of the Western Ethiopian Shield (WES), indicating pulses of magmatism from ca. 850 to 820 Ma (Ayalew and Peccerillo, 1998; Blades et al., 2015), although the precise spatial relationship of the WES to both the SM and ANS prior to the East African Orogeny is still uncertain. Minor arc accretion was occurring in the ANS (e.g. Johnson and Woldehaimanot, 2003; Johnson et al., 2011), although subduction in Azania corresponding with the formation of the extensive Imorona-Itsindro suite from ca. 850 Ma is suggested to be the primary driver of pulling C-SF northwards (Handke et al., 1999; Archibald et al., 2016, in press). Due to the scope of this study, we simplify the accretion of the terranes in the ANS to an extensive subduction zone, since spreading was likely small scale and preserved in back-arc basins while the dominant tectonic regime, suggested through the synthesis of broadscale geological evidence and palaeomagnetic data (assuming a fixed SM-C-SF Plate), is subduction. We propose that future work and regional studies can focus on building a consistent plate model of the different terranes in the area that can be integrated into this larger global model and note that more palaeomagnetic data are needed to better constrain rifting time and the motion of C-SF.

India and South China were located at polar latitudes (on the 'north' pole) by 850 Ma (Figs. 4, 7), and subduction in the Eastern Ghats had ceased, although there was still some minor tectonic activity occurring. The motion of the Indian and South China Plate during the late Tonian reached its zenith at 820 Ma with South China sitting on the pole. After this time, India and South China begin their southward drift towards Gondwana. Geologically, the Yangtze and north-western India were fully assembled, and subduction is inferred to have entered a hiatus between 850 and 800 Ma when magmatism along the southern margin of India (Tucker et al., 2001), in the Seychelles (Sato et al., 2010) and on the (present-day) northern margin of the Yangtze Craton (Yan et al., 2004; Zhou et al., 2002) started again.

7.4. 800–750 Ma, Rodinia breakup initiates

The first stage of Rodinia breakup began around ca. 800 Ma, with the opening of the Proto-Pacific Ocean between Australia-Antarctica-Tarim and Laurentia, which had returned to an equatorial-low latitude

position, with Baltica-Amazonia-WAC located in mid latitudes further south (Figs. 4 and 9a). The spreading system separating Laurentia and Australia likely extended further north, and is inferred to be the spreading ridge associated with Siberia's dextral movement against Laurentia between 800 and 700 Ma (Pisarevsky et al., 2013). The accommodation of the motion of the Australian Plate away from Laurentia is by inferred subduction outboard of Australia and Antarctica. Assuming a close spatial relationship between Tarim and Australia, the change to retreating subduction preserved in the western Kuruktag area of Tarim (Ge et al., 2014) suggests that the Australian Plate was the overriding one.

The absence of preserved early Cryogenian arcs in Australia could be accounted for by placing the Lhasa terrane against the west coast of Australia as it records Tonian and Cryogenian aged magmatism (Guynn et al., 2006; Qi et al., 2012; Zhang et al., 2012a,b, 2014). In Antarctica, snow and ice cover the suture between Mawson and the other Precambrian constituents of Antarctica, but a prediction of this model is that a series of 800–700 Ma arc related rocks exist, separated by N-S sutures between the parts of Antarctica associated with the Mawson craton and Neoproterozoic India (e.g. Chron Craton of Boger, 2011).

Siberia's motion is accommodated by a cessation of subduction along Greenland (the Valhalla Orogeny), with the main subduction of oceanic crust between Siberia and Baltica occurring outboard of Baltica, although the presence of this arc is unknown. The (present day) eastern and southern margins of Laurentia remained mostly intact during this time, although separation due to small scale spreading of WAC and Amazonia is inferred from the presence of a ca. 757 Ma ophiolite preserved in the Araguaia Belt between Amazonia and the WAC (Paixão et al., 2008). Kalahari remained attached to Laurentia, and its relationship with the Australian Plate is along a transform fault, based on Cryogenian palaeomagnetic data from Australia that show it remained in low-mid latitudes (Fig. 4). This boundary accounts for the absence of passive margin sedimentation along the (present-day) eastern margin of the Kalahari Craton. During this time, subduction in the ANS was (present-day) N-S aligned with the amalgamation of the western oceanic domain by ca. 750 Ma, inboard of the Afif-Abas Block.

India and South China were located at mid-high latitudes at 800 Ma and palaeomagnetic data suggests that they underwent a ~35° counterclockwise rotation by 720 Ma. Subduction had ceased on the (present-day) eastern margin of India, although the western margin records magmatism in the Seychelles and the Malani Igneous Suite (e.g. Tucker et al., 2001) until ca. 750 Ma, and along the Yangtze Craton, but not on the north-western margin of India, hence the two subduction zones are offset by a small transform fault. The preservation of an ophiolite in the Manumedu Complex of southern India indicates that subduction extended to the southern margin of India and is interpreted here as the initiation of the closure of the Mozambique Ocean and the onset of Gondwana amalgamation. The breakup of Rodinia and onset of southerly growth, motion and subduction of India is inferred to alter the paradigm of seafloor spreading in the Mirovoi Ocean (analogous to how Pangaea breakup changed Panthalassa spreading?), and the triple junction that existed until now in the Mirovoi Ocean is replaced a by a single ridge system.

7.5. 750–700 Ma, Congo-São Francisco rifting

By 750 Ma C-SF is located adjacent to the Kalahari Craton in a position similar to Li et al. (2008) to fit palaeomagnetic data (Figs 4, 10a and b). The Proto-Pacific spreading system separating the Australian Plate from Rodinia extended further southwards, breaking C-SF from the Kalahari. We posit that this is plausible as Australia is inferred to have 'unzipped' from Laurentia from the north towards the south in order to maintain a low latitude position and to necessitate the 'fan-like collapse' of Rodinia during the transition to Gondwana (Hoffman, 1991). The southerly extent of this unzipping is the equatorial and most distant craton from the Rodinian core, C-SF. The extension of the spreading ridge would most likely occur on a pre-existing zone of

weakness, in this case the transform fault that separated the C-SF plate from Kalahari. From 750 Ma, the combined C-SF and SM plate is almost completely surrounded by subduction, with only the (present-day) southern margin of the Congo Craton preserving a passive margin (e.g. McGee et al., 2012a). There is evidence of subduction preserved in the northern ANS with the final suturing of the central and western terranes. Assuming a close spatial relationship between the ANS and SM, we continue this subduction zone outboard of the SM (early development of peri-Gondwanan terranes?) and into Hoggar, where the (oblique) subduction and accretion of the LATEA and Iskel terranes were taking place (Caby, 2003; Liégeois et al., 2003). Subduction outboard of the (present day) northern SM margin is inferred, partly to accommodate C-SF spreading from Rodinia, and partly to link the subduction on each side of its margin. Similar to our simplification of the early tectonism in the ANS as a primarily convergent regime, we depict the assembly of Hoggar and LATEA as a convergence dominated tectonic regime with the expectation that future iterations of the reconstruction can more closely model the terrane amalgamation.

The Australian plate continued to grow from the spreading centre between it and Laurentia. At the same time, the Mawson Sea (between India and Australia-Antarctica) shrunk. India and South China remained at similar latitudes as their 35° counter-clockwise rotation finished by ca. 720 Ma, with subduction ceasing on its northern margin along the Yangtze, and occurring solely on its southern margin (e.g. Collins et al., 2014; Yellappa et al., 2010).

On the eastern margin of Rodinia, Amazonia-Baltica-Laurentia continued to remain stable, with the proto-Avalonian and Cadomian arcs developing outboard of West Africa and Baltica. Sedimentation outboard of Greenland continued (e.g. Malone et al., 2014), and also outboard of the Timan margin of Baltica (e.g. Siedlecka et al., 2004) during the Cryogenian, indicating that there was no arc-continent collision here at this time. We follow the depiction of Malone et al. (2014) by extending the Valhalla Orogeny outboard of this margin, allowing for a thick passive margin, while preserving the cirucm-Rodinia subduction system. The remaining portion of Rodinia finishes a (subtle) 20° clockwise rotation to better fit the Franklin Dyke Swarm's palaeomagnetic pole at ca. 720 Ma, with West Africa occupying a polar latitude, and Amazonia and Baltica in mid latitudes (Figs. 4 and 11a).

7.6. 700–600 Ma, Kalahari rifting

Rodinia remains in a similar position, with Laurentia in equatorial-low latitudes, Baltica-Amazonia in mid latitudes and West Africa in high latitudes (Fig. 4). Rifting between the Kalahari Craton and Laurentia occurred at 700 Ma, although this is not constrained palaeomagnetically, and poorly constrained geologically, such that rifting time anywhere from 725 to 675 Ma is acceptable. We opted for 700 Ma for three reasons; firstly, the earliest evidence of subduction in the Damara-Lufilian-Zambezi Belt is ca. 675 Ma (John et al., 2004a). Secondly, assuming a Neoproterozoic connection between Kalahari and Laurentia, later rifting (post 650 Ma) of Kalahari is problematic, as Rodinia begins a clockwise rotation to fit 615 Ma palaeomagnetic data (Long Range and Egersund Dykes from Laurentia and Baltica respectively), which moves the (present-day) southern margin of Laurentia away from Gondwana. If Kalahari remains attached in its 'usual' position, then the ocean basin requiring closure becomes incredibly large (~9000 km) and narrow, due to the proximity of Australia-Antarctica, something we consider unlikely given the distribution of plate boundaries at this time. Finally, as Australia-Antarctica occupy a similar relative palaeolongitude (based on spreading rates) and since the trajectory of Australia-Antarctica spreading must change in order for it fit Ediacaran palaeomagnetic data, we infer a ridge jump for Australia, with the new orientation of the spreading ridge matching the inferred rifting trajectory of Kalahari off Laurentia. Following the unzipping of the supercontinent, we infer that the extension of this rift to the south continued along the RDLP and Amazonian margin of Rodinia, possibly rifting off other micro-

blocks or terranes from Rodinia and transferring them to the C-SF. We currently infer that the Paranapanema Block to be one of these, based on the collisional orogenies that ring it (e.g. Riberia belt against São Francisco Craton, Brasília Belt against Amazonia), suggesting that it was, for a time in the Neoproterozoic, unconnected to the larger South American cratons that are presently juxtaposed against it.

The C-SF and SM plate is surrounded by subduction by 680 Ma. As mentioned above, the earliest evidence for subduction in the Damara-Lufilian-Zambezi Belt between Congo and Kalahari is preserved in eclogitic oceanic crust in the Zambezi Belt, dated to between 675 and 590 Ma (John et al., 2003, 2004a). Subduction along the southern margin of São Francisco is preserved in the Ribeira Belt, inferred here to represent collision of the Paraná Block with São Francisco by 630 Ma. The collision of the Coastal Terrane from 650 Ma in the Kaoko Belt, outboard of Congo, is synchronous with the collision of the Oriental Terrane slightly further north in the Ribeira Belt, outboard of São Francisco. The tectonic evolution of the Dom Feliciano Belt, which preserves long lived subduction from the Cryogenian through to the Cambrian, is more difficult to untangle in a global context and would likely benefit from a more detailed regional model. Two key issues are where the Dom Feliciano Belt developed (adjacent to the RDLP or as small continental terranes in an open ocean) and how the belt preserves sinistral deformation given that the overwhelming regime of transition from eastern Rodinia to western Gondwana is dextral (e.g. Transbrasiliano lineament). If it developed purely on the margin, or slightly outboard, of the RDLP (where it is preserved) the traditional position of RDLP in Rodinia (e.g. Gaucher et al., 2011) would not be valid as it is surrounded by other portions of cratonic crust until the opening of the Iapetus Ocean, and experienced extension rather than convergence at this time. Alternatively, having the RDLP as a 'separate' cratonic element to Rodinia is problematic in a plate-modelling scenario as there are no palaeomagnetic data to constrain its position, and so it would become essentially a 'ghost' craton somewhere in an ocean. A third option is to have the Dom Feliciano Belt evolve in a position completely removed from RDLP, and their close spatial relationship be a consequence of late Ediacaran-early Cambrian tectonics that juxtaposed them (e.g. Rapela et al., 2011). We opt to leave RDLP as part of Rodinia and have the Dom Feliciano Belt evolve outboard within the Adamastor Ocean until 600 Ma, perhaps as a consequence of rifting between C-SF-Kalahari at 750 Ma, and perhaps acting as the (most) southerly extension of the Kaoka and Ribeira belts from 700 Ma. Here the exotic (to RDLP) Nico Perez Terrane was perhaps a micro-continental slither that rifted off Rodinia and became the locus for subduction. If so, it could be tectonically related to both the Coastal and Oriental terranes further north. Rapela et al. (2011) showed that most of the sinistral transpression deformation occurred post 600 Ma, and inferred the ca. 540 to 520 Ma RDLP collision with Kalahari to be the driver of this deformation. This is somewhat problematic, given RDLP's position in Rodinia, since it should be approaching from the (present day) south, along a similar path to the Kalahari Craton, and not sliding from the north (as if it were adjacent to C-SF). Instead, we suggest that the sinistral deformation evident here is driven by closure of the Araçuaí Ocean between Paraná-São Francisco and Congo that closed mostly between 600 and 570 Ma, leading to tectonic escape towards the south.

Subduction on the western margin of São Francisco in the Brasília Belt was underway with the development of the Goiás magmatic arc and accretion of the Goiás Massif. The relationship of the Goiás Arc and massif to the broader palaeogeography beyond their suturing to São Francisco is unknown. Palaeomagnetic data between 750 and 720 Ma place Amazonia (palaeomagnetic constraints from Franklin-Natkusiak in Laurentia) and C-SF (Mbozi Complex) orthogonal to one another and separated by ~30° of latitude. By ca. 650 Ma with the C-SF rifting from the southern margin of Rodinia, even assuming slow spreading (20 mm/yr), a ~2000 km ocean basin would separate the two. Furthermore, the separation of the Brasília Belt and younger Araguaia and Paraguay belts by the Transbrasiliano Lineament, suggests

that the late Cryogenian-Ediacaran development of the Brasília Belt was probably unrelated to events occurring on the margin of Rodinia during this time, and that the Goiás Arc and massif evolved away from Amazonia. Assuming a (relatively) close and fixed spatial position between the C-SF and the SM-Borborema-Hoggar cratons, the juvenile, oceanic Goiás magmatic arc, and Archaean Goiás Massif would act as a southerly extension of the magmatism and accretion of terranes in the Hoggar Shield. Here also, juvenile arc development is associated with accretion of older thin slithers of Archaean and Palaeopoterozoic terranes (e.g. Caby, 2003; Liégeois et al., 2003). We (tentatively) propose a correlation between the westerly growth of the two areas. We infer that this subduction is preserved in between these areas along the margin of Borborema, where arc-related granitoids are preserved from 670 Ma, and detrital zircons with an age range of 780 to 617 Ma and a peak at ca. 690 Ma suggest that subduction could be traced back to the early Cryogenian (Ganade de Araujo et al., 2016). We depict some transform motion (i.e. Transbrasiliano Belt) between the growing Gondwana and dwindling Rodinia from 650 Ma due to the clockwise rotation of Rodinia to fit palaeomagnetic data. The 650 Ma Bassaride Belt on the (present-day) southwestern margin of the WAC formed with the closure of the narrow ocean basin between it and Amazonia.

Closure of the Mozambique Ocean under Azania and the ANS, and closure of the Neomozambique Ocean, under Congo and SM, were occurring, with India and South China being pulled south. Subduction outboard of Australia, and closure of the Mawson Sea is inferred to have ceased by 670 Ma due to proximity, without collision, between Australia and India. From ca. 650 Ma India begins sliding past Australia along the sinistral Darling Fault (Collins, 2003; Fitzsimons, 2003), and we rotate Australia counter-clockwise to help this motion and also to maintain its low latitude and to match its APWP during the Ediacaran, which

concludes with the ca. 570 Ma Wonoka Pole and suggests an almost 180° rotation from its position in Rodinia. The inferred mid ocean ridge that, in part, drives the rotation of Rodinia is extended through to Australia (Fig. 12). In the east, it creates some small-scale displacement, (perhaps accounting for sedimentation on the eastern margin of Australia) and is offset via a transform fault from here, northwards, to between cratonic Australia (+Lhasa?) and Tarim. This spreading forces the 40° intraplate rotation of Li and Evans (2011) of the NAC to the SAC and forms the Petermann and Paterson Orogenies (Bagas, 2004; Raimondo et al., 2010) and also causes the rifting of Tarim away from Australia by Cambrian times.

Juvenile arcs in the Avalonian and Cadomian terranes formed then slowly moved towards Baltica, West Africa and Amazonia. Avalonia collided with Amazonia by 650 Ma, as exhibited by the timing of peak metamorphism. Subduction remained ongoing after this collision, likely stepping away from the suture zone to form a continental margin. Cadomia is less well known, but a similar event is inferred (Garfunkel, 2015; Murphy et al., 2013; Nance et al., 2008). There is some minor, small-scale separation and rotation between Baltica and Amazonia between 615 and 600 Ma, although the Iapetus Ocean remained closed during this time. On the other side of Laurentia, rifting of Siberia and North China away from Rodinia started. There was a large counter-clockwise rotation of Siberia to fit Ediacaran- to Cambrian-aged palaeomagnetic data (Pisarevsky et al., 1997), necessitating large sinistral faults against northern Laurentia. This was driven, in part, by spreading between Siberia and an unknown craton, inferred here to be North China, as Baltica remained attached to Laurentia. However, North China is inferred out of convention and tradition rather than from data, since there are no palaeomagnetic constraints on it for this time. In the Cryogenian, subduction outboard of the Siberian margins
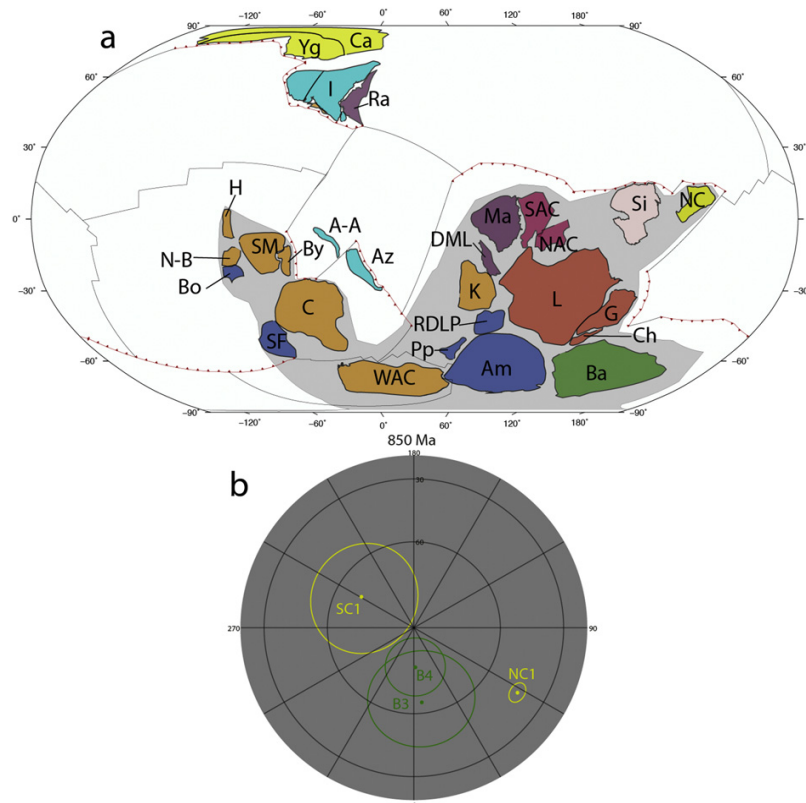

Fig. 8. (a) Tectonic geography at 850 Ma; Yg, Yangtze Craton (South China), for other abbreviations see Figs. 5 and 6. (b) Palaeomagnetic poles around 850 Ma.

(e.g. Yenesei Ridge) occurred, with the accretion of a series of terranes (e.g. Kara, Angara; Metelkin et al., 2012, Vernikovsky et al., 2004) that continued from this time right up to the Cambrian.

7.7. 600–520 Ma, opening of Iapetus Ocean and Gondwana amalgamation

By 600 Ma, most of the subduction zones that facilitated Gondwana amalgamation had formed. However, the opening of the Iapetus and the motion of Amazonia and the WAC into the C-SF and the SM drove the youngest Gondwana-forming orogenies (Figs. 13 and 14). The eastern Iapetus (between Baltica and Laurentia) opened first at ca. 600 Ma, with small degrees of extension between Amazonia and Baltica. The western arm of Iapetus, between Amazonia and Laurentia, began rifting at 590 Ma. In the WAC, the extensive oceanic crust that developed outboard of its Tonian-Cryogenian passive margin acted as a strong pulling force as it subducted, dragging it towards the SM and closing the Pharusian Ocean. Here subduction dipped away from WAC, beneath the growing Gondwana, and transpressive tectonics and oblique convergence are inferred to have occurred between 610 and 580 Ma in both the Dahomeyide and Pharuside belts (e.g. Caby, 2003; Paquette et al., 1998; Berger et al., 2014). Some minor motion between Amazonia and WAC is invoked to shift the WAC from its suture against Amazonia preserved in the Bassaride Belt, to the more southerly 550 Ma Rokelide Belt. The Araguaia and Paraguay belts, along the present day eastern margin of Amazonia, were also active during this time. The (present-day) northerly movement of the WAC and Amazonia into Gondwana is here used to account for the stronger deformation and higher metamorphic grade preserved in the Araguaia Belt than is seen in the Paraguay Belt, as it was on the leading edge of the plate when it collided with C-SF. The Paraguay Belt only preserves greenschist facies

metamorphism (Pimentel et al., 1996), which is explained by its location on a trailing or peripheral margin of the plate. The poorly dated rift-drift transition that is preserved in the Paraguay Belt could represent a motion of RDLP away from Amazonia (as RDLP sits adjacent to the location of the Paraguay belt in Rodinia), and the late deformation (550–520 Ma) here could be a response to the collision of RDLP with the rest of Gondwana and closure of the Adamastor Ocean along the 550–540 Gariep belt (e.g. Frimmel and Frank, 1998). The Araguaia Belt, which preserves a ca. 750 Ma ophiolite, records a slightly longer history of sedimentation and deformation than the Paraguay Belt, and the timing of collision here, at 550 Ma, is inferred to represent the primary suture between the two largest cratonic crust components of Gondwana (C-SF and Amazonia-WAC). The dextral Transbrasiliano Lineament is the structural boundary that separates the two sections of crust (Figs. 11 and 12). We acknowledge that the notion of a long (~6000 km!) strike-slip fault is problematic, although it accounts quite well for the relative motion between Laurentia-Amazonia-WAC and Gondwana during the Ediacaran, both during the subtle clockwise rotation of Rodinia to fit 615 Ma palaeomagnetic data, and in juxtaposing Amazonia-WAC in their Gondwana configuration from an equatorial Laurentia. It is our expectation that the lineament probably espouses some component of oblique subduction, and that a more realistic interpretation would be a series of small transform faults linking and offsetting oblique subduction in the Paraguay, Araguaia and Brasília belts, and perhaps the Dom Feliciano and Dahomeyide belts. Such a scenario would benefit from further untangling the spatial and temporal relationships of the small exotic terranes caught up in the orogenies along the margins of the (present day) African cratons (e.g. Coastal, Oriental, Nico Perez terranes) to create a more nuanced model for the amalgamation of western Gondwana. Further east, closure of the Khomas Ocean
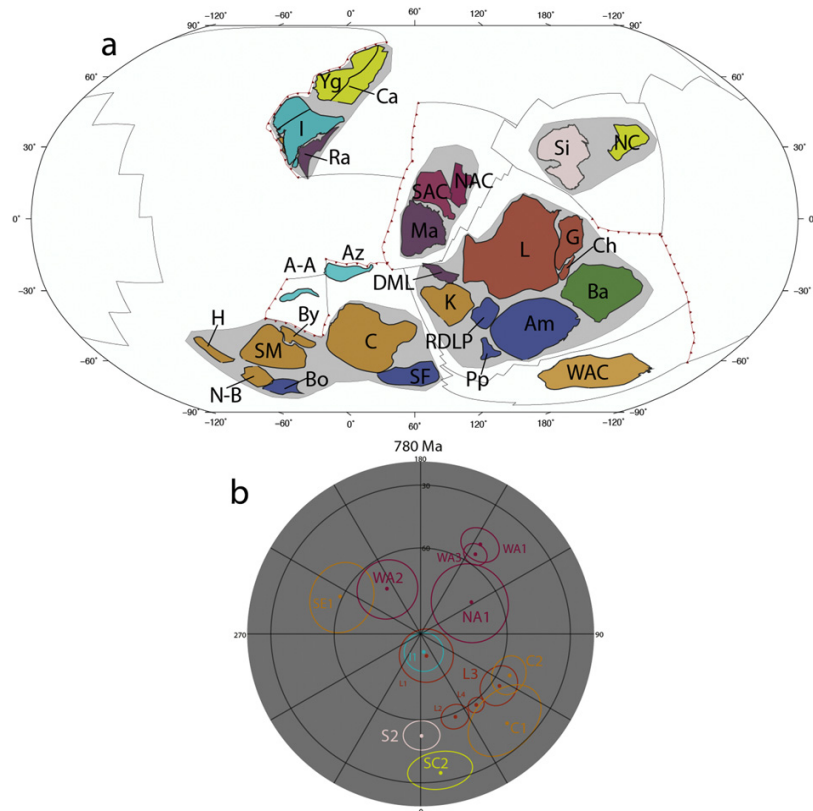

Fig. 9. (a) Tectonic geography at 780 Ma, see Figs. 5, 6 and 7 for abbreviations. (b) Palaeomagnetic poles around 780 Ma.

between Congo and Kalahari was completed by 550 Ma with the development of the Damara-Lufilian-Zambezi Orogeny, although some later transpressive deformation may have occurred with the collision of RDLP along the Mwembeshi Shear Zone (e.g. Naydenov et al., 2014).

The relationship and suture between Australia-Antarctica and Dronning Maud Land (attached to Kalahari) is unknown due to ice cover. However, from permissible positions of each craton from palaeomagnetic data (e.g. Wonoka Pole, mean Gondwana APWP), indicate that the motion would be along a transform fault as their latitudes prior to collision preserved in the Pinjarra Orogeny are similar to their Gondwana fit (Fig. 4). The enigmatic Coats Land Block and Crohn Craton of Boger (2011) could perhaps record some of this deformation and collision, although otherwise the suturing of Australia-Antarctica to Gondwana at 520 Ma marks the final major Gondwana building orogen (Fig. 14). Further north in Australia, the intraplate rotation of the NAC into the SAC finishes by 550 Ma, a similar time to the closure of the Neomozambique and Mozambique oceans between Azania and Congo, and India and Azania, respectively. Further north (present day), the ANS finished assembly by 550 Ma and is accreted onto the SM. Outboard on the (present-day) northern margin of the SM, WAC and Amazonia the peri-Gondwanian terranes are developing (e.g. Avalonia and Cadomia, Armorica, Florida, Iberia etc.).

Finally, the kinematic evolution of the non-Gondwanan constituents (Laurentia, Siberia and Baltica) suffers from two key problems. Firstly, the current 'Ediacaran nightmare' (cf. Meert, 2014b) of palaeomagnetic data from both areas makes it difficult to reliably trace the latitudinal wandering of these continents. Secondly, a lack of continent-continent collisions during the Ediacaran and early Cambrian makes it difficult to pin them to a tectonic environment or to another continent (especially Baltica and Siberia). Thus, the motion of Baltica, post Iapetus opening,

is problematic and forms one of the most poorly constrained motions of any major continent in the model. An appropriate solution is probably to look at the post-Iapetus opening evolution of Baltica as a single entity. Here we have its motion between 550 and 520 Ma depicted to connect to its 500 Ma position described in Domeier (2016). Baltica rifts off from Laurentia at mid-high latitude and moves towards an equatorial position, to fit high quality ca. 550 Ma palaeomagnetic data (e.g. Lubnina et al., 2014), in close proximity to Siberia. We infer two drivers for this motion, firstly subduction in the Timan area of Baltica acts as the leading edge, with slab roll-back pulling Baltica northwards. Secondly, the opening of the ocean between Gondwana and Baltica (orthogonal to the Iapetus Ocean) is inferred to exert more pushing force on Baltica than the rift between Baltica and Laurentia, leading to a northerly motion of Baltica. Nonetheless, this position is puzzling, as with two large continents (Baltica and Siberia) so close to one another, we would expect an eventual collision. By 550 Ma Siberia is finishing its large rotation to fit the palaeomagnetic pole from the Kesyussa Formation (Pisarevsky et al., 1997). From this point we infer a spreading system opening between Siberia and Laurentia to begin pushing Siberia further east to collide with Chinese blocks that rift from Gondwana during the Palaeozoic (e.g. Domeier and Torsvik, 2014). This re-organisation and spreading ridge is (loosely) inferred to act as a driver to push Baltica away from both Siberia and Laurentia and back towards high latitude and its 500 Ma position.

8. Discussion

Below we briefly summarise some characteristics of the plate model that have relevance to geodynamic understanding of plate tectonics in the Neoproterozoic. Complete topological plate reconstructions can be
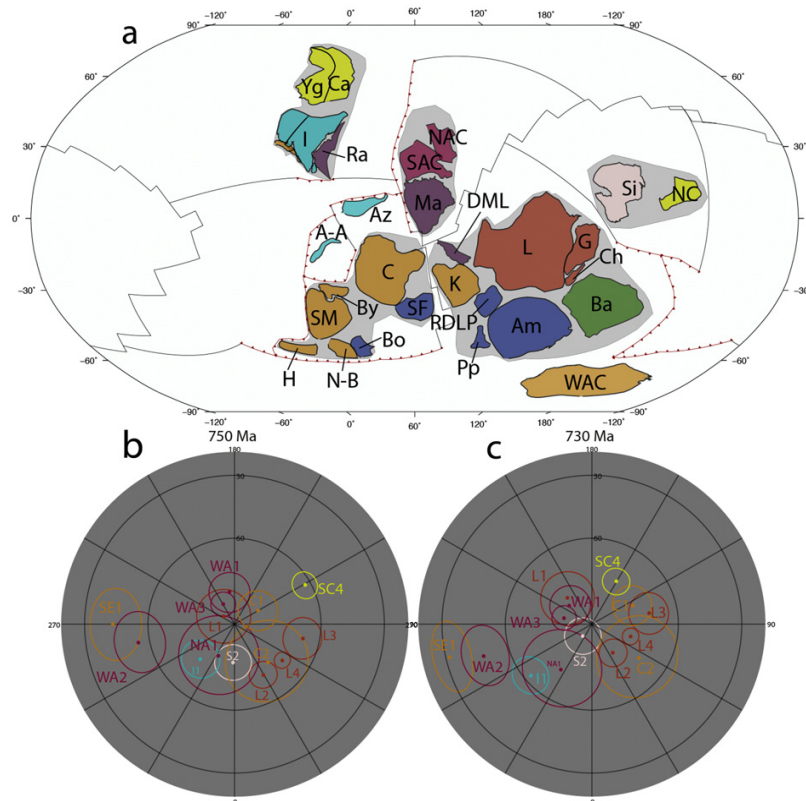

Fig. 10. (a) Tectonic geography at 750 Ma, see Figs. 5, 6 and 7 for abbreviations. (b) Palaeomagnetic poles around 750 Ma and (c) palaeomagnetic poles around 730 Ma.

used to compute a number of characteristics that describe the behaviour of plates and plate boundaries and these quantities for our Proterozoic reconstruction can be compared to models both for the Phanerozoic and for the present-day Earth. We divide the characteristics into two classes; those based on plate geometries, and those based on plate kinematics, the latter being more directly dependent on the motions of the continents. As shown by Domeier and Torsvik (2014), True Polar Wander (TPW) corrections will affect computed plate velocities, and our results here do not consider TPW effects. Considering the large overall uncertainties and that oceanic plates and mid-ocean ridges are artificial and inferred rather than observed, the plate model characteristics must be treated with a high level of caution. We thus offer the comments below as a way of comparison with Phanerozoic reconstructions (e.g. Domeier and Torsvik, 2014; Matthews et al., 2016), with the aim of illustrating the degree to which our reconstructions share similar characteristics, as well highlighting areas of future improvement. We extract velocity values only from cratonic crust and not from full topological plates due to the uncertainty surrounding pre-Pangaea oceanic domains, as well as absence of hard evidence of plate boundaries in the oceanic domain.

8.1. Plate geometries

8.1.1. Number and size of plates

The total number of plates modelled in the Neoproterozoic varies from six to twenty, with a smaller number of plates more common in the early Neoproterozoic, and a higher number more prevalent just prior to Gondwana amalgamation (Fig. 15a). The least number of plates occurs in the intervals 860 and 850 Ma and 820 and 800 Ma, both times during the life span of Rodinia. The largest number of plates occur in the

transition between the two supercontinents (ca. 600 to 580 Ma). While this represents fewer plates than were modelled for the Palaeozoic (e.g. Domeier and Torsvik, 2014) and for the Cenozoic and Mesozoic (Mallard et al., 2016; Matthews et al., 2016; Morra et al., 2013, Fig. 15b), the change in number of plates associated with the supercontinent cycle is broadly similar. Unsurprisingly, the number of plates is lowest during times of supercontinent existence, (e.g. 1000–800 Ma and 560–520 Ma), while during dispersal and assembly the number is typically higher. Matthews et al. (2016) suggested that missing plates could be accounted for, in part, by the lack of regional analyses some areas receive, such that the evolution of back-arc basins and areas of regional accretion could account for a subset of missing plates. The model presented here is a simplification that excludes smaller micro-plate accretion and instead focusses on the major constituents of continental crust to produce a global model, within which, regional improvements can be anchored (and, ideally, improve the global model). Specifically, a number of tectonically complex areas that are likely made up of small plates were simplified (e.g. Hoggar Shield, ANS, Kara and Angara microterranes, Lhasa, Indochina). More complex tectonics in most, if not all, of these areas likely occurred through the entire supercontinent cycle (e.g. Caby, 2003; Fritz et al., 2013; Johnson et al., 2011, Metelkin et al., 2012; Vernikovsky et al., 2016; Robinson et al., 2014).

The comparison of plate size, and the relationship between this and the number of plates, is slightly more nuanced and informative about shortcomings in the model. The size of the largest plate during the Neoproterozoic is slightly larger than that seen during the past 200 Ma (e.g. Morra et al., 2013). From here, however, plate size decreases more rapidly than that predicted during younger times, and the trend identified by both Morra et al. (2013) and Matthews et al. (2016) of ~8 large plates, with the rest being of considerably smaller
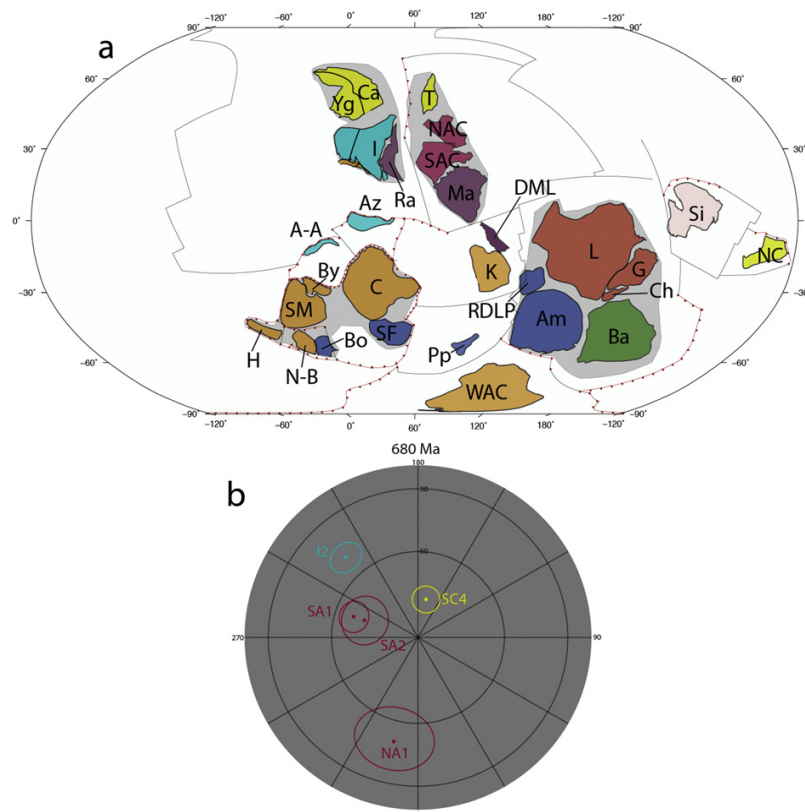

Fig. 11. (a) Tectonic geography at 680 Ma; T, Tarim, for other abbreviations see Figs. 5, 6 and 7. (b) Palaeomagnetic poles around 680 Ma.
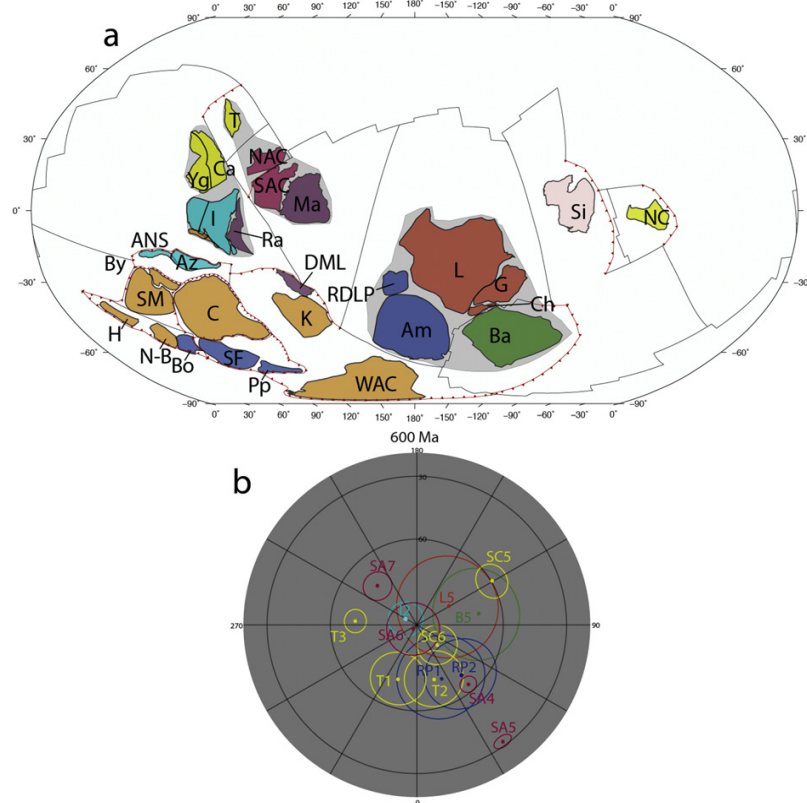
Fig. 12. (a) Tectonic geography at 600 Ma, see Figs. 5, 6, 7 and 10 for abbreviations. (b) Palaeomagnetic poles around 600 Ma.

size, is not observed here (i.e. there is no inflexion point after eight plates). For earlier times (1000–800 Ma) the inflexion point leading to a notable decrease in plate size occurs after the largest four plates. Comparably, in younger times (e.g. 700–520 Ma) the inflexion does not occur until the ultimate or penultimate smallest plate (i.e. there is a linear trend of cumulative plate count vs. plate size). We also find a similar trend with homogenous vs. heterogeneous tessellation of plates during the Neoproterozoic (Fig. 15c). Morra et al. (2013) proposed that immediately after supercontinent breakup the global system developed towards a homogenous organisation of plates, where the large plates were all of a similar size (i.e. a low standard deviation of plate size amongst the largest eight plates). This relaxes over 50–100 Myr to a heterogeneous distribution of plates with a high standard deviation more commonly associated with a growing supercontinent (i.e. one large plate). This is analogous to supercontinent breakup modelled here, as we 'unzip Rodinia' from the outside. Here, as one large supercontinent consisting of >80% of the available continental crust (heterogeneous tessellation) broke-up, smaller continental fragments rifted off incrementally at similar times from the outside (i.e. Australia first, then C-SF, then Kalahari), leading to a homogenous distribution of large plate sizes. Early in this process the bulk of the supercontinent remains (e.g. Fig. 9, Australia and Siberia have rifted off, but the rest of Rodinia is intact). Hence, the remaining supercontinent then still forms a large plate. As rifting and break-up continues, the size of the remnant supercontinent diminishes, and is taken up by other plates that continue rifting. For example, at 680 Ma (Fig. 11), Australia, C-SF, Kalahari, Siberia all occupy their own plates, and the remnant Rodinia is much smaller, now consisting only of Baltica, Laurentia and Amazonia, leading to plate sizes that are more similar.

The plate size and number of plates are inherently linked. We expect our oversimplified model to underestimate the number of plates, and that in more detailed future analyses the number of small plates in such a model will increase. Mallard et al. (2016), demonstrated that ongoing subduction at the margin of larger continental plates is a driver of plate fragmentation. Therefore, we expect that continent-margin subduction would create an ensemble of smaller plates. An example of this in the model may be the large oceanic embayment from 1000 to 850 Ma in Rodinia, just north of the WAC, where it joins the Congo Craton, which is here assigned to Rodinia, but could be subdivided into smaller plates (for example by further extending Azania).

8.1.2. Length of plate boundaries

We extracted the length of plate boundaries throughout the Neoproterozoic (Fig. 16) and compared them with estimates from Phanerozoic reconstructions. We evaluate the total length of subduction zones, and also the combined total length of mid ocean ridge (MOR) and transform boundaries - we refrain from specifically extracting ridge and transform lengths, due to the largely synthetic construction of divergent plate boundaries into ridge and transform segments within pre-Pangaea reconstructions.

The model presented here exhibits, on average, slightly less subduction than is evident at present-day, and ~60% of the total length of present-day MORs and transform boundaries. It is reasonable to consider our computed lengths as conservative estimates, as we do not include regional accretion models that may incorporate a series of back-arc basin opening and closures (e.g. Turaeg Shield, Avalonia, Cadomia, Western Ethiopian Shield, ANS), which account for a small amount of
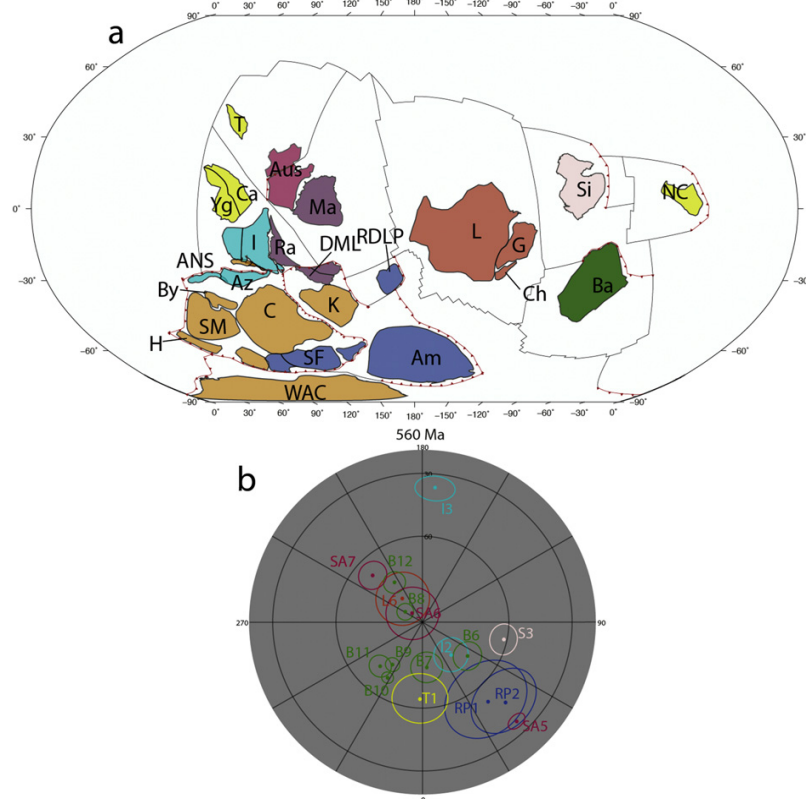
Fig. 13. (a) Tectonic geography at 560 Ma; Aus, Australia, for other abbreviations see Figs. 5, 6, 7 and 10. (b) Palaeomagnetic poles around 560 Ma.

global subduction, and we have little evidence to constrain oceanic-oceanic subduction zones.

The Neoproterozoic model has a similar length of plate boundaries to that of the Palaeozoic, and, in particular, the evolution of MORs and transform boundaries during the Neoproterozoic follows a similar, but slightly more protracted, trend (Fig. 16). There is a gradual increase in the length of MORS and transform boundaries until 600 Ma, reflecting the breakup of Rodinia and culminating with the opening of the Iapetus Ocean and the inversion of the ocean basins between the cratonic constituents of Gondwana (e.g. Fig. 11a), a pattern similar to the Mesozoic increase in total plate boundary length during the breakup of Pangaea and initiation of many new MORs. The peak in the mid Tonian is associated with the motion of the C-SF plate (e.g. Figs. 7a and 8a). The decrease post 600 Ma is due to the amalgamation of Gondwana, and is likely exacerbated by the uncertainty of the evolution of the Panthalassa Ocean, and could be rectified by models of the Early Palaezoic that map the evolution of the Panthalassa Ocean backwards in time from the Late Palaeozoic.

Our length of subduction zones also shows a similar trend to the estimates of continental arc length presented by Cao et al. (2017), although these authors presented their synthesis of geological data using a different reconstruction model (Scotese, 2016). They depict a doubling of arc length from 750 to 550 Ma, where it drops abruptly (associated with collision of India and Africa), before dropping again at 530–520 Ma, associated with the collision of Australia and Gondwana (Figs. 11a, 12a and 16). Cao et al. (2017) record the length of continental arcs during the height of Gondwana building (650–550 Ma) as being roughly equal to the length of continental arcs at the present day. We find a similar relationship for the total subduction zone lengths within our model; from 750 to 550 Ma, the length of subduction zones double,

with total subduction length between 600 and 550 Ma roughly the same length as total subduction at present-day (~55,000 km). Assuming that the proportion of continental vs. oceanic arcs remains stable over time, their measurements are, proportionally, in good agreement with our own.

8.2. Plate kinematics

8.2.1. Latitudinal distribution of subduction

The concept of inertial-interchange true polar wander (IITPW) describes the process where mantle instabilities arising from mass distributions at different latitudes, acting to reduce (or destabilise) the angular velocity of the earth on its spin axis, the outer layers of the earth (crust and mantle) can rotate relative to the spin axis (Evans, 2003; Goldreich and Toomre, 1969). Centrifugal forces due to the rotation of the Earth push positive inertia anomalies to the minimum moment of inertia (around the Equator). Two important processes that redistribute mass within the Earth are subduction, the process of introducing cold, dense material into the mantle, and plume upwellings, the process of pushing hot, buoyant material further away from the centre of the earth (Raub et al., 2007).

Raub et al. (2007) postulated that superplumes (like those arising from the thermal insulation of a supercontinent) would have a stronger effect on IITPW than individual sinking slabs due to the concentration of mass differentials. Hence, high latitudinal superplumes would encourage IITPW; as would extensive low latitude subduction if there was a high latitude positive anomaly as well. Conversely, low latitude superplumes stabilise the moment of inertia, negating IITPW. Critically, the thermal insulation that a supercontinent creates in the mantle (e.g. Ganne et al., 2016) will generate a positive inertia anomaly. Typically,
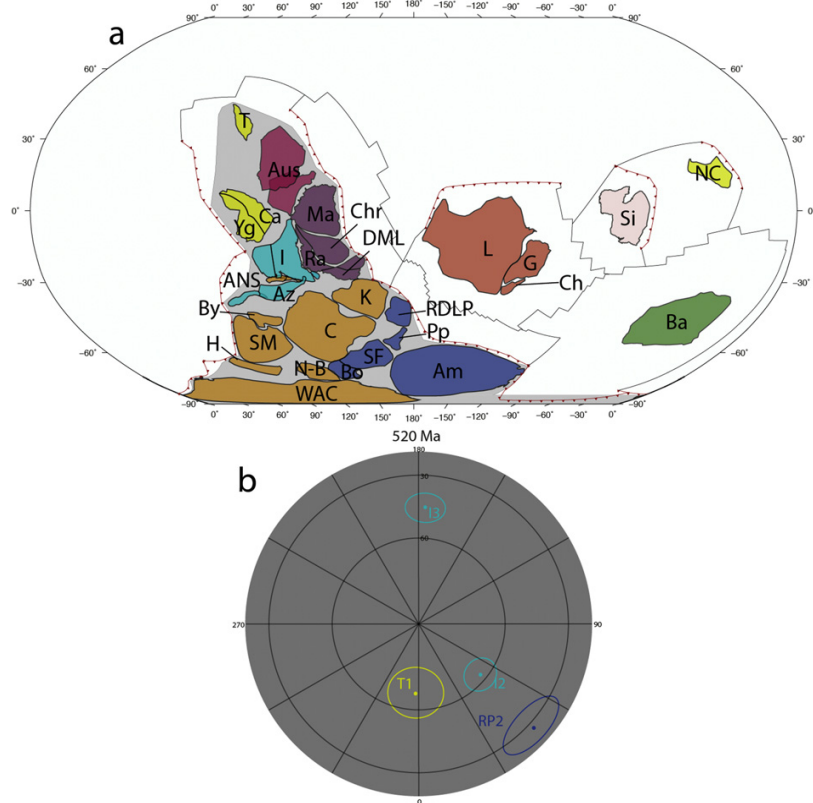
Fig. 14. (a) Tectonic geography at 520 Ma; Chr, Chron Craton, for other abbreviations see Figs. 5, 6, 7, 10 and 12. (b) Palaeomagnetic poles around 520 Ma.

TPW is inferred through measuring abrupt latitudinal changes of palaeomagnetic data within APWPs across the entire globe. Such episodes been interpreted in Phanerozoic times (e.g. Steinberger and Torsvik, 2008; Steinberger et al., 2017) and are suspected during the Neoproterozoic (e.g. Evans, 2003).

Our reconstruction provides an estimate the spatial and temporal distribution of subduction zones, (albeit with the caveats concerning interpolation of plate boundaries outlined previously), which may hold clues to redistributions of mass within the deep Earth and related true polar wander episodes. The latitudinal distribution of subduction zones through the Neoproterozoic is shown in Fig. 17. Low latitude subduction is prevalent throughout the Tonian, evident in the equatorial Valhalla Orogeny and early subduction in Azania and the ANS, and by the mid-latitude accretion of India-South China. In particular, there is a relative dearth of high latitude subduction between 850 and 700 Ma, one of the key times postulated to be affected by IITPW (e.g. Evans, 2003; Li et al., 2004).

Li and Zhong (2009) proposed that a scenario where a supercontinent that is surrounded by a girdle of subduction can generate antipodal superplumes, one of which will form beneath the supercontinent itself. Superplumes forming beneath a supercontinent at high latitudes (e.g. Li et al., 2008) would be more likely to generate episodes of IITPW. Our model omits both South China and India from Rodinia (and thus any requirement to fit Rodinia to palaeomagnetic data from these regions), with the consequence that Rodinia lies at low latitudes throughout the time that any superplume may have developed beneath it. Palaeomagentic constraints on the Congo have been respected by not having Rodinia form until ca. 750 Ma, immediately before it begins to break-up. The geological evidence used to argue for the existence of a superplume in Rodinia between 850 and 750 Ma relate predominantly to dyke swarms throughout Australia, eastern Laurentia and South China, bimodal magmatism in South China and magmatic activity throughout India (Li et al., 2003, 2008). As our model separates India and South China from Rodinia, we suggest that the magmatic record through this period needs to be objectively investigated to ensure that a 'smoking-gun' for the proposed superplume exists. We also suggest that a significant amount of this magmatism should be within the core of Rodinia (east Australia, west Laurentia, south Congo, Kalahari, Rio de la Plata), rather than on the periphery where voluminous subduction-related arc magmatism occurred.

During the Ediacaran, nearly every piece of known continental crust, along with nearly all subduction zones constrained by observations from the geological record, were in the southern hemisphere (e.g. Figs. 13a, 14a and 17). Given the conventional interpretation of palaeomagnetic data and the position of continents, the northern hemisphere of the globe, and particularly the medium-high latitudes, consisted primarily of oceanic plates at this time. While determining the nature of IITPW during this time is elusive, in part, because of discrepancies in palaeomagnetic data (e.g. the 'Ediacaran nightmare' of Baltica and Laurentia; Meert, 2014b, compared to Australia which has a relatively consistent APWP that does not seem to exhibit IITPW; Schmidt, 2014), the shift towards a monohemispheric distribution of continental crust and subduction zones, creates implications for both the mass distribution of the Earth and, consequently, TPW.

8.2.2. Plate velocities

The concept of a 'plate tectonic speed limit' has been proposed for plate motions since the Jurassic (e.g. Zahirovic et al., 2015), although it is less certain whether the same limits apply for earlier times (e.g. Gurnis and Torsvik, 1994; Meert et al., 1993). Limits derived from reconstruction
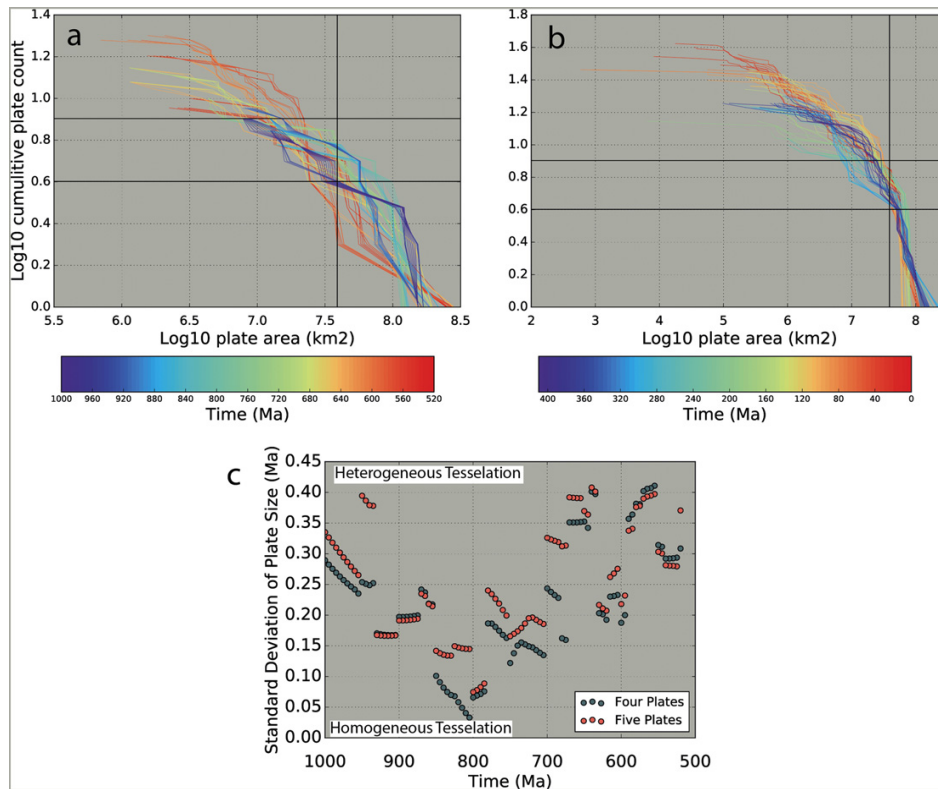
Fig. 15. Log$_{10}$ of plate size vs. log$_{10}$ of cumulative plate count (from largest to smallest) for; (a) Neoproterozoic model presented here; (b) the Late Palaeozoic, Mesozoic and Cenozoic after Matthews et al. (2016); and (c) standard deviation of the largest four and five plates vs. time for the Neoproterozoic model. Straight black lines in (a) and (b) represent markers for log$_{10}$(4) and log$_{10}$(8) (horizontal lines) and the vertical line represents the cut off of area for large vs. small plates after Mallard et al. (2016) (7.59 on the scale). Sizes are extracted at 5 Myr intervals.

models of the Cenozoic and Mesozoic suggest a maximum velocity of ~200 mm/yr for plates consisting of less than 50% continental crust, with cratonic and continental crust typically moving no faster than ~150 mm/yr (Zahirovic et al., 2015). Furthermore, Root-Mean Square (RMS) velocities of plates consisting of >25% cratonic crust are ~28 mm/yr, and plates with any amount of continental crust have a RMS velocities of ~58 mm/yr. Models of the Palaeozoic (Domeier and Torsvik, 2014), Matthews et al. (2016) indicate that the global RMS velocity of continental crust peaked at ~140 mm/yr at ca. 360 Ma, but otherwise averaged around ~100 mm/yr. Fig. 18 depicts the RMS velocities of

continental crust extracted from the model for the Neoproterozoic. The model presented here maintains an average RMS velocity for continental crust of ~37 mm/yr, roughly in line with plate motions over the past 200 Ma.

The lower global RMS velocity that we have extracted from the Neoproterozoic compared to the Palaeozoic may be a consequence of both the fewer amount of palaeomagnetic data available for the Neoproterozoic, as well as a lesser quality of poles from the available poles (e.g. Domeier, 2016; Domeier and Torsvik, 2014, are based on a compilation of Torsvik et al., 2012, consisting of 150 + quality filtered
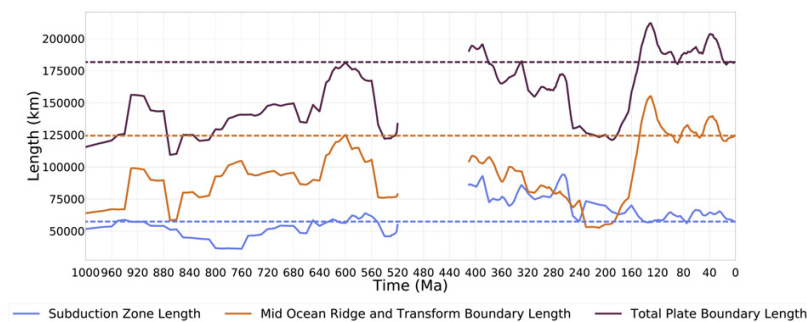

Fig. 16. Length of plate boundaries, extracted at 1 Myr intervals and calculated as 10 Myr rolling average. The present-day length of plate boundaries are plotted as straight dashed lines. Boundary lengths are from the model presented here and the model from Matthews et al. (2016), which is a compilation of the Domeier and Torsvik (2014) and Müller et al. (2016) models.
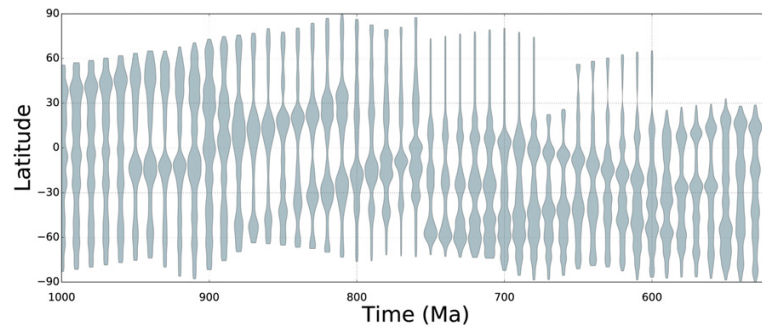
70

Fig. 17. Latitudinal distribution of subduction zones through the Neoproterozoic.

poles, comparatively we use 51). In particular, omitting poles from Baltica and Laurentia in the Late Ediacaran and Cambrian (Section 6.1) simplified the motions of the both plates. A stricter fitting of palaeomagnetic poles here would dramatically increase the distance that each continent moved, increasing their velocity.

Peaks of global RMS velocity occur following the rifting of plates that have a significant constituent of inferred oceanic crust. For example, Australia and Siberia, both moving relative to Laurentia from 800 Ma, have significant lengths of modelled oceanic subduction along their leading edges (as there is no preserved subduction on the appropriate continental margins) (e.g. Figs. 9a and 10a). Similarly, the increase of RMS velocity at 700 Ma is associated with the rifting of Kalahari and the initiation of the closure of the Khomas Ocean, where a tectonic plate with a leading edge of oceanic crust was subducted (e.g. Figs. 11a and 12a). Comparatively, the rifting of C-SF-SM at 750 Ma had limited oceanic crust due to (preserved) subduction on its leading edges (e.g. ANS, SM, Hoggar region, Figs. 10a and 11a), so there is no increase in RMS velocity. The peak at ca. 670 Ma is likely the result of inferred southerly subduction of India and closure of the Mozambique and Neomozambique Ocean (e.g. Fig. 11a), where the lead of the plate also consisted of oceanic crust, perhaps analogous to the closure of the Neo-Tethys in the Cenozoic.

We also extracted the velocity from centroid points of individual cratons (Fig. 19a–e), to more clearly identify phases of rapid continental motion and discuss how well constrained these phases of motion are. Generally, the velocities are less than 80 mm/yr, although there are some exceptions where individual plate velocities extend up to ~120 mm/yr. For example, the Congo Craton (and Borborema, São Francisco, the SM, Hoggar, Nigeria-Benin and Bayuda blocks, which are children of Congo within the plate hierarchy) exhibits a phase of rapid motion between 780 and 750 Ma. Although the velocity is high for such a large plate (~120 mm/yr), the speed is required to satisfy palaeomagnetic data and known geological constraints, though dating on many of the sedimentary sequences is poor (Section 3.5). Shifting the rifting time to before 900 Ma, with a transition to drift by 850 Ma (still permitted by palaeomagnetic data), would reduce the velocity, however, we have opted to constrain the movement to a time coeval with the onset of the Imorona-Itsindro subduction zone outboard of Azania (Handke et al., 1999; Archibald et al., 2016, in press).

Siberia and North China (also linked in the reconstruction hierarchy) record a phase of rapid motion at a similar time (ca. 780 Ma) (Fig. 9a). The rapid Siberia and North China motion (~110 mm/yr) follows their displacement along the (present-day) northern margin of Laurentia as a response to the 800 Ma rifting of Australia from the west coast of Laurentia. This motion is constrained by palaeomagnetic data (e.g. Pisarevsky et al., 2013) suggesting that Siberia was located closer to Laurentia at 760 Ma than in the Tonian (e.g. Figs. 9a and 10a). As with C-SF, earlier rifting of Siberia would reduce the velocity. The location of the Euler Pole for the rifting of Australia from Laurentia, suggests that rifting initiated to the (present-day) north of Australia, closer to

Siberia, and moved south as it progressed (i.e. the fan-like collapse). This phase of rapid motion could be reduced by modelling the opening of the ocean basin between Australia and Laurentia further north (ca. 825 Ma), outboard (and west) of Siberia, then propagated southwards to initiate rifting of Australia from Laurentia by 800 Ma (Fig. 9a).

Rapid phases of motion are modelled for both India-South China-Rayner (100 cm/yr at ca. 650 Ma), and the RDLP (120 mm/yr at ca. 520 Ma), both implied within our model to result from a similar mechanism (Figs. 13a and 14a). In both cases, the cratons are initially separated from a growing supercontinent by an ocean basin; then, subduction initiates around the supercontinent periphery resulting in closure of the ocean basins and pulling the smaller continental blocks towards Gondwana. In both cases, the leading edge of the plate is inferred to consist of a significant area of oceanic crust, similar to the evolution of India in the Cenozoic. This creates a strong pulling force and can explain the faster than expected motions. Finally, Baltica exhibits extremely fast motions in the latest Ediacaran and early Cambrian (Fig. 14a); we note that this is partly a reflection of uncertainties with palaeomagnetic data from both Baltica and Laurentia during this time and the subsequent uncertainty about their position. For example, Domeier (2016) depicts a high latitude Baltica at 500 Ma outboard of Gondwana (our 520 Ma position is in transition to this position), but this necessitates a fast transition and rotation from the reliable 560 Ma poles that place the continent at a lower latitude.

9. Future work

The study that we present here is, by necessity, incomplete and therefore, represents just a first approximation to the true tectonic geography of the nearly half a billion years of Earth history represented by the Neoproterozoic. We do assert, however, that this methodology is an important way to test the numerous speculated links between Neoproterozoic plate tectonics and the greater Earth system. We also confident that this is the most complete attempt to date at merging
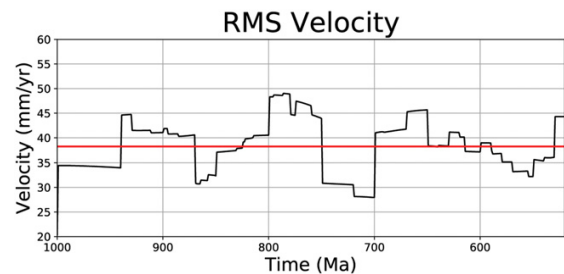

Fig. 18. RMS velocity of continental crust in the Neoproterozoic. The black line is the average from all continents extracted at a 5 Myr interval. The red line is the average across the Neoproterozoic.

tectono-geographic data derived from geology with palaeomagnetic data for the Neoproterozoic and, to our knowledge, this is the first attempt at amalgamating these into a full globe, whole-plate topological model of the planet over this critical period of Earth history. We hope that this will stimulate many improvements to palaeogeographical reconstructions over the next few years.

Beyond the gathering of more (and better quality) palaeomagnetic and geological data, we identify three key steps that should be undertaken in the future to improve the reconstruction presented here. Firstly, we are conservative with the amount of subduction occurring during the Neoproterozoic, relative to what we know occurs at the present-day. Assuming that Neoproterozoic subduction systems were similar

to the modern Earth, there is a considerable scope for uncovering other subduction systems during this time. Part of this will be through developing more tectonically complex and complete regional models for key areas (e.g. Azania, SM, ANS and Siberia) that more closely approximate the spatial and temporal constraints of arc collision, back-arc rifting and subduction initiation. This could be achieved by the coupling of models with whole earth system databases, such as a global geochemistry database. Secondly, the development of alternate models to test end member scenarios is critically important to completely evaluate the reliability of this (and any other model), especially with respect to times with more accessible to data (e.g. 650–500 Ma). Finally, the coupling of this reconstruction to younger models for the Phanerozoic
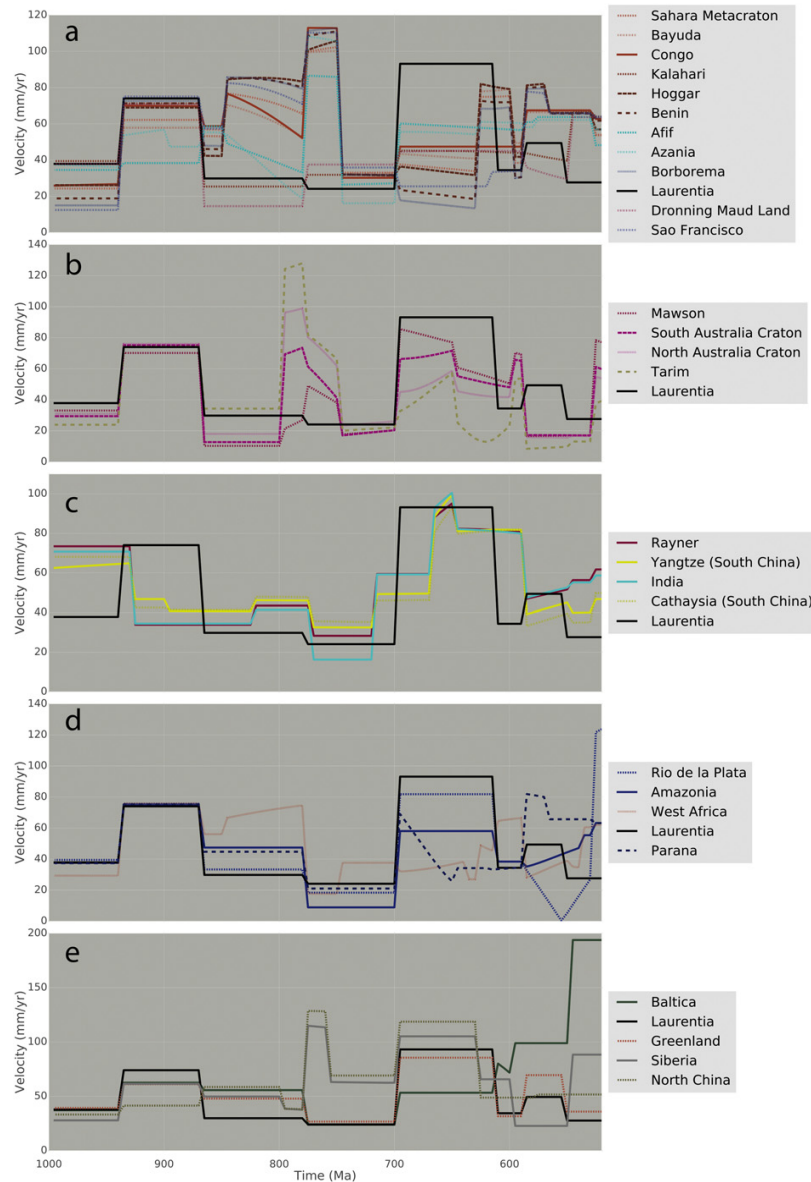
Fig. 19. Velocity of continental crust fragments in the Neoproterozoic. Velocities were calculated from the centroid of each portion of continental crust. Each panel broadly reflects a common Neoproterozoic journey; (a) Congo-São Francisco and the Sahara Metacraton (extra south Rodinia); (b) Australia and Mawson (west Rodinia); (c) India and South China; (d) Amazonia (east Rodinia); (e) Laurentia and northern Rodinia. Colour is based on present day geographical position; red – North America; dark blue – South American; green, Europe; grey, Siberia; light blue, India, Madagascar and the Middle East; yellow, China; purple, Australia and Antarctica. Laurentia is plotted in black in each panel as it is considered the heart of Rodinia.

paves the way for the first full plate models that encompass entire supercontinent cycles and will be instrumental for further understanding the long-term nature of the mantle. So, a priority and future studies should prioritise linking Neoproterozoic reconstructions with the younger Palaeozoic models (e.g. Domeier, 2016; Domeier and Torsvik, 2014).

10. Conclusions

The Neoproterozoic was dominated by a supercontinent cycle beginning with the formation of Rodinia, its subsequent breakup, and the consequent amalgamation of Gondwana. Here we have presented the first full plate global reconstruction of the Neoproterozoic that synthesises both palaeomagnetic and geological data with plate tectonic theory to model the evolution of plate boundaries and plates during this time. We present an updated set of Euler rotations for the kinematic motion of these plates during the Neoproterozoic. In particular, we present a new model for India and South China that reconciles the similar accretionary histories of the two cratons in the Tonian and fits the sparse palaeomagnetic data available from both cratons. This places South China in a position similar to its Gondwana position in the Cambrian, just north of India. A new model for the Congo-São Francisco craton is also proposed that ties disparate palaeomagnetic data (from the Tonian and Cryogenian) with a rifting event and counter-clockwise rotation of C-SF relative to Rodinia, helping explain the thick mid-Tonian sedimentation evident on the southern margin of Congo and eastern margin of the WAC, 50 Ma before the earliest inferred Rodinia rifting.

A key contribution of the reconstruction presented here is to model plate boundaries through time, and, by extension, model tectonic plates. From this we are able to extract basic data about the geometries and kinematics of these boundaries and plates, and make decisions about plate motions that minimise factors such as velocity, whilst also fitting palaeomagnetic and geological constraints. Our model maintains an average RMS velocity of continental crust during the Neoproterozoic of ~3.8 cm/yr.

The methodology has also allowed us to investigate the lengths of plate boundaries through time. We note that, relative to present-day, we have underestimated the length of subduction zones by 5000 to 10,000 km. This probable underestimation is likely due to poorly preserved subduction missing from the geological record (e.g. ocean-ocean convergence), and the oversimplification of key areas of subduction in the Neoproterozoic that we incorporated into this initial model. We expect that this model will be useful and act as a foundation, for future regional studies in poorly constrained areas of the Neoproterozoic, as well as providing an essential plate tectonic model that can be used to investigate the link between plate tectonics and other Earth systems, such as climate, biological evolution, oceanography and mantle geodynamics.

Acknowledgements

Appendix A. Supplementary data

Supplementary data to this article can be found online at http://dx.doi.org/10.1016/j.gr.2017.04.001.

References

Abdallah, N., Liégeois, J.P., De Waele, B., Fezaa, N., Ouabadi, A., 2007. The Temaguessine Fe-cordierite orbicular granite (Central Hoggar, Algeria): U–Pb SHRIMP age, petrology, origin and geodynamical consequences for the late Pan-African magmatism of the Tuareg shield. Journal of African Earth Sciences 49 (4), 153–178.

Abdelsalam, M.G., Liégeois, J.P., Stern, R.J., 2002. The Saharan Metacraton. Journal of African Earth Sciences 34 (3), 119–136.

Abdelsalam, M.G., Stern, R.J., Copeland, P., Elfaki, E.M., Elhur, B., Ibrahim, F.M., 1998. The Neoproterozoic Keraf Suture in NE Sudan: sinistral transpression along the eastern margin of West Gondwana. The Journal of Geology 106 (2), 133–148.

Abreu, F.A.M., Gorayeb, P.S.S., Hasui, Y., 1994. Tectônica e inversão metamórfica no Cinturão Araguaia. SBG/Grupo Norte, Simpósio de Geologia da Amazônia. 4, pp. 1–4.

Acharyya, S.K., 2003. The nature of Mesoproterozoic Central Indian Tectonic Zone with exhumed and reworked older granulites. Gondwana Research 6 (2), 197–214.

Aleinikoff, J.N., Zartman, R.E., Walter, M., Rankin, D.W., Lyttle, P.T., Burton, W.C., 1995. U-Pb ages of metarhyolites of the Catoctin and Mount Rogers Formations, central and southern Appalachians: evidence for two pulses of Iapetan rifting. American Journal of Science 295 (4), 428–454.

Alessio, B., Blades, M., Murray, G., Thorpe, B., Collins, A.S., Kelsey, D., Foden, J., Payne, J., Al Khirbash, S., Jourdan, F., 2017. Origin and tectonic evolution of the north-east basement of Oman – a window into the Neoproterozoic accretionary growth of India? Geological Magazine http://dx.doi.org/10.1017/S0016756817000061 (in press).

Alkmim, F.F., Marshak, S., Pedrosa-Soares, A.C., Peres, G.G., Cruz, S.C.P., Whittington, A., 2006. Kinematic evolution of the Araçuaí-West Congo orogen in Brazil and Africa: nutcracker tectonics during the Neoproterozoic assembly of Gondwana. Precambrian Research 149 (1), 43–64.

Allen, P.A., 2007. The Huqf Supergroup of Oman: basin development and context for Neoproterozoic glaciation. Earth-Science Reviews 84 (3), 139–185.

Allen, J.S., Thomas, W.A., Lavoie, D., 2010. The Laurentian margin of northeastern North America. Geological Society of America Memoirs 206, 71–90.

Alvarenga, C.J., Boggiani, P.C., Babinski, M., Dardenne, M.A., Figueiredo, M., Santos, R.V., Dantas, E.L., 2009. The Amazonian palaeocontinent. Developments in Precambrian Geology 16, pp. 15–28.

Alvarenga, C.J., Dardenne, M.A., Santos, R.V., Brod, E.R., Gioia, S.M., Sial, A.N., Dantas, E.L., Ferreira, V.P., 2008. Isotope stratigraphy of Neoproterozoic cap carbonates in the Araras Group, Brazil. Gondwana Research 13 (4), 469–479.

Alvarenga, C.J., Figueiredo, M.F., Babinski, M., Pinho, F.E., 2007. Glacial diamictites of Serra Azul Formation (Ediacaran, Paraguay belt): evidence of the Gaskiers glacial event in Brazil. Journal of South American Earth Sciences 23 (2), 236–241.

Alvarenga, C.D., Moura, C.V., Gorayeb, P.D.S., Abreu, F.D., 2000. Paraguay and Araguaia belts. Tectonic Evolution of South America. 31, pp. 183–193.

Alvarenga, C.J., Santos, R.V., Dantas, E.L., 2004. C–O–Sr isotopic stratigraphy of cap carbonates overlying Marinoan-age glacial diamictites in the Paraguay Belt, Brazil. Precambrian Research 131 (1), 1–21.

Álvaro, J.J., Pouclet, A., Ezzouhairi, H., Soulaimani, A., Bouougri, E.H., Imaz, A.G., Fekkak, A., 2014. Early Neoproterozoic rift-related magmatism in the Anti-Atlas margin of the West African craton, Morocco. Precambrian Research 255, 433–442.

Alves, C.L., 2006. Petrologia, geoquímica e geocronologia do granito Ramal do Lontra e sua relação com a tectônica e metamorfismo do Cinturão Araguaia, Xambioá (TO). (Unpublished MSc). Thesis Universidade Federal do Pará.

An, M., Wiens, D.A., Zhao, Y., Feng, M., Nyblade, A.A., Kanao, M., Li, Y., Maggi, A., Lévêque, J.J., 2015. S-velocity model and inferred Moho topography beneath the Antarctic Plate from Rayleigh waves. Journal of Geophysical Research, Solid Earth 120 (1), 359–383.

Appel, P., Schenk, V., 1998. High-pressure granulite facies metamorphism in the Pan-African belt of eastern Tanzania: P–T–t evidence against granulite formation by continent collision. Journal of Metamorphic Geology 16 (4), 491–509.

Archibald, D.B., Collins, A.S., Foden, J.D., Payne, J.L., Holden, P., Razakamanana, T., De Waele, B., Thomas, R.J., Pitfield, P.E., 2016. Genesis of the Tonian Imorona-Itsindro Magmatic Suite in central Madagascar: insights from U-Pb, oxygen and hafnium isotopes in zircon. Precambrian Research 281, 312–337.

Archibald, D.B., Collins, A.S., Foden, J.D., Razakamanana, T., 2017. Petrogenesis of the Tonian Imorona-Itsindro Suite. Journal of Geology http://dx.doi.org/10.1086/691185 (in press).

Armstrong, R.A., Master, S., Robb, L.J., 2005. Geochronology of the Nchanga Granite, and constraints on the maximum age of the Katanga Supergroup, Zambian Copperbelt. Journal of African Earth Sciences 42 (1), 32–40.

Arthaud, M.H., Caby, R., Fuck, R.A., Dantas, E.L., Parente, C.V., 2008. Geology of the northern Borborema Province, NE Brazil and its correlation with Nigeria, NW Africa. Geological Society, London, Special Publications 294 (1), 49–67.

Attoh, K., Dallmeyer, R.D., Affaton, P., 1997. Chronology of nappe assembly in the Pan-African Dahomeyide orogen, West Africa: evidence from [40]Ar[39]Ar mineral ages. Precambrian Research 82 (1), 153–171.

Attoh, K., Samson, S., Agbossoumondé, Y., Nude, P.M., Morgan, J., 2013. Geochemical characteristics and U–Pb zircon LA-ICPMS ages of granitoids from the Pan-African Dahomeyide orogen, West Africa. Journal of African Earth Sciences 79, 1–9.

Austermann, J., Ben-Avraham, Z., Bird, P., Heidbach, O., Schubert, G., Stock, J.M., 2011. Quantifying the forces needed for the rapid change of Pacific plate motion at 6 Ma. Earth and Planetary Science Letters 307 (3), 289–297.

Ayalew, T., Bell, K., Moore, J.M., Parrish, R.R., 1990. U-Pb and Rb-Sr geochronology of the western Ethiopian shield. Geological Society of America Bulletin 102 (9), 1309–1316.

Ayalew, T., Peccerillo, A., 1998. Petrology and geochemistry of the Gore-Gambella plutonic rocks: implications for magma genesis and the tectonic setting of the Pan-African Orogenic Belt of western Ethiopia. Journal of African Earth Sciences 27 (3), 397–416.

Babinski, M., Boggiani, P.C., Fanning, C.M., Fairchild, T.R., Simon, C.M., Sial, A.N., 2008. U-Pb shrimp geochronology and isotope chemostratigraphy (C, O, Sr) of the Tamengo Formation, southern Paraguay belt, Brazil. South American Symposium on Isotope Geology. vol. 6.

Babinski, M., Boggiani, P.C., Trindade, R.I.F., Fanning, C.M., 2013. Detrital zircon ages and geochronological constraints on the Neoproterozoic Puga diamictites and associated BIFs in the southern Paraguay Belt, Brazil. Gondwana Research 23 (3), 988–997.

Bagas, L., 2004. Proterozoic evolution and tectonic setting of the northwest Paterson Orogen, Western Australia. Precambrian Research 128 (3), 475–496.

Bandeira, J., McGee, B., Nogueira, A.C., Collins, A.S., Trindade, R., 2012. Sedimentological and provenance response to Cambrian closure of the Clymene ocean: the upper Alto Paraguai Group, Paraguay belt, Brazil. Gondwana Research 21 (2), 323–340.

Barley, M.E., Groves, D.I., 1992. Supercontinent cycles and the distribution of metal deposits through time. Geology 20 (4), 291–294.

Basei, M.A.S., Frimmel, H.E., Nutman, A.P., Preciozzi, F., Jacob, J., 2005. A connection between the Neoproterozoic Dom Feliciano (Brazil/Uruguay) and Gariep (Namibia/South Africa) orogenic belts–evidence from a reconnaissance provenance study. Precambrian Research 139 (3), 195–221.

Basei, M.A.S., Siga Jr., O., Masquelin, H., Harara, O.M., Reis Neto, J.M., Preciozzi Porta, F., 2000. The Dom Feliciano Belt and the Rio de la Plata Craton: tectonic evolution and correlation with similar provinces of southwestern Africa. Tectonic Evolution of South America. 31.

Bassot, J.P., Vachette, M., 1983. Données nouvelles sur l'âfe du massif de granitoïdes du Niokolo–Koba (Sénégal oriental); implications sur l'âge du stade précoce de la chaîne des uritanides. Journal of African Earth Science 1, 159–165.

Becker, T., Garoeb, H., Ledru, P., Milesi, J.P., 2005. The Mesoproterozoic event within the Rehoboth Basement Inlier of Namibia: review and new aspects of stratigraphy, geochemistry, structure and plate tectonic setting. South African Journal of Geology 108 (4), 465–492.

Becker, T., Schalk, K.E.L., 2008. The Sinclair Supergroup of the Rehoboth volcanic arc from the Sossusvlei-Gamsberg area to the Gobabis region. In: McG Miller, R. (Ed.), The Geology of Namibia. Archaean to Mesoproterozoic vol. 1, pp. 8.68–8.104.

Be'eri-Shlevin, Y., Eyal, M., Eyal, Y., Whitehouse, M.J., Litvinovsky, B., 2012. The Sa'al volcano-sedimentary complex (Sinai, Egypt): a latest Mesoproterozoic volcanic arc in the northern Arabian Nubian Shield. Geology 40 (5), 403–406.

Beeson, J., Harris, L.B., Delor, C.P., 1995. Structure of the western Albany Mobile Belt (southwestern Australia): evidence for overprinting by Neoproterozoic shear zones of the Darling Mobile Belt. Precambrian Research 75 (1), 47–63.

Berger, J., Ouzegane, K., Bendaoud, A., Liegeois, J.P., Kienast, J.R., Bruguier, O., Caby, R., 2014. Continental subduction recorded by Neoproterozoic eclogite and garnet amphibolites from Western Hoggar (Tassendjanet terrane, Tuareg Shield, Algeria). Precambrian Research 247, 139–158.

Bhowmik, S.K., Bernhardt, H.J., Dasgupta, S., 2010. Grenvillian age high-pressure upper amphibolite-granulite metamorphism in the Aravalli-Delhi Mobile Belt, Northwestern India: new evidence from monazite chemical age and its implication. Precambrian Research 178 (1), 168–184.

Bhowmik, S.K., Wilde, S.A., Bhandari, A., Pal, T., Pant, N.C., 2012. Growth of the Greater Indian Landmass and its assembly in Rodinia: geochronological evidence from the Central Indian Tectonic Zone. Gondwana Research 22 (1), 54–72.

Bierlein, F.P., Groves, D.I., Cawood, P.A., 2009. Metallogeny of accretionary orogens—the connection between lithospheric processes and metal endowment. Ore Geology Reviews 36 (4), 282–292.

Bingen, B., Demaiffe, D., Breemen, O.V., 1998. The 616 Ma old Egersund basaltic dike swarm, SW Norway, and late Neoproterozoic opening of the Iapetus Ocean. The Journal of Geology 106 (5), 565–574.

Bingen, B., Jacobs, J., Viola, G., Henderson, I.H.C., Skår, Ø., Boyd, R., Thomas, R.J., Solli, A., Key, R.M., Daudi, E.X.F., 2009. Geochronology of the Precambrian crust in the Mozambique belt in NE Mozambique, and implications for Gondwana assembly. Precambrian Research 170 (3), 231–255.

Bingen, B., Nordgulen, O., Viola, G., 2008. A four-phase model for the Sveconorwegian orogeny, SW Scandinavia. Norsk Geologisk Tidsskrift 88 (1), 43.

Black, R., Latouche, L., Liégeois, J.P., Caby, R., Bertrand, J.M., 1994. Pan-African displaced terranes in the Tuareg shield (central Sahara). Geology 22 (7), 641–644.

Black, L.P., Sheraton, J.W., Tingey, R.J., Mcculloch, M.T., 1992. New U-Pb zircon ages from the Denman Glacier area, East Antarctica, and their significance for Gondwana reconstruction. Antarctic Science 4 (04), 447–460.

Blades, M.L., Collins, A.S., Foden, J., Payne, J.L., Xu, X., Alemu, T., Woldetinsae, G., Clark, C., Taylor, R.J., 2015. Age and hafnium isotopic evolution of the Didesa and Kemashi Domains, western Ethiopia. Precambrian Research 270, 267–284.

Bogdanova, S., Gorbatschev, R., Skridlaite, G., Soesoo, A., Taran, L., Kurlovich, D., 2015. Trans-Baltic Palaeoproterozoic correlations towards the reconstruction of supercontinent Columbia/Nuna. Precambrian Research 259, 5–33.

Boger, S.D., 2011. Antarctica—before and after Gondwana. Gondwana Research 19 (2), 335–371.

Boger, S.D., Hirdes, W., Ferreira, C.A.M., Schulte, B., Jenett, T., Fanning, C.M., 2014. From passive margin to volcano–sedimentary forearc: the Tonian to Cryogenian evolution of the Anosyen Domain of southeastern Madagascar. Precambrian Research 247, 159–186.

Boger, S.D., Maas, R., Fanning, C.M., 2008. Isotopic and geochemical constraints on the age and origin of granitoids from the central Mawson Escarpment, southern Prince Charles Mountains, East Antarctica. Contributions to Mineralogy and Petrology 155 (3), 379–400.

Boger, S.D., Wilson, C.J.L., Fanning, C.M., 2001. Early Paleozoic tectonism within the East Antarctic craton: the final suture between east and west Gondwana? Geology 29 (5), 463–466.

Bouougri, E.H., Saquaque, A., 2004. Lithostratigraphic framework and correlation of the Neoproterozoic northern West African Craton passive margin sequence (Siroua–Zenaga–Bouazzer Elgraara inliers, central Anti-Atlas, Morocco): an integrated approach. Journal of African Earth Sciences 39 (3), 227–238.

Bouyo, M.H., Penaye, J., Barbey, P., Toteu, S.F., Wandji, P., 2013. Petrology of high-pressure granulite facies metapelites and metabasites from Tcholliré and Banyo regions: geodynamic implication for the Central African Fold Belt CAFB of north-central Cameroon. Precambrian Research 224, 412–433.

Bowring, S.A., Grotzinger, J.P., Condon, D.J., Ramezani, J., Newall, M.J., Allen, P.A., 2007. Geochronologic constraints on the chronostratigraphic framework of the Neoproterozoic Huqf Supergroup, Sultanate of Oman. American Journal of Science 307 (10), 1097–1145.

Bradley, D.C., 2011. Secular trends in the geologic record and the supercontinent cycle. Earth-Science Reviews 108 (1), 16–33.

Brito Neves, B.B., Fuck, R.A., Pimentel, M.M., 2016. A colagem Brasiliana na América do Sul: uma revisão. Brazilian Journal of Geology 44 (3), 493–518.

Brito Neves, B.B., Santos, E.J., Van Schmus, W.R., 2000. Tectonic history of the Borborema Province, northeastern Brazil. Tectonic evolution of the South America, pp. 151–182.

Brito Neves, B.D., Van Schmus, W.R., Dos Santos, E.J., Neto, M.C., Kozuch, M., 1995. O evento Cariris Velhos na Província Borborema: integração de dados, implicações e perspectivas. Brazilian Journal of Geology 25 (4), 279–296.

Brookfield, M.E., 1993. Neoproterozoic Laurentia-Australia fit. Geology 21 (8), 683–686.

Buchan, K.L., Dunlop, D.J., 1976. Paleomagnetism of the Haliburton intrusions: superimposed magnetizations, metamorphism, and tectonics in the late Precambrian. Journal of Geophysical Research 81 (17), 2951–2967.

Bueno, J.F., Oliveira, E.P., McNaughton, N.J., Laux, J.H., 2009. U–Pb dating of granites in the Neoproterozoic Sergipano Belt, NE-Brazil: implications for the timing and duration of continental collision and extrusion tectonics in the Borborema Province. Gondwana Research 15 (1), 86–97.

Bull, S., Selley, D., Broughton, D., Hitzman, M., Cailteux, J., Large, R., McGoldrick, P., 2011. Sequence and carbon isotopic stratigraphy of the Neoproterozoic Roan Group strata of the Zambian copperbelt. Precambrian Research 190 (1), 70–89.

Burrett, C., Berry, R., 2000. Proterozoic Australia–Western United States (AUSWUS) fit between Laurentia and Australia. Geology 28 (2), 103–106.

Burrett, C., Berry, R., 2002. A statistical approach to defining Proterozoic crustal provinces and testing continental reconstructions of Australia and Laurentia-SWEAT or AUSWUS? Gondwana Research 5 (1), 109–122.

Burrett, C., Zaw, K., Meffre, S., Lai, C.K., Khositanont, S., Chaodumrong, P., Udchachon, M., Ekins, S., Halpin, J., 2014. The configuration of Greater Gondwana—evidence from LA ICPMS, U–Pb geochronology of detrital zircons from the Palaeozoic and Mesozoic of Southeast Asia and China. Gondwana Research 26 (1), 31–51.

Butterworth, N., Steinberg, D., Müller, R.D., Williams, S., Merdith, A.S., Hardy, S., 2016. Tectonic environments of South American porphyry copper magmatism through time revealed by spatiotemporal data mining. Tectonics 35:2847–2862. http://dx.doi.org/10.1002/2016TC004289.

Caby, R., 1989. Precambrian terranes of Benin-Nigeria and northeast Brazil and the Late Proterozoic south Atlantic fit. Geological Society of America Special Papers 230, 145–158.

Caby, R., 2003. Terrane assembly and geodynamic evolution of central–western Hoggar: a synthesis. Journal of African Earth Sciences 37 (3), 133–159.

Caby, R., Monié, P., 2003. Neoproterozoic subductions and differential exhumation of western Hoggar (southwest Algeria): new structural, petrological and geochronological evidence. Journal of African Earth Sciences 37 (3), 269–293.

Campos Neto, M.D.C., Caby, R., 1999. Neoproterozoic high-pressure metamorphism and tectonic constraint from the nappe system south of the São Francisco Craton, southeast Brazil. Precambrian Research 97 (1), 3–26.

Candan, O., Koralay, O.E., Topuz, G., Oberhänsli, R., Fritz, H., Collins, A.S., Chen, F., 2016. Late Neoproterozoic gabbro emplacement followed by early Cambrian eclogite-facies metamorphism in the Menderes Massif (W. Turkey): implications on the final assembly of Gondwana. Gondwana Research 34, 158–173.

Cande, S.C., Stegman, D.R., 2011. Indian and African plate motions driven by the push force of the Reunion plume head. Nature 4757354, 47–52.

Cao, W., Lee, C.T.A., Lackey, J.S., 2017. Episodic nature of continental arc activity since 750 Ma: a global compilation. Earth and Planetary Science Letters 461, 85–95.

Cardona, A., Chew, D., Valencia, V.A., Bayona, G., Mišković, A., Ibañez-Mejía, M., 2010. Grenvillian remnants in the Northern Andes: Rodinian and Phanerozoic paleogeographic perspectives. Journal of South American Earth Sciences 29 (1), 92–104.

Carvalho, M.J., Oliveira, E.P., Dantas, E.L., McNaughton, N., 2005. Evolução Tectônica do Domínio Marancó-Poço Redondo: registro das orogêneses Cariris Velhos e Brasililana na margem norte da Faixa Sergipana. SBG, Simpósio sobre o Cráton do São Francisco. 3, pp. 204–207.

Castaing, C., Feybesse, J.A., Thiéblemont, D., Triboulet, C., Chevremont, P., 1994. Palaeogeographic reconstructions of the Pan-African/Brasiliano orogen: closure of an oceanic domain or intracontinental convergence between major blocks? Precambrian Research 69 (1–4), 327–344.

Castaing, C., Triboulet, C., Feybesse, J.L., Chevremont, P., 1993. Tectonometamorphic evolution of Ghana, Togo and Benin in the light of the Pan-African/Brasiliano orogeny. Tectonophysics 218 (4), 323–342.

Cawood, P.A., 2005. Terra Australis Orogen: Rodinia breakup and development of the Pacific and Iapetus margins of Gondwana during the Neoproterozoic and Paleozoic. Earth-Science Reviews 69 (3), 249–279.

Cawood, P.A., McCausland, P.J., Dunning, G.R., 2001. Opening Iapetus: constraints from the Laurentian margin in Newfoundland. Geological Society of America Bulletin 113 (4), 443–453.

Cawood, P.A., Nemchin, A.A., Strachan, R., Prave, T., Krabbendam, M., 2007. Sedimentary basin and detrital zircon record along East Laurentia and Baltica during assembly and breakup of Rodinia. Journal of the Geological Society 164 (2), 257–275.

Cawood, P.A., Pisarevsky, S.A., 2006. Was Baltica right-way-up or upside-down in the Neoproterozoic? Journal of the Geological Society 163 (5), 753–759.

Cawood, P.A., Strachan, R., Cutts, K., Kinny, P.D., Hand, M., Pisarevsky, S., 2010. Neoproterozoic orogeny along the margin of Rodinia: Valhalla orogen, North Atlantic. Geology 38 (2), 99–102.

Cawood, P.A., Strachan, R.A., Pisarevsky, S.A., Gladkochub, D.P., Murphy, J.B., 2016. Linking collisional and accretionary orogens during Rodinia assembly and breakup: implications for models of supercontinent cycles. Earth and Planetary Science Letters 449, 118–126.

Cawood, P.A., Wang, Y., Xu, Y., Zhao, G., 2013. Locating South China in Rodinia and Gondwana: a fragment of greater India lithosphere? Geology 41 (8), 903–906.

Caxito, F.D., Uhlein, A., Dantas, E.L., 2014. The Afeição augen-gneiss Suite and the record of the Cariris Velhos Orogeny (1000–960 Ma) within the Riacho do Pontal fold belt, NE Brazil. Journal of South American Earth Sciences 51, 12–27.

Chen, X., Rong, J.Y., 1992. Ordovician plate tectonics of China and its neighbouring regions. Global Perspectives on Ordovician Geology, pp. 277–291.

Chen, Y., Xu, B., Zhan, S., Li, Y., 2004. First mid-Neoproterozoic paleomagnetic results from the Tarim Basin (NW China) and their geodynamic implications. Precambrian Research 133 (3), 271–281.

Clark, C., Healy, D., Johnson, T., Collins, A.S., Taylor, R.J., Santosh, M., Timms, N.E., 2015. Hot orogens and supercontinent amalgamation: a Gondwanan example from southern India. Gondwana Research 28 (4), 1310–1328.

Cocks, L.R.M., Torsvik, T.H., 2002. Earth geography from 500 to 400 million years ago: a faunal and palaeomagnetic review. Journal of the Geological Society 159 (6), 631–644.

Collett, S., Faryad, S.W., Mosazai, A.M., 2015. Polymetamorphic evolution of the granulite-facies Paleoproterozoic basement of the Kabul Block, Afghanistan. Mineralogy and Petrology 109 (4), 463–484.

Collins, A.S., 2003. Structure and age of the northern Leeuwin Complex, Western Australia: constraints from field mapping and U–Pb isotopic analysis. Australian Journal of Earth Sciences 50 (4), 585–599.

Collins, A.S., 2006. Madagascar and the amalgamation of Central Gondwana. Gondwana Research 9 (1), 3–16.

Collins, A.S., Clark, C., Plavsa, D., 2014. Peninsular India in Gondwana: the tectonothermal evolution of the Southern Granulite Terrain and its Gondwanan counterparts. Gondwana Research 25 (1), 190–203.

Collins, A.S., Clark, C., Sajeev, K., Santosh, M., Kelsey, D.E., Hand, M., 2007b. Passage through India: the Mozambique Ocean suture, high-pressure granulites and the Palghat-Cauvery shear zone system. Terra Nova 19 (2), 141–147.

Collins, A.S., Fitzsimons, I.C.W., 2001. Structural, isotopic and geochemical constraints on the evolution of the Leeuwin Complex, southwest Australia. Geological Society of Australia Abstracts. vol. 65. Geological Society of Australia; 1999, pp. 16–19.

Collins, A.S., Kinny, P.D., Razakamanana, T., 2012. Depositional age, provenance and metamorphic age of metasedimentary rocks from southern Madagascar. Gondwana Research 21 (2), 353–361.

Collins, A.S., Kröner, A., Fitzsimons, I.C., Razakamanana, T., 2003. Detrital footprint of the Mozambique Ocean: U–Pb SHRIMP and Pb evaporation zircon geochronology of metasedimentary gneisses in eastern Madagascar. Tectonophysics 375 (1), 77–99.

Collins, A.S., Pisarevsky, S.A., 2005. Amalgamating eastern Gondwana: the evolution of the Circum-Indian Orogens. Earth-Science Reviews 71 (3), 229–270.

Collins, A.S., Santosh, M., Braun, I., Clark, C., 2007a. Age and sedimentary provenance of the Southern Granulites, South India: U-Th-Pb SHRIMP secondary ion mass spectrometry. Precambrian Research 155 (1), 125–138.

Collins, A.S., Windley, B.F., 2002. The tectonic evolution of central and northern Madagascar and its place in the final assembly of Gondwana. The Journal of Geology 110 (3), 325–339.

Condie, K.C., Rosen, O.M., 1994. Laurentia-Siberia connection revisited. Geology 22 (2), 168–170.

Conrad, C.P., Lithgow-Bertelloni, C., 2002. How mantle slabs drive plate tectonics. Science 2985591, 207–209.

Cordani, U.G., D'Agrella-Filho, M.S., Brito-Neves, B.D., Trindade, R.I.F., 2003. Tearing up Rodinia: the Neoproterozoic palaeogeography of South American cratonic fragments. Terra Nova 15 (5), 350–359.

Cordani, U.G., Pimentel, M.M., Araújo, C.E.G.D., Fuck, R.A., 2013. The significance of the Transbrasiliano-Kandi tectonic corridor for the amalgamation of West Gondwana. Brazilian Journal of Geology 43 (3), 583–597.

Corvino, A.F., Boger, S.D., Henjes-Kunst, F., Wilson, C.J., Fitzsimons, I.C., 2008. Superimposed tectonic events at 2450 Ma, 2100 Ma, 900 Ma and 500 Ma in the North Mawson Escarpment, Antarctic Prince Charles Mountains. Precambrian Research 167 (3), 281–302.

Cox, G.M., Halverson, G.P., Stevenson, R.K., Vokaty, M., Poirier, A., Kunzmann, M., Li, Z.X., Denyszyn, S.W., Strauss, J.V., Macdonald, F.A., 2016. Continental flood basalt weathering as a trigger for Neoproterozoic Snowball Earth. Earth and Planetary Science Letters 446, 89–99.

Cox, G.M., Lewis, C.J., Collins, A.S., Halverson, G.P., Jourdan, F., Foden, J., Nettle, D., Kattan, F., 2012. Ediacaran terrane accretion within the Arabian–Nubian Shield. Gondwana Research 21 (2), 341–352.

Cozzi, A., Rea, G., Craig, J., 2012. From global geology to hydrocarbon exploration: Ediacaran-Early Cambrian petroleum plays of India, Pakistan and Oman. Geological Society, London, Special Publications 366 (1), 131–162.

Culver, S.J., Repetski, J.E., Pojeta, J., Hunt, D., 1996. Early and Middle(?) Cambrian metazoan and protistan fossils from West Africa. Journal of Paleontology 70 (01), 1–6.

Curto, J.B., Vidotti, R.M., Fuck, R.A., Blakely, R.J., Alvarenga, C.J., Dantas, E.L., 2014. The tectonic evolution of the Transbrasiliano Lineament in northern Paraná Basin, Brazil, as inferred from aeromagnetic data. Journal of Geophysical Research, Solid Earth 119 (3), 1544–1562.

Cutts, K.A., Hand, M., Kelsey, D.E., Wade, B., Strachan, R.A., Clark, C., Netting, A., 2009. Evidence for 930 Ma metamorphism in the Shetland Islands, Scottish Caledonides: implications for Neoproterozoic tectonics in the Laurentia–Baltica sector of Rodinia. Journal of the Geological Society 166 (6), 1033–1047.

da Silva, L.C., McNaughton, N.J., Armstrong, R., Hartmann, L.A., Fletcher, I.R., 2005. The Neoproterozoic Mantiqueira Province and its African connections: a zircon-based U–Pb geochronologic subdivision for the Brasiliano/Pan-African systems of orogens. Precambrian Research 136 (3), 203–240.

da Silva, L.C., McNaughton, N.J., Hartmann, L.A., Fletcher, I.R., 2003. Zircon U-Pb SHRIMP dating of Serra dos Orgos and Rio de Janeiro gneissic granitic suites: implications for the (560 Ma) Brasiliano/Pan-African collage. Revista Brasileira de Geociencias 33 (2), 237–244.

D'Agrella-Filho, M.S., Pacca, I.G., Renne, P.R., Onstott, T.C., Teixeira, W., 1990. Paleomagnetism of Middle Proterozoic (1.01 to 1.08 Ga) mafic dykes in southeastern Bahia State—São Francisco craton, Brazil. Earth and Planetary Science Letters 101 (2–4), 332–348.

D'Agrella-Filho, M.S., Pacca, I.I., Trindade, R.I., Teixeira, W., Raposo, M.I.B., Onstott, T.C., 2004. Paleomagnetism and ^{40}Ar/^{39}Ar ages of mafic dikes from Salvador (Brazil): new constraints on the São Francisco craton APW path between 1080 and 1010 Ma. Precambrian Research 132 (1), 55–77.

Dallmeyer, R.D., Caen-Vachette, M., Villeneuve, M., 1987. Emplacement age of post-tectonic granites in southern Guinea (West Africa) and the peninsular Florida subsurface: implications for origins of southern Appalachian exotic terranes. Geological Society of America Bulletin 99 (1), 87–93.

Dalziel, I.W.D., 1991. Pacific margins of Laurentia and East Antarctica-Australia as a conjugate rift pair: evidence and implications for an Eocambrian supercontinent. Geology 19 (6), 598–601.

Dalziel, I.W.D., 1992. On the organization of American plates in the Neoproterozoic and the breakout of Laurentia. GSA Today 2 (11), 237–241.

Dalziel, I.W.D., 1997. Overview: Neoproterozoic-Paleozoic geography and tectonics: review, hypothesis, environmental speculation. Geological Society of America Bulletin 109 (1), 16–42.

Dantas, E.L., de Alvarenga, C.J.S., Santos, R.V., Pimentel, M.M., 2009. Using Nd isotopes to understand the provenance of sedimentary rocks from a continental margin to a foreland basin in the Neoproterozoic Paraguay Belt, Central Brazil. Precambrian Research 170 (1), 1–12.

Dardenne, M.A., 2000. The Brasília fold belt. In: Cordani, U.G., Milani, E.J., Thomaz Filho, A., Campos, D.A. (Eds.), 31st International Tectonic Evolution of South America.

Dasgupta, S., Bose, S., Das, K., 2013. Tectonic evolution of the Eastern Ghats belt, India. Precambrian Research 227, 247–258.

Davis, J.K., Meert, J.G., Pandit, M.K., 2014. Paleomagnetic analysis of the Marwar Supergroup, Rajasthan, India and proposed interbasinal correlations. Journal of Asian Earth Sciences 91, 339–351.

Davison, I., Dos Santos, R.A., 1989. Tectonic evolution of the Sergipano fold belt, NE Brazil, during the Brasiliano orogeny. Precambrian Research 45 (4), 319–342.

de Waele, B., Johnson, S.P., Pisarevsky, S.A., 2008. Palaeoproterozoic to Neoproterozoic growth and evolution of the eastern Congo Craton: its role in the Rodinia puzzle. Precambrian Research 160 (1), 127–141.

de Waele, B., Wingate, M.T., Fitzsimons, I.C., Mapani, B.S., 2003. Untying the Kibaran knot: a reassessment of Mesoproterozoic correlations in southern Africa based on SHRIMP U-Pb data from the Irumide belt. Geology 31 (6), 509–512.

de Wit, M.J., Linol, B., 2015. Precambrian basement of the Congo Basin and its flanking terrains. Geology and Resource Potential of the Congo Basin. Springer Berlin Heidelberg, pp. 19–37.

de Wit, M.J., Stankiewicz, J., Reeves, C., 2008. Restoring Pan-African-Brasiliano connections: more Gondwana control, less Trans-Atlantic corruption. In: Pankhurst, R.J., RAJ, Trouw, Brito Neves, B.B., de Wit, M.J. (Eds.), West Gondwana: Pre-Cenozoic Correlations Across the South Atlantic Region. vol. 294. Geological Society of London, London, pp. 399–412 (Special Publications).

Delor, C., Lafon, J.M., Milesi, J.P., Fanning, M., 2003. First evidence of 560–575 Ma granulites and syn-tectonic magmatism in the Rockelides belt: geology, geochronology and geodynamic implications. 19th CAG, March, 19–22.

Denyszyn, S.W., Halls, H.C., Davis, D.W., Evans, D.A.D., 2009. Paleomagnetism and U-Pb geochronology of Franklin dykes in High Arctic Canada and Greenland: a revised age and paleomagnetic pole constraining block rotations in the Nares Strait region. Canadian Journal of Earth Sciences 46, 689–705.

Deynoux, M., Affaton, P., Trompette, R., Villeneuve, M., 2006. Pan-African tectonic evolution and glacial events registered in Neoproterozoic to Cambrian cratonic and foreland basins of West Africa. Journal of African Earth Sciences 46 (5), 397–426.

Dobmeier, C.J., Raith, M.M., 2003. Crustal architecture and evolution of the Eastern Ghats Belt and adjacent regions of India. Geological Society, London, Special Publications 206 (1), 145–168.

Dobmeier, C., Simmat, R., 2002. Post-Grenvillean transpression in the Chilka Lake area, Eastern Ghats Belt—implications for the geological evolution of peninsular India. Precambrian Research 113 (3), 243–268.

Doebrich, J.L., Al-Jehani, A.M., Siddiqui, A.A., Hayes, T.S., Wooden, J.L., Johnson, P.R., 2007. Geology and metallogeny of the Ar Rayn terrane, eastern Arabian shield: evolution of a Neoproterozoic continental-margin arc during assembly of Gondwana within the East African Orogen. Precambrian Research 158 (1), 17–50.

Domeier, M., 2016. A plate tectonic scenario for the Iapetus and Rheic oceans. Gondwana Research 36, 275–295.

Domeier, M., Torsvik, T.H., 2014. Plate tectonics in the late Paleozoic. Geoscience Frontiers 5 (3), 303–350.

Dong, Y., Santosh, M., 2016. Tectonic architecture and multiple orogeny of the Qinling Orogenic Belt, Central China. Gondwana Research 29 (1), 1–40.

Dong, X., Zhang, Z., Liu, F., Wang, W., Yu, F., Shen, K., 2011. Zircon U–Pb geochronology of the Nyainqêntanglha Group from the Lhasa terrane: new constraints on the Triassic orogeny of the south Tibet. Journal of Asian Earth Sciences 42 (4), 732–739.

Droser, M.L., Gehling, J.G., 2015. The advent of animals: the view from the Ediacaran. Proceedings of the National Academy of Sciences 112 (16), 4865–4870.

Egal, E., Guerrot, C., Le Goff, E., Thiéblemont, D., Chantraine, J., 1996. The Cadomian Orogeny Revisited in Northern Brittany (France). Special Papers - Geological Society of America, pp. 281–318.

El Desouky, H.A., Muchez, P., Boyce, A.J., Schneider, J., Cailteux, J.L., Dewaele, S., von Quadt, A., 2010. Genesis of sediment-hosted stratiform copper–cobalt mineralization at Luiswishi and Kamoto, Katanga Copperbelt (Democratic Republic of Congo). Mineralium Deposita 45 (8), 735–763.

Elming, S.-Å., Pisarevsky, S.A., Layer, P., Bylund, G., 2014. A palaeomagnetic and $^{40}Ar/^{39}Ar$ study of mafic dykes in southern Sweden: a new Early Neoproterozoic key-pole for the Baltic Shield and implications for Sveconorwegian and Grenville loops. Precambrian Research 244, 192–206.

Embleton, B.J.J., Schmidt, P.W., 1985. Age and significance of magnetizations in dolerite dykes from the Northampton Block, Western Australia. Australian Journal of Earth Sciences 32 (3), 279–286.

Embleton, B.J.J., Williams, G.E., 1986. Low paleolatitude of deposition for Late Precambrian periglacial varvites in South Australia: implications for paleoclimatology. Earth and Planetary Science Letters 79, 419–430.

Ennih, N., Liégeois, J.P., 2001. The Moroccan Anti-Atlas: the West African craton passive margin with limited Pan-African activity. Implications for the northern limit of the craton. Precambrian Research 112 (3), 289–302.

Ernst, R.E., Bleeker, W., Söderlund, U., Kerr, A.C., 2013. Large Igneous Provinces and supercontinents: toward completing the plate tectonic revolution. Lithos 174, 1–14.

Ernst, R.E., Hamilton, M.A., Söderlund, U., Hanes, J.A., Gladkochub, D.P., Okrugin, A.V., Kolotilina, T., Mekhonoshin, A.S., Bleeker, W., LeCheminant, A.N., Buchan, K.L., 2016. Long-lived connection between southern Siberia and northern Laurentia in the Proterozoic. Nature Geoscience 9 (6), 464–469.

Ernst, R.E., Wingate, M.T.D., Buchan, K.L., Li, Z.X., 2008. Global record of 1600–700 Ma Large Igneous Provinces LIPs: implications for the reconstruction of the proposed Nuna (Columbia) and Rodinia supercontinents. Precambrian Research 160 (1), 159–178.

Evans, D.A., 1998. True polar wander, a supercontinental legacy. Earth and Planetary Science Letters 157 (1), 1–8.

Evans, D.A., 2003. True polar wander and supercontinents. Tectonophysics 362.

Evans, D.A., 2009. The palaeomagnetically viable, long-lived and all-inclusive Rodinia supercontinent reconstruction. Geological Society, London, Special Publications 327 (1), 371–404.

Evans, D.A., 2013. Reconstructing pre-Pangean supercontinents. Geological Society of America Bulletin 125 (11−12), 1735–1751.

Evans, D.A.D., Li, Z.X., Kirschvink, J.L., Wingate, M.T.D., 2000. A high quality mid-Neoproterozoic paleomagnetic pole from South China, with implications for ice ages and the breakup configuration of Rodinia. Precambrian Research 100, 313–334.

Evans, D.A.D., Trindade, R.I.F., Catelani, E.L., D'Agrella-Filho, M.S., Heaman, L.M., Oliveira, E.P., Soderlund, U., Ernst, R.E., Smirnov, A.V., Salminen, J.M., 2016b. Return to Rodinia? Moderate to high palaeolatitude of the Sao Francisco/Congo craton at 920 Ma. In: Li, Z.X., Evans, D.A.D., Murphy, J.B. (Eds.), Supercontinent Cycles Through Earth History. Geol. Soc. London Spec. Publ. 424, pp. 167–190.

Evans, D.A., Veselovsky, R.V., Petrov, P.Y., Shatsillo, A.V., Pavlov, V.E., 2016a. Paleomagnetism of Mesoproterozoic margins of the Anabar Shield: a hypothesized billion-year partnership of Siberia and northern Laurentia. Precambrian Research 281, 639–655.

Evuk, D., Franz, G., Frei, D., Lucassen, F., 2014. The Neoproterozoic evolution of the central-eastern Bayuda Desert (Sudan). Precambrian Research 240, 108–125.

Eyal, M., Be'eri-Shlevin, Y., Eyal, Y., Whitehouse, M.J., Litvinovsky, B., 2014. Three successive Proterozoic island arcs in the Northern Arabian–Nubian Shield: evidence from SIMS U–Pb dating of zircon. Gondwana Research 25 (1), 338–357.

Faccenna, C., Becker, T.W., Lallemand, S., Steinberger, B., 2012. On the role of slab pull in the Cenozoic motion of the Pacific plate. Geophysical Research Letters 39 (3).

Fairhead, J.D., Maus, S., 2003. CHAMP satellite and terrestrial magnetic data help define the tectonic model for South America and resolve the lingering problem of the pre-break-up fit of the South Atlantic Ocean. The Leading Edge 22 (8), 779–783.

Faryad, S.W., Collett, S., Finger, F., Sergeev, S.A., Čopjaková, R., Siman, P., 2016. The Kabul Block (Afghanistan), a segment of the Columbia Supercontinent, with a Neoproterozoic metamorphic overprint. Gondwana Research 34, 221–240.

Fekkak, A., Pouclet, A., Ouguir, H., Badra, L., Gasquet, D., 1999. Le groupe du Neoproterozoique inferieur de Kelaat Mgouna (Saghro, Anti-Atlas, Maroc); temoin d'un stade precoce de l'extension pre-panafricaine. Bulletin de la Société Géologique de France 170 (6), 789–797.

Fernandes, G.L.D.F., da Silva Schmitt, R., Bongiolo, E.M., Basei, M.A., Mendes, J.C., 2015. Unraveling the tectonic evolution of a Neoproterozoic–Cambrian active margin in

the Ribeira Orogen (se Brazil): U–Pb and Lu–Hf provenance data. Precambrian Research 266, 337–360.

Ferraccioli, F., Finn, C.A., Jordan, T.A., Bell, R.E., Anderson, L.M., Damaske, D., 2011. East Antarctic rifting triggers uplift of the Gamburtsev Mountains. Nature 4797373, 388–392.

Fezaa, N., Liégeois, J.P., Abdallah, N., Cherfouh, E.H., De Waele, B., Bruguier, O., Ouabadi, A., 2010. Late Ediacaran geological evolution (575–555 Ma) of the Djanet Terrane, Eastern Hoggar, Algeria, evidence for a Murzukian intracontinental episode. Precambrian Research 180 (3), 299–327.

Fitzsimons, I.C.W., 2000a. Grenville-age basement provinces in East Antarctica: evidence for three separate collisional orogens. Geology 28 (10), 879–882.

Fitzsimons, I.C.W., 2000b. A review of tectonic events in the East Antarctic Shield and their implications for Gondwana and earlier supercontinents. Journal of African Earth Sciences 31 (1), 3–23.

Fitzsimons, I.C.W., 2003. Proterozoic basement provinces of southern and southwestern Australia, and their correlation with Antarctica. Geological Society, London, Special Publications 206 (1), 93–130.

Fitzsimons, I.C.W., Hulscher, B., 2005. Out of Africa: detrital zircon provenance of central Madagascar and Neoproterozoic terrane transfer across the Mozambique Ocean. Terra Nova 17 (3), 224–235.

Foden, J., Elburg, M.A., Dougherty-Page, J., Burtt, A., 2006. The timing and duration of the Delamerian Orogeny: correlation with the Ross Orogen and implications for Gondwana assembly. The Journal of Geology 114 (2), 189–210.

Fortey, R.A., Cocks, L.R.M., 1998. Biogeography and palaeogeography of the Sibumasu terrane in the Ordovician: a review. Biogeography and Geological Evolution of SE Asia, pp. 43–56.

Frimmel, H.E., Basei, M.S., Gaucher, C., 2011. Neoproterozoic geodynamic evolution of SW-Gondwana: a southern African perspective. International Journal of Earth Sciences 100 (2–3), 323–354.

Frimmel, H.E., Fölling, P.G., 2004. Late Vendian closure of the Adamastor Ocean: timing of tectonic inversion and syn-orogenic sedimentation in the Gariep Basin. Gondwana Research 7 (3), 685–699.

Frimmel, H.E., Fölling, P.G., Eriksson, P.G., 2002. Neoproterozoic tectonic and climatic evolution recorded in the Gariep Belt, Namibia and South Africa. Basin Research 14 (1), 55–67.

Frimmel, H.E., Frank, W., 1998. Neoproterozoic tectono-thermal evolution of the Gariep Belt and its basement, Namibia and South Africa. Precambrian Research 90 (1), 1–28.

Fritz, H., Abdelsalam, M., Ali, K.A., Bingen, B., Collins, A.S., Fowler, A.R., Ghebreab, W., Hauzenberger, C.A., Johnson, P.R., Kusky, T.M., Macey, P., 2013. Orogen styles in the East African Orogen: a review of the Neoproterozoic to Cambrian tectonic evolution. Journal of African Earth Sciences 86, 65–106.

Frost, B.R., Avchenko, O.V., Chamberlain, K.R., Frost, C.D., 1998. Evidence for extensive Proterozoic remobilization of the Aldan shield and implications for Proterozoic plate tectonic reconstructions of Siberia and Laurentia. Precambrian Research 89 (1), 1–23.

Fu, X., Zhang, S., Li, H., Ding, J., Li, H., Yang, T., Wu, H., Yuan, H., Lv, J., 2015. New paleomagnetic results from the Huaibei Group and Neoproterozoic mafic sills in the North China Craton and their paleogeographic implications. Precambrian Research 269, 90–106.

Fuck, R.A., Neves, B.B.B., Schobbenhaus, C., 2008. Rodinia descendants in South America. Precambrian Research 160 (1), 108–126.

Ganade de Araujo, C.E., Cordani, U.G., Agbossoumounde, Y., Caby, R., Basei, M.A., Weinberg, R.F., Sato, K., 2016. Tightening-up NE Brazil and NW Africa connections: new U–Pb/Lu–Hf zircon data of a complete plate tectonic cycle in the Dahomey belt of the West Gondwana Orogen in Togo and Benin. Precambrian Research 276, 24–42.

Ganade de Araujo, C.E., Cordani, U.G., Basei, M.A., Castro, N.A., Sato, K., Sproesser, W.M., 2012. U–Pb detrital zircon provenance of metasedimentary rocks from the Ceará Central and Médio Coreaú Domains, Borborema Province, NE-Brazil: tectonic implications for a long-lived Neoproterozoic active continental margin. Precambrian Research 206, 36–51.

Ganade de Araujo, C.E., Cordani, U.G., Weinberg, R.F., Basei, M.A., Armstrong, R., Sato, K., 2014a. Tracing Neoproterozoic subduction in the Borborema Province (NE-Brazil): clues from U-Pb geochronology and Sr-Nd-Hf-O isotopes on granitoids and migmatites. Lithos 202, 167–189.

Ganade de Araujo, C.E., Weinberg, R.F., Cordani, U.G., 2014b. Extruding the Borborema Province (NE-Brazil): a two-stage Neoproterozoic collision process. Terra Nova 26 (2), 157–168.

Ganne, J., Feng, X., Rey, P., De Andrade, V., 2016. Statistical petrology reveals a link between supercontinents cycle and mantle global climate. American Mineralogist 101 (12), 2768–2773.

Garfunkel, Z., 2015. The relations between Gondwana and the adjacent peripheral Cadomian domain—constrains on the origin, history, and paleogeography of the peripheral domain. Gondwana Research 28 (4), 1257–1281.

Gasquet, D., Levresse, G., Cheilletz, A., Azizi-Samir, M.R., Mouttaqi, A., 2005. Contribution to a geodynamic reconstruction of the Anti-Atlas (Morocco) during Pan-African times with the emphasis on inversion tectonics and metallogenic activity at the Precambrian–Cambrian transition. Precambrian Research 140 (3), 157–182.

Gaucher, C., Finney, S.C., Poiré, D.G., Valencia, V.A., Grove, M., Blanco, G., Pamoukaghlián, K., Peral, L.G., 2008. Detrital zircon ages of Neoproterozoic sedimentary successions in Uruguay and Argentina: insights into the geological evolution of the Río de la Plata Craton. Precambrian Research 167 (1), 150–170.

Gaucher, C., Frei, R., Chemale Jr., F., Frei, D., Bossi, J., Martínez, G., Chiglino, L., Cernuschi, F., 2011. Mesoproterozoic evolution of the Río de la Plata Craton in Uruguay: at the heart of Rodinia? International Journal of Earth Sciences 100 (2–3), 273–288.

Ge, R., Zhu, W., Wilde, S.A., 2016. Mid-Neoproterozoic (ca. 830–800 Ma) metamorphic P-T paths link Tarim to the circum-Rodinia subduction-accretion system. Tectonics 35 (6), 1465–1488.

Ge, R., Zhu, W., Wilde, S.A., He, J., Cui, X., Wang, X., Bihai, Z., 2014. Neoproterozoic to Paleozoic long-lived accretionary orogeny in the northern Tarim Craton. Tectonics 33 (3), 302–329.

Gee, D.G., Teben'kov, A.M., 1996. Two major unconformities beneath the Neoproterozoic Murchisonfjorden Supergroup in the Caledonides of central Nordaustlandet, Svalbard. Polar Research 15 (1), 81–91.

Gernon, T.M., Hincks, T.K., Tyrrell, T., Rohling, E.J., Palmer, M.R., 2016. Snowball Earth ocean chemistry driven by extensive ridge volcanism during Rodinia breakup. Nature Geoscience 9 (3), 242–248.

Gladkochub, D.P., Donskaya, T.V., Wingate, M.T.D., Mazukabzov, A.M., Pisarevsky, S.A., Sklyarov, E.V., Stanevich, A.M., 2010a. A one-billion-year gap in the Precambrian history of the southern Siberian Craton and the problem of the Transproterozoic supercontinent. American Journal of Science 310 (9), 812–825.

Gladkochub, D.P., Pisarevsky, S.A., Donskaya, T.V., Ernst, R.E., Wingate, M.T., Söderlund, U., Mazukabzov, A.M., Sklyarov, E.V., Hamilton, M.A., Hanes, J.A., 2010b. Proterozoic mafic magmatism in Siberian craton: an overview and implications for paleocontinental reconstruction. Precambrian Research 183 (3), 660–668.

Goddéris, Y., Donnadieu, Y., Nédélec, A., Dupré, B., Dessert, C., Grard, A., Ramstein, G., Francois, L.M., 2003. The Sturtian 'snowball' glaciation: fire and ice. Earth and Planetary Science Letters 211 (1), 1–12.

Goldreich, P., Toomre, A., 1969. Some remarks on polar wandering. Journal of Geophysical Research 74 (10), 2555–2567.

Goscombe, B., Armstrong, R., Barton, J.M., 2000. Geology of the Chewore Inliers, Zimbabwe: constraining the Mesoproterozoic to Palaeozoic evolution of the Zambezi Belt. Journal of African Earth Sciences 30 (3), 589–627.

Goscombe, B.D., Gray, D.R., 2008. Structure and strain variation at mid-crustal levels in a transpressional orogen: a review of Kaoko Belt structure and the character of West Gondwana amalgamation and dispersal. Gondwana Research 13 (1), 45–85.

Goscombe, B., Hand, M., Gray, D., 2003b. Structure of the Kaoko Belt, Namibia: progressive evolution of a classic transpressional orogen. Journal of Structural Geology 25 (7), 1049–1081.

Goscombe, B., Hand, M., Gray, D., Mawby, J., 2003a. The metamorphic architecture of a transpressional orogen: the Kaoko Belt, Namibia. Journal of Petrology 44 (4), 679–711.

Gray, D.R., Foster, D.A., Meert, J.G., Goscombe, B.D., Armstrong, R., Trouw, R.A.J., Passchier, C.W., 2008. A Damara Orogen perspective on the assembly of southwestern Gondwana. Geological Society, London, Special Publications 294 (1), 257–278.

Gregory, L.C., Meert, J.G., Bingen, B., Pandit, M.K., Torsvik, T.H., 2009. Paleomagnetism and geochronology of the Malani Igneous Suite, Northwest India: implications for the configuration of Rodinia and the assembly of Gondwana. Precambrian Research 170 (1), 13–26.

Gregory, L.C., Meert, J.G., Pradhan, V., Pandit, M.K., Tamrat, E., Malone, S.J., 2006. A paleomagnetic and geochronologic study of the Majhgawan kimberlite, India: implications for the age of the Upper Vindhyan Supergroup. Precambrian Research 149 (1), 65–75.

Gupta, S., 2012. Strain localization, granulite formation and geodynamic setting of 'hot orogens': a case study from the Eastern Ghats Province, India. Geological Journal 47 (2–3), 334–351.

Gurnis, M., Torsvik, T.H., 1994. Rapid drift of large continents during the late Precambrian and Paleozoic: paleomagnetic constraints and dynamic models. Geology 22 (11), 1023–1026.

Gurnis, M., Turner, M., Zahirovic, S., DiCaprio, L., Spasojevic, S., Müller, R.D., Boyden, J., Seton, M., Manea, V.C., Bower, D.J., 2012. Plate tectonic reconstructions with continuously closing plates. Computers & Geosciences 38 (1), 35–42.

Gutiérrez-Alonso, G., Fernández-Suárez, J., Collins, A.S., Abad, I., Nieto, F., 2005. Amazonian Mesoproterozoic basement in the core of the Ibero-Armorican Arc: $^{40}Ar/^{39}Ar$ detrital mica ages complement the zircon's tale. Geology 33 (8), 637–640.

Guynn, J., Kapp, P., Gehrels, G.E., Ding, L., 2012. U–Pb geochronology of basement rocks in central Tibet and paleogeographic implications. Journal of Asian Earth Sciences 43 (1), 23–50.

Guynn, J.H., Kapp, P., Pullen, A., Heizler, M., Gehrels, G., Ding, L., 2006. Tibetan basement rocks near Amdo reveal "missing" Mesozoic tectonism along the Bangong suture, central Tibet. Geology 34 (6), 505–508.

Hadj-Kaddour, Z., Liegeois, J.P., Demaiffe, D., Caby, R., 1998. The alkaline–peralkaline granitic post-collisional Tin Zebane dyke swarm (Pan-African Tuareg shield, Algeria): prevalent mantle signature and late agpaitic differentiation. Lithos 45 (1), 223–243.

Halls, H.C., Lovette, A., Hamilton, M., Söderlund, U., 2015. A paleomagnetic and U–Pb geochronology study of the western end of the Grenville dyke swarm: rapid changes in paleomagnetic field direction at ca. 585 Ma related to polarity reversals? Precambrian Research 257, 137–166.

Halpin, J.A., Crawford, A.J., Direen, N.G., Coffin, M.F., Forbes, C.J., Borissova, I., 2008. Naturaliste Plateau, offshore Western Australia: a submarine window into Gondwana assembly and breakup. Geology 36 (10), 807–810.

Halverson, G.P., Dudás, F.Ö., Maloof, A.C., Bowring, S.A., 2007. Evolution of the $^{87}Sr/^{86}Sr$ composition of Neoproterozoic seawater. Palaeogeography, Palaeoclimatology, Palaeoecology 256 (3), 103–129.

Halverson, G.P., Hurtgen, M.T., Porter, S.M., Collins, A.S., 2009. Neoproterozoic-Cambrian biogeochemical evolution. In: Gaucher, C., Sial, A.N., Halverson, G.P., Frimmel, H.E. (Eds.), Neoproterozoic-Cambrian Tectonics, Global Change and Evolution: A Focus on Southwestern Gondwana. Developments in Precambrian Geology vol. 16. Elsevier, pp. 351–365.

Halverson, G.P., Maloof, A.C., Hoffman, P.F., 2004. The Marinoan glaciation (Neoproterozoic) in northeast Svalbard. Basin Research 16 (3), 297–324.

Handke, M.J., Tucker, R.D., Ashwal, L.D., 1999. Neoproterozoic continental arc magmatism in west-central Madagascar. Geology 27 (4), 351–354.

Hanson, R.E., 2003. Proterozoic geochronology and tectonic evolution of southern Africa. Geological Society, London, Special Publications 206 (1), 427–463.

Hanson, R.E., Harmer, R.E., Blenkinsop, T.G., Bullen, D.S., Dalziel, I.W.D., Gose, W.A., Hall, R.P., Kampunzu, A.B., Key, R.M., Mukwakwami, J., Munyanyiwa, H., 2006. Mesoproterozoic intraplate magmatism in the Kalahari Craton: a review. Journal of African Earth Sciences 46 (1), 141–167.

Hardie, L.A., 1996. Secular variation in seawater chemistry: an explanation for the coupled secular variation in the mineralogies of marine limestones and potash evaporites over the past 600 my. Geology 24 (3), 279–283.

Harlan, S.S., Geissman, J.W., Snee, L.W., 2008. Paleomagnetism of Proterozoic mafic dikes from the Tobacco Root Mountains, southwest Montana. Precambrian Research 163, 239–264.

Harris, L.B., 1994. Neoproterozoic sinistral displacement along the Darling mobile belt, Western Australia, during Gondwanaland assembly. Journal of the Geological Society 151 (6), 901–904.

Harris, L.B., Beeson, J., 1993. Gondwanaland significance of Lower Palaeozoic deformation in central India and SW Western Australia. Journal of the Geological Society 150 (5), 811–814.

Hartmann, L.A., Campal, N., Santos, J.O.S., McNaughton, N.J., Bossi, J., Schipilov, A., Lafon, J.M., 2001. Archean crust in the Rio de la Plata Craton, Uruguay—SHRIMP U–Pb zircon reconnaissance geochronology. Journal of South American Earth Sciences 14 (6), 557–570.

Hartmann, O., Hoffer, E., Haack, U., 1983. Regional metamorphism in the Damara orogen: interaction of crustal motion and heat transfer. Special Publication of the Geological Society of South Africa. 11, pp. 233–241.

Hartmann, L.A., Santos, J.O.S., Bossi, J., Campal, N., Schipilov, A., McNaughton, N.J., 2002. Zircon and titanite U–Pb SHRIMP geochronology of Neoproterozoic felsic magmatism on the eastern border of the Rio de la Plata Craton, Uruguay. Journal of South American Earth Sciences 15 (2), 229–236.

Hauzenberger, C.A., Bauernhofer, A.H., Hoinkes, G., Wallbrecher, E., Mathu, E.M., 2004. Pan-African high pressure granulites from SE-Kenya: petrological and geothermobarometric evidence for a polycyclic evolution in the Mozambique belt. Journal of African Earth Sciences 40 (5), 245–268.

Hauzenberger, C.A., Sommer, H., Fritz, H., Bauernhofer, A., Kröner, A., Hoinkes, G., Wallbrecher, E., Thöni, M., 2007. SHRIMP U–Pb zircon and Sm–Nd garnet ages from the granulite-facies basement of SE Kenya: evidence for Neoproterozoic polycyclic assembly of the Mozambique Belt. Journal of the Geological Society 164 (1), 189–201.

Heilbron, M., Duarte, B.P., de Morisson Valeriano, C., Simonetti, A., Machado, N., Nogueira, J.R., 2010. Evolution of reworked Paleoproterozoic basement rocks within the Ribeira belt (Neoproterozoic), SE-Brazil, based on U–Pb geochronology: implications for paleogeographic reconstructions of the São Francisco-Congo paleocontinent. Precambrian Research 178 (1), 136–148.

Heilbron, M., Machado, N., 2003. Timing of terrane accretion in the Neoproterozoic–Eopaleozoic Ribeira orogen (SE Brazil). Precambrian Research 125 (1), 87–112.

Heilbron, M., Machado, N., Simonetti, A., Duarte, P.B., 2003. A Paleoproterozoic orogen reworked within the Neoproterozoic Ribeira Belt, Southeastern Brazil. Short Papers IV South American Symposium on Isotope Geology, Salvador, Bahia, Brazil, pp. 186–189.

Heilbron, M., Valeriano, C.M., Tassinari, C.C.G., Almeida, J., Tupinambá, M., Siga, O., Trouw, R., 2008. Correlation of Neoproterozoic terranes between the Ribeira Belt, SE Brazil and its African counterpart: comparative tectonic evolution and open questions. Geological Society, London, Special Publications 294 (1), 211–237.

Henderson, B.J., Collins, W.J., Murphy, J.B., Gutierrez-Alonso, G., Hand, M., 2016. Gondwanan basement terranes of the Variscan–Appalachian orogen: Baltican, Saharan and West African hafnium isotopic fingerprints in Avalonia, Iberia and the Armorican Terranes. Tectonophysics 681, 278–304.

Henderson, B., Collins, A.S., Payne, J., Forbes, C., Saha, D., 2014. Geologically constraining India in Columbia: the age, isotopic provenance and geochemistry of the protoliths of the Ongole Domain, Southern Eastern Ghats, India. Gondwana Research 26 (3), 888–906.

Henry, B., Liégeois, J.P., Nouar, O., Derder, M.E.M., Bayou, B., Bruguier, O., Ouabadi, A., Belhai, D., Amenna, M., Hemmi, A., Ayache, M., 2009. Repeated granitoid intrusions during the Neoproterozoic along the western boundary of the Saharan metacraton, Eastern Hoggar, Tuareg shield, Algeria: an AMS and U–Pb zircon age study. Tectonophysics 474 (3), 417–434.

Higgins, M.D., van Breemen, O., 1998. The age of the Sept Iles layered mafic intrusion, Canada: implications for the late Neoproterozoic/Cambrian history of southeastern Canada. The Journal of Geology 106 (4), 421–432.

Hodych, J.P., Cox, R.A., Košler, J., 2004. An equatorial Laurentia at 550 Ma confirmed by Grenvillian inherited zircons dated by LAM ICP-MS in the Skinner Cove volcanics of western Newfoundland: implications for inertial interchange true polar wander. Precambrian Research 129 (1), 93–113.

Hoffman, P.F., 1991. Did the breakout of Laurentia turn Gondwanaland inside-out. Science 2525011, 1409–1412.

Hoffman, P.F., Hawkins, D.P., Isachsen, C.E., Bowring, S.A., 1996. Precise U-Pb zircon ages for early Damaran magmatism in the Summas Mountains and Welwitschia Inlier, northern Damara belt, Namibia. Communications of the Geological Survey of Namibia. 11, pp. 47–52.

Hoffman, P.F., Kaufman, A.J., Halverson, G.P., Schrag, D.P., 1998a. A Neoproterozoic snowball earth. Science 2815381, 1342–1346.

Hoffman, P.F., Kaufman, A.J., Halverson, G.P., Schrag, D.P., 1998b. Comings and goings of global glaciations on a Neoproterozoic tropical platform in Namibia. GSA Today 8 (5), 1–9.

Hoffmann, K.H., Condon, D.J., Bowring, S.A., Crowley, J.L., 2004. U-Pb zircon date from the Neoproterozoic Ghaub Formation, Namibia: constraints on Marinoan glaciation. Geology 32 (9), 817–820.

Huang, B., Xu, B., Zhang, C., Li, Y.A., Zhu, R., 2005. Paleomagnetism of the Baiyisi volcanic rocks (ca. 740 Ma) of Tarim, Northwest China: a continental fragment of Neoproterozoic Western Australia? Precambrian Research 142 (3), 83–92.

Hyodo, H., Dunlop, D.J., 1993. Effect of anisotropy on the paleomagnetic contact test for a Grenville dike. Journal of Geophysical Research, Solid Earth 98 (B5), 7997–8017.

Iglesia Llanos, M.P., Tait, J.A., Popov, V., Abalmassova, A., 2005. Palaeomagnetic data from Ediacaran (Vendian) sediments of the Arkhangelsk region, NW Russia: an alternative apparent polar wander path of Baltica for the Late Proterozoic-Early Palaeozoic. Earth and Planetary Science Letters 240, 732–747.

Inglis, J.D., Samson, S.D., D'lemos, R.S., Miller, B.V., 2005. Timing of Cadomian deformation and magmatism within La Hague, NW France. Journal of the Geological Society 162 (2), 389–400.

Jacobs, J., Elburg, M., Läufer, A., Kleinhanns, I.C., Henjes-Kunst, F., Estrada, S., Ruppel, A.S., Damaske, D., Montero, P., Bea, F., 2015. Two distinct Late Mesoproterozoic/Early Neoproterozoic basement provinces in central/eastern Dronning Maud Land, East Antarctica: the missing link, 15–21 E. Precambrian Research 265, 249–272.

Jacobs, J., Pisarevsky, S., Thomas, R.J., Becker, T., 2008. The Kalahari Craton during the assembly and dispersal of Rodinia. Precambrian Research 160 (1), 142–158.

Jardim de Sá, E.F., Moraes, J.A.C., D'el-Rey Silva, L.J.H., 1986. Tectônica tangencial na Faixa Sergipana. 34° Congresso Brasileiro de Geologia 3, pp. 1246–1259 (Abstracts).

Jing, X., Yang, Z., Tong, Y., Han, Z., 2015. A revised paleomagnetic pole from the mid-Neoproterozoic Liantuo Formation in the Yangtze block and its paleogeographic implications. Precambrian Research 268, 194–211.

Johansson, Å., 2009. Baltica, Amazonia and the SAMBA connection—1000 million years of neighbourhood during the Proterozoic? Precambrian Research 175 (1), 221–234.

Johansson, Å., 2014. From Rodinia to Gondwana with the 'SAMBA' model—a distant view from Baltica towards Amazonia and beyond. Precambrian Research 244, 226–235.

John, T., Schenk, V., Haase, K., Scherer, E., Tembo, F., 2003. Evidence for a Neoproterozoic ocean in south-central Africa from mid-oceanic-ridge–type geochemical signatures and pressure-temperature estimates of Zambian eclogites. Geology 31 (3), 243–246.

John, T., Schenk, V., Mezger, K., Tembo, F., 2004b. Timing and PT evolution of whiteschist metamorphism in the Lufilian Arc–Zambezi Belt orogen (Zambia): implications for the assembly of Gondwana. The Journal of Geology 112 (1), 71–90.

John, T., Scherer, E.E., Haase, K., Schenk, V., 2004a. Trace element fractionation during fluid-induced eclogitization in a subducting slab: trace element and Lu–Hf–Sm–Nd isotope systematics. Earth and Planetary Science Letters 227 (3), 441–456.

Johnson, P.R., Andresen, A., Collins, A.S., Fowler, A.R., Fritz, H., Ghebreab, W., Kusky, T., Stern, R.J., 2011. Late Cryogenian–Ediacaran history of the Arabian–Nubian Shield: a review of depositional, plutonic, structural, and tectonic events in the closing stages of the northern East African Orogen. Journal of African Earth Sciences 61 (3), 167–232.

Johnson, T.E., Clark, C., Taylor, R.J., Santosh, M., Collins, A.S., 2015. Prograde and retrograde growth of monazite in migmatites: an example from the Nagercoil Block, southern India. Geoscience Frontiers 6 (3), 373–387.

Johnson, S.P., De Waele, B., Liyungu, K.A., 2006. U-Pb sensitive high-resolution ion microprobe (SHRIMP) zircon geochronology of granitoid rocks in eastern Zambia: terrane subdivision of the Mesoproterozoic Southern Irumide Belt. Tectonics 25 (6).

Johnson, S.P., De Waele, B., Tembo, F., Katongo, C., Tani, K., Chang, Q., Iizuka, T., Dunkley, D., 2007. Geochemistry, geochronology and isotopic evolution of the Chewore–Rufunsa Terrane, Southern Irumide Belt: a Mesoproterozoic continental margin arc. Journal of Petrology 48 (7), 1411–1441.

Johnson, E.L., Phillips, G., Allen, C.M., 2016. Ediacaran–Cambrian basin evolution in the Koonenberry Belt (eastern Australia): implications for the geodynamics of the Delamerian Orogen. Gondwana Research 37, 266–284.

Johnson, S.P., Rivers, T., De Waele, B., 2005. A review of the Mesoproterozoic to early Palaeozoic magmatic and tectonothermal history of south–central Africa: implications for Rodinia and Gondwana. Journal of the Geological Society 162 (3), 433–450.

Johnson, P.R., Stewart, I.C., 1995. Magnetically inferred basement structure in central Saudi Arabia. Tectonophysics 245 (1), 37–52.

Johnson, P.R., Woldehaimanot, B., 2003. Development of the Arabian-Nubian Shield: perspectives on accretion and deformation in the northern East African Orogen and the assembly of Gondwana. Geological Society, London, Special Publications 206 (1), 289–325.

Jöns, N., Schenk, V., 2008. Relics of the Mozambique Ocean in the central East African Orogen: evidence from the Vohibory Block of southern Madagascar. Journal of Metamorphic Geology 26 (1), 17–28.

Jung, S., Hoernes, S., Mezger, K., 2000. Geochronology and petrogenesis of Pan-African, syn-tectonic, S-type and post-tectonic A-type granite (Namibia): products of melting of crustal sources, fractional crystallization and wall rock entrainment. Lithos 50 (4), 259–287.

Jung, S., Mezger, K., 2003. U-Pb garnet chronometry in high-grade rocks—case studies from the central Damara orogen (Namibia) and implications for the interpretation of Sm-Nd garnet ages and the role of high U-Th inclusions. Contributions to Mineralogy and Petrology 146 (3), 382–396.

Kalsbeek, F., Affaton, P., Ekwueme, B., Frei, R., Thrane, K., 2012. Geochronology of granitoid and metasedimentary rocks from Togo and Benin, West Africa: comparisons with NE Brazil. Precambrian Research 196, 218–233.

Kamo, S.L., Gower, C.F., 1994. Note: U-Pb baddeleyite dating clarifies age of characteristic paleomagnetic remanence of Long Range dykes, southeastern Labrador. Atlantic Geology 30, 259–262.

Kamo, S.L., Krogh, T.E., Kumarapeli, P.S., 1995. Age of the Grenville dyke swarm, Ontario-Quebec: implications for the timing of Lapetan rifting. Canadian Journal of Earth Sciences 32 (3), 273–280.

Karlstrom, K.E., Åhäll, K.I., Harlan, S.S., Williams, M.L., McLelland, J., Geissman, J.W., 2001. Long-lived (1.8–1.0 Ga) convergent orogen in southern Laurentia, its extensions to Australia and Baltica, and implications for refining Rodinia. Precambrian Research 111 (1), 5–30.

Karlstrom, K.E., Williams, M.L., McLelland, J., Geissman, J.W., Ahall, K., 1999. Refining Rodinia: geologic evidence for the Australia-Western US connection in the Proterozoic. GSA Today 9, 1–7.

Karmakar, S., Schenk, V., 2015. Neoarchean UHT metamorphism and Paleoproterozoic UHT reworking at Uweinat in the East Sahara Ghost Craton, SW Egypt: evidence from petrology and texturally controlled in situ monazite dating. Journal of Petrology 56 (9), 1703–1742.

Karmakar, S., Schenk, V., 2016. Mesoproterozoic UHT metamorphism in the Southern Irumide Belt, Chipata, Zambia: petrology and in situ monazite dating. Precambrian Research 275, 332–356.

Kasch, K.W., 1983. Regional PT variations in the Damara Orogen with particular reference to early high-pressure metamorphism along the southern margin. Evolution of the Damara Orogen of South West Africa/Namibia. 11, pp. 243–253.

Katz, M.B., 1989. Sri Lanka-Indian eastern Ghats-east Antarctica and the Australian Albany Fraser mobile belt: gross geometry, age relationships, and tectonics in Precambrian Gondwanaland. The Journal of Geology 97 (5), 646–648.

Kelsey, D.E., Hand, M., Clark, C., Wilson, C.J.L., 2007. On the application of in situ monazite chemical geochronology to constraining P–T–t histories in high-temperature (>850 °C) polymetamorphic granulites from Prydz Bay, East Antarctica. Journal of the Geological Society 164 (3), 667–683.

Keppie, J.D., Dostal, J., Dallmeyer, R.D., Doig, R., 2000. Superposed Neoproterozoic and Silurian magmatic arcs in central Cape Breton Island, Canada: geochemical and geochronological constraints. Geological Magazine 137 (02), 137–153.

Keppie, J.D., Ortega-Gutiérrez, F., 2010. 1.3–0.9 Ga Oaxaquia (Mexico): remnant of an arc/backarc on the northern margin of Amazonia. Journal of South American Earth Sciences 29 (1), 21–27.

Kirschvink, J.L., 1992. Late Proterozoic Low-latitude Global Glaciation: The Snowball Eart.

Klein, R., Salminen, J., Mertanen, S., 2015. Baltica during the Ediacaran and Cambrian: a paleomagnetic study of Hailuoto sediments in Finland. Precambrian Research 267, 94–105.

Knesel, K.M., Cohen, B.E., Vasconcelos, P.M., Thiede, D.S., 2008. Rapid change in drift of the Australian plate records collision with Ontong Java plateau. Nature 4547205, 754–757.

Koester, E., Porcher, C.C., Pimentel, M.M., Fernandes, L.A.D., Vignol-Lelarge, M.L., Oliveira, L.D., Ramos, R.C., 2016. Further evidence of 777 Ma subduction-related continental arc magmatism in Eastern Dom Feliciano Belt, southern Brazil: the Chácara das Pedras Orthogneiss. Journal of South American Earth Sciences 68, 155–166.

Korhonen, F.J., Clark, C., Brown, M., Bhattacharya, S., Taylor, R., 2013. How long-lived is ultrahigh temperature (UHT) metamorphism? Constraints from zircon and monazite geochronology in the Eastern Ghats orogenic belt, India. Precambrian Research 234, 322–350.

Kumar, T.V., Rao, Y.B., Plavsa, D., Collins, A.S., Tomson, J.K., Gopal, B.V., Babu, E.V.S.S.K., 2016. Zircon U-Pb ages and Hf isotopic systematics of charnockite gneisses from the Ediacaran—Cambrian high-grade metamorphic terranes, southern India: Constraints on crust formation, recycling, and Gondwana correlations. GSA Bulletin, B31474-1.

Küster, D., Liégeois, J.P., 2001. Sr, Nd isotopes and geochemistry of the Bayuda Desert high-grade metamorphic basement (Sudan): an early Pan-African oceanic convergent margin, not the edge of the East Saharan ghost craton? Precambrian Research 109 (1), 1–23.

Küster, D., Liégeois, J.P., Matukov, D., Sergeev, S., Lucassen, F., 2008. Zircon geochronology and Sr, Nd, Pb isotope geochemistry of granitoids from Bayuda Desert and Sabaloka (Sudan): evidence for a Bayudian event (920–900 Ma) preceding the Pan-African orogenic cycle (860–590 Ma) at the eastern boundary of the Saharan Metacraton. Precambrian Research 164 (1), 16–39.

Kwékam, M., Liégeois, J.P., Njonfang, E., Affaton, P., Hartmann, G., Tchoua, F., 2010. Nature, origin and significance of the Fomopéa Pan-African high-K calc-alkaline plutonic complex in the Central African fold belt (Cameroon). Journal of African Earth Sciences 57 (1), 79–95.

Lan, C.Y., Chung, S.L., Van Long, T., Lo, C.H., Lee, T.Y., Mertzman, S.A., Jiun-San Shen, J., 2003. Geochemical and Sr–Nd isotopic constraints from the Kontum massif, central Vietnam on the crustal evolution of the Indochina block. Precambrian Research 122 (1), 7–27.

Landing, E., 2005. Early Paleozoic Avalon–Gondwana unity: an obituary—response to "Palaeontological evidence bearing on global Ordovician–Silurian continental reconstructions" by RA Fortey and LRM Cocks. Earth-Science Reviews 69 (1), 169–175.

Lavoie, D., Burden, E., Lebel, D., 2003. Stratigraphic framework for the Cambrian Ordovician rift and passive margin successions from southern Quebec to western Newfoundland. Canadian Journal of Earth Sciences 40 (2), 177–205.

Lehmann, J., Saalmann, K., Naydenov, K.V., Milani, L., Belyanin, G.A., Zwingmann, H., Charlesworth, G., Kinnaird, J.A., 2016. Structural and geochronological constraints on the Pan-African tectonic evolution of the northern Damara Belt, Namibia. Tectonics 35 (1), 103–135.

Leite, J.A., Hartman, L.A., Mcnaughton, N.J., Chemale Jr., F., 1998. SHRIMP U/Pb zircon geochronology of Neoproterozoic juvenile and crustal-reworked terranes in southernmost Brazil. International Geology Review 40 (8), 688–705.

Lenz, C., Porcher, C.C., Fernandes, L.A.D., Masquelin, H., Koester, E., Conceição, R.V., 2013. Geochemistry of the Neoproterozoic (800–767 Ma) Cerro Bori orthogneisses, Dom Feliciano Belt in Uruguay: tectonic evolution of an ancient continental arc. Mineralogy and Petrology 107 (5), 785–806.

Levashova, N.M., Bazhenov, M.L., Meert, J.G., Kuznetsov, N.B., Golovanov, I.V., Danukalov, K.N., Fedorova, N.M., 2013. Paleogeography of Baltica in the Ediacaran: paleomagnetic

and geochronological data from the clastic Zigan Formation, South Urals. Precambrian Research 236, 16–30.

Li, Z.X., 2000. New palaeomagnetic results from the 'cap dolomite' of the Neoproterozoic Walsh Tillite, northwestern Australia. Precambrian Research 100 (1), 359–370.

Li, Z.X., Bogdanova, S.V., Collins, A.S., Davidson, A., De Waele, B., Ernst, R.E., Fitzsimons, I.C.W., Fuck, R.A., Gladkochub, D.P., Jacobs, J., Karlstrom, K.E., Lu, S., Natapov, L.M., Pease, V., Pisarevsky, S.A., Thrane, K., Vernikovsky, V., 2008. Assembly, configuration, and break-up history of Rodinia: a synthesis. Precambrian Research 160 (1), 179–210.

Li, Z.X., Evans, D.A., 2011. Late Neoproterozoic 40° intraplate rotation within Australia allows for a tighter-fitting and longer-lasting Rodinia. Geology 39 (1), 39–42.

Li, Z.X., Evans, D.A., Halverson, G.P., 2013. Neoproterozoic glaciations in a revised global palaeogeography from the breakup of Rodinia to the assembly of Gondwanaland. Sedimentary Geology 294, 219–232.

Li, Z.X., Evans, D.A.D., Zhang, S., 2004. A 90 spin on Rodinia: possible causal links between the Neoproterozoic supercontinent, superplume, true polar wander and low-latitude glaciation. Earth and Planetary Science Letters 220 (3), 409–421.

Li, Z.X., Li, X.H., Kinny, P.D., Wang, J., 1999. The breakup of Rodinia: did it start with a mantle plume beneath South China? Earth and Planetary Science Letters 173 (3), 171–181.

Li, Z.X., Li, X.H., Kinny, P.D., Wang, J., Zhang, S., Zhou, H., 2003. Geochronology of Neoproterozoic syn-rift magmatism in the Yangtze Craton, South China and correlations with other continents: evidence for a mantle superplume that broke up Rodinia. Precambrian Research 122 (1), 85–109.

Li, L., Tull, J.F., 1998. Cover stratigraphy and structure of the southernmost external basement massifs in the Appalachian Blue Ridge; evidence for two-stage late Proterozoic rifting. American Journal of Science 298 (10), 829–867.

Li, Z.X., Zhang, L., Powell, C.M., 1995. South China in Rodinia: part of the missing link between Australia–East Antarctica and Laurentia? Geology 23 (5), 407–410.

Li, Z.X., Zhang, L., Powell, C.M., 1996. Positions of the East Asian cratons in the Neoproterozoic supercontinent Rodinia. Australian Journal of Earth Sciences 43 (6), 593–604.

Li, Z.X., Zhong, S., 2009. Supercontinent–superplume coupling, true polar wander and plume mobility: plate dominance in whole-mantle tectonics. Physics of the Earth and Planetary Interiors 176 (3), 143–156.

Liégeois, J.P., Abdelsalam, M.G., Ennih, N., Ouabadi, A., 2013. Metacraton: nature, genesis and behavior. Gondwana Research 23 (1), 220–237.

Liégeois, J.P., Black, R., Navez, J., Latouche, L., 1994. Early and late Pan-African orogenies in the air assembly of terranes (Tuareg Shield, Niger). Precambrian Research 67 (1), 59–88.

Liégeois, J.P., Latouche, L., Boughrara, M., Navez, J., Guiraud, M., 2003. The LATEA metacraton (Central Hoggar, Tuareg shield, Algeria): behaviour of an old passive margin during the Pan-African orogeny. Journal of African Earth Sciences 37 (3), 161–190.

Likhanov, I.I., Nozhkin, A.D., Reverdatto, V.V., Kozlov, P.S., 2014. Grenville tectonic events and evolution of the Yenisei Ridge at the western margin of the Siberian Craton. Geotectonics 48 (5), 371–389.

Likhanov, I.I., Reverdatto, V.V., Kozlov, P.S., Khiller, V.V., Sukhorukov, V.P., 2015. P–T–t constraints on polymetamorphic complexes of the Yenisey Ridge, East Siberia: implications for Neoproterozoic paleocontinental reconstructions. Journal of Asian Earth Sciences 113, 391–410.

Linnemann, U., Pereira, F., Jeffries, T.E., Drost, K., Gerdes, A., 2008. The Cadomian Orogeny and the opening of the Rheic Ocean: the diacrony of geotectonic processes constrained by LA-ICP-MS U–Pb zircon dating (Ossa-Morena and Saxo-Thuringian Zones, Iberian and Bohemian Massifs). Tectonophysics 461 (1), 21–43.

Litherland, M., Power, G., 1989. The geologic and geomorphologic evolution of Serrania Huanchaca, eastern Bolivia: the legendary "Lost World". Journal of South American Earth Sciences 2 (1), 1–17.

Liu, X.C., Jahn, B.M., Zhao, Y., Li, M., Li, H., Liu, X., 2006. Late Pan-African granitoids from the Grove Mountains, East Antarctica: age, origin and tectonic implications. Precambrian Research 145 (1), 131–154.

Liu, X.C., Zhao, Y., Hu, J., 2013. The c. 1000–900 Ma and c. 550–500 Ma tectonothermal events in the Prince Charles Mountains–Prydz Bay region, East Antarctica, and their relations to supercontinent evolution. Geological Society, London, Special Publications 383 (1), 95–112.

Liu, X.C., Zhao, Y., Song, B., Liu, J., Cui, J., 2009. SHRIMP U–Pb zircon geochronology of high-grade rocks and charnockites from the eastern Amery Ice Shelf and southwestern Prydz Bay, East Antarctica: constraints on Late Mesoproterozoic to Cambrian tectonothermal events related to supercontinent assembly. Gondwana Research 16 (2), 342–361.

Liu, Q., Zhao, G., Sun, M., Eizenhöfer, P.R., Han, Y., Hou, W., Zhang, X., Wang, B., Liu, D., Xu, B., 2015. Ages and tectonic implications of Neoproterozoic ortho-and paragneisses in the Beishan Orogenic Belt, China. Precambrian Research 266, 551–578.

Liu, X.C., Zhao, Z., Zhao, Y., Chen, J., Liu, X.H., 2003. Pyroxene exsolution in mafic granulites from the Grove Mountains, East Antarctica. European Journal of Mineralogy 15 (1), 55–65.

Loewy, S.L., Dalziel, I.W.D., Pisarevsky, S., Connelly, J.N., Tait, J., Hanson, R.E., Bullen, D., 2011. Coats Land crustal block, East Antarctica: a tectonic tracer for Laurentia? Geology 39 (9), 859–862.

Longridge, L., 2012. Tectonothermal Evolution of the Southwestern Central Zone, Damara Belt, Namibia. (Unpublished PhD thesis). University of the Witwatersrand, Johannesburg, South Africa (525 pp.).

Longridge, L., Kinnaird, J.A., Gibson, R.L., Armstrong, R.A., 2014. Amphibolites of the Central Zone: new SHRIMP U-Pb ages and implications for the evolution of the Damara Orogen, Namibia. South African Journal of Geology 117 (1), 67–86.

Lubnina, N.V., Pisarevsky, S.A., Puchkov, V.N., Kozlov, V.I., Sergeeva, N.D., 2014. New paleomagnetic data from Late Neoproterozoic sedimentary successions in Southern Urals, Russia: implications for the Late Neoproterozoic paleogeography of the Iapetan realm. International Journal of Earth Sciences 103 (5), 1317–1334.

Mallard, C., Coltice, N., Seton, M., Müller, R.D., Tackley, P.J., 2016. Subduction controls the distribution and fragmentation of Earth's tectonic plates. Nature 535, 140–143.

Mallard, L.D., Rogers, J.J., 1997. Relationship of Avalonian and Cadomian terranes to Grenville and Pan-African events. Journal of Geodynamics 23 (3), 197–221.

Malone, S.J., McClelland, W.C., von Gosen, W., Piepjohn, K., 2014. Proterozoic evolution of the North Atlantic–Arctic Caledonides: insights from detrital zircon analysis of metasedimentary rocks from the Pearya Terrane, Canadian High Arctic. The Journal of Geology 122 (6), 623–647.

Martin, M.W., Grazhdankin, D.V., Bowring, S.A., Evans, D.A.D., Fedonkin, M.A., Kirschvink, J.L., 2000. Age of Neoproterozoic bilatarian body and trace fossils, White Sea, Russia: implications for metazoan evolution. Science 2885467, 841–845.

Masberg, P., Mihm, D., Jung, S., 2005. Major and trace element and isotopic (Sr, Nd, O) constraints for Pan-African crustally contaminated grey granite gneisses from the southern Kaoko belt, Namibia. Lithos 84 (1), 25–50.

Matteini, M., Junges, S.L., Dantas, E.L., Pimentel, M.M., Bühn, B., 2010. In situ zircon U–Pb and Lu–Hf isotope systematic on magmatic rocks: insights on the crustal evolution of the Neoproterozoic Goiás Magmatic Arc, Brasília belt, Central Brazil. Gondwana Research 17 (1), 1–12.

Matthews, K.J., Maloney, K.T., Zahirovic, S., Williams, S.E., Seton, M., Müller, R.D., 2016. Global plate boundary evolution and kinematics since the late Paleozoic. Global and Planetary Change 146, 226–250.

Matthews, K.J., Seton, M., Müller, R.D., 2012. A global-scale plate reorganization event at 105 − 100 Ma. Earth and Planetary Science Letters 355, 283–298.

Maurin, J.C., 1993. La chaine panafricaine ouest-congolienne; correlation avec le domaine est-bresilien et hypothese geodynamique. Bulletin de la Société Géologique de France 164 (1), 51–60.

McCausland, P.J., Hankard, F., Van der Voo, R., Hall, C.M., 2011. Ediacaran paleogeography of Laurentia: paleomagnetism and 40Ar–39Ar geochronology of the 583 Ma Baie des Moutons syenite, Quebec. Precambrian Research 187 (1), 58–78.

McCausland, P.J.A., Hodych, J.P., 1998. Paleomagnetism of the 550 Ma Skinner Cove volcanics of western Newfoundland and the opening of the Iapetus Ocean. Earth and Planetary Science Letters 163, 15–29.

McCausland, P.J.A., Hodych, J.P., Dunning, G.R., 1997. Evidence from western Newfoundland for the final breakup of Rodinia? U-Pb age and palaeolatitude of the Skinner Cove volcanics. In: Ottawa, A. (Ed.), Geological Association of Canada and Mineralogical Association of Canada Annual Meeting. vol. 99 (Abstracts).

McElhinny, M.W., Cowley, J.A., Edwards, D.J., 1978. Palaeomagnetism of some rocks from peninsular India and Kashmir. Tectonophysics 50, 41–54.

McGee, B., Collins, A.S., Trindade, R.I., 2012b. G'day Gondwana—the final accretion of a supercontinent: U–Pb ages from the post-orogenic São Vicente Granite, northern Paraguay Belt, Brazil. Gondwana Research 21 (2), 316–322.

McGee, B., Collins, A.S., Trindade, R.I., 2013. A glacially incised canyon in Brazil: further evidence for mid-Ediacaran glaciation? The Journal of Geology 121 (3), 275–287.

McGee, B., Collins, A.S., Trindade, R.I., Jourdan, F., 2015a. Investigating mid-Ediacaran glaciation and final Gondwana amalgamation using coupled sedimentology and 40Ar/39Ar detrital muscovite provenance from the Paraguay Belt, Brazil. Sedimentology 62 (1), 130–154.

McGee, B., Collins, A.S., Trindade, R.I., Payne, J., 2015b. Age and provenance of the Cryogenian to Cambrian passive margin to foreland basin sequence of the northern Paraguay Belt, Brazil. Geological Society of America Bulletin 127 (1–2), 76–86.

McGee, B., Halverson, G.P., Collins, A.S., 2012a. Cryogenian rift-related magmatism and sedimentation: South-western Congo Craton, Namibia. Journal of African Earth Sciences 76, 34–49.

McMenamin, M.A., McMenamin, D.L.S., 1990. The Emergence of Animals: The Cambrian Breakthrough. Columbia University Press.

McWilliams, M.O., 1981. Palaeomagnetism and Precambrian tectonic evolution of Gondwana. Developments in Precambrian Geology. 4, pp. 649–687.

Meert, J.G., 2003. A synopsis of events related to the assembly of eastern Gondwana. Tectonophysics 362 (1), 1–40.

Meert, J.G., 2014a. Strange attractors, spiritual interlopers and lonely wanderers: the search for pre-Pangean supercontinents. Geoscience Frontiers 5 (2), 155–166.

Meert, J.G., 2014b. Ediacaran–Early Ordovician paleomagnetism of Baltica: a review. Gondwana Research 25 (1), 159–169.

Meert, J.G., Lieberman, B.S., 2004. A palaeomagnetic and palaeobiogeographical perspective on latest Neoproterozoic and early Cambrian tectonic events. Journal of the Geological Society 161 (3), 477–487.

Meert, J.G., Lieberman, B.S., 2008. The Neoproterozoic assembly of Gondwana and its relationship to the Ediacaran–Cambrian radiation. Gondwana Research 14 (1), 5–21.

Meert, J.G., Pandit, M., Kamenov, G.D., 2013. Further geochronological and paleomagnetic constraints on Malani (and pre-Malani) magmatism in NW India. Tectonophysics 608, 1254–1267.

Meert, J.G., Pandit, M.K., Pradhan, V.R., Banks, J., Sirianni, R., Stroud, M., Newstead, B., Gifford, J., 2010. Precambrian crustal evolution of peninsular India: a 3.0 billion year odyssey. Journal of Asian Earth Sciences 39 (6), 483–515.

Meert, J.G., Torsvik, T.H., 2003. The making and unmaking of a supercontinent: Rodinia revisited. Tectonophysics 375 (1), 261–288.

Meert, J.G., Van Der Voo, R., 1997. The assembly of Gondwana 800–550 Ma. Journal of Geodynamics 23 (3), 223–235.

Meert, J.G., Van der Voo, R., Ayub, S., 1995. Paleomagnetic investigation of the Neoproterozoic Gagwe lavas and Mbozi complex, Tanzania and the assembly of Gondwana. Precambrian Research 74 (4), 225–244.

Meert, J.G., Van der Voo, R., Powell, C.M., Li, Z.X., McElhinny, M.W., Chen, Z., Symons, D.T.A., 1993. A plate-tectonic speed limit? Nature 363, 216–217.

Metcalfe, I., 2006. Palaeozoic and Mesozoic tectonic evolution and palaeogeography of East Asian crustal fragments: the Korean Peninsula in context. Gondwana Research 9 (1), 24–46.

Metcalfe, I., 2011. Palaeozoic–Mesozoic history of SE Asia. Geological Society, London, Special Publications 355 (1), 7–35.

Metcalfe, I., 2013. Gondwana dispersion and Asian accretion: tectonic and palaeogeographic evolution of eastern Tethys. Journal of Asian Earth Sciences 66, 1–33.

Metelkin, D.V., Vernikovsky, V.A., Kazansky, A.Y., 2012. Tectonic evolution of the Siberian paleocontinent from the Neoproterozoic to the Late Mesozoic: paleomagnetic record and reconstructions. Russian Geology and Geophysics 53 (7), 675–688.

Meyer, C., 1988. Ore deposits as guides to geologic history of the Earth. Annual Review of Earth and Planetary Sciences 16, 147.

Mezger, K., Cosca, M.A., 1999. The thermal history of the Eastern Ghats Belt (India) as revealed by U–Pb and ^{40}Ar/^{39}Ar dating of metamorphic and magmatic minerals: implications for the SWEAT correlation. Precambrian Research 94 (3), 251–271.

Mikhalsky, E.V., Sheraton, J.W., 2011. The Rayner tectonic province of East Antarctica: compositional features and geodynamic setting. Geotectonics 45 (6), 496–512.

Mikhalsky, E.V., Sheraton, J.W., Kudriavtsev, I.V., Sergeev, S.A., Kovach, V.P., Kamenev, I.A., Laiba, A.A., 2013. The Mesoproterozoic Rayner Province in the Lambert Glacier area: its age, origin, isotopic structure and implications for Australia–Antarctica correlations. Geological Society, London, Special Publications 383 (1), 35–57.

Miller, R.M., 1983. The Pan-African Damara Orogen of South West Africa/Namibia. Evolution of the Damara Orogen of South West Africa/Namibia.

Miller, R.M., 2008. The Geology of Namibia. Geological Survey of Namibia, Windhoek.

Miller, R.M., 2013. Comparative stratigraphic and geochronological evolution of the Northern Damara Supergroup in Namibia and the Katanga Supergroup in the Lufilian Arc of Central Africa. Geoscience Canada 40 (2), 118–140.

Miller, B.V., Barr, S.M., 2004. Metamorphosed gabbroic dikes related to opening of Iapetus Ocean at the St. Lawrence promontory: Blair River Inlier, Nova Scotia, Canda. The Journal of Geology 112 (3), 277–288.

Miller, R.M., Becker, T., 2008. The Geology of Namibia: Neoproterozoic to Lower Palaeozoic. vol. 2. Ministry of Mines and Energy Geological Survey of Namibia.

Miller, K.C., Hargraves, R.B., 1994. Paleomagnetism of some Indian kimberlites and lamproites. Precambrian Research 69 (1–4), 259–267.

Mishra, D.C., Singh, B., Tiwari, V.M., Gupta, S.B., Rao, M.B.S.V., 2000. Two cases of continental collisions and related tectonics during the Proterozoic period in India—insights from gravity modelling constrained by seismic and magnetotelluric studies. Precambrian Research 99 (3), 149–169.

Mitchell, R.N., Kilian, T.M., Evans, D.A., 2012. Supercontinent cycles and the calculation of absolute palaeolongitude in deep time. Nature 4827384, 208–211.

Moores, E.M., 1991. Southwest US-East Antarctic (SWEAT) connection: a hypothesis. Geology 19 (5), 425–428.

Moraes, R., Brown, M., Fuck, R.A., Camargo, M.A., Lima, T.M., 2002. Characterization and P–T evolution of melt-bearing ultrahigh-temperature granulites: an example from the Anápolis–Itauçu Complex of the Brasília Fold Belt, Brazil. Journal of Petrology 43 (9), 1673–1705.

Morra, G., Seton, M., Quevedo, L., Müller, R.D., 2013. Organization of the tectonic plates in the last 200 Myr. Earth and Planetary Science Letters 373, 93–101.

Moura, C.A., Gaudette, H., 1993. Evidence of Brasiliano/Panafrican deformation in the Araguaia belt: implication for Gondwana evolution. Revista Brasileira de Geociencias 23 (2), 117–123.

Moura, C.A.V., Pinheiro, B.L.S., Nogueira, A.C.R., Gorayeb, P.S.S., Galarza, M.A., 2008. Sedimentary provenance and palaeoenvironment of the Baixo Araguaia Supergroup: constraints on the palaeogeographical evolution of the Araguaia Belt and assembly of West Gondwana. Geological Society, London, Special Publications 294 (1), 173–196.

Moussine-Pouchkine, A., Bertrand-Sarfati, J., 1978. Le Gourma; un aulacogene du Precambrien superieur? Bulletin de la Société Géologique de France 7 (6), 851–855.

Müller, R.D., Seton, M., Zahirovic, S., Williams, S.E., Matthews, K.J., Wright, N.M., Shephard, G.E., Maloney, K.T., Barnett-Moore, N., Hosseinpour, M., Bower, D.J., 2016. Ocean basin evolution and global-scale plate reorganization events since Pangea breakup. Annual Review of Earth and Planetary Sciences 44 (1), 107–138.

Murphy, J.B., Keppie, J.D., Dostal, J., Nance, R.D., 1999. Neoproterozoic-Early Paleozoic evolution of Avalonia. Laurentia-Gondwana Connections Before Pangea. 336, p. 253.

Murphy, J.B., Nance, R.D., 1989. Model for the evolution of the Avalonian-Cadomian belt. Geology 17 (8), 735–738.

Murphy, J.B., Pisarevsky, S., Nance, R.D., 2013. Potential geodynamic relationships between the development of peripheral orogens along the northern margin of Gondwana and the amalgamation of West Gondwana. Mineralogy and Petrology 107 (5), 635–650.

Murphy, J.B., Pisarevsky, S.A., Nance, R.D., Keppie, J.D., 2004. Neoproterozoic—Early Paleozoic evolution of peri-Gondwanan terranes: implications for Laurentia-Gondwana connections. International Journal of Earth Sciences 93 (5), 659–682.

Murphy, J.B., Strachan, R.A., Nance, R.D., Parker, K.D., Fowler, M.B., 2000. Proto-Avalonia: a 1.2–1.0 Ga tectonothermal event and constraints for the evolution of Rodinia. Geology 28 (12), 1071–1074.

Murthy, G.S., Gower, C., Tubett, M., Patzold, R., 1992. Paleomagnetism of Eocambrian Long Range dykes and Double Mer Formation from Labrador, Canada. Canadian Journal of Earth Sciences 29, 1224–1234.

Nagy, E.A., Schärer, U., Minh, N.T., 2000. Oligo-Miocene granitic magmatism in central Vietnam and implications for continental deformation in Indochina. Terra Nova 12 (2), 67–76.

Nance, R.D., Murphy, J.B., 2013. Origins of the supercontinent cycle. Geoscience Frontiers 4 (4), 439–448.

Nance, R.D., Murphy, J.B., Keppie, J.D., 2002. A Cordilleran model for the evolution of Avalonia. Tectonophysics 352 (1), 11–31.

Nance, R.D., Murphy, J.B., Santosh, M., 2014. The supercontinent cycle: a retrospective essay. Gondwana Research 25 (1), 4–29.

Nance, R.D., Murphy, J.B., Strachan, R.A., D'Lemos, R.S., Taylor, G.K., 1991. Late Proterozoic tectonostratigraphic evolution of the Avalonian and Cadomian terranes. Precambrian Research 53 (1–2), 41–78.

Nance, R.D., Murphy, J.B., Strachan, R.A., Keppie, J.D., Gutiérrez-Alonso, G., Fernández-Suárez, J., Quesada, C., Linnemann, U., D'lemos, R., Pisarevsky, S.A., 2008. Neoproterozoic-early Palaeozoic tectonostratigraphy and palaeogeography of the peri-Gondwanan terranes: Amazonian v. West African connections. Geological Society, London, Special Publications 297 (1), 345–383.

Nanda, J., Gupta, S., Dobmeier, C.J., 2008. Metamorphism of the Koraput Alkaline Complex, Eastern Ghats Province, India—evidence for reworking of a granulite terrane. Precambrian Research 165 (3), 153–168.

Nascimento, R.S., Oliveira, E.P., Carvalho, M.J., McNaughton, N., 2005. Evolução tectônica do Domínio Canindé, Faixa Sergipana, NE do Brasil. Simpósio sobre o Cráton do São Francisco. 3, pp. 239–242.

Naydenov, K.V., Lehmann, J., Saalmann, K., Milani, L., Kinnaird, J.A., Charlesworth, G., Frei, D., Rankin, W., 2014. New constraints on the Pan-African Orogeny in Central Zambia: a structural and geochronological study of the Hook Batholith and the Mwembeshi Zone. Tectonophysics 637, 80–105.

Neves, S.P., da Silva, J.M.R., Bruguier, O., 2016. The transition zone between the Pernambuco-Alagoas Domain and the Sergipano Belt (Borborema Province, NE Brazil): geochronological constraints on the ages of deposition, tectonic setting and metamorphism of metasedimentary rocks. Journal of South American Earth Sciences 72, 266–278.

Niu, J., Li, Z.X., Zhu, W., 2016. Palaeomagnetism and geochronology of mid-Neoproterozoic Yanbian dykes, South China: implications for a c. 820–800 Ma true polar wander event and the reconstruction of Rodinia. In: Li, Z.X., Evans, D.A.D., Murphy, J.B. (Eds.), Supercontinent Cycles Through Earth History. Geol. Soc. London Spec. Publ. 424, pp. 191–211.

Nkoumbou, C., Barbey, P., Yonta-Ngouné, C., Paquette, J.L., Villiéras, F., 2014. Pre-collisional geodynamic context of the southern margin of the Pan-African fold belt in Cameroon. Journal of African Earth Sciences 99, 245–260.

Novak, S.W., Rankin, D.W., 2004. Compositional zoning of a Neoproterozoic ash-flow sheet of the Mount Rogers Formation, southwestern Virginia Blue Ridge, and the aborted rifting of Laurentia. Geological Society of America Memoirs 197, 571–600.

Nozhkin, A.D., Turkina, O.M., Bibikova, E.V., Terleev, A.A., Khomentovsky, V.V., 1999. Riphean granite-gneiss domes of the Yenisei Range: geological structure and U-Pb isotopic age. Geologiya i Geofizika 40, 1305–1313.

Oliveira, E.P., Bueno, J.F., McNaughton, N.J., Silva Filho, A.F., Nascimento, R.S., Donatti-Filho, J.P., 2015. Age, composition, and source of continental arc-and syn-collision granites of the Neoproterozoic Sergipano Belt, Southern Borborema Province, Brazil. Journal of South American Earth Sciences 58, 257–280.

Oliveira, E.P., Tarney, J., 1990. Petrogenesis of the Canindé de São Francisco Complex: a major Late Proterozoic gabbroic body in the Sergipe Foldbelt, northeastern Brazil. Journal of South American Earth Sciences 3 (2), 125–140.

Oliveira, E.P., Windley, B.F., Araújo, M.N., 2010. The Neoproterozoic Sergipano orogenic belt, NE Brazil: a complete plate tectonic cycle in western Gondwana. Precambrian Research 181 (1), 64–84.

Olovyanishnikov, V.G., Roberts, D., Siedlecka, A., 2000. Tectonics and sedimentation of the Meso-to Neoproterozoic Timan-Varanger Belt along the northeastern margin of Baltica. Polarforschung 68, 267–274.

Owona, S., Schulz, B., Ratschbacher, L., Ondoa, J.M., Ekodeck, G.E., Tchoua, F.M., Affaton, P., 2011. Pan-African metamorphic evolution in the southern Yaounde Group (Oubanguide Complex, Cameroon) as revealed by EMP-monazite dating and thermobarometry of garnet metapelites. Journal of African Earth Sciences 59 (1), 125–139.

Oyhantçabal, P., Siegesmund, S., Wemmer, K., Frei, R., Layer, P., 2007. Post-collisional transition from calc-alkaline to alkaline magmatism during transcurrent deformation in the southernmost Dom Feliciano Belt (Braziliano–Pan-African, Uruguay). Lithos 98 (1), 141–159.

Oyhantçabal, P., Siegesmund, S., Wemmer, K., Passchier, C.W., 2011. The transpressional connection between Dom Feliciano and Kaoko belts at 580–550 Ma. International Journal of Earth Sciences 100 (2–3), 379–390.

Oyhantçabal, P., Siegesmund, S., Wemmer, K., Presnyakov, S., Layer, P., 2009. Geochronological constraints on the evolution of the southern Dom Feliciano Belt (Uruguay). Journal of the Geological Society 166 (6), 1075–1084.

Paciullo, F.V.P., Ribeiro, A., Andreis, R.R., Trouw, R.A.J., 2000. The Andrelândia basin, a Neoproterozoic intraplate continental margin, southern Brasília Belt, Brazil. Brazilian Journal of Geology 30 (1), 200–202.

Paixão, M.A.P., Nilson, A.A., Dantas, E.L., 2008. The Neoproterozoic Quatipuru ophiolite and the Araguaia fold belt, central-northern Brazil, compared with correlatives in NW Africa. Geological Society, London, Special Publications 294 (1), 297–318.

Paquette, J., Caby, R., Djouadi, M.T., Bouchez, J.L., 1998. U–Pb dating of the end of the Pan-African orogeny in the Tuareg shield: the post-collisional syn-shear Tioueine pluton (Western Hoggar, Algeria). Lithos 45 (1), 245–253.

Park, J.K., Buchan, K.L., Harlan, S.S., 1995. A proposed giant radiating dyke swarm fragmented by the separation of Laurentia and Australia based on paleomagnetism of ca. 780 Ma mafic intrusions in western North America. Earth and Planetary Science Letters 132 (1), 129–139.

Patranabis-Deb, S., 2004. Lithostratigraphy of the Neoproterozoic Chattisgarh Sequence, its bearing on the tectonics and palaeogeography. Gondwana Research 7 (2), 323–337.

Patriat, P., Achache, J., 1984. India–Eurasia collision chronology has implications for crustal shortening and driving mechanism of plates. Nature 311, 615–621.

Pavlov, V.E., Gallet, Y., Petrov, P.Y., Zhuravlev, D.Z., Shatsillo, A.V., 2002. The Ui Group and Late Riphean sills in the Uchur-Maya area: isotopic and paleomagnetic data and the problem of the Rodinia supercontinent. Fizika Zemli 38, 26–41.

Pavlov, V.E., Shatsillo, A.V., Petrov, P.Y., 2015. Paleomagnetism of the upper Riphean deposits in the Turukhansk and Olenek uplifts and Uda Pre-Sayan region and the neoproterozoic drift of the Siberian Platform. Izvestiya Physics of the Solid Earth 51 (5), 716–747.

Payne, J.L., Hand, M., Barovich, K.M., Reid, A., Evans, D.A., 2009. Correlations and reconstruction models for the 2500–1500 Ma evolution of the Mawson Continent. Geological Society, London, Special Publications 323 (1), 319–355.

Pedrsoa-Soares, A.C., Noce, C.M., Vidal, P., Monteiro, R.L.B.P., Leonardos, O.H., 1992. Toward a new tectonic model for the late Proterozoic Araçuaí (SE Brazil)-West Congolian (SW Africa) belt. Journal of South American Earth Sciences 6 (1), 33–47.

Pedrosa-Soares, A.C., Noce, C.M., Wiedemann, C.M., Pinto, C.P., 2001. The Araçuaí-West-Congo Orogen in Brazil: an overview of a confined orogen formed during Gondwanaland assembly. Precambrian Research 110 (1), 307–323.

Pedrosa-Soares, A.C., Wiedemann-Leonardos, C.M., 2000. Evolution of the Araçuaí Belt and its connection to the Ribeira Belt, eastern Brazil. Tectonic Evolution of South America. 31, pp. 265–310.

Pehrsson, S.J., Eglington, B.M., Evans, D.A., Huston, D., Reddy, S.M., 2016. Metallogeny and its link to orogenic style during the Nuna supercontinent cycle. Geological Society, London, Special Publications 424 (1), 83–94.

Pimentel, M.M., Fuck, R.A., de Alvarenga, C.J., 1996. Post-Brasiliano (Pan-African) high-K granitic magmatism in Central Brazil: the role of Late Precambrian-early Palaeozoic extension. Precambrian Research 80 (3), 217–238.

Pimentel, M.M., Fuck, R.A., Jost, H., Ferreira Filho, C.F., Araújo, S.D., 2000. The basement of the Brasília fold belt and the Goiás magmatic arc. Tectonic Evolution of South America. 31, pp. 195–229.

Pimentel, M.M., Jost, H., Fuck, R.A., 2004. O embasamento da Faixa Brasília e o arco Magmático de Goiás. In: Mantesso-Neto, V., Bartorelli, A., Dal Ré, Carneiro C., Brito-Neves BB Org (Eds.), Geologia do Continente Sul-Americano: evolução da obra de Fernando Flávio Marques de Almeida. Beca, São Paulo, pp. 355–368.

Pimentel, M.M., Rodrigues, J.B., DellaGiustina, M.E.S., Junges, S., Matteini, M., Armstrong, R., 2011. The tectonic evolution of the Neoproterozoic Brasília Belt, central Brazil, based on SHRIMP and LA-ICPMS U–Pb sedimentary provenance data: a review. Journal of South American Earth Sciences 31 (4), 345–357.

Pin, C., Poidevin, J.L., 1987. U-Pb zircon evidence for a pan-African granulite facies metamorphism in the Central African Republic. A new interpretation of the high-grade series of the northern border of the Congo craton. Precambrian Research 36 (3), 303–312.

Piper, J.D.A., Beckmann, G.E.J., Badham, J.P.N., 1976. Palaeomagnetic evidence for a Proterozoic super-continent [and discussion]. Philosophical Transactions of the Royal Society of London A 2801298, 469–490.

Pisarevsky, S.A., Bylund, G., 2006. Palaeomagnetism of 935 Ma mafic dykes in southern Sweden and implications for the Sveconorwegian Loop. Geophysical Journal International 166, 1095–1104.

Pisarevsky, S.A., Elming, S.Å., Pesonen, L.J., Li, Z.X., 2014. Mesoproterozoic paleogeography: supercontinent and beyond. Precambrian Research 244, 207–225.

Pisarevsky, S.A., Gladkochub, D.P., Konstantinov, K.M., Mazukabzov, A.M., Stanevich, A.M., Murphy, J.B., Tait, J.A., Donskaya, T.V., Konstantinov, I.K., 2013. Paleomagnetism of Cryogenian Kitoi mafic dykes in South Siberia: implications for Neoproterozoic paleogeography. Precambrian Research 231, 372–382.

Pisarevsky, S.A., Gurevich, E.L., Khramov, A.N., 1997. Palaeomagnetism of Lower Cambrian sediments from the Olenek River section (northern Siberia): palaeopoles and the problem of magnetic polarity in the Early Cambrian. Geophysical Journal International 130, 746–756.

Pisarevsky, S.A., Murphy, J.B., Cawood, P.A., Collins, A.S., 2008a. Late Neoproterozoic and Early Cambrian palaeogeography: models and problems. Geological Society, London, Special Publications 294 (1), 9–31.

Pisarevsky, S.A., Natapov, L.M., 2003. Siberia and Rodinia. Tectonophysics 375 (1), 221–245.

Pisarevsky, S.A., Natapov, L.M., Donskaya, T.V., Gladkochub, D.P., Vernikovsky, V.A., 2008b. Proterozoic Siberia: a promontory of Rodinia. Precambrian Research 160 (1), 66–76.

Pisarevsky, S.A., Wingate, M.T., Powell, C.M., Johnson, S., Evans, D.A., 2003. Models of Rodinia assembly and fragmentation. Geological Society, London, Special Publications 206 (1), 35–55.

Pisarevsky, S.A., Wingate, M.T.D., Stevens, M.K., Haines, P.W., 2007. Paleomagnetic results from the Lancer-1 stratigraphic drill hole, Officer Basin, Western Australia, and implications for Rodinia reconstructions. Australian Journal of Earth Sciences 54, 561–572.

Piuzana, D., Pimentel, M.M., Fuck, R.A., Armstrong, R., 2003. Neoproterozoic granulite facies metamorphism and coeval granitic magmatism in the Brasilia Belt, Central Brazil: regional implications of new SHRIMP U–Pb and Sm–Nd data. Precambrian Research 125 (3), 245–273.

Plavsa, D., Collins, A.S., Foden, J.D., Clark, C., 2015. The evolution of a Gondwanan collisional orogen: a structural and geochronological appraisal from the Southern Granulite Terrane, South India. Tectonics 34 (5), 820–857.

Plavsa, D., Collins, A.S., Foden, J.F., Kropinski, L., Santosh, M., Chetty, T.R.K., Clark, C., 2012. Delineating crustal domains in peninsular India: age and chemistry of orthopyroxene-bearing felsic gneisses in the Madurai block. Precambrian Research 198, 77–93.

Plavsa, D., Collins, A.S., Payne, J.L., Foden, J.D., Clark, C., Santosh, M., 2014. Detrital zircons in basement metasedimentary protoliths unveil the origins of southern India. Geological Society of America Bulletin 126 (5–6), 791–811.

Poidevin, J.L., 1985. Le Proterozoic supérieur de la Républic Centrafricaine. Annales du Musée Royal de l'Afrique centrale, Tervuren (Belgique), Serie in-8, Sciences Geologiques. 91 (75 pp.).

Popov, N.V., 2001. A tectonic model of the Early Precambrian evolution of the south Yenisey Ridge. Russian Geology and Geophysics 42, 1028–1041.

Popov, V., Iosifidi, A., Khramov, A., Tait, J., Bachtadse, V., 2002. Paleomagnetism of Upper Vendian sediments from the Winter Coast, White Sea region, Russia: implications for the paleogeography of Baltica during Neoproterozoic times. Journal of Geophysical Research 107 (B11):2315. http://dx.doi.org/10.1029/2001JB001607.

Popov, V.V., Khramov, A.N., Bachtadse, V., 2005. Palaeomagnetism, magnetic stratigraphy, and petromagnetism of the Upper Vendian sedimentary rocks in the sections of the Zolotitsa River and in the Verkhotina Hole, Winter Coast of the White Sea, Russia. Russian Journal of Earth Sciences 7 (2), 1–29.

Porada, H., Berhorst, V., 2000. Towards a new understanding of the Neoproterozoic-Early Palaeozoic Lufilian and northern Zambezi Belts in Zambia and the Democratic Republic of Congo. Journal of African Earth Sciences 30 (3), 727–771.

Powell, C.M., Dalziel, I.W.D., Li, Z.X., McElhinny, M.W., 1995. Did Pannotia, the latest Neoproterozoic southern supercontinent, really exist? Eos (Transactions, American Geophysical Union), Fall Meeting. vol. 76, no. 46, p. 172

Powell, C.M., Li, Z.X., McElhinny, M.W., Meert, J.G., Park, J.K., 1993. Paleomagnetic constraints on timing of the Neoproterozoic breakup of Rodinia and the Cambrian formation of Gondwana. Geology 21 (10), 889–892.

Powell, C.M., Pisarevsky, S.A., 2002. Late Neoproterozoic assembly of east Gondwana. Geology 30 (1), 3–6.

Pradhan, V.R., Meert, J.G., Pandit, M.K., Kamenov, G., Gregory, L.C., Malone, S.J., 2010. India's changing place in global Proterozoic reconstructions: a review of geochronologic constraints and paleomagnetic poles from the Dharwar, Bundelkhand and Marwar cratons. Journal of Geodynamics 50 (3), 224–242.

Pradhan, V.R., Pandit, M.K., Meert, J.G., 2008. A cautionary note on the age of the paleomagnetic pole obtained from the Harohalli dyke swarms, Dharwar craton, southern India. Indian Dykes: Geochemistry, Geophysics, and Geochronology. Narosa Publishing Ltd., New Delhi, India, pp. 339–352.

Preiss, W.V., 2000. The Adelaide Geosyncline of South Australia and its significance in Neoproterozoic continental reconstruction. Precambrian Research 100 (1), 21–63.

Pu, J.P., Bowring, S.A., Ramezani, J., Myrow, P., Raub, T.D., Landing, E., Mills, A., Hodgin, E., Macdonald, F.A., 2016. Dodging snowballs: geochronology of the Gaskiers glaciation and the first appearance of the Ediacaran biota. Geology 44 (11), 955–958.

Puffer, J.H., 2002. A Late Neoproterozoic eastern Laurentian superplume: location, size, chemical composition, and environmental impact. American Journal of Science 302 (1), 1–27.

Qi, X., Santosh, M., Zhu, L., Zhao, Y., Hu, Z., Zhang, C., Ji, F., 2014. Mid-Neoproterozoic arc magmatism in the northeastern margin of the Indochina block, SW China: geochronological and petrogenetic constraints and implications for Gondwana assembly. Precambrian Research 245, 207–224.

Qi, X., Zeng, L., Zhu, L., Hu, Z., Hou, K., 2012. Zircon U–Pb and Lu–Hf isotopic systematics of the Daping plutonic rocks: implications for the Neoproterozoic tectonic evolution of the northeastern margin of the Indochina block, Southwest China. Gondwana Research 21 (1), 180–193.

Queiroz, C.L., Jost, H., da Silva, L.C., McNaughton, N.J., 2008. U–Pb SHRIMP and Sm–Nd geochronology of granite–gneiss complexes and implications for the evolution of the Central Brazil Archean Terrain. Journal of South American Earth Sciences 26 (1), 100–124.

Raimondo, T., Collins, A.S., Hand, M., Walker-Hallam, A., Smithies, R.H., Evins, P.M., Howard, H.M., 2010. The anatomy of a deep intracontinental orogen. Tectonics http://dx.doi.org/10.1029/2009TC002504.

Rainaud, C., Master, S., Armstrong, R.A., Phillips, D., Robb, L.J., 2005. Monazite U–Pb dating and ^{40}Ar–^{39}Ar thermochronology of metamorphic events in the Central African Copperbelt during the Pan-African Lufilian Orogeny. Journal of African Earth Sciences 42 (1), 183–199.

Rainbird, R.H., Jefferson, C.W., Young, G.M., 1996. The early Neoproterozoic sedimentary Succession B of northwestern Laurentia: correlations and paleogeographic significance. Geological Society of America Bulletin 108 (4), 454–470.

Rainbird, R.H., Stern, R.A., Khudoley, A.K., Kropachev, A.P., Heaman, L.M., Sukhorukov, V.I., 1998. U–Pb geochronology of Riphean sandstone and gabbro from southeast Siberia and its bearing on the Laurentia–Siberia connection. Earth and Planetary Science Letters 164 (3), 409–420.

Ramakrishnan, M., Nanda, J.K., Augustine, P.F., 1998. Geological evolution of the Proterozoic Eastern Ghats mobile belt. Geological Survey of India Special Publication 44, 1–21.

Ramos, V.A., Vujovich, G., Martino, R., Otamendi, J., 2010. Pampia: a large cratonic block missing in the Rodinia supercontinent. Journal of Geodynamics 50 (3), 243–255.

Rao, V.V., Krishna, V.G., 2013. Evidence for the Neoproterozoic Phulad Suture Zone and Genesis of Malani Magmatism in the NW India from deep seismic images: implications for assembly and breakup of the Rodinia. Tectonophysics 589, 172–185.

Rapalini, A.E., 2006. New late Proterozoic paleomagnetic pole for the Rio de la Plata craton: implications for Gondwana. Precambrian Research 147, 223–233.

Rapalini, A.E., Tohver, E., Sánchez Bettucci, L., Lossada, A.C., Barcelona, H., Pérez, C., 2015. The late Neoproterozoic Sierra de las Ánimas Magmatic Complex and Playa Hermosa Formation, southern Uruguay, revisited: Paleogeographic implications of new paleomagnetic and precise geochronologic data. Precambrian Research 259, 143–155.

Rapela, C.W., Fanning, C.M., Casquet, C., Pankhurst, R.J., Spalletti, L., Poiré, D., Baldo, E.G., 2011. The Rio de la Plata craton and the adjoining Pan-African/brasiliano terranes: their origins and incorporation into south-west Gondwana. Gondwana Research 20 (4), 673–690.

Rapela, C.W., Pankhurst, R.J., Casquet, C., Baldo, E., Saavedra, J., Galindo, C., Fanning, C.M., 1998. The Pampean Orogeny of the southern proto-Andes: Cambrian continental collision in the Sierras de Córdoba. Geological Society, London, Special Publications 142 (1), 181–217.

Rapela, C.W., Pankhurst, R.J., Casquet, C., Fanning, C.M., Baldo, E.G., González-Casado, J.M., Galindo, C., Dahlquist, J., 2007. The Río de la Plata craton and the assembly of SW Gondwana. Earth-Science Reviews 83 (1), 49–82.

Raub, T.D., Kirschvink, J.L., Evans, D.A.D., 2007. True polar wander: linking deep and shallow geodynamics to hydro-and biospheric hypotheses. Treatise on Geophysics. 5, pp. 565–589.

Rekha, S., Upadhyay, D., Bhattacharya, A., Kooijman, E., Goon, S., Mahato, S., Pant, N.C., 2011. Lithostructural and chronological constraints for tectonic restoration of Proterozoic accretion in the Eastern Indian Precambrian shield. Precambrian Research 187 (3), 313–333.

Renne, P.R., Onstott, T.C., D'Agrella-Filho, M.S., Pacca, I.G., Teixeira, W., 1990. $^{40}Ar/^{39}Ar$ dating of 1.0–1.1 Ga magnetizations from the Saõ Francisco and Kalahari cratons: tectonic implications for Pan-African and Brasiliano mobile belts. Earth and Planetary Science Letters 101 (2–4), 349–366.

Rickers, K., Mezger, K., Raith, M.M., 2001. Evolution of the continental crust in the Proterozoic Eastern Ghats Belt, India and new constraints for Rodinia reconstruction: implications from Sm–Nd, Rb–Sr and Pb–Pb isotopes. Precambrian Research 112 (3), 183–210.

Roberts, N.M., 2013. The boring billion?–lid tectonics, continental growth and environmental change associated with the Columbia supercontinent. Geoscience Frontiers 4 (6), 681–691.

Robinson, F.A., Foden, J.D., Collins, A.S., 2015a. Zircon geochemical and geochronological constraints on contaminated and enriched mantle sources beneath the Arabian Shield, Saudi Arabia. The Journal of Geology 123 (5), 463–489.

Robinson, F.A., Foden, J.D., Collins, A.S., 2015b. Geochemical and isotopic constraints on island arc, synorogenic, post-orogenic and anorogenic granitoids in the Arabian Shield, Saudi Arabia. Lithos 220, 97–115.

Robinson, F.A., Foden, J.D., Collins, A.S., Payne, J.L., 2014. Arabian Shield magmatic cycles and their relationship with Gondwana assembly: insights from zircon U–Pb and Hf isotopes. Earth and Planetary Science Letters 408, 207–225.

Rolin, P., 1995. Carte tectonique de la Republique centrafricaine, au 1: 1.500. 000.

Rong, Jia-Yu, Boucot, A.J., Su, Yang-Zheng, Strusz, D.L., 1995. Biogeographical analysis of Late Silurian brachiopod faunas, chiefly from Asia and Australia. Lethaia 28 (1), 39–60.

Rooney, A.D., Strauss, J.V., Brandon, A.D., Macdonald, F.A., 2015. A Cryogenian chronology: two long-lasting synchronous Neoproterozoic glaciations. Geology 43 (5), 459–462.

Roy, A., Kagami, H., Yoshida, M., Roy, A., Bandyopadhyay, B.K., Chattopadhyay, A., Khan, A.S., Huin, A.K., Pal, T., 2006. Rb–Sr and Sm–Nd dating of different metamorphic events from the Sausar Mobile Belt, central India: implications for Proterozoic crustal evolution. Journal of Asian Earth Sciences 26 (1), 61–76.

Roy, A., Prasad, M.H., 2003. Tectonothermal events in Central Indian Tectonic Zone CITZ and its implications in Rodinian crustal assembly. Journal of Asian Earth Sciences 22 (2), 115–129.

Roy, J.L., Robertson, W.A., 1978. Paleomagnetism of the Jacobsville Formation and the apparent polar path for the interval −1100 to −670 my for North America. Journal of Geophysical Research, Solid Earth 83 (B3), 1289–1304.

Saalmann, K., Remus, M.V.D., Hartmann, L.A., 2006. Tectonic evolution of the Neoproterozoic Sao Gabriel block, southern Brazil: constraints on Brasiliano orogenic evolution of the Rio de la Plata cratonic margin. Journal of South American Earth Sciences 21 (3), 204–227.

Sadowski, G.R., Bettencourt, J.S., 1996. Mesoproterozoic tectonic correlations between eastern Laurentia and the western border of the Amazon Craton. Precambrian Research 76 (3), 213–227.

Saha, D., Patranabis-Deb, S., Collins, A.S., 2016. Proterozoic stratigraphy of southern Indian cratons and global context. In: Montenari, M. (Ed.), Stratigraphy & Timescales, pp. 1–59.

Samson, S.D., D'Lemos, R.S., 1998. U–Pb geochronology and Sm–Nd isotopic composition of Proterozoic gneisses, Channel Islands, UK. Journal of the Geological Society 155 (4), 609–618.

Samson, S.D., D'Lemos, R.S., 1999. A precise late Neoproterozoic U–Pb zircon age for the syntectonic Perelle quartz diorite, Guernsey, Channel Islands, UK. Journal of the Geological Society 156 (1), 47–54.

Samson, S.D., Inglis, J.D., D'Lemos, R.S., Admou, H., Blichert-Toft, J., Hefferan, K., 2004. Geochronological, geochemical, and Nd–Hf isotopic constraints on the origin of Neoproterozoic plagiogranites in the Tasriwine ophiolite, Anti-Atlas orogen, Morocco. Precambrian Research 135 (1), 133–147.

Sanchez Bettucci, L., Peel, E., Masquelin, H., 2010. Neoproterozoic tectonic synthesis of Uruguay. International Geology Review 52 (1), 51–78.

Santos, T.J.S., Fetter, A.H., Neto, J.N., 2008b. Comparisons between the northwestern Borborema Province, NE Brazil, and the southwestern Pharusian Dahomey Belt, SW Central Africa. Geological Society, London, Special Publications 294 (1), 101–120.

Santos, J.O.S., Hartmann, L.A., Gaudette, H.E., Groves, D.I., Mcnaughton, N.J., Fletcher, I.R., 2000. A new understanding of the provinces of the Amazon Craton based on integration of field mapping and U-Pb and Sm-Nd geochronology. Gondwana Research 3 (4), 453–488.

Santos, J.O.S., Rizzotto, G.J., Potter, P.E., McNaughton, N.J., Matos, R.S., Hartmann, L.A., Chemale, F., Quadros, M.E.S., 2008a. Age and autochthonous evolution of the Sunsás Orogen in West Amazon Craton based on mapping and U–Pb geochronology. Precambrian Research 165 (3), 120–152.

Santos, E.J., Van Schmus, W.R., Kozuch, M., de Brito Neves, B.B., 2010. The Cariris Velhos tectonic event in northeast Brazil. Journal of South American Earth Sciences 29 (1), 61–76.

Sassi, F.P., Visona, D., Ferrara, G., Gatto, G.O., Ibrahim, H.A., Said, A.A., Tonarini, S., 1993. The crystalline basement of Northern Somalia: lithostratigraphy and sequence of events. Geology and mineral resources of Somalia and surrounding regions. 1st Agron Oltemare, Firenze, Relaz. Monogr. 113, pp. 3–40.

Sato, K., Santosh, M., Tsunogae, T., Kon, Y., Yamamoto, S., Hirata, T., 2010. Laser ablation ICP mass spectrometry for zircon U–Pb geochronology of ultrahigh-temperature gneisses and A-type granites from the Achankovil Suture Zone, southern India. Journal of Geodynamics 50 (3), 286–299.

Schersten, A., Areback, H., Cornell, D., Hoskin, P., Aberg, A., Armstrong, R., 2000. Dating mafic-ultramafic intrusions by ion-microprobing contact-melt zircon: examples from SW Sweden. Contributions to Mineralogy and Petrology 139, 115–125.

Schmidt, P.W., 2014. A review of Precambrian palaeomagnetism of Australia: palaeogeography, supercontinents, glaciations and true polar wander. Gondwana Research 25 (3), 1164–1185.

Schmidt, A., Wedepohl, K.H., 1983. Chemical composition and genetic relations of the Matchless amphibolite (Damara orogenic belt). Evolution of the Damara Orogen of South West Africa/Namibia.

Schmidt, P.W., Williams, G.E., 1995. The Neoproterozoic climatic paradox: equatorial palaeolatitude for Marinoan glaciation near sea level in South Australia. Earth and Planetary Science Letters 134, 107–124.

Schmidt, P.W., Williams, G.E., 1996. Palaeomagnetism of the ejecta-bearing Bunyeroo Formation, late Neoproterozoic, Adelaide fold belt, and the age of the Acraman impact. Earth and Planetary Science Letters 144, 347–357.

Schmidt, P.W., Williams, G.E., 2010. Ediacaran palaeomagnetism and apparent polar wander path for Australia: no large true polar wander. Geophysical Journal International 182, 711–726.

Schmidt, P.W., Williams, G.E., McWilliams, M.O., 1991. Palaeomagnetism and magnetic anisotropy of late Neoproterozoic strata, South Australia: implications for the palaeolatitude of late Cryogenian glaciation, cap carbonate and the Ediacaran System. Precambrian Research 174, 35–52.

Schmidt, P.W., Williams, G.E., McWilliams, M.O., 2009. Palaeomagnetism and magnetic anisotropy of late Neoproterozoic strata, South Australia: implications for the palaeolatitude of late Cryogenian glaciation, cap carbonate and the Ediacaran System. Precambrian Research 174, 35–52.

Schmitt, R.S., Trouw, R.A.J., Van Schmus, W.R., Passchier, C.W., 2008. Cambrian orogeny in the Ribeira Belt (SE Brazil) and correlations within West Gondwana: ties that bind underwater. Geological Society, London, Special Publications 294 (1), 279–296.

Scotese, C.R., 2016. PALEOMAP PaleoAtlas for GPlates and the PaleoDataPlotter Program, Geological Society of America, North-Central Section. 50th Annual Meeting, April 18–19, 2016. University of Illinois, Champaign-Urbana, IL.

Seer, H.J., Brod, J.A., Fuck, R.A., Pimentel, M.M., Boaventura, G.R., Dardenne, M.A., 2001. Grupo Araxá em sua área tipo: um fragmento de crosta oceânica neoproterozóica na Faixa de Dobramentos Brasília. Revista Brasileira de Geociências 31 (3), 385–396.

Seer, H.J., Brod, J.A., Valeriano, C.M., Fuck, R.A., 2005. Leucogranitos intrusivos no Grupo Araxá: registro de um evento magmático durante colisão Neoproterozóica na porção meridional da Faixa Brasília. Revista Brasileira de Geociências 35 (1), 33–42.

Seer, H.J., Dardenne, M.A., 2000. Tectonostratigraphic terrane analysis on neoproterozoic times: the case study of Araxa Synform, Minas Gerais State, Brazil; implications to the final collage of the Gondwanaland. Revista Brasileira de Geociências 30, 78–81.

Seton, M., Flament, N., Whittaker, J., Müller, R.D., Gurnis, M., Bower, D.J., 2015. Ridge subduction sparked reorganization of the Pacific plate-mantle system 60–50 million years ago. Geophysical Research Letters 42 (6), 1732–1740.

Seton, M., Müller, R.D., Zahirovic, S., Gaina, C., Torsvik, T., Shephard, G., Talsma, A., Gurnis, M., Turner, M., Maus, S., Chandler, M., 2012. Global continental and ocean basin reconstructions since 200 Ma. Earth-Science Reviews 113 (3), 212–270.

Seymour, K.S., Kumarapeli, P.S., 1995. Geochemistry of the Grenville dyke swarm: role of plume-source mantle in magma genesis. Contributions to Mineralogy and Petrology 120 (1), 29–41.

Shu, L.S., Deng, X.L., Zhu, W.B., Ma, D.S., Xiao, W.J., 2011. Precambrian tectonic evolution of the Tarim Block, NW China: new geochronological insights from the Quruqtagh domain. Journal of Asian Earth Sciences 42 (5), 774–790.

Siedlecka, A., Roberts, D., Nystuen, J.P., Olovyanishnikov, V.G., 2004. Northeastern and northwestern margins of Baltica in Neoproterozoic time: evidence from the Timanian and Caledonian Orogens. Geological Society, London, Memoirs 30 (1), 169–190.

Silva Filho, M.A., 1976. A suíte ofiolítica da Geossinclinal de Propriá. Proceedings of the XXIX Congresso Brasileiro Geologia. vol. 4, pp. 51–58.

Silva Filho, A.F., Guimarães, I.P., Lyra De Brito, M.E., Plmentel, M.M., 1997. Geochemical signatures of main Neoproterozoic late-tectonic granitoids from the Proterozoic Sergipano fold belt, Brazil: significance for the Brasiliano orogeny. International Geology Review 39 (7), 639–659.

Smethurst, M.A., Khramov, A.N., Torsvik, T.H., 1998. The Neoproterozoic and Palaeozoic palaeomagnetic data for the Siberian platform: from Rodinia to Pangea. Earth-Science Reviews 43 (1), 1–24.

Sohl, L.E., Christie-Block, N., Kent, D.E., 1999. Paleomagnetic polarity reversals in Marinoan (ca. 600 Ma) glacial deposits of Australia: implications fot the duration of low-latitude glaciation in Neoproterozoic time. Geological Society of America Bulletin 111, 1120–1139.

Song, S., Su, L., Li, X.H., Niu, Y., Zhang, L., 2012. Grenville-age orogenesis in the Qaidam-Qilian block: the link between South China and Tarim. Precambrian Research 220, 9–22.

Stacey, J., Hedge, C.E., 1984. Geochronological and isotopic evidence for early Proterozoic crust in the eastern Arabian Shield. Geology 12 (5), 310–313.

Stearn, J.E.F., Piper, J.D.A., 1984. Palaeomagnetism of the Sveconorwegian mobile belt of the Fennoscandian Shield. Precambrian Research 23, 201–246.

Stein, H., Hannah, J., Zimmerman, A., Markey, R., 2006. Mineralization and deformation of the Malanjkhand terrane (2,490–2,440 Ma) along the southern margin of the Central Indian Tectonic Zone. Mineralium Deposita 40 (6–7), 755–765.

Steinberger, B., Seidel, M.L., Torsvik, T.H., 2017. Limited true polar wander as evidence that Earth's nonhydrostatic shape is persistently triaxial. Geophysical Research Letters 44, 827–834.

Steinberger, B., Torsvik, T.H., 2008. Absolute plate motions and true polar wander in the absence of hotspot tracks. Nature 4527187, 620–623.

Stephens, W.E., Jemielita, R.A., Davis, D., 1997. Evidence for ca. 750 Ma intra-plate extensional tectonics from granite magmatism on the Seychelles: new geochronological data and implications for Rodinia reconstructions and fragmentation. Terra Nova 9, 166.

Stern, R.J., 1994. Arc-assembly and continental collision in the Neoproterozoic African orogen: implications for the consolidation of Gondwanaland. Annual Review of Earth and Planetary Sciences 22, 319–351.

Stern, R.J., Avigad, D., Miller, N., Beyth, M., 2008. From volcanic winter to snowball earth: an alternative explanation for Neoproterozoic biosphere stress. Links Between

Geological Processes, Microbial Activities & Evolution of Life. Springer Netherlands, pp. 313–337.

Stern, R.J., Kröner, A., Manton, W.I., Reischmann, T., Mansour, M., Hussein, I.M., 1989. Geochronology of the late Precambrian Hamisana shear zone, Red Sea Hills, Sudan and Egypt. Journal of the Geological Society 146 (6), 1017–1029.

Stoeser, D.B., Frost, C.D., 2006. Nd, Pb, Sr, and O isotopic characterization of Saudi Arabian shield terranes. Chemical Geology 226 (3), 163–188.

Stoeser, D.B., Whitehouse, M.J., Stacey, J.S., 2001. The Khida terrane—geology of Paleoproterozoic rocks in the Muhayil area, eastern Arabian Shield, Saudi Arabia. Gondwana Research 4 (2), 192–194.

Strachan, R.A., Collins, A.S., Buchan, C., Nance, R.D., Murphy, J.B., D'Lemos, R.S., 2007. Terrane analysis along a Neoproterozoic active margin of Gondwana: insights from U–Pb zircon geochronology. Journal of the Geological Society 164 (1), 57–60.

Strachan, R.A., Nance, R.D., Dallmeyer, R.D., D'lemos, R.S., Murphy, J.B., Watt, G.R., 1996. Late Precambrian tectonothermal evolution of the Malverns Complex. Journal of the Geological Society 153 (4), 589–600.

Strachan, R.A., Nutman, A.P., Friderichsen, J.D., 1995. SHRIMP U-Pb geochronology and metamorphic history of the Smallefjord sequence, NE Greenland Caledonides. Journal of the Geological Society 152 (5), 779–784.

Strachan, R.A., Treloar, P.J., Brown, M., D'Lemos, R.S., 1989. Short paper: Cadomian terrane tectonics and magmatism in the Armorican Massif. Journal of the Geological Society 146 (3), 423–426.

Su, W.B., Li, H.K., Xu, L., Jia, S.H., Geng, J.Z., Zhou, H.Y., Wang, Z.H., Pu, H.Y., 2012. Luoyu and Ruyang Group at the south margin of the North China Craton (NCC) should belong in the Mesoproterozoic Changchengian System: direct constraints from the LA-MC-ICPMS U-Pb age of the tuffite in the Luoyukou Formation, Ruzhou, Henan, China. Geological Survey and Research 35 (2), 96–108.

Swanson-Hysell, N.L., Maloof, A.C., Kirschvink, J.L., Evans, D.A.D., Halverson, G.P., Hurtgen, M.T., 2012. Constraints on Neoproterozoic paleogeography and Paleozoic orogenesis from paleomagnetic records of the Bitter Springs Formation, Amadeus basin, central Australia. American Journal of Science 312, 817–884.

Symons, D.T.A., Chiasson, A.D., 1991. Paleomagnetism of the Callander Complex and the Cambrian apparent polar wander path for North America. Canadian Journal of Earth Sciences 28 (3), 355–363.

Tackley, P.J., 2000. Self-consistent generation of tectonic plates in time-dependent, three-dimensional mantle convection simulations. Geochemistry, Geophysics, Geosystems 1 (8).

Taylor, R.J., Clark, C., Johnson, T.E., Santosh, M., Collins, A.S., 2015. Unravelling the complexities in high-grade rocks using multiple techniques: the Achankovil Zone of southern India. Contributions to Mineralogy and Petrology 169 (5), 1–19.

Teixeira, W., Pinese, J.P.P., Iacumin, M., Girardi, V.A.V., Piccirillo, E.M., Echeveste, H., Ribot, A., Fernandez, R., Renne, P.R., Heaman, L.M., 2002. Calc-alkaline and tholeiitic dyke swarms of Tandilia, Rio de la Plata craton, Argentina: U–Pb, Sm–Nd, and Rb–Sr ^{40}Ar/^{39}Ar data provide new clues for intraplate rifting shortly after the Trans-Amazonian orogeny. Precambrian Research 119 (1), 329–353.

Tenczer, V., Hauzenberger, C., Fritz, H., Hoinkes, G., Muhongo, S., Klötzli, U., 2013. Crustal age domains and metamorphic reworking of the deep crust in Northern-Central Tanzania: a U/Pb zircon and monazite age study. Mineralogy and Petrology 107 (5), 679–707.

Thomas, R.J., Chevallier, L.P., Gresse, P.G., Harmer, R.E., Eglington, B.M., Armstrong, R.A., De Beer, C.H., Martini, J.E.J., De Kock, G.S., Macey, P.H., Ingram, B.A., 2002. Precambrian evolution of the Sirwa window, Anti-Atlas orogen, Morocco. Precambrian Research 118 (1), 1–57.

Thomas, R.J., De Waele, B., Schofield, D.I., Goodenough, K.M., Horstwood, M., Tucker, R., Bauer, W., Annells, R., Howard, K., Walsh, G., Rabarimanana, M., 2009. Geological evolution of the Neoproterozoic Bemarivo Belt, northern Madagascar. Precambrian Research 172 (3), 279–300.

Thomas, R.J., Fekkak, A., Ennih, N., Errami, E., Loughlin, S.C., Gresse, P.G., Chevallier, L.P., Liégeois, J.P., 2004. A new lithostratigraphic framework for the Anti-Atlas Orogen, Morocco. Journal of African Earth Sciences 39 (1), 217–226.

Tohver, E., Trindade, R.I.F., Solum, J.G., Hall, C.M., Riccomini, C., Nogueira, A.C., 2010. Closing the Clymene Ocean and bending a Brasiliano belt: evidence for the Cambrian formation of Gondwana, southeast Amazon craton. Geology 38 (3), 267–270.

Tohver, E., Van der Pluijm, B.A., Mezger, K., Scandolara, J.E., Essene, E.J., 2005a. Two stage tectonic history of the SW Amazon craton in the late Mesoproterozoic: identifying a cryptic suture zone. Precambrian Research 137 (1), 35–59.

Tohver, E., Van Der Pluijm, B.A., Scandolara, J.E., Essene, E.J., 2005b. Late Mesoproterozoic deformation of SW Amazonia (Rondônia, Brazil): geochronological and structural evidence for collision with southern Laurentia. The Journal of Geology 113 (3), 309–323.

Töpfner, C., 1996. Brasiliano-Granitoide in den Bundesstaaten São Paulo und Minas Gerais, Brasilien: eine vergleichende Studie; Zirkontypologie, U-(Th)-Pb-und Rb-Sr-Altersbestimmungen. Inst. für Allg. u. Angewandte Geologie d. Ludwig-Maximilians-Univ.

Torsvik, T.H., Ashwal, L.D., Tucker, R.D., Eide, E.A., 2001b. Neoproterozoic geochronology and palaeogeography of the Seychelles microcontinent: the India link. Precambrian Research 110 (1), 47–59.

Torsvik, T.H., Carter, L.M., Ashwal, L.D., Bhushan, S.K., Pandit, M.K., Jamtveit, B., 2001a. Rodinia refined or obscured: palaeomagnetism of the Malani igneous suite (NW India). Precambrian Research 108 (3), 319–333.

Torsvik, T.H., Smethurst, M.A., Meert, J.G., Van der Voo, R., McKerrow, W.S., Brasier, M.D., Sturt, B.A., Walderhaug, H.J., 1996. Continental break-up and collision in the Neoproterozoic and Palaeozoic—a tale of Baltica and Laurentia. Earth-Science Reviews 40 (3), 229–258.

Torsvik, T.H., Van der Voo, R., Preeden, U., Mac Niocaill, C., Steinberger, B., Doubrovine, P.V., van Hinsbergen, D.J., Domeier, M., Gaina, C., Tohver, E., Meert, J.G., 2012. Phanerozoic polar wander, palaeogeography and dynamics. Earth-Science Reviews 114 (3), 325–368.

Toteu, S.F., Fouateu, R.Y., Penaye, J., Tchakounte, J., Mouangue, A.C.S., Van Schmus, W.R., Deloule, E., Stendal, H., 2006. U-Pb dating of plutonic rocks involved in the nappe tectonic in southern Cameroon: consequence for the Pan-African orogenic evolution of the central African fold belt. Journal of African Earth Sciences 44 (4–5), 479–493.

Toteu, S.F., Penaye, J., Djomani, Y.P., 2004. Geodynamic evolution of the Pan-African belt in central Africa with special reference to Cameroon. Canadian Journal of Earth Sciences 41 (1), 73–85.

Toteu, S.F., Van Schmus, W.R., Penaye, J., Michard, A., 2001. New U-Pb and Sm-Nd data from north-central Cameroon and its bearing on the pre-Pan African history of central Africa. Precambrian Research 108 (1–2), 45–73.

Toteu, S.F., Van Schmus, W.R., Penaye, J., Nyobe, J.B., 1994. U-Pb and Sm-Nd evidence for Eburnian and Pan-African high-grade metamorphism in cratonic rocks of southern Cameroon. Precambrian Research 67 (3–4), 321–347.

Trompette, R., 1994. Geology of Western Gondwana (2000–500 Ma). Pan-African-Brasiliano Aggregation of South America and Africa. 350. Balkema.

Trouw, R.A.J., Heilbron, M., Ribeiro, A., Paciullo, F., Valeriano, C.M., Almeida, J.C.H., Tupinambá, M., Andreis, R.R., 2000. The central segment of the Ribeira Belt. Tectonic Evolution of South America. 31, pp. 287–310.

Tucker, R.D., Ashwal, L.D., Handke, M.J., Hamilton, M.A., Le Grange, M., Rambeloson, R.A., 1999. U-Pb geochronology and isotope geochemistry of the Archean and Proterozoic rocks of north-central Madagascar. The Journal of Geology 107 (2), 135–153.

Tucker, R.D., Ashwal, L.D., Torsvik, T.H., 2001. U–Pb geochronology of Seychelles granitoids: a Neoproterozoic continental arc fragment. Earth and Planetary Science Letters 187 (1), 27–38.

Tucker, R.D., Kusky, T.M., Buchwaldt, R., Handke, M.J., 2007. Neoproterozoic nappes and superposed folding of the Itremo Group, west-central Madagascar. Gondwana Research 12 (4), 356–379.

Tucker, R.D., Roig, J.Y., Macey, P.H., Delor, C., Amelin, Y., Armstrong, R.A., Rabarimanana, M.H., Ralison, A.V., 2011. A new geological framework for south-central Madagascar, and its relevance to the "out-of-Africa" hypothesis. Precambrian Research 185 (3), 109–130.

Tucker, R.D., Roig, J.Y., Moine, B., Delor, C., Peters, S.G., 2014. A geological synthesis of the Precambrian shield in Madagascar. Journal of African Earth Sciences 94, 9–30.

Tupinamba, M.A., 1999. Evolução tectônica e magmática da Faixa Ribeira na região serrana do Estado do Rio de Janeiro (Doctoral dissertation).

Tupinambá, M., Heilbron, M., Valeriano, C., Júnior, R.P., de Dios, F.B., Machado, N., do Eirado Silva, L.G. and de Almeida, J.C.H., 2012. Juvenile contribution of the Neoproterozoic Rio Negro Magmatic Arc (Ribeira Belt, Brazil): implications for Western Gondwana amalgamation. Gondwana Research 21 (2), 422–438.

Usuki, T., Lan, C.Y., Wang, K.L., Chiu, H.Y., 2013. Linking the Indochina block and Gondwana during the Early Paleozoic: evidence from U–Pb ages and Hf isotopes of detrital zircons. Tectonophysics 586, 145–159.

Valentine, J.W., Moores, E.M., 1972. Global tectonics and the fossil record. The Journal of Geology 167–184.

Valeriano, C.M., Machado, N., Simonetti, A., Valladares, C.S., Seer, H.J., Simões, L.S.A., 2004. U–Pb geochronology of the southern Brasília belt (SE-Brazil): sedimentary provenance, Neoproterozoic orogeny and assembly of West Gondwana. Precambrian Research 130 (1), 27–55.

Valeriano, C.M., Pimentel, M.M., Heilbron, M., Almeida, J.C.H., Trouw, R.A.J., 2008. Tectonic evolution of the Brasília Belt, Central Brazil, and early assembly of Gondwana. Geological Society, London, Special Publications 294 (1), 197–210.

Valladares, C.S., Machado, N., Heilbron, M., Gauthier, G., 2004. Ages of detrital zircon from siliciclastic successions south of the São Francisco Craton, Brazil: implications for the evolution of Proterozoic basins. Gondwana Research 7 (4), 913–921.

Van der Voo, R., 1990. The reliability of paleomagnetic data. Tectonophysics 184 (1), 1–9.

van Hinsbergen, D.J., Steinberger, B., Doubrovine, P.V., Gassmöller, R., 2011. Acceleration and deceleration of India-Asia convergence since the Cretaceous: roles of mantle plumes and continental collision. Journal of Geophysical Research, Solid Earth 116 (B6).

Van Schmus, W.R., Oliviera, E.P., Silva Filho, A.F., Toteu, S.F., Penaye, J., Guimares, I.P., 2008. Proterozoic links between the Borborema Province, NE Brazil, and the Central African Fold Belt. In: Pankurst, R.J., RAJ, Trouw, Brito Neves, B.B., de Wit, M.J. (Eds.), West Gondwana: Pre-Cenozoic Correlations Across the South Atlantic Region, 294th ed. Geological Society of London, London, pp. 69–100 (Special Publications).

Vernikovsky, V.A., Metelkin, D.V., Vernikovskaya, A.E., Matushkin, N.Y., Kazansky, A.Y., Kadilnikov, P.I., Romanova, I.V., Wingate, M.T.D., Larionov, A.N., Rodionov, N.V., 2016. Neoproterozoic tectonic structure of the Yenisei Ridge and formation of the western margin of the Siberian craton based on new geological, paleomagnetic, and geochronological data. Russian Geology and Geophysics 57 (1), 47–68.

Vernikovsky, V.A., Vernikovskaya, A.E., Pease, V.L., Gee, D.G., 2004. Neoproterozoic orogeny along the margins of Siberia. Geological Society, London, Memoirs 30 (1), 233–248.

Villeneuve, M., 1984. Etude Géologique de la Bordure SW du Craton Ouest Africain. These d'État, Université dAix-Marseille III.

Villeneuve, M., 2008. Review of the orogenic belts on the western side of the West African craton: the Bassarides, Rokelides and Mauritanides. Geological Society, London, Special Publications 297 (1), 169–201.

Villeneuve, M., Bassot, J.P., Robineau, B., Dallmeyer, R.D., Ponsard, J.F., 1991. The Bassaride Orogen. The West African Orogens and Circum-atlantic Correlatives. Springer Berlin Heidelberg, pp. 151–185.

Vogel, M.B., Ireland, T.R., Weaver, S.D., 2002. The multistage history of the Queen Maud Batholith, La Gorce Mountains, central Transantarctic Mountains. Antarctica at the Close of a Millennium: Proceedings of the 8th International Symposium on Antarctic Earth Sciences, Wellington 1999.

Volobuev, M.I., 1993. Riphean ophiolite complex of the Yenisei Ridge. Geotektonika 6, 82–87.

Walderhaug, H.J., Torsvik, T.H., Eide, E.A., Sundvoll, B., Bingen, B., 1999. Geochronology and palaeomagnetism of the Hunnendalen dykes, SW Norway: implications for the Sveconorwegian apparent polar wander loop. Earth and Planetary Science Letters 169, 71–83.

Walderhaug, H.J., Torsvik, T.H., Halvorsen, E., 2007. The Egersund dykes (SW Norway): a robust Early Ediacaran (Vendian) palaeomagnetic pole from Baltica. Geophysical Journal International 168, 935–948.

Wang, Y., Liu, D., Chung, S.L., Tong, L., Ren, L., 2008. SHRIMP zircon age constraints from the Larsemann Hills region, Prydz Bay, for a Late Mesoproterozoic to Early Neoproterozoic tectono-thermal event in East Antarctica. American Journal of Science 308 (4), 573–617.

Wang, J.Q., Shu, L.S., Santosh, M., Xu, Z.Q., 2015. The Pre-Mesozoic crustal evolution of the Cathaysia Block, South China: insights from geological investigation, zircon U–Pb geochronology, Hf isotope and REE geochemistry from the Wugongshan complex. Gondwana Research 28 (1), 225–245.

Wang, H., Wu, Y.B., Gao, S., Liu, X.C., Gong, H.J., Li, Q.L., Li, X.H., Yuan, H.L., 2011. Eclogite origin and timings in the North Qinling terrane, and their bearing on the amalgamation of the South and North China blocks. Journal of Metamorphic Geology 29 (9), 1019–1031.

Ward, R., Stevens, G., Kisters, A., 2008. Fluid and deformation induced partial melting and melt volumes in low-temperature granulite-facies metasediments, Damara Belt, Namibia. Lithos 105 (3), 253–271.

Warnock, A.C., Kodama, K.P., Zeitler, P.K., 2000. Using thermochronometry and low-temperature demagnetization to accurately date Precambrian paleomagnetic poles. Journal of Geophysical Research, Solid Earth 105 (B8), 19435–19453.

Wegener, A., 1912. Die entstehung der kontinente. Geologische Rundschau 3 (4), 276–292.

Weil, A.B., Geissman, J.W., Ashby, J.M., 2006. A new paleomagnetic pole for the Neoproterozoic Uinta Mountain supergroup, Central Rocky Mountain States, USA. Precambrian Research 147, 234–259.

Weil, A.B., Geissman, J.W., Van der Voo, R., 2004. Paleomagnetism of the Neoproterozoic Chuar Group, Grand Canyon Supergroup, Arizona: implications for Laurentia's Neoproterozoic APWP and Rodinia break-up. Precambrian Research 129, 71–92.

Weil, A.B., Van der Voo, R., Mac Niocaill, C., Meert, J.G., 1998. The Proterozoic supercontinent Rodinia: paleomagnetically derived reconstructions for 1100 to 800 Ma. Earth and Planetary Science Letters 154 (1), 13–24.

Wen, B., Evans, D.A., Li, Y.X., 2017. Neoproterozoic paleogeography of the Tarim Block: an extended or alternative "missing-link" model for Rodinia? Earth and Planetary Science Letters 458, 92–106.

Wen, B., Li, Y.X., Zhu, W., 2013. Paleomagnetism of the Neoproterozoic diamictites of the Qiaoenbrak formation in the Aksu area, NW China: constraints on the paleogeographic position of the Tarim Block. Precambrian Research 226, 75–90.

Whitehouse, M.J., Pease, V., Al-Khirbash, S., 2016. Neoproterozoic crustal growth at the margin of the East Gondwana continent–age and isotopic constraints from the easternmost inliers of Oman. International Geology Review 58 (16), 2046–2064.

Whitehouse, M.J., Stoeser, D.B., Stacey, J.S., 2001. The Khida terrane—geochronological and isotopic evidence for Paleoproterozoic and Archean crust in the eastern Arabian Shield of Saudi Arabia. Gondwana Research 4 (2), 200–202.

Whitehouse, M.J., Windley, B.F., Ba-Bttat, M.A., Fanning, C.M., Rex, D.C., 1998. Crustal evolution and terrane correlation in the eastern Arabian Shield, Yemen: geochronological constraints. Journal of the Geological Society 155 (2), 281–295.

Whittaker, J.M., Müller, R.D., Leitchenkov, G., Stagg, H., Sdrolias, M., Gaina, C., Goncharov, A., 2007. Major Australian-Antarctic plate reorganization at Hawaiian-Emperor bend time. Science 3185847, 83–86.

Williams, G.E., Schmidt, P.W., 2015. Low paleolatitude for the late Cryogenian interglacial succession, South Australia: paleomagnetism of the Angepena Formation, Adelaide Geosyncline. Australian Journal of Earth Sciences 62, 243–253.

Windley, B.F., Whitehouse, M.J., Ba-Bttat, M.A., 1996. Early Precambrian gneiss terranes and Pan-African island arcs in Yemen: crustal accretion of the eastern Arabian Shield. Geology 24 (2), 131–134.

Wingate, M.T., Campbell, I.H., Compston, W., Gibson, G.M., 1998. Ion microprobe U–Pb ages for Neoproterozoic basaltic magmatism in south-central Australia and implications for the breakup of Rodinia. Precambrian Research 87 (3), 135–159.

Wingate, M.T., Giddings, J.W., 2000. Age and palaeomagnetism of the Mundine Well dyke swarm, Western Australia: implications for an Australia–Laurentia connection at 755 Ma. Precambrian Research 100 (1), 335–357.

Wingate, M.T.D., Pisarevsky, S.A., De Waele, B., 2010. Paleomagnetism of the 765 Ma Luakela Volcanics in northwest Zambia and implications for Neoproterozoic positions of the Congo Craton. American Journal of Science 310, 1333–1344.

Wingate, M.T., Pisarevsky, S.A., Evans, D.A., 2002. Rodinia connections between Australia and Laurentia: no SWEAT, no AUSWUS? Terra Nova 14 (2), 121–128.

Worsley, T.R., Kidder, D.L., 1991. First-order coupling of paleogeography and CO$_2$, with global surface temperature and its latitudinal contrast. Geology 19 (12), 1161–1164.

Worsley, T.R., Nance, D., Moody, J.B., 1984. Global tectonics and eustasy for the past 2 billion years. Marine Geology 58 (3), 373–400.

Xu, B., Jian, P., Zheng, H., Zou, H., Zhang, L., Liu, D., 2005. U–Pb zircon geochronology and geochemistry of Neoproterozoic volcanic rocks in the Tarim Block of northwest China: implications for the breakup of Rodinia supercontinent and Neoproterozoic glaciations. Precambrian Research 136 (2), 107–123.

Xu, B., Zou, H., Chen, Y., He, J., Wang, Y., 2013. The Sugetbrak basalts from northwestern Tarim Block of northwest China: geochronology, geochemistry and implications for Rodinia breakup and ice age in the Late Neoproterozoic. Precambrian Research 236, 214–226.

Yan, Q., Hanson, A.D., Wang, Z., Druschke, P.A., Yan, Z., Wang, T., Liu, D., Song, B., Jian, P., Zhou, H., Jiang, C., 2004. Neoproterozoic subduction and rifting on the northern margin of the Yangtze Plate, China: implications for Rodinia reconstruction. International Geology Review 46 (9), 817–832.

Yao, J., Cawood, P.A., Shu, L., Santosh, M., Li, J., 2016. An Early Neoproterozoic accretionary prism ophiolitic mélange from the Western Jiangnan Orogenic Belt, South China. The Journal of Geology 124 (5), 587–601.

Yellappa, T., Chetty, T.R.K., Tsunogae, T., Santosh, M., 2010. The Manamedu Complex: geochemical constraints on Neoproterozoic suprasubduction zone ophiolite formation within the Gondwana suture in southern India. Journal of Geodynamics 50 (3), 268–285.

Young, G.M., 1981. Upper Proterozoic supracrustal rocks of North America: a brief review. Precambrian Research 15 (3), 305–330.

Young, G.M., Jefferson, C.W., Delaney, G.D., Yeo, G.M., 1979. Middle and late Proterozoic evolution of the northern Canadian Cordillera and Shield. Geology 7 (3), 125–128.

Yu, S., Zhang, J., del Real, P.G., Zhao, X., Hou, K., Gong, J., Li, Y., 2013. The Grenvillian orogeny in the Altun–Qilian–North Qaidam mountain belts of northern Tibet Plateau: constraints from geochemical and zircon U–Pb age and Hf isotopic study of magmatic rocks. Journal of Asian Earth Sciences 73, 372–395.

Zahirovic, S., Müller, R.D., Seton, M., Flament, N., 2015. Tectonic speed limits from plate kinematic reconstructions. Earth and Planetary Science Letters 418, 40–52.

Zhan, S., Chen, Y., Xu, B., Wang, B., Faure, M., 2007. Late Neoproterozoic paleomagnetic results from the Sugetbrak Formation of the Aksu area, Tarim basin (NW China) and their implications to paleogeographic reconstructions and the snowball Earth hypothesis. Precambrian Research 154, 143–158.

Zhang, Z., Dong, X., Liu, F., Lin, Y., Yan, R., He, Z., Santosh, M., 2012b. The making of Gondwana: discovery of 650 Ma HP granulites from the North Lhasa, Tibet. Precambrian Research 212, 107–116.

Zhang, Z.M., Dong, X., Santosh, M., Zhao, G.C., 2014. Metamorphism and tectonic evolution of the Lhasa terrane, Central Tibet. Gondwana Research 25 (1), 170–189.

Zhang, S., Evans, D.A., Li, H., Wu, H., Jiang, G., Dong, J., Zhao, Q., Raub, T.D., Yang, T., 2013. Paleomagnetism of the late Cryogenian Nantuo Formation and paleogeographic implications for the South China Block. Journal of Asian Earth Sciences 72, 164–177.

Zhang, S., Li, Z.X., Evans, D.A., Wu, H., Li, H., Dong, J., 2012a. Pre-Rodinia supercontinent Nuna shaping up: a global synthesis with new paleomagnetic results from North China. Earth and Planetary Science Letters 353, 145–155.

Zhang, S., Li, H., Jiang, G., Evans, D.A.D., Dong, J., Wu, H., Yang, T., Liu, P., Xiao, Q., 2015. New paleomagnetic results from the Ediacaran Doushantuo Formation in South China and their paleogeographic implications. Precambrian Research 259, 130–142.

Zhang, C.L., Li, X.H., Li, Z.X., Lu, S.N., Ye, H.M., Li, H.M., 2007. Neoproterozoic ultramafic–mafic-carbonatite complex and granitoids in Quruqtagh of northeastern Tarim Block, western China: geochronology, geochemistry and tectonic implications. Precambrian Research 152 (3), 149–169.

Zhang, C.L., Li, Z.X., Li, X.H., Ye, H.M., 2009. Neoproterozoic mafic dyke swarms at the northern margin of the Tarim Block, NW China: age, geochemistry, petrogenesis and tectonic implications. Journal of Asian Earth Sciences 35 (2), 167–179.

Zhang, S., Li, Z.X., Wu, H., 2006. New Precambrian palaeomagnetic constraints on the position of the North China Block in Rodinia. Precambrian Research 144 (3), 213–238.

Zhang, S., Li, Z.X., Wu, H., Wang, H., 2000. New paleomagnetic results from the Neoproterozoic successions in southern North China Block and paleogeographic implications. Science in China Series D: Earth Sciences 43 (1), 233–244.

Zhang, Q.R., Piper, J.D.A., 1997. Palaeomagnetic study of Neoproterozoic glacial rocks of the Yangzi Block: palaeolatitude and configuration of South China in the late Proterozoic supercontinent. Precambrian Research 85, 173–199.

Zhao, P., Chen, Y., Zhan, S., Xu, B., Faure, M., 2014. The apparent polar wander path of the Tarim block (NW China) since the Neoproterozoic and its implications for a long-term Tarim–Australia connection. Precambrian Research 242, 39–57.

Zhao, X., Coe, R.S., Liu, C., Zhou, Y., 1992. New Cambrian and Ordovician paleomagnetic poles for the North China Block and their paleogeographic implications. Journal of Geophysical Research, Solid Earth 97 (B2), 1767–1788.

Zhao, Y., Liu, X.C., Fanning, C.M., Liu, X.H., 2000. The Grove Mountains, a segment of a Pan-African orogenic belt in East Antarctica. Abstract Volume of the 31th IGC, Rio de Janeiro, Brazil.

Zhao, Y., Liu, X., Song, B., Zhang, Z., Li, J., Yao, Y., Wang, Y., 1995. Constraints on the stratigraphic age of metasedimentary rocks from the Larsemann Hills, East Antarctica: possible implications for Neoproterozoic tectonics. Precambrian Research 75 (3), 175–188.

Zhou, M.F., Kennedy, A.K., Sun, M., Malpas, J., Lesher, C.M., 2002. Neoproterozoic arc-related mafic intrusions along the northern margin of South China: implications for the accretion of Rodinia. The Journal of Geology 110 (5), 611–618.

Zhu, W., Zhang, Z., Shu, L., Lu, H., Su, J., Yang, W., 2008. SHRIMP U–Pb zircon geochronology of Neoproterozoic Korla mafic dykes in the northern Tarim Block, NW China: implications for the long-lasting breakup process of Rodinia. Journal of the Geological Society 165 (5), 887–890.

Zhu, D.C., Zhao, Z.D., Niu, Y., Dilek, Y., Mo, X.X., 2011. Lhasa terrane in southern Tibet came from Australia. Geology 39 (8), 727–730.

Zonenshain, L.P., Kuzmin, M.I., Natapov, L.M., Page, B.M., Lewandowski, M., 1993. Geology of the USSR: a plate-tectonic synthesis. Pure and Applied Geophysics 140 (4), 744.

Andrew S. Merdith is a PhD candidate at the University of Sydney, where he completed a Bachelor of Education and a Bachelor of Science (Honours) in 2012, looking at the formation and distribution of sedimentary opal deposits in Australia. He enjoys puzzles, coffee and piecing together the tectonic geography of the world by integrating ground based, geological and geophysical observations and measurements within a digital framework. He is particularly interested in the deep time tectonic evolution of plate configurations and orogens during the supercontinent cycle.

Alan S. Collins has been studying the tectonic geography of the Neoproterozoic for the last 20 years. He has worked extensively in Madagascar, Arabia, Ethiopia, Brazil, East Africa and India where he has had the pleasure of working with stimulating colleagues on the tectonic evolution of Gondwana amalgamation. He is full professor at The University of Adelaide and for the last four years has held an Australian Research Council Future Fellowship.

Simon E. Williams joined the School of Geosciences at the University of Sydney in January 2010. He obtained a PhD in geophysics from the University of Leeds, having completed a degree in geology at Liverpool University. From 2004 to 2009 he worked as a geophysicist at GETECH in the UK, a potential-field geophysics consultancy. Since arriving in Sydney, his research has concentrated both on marine geoscience and global-scale plate tectonics and geodynamics. He has been chief scientist for two research voyages on the CSIRO Marine National Facility, in 2011 discovering microcontinents in the Indian Ocean and in 2016 collecting samples from the submerged continent Zealandia.

Sergei Pisarevsky obtained his MSc in geophysics from Leningrad State University in 1976, and PhD in geophysics from the same University in 1983. He moved to the Tectonics Special Research Centre at the School of Earth and Geographical Sciences of the University of Western Australia (UWA) in 1998. In 2007 he moved to the University of Edinburgh and returned to UWA in 2010. He works in Curtin University since 2011. Particular research areas include: palaeomagnetism, Precambrian geology, plate tectonics and global palaeogeography.

John D. Foden is a geochemist, petrologist and isotope geochemist educated at ANU and the University of Tasmania, with 35 years of post-PhD experience as a researcher and university educator. With >120 research publications, he has wide ranging international field and research experience.

Donnelly B. Archibald is an Instructor in the Department of Earth Sciences at St. Francis Xavier University, Canada. He graduated with a BSc Honours (Earth Science) in 2010 from St. Francis Xavier University, an MSc (Geology) in 2012 from Acadia University, Canada and attained a PhD from the University of Adelaide, Australia in 2016. He is currently the Secretary of the Volcanology and Igneous Petrology Division of the Geological Association of Canada. His particular interests are focussed in applying igneous petrology, isotope geochemical and geochronological techniques to unravel tectonic problems. His research areas include Neoproterozoic palaeogeography and tectonics, the Precambrian geological history of Madagascar, and Appalachian Orogenesis.

Morgan L. Blades is a Ph.D. candidate at the University of Adelaide using geochronology and geochemistry to unravel the Neoproterozoic evolution of the northern East African Orogen, a major Gondwana forming collisional zone, giving insight into the paleogeography of Gondwana. Her research is mainly focussed in the Western Ethiopian Shield, Oman, Chad and Sudan.

Brandon L. Alessio completed his undergraduate degrees at the University of Adelaide. During his Honours year he investigated the tectonic evolution of Oman's Neoproterozoic basement, looking at the implications this evolution had on pre-Gondwana palaeogeography. Currently working on a PhD at the University of Adelaide, Brandon is continuing to investigate Neoproterozoic palaeogeography, though is now doing so by constraining the evolution of the Southern Irumide Belt in Zambia.

Sheree Armistead is a PhD candidate at the University of Adelaide. She received her BSc. Hons from Monash University in 2013 looking at structural controls of IOCG deposits in the Curnamona Province of Australia. She subsequently worked as a geochronologist and mineral systems geologist at Geoscience Australia in Canberra working on the Tasmanides of eastern Australia. Her PhD research is on the Neoproterozoic amalgamation of central Gondwana with a particular focus on regions in Madagascar and India. She is particularly interested in structural geology and isotope geochemistry, as well as using a range of techniques to analyse large datasets both temporally and spatially.

Diana Plavsa is a University of Adelaide BSc Hons graduate where she combined magnetotelluric data with geological information in the Pine Creek Orogen for her Honours thesis, she then worked as a coal and gold geologist before seeing the light and returning to do a PhD on the tectonic evolution of the Southern Granulite Terrane of India that she graduated from in 2014. Since then she moved to Curtin University in Perth where she has been working on geochemical and isotopic footprints of buried mineralisation in the Capricorn orogeny.
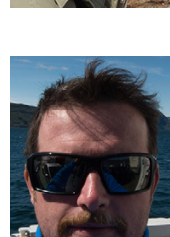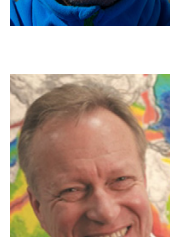
Chris Clark is an Associate Professor in metamorphic geology and geochronology at Curtin University in Western Australia. His main research interests are in the linking of geochronology, specifically U–Pb using zircon and monazite, with the development of metamorphic assemblages in order to constrain the durations of mountain-building events in high-grade metamorphic terranes.

R. Dietmar Müller received his PhD in Earth Science from the Scripps Institution of Oceanography in La Jolla/California in 1993. After joining the University of Sydney in the same year he started building the EarthByte e-research group. The EarthByters are pursuing open innovation, involving the collaborative development of open-source software as well as global digital data sets made available under a creative commons license. One of the fundamental aims of the EarthByte Group is geodata synthesis through space and time, assimilating the wealth of disparate geological and geophysical data into a four-dimensional Earth model. Currently his research is focussed on building a prototype for a Virtual Geological Observatory built around the GPlates open innovation platform.

Chapter Four

Quantifying the link between subduction and continental rifting across two supercontinent cycles

Quantifying the link between subduction and continental rifting across two supercontinent cycles

Merdith, A.S.[1,2], Williams, S.E.[1], Brune, S.[3], Collins, A.S.[4], Riggs, R.A.[1] and Müller, R.D.[1]

[1] EarthByte Group, School of Geosciences, The University of Sydney, Madsen Building F09, Camperdown, NSW 2006, Australia
[2] Data61, CSIRO, Australian Technology Park, Eveleigh, NSW 2015, Australia
[3] German Research Centre for Geosciences GFZ, 14473 Potsdam, Germany
[4] Centre for Tectonics, Resources and Exploration (TRaX), Department of Earth Sciences, The University of Adelaide, Adelaide, SA 5005, Australia.

Abstract

Data constraining continental rifts and subduction outboard of continental lithosphere over successive supercontinent cycles provide insights into the long term evolution of the mantle and the mechanisms behind supercontinent cycles. However, until now, only 'snapshots' of times of interest have been analysed and projected forwards or backwards until the next snapshot, rather than mapping continental rifts and subduction zones continuously through time. Using recently published plate models with continuously closing boundaries for the Neoproterozoic and Phanerozoic, we estimate how rift and continent-margin arc length vary from 1 Ga to present. We relate this to the supercontinent cycle by extracting a measure of continental perimeter (i.e. length of margin between continental and oceanic lithosphere) as a proxy for the existence of a supercontinent under the hypothesis that during times of supercontinent existence the total perimeter length should be low, and during assembly and dispersal it should be high. Our model clearly distinguishes times of supercontinent existence from the perimeter-to-area ratio, the amalgamation of Gondwana from changes in the length of continent-margin arc and the breakup of Rodinia and Pangea from rift lengths. It is difficult to define the assembly of Pangea from our results; instead the assembly of Gondwana (ca. 520 Ma) marks the most prominent change in arc length and perimeter-to-area ratio. These results suggest that the traditional understanding of the supercontinent cycle whereby supercontinent existence for short periods of time before dispersing and re-accreting may be incomplete to fully describe the cycle. Our results suggest instead that either a two-stage supercontinent cycle after Condie (2002) could be a more appropriate understanding, or that the time period of 1000 to 0 Ga is dominated by supercontinent existence, with brief periods of dispersal and amalgamation. The temporal and spatial relationship between continent-margin arc and rift length suggests that subduction occurring around the periphery of a supercontinent plays an important role in the initial breakup of a supercontinent, but does not necessarily contribute to ongoing dispersal. A geodynamic definition of a supercontinent is proposed, whereby an abrupt decrease in global continent-margin arc length marks the point of supercontinent assembly. This would have the added benefit of explicitly linking our understanding of a supercontinent with the mantle, and could be a pertinent framework to continue to unravel the relationship between crust and mantle

1 Introduction

The supercontinent cycle, the theory that over time continental lithosphere aggregates into one body, then eventually breaks up into smaller continents before subsequently re-aggregating into the next supercontinent has been well established over the past thirty years. However, the mechanisms controlling how and why continents assemble and disperse are less well understood. The theory was established on the notable temporal episodicity of global tectonic events, such as orogenies and ocean basin openings and closures, that had been discovered during the Proterozoic and Phanerozoic (see Nance and Murphy, 2013 and Nance et al., 2014 for summaries), with Worsley et al. (1984) first clearly proposing a model for a supercontinent cycle. Their hypothesis was proposed on the basis that geological time is punctuated by episodic peaks of collision (marking assembly) and peaks of mafic dyke swarms (marking breakup) (Worsley et al., 1984). While the existence and breakup of the most recent supercontinent, Pangea, was well established since early in the 20th century, the proposal of Precambrian supercontinents only occurred from the 1970's (e.g. Piper et al., 1976; Valentine and Moores, 1970). These were based on matching apparent polar wander paths (APWPs) from palaeomagnetic data from various components of Archaean-Proterozoic aged cratonic crust and similar ages of large orogens. Recognition of these periodic trends led to the proposal of two supercontinents prior to Pangea: Rodinia, the latest Mesoproterozoic-Early Neoproterozoic (1100-800 Ma, e.g. Dalziel, 1991; Hoffman, 1991; McMenamin and McMenamin, 1990; Moores, 1991) supercontinent; and Nuna (also known as Columbia) the Palaeoproterozoic-Mesoproterozoic (1650-1500 Ma, Rogers and Santosh, 2002; Meert, 2002; Zhao et al., 2004) supercontinent.

Problems in assessing the importance of the supercontinent cycle relate to being able to clearly define what constitutes a supercontinent. A supercontinent is typically thought or expressed as one continent comprising all land on the earth, however even in Pangea there were portions of continental lithosphere not part of the supercontinent (e.g. Tethyan terranes). While this is definitely true of Pangea, uncertainties in deeper time make it difficult to determine whether this definition is also applicable, even by adding qualifiers such as 'most of', 'virtually all of' or '75%' of the continental lithosphere (e.g. Hoffman, 1999; Meert, 2012; Rogers and Santosh, 2003), there are still problems. For example, the recent Merdith et al. (2017) model excludes India and South China from Rodinia, and has a rotation of the Congo-Saõ Francisco plate relative to Rodinia during the Tonian, meaning that during the mid-Toninan Rodinia was located on two separate plates. Previous models by Li et al. (2008; 2013) did have a Rodinia that consisted of all continental lithosphere, but it was fleeting, existing for only ca. 50 Myr before India rifted off. Alternatively, models by Pisarevsky et al. (2003) remove the Congo-Saõ Francisco craton from Rodinia completely. So while a definition of 'most of the continental lithosphere' may be applicable to Pangea, the removal of large portions of (present day) cratonic lithosphere from Rodinia in some models would suggest that the earlier supercontinents would fail this definition. Furthermore, Gondwana has partly defied classification and posed problems for the supercontinent cycle, as even though it consisted of an incredibly large portion of lithosphere, it would fail the 'most of the continental lithosphere' criteria (or any more stringent criteria), as it did not include Baltica, Siberia and Laurentia. However, it otherwise has characteristics reminiscent of a supercontinent, such as the development of large continental-continental orogens during its formation and a was encircled by a long lived, continuous continent-margin arc (here used to described subduction where the ove-riding plate is predominantly continental lithosphere, but where a continental arc is not necessarily produced due to subduction occurring outboard of the continent) persisting until its breakup (Cawood, 2005). Bradley (2011) proposed a more inclusive definition of a supercontinent, by which a supercontinent is a grouping of a formerly dispersed continents, which would make Gondwana a supercontinent, but could also be used to argue that Laurussia (consisting of formerly dispersed continents, Laurentia, Baltica and Siberia) would also be a supercontinent. Having an effective definition of what constitutes a supercontinent is incredibly important, as it has significant ramifications for how earth scientists interpret the cyclicity of plate tectonics, and it carries implications for understanding the long-term interaction

between mantle and surface.

Conceptually, models of supercontinent breakup tend to advocate a dual mechanism between a build-up of heat underneath the supercontinent (typically inferred to occur from a superplume, (e.g. Li and Zhong, 2009; Zhong et al., 2007) leading to lithospheric thinning, generation of large igneous provinces (LIPs) and rifting (Gurnis, 1988; White and McKenzie, 1989), and a circum-supercontinent subduction girdle that creates a pulling force due to slab roll back (e.g. Bercovici and Long, 2014; Cawood et al., 2016; Dal Zilio et al., 2017; Lowman and Jarvis, 1999), as the stresses supplied just by plumes are insufficient to induce continental breakup (e.g. Hill, 1991). However, there is still a large disconnect between mantle modelling and the geological observations that constrain supercontinent breakup. For instance, heat under a supercontinent has been proposed from both a deep (e.g. plume theory, up-wellings; White and McKenzie, 1989) and shallow (e.g. thermal insulation, Coltice et al., 2009) mantle source; supercontinent breakup has been suggested to be driven solely by plumes (e.g. Li et al., 1999; 2003) or by plate driving forces, which may be, in part, affected by plume arrival (e.g. Hill, 1991; Murphy et al., 2009). Additionally, while the importance of subduction in supercontinent breakup was established earlier (e.g. Collins, 2003; Lowman and Jarvis, 1999), only recently has the role that subduction plays in creating both heat anomalies underneath supercontinents (e.g. Heron and Lowman, 2011), and in controlling the fragmentation of tectonic plates throughout a supercontinent cycle (Mallard et al., 2016), been demonstrated. Subsequently, a subduction girdle around a supercontinent is now considered to be important for the breakup of supercontinents to initiate (e.g. Keppie, 2015), but whether it plays a role in the continual fragmentation of a supercontinent is ambiguous (Dal Zilio et al., 2017).

For Pangea, evidence of this subduction girdle and (some) of the slabs subducted are still easily recognisable today in the geological record (e.g. Andes, Eastern Australia, northwest Pacific) and in mantle tomography (e.g. van der Meer et al., 2010; 2012). Unfortunately, while the existence of the pre-Pangea supercontinents is reasonably well established, the dearth of data from the Proterozoic has left both their

precise configuration, and the extent of subduction and rifting around, and inside, each supercontinent more fleeting. Consequently, while the 'lifespan' of Rodinia and Nuna (amalgamation, supercontinent drift, breakup) can be broadly constrained, the underlying mechanisms, and spatial and temporal relationships between subduction and rifting are more difficult to quantitatively determine. A mantle superplume was proposed to exist underneath Rodinia due to extensive dyke swarms preserved in Australia, Laurentia and South China (± India) that intruded over a protracted (ca. 85 Ma) length of time (e.g. Li et al., 1999; 2003). This superplume was linked to episodes of true polar wander (e.g. Li et al., 2004; 2008; Mitchell et al., 2012 - though this argument is tied to a particular configuration ("Missing-Link") of Laurentia, Australia and South China (Li et al., 1995)) and was suggested to be a driving force that broke Rodinia apart due to its ubiquity across a large extent of continental crust between 820 and 700 Ma. Recent proposals of Rodinia's configuration have moved away from the Missing-Link configuration (e.g. Cawood et al., 2013; Collins and Pisarevsky, 2005; Merdith et al., 2017; Pisarevsky et al., 2003) due to contrasting geochemical evidence suggesting that the northern and northwestern margins of South China were active during the Tonian-Cryogenian and faced an open ocean (e.g. Yan et al., 2004; Zhao et al., 2015; Zhou et al., 2002), palaeomagnetic evidence that require South China to be at high latitude when Rodinia is at low latitudes (e.g. 812 to 792 Ma Xiaofeng Dykes from South China (Li et al., 2004) vs. the 800 to 750 Ma Unita Formation from Laurentia (Weil et al., 2006, though episodes of true polar wander (TPW) can account for this) and geological data that tie it to India during the Neoproterozoic (e.g. Cawood et al., 2013; 2017; Jiang et al., 2003; Merdith et al., 2017). Consequently, while more recent proposals do not rule out a superplume, the size, timing and location of such an event needs to be re-addressed. Irrespective of the nature of a Neoproterozoic superplume, there is geological evidence for both a series of rifting events throughout the Neoproterozoic (e.g. Bradley, 2008), and the existence of continent-margin arcs around the periphery of Rodinia (Cawood et al., 2016; Merdith et al., 2017).

Using a recently published global plate tectonic

model of the Neoproterozoic (Merdith et al., 2017), part-global models of the Early Palaeozoic (Domeier, 2016) and global models of the Phanerozoic (Domeier and Torsvik, 2014; Matthews et al., 2016; Müller et al., 2016), all of which model the evolution of plate boundaries through this time, we extract both continent-margin arc length and rift length for the past 1000 Ma. We do this to investigate the relationship between the two, to what extent they are interrelated and correlated, and how this relates to conceptual models for the forces driving supercontinent assembly and breakup. We also extract the perimeter-to-area ratio for continental lithosphere for the same time period to use as a proxy for the connectedness of the continental lithosphere (i.e. is there a supercontinent?), to see how rifting and continent-margin arc length change through an entire supercontinent cycle, and what implications these carry for our understanding of a 'supercontinent'. We also use our results to test competing hypotheses of processes resulting in supercontinent breakup, particularly whether 'top down' methods relating to subduction, or 'bottom up' methods relating to superlume arrival, more easily explain our results.

2 Methodology

To complete our analyses of plate boundary lengths from 1 Ga to present, we require a plate tectonic model of this time. However, there is currently no suitable published reconstruction that continuously covers this time period, so we constructed a model from a synthesis of existing models covering different time periods within the Neoproterozoic, mid-late Palaeozoic, Mesozoic and Cenozoic. The two deeper time plate models used for the analysis; Merdith et al. (2017) and Domeier (2016) (hereafter Mer17 and Dom16), have been linked, with minor adjustments to both models summarised further below. As the Dom16 model only maps the Iapetus and Rheic realms, the Mer17 model has been forward extended, using the Dom16 rotations, terrane shapes and boundaries. The 410 Ma position of crustal elements and plate boundaries of the model used reflects the plate positions of a revised model for plate motions between 410 and 250 Ma (Young et al., in prep). Rotations for the other continental lithosphere components (North China, South China, Tarim and Siberia) have been constructed for the

Early Palaeozoic, as have some key terranes of the Central Asian Orogenic Belt, to provide a complete global model (also summarised below). The model presented here is an extension of a Precambrian model that maps the motion of cratonic lithosphere and an estimate of well preserved plate boundaries (i.e. boundaries occurring close to continental lithosphere), rather than a detailed interpretation of Palaeozoic geology. The younger time model used is from Matthews et al. (2016) (hereafter Mat16), which is a compilation of the Domeier and Torsvik (2014) model for the Middle and Late Palaeozoic, and the Müller et al. (2016) model of the Mesozoic and Cenozoic. Previous measures of a supercontinent involve either strict geological criteria such as defined cratonic blocks within the supercontinent, sutures from the amalgamation process and passive margins (e.g. Evans, 2013), though it is difficult to extract a metric from qualitative criteria to measure the existence of a supercontinent through time. Zaffos et al. (2017) used a fragmentation index between 0 and 1 to measure continental fragmentation through the Phanerozoic, whereby a 1 constitutes all continental blocks separate and 0 represents them all together. They used a continuous model for the Phanerozoic (including terranes and cratonic crust), which is not suitable for us as the Mer17 model only model Precambrian cratonic crust. Therefore, to act as a proxy for the existence of a supercontinent we extract the perimeter-to-area ratio from continental lithosphere between 1000 and 0 Ma. Hawkesworth et al. (2013; 2016) and Cawood et al. (2013) compare crustal growth models and show that by the Neoproterozoic most models depict that 80% of the volume of present day crust had already formed. Consequently we think that calculating a measure of a supercontinent based on present-day cratonic outlines would give a reasonable approximation of 'connectedness' of continental lithosphere.

2-1 Deriving a continuous reconstruction model from 1 Ga to present

2-1-1 Modifications to plate model between 1000 and 520 Ma

A small number of changes have been made from the Neoproterozoic model published by Merdith et al. (2017) to better account for Palaeozoic positions
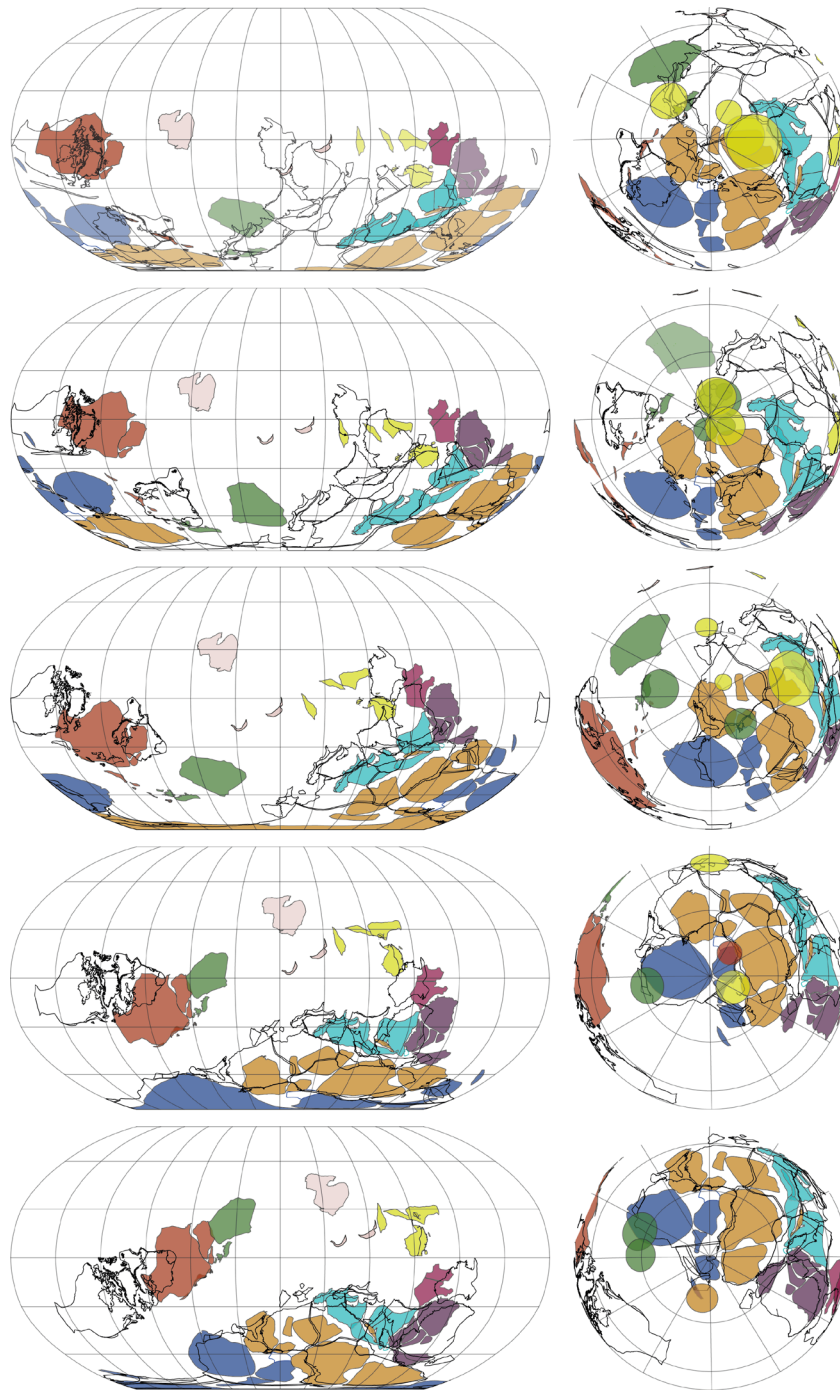
Figure 1 - Comparison of changes made to Dom16 to integrate it into the Mer17 model by extending it forward into the Early Palaeozoic. Solid black blocks are Dom16, coloured blocks are changes presented here. Longitudinal constraints are valid for only the Dom16 model. (a) 500 Ma; (b) 475 Ma; (c) 450 Ma; (d) 425 Ma, and; (e) 410 Ma. By ca. 440 Ma the Mer17 model has a similar longitude for Gondwana as Dom16. There is some variation in the longitudinal position of Laurentia-Baltica in the Silurian-Devonian, though the relative rotation between them is preserved.

of cratonic crust. The palaeolatitude and palaeolongitude of Gondwana at 520 Ma was adjusted to more closely resemble the Gondwana location modelled in Dom16. Faunal, palaeomagnetic and geological data suggest North China to be in close proximity to Australia during the Palaeozoic, until the mid-Ordovician (e.g. Burrett et al., 1990; 2014; Huang et al.,

1999; Metcalfe, 2013). To accommodate this position of North China, Tarim is shifted slightly further south on the northwest Australian margin, to allow room for North China to sit along the northern margin (Figure 1a). We allude this position for North China in Rodinia due, in part, to the redating of Neoproterozoic palaeomagnetic data from North China

that suggested the poles originally used to argue for its position outboard of Siberia are now Mesoproterozoic (Su et al., 2012). We note that the rifting length will not differ at all, and the continent-margin arc length is likely to differ by less than 1000 km as North China contains only a small portion of crust relative to the rest of Rodinia. Otherwise, we follow Merdith et al. (2017) with Tarim diverging from Australia during the latest Neoproterozoic is as a response to the closure of the Mawson Sea between Australia-Antarctica and Gondwana, and the Paterson and Petermann orogenies forming from the intraplate rotation of Australia (Li and Evans, 2011; Martin et al. 2017). North China also diverges from Australia slightly to accommodate Tarim's departure, but otherwise remains close enough to Australia to share faunal patterns until ca. 470 Ma, when diverging fauna and stratigraphy (Metcalfe, 2013) begin to suggest a further separation. The prolonged proximity between North China and Australia (until the Ordovician), even after an onset of rifting in the Cambrian could be accounted for by its clockwise rotation against Gondwana, which requires a somewhat transverse motion against the Australian margin. Some problems remain with the model, specifically the mid-latitude of the southern and eastern margin of Congo during the Ediacaran is at odds with geochemical data of carbonates that necessitate warm, equatorial water for precipitation, though we note that this will not impact the length of rifts, continent-margin arcs or perimeter-to-area ratio.

2-1-2 Modifications to plate model between 520 and 410 Ma

The position of Gondwana at 510 Ma is longitudinally, approximately 90° away from Dom16. It rotates slowly during the Early Palaeozoic to be consistent with Dom16 by ca. 440 to 430 Ma. Baltica and Laurentia have been altered more significantly. Laurentia and Baltica (Laurussia) are shifted ~60° degrees longitudinally at 410 Ma, as their position at this time in the model used here is closer to Laurussia's position in Pangea (compared to Dom16). The position of Baltica in Dom16, especially during the Cambrian and Ordovician, reflects its position in Torsvik et al. (2012), who presuppose an inverted connection between Baltica and Laurentia during the Neoproterozoic (cf. Hartz and Torsvik, 2002). As

Mer17 models the 'right-way up' interpretation (cf. Cawood and Pisarevsky, 2006), we slightly alter the position of Baltica, predominantly between 510 and 450 Ma to better reflect a different start-time position at the opening of the Iapetus. The motions of the peri-Gondwanan terranes remain the same relative to Gondwana. All changes remain supported by palaeomagnetic data, but the model no longer has the absolute palaeolongitudinal constraints that were originally imposed by Domeier (2016) (Figure 1).

2-1-3 New Early Palaeozoic rotations

Our extended, simplified model for the Early Palaeozoic broadly follows Golonka (2007), where oceanic-oceanic subduction exists outboard of the northern margin of Gondwana. This subduction zone rolls back, away from Gondwana, as terranes start to accrete and build, and the first generation of Tethyan Ocean opens. We represent this subduction zone with two terranes, that lie, in a reconstructed Gondwana, from north to south; the Central Tien Shan Terrane, that preserves subduction on its northern margin (facing Siberia) and southern margin (facing Tarim) and collided with the northern margin of Tarim in the Palaeozoic (Xiao et al., 2013), and the Precambrian Chu-Ili terrane of Kazakhstan (e.g. Kröner et al., 2007), that collided with the Siberia craton during the Late Palaeozoic, but otherwise shares Early Palaeozoic faunal assemblages with Gondwana (Popov et al., 2009). As their position in Pangea is between the Chinese cratons and Siberia, we infer that they developed outboard of Tarim and North China in the Palaeo Asian Ocean, consequently we depict a spreading ridge separating these terranes from Gondwana, in part, as an easterly extension of the spreading ridge that opened the Rheic Ocean. Another terrane, the Qiadam block, that rifted off North China in the early Palaeozoic, before re-accreting in the Ordovician (e.g. Dong and Santosh, 2016), is also depicted. Palaeomagnetic data for Tarim, North China and South China is summarised in Table 1; data for Gondwana, Laurentia, Baltica and the Avalonian terranes from Torsvik et al. (2012) and Domeier (2016)

The ridge separating the outboard Kazakhstan terranes jumped at some point in the Palaeozoic, and began to further separate North China and South

China from Gondwana, as evidenced by the subtle shallowing of South China's palaeomagnetic data (Table 1, Han et al., 2015; Huang et al., 2000; Yang et al., 2004), and also by the removal of Gondwanan fauna from the chinese blocks during the Ordovician-Silurian (e.g. Metcalfe, 2013). Our Ediacaran-Cambrian configuration of (from north to south along the northwestern Australian margin towards the northern Indian margin) North China, Tarim and South China is similar to that of Metcalfe (2013), with Tarim diverging from Gondwana initially, followed by North China, and finally South China. As noted by Domeier (2017), from the latest Cambrian to the Silurian, the allowable palaeolatitudes of these blocks overlap one another, suggesting that by the Ordovician-Silurian boundary all three need to be in their correct palaeolongitudinal order (i.e. Tarim in the west, then South China in the centre and North China in the east) (Figure 4 - Huang et al., 1999; Zhao et al., 1992). Siberia remained nearly completely ringed by subduction during this time, though interestingly, they were mostly oceanic-oceanic arcs, or developing on small slithers of crust away from the Precambrian cratonic core (e.g. Cocks and Torsvik, 2007; Metelkin et al., 2012). Palaeomagnetic data suggest it drifted northwards slowly, and rotated clockwise from its break-out against Laurentia in the Cryogenian (Metelkin et al., 2012; Pisarevsky et al., 1997). Similarly to Mer17 and Dom16, connected and evolving plate boundaries are provided with this model as a requirement of plate tectonic theory, though we note firstly; that they are preliminary and more work must be done to better model the tectonic evolution of this time period (e.g. Domeier, 2017), and, secondly, as the focus of this paper is on rifting and subduction length, plate boundaries in the oceanic realm (either spreading or subduction) are not considered for the analysis presented here.

Table 1 - Palaeomagnetic data from South China, Tarim and North China. Slat, Site latitude; Slon, Site longitude; Plat, pole latitude; Plon, pole longitude. *these poles reported in Zhao et al. (2014) but original articles are in Chinese and the authors did not have access to them.

Block	Name	Age	Slat	Slon	Plat	Plon	a95	Reference
North China	Hebei and Shandong Sediments	Cambrian	36	118	-21.2	155.2	12.4	Zhao et al. (1992)
North China	NE Sino-Korean Massif	Cambrian	35.6	110.5	-26.8	154.5	8.9	Gao et al. (1983) (recalculated by Zhou et al., 1992)
North China	Zhangxia and Xuzhuang Fms	Middle Cambrian	35.6	110.5	-37	146.7	5.5	Huang et al. (1999)
North China	Changshan and Gushan Fms	Late Cambrian	35.6	110.5	-31.7	149.6	5.4	Huang et al. (1999)
North China	Hebei and Shandong Sediments	Ordovician	36	118	-28.8	130.9	12.3	Zhao et al. (1992)
North China	Liangjiashan and Lower Majiagou Fm	Early Ordovician	35.6	110.5	-37.4	144.3	8.5	Huang et al. (1999)
North China	Jinghe	Middle Ordovician	35.6	110.5	-31.5	147.7	7	Huang et al. (1999)
North China	Upper Majiagou Formation	Middle Ordovician	35.6	110.5	-27.9	130.4	9.2	Yang et al. (1996)
South China	Douposi Formation	Middle Cambrian	32.4	106.3	-51.3	166	8.3	Yang et al. (2004)
South China	Shiqian Redbeds	Silurian	27.5	108	-14.9	16.1	5.1	Huang et al. (2000)
South China	Pagoda Formation	Late Ordovician	32.4	106.3	-45.8	191.3	3.6	Han et al. (2015)
Tarim	*	Early Ordovician	41.3	83.4	-20.4	180.6	8.5	Fang et al. (1996)
Tarim	*	Late Ordovician	40.6	78.9	-40.7	183.3	4.8	Sun and Huang (2009)
Tarim	Red Sandstone	Silurian	40.6	79.4	-12.8	-20.2	7.3	Zhao et al. (2014) - average of three poles from Fang et al. (1996; 1998); Li et al. (1990)

2-2 Extracting continent-margin arc and rift length, and continental perimeter-to-area ratio

2-2-1 Rift length

The spatio-temporal distribution of continental rifting is difficult to precisely date in the Neoproterozoic, though the geological record of rifting is more complete than other plate boundary types (e.g. mid ocean ridges). Initiation of extension is often determined by the onset of sedimentation dominated by siliciclastic sediments deposited in a lacustrine or fluvial environment accompanied by mafic intrusions and graben development as extensions progresses (e.g. Bradley, 2008). The cessation of rifting

times it is more difficult, and the rift-drift transition is usually marked by the preservation of turbidites overlain by a thick carbonate platform and/or a transition to deep water sedimentation (e.g. Bradley, 2008; Condie, 2003). However, the reliance on sedimentary facies for constraining times of rifting and drifting, in particular for the Precambrian, is problematic due to difficulties on absolute dating methods of sedimentary rock and the absence of fossils for relative dating. An alternative method to infer the history of rift formation is to use comprehensive global plate kinematic models that integrate geological, palaeomagnetic and geodynamic observations to simulate the motion of (primarily) continental lithosphere (and/or tectonics plates) through time, whereby if two portions of continental crust separate, a rift basin is inferred to have occurred.
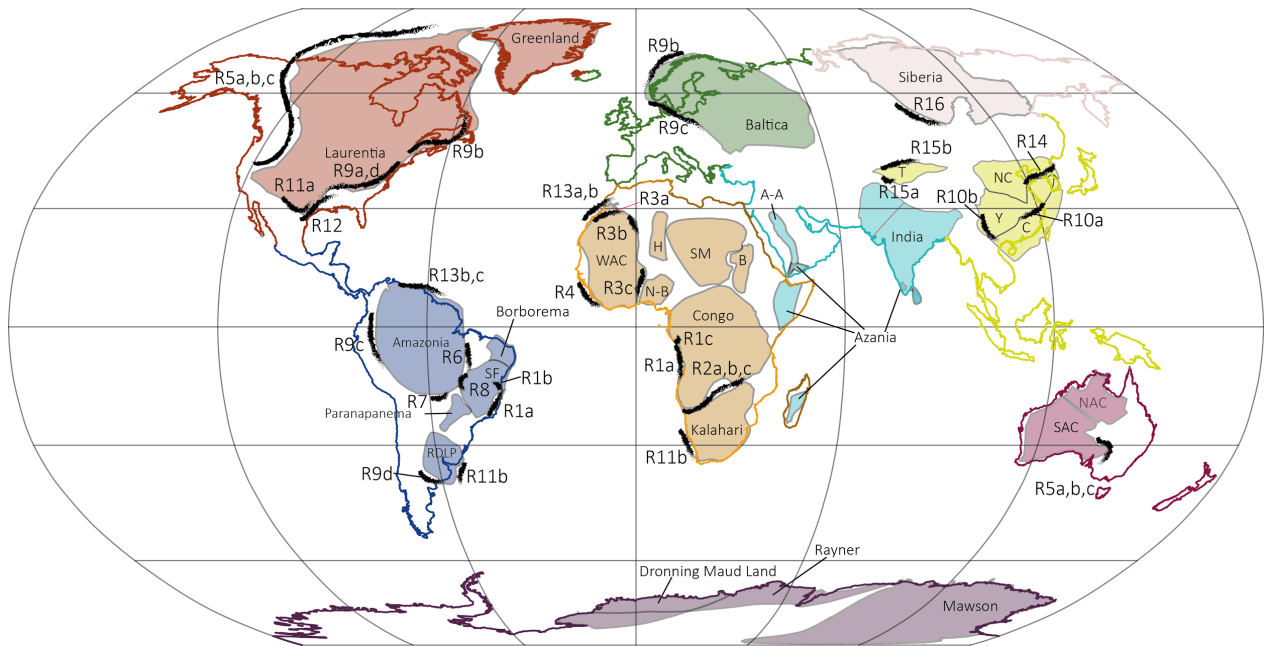
Figure 2 - Distribution of Neoproterozoic to Early Palaeozoic rifts used in the analysis (some conjugate rifts are also highlighted). Use key in Table 1 to identify rifts (R1-R16). Cratonic crust is colour coded according to present day location. A-A, Afif-Abas terrane; B, Bayuda block; C, Cathaysia (South China craton); H, Hoggar; NAC, North Australian craton; N-B, Nigeria-Benin block; NC, North China craton; RDLP, Rio de la Plata; SAC, South Australian craton; SF, Saõ Francisco craton; SM, Sahara Metacraton; T, Tarim; Y, Yangtze (South China craton)

and transition to drift is recorded by the onset of formation of oceanic lithosphere and the subsequent development of conjugate passive margins (Bradley, 2008; Condie, 2002; 2003). For post-Pangea times, the preservation of oceanic crust in situ makes it possible to date the rift-drift transition to within a few Myr (e.g. Brune et al., 2016). For pre-Pangea

We have identified 33 rifts during the Neoproterozoic which are both contained within the Mer17 reconstruction as locations of continental breakup, and which are supported by the geological record of rifting and passive margin development (e.g. Bradley, 2008). We also infer one other rift occurring from the Mer17 model, for which geological evi-

Table 2: Summary of rifts used in the analysis. See Supplementary Material 1 for a discussion of our age of rifting and rift-drift transitions.
^ indicates age based purely from plate model
* indicates modelling used in age determination (along with geological constraints)
** indicates rift inferred by model only

ID	Geological identification	Craton	Rift initiation (Ma)	Rift cessation (break-up or failure) (Ma)	Key Reference(s)
R1a	Macaúbas Basin	Congo - São Francisco	1000	900	Alkmim et al., 2006; Pedrosa-Soares et al., 2001
R1b	Paramirim Aulacogen	Saõ Francisco	1000	900	Pedorsa-Soares et al., 2001
R1c	Sangha Aulacogen	Congo Craton	1000	900	Pedorsa-Soares et al., 2001
R2a	Katanga Supergroup	Congo	880	820	Johnson et al., 2005
R2b	Khomas Ocean (eastern extent)	Congo	760	670	Halverson et al., 2005
R2c	Khomas Ocean (western extent)	Congo	760	670	
R3a	Anit-Atlas	West African Craton	880^	800	Ennih and Liégeois, 2001
R3b	Ougarta Aulacogen	West African Craton	880^	800	Ennih and Liégeois, 2001
R3c	Gourma Aulacogen	West African Craton	880^	800	Ennih and Liégeois, 2001
R4	Bassaride Sea	West African Craton	850	800	Villeneuve, 2008
R5a	Proto-pacific ocean	Australia-Laurentia	830	775	Preiss, 2000
R5b		Australia-Laurentia	720	670	Yonkee et al., 2014
R5c		Australia-Laurentia	580	540	Yonkee et al., 2014
R6	Araguaia Belt	Amazonia	850*	800	Moura et al., 2008; Paixão et al., 2008
R7	Paraguay Belt	Amazonia	700	640	Babinski et al., 2013
R8	Goiás Arc	Saõ Francisco	850*	745	Babinski et al., 2007; Valeriano et al., 2004
R9a	Failed rift	Laurentia	760	700	Aleinkoff et al., 1995; Li and Tull, 1998
R9b	Northern Iapetus Ocean	Laurentia-Baltica	615	540	Cawood et al., 2001
R9c	Torniquest Sea	Baltica-Amazonia	615	540	Cawood et al., 2001
R9d	Southern Iapetus Ocean	Laurentia-Amazonia	590	540	Cawood et al., 2001
R9e	Southern Iapetus Ocean	Laurentia-RDLP	590	540	Cawood et al., 2001
R10a	Nanhua basin	South China	830	750	Wang and Li, 2003
R10b	Kangdian basin	South China-India	830	550	Jiang et al. 2003
R11a	Adamastor ocean	Laurentia-Kalahari	750**,^	690	
R11b	Gariep Belt	RDLP-Kalahari	750	690	Frimmell et al., 2002; Macdonald et al., 2010
R12	Argentine Precordillera	Laurentia-Cuyania Terrane	540	515	Thomas and Astini, 1996
R13a	Rheic Ocean	Avalonia	550	490	Nance et al., 2008
R13b	Rheic Ocean	Ganderia	570	505	Nance et al., 2008; Schulz et al., 2008
R13c	Rheic Ocean	Carolinia	550	490	Nance et al., 2008
R14	Proto-Tethys Ocean	North China	550	480	Ryu et al., 2005?
R15a	??Proto-pacific Ocean	Tarim	880	780	Wang et al., 2015
R15b	Aksu area, ?Palaeo Asian Ocean?	Tarim	615	550	Xu et al., 2009; Zhao et al., 2014

dence is lacking, but which are invoked on the basis of affinities between now-separated blocks within past reconstructions (e.g. Li et al., 2008; Merdith et al., 2017; Table 1, Figure 2). Of the 34 total rifts, four have ages constrained purely from the plate model and two use the plate model to approximate age in accordance with geological data.

We include failed rifts in our analysis as they preserve evidence of extension and may also be important to some auxiliary processes of interest such as changes in climate (e.g. Brune et al. 2017, in press). Failed rifts are locations where there is geological evidence of rifting (magmatic intrusions, crustal thinning, graben development, sedimentation etc.) without evidence of it progressing to seafloor spreading. Failed rifts can be preserved as aulacogens, or they can become the sites of further phases of rifting that lead to seafloor spreading (see Supplementary Material 1 (SM1)). For times prior to Pangea, failed rifts are dif-

ficult to determine in the geological record because they are not revealed through palaeomagnetic data or plate models and are often deformed or covered by younger sedimentary sequences. This makes dating them difficult and interpretations of their structure, which can help resolve whether the sedimentary rocks represent a failed rift or an intracratonic sag basin, are resolved through non-direct geophysical methods such as seismic surveys or gravity anomaly maps (e.g. Nunn and Aires, 1988). During the Palaeozoic times not covered by Mer17 (520-410 Ma) the rifts analysed were constrained to being represented in the Dom16 model. Thus, within the Palaeozoic, only the Iapetus and Rheic realms were considered. For younger times (450-0 Ma), the compilation of rift length by Şengör and Natal'in (2001) was used for the analysis. This was done because they also include a measure of failed rift length in their analysis. Ages or rifting events from the Mer17 and Dom16 models are summarised succinctly in Table 2 and a discussion of the times we have used for each rift is provided in SM1.

Once each rift and its duration had been identified, a polyline was digitised in GPlates (www.gplates.org) within the tectonic models. The length of the

polyline was matched as best as possible from published studies depicting the length of either the preserved passive margin (interpreted to be representative of the length of the rifted margin), or the fold belt where the sediments deposited in the rift basin are preserved. Extraction and analysis of data was done using the pyGPlates (www.pygplates.org) library for python.

2-2-2 Continent-to-area ratio

Polygons representing the extent of inferred continental lithosphere (i.e. artificial continent-ocean boundaries) were digitised in GPlates around each coherent tectonic plate between 1000 and 410 Ma (Figure 2, also see Supplementary Material 2 (SM2) for an animation). Where plate boundaries are preserved in the geological record, which is typically close to the craton boundary, the estimated extent of continental lithosphere is more reliable. Away from active plate boundaries we have interpreted as best as possible an approximate outline for the continental lithosphere not represented by the cratonic component. Between 410 to 0 Ma we used continent-ocean boundaries digitised by Matthews et al. (2016) to act as the extent of continental area. We create variance
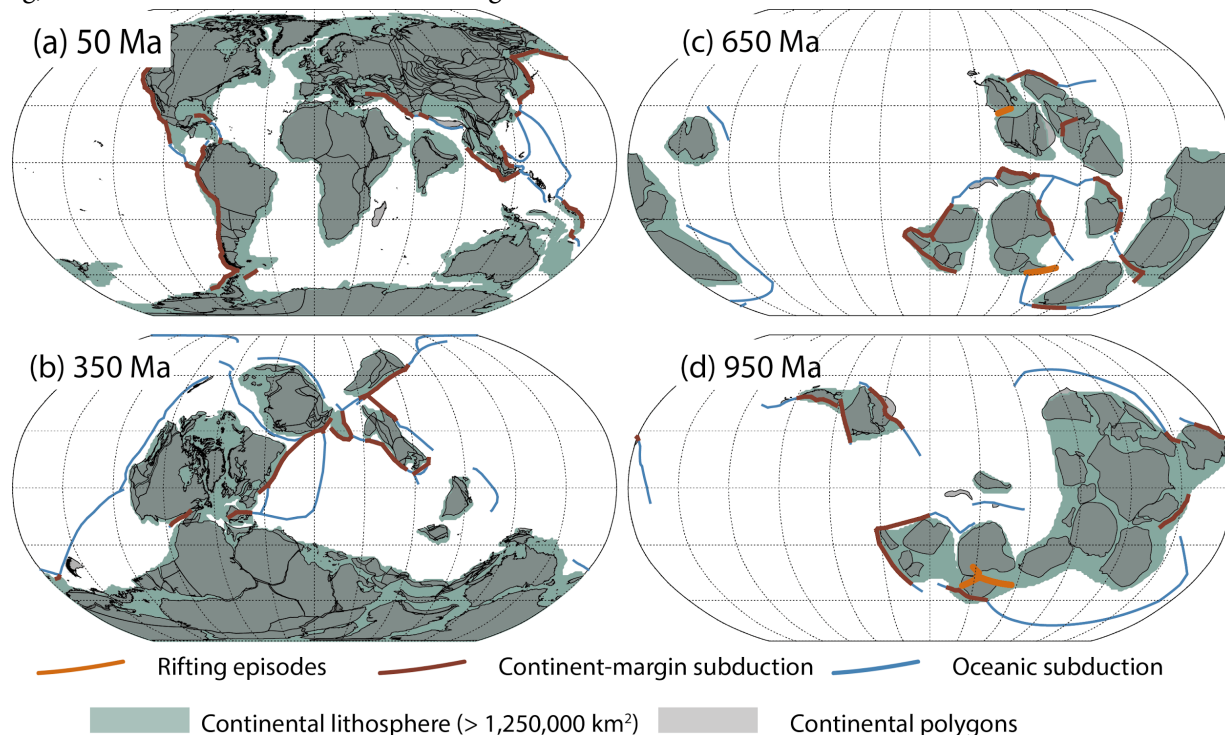

Figure 3 - Examples of continents used for select timeslices. Continent-margin subduction and oceanic subduction are determined by a 150 km threshold to the nearest continent greater than 1,250,000 km2. See Supplementary Material 2 for a full animation from 1000 to 0 Ma.

in the continent-to-area ratio by thresholding the minimum area of lithosphere to qualify as 'continental lithosphere' , either 10,000 km^2 (which captures nearly everything) or 1,250,000 km^2 (which captures predominantly only cratonic lithosphere and ignores many smaller terranes and island arcs, especially as is depicted in the Mat16 model, e.g. Figure 2a, b). We use the larger threshold, as the smaller threshold includes terranes, hot spot chain, island arcs and juvenile crust. As we calculate this iteratively over time, once (or if) these smaller terranes and arcs collide with a larger landmass, their contribution towards the continental area and perimeter are included in the analysis, as the continent-ocean boundary of the larger continent is extended outwards into the oceanic domain for subsequent younger times. These perimeter lengths are then used for two purposes:

i) to provide an estimate of the changes in size of land mass through the Neoproterozoic as a proxy for the supercontinent cycle
ii) to facilitate the extraction of length of continent-margin arcs from the Mer17, Dom16 and Mat16 models

2-2-3 Continent-margin arc lengths

We extract continent-margin arc length from the topological models by measuring the distance from the constructed continental perimeters (Section 2-2-2) to the nearest subduction zone. This was done in order to only capture subduction that occurs close to a continent margin, including both continental arcs and subduction where there is no intermediary plate boundary between the arc and continental lithosphere (i.e. the arc is around a continental margin, but not strictly a continental arc), and also to ensure our analysis does not capture oceanic-oceanic arcs (e.g. Cao et al. 2017). We vary the distance thresholds from the continental polygons (Figure 2) to subduction zones from the models to extract a variety of lengths based on proximity to continental lithosphere. We do this because both the (original) location of subduction zones are, in many cases, poorly known, and the spatial extent of cratonic crust at any location at a times is poorly unknown (Mer17 models principally present day cratonic crust, Dom16 and Mat16 model cratonic crust and terranes) and because arcs that are not specifically continental

arcs can still impart forces onto the overriding plate if they are in close proximity to the margin, such as through the generation of large scale convection (e.g. Dal Zilio et al., 2017). Consequently, there is a degree of uncertainty as to whether some subduction zones are close to the margin of a continent or oceanic. This is especially where, in the reconstructions, subduction is interpreted to occur away from a craton or continent, where subduction has been inferred to link other plate boundaries together (as per plate tectonic theory) or where subduction has been modelled to accommodate plate motions suggested by palaeomagnetic data or rifting. We extract lengths in various thresholds, and hypothesise that we should see exponentially smaller increases in continent-margin arc length until a point where there is a large increase. The smaller increases are expected to come from arcs that are modelled to extend into an ocean away from a craton, to meet another plate boundary. The large increase should come at a point where the distance threshold is sufficient to begin capturing oceanic-oceanic subductions (either modelled or preserved).

3 Results

3-1 Arc and rift length of the Neoproterozoic-Early Palaeozoic

The length of rifts through the Neoproterozoic are depicted in Figure 4a; here we depict all compiled rifts to show the individual contributions of each individual rift to the total length. The rifted margins of Laurentia, in particular, the western, Proto-pacific margin, and the eastern, Iapetus margin, contribute two of the longest rift margins preserved from this time. We also can identify three clear times of rift initiation in the history of Rodinia (irrespective of whether they progressed to full breakup): (i) late Tonain, (ii) mid Cryogenian, and (iii) mid Ediacaran. These events correspond to the (i) counter-clockwise rotation of C-SF to Rodinia, and the initiation of rifting along the western margin of Laurentia, (ii) the progressive unzipping of cratonic elements of Rodinia (Congo, Kalahari), and (iii) the opening of the Iapetus Ocean. There are only two times where there is no ongoing rifting - the mid-Tonian, and during the Ordovician and Silurian. This younger apparent hiatus in rift activity is likely because we have not
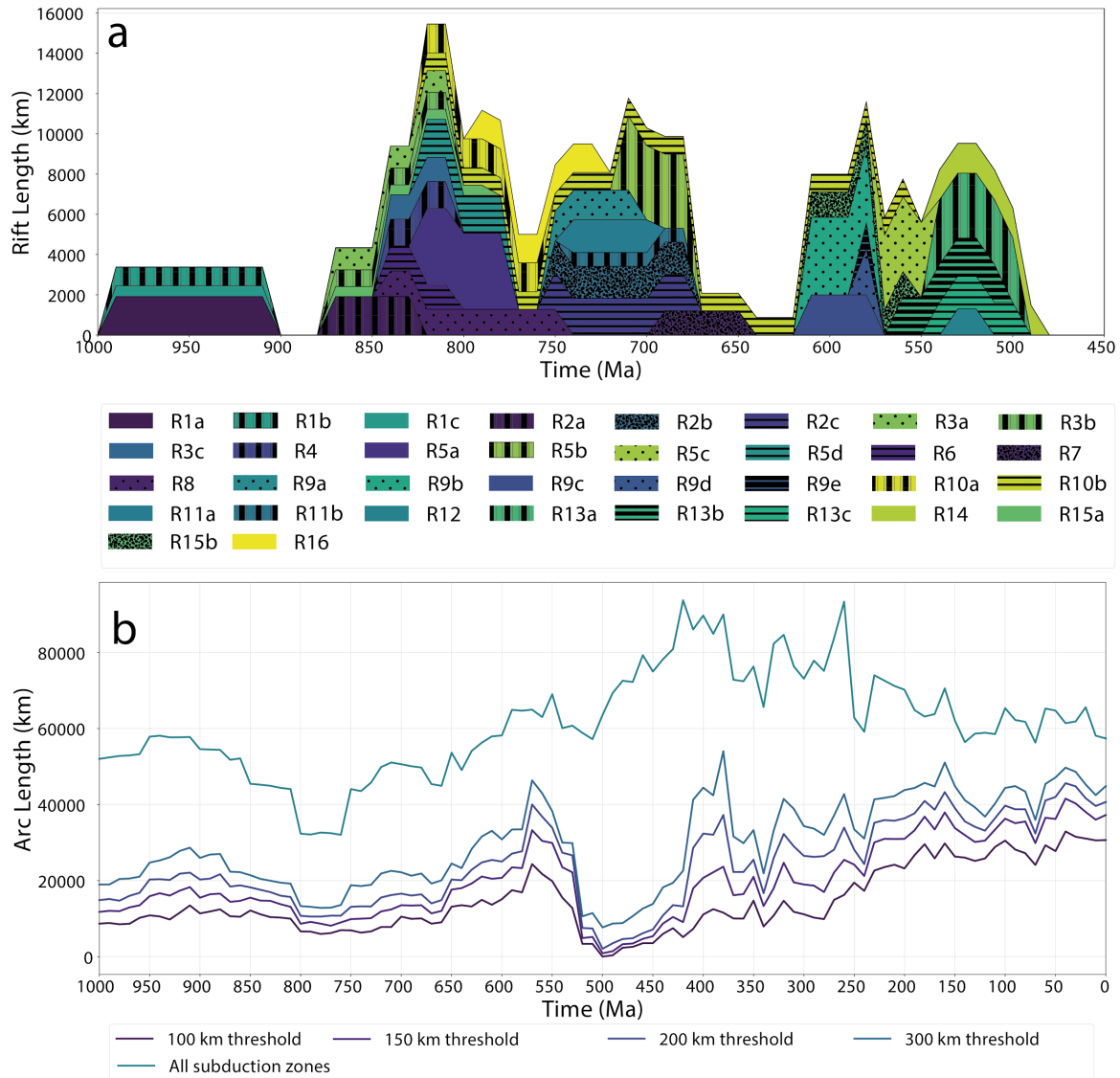
Figure 4 - (a) stack plot of rift length during the Neoproterozoic showing the individual contributions of different rifting events. We note three main pulses of rifting relating to Rodinia breakup: (i) Tonian, (ii) late Tonian to Cryogenian, and (iii) Ediacaran. (b) length of continent-margin arcs extracted from the Mer17, Dom16 and Mat16 models based on thresholded distance to nearest COB.

included any rifting from the Early Palaeozoic except for what is constrained in Dom16 or taken from Şengör and Natal'in (2001).

Figure 4a depicts the length of continent-margin arcs with varying thresholds from the 1000 to 0 Ma model (see also Figure 5 and SM3 for a map view of subduction zones). We pick 150 km (bold line in the figure) as an appropriate threshold, noting that slightly larger threshold distances of 200 and 300 km exhibit the same relative trends, suggesting that we have captured a reasonable approximation of continent-margin arc length, as expressed in the Mer17, Dom16 and Mat16 models. We also extract the length of all subduction zones in the models (including oceanic subduction) to act as a reference. There are a number of peaks evident in the continent-margin arc length. Firstly, the early hump of subduction between 950 and 900 Ma corresponds to the circum-Rodinia subduction girdle (e.g. Figure 5a,b). Secondly, there is a gradual increase in continent-margin arc length from the ca. 750 Ma, leading to a peak between 570 and 550 Ma (Figure 5e,f). This corresponds with the amalgamation of Gondwana, culminating with the closure of the Mozambique and Brasilia ocean, between India and Congo, and between Amazonia and Congo respectively (e.g. Collins and Pisarevsky, 2005). The third peak, occurring post Gondwana amalgamation during the Silurian-Devonian (ca. 450 Ma), marks the closure of the Iapetus Ocean, and development of Terra Australis subduction system that
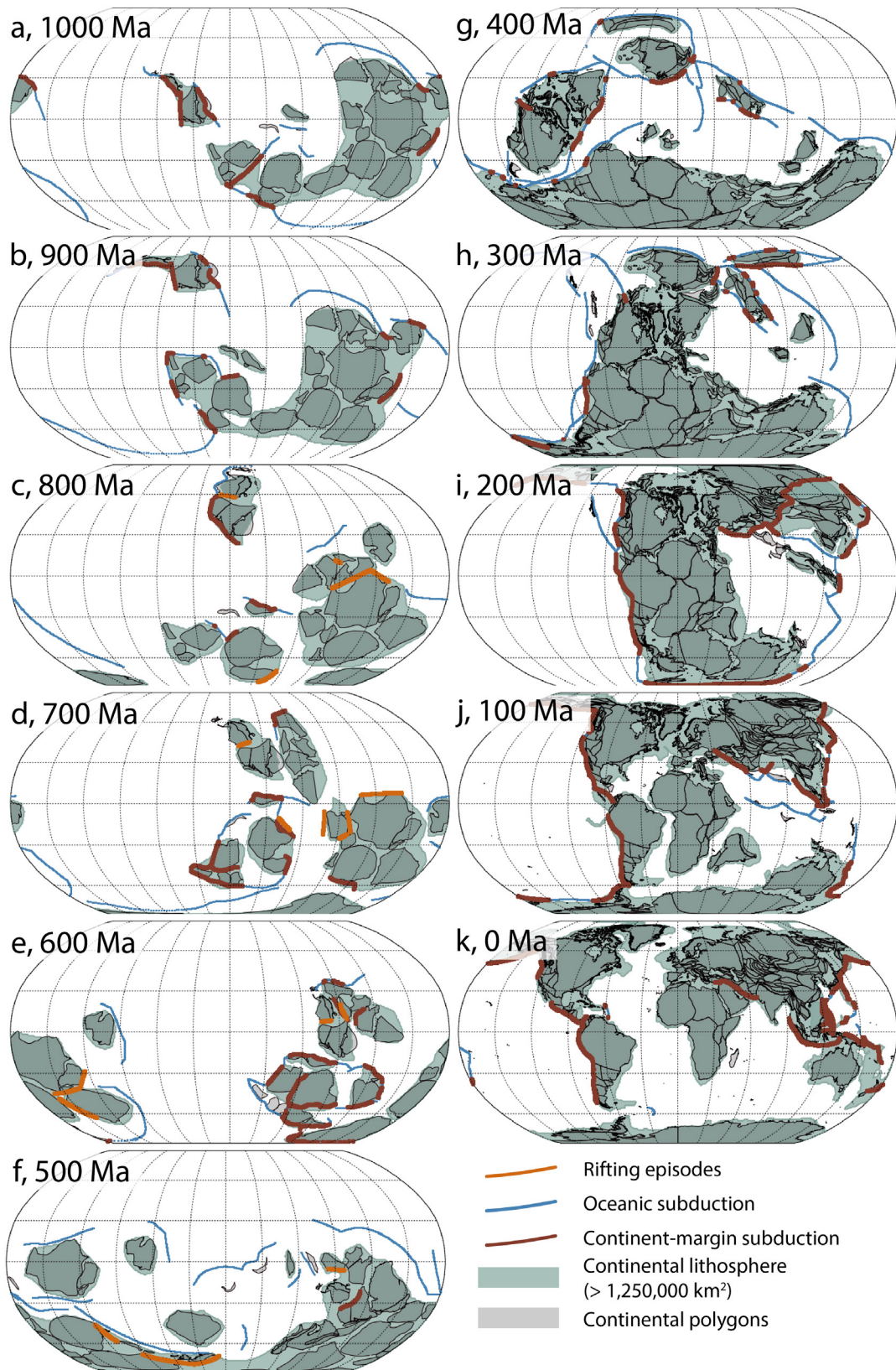
Figure 5 - Summary of reconstruction from 1000 to 0 Ma (see digital data for an animation in 10 Ma increments). Continent-margin subduction is any subduction zone within 150 km distance from the nearest piece of continental lithosphere greater than 1,250,000 km2 (e.g. Figures 4b and 5b).

persists, in parts (e.g. Andes - Figure 5g-k), to the present day (e.g. Cawood 2005). Subsequent peaks from 400 to 350 Ma reflect the suturing of Siberia to Laurentia and Baltica, and then this land mass with Gondwana, forming Pangea by 350 Ma (e.g. Figure 5g,h). Continent-margin arc length increases from 300 to 200 Ma (interpreted to correspond with the development of the circum-Pangea subduction girdle, e.g. Figure 5i), before plateauing from 200 Ma to present (there is some uncertainty here due to the increase in model resolution from ca. 250 Ma to present). A slight increase in continent-margin arc length from 200 Ma to present day could be similar to the gradual increase of arc length prior to Gondwana's amalgamation and records the collisions of the present-day continents prior to the formation of the next supercontinent.

3-2 Continental perimeter-to-area ratio

To help account for resolution changes between models (especially comparing the resolution of models during Cenozoic with models during the Tonian) we extract a ratio of the global perimeter of continental polygont al., 2012), and this is evident within our results (Figures 5j).

4 Discussion

4-1 Robustness of arc and rift length estimates

Our estimates for the total lengths of continent-margin arcs are broadly similar to those of Cao et al., (2017), though we extract a continent-margin arc length that is longer by ~5000-7500 km between 650 and 520 Ma and from 410 until 70 Ma, and a shorter continent-margin arc length between 520 and 410 Ma (e.g. Figures 5e, 6b). We attribute the differences to both the reconstructions and the methodology for defining arc extent. Firstly, we have used a reconstruction model that incorporates additional detail such as modelling a two stage collision of India-Azania-Congo during Gondwana amalgamation, and the closure of the Araçuai Basin between the Saõ-Francisco and Congo cratons (see Figure 5d,e and Supplementary Material 2). Secondly, Cao et al. (2017) limit their definition of continental arcs to those preserved within geological maps and

magmatic episodes (i.e. they explicity extract continental-arc length), whereas we extrapolate plate boundaries between discrete areas of ground-truth along continental outlines. For example, magmatism is not continuously preserved along the Andean margin for the Cenozoic where inferred flat-slab subduction occured (e.g. Ramos and Folguera, 2009) so they depict a series of broken subduction zones, while we interpelate that subduction was still occurring, the western coast of North America has experienced interplay between ridges and subduction over the last 40 Ma leading to slightly different models about the spatial extent of subduction (e.g. Schellart et al., 2010). Explaining our lower measures of continent-margin arc length in our results between 520 and 410 Ma is grounded in the rudimentary model for the Central Asian Orogenic Belt that we have implemented within this model, where continent-margin subduction is preserved only towards the late Devonian, and otherwise the 520 to 410 Ma period is dominated by oceanic arcs (e.g. Figure 6b).

Our results also corroborate with the detrital zircon record from Voice et al. (2011) (Figure 6c). Both continent-margin arc length and the detrital zircon record exhibit a lull during the Cryogenian (corresponding to the initial and prolonged breakup of Rodinia, and the turn-down in length of continen-marginl arcs) and a gradual increase leading to a peak at ca. 650 to 550 Ma during amalgamation of Gondwana (Figure 6b,c). The mid-late Palaeozoic is marked by a decrease in recorded zircon production, though small peaks at ca. 350 and 250 Ma (e.g. Condie and Aster, 2010; Voice et al., 2011 - Figure 6b,c), corresponding to the collision of Siberia with Laurussia, and then the final amalgamation of Pangea respectively, are also captured by our analysis (and that of Cao et al., 2017) of continent-margin arc length. Our aforementioned longer continent-margin arc length between 410 and 380 Ma is accounted for by the reconstruction we use here (Matthews et al. (2016), which uses the Domeier and Torsvik (2014), reconstruction for the early Palaeozoic). This reconstruction models the collision of some of the peri-Siberian arcs with the Siberian platform (e.g. Magnitogorsk Arc), and also with the development of oppositely dipping subduction zones closing the Rheic ocean on each of its margins, prior to the collision of Laurussia with Siberia and Gondwana (e.g. Figure 6a in
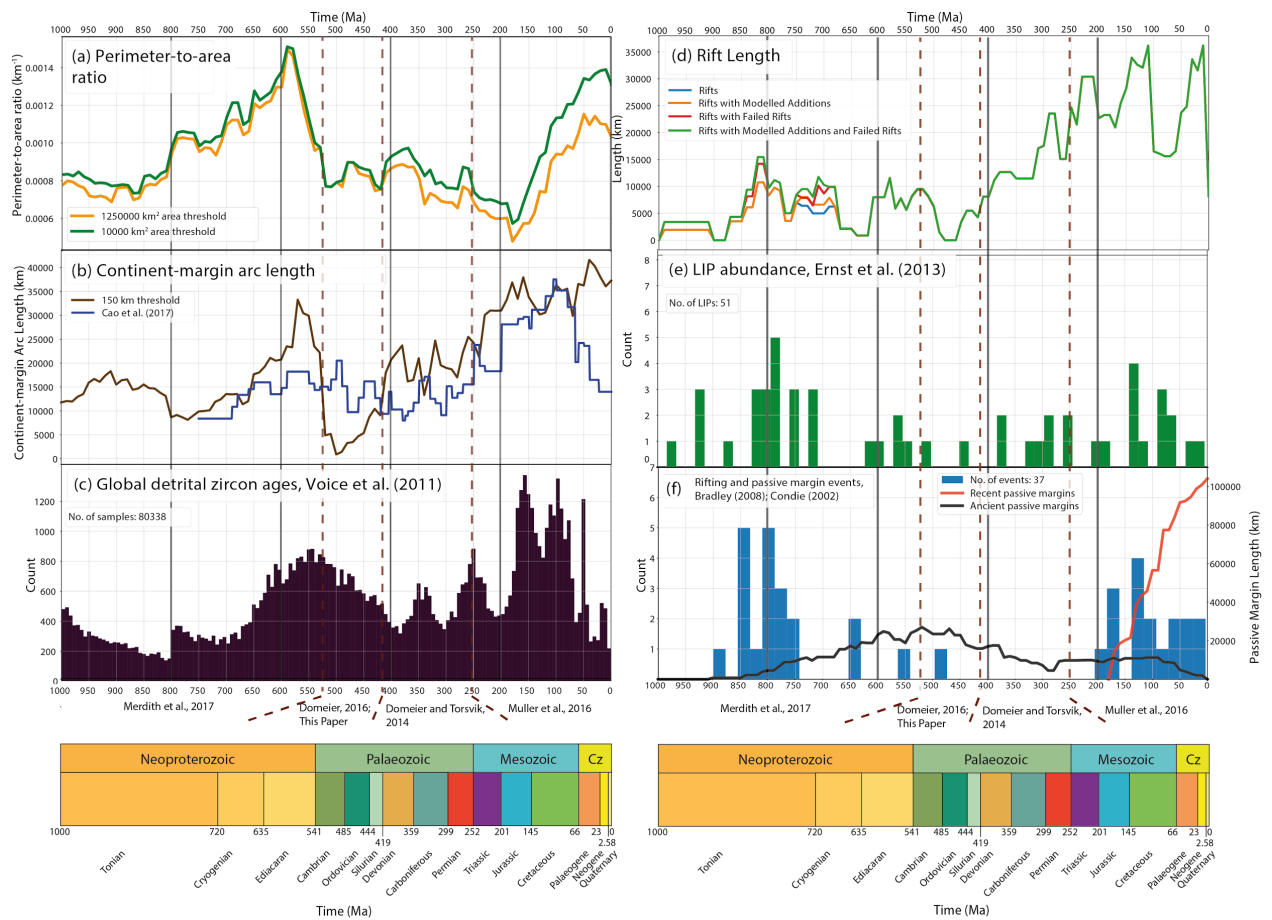
Figure 6 - (a) Perimeter-to-area ratio; (b) continent-margin arc length extracted here, and from Cao et al., (2017); (c) global detrital zircon ages from Voice et al. (2011); (d) rift length; (e) LIP abundance from Ernst et al. (2013), and; (f) Rifting events from Condie (2002) and passive margin lengths from Bradley (2008). The black line in panel F records the length of ancient passive margins that have are no longer preserved in situ (hence their length at present day is 0 km). The red line in panel F represents modern passive margins that are still preserved in situ. Cz is Cenozoic, ages come from the International Chronostratigraphic Chart v. 2017/02 (Cohen et al., 2013). Dashed red lines indicate the temporal extents of each model used for this analysis.

Domeier and Torsvik, 2014) over this time period, whereas Cao et al. (2017) model the closure of the Rheic ocean through a single sided subduction zone, and do not have the collision of oceanic arcs with Siberia until later.

The three major rifting phases associated here with the breakup Rodinia (Figure 6d) differ slightly from earlier studies (e.g. Condie, 2002; 2003). Condie (2002) measured frequency of distinct rifts that lead to breakup over the past 1 Ga (Figure 6f), noting two key clusters related to Rodinia breakup, at ca. 800 Ma and ca. 600 Ma (Condie 2002; 2003). The youngest phase outlined by Condie (2002) is correlative to our analysis, representing the opening of the Iapetus Ocean (e.g. Figure 5f,g), and we also infer that our earliest (ca. 850 to 800 Ma) phase of rifting correlates to the other rifting phase in Condie (2002), representing early rifting of Rodinia (e.g. Katanga

Supergroup in Congo, Adelaidian units in Australia). Our mid-rifting phase (ca. 720 to 680 Ma) is not represented in the results of Condie (2002), as the majority of rifts during this phase did not result in breakup (compare green vs. blue line Figure 5d). Additionally, because we measure rift length (as opposed to number of rifting events), the identification of two extensive failed rifting events, one on the western margin of Laurentia between 720 and 680 Ma (e.g. Colpron et al., 2002; Prave, 1999; Yonkee et al., 2014), and the other on the eastern margin of Laurentia (e.g. Aleinkoff et al., 1995; Li and Tull, 1998) would contribute significantly to the overall length of rifting during this phase (e.g. Figure 4b, 6c) at a time when Condie (2002) depicts no rifting.

For Neoproterozoic and Palaeozoic times we observe good correlation between increasing passive margin length and the timing of rifting pulses (Figure 6f).

100

Passive margins are particularly useful as their initiation corresponds to rifting (in that successful rifting results in a passive margin), and their destruction corresponds to continental arc production (Bradley (2008) marks the cessation at continent-continent collision and subduction of the continent-ocean boundary). Passive margin length increases from 850 Ma, with a steeper gradient occurring at ca. 800 Ma and 720 Ma (Figure 6f) (corresponding the the cessation of rifting we record just prior to these times, e.g. Figure 4a and 6d). The data from Bradley (2008) show a gradual increase of passive margin length up until ca. 550 Ma (Figure 6f), where it begins to decrease (Figure 6f). This is correlated with the increase in continent-margin length corresponding with the amalgamation of Gondwana. The decrease in passive margin length occurs between 600 and 550 Ma, coinciding with the collisions of Amazonia, India and Kalahari with Congo, and also between 520 to 500 Ma, corresponding to the collision of Australia and Rio de la Plata with Gondwana, while the intermittent rise in passive margin length from 500 to 450 Ma is related to the opening of the Rheic Ocean.

For younger times we see similar episodicity of rifting pulses during the Neoproterozoic and Mesozoic-Cenozoic, with both Rodinia and Pangea are characterised by a series of rifting pulses (each lasting for 30 to 50 Myr), rather than a single, protracted rifting event. Rodinia experienced three pulses of rifting (ca. 850 to 800 Ma, 720 to 680 Ma and 620 to 570 Ma). If we consider the East African Rift system (e.g. Şengör and Natal'in, 2001) the final breakup event of Pangea, then Pangea has also experienced three clear rifting episodes — ca. 230 to 200, corresponding to rifting between North and Central America and Europe, Greenland and Africa; 150 to 100 Ma, corresponding to rifting between Antarctica, India and Australia, and South American and Southern Africa, and ca. 50 to 0 Ma, corresponding to ongoing rifting within the East African Rift System (Brune et al., in press; Şengör and Natal'in, 2001). One notable difference is that rift lengths during Pangea breakup are considerably longer than during Rodinia breakup, this is likely due to preservation bias, whereby ocean basins, undeformed passive margins and matching coastlines allow for a much more detailed and realistic reconstruction, easier dating of key transitions,

and, subsequently, give more accurate representations of rift length and duration.

The continent-margin length from our results has been steadily increasing since the initiation of Pangea rifting (ca. 250 Ma, Figure 6b) without a prominent peak (for example, as are observed at 600 and, perhaps, at 400 Ma), which is similar to the gradual increase of arc length between 800 and 600 Ma (Figure 5b). Our results diverge from Cao et al. (2017) for this time, and also from the zircon record of Voice et al. (2011) by recording a greater amount of subduction. A particular point of difference is that at 70 Ma our estimates of continental arc length increase, while Cao et al. (2017) (and zircon data) show a decrease (e.g. animation in SM3). This is likely a limitation of our methodology, where we define continent-margin arcs as any subduction within a 150 km proximity of continental lithosphere with area larger than 1,250,000 km2. Between 70 and 60 Ma we depict a larger area of continental lithosphere than Cao et al. (2017) – for example we depict a larger greater India than they do, and also include 'Zealandia' as an extent of continental lithosphere – hence subduction on India's northern margin, and amongst New Zealand counts towards the total continent-margin arc length in our analysis, but does not for their analysis.

4-2 Measuring the 'supercontinent cycle'

The original proposal of the supercontinent cycle was suggested on the cyclicity of collisional and rifting events (Worsley et al., 1984). There are a series of cyclical events within our data of collision (i.e. peaks of continent-margin arcs), dispersal (i.e. peaks of rifting) and perimeter-to-area ratio (Figure 5), though interpretation the data as a single cycle is difficult to discern as the cyclicity within each parameter is not consistent through the others. What can be (somewhat clearly) discerned are times of supercontinent existence from the perimeter-to-area ratio (Figure 7a), the amalgamation of Gondwana from changes in continent-margin arc lengths (Figure 7b - possibly also the assembly of Pangea?) and the breakup of Rodinia and Pangea from rift lengths (e.g. Figure 7c). Interestingly, while we can clearly observe the breakup of Rodinia, it is difficult to determine the assembly of Pangea, instead the assembly of Gondwa-
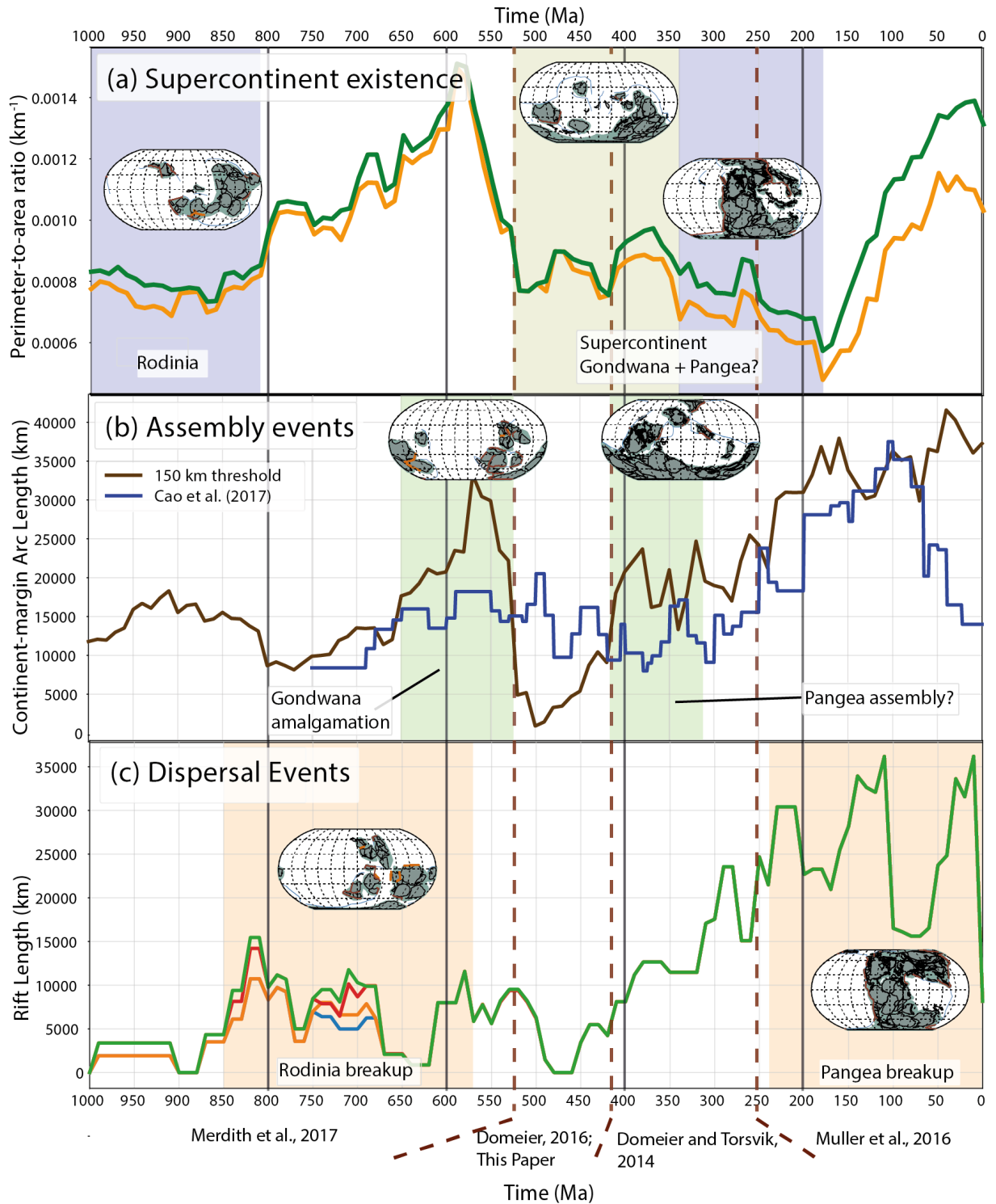
Figure 7 - Results from Figure 5 with key supercontinent times overlain (see Figure 5 for details). (a) Supercontinent cycle, blue shaded regions depict the 'traditional' periods of supercontinent existence, separated by periods of amalgamation and dispersal, the yellow shaded region represents Gondwana existence. (b) Amalgamation and assembly events of Gondwana and Pangea respectively. (c) Dispersal events of Rodinia and Pangea (Gondwana's breakup is synchronous with Pangea's)

na marks the most obvious change in arc length and perimeter-to-area ratio. This suggests either that the supercontinent Pangea began with Gondwana at ca. 520 Ma and existed up until its breakup (as Pangea) at 200 Ma, or that Gondwana exists as a superconti-

nent in its own right, and there is a second stage of the supercontinent cycle, typified by the transition of Gondwana to Pangea through incomplete breakup and slow accumulation of (more) continental lithosphere (e.g. Condie, 2002).
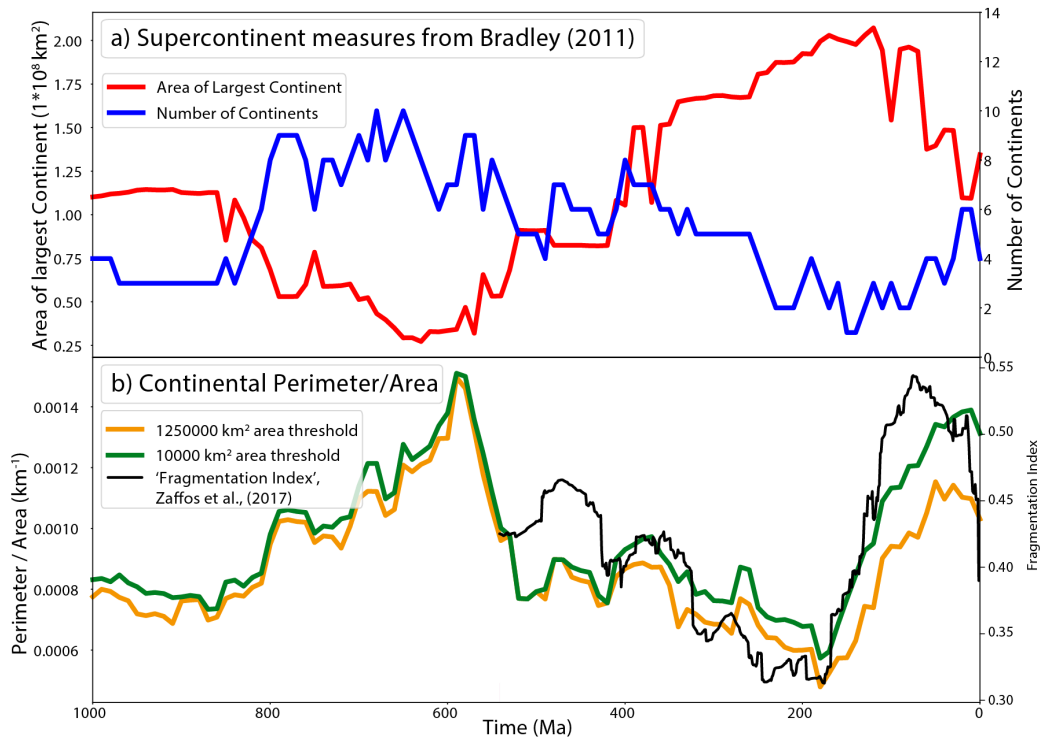
Figure 8 - Measure of supercontinent after (a) Bradley (2011) and (b) this paper (black line is the 'fragmentation index' of Zaffos et al., 2017).

The continental perimeter-to-area ratio could be a useful metric for helping quantify the 'connectedness' or 'fragmentation' (e.g. Zaffos et al., 2017) of continents through time (Figure 6a). Bradley (2011) suggested two other possible quantitative mechanisms for tracing the evolution of a supercontinent; area of the largest plate, and number of separate continents (Figure 8), and Zaffos et al., (2017) used a similar concept by normalising perimeter length through time as a 'fragmentation index'. However, as we are using separate models each with distinct differences in number resolution and size of terranes and continents, perimeter length by itself would be insufficient as it is partly dependent on model resolution. Times of supercontinent existence are obvious in all measures described above (Figure 8), being typified by large peaks in area of the largest continent and troughs of the number of continents (Figure 8a) and when there are troughs in perimeter-to-area ratio and the fragmentation index (Figure 8b). In these graphs the first order cyclicity is more obvious than in rift and continent-margin arc lengths, suggesting that on a palaeogeographic basis a single-stage supercontinent cycle is appropriate. Interestingly, the first order cyclicity can encompasses the two-stage cycle of Condie (2002), as there is no clear distinc-

tion (by any of the methods) between Gondwana and Pangea. Rather, Gondwana (amalgamation ca. 500 Ma) is the initiation of the 'supercontinent' part of the cycle, and it concludes with Pangea breakup, supporting the idea that every second supercontinent transition involves the gradual building from one supercontinent to another without full breakup.

Under the two-stage scheme of the supercontinent cycle (Condie, 2002), the first stage represents the 'traditional' cycle, involving the breakup of one supercontinent and re-amalgamation into the next, and is represented here by the transition from Rodinia to Gondwana (Figure 5c-f). The second stage of the cycle suggests that Rodinia formed from the continual growth of Nuna (the supercontinent prior to Rodinia) with minor re-adjustments (e.g. Meert, 2014; Roberts, 2013), and Pangea was formed from the continual aggregation of crust to Gondwana (with minor adjustments, e.g. Figure 5f-i), rather than a full breakup of the respective Nuna and Gondwana constituent continents (Condie, 2002). Using this understanding of the supercontinent cycle, we would expect to see a continual progression of increasing continent-margin arc length between 520 Ma (marking the amalgamation of Gondwana) and 350 Ma (marking the final assembly of Pangea) coupled with

no peaks of rift length (some rifting could be expected regionally, but there should not be a global pulse of rifting, as we would expect (and is evident) in the breakup of Rodinia and Pangea). This is because there is no full breakup of the prior supercontinent. We observe this in our results, both palaeogeographically (e.g. Figure 5f-i) and in the changes in arc and rift length from 500 to 200 Ma (Figure 6). During this period of time we observe a gradual increase in continent-margin arc length and no notable pulses of rifting suggesting that a supercontinent is fragmenting (e.g. Figure 6d). In particular, we do not see a large, abrupt decrease in continent-margin arc length upon Pangea amalgamation, as we see marking the amalgamation of Gondwana. The absence of rifting pulses is also reflected in the dearth of rifting events compiled by Condie (2002), and the decrease in passive margin length of Bradley (2008) (Figure 6f). However, we note that our above comments are not definitive proof of this conception of the supercontinent cycle, rather they articulate that the simple conceptual model of accretion-drift-dispersal may not be adequate to fully explain the supercontinent cycle. To better explore the cycle, an understanding of what constitutes a supercontinent beyond palaeogeographical constraints may be necessary. In particular, identifying the geodynamic implications of a supercontinent, relating them to temporal geological evidence (e.g. rift length, arc length) and comparing them to a palaeogeographical understanding of a supercontinent are important, as it could, for example, influence whether Gondwana is considered a supercontinent or just a large aggregation of continental lithosphere.

An alternative to the two-stage scheme is to explicitly consider Gondwana as part of the same period of supercontinent existence as Pangea, which would require the re-conception of the supercontinent cycle. Traditionally, the cycle consists of brief periods of supercontinent existence (e.g. 1000 to 850 Ma for Rodinia, 340 to 180 Ma for Pangea) with longer times of dispersal and accretion in between. However, if Gondwana is explicitly considered part of the Pangean supercontinent phase, then it would suggest that the cycle consists of longer times of supercontinent existence (e.g. 520 to 180 Ma, Gondwana amalgamation to Pangea dispersal, Figures 5i-j, 8a) punctuated by shorter times of dispersal and amal-

gamation. This would require that part of the 'supercontinent existence' phase involves the continual accretion of more crust to the nucleus (as suggested by continent-margin arc length, Figure 6b). In this case – with Gondwana and Pangea forming part of the same supercontinent cycle (as, potentially, did Nuna and Rodinia) – Gondwana reflects the initialisation of the supercontinent (Figure 8b), and Pangea is the culmination of a long accretionary process, as suggested by the continental-to-perimeter ratio (Figure 8a)

An alternative to palaeogeographical-based conceptions of the supercontinent cycle could be to use variation within the length of continent-margin arcs, as these may be better constrained by the geological record, and more easily verifiable by geological data such as preserved arc rocks (e.g. Cao et al., 2017; Cawood et al., 2016; Merdith et al., 2017). Rifts, though they are more ambiguous in deep geological time, could also be used to mark the endpoint of a supercontinent. In this case, the criteria of a supercontinent would be that its amalgamation causes a (geologically) rapid and pronounced decrease in the total length of global continent-margin arcs as subduction resets to the periphery of the supercontinent (Cawood and Buchan, 2007; Figure 8b), and its breakup creates a series of global peaks in rifting length (with the first global pulse of rifting representing the beginning of dispersal, Figure 8c). The global ubiquity of both continent-margin arc and rifting lengths are the keys to these criteria, as if only a regional reduction or increase (respectively) is observed it is likely to either reflect a small-scale plate boundary re-organisation (e.g. terrane collision resulting in subduction cessation), or the opening of an internal ocean and terrane migration (e.g. Rheic and Tethyan oceans, Figure 5h-j).

4-3 Hypotheses of supercontinent breakup

The processes that drive supercontinent breakup have been proposed to be dominated by subduction ('top-down'), or mantle dynamics ('bottom-up'). Typically, top-down models invoke slab pull and long-lived subduction on the periphery of a supercontinent to eventually induce enough strain to break continental
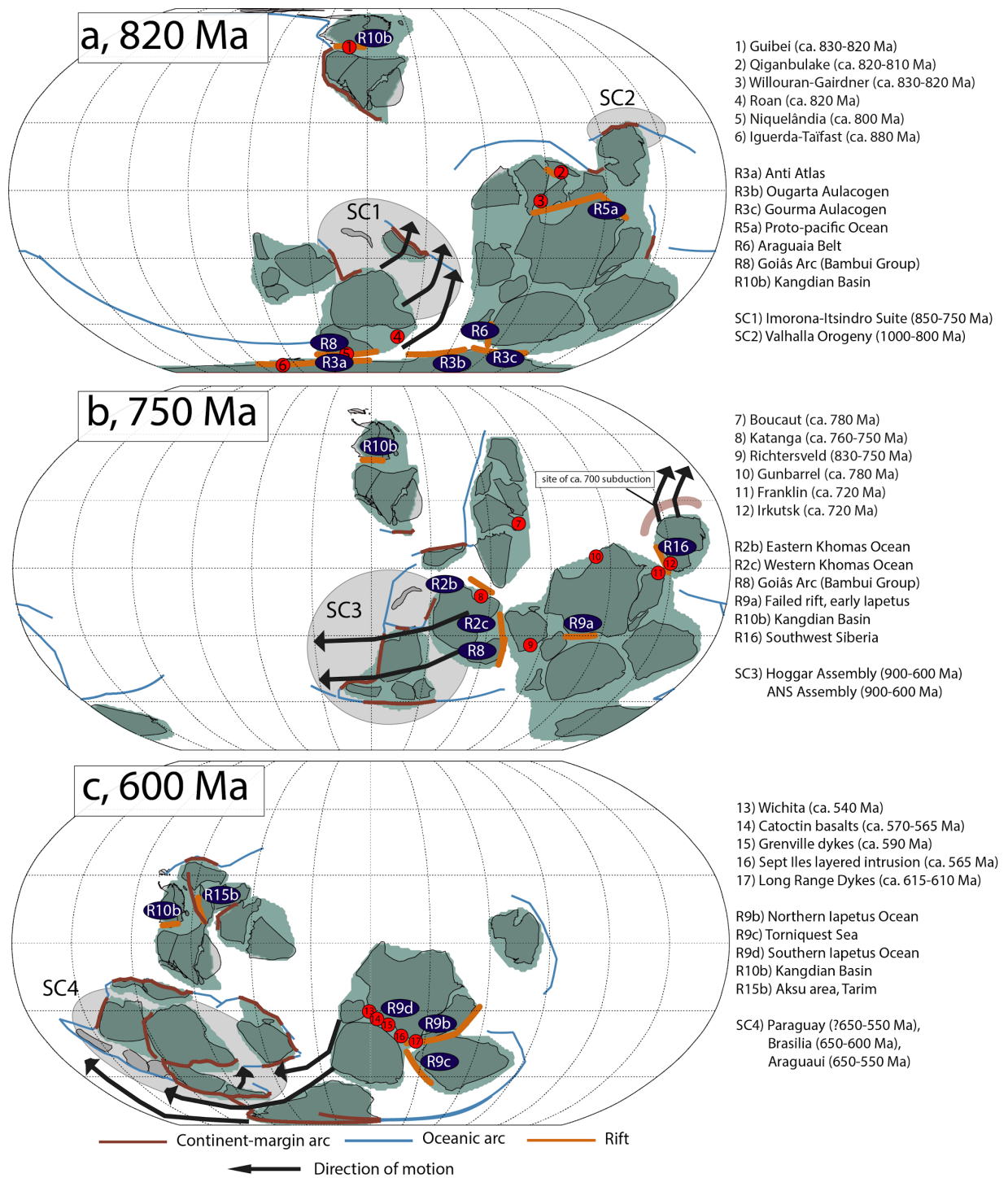
Figure 9 - Snapshots of rifting times during the breakup of Rodinia (a) 820 Ma; (b) 750 Ma, and; (c) 600 Ma. Tectonic events – LIPs, rifting events, subduction complexes (SC) – around each time are displayed.

lithosphere and induce dispersal (e.g. Cawood and Buchan, 2007; Collins 2003). Conversely, bottom-up models suggest that arrival of superplumes (suggested by the presence of LIPs) are the primary driver of rifting and supercontinent breakup (e.g. Li et al., 1999; 2003). These two models are not mutually exclusive, and during supercontinent dispersal both may be acting in some capacity (at different scales)

to drive breakup or amalgamation (e.g. Murphy et al., 2009). For example, a subduction girdle (i.e. 'top-down') might provide the strain to break the supercontinent, while a superplume (i.e. 'bottom-up') might control where rifting localises (c.f. Cawood et al., 2016; Courtillot et al., 1999). In order to test these ideas we depict key breakup times of Rodinia with position of LIPs overlain (taken from Ernst et

al., 2013) (Figure 9).

Our results of rifting pulses corroborate with the large igneous province (LIP) record of Ernst et al. (2013) which show abundant LIP emplacement in the Neoproterozoic between 850 and 800 Ma, and between 620 and 570 Ma (Figures 6f, 9a,c). Large igneous provinces (LIPs) are associated with super-continent breakup. The middle pulse of rifting in our analysis (e.g. 750-680 Ma, Figure 5d) is correlated with LIP formation for the earlier part of rifting (e.g. ca. 750 Ma), however few recorded LIPs were generated during the tail end of this rifting pulse (720 to 680 Ma, Figure 9b). LIPs mark the rifting phase (prior to development of a passive margin) and are typically related to continental breakup (e.g. Courtillot et al., 2001; Ernst and Bleeker, 2010), and not failed rifting events. Consequently, we attribute the presence of ca. 750 Ma LIPs to rifting that lead to the rifting of Congo and Rodinia, and the absence of 720 to 680 Ma LIPs to the dominance of failed rifting events that were more prevalent during this pulse of rifting of Rodinia (e.g. Figure 6d, 9b).

The temporal displacement between the peak of continent-margin arc length from 950 and 850 Ma and large pulse of rifting and LIP generation between 850 and 780 Ma lends supports the hypothesis that supercontinent breakup is, in part, driven by rollback of long-lived subduction around the periphery of the supercontinent (e.g. Bercovici and Long, 2014; Cawood et al., 2016). We can also observe, for Rodinia, that the rifting present at 850 to 800 Ma is predominantly constrained to around the West African and Congo cratons, and along the suture between Australia and Laurentia (e.g. Figure 9a). Continental arcs are preserved in the Imorona-Itsindro Suite of Azania (present day Madagascar - Collins and Pisarevsky, 2005) from ca. 850 to 750 Ma (e.g. Archibald et al., 2016; 2017, Figure 5c, 8a, SM3) and is interpreted to be reminiscent of an Andean style continental arc (Archibald et al., 2017). Subduction outboard of Australia is more difficult to determine, though reconstructing both Tarim and North China to a position near Australia would suggest some arc activity, and Merdith et al. (2017) suggested that slightly younger subduction could be preserved here within some fragments of crust now located in southeast Asia. Importantly, all LIPs, especially in the

Congo-Saõ Francisco cratons (C-SF), post-date the initiation of rifting. Younger pulses of rifting of Rodinia exhibit a similar story. Subduction preserved in the Valhalla orogen of Siberia (e.g. Cawood et al., 2011; Likhanov et al., 2015) predates rifting and LIP emplacement at ca. 720 to 700 Ma (Figure 9b), and the initiation of extensive subduction zones around C-SF from 700 Ma (e.g. Figure 5d,e) clearly predate the opening of the Iapetus Ocean and emplacement of LIPs there (e.g. Figure 9c). Cawood et al. (2016) suggested that most LIPs and dyking events correlated to Rodinia's breakup could be easily explained through rifting, rather than superplume arrival. Our results suggest the establishment of rifting prior to LIP formation, which, while not discounting the presence of a superplume, nor the possibility that it does contribute to breakup, would indicate that superplume arrival does not necessarily induce rifting, in agreement with previous studies (Brune et al., 2013; Cawood et al., 2016).

Relating these comments to the mechanism of breakup we observe that the closure of interior oceans leading to the formation of a supercontinent (e.g. Gondwana amalgamation, Figure 5d-f) results in a resetting of subduction to outboard of the supercontinent forming a girdle of subduction (e.g. Cawood and Buchan, 2007; Collins, 2003; Collins et al., 2011) (Figure 5a-d,h,i). This girdle is likely to exert a stronger pulling force than the alternative – the closure of interior oceans – because the circum-supercontinent girdle is more likely to involve long lived subduction (i.e. until an eventual continent-continent collision) that generates a constant slab-pull force (Collins, 2003). It also creates a strong negative buoyancy anomaly in the mantle, meaning that while some roll back and opening of back-arc basins could be expected, it is difficult for the subduction zone to move far away from the margin (e.g. eastern Australia during the Palaeozoic).

Dal Zilio et al. (2017) proposed a mechanism to explain fragmentation of a supercontinent, relating duration of subduction to breakup. They suggested that long-lived subduction increases the volume of subducted crust that can penetrate the lower mantle (after stagnating at the 660 km viscosity discontinuity) in the mantle due to slab build up and folding (e.g. Sigloch and Mihalynuk, 2013). Consequently, this

creates a larger cell of convection and can localise stress at a further distance from the margin, allowing supercontinent dispersal to occur (Dal Zilio et al., 2017). Alternatively, shorter lived subduction, such as within interior oceans that close and subduction ceases over 100 Myr (e.g. Iapetus and Rheic oceans - Figure 5e-g; Domeier 2016; Domeier and Torsvik, 2014; Tethyan realms, Metcalfe 2013), are less likely to have the same volume of slabs penetrating the lower mantle. Hence, they create smaller cells of convection and may be less likely to be able to disperse a supercontinent, rather they create marginal basins and smaller oceanic realms (Dal Zilio et al., 2017). As cessation of subduction zone should produce abrupt downturns in arc length, we can see from our results (e.g. Figure 4b, 5b) that during the Neoproterozoic cessation primarily occurs post Gondwana amalgamation (reductions in continent-marginl arc length prior to this are around 2000 to 3000 km in length), suggesting that most of the subduction around Rodinia was semi-continuous (see also Cawood et al., 2016).

Dal Zilio et al. (2017) noted that this concept is also controlled by the strength of the overriding lithosphere and the presence and/or position of any pre-existing weaknesses (typically determined by the presence of thick, old cratonic crust with a deep lithospheric root or a large orogenic event), hence margins of a supercontinent put under stress by long-lived subduction may be preserved and not result in breakup, A potential example of this is evident in comparing Laurentia-Greenland with Laurentia-Siberia connection. Northern Laurentia and Greenland were sutured along the Trans-Hudson Orogen at ca. 1.9 to 1.8 Ga (Bickford et al., 1990) and did not breakup during Rodinia dispersal. Comparably, there is currently no known suture between Siberia and Laurentia for their fits during Nuna and Rodinia, and the two commonly proposed configurations simply juxtapose their coastlines and breakup did occur during Rodinia's dispersal. The two configurations either argue for a tighter configuration from ca. 1.9 Ga with ~ 500 km between their margins (cf. Ernst et al., 2016) or a looser configuration from ca. 1.5 Ga with ~ 3000 km between their margins, (cf. Pisarevsky and Natapov, 2003, though the timing of this configuration is predominantly based on palaeomagnetic data, e.g. Pisarevsky et al., 2014).

The alternative idea implicit within Dal Zilio's et al., (2017) study is that short-lived subduction leads to a series of rifted terranes without supercontinent breakup. We observe this along the northern margin of Gondwana from ca. 520 Ma, where the length of continent-margin arc exhibits more local peaks while steadily increasing, suggesting that there is both a large long lived subduction zone, and a series of smaller subduction zones that periodically initiate then cease (Figure 4b, 5b). A large subduction zone initiates outboard of Gondwana (e.g. Ross-Delamarian orogeny, proto-Andes, Figure 5f,e), likely as a response to closure of interior oceans during Gondwana's amalgamation - cf. Cawood and Buchan, 2007), and this subduction zone is still preserved today in South America and the southwest Pacific (e.g. Figure 5j,k). Comparably, a series of subduction zones open and close over ca. 100 Ma timescales on the northern (Iapetus-Tethyan) margins of Gondwana, and a series of terranes rift off and begin coalescing against Laurussia and Siberia to form the Central Asian Orogenic Belt (e.g. Figure 5f-d).

For the later pulses of rifting associated with Rodinia and Pangea breakup, there is no notable increase of continent-margin arc length relative to the length prior to the initial pulse of rifting. Rather the subsequent pulses of rifting, which exhibit a similar magnitude to the initial pulse, occur without a peak of continent-margin arc formation preceding them. This could mean that while subduction is required for supercontinent breakup, once breakup has progressed to seafloor spreading, the system becomes less dependent on a girdle of subduction occurring around the periphery of the (remaining) supercontinent to continue to fragment the continental crust. In this case, accretion and assembly of the subsequent supercontinent could be driven more locally by either slab pull of a single subduction zone dragging continental lithosphere towards a downwelling or geoid low (e.g. Anderson, 1994) or through the effects of plume arrival creating a geoid high in an exterior ocean, forcing the preferential closure of interior oceans (e.g. Murphy et al., 2009).

5 Conclusions

The last 1 Ga of Earth history has been punctuated

by the formation and breakup of at least two supercontinents, Rodinia and Pangea. Here we have used full plate, topological plate models to extract a continuous estimate of the length of continent-margin arcs, rifts and continental perimeter-to-area ratio in order to better understand the long-term evolution of the surface of the earth and to investigate how it relates to the supercontinent cycle. A simple first degree supercontinent cycle is not supported by variations within continent-margin arc and rifting length. Consequently, we suggest either a two-stage supercontinent cycle, or a cycle wherein the period of 'supercontinent existence' (distinct from supercontinent dispersal or assembly) covers a larger period of time than previously thought, such that Gondwana to Pangea encompasses the gradual accretion of continental lithosphere to an already existing supercontinent. Under this concept, supercontinent assembly is marked by a pronounced and abrupt drop in the global length of continent-margin arcs, as is evident for the amalgamation of Gondwana. This is seen for Pangea and also Gondwana, leading us to propose this as a general geodynamic definition of a supercontinent, in addition to palaeogeographical definitions about the amount of lithosphere connected on a single tectonic plate. This has a benefit of defining a supercontinent by a geodynamic criterion, in addition to just a palaeogeographic criteria of land mass. Our results suggest a correlation between subduction prior to the initial rifting of supercontinents (both Rodinia and Pangea), agreeing with previous studies that suggested supercontinent rifting and breakup is driven by a circum-supercontinent subduction girdle, and not by the presence of a superplume, evidenced by LIP emplacement. However, our results do not show subsequent subduction driving continual fragmentation of a supercontinent, suggesting that once initial breakup occurs other forces contribute more strongly than the initial subduction girdle. We include with this publication an extension of a full plate Neoproterozoic model until 410 Ma. The Early Palaeozoic portion (520-410 Ma) should be treated cautiously, as we have only modelled Precambrian cratonic crust and not the terranes that make up the Central Asian Orogenic Belt.

6 References

Aleinikoff, J.N., Zartman, R.E., Walter, M., Rankin, D.W., Lyttle, P.T. and Burton, W.C., 1995. U-Pb ages of metarhyolites of the Catoctin and Mount Rogers Formations, central and southern Appalachians: Evidence for two pulses of Iapetan rifting. American Journal of Science, 295(4), pp.428-454.

Alkmim, F.F., Marshak, S., Pedrosa-Soares, A.C., Peres, G.G., Cruz, S.C.P. and Whittington, A., 2006. Kinematic evolution of the Araçuaí-West Congo orogen in Brazil and Africa: Nutcracker tectonics during the Neoproterozoic assembly of Gondwana. Precambrian research, 149(1), pp.43-64.

Anderson, D.L., 1994. Superplumes or supercontinents?. Geology, 22(1), pp.39-42.

Archibald, D.B., Collins, A.S., Foden, J.D. and Razakamanana, T., 2017. Tonian Arc Magmatism in Central Madagascar: The Petrogenesis of the Imorona-Itsindro Suite. The Journal of Geology, 125(3), pp.271-297.

Archibald, D.B., Collins, A.S., Foden, J.D., Payne, J.L., Holden, P., Razakamanana, T., De Waele, B., Thomas, R.J. and Pitfield, P.E., 2016. Genesis of the Tonian Imorona–Itsindro magmatic Suite in central Madagascar: Insights from U–Pb, oxygen and hafnium isotopes in zircon. Precambrian Research, 281, pp.312-337.

Babinski, M., Boggiani, P.C., Trindade, R.I.F. and Fanning, C.M., 2013. Detrital zircon ages and geochronological constraints on the Neoproterozoic Puga diamictites and associated BIFs in the southern Paraguay Belt, Brazil. Gondwana Research, 23(3), pp.988-997.

Babinski, M., Vieira, L.C. and Trindade, R.I., 2007. Direct dating of the Sete Lagoas cap carbonate (Bambuí Group, Brazil) and implications for the Neoproterozoic glacial events. Terra Nova, 19(6), pp.401-406.

Bercovici, D. and Long, M.D., 2014. Slab rollback instability and supercontinent dispersal. Geophysical Research Letters, 41(19), pp.6659-6666.

Bickford, M.E., Collerson, K.D., Lewry, J.F., Van Schmus, W.R. and Chiarenzelli, J.R., 1990. Proterozoic collisional tectonism in the Trans-Hudson orogen, Saskatchewan. Geology, 18(1), pp.14-18.

Bradley, D.C., 2008. Passive margins through earth history. Earth-Science Reviews, 91(1), pp.1-26.

Bradley, D.C., 2011. Secular trends in the geologic record and the supercontinent cycle. Earth-Science Reviews, 108(1), pp.16-33.

Brune, S., Popov, A.A., and Sobolev, S.V., 2013, Quantifying the thermo-mechanical impact of plume arrival on continental break-up: Tectonophysics, v. 604, p. 51–59, doi: 10.1016/j.tecto.2013.02.009.

Brune, S., Williams, S.E., Butterworth, N.P. and Müller, R.D., 2016. Abrupt plate accelerations shape rifted continental margins. Nature, 536(7615), pp.201-204.

Burrett, C., Long, J. and Stait, B., 1990. Early-Middle Palaeozoic biogeography of Asian terranes derived from Gondwana. Geological Society, London, Memoirs, 12(1), pp.163-174.

Burrett, C., Zaw, K., Meffre, S., Lai, C.K., Khositanont, S., Chaodumrong, P., Udchachon, M., Ekins, S. and Halpin, J., 2014. The configuration of Greater Gondwana—evidence from LA ICPMS, U–Pb geochronology of detrital zircons from the Palaeozoic and Mesozoic of Southeast Asia and China. Gondwana Research, 26(1), pp.31-51.

Cao, W., Lee, C.T.A. and Lackey, J.S., 2017. Episodic nature of continental arc activity since 750 Ma: A global compilation. Earth and Planetary Science Letters, 461, pp.85-95.

Cawood, P.A. and Buchan, C., 2007. Linking accretionary orogenesis with supercontinent assembly. Earth-Science Reviews, 82(3), pp.217-256.

Cawood, P.A. and Pisarevsky, S.A., 2006. Was Baltica right-way-up or upside-down in the Neoproterozoic?. Journal of the Geological Society, 163(5), pp.753-759.

Cawood, P.A., 2005. Terra Australis Orogen: Rodinia breakup and development of the Pacific and Iapetus margins of Gondwana during the Neoproterozoic and Paleozoic. Earth-Science Reviews, 69(3), pp.249-279.

Cawood, P.A., Hawkesworth, C.J. and Dhuime, B., 2013. The continental record and the generation of continental crust. Geological Society of America Bulletin, 125(1-2), pp.14-32.

Cawood, P.A., McCausland, P.J. and Dunning, G.R., 2001. Opening Iapetus: constraints from the Laurentian margin in Newfoundland. Geological Society of America Bulletin, 113(4), pp.443-453.

Cawood, P.A., Strachan, R., Cutts, K., Kinny, P.D., Hand, M. and Pisarevsky, S., 2010. Neoproterozoic orogeny along the margin of Rodinia: Valhalla orogen, North Atlantic. Geology, 38(2), pp.99-102.

Cawood, P.A., Strachan, R.A., Pisarevsky, S.A., Gladkochub, D.P. and Murphy, J.B., 2016. Linking collisional and accretionary orogens during Rodinia assembly and breakup: Implications for models of supercontinent cycles. Earth and Planetary Science Letters, 449, pp.118-126.

Cawood, P.A., Wang, Y., Xu, Y. and Zhao, G., 2013. Locating South China in Rodinia and Gondwana: A fragment of greater India lithosphere?. Geology, 41(8), pp.903-906.

Cawood, P.A., Zhao, G., Yao, J., Wang, W., Xu, Y. and Wang, Y., 2017. Reconstructing South China in Phanerozoic and Precambrian supercontinents. Earth-Science Reviews.

Cocks, L.R.M. and Torsvik, T.H., 2007. Siberia, the wandering northern terrane, and its changing geography through the Palaeozoic. Earth-Science Reviews, 82(1), pp.29-74.

Collins, A.S. and Pisarevsky, S.A., 2005. Amalgamating eastern Gondwana: the evolution of the Circum-Indian Orogens. Earth-Science Reviews, 71(3), pp.229-270.

Collins, W.J., 2003. Slab pull, mantle convection, and Pangaean assembly and dispersal. Earth and Planetary Science Letters, 205(3), pp.225-237.

Collins, W.J., Belousova, E.A., Kemp, A.I. and Murphy, J.B., 2011. Two contrasting Phanerozoic orogenic systems revealed by hafnium isotope data. Nature Geoscience, 4(5), p.333.

Colpron, M., Logan, J.M. and Mortensen, J.K., 2002. U-Pb zircon age constraint for late Neoproterozoic rifting and initiation of the lower Paleozoic passive margin of western Laurentia. Canadian Journal of Earth Sciences, 39(2), pp.133-143.

Coltice, N., Bertrand, H., Rey, P., Jourdan, F., Phillips, B.R. and Ricard, Y., 2009. Global warming of the mantle beneath continents back to the Archaean. Gondwana Research, 15(3), pp.254-266.

Condie, K.C. and Aster, R.C., 2010. Episodic zircon age spectra of orogenic granitoids: the supercontinent connection and continental growth. Precambrian Research, 180(3), pp.227-236.

Condie, K.C., 2002. The supercontinent cycle: are there two patterns of cyclicity?. Journal of African Earth Sciences, 35(2), pp.179-183.

Condie, K.C., 2003. Supercontinents, superplumes and continental growth: the Neoproterozoic record. Geological Society, London, Special Publications, 206(1), pp.1-21.

Courtillot, V., Jaupart, C., Manighetti, I., Tapponnier, P. and Besse, J., 1999. On causal links between flood basalts and continental breakup. Earth and Planetary Science Letters, 166(3), pp.177-195.

Dal Zilio, L., Faccenda, M. and Capitanio, F., 2017. The role of deep subduction in supercontinent breakup. Tectonophysics.

Dalziel, I.W., 1991. Pacific margins of Laurentia and East Antarc-

tica-Australia as a conjugate rift pair: Evidence and implications for an Eocambrian supercontinent. Geology, 19(6), pp.598-601.

Domeier, M. and Torsvik, T.H., 2014. Plate tectonics in the late Paleozoic. Geoscience Frontiers, 5(3), pp.303-350.

Domeier, M., 2016. A plate tectonic scenario for the Iapetus and Rheic Oceans. Gondwana Research, 36, pp.275-295.

Domeier, M., 2017, April. Early Paleozoic tectonics of Asia: A preliminary full-plate model. In EGU General Assembly Conference Abstracts (Vol. 19, p. 10167).

Dong, Y. and Santosh, M., 2016. Tectonic architecture and multiple orogeny of the Qinling Orogenic Belt, Central China. Gondwana Research, 29(1), pp.1-40.

Ennih, N. and Liégeois, J.P., 2001. The Moroccan Anti-Atlas: the West African craton passive margin with limited Pan-African activity. Implications for the northern limit of the craton. Precambrian Research, 112(3), pp.289-302.

Ernst, R., and Bleeker, W., 2010, Large igneous provinces (LIPs), giant dyke swarms, and mantle plumes: Signifi- cance for breakup events within Canada and adjacent regions from 2.5 Ga to the Present: Canadian Journal of Earth Sciences, v. 47, p. 695–739.

Ernst, R.E., Bleeker, W., Söderlund, U. and Kerr, A.C., 2013. Large Igneous Provinces and supercontinents: Toward completing the plate tectonic revolution.

Ernst, R.E., Hamilton, M.A., Söderlund, U., Hanes, J.A., Gladkochub, D.P., Okrugin, A.V., Kolotilina, T., Mekhonoshin, A.S., Bleeker, W., LeCheminant, A.N. and Buchan, K.L., 2016. Long-lived connection between southern Siberia and northern Laurentia in the Proterozoic. Nature Geoscience, 9(6), pp.464-469.

Evans, D.A., 2013. Reconstructing pre-Pangean supercontinents. Geological Society of America Bulletin, 125(11-12), pp.1735-1751.

Fang, D.J., Jin, G.H., Jiang, L.P., Wang, P.Y., Wang, Z.L., 1996. Paleozoic paleomagnetic results and the tectonic significance of Tarim palte. Acta Geophys. Sin. 39 (4), 522–532 (in Chinese with English abstract).

Fang, D.J., Wang, P.Y., Shen, Z.Y., Tan, X.D., 1998. Paleomagnetic results and Phanero- zoic apparent polar wandering path of Tarim block. Sci. China Ser. D 41 (Suppl.), 105–112.

Frimmel, H.E., Fölling, P.G. and Eriksson, P.G., 2002. Neoproterozoic tectonic and climatic evolution recorded in the Gariep Belt, Namibia and South Africa. Basin Research, 14(1), pp.55-67.

Gao, R.F., Huang, H.L., Zhu, Z.W., Liu, H.S., Fan, Y.Q. and Qing, X.J., 1983. The study of paleomagnetism in northeastern Sino-Korean massif during Pre-late Paleozoic. Contribution to Project of Plate Tectonics of Northern China, 1, pp.264-274.

Gladkochub, D.P., Wingate, M.T.D., Pisarevsky, S.A., Donskaya, T.V., Mazukabzov, A.M., Ponomarchuk, V.A. and Stanevich, A.M., 2006. Mafic intrusions in southwestern Siberia and implications for a Neoproterozoic connection with Laurentia. Precambrian Research, 147(3), pp.260-278.

Golonka, J., 2009. Phanerozoic paleoenvironment and paleolithofacies maps: early Paleozoic. Geologia/Akademia Górniczo-Hutnicza im. Stanisława Staszica w Krakowie, 35, pp.589-654.

Gurnis, M., 1988. Large-scale mantle convection and the aggregation and dispersal of supercontinents. Nature, 332(6166), pp.695-699.

Halverson, G.P., Hoffman, P.F., Schrag, D.P., Maloof, A.C. and Rice, A.H.N., 2005. Toward a Neoproterozoic composite carbon-isotope record. Geological Society of America Bulletin, 117(9-10), pp.1181-1207.

Han, Z., Yang, Z., Tong, Y. and Jing, X., 2015. New paleomagnetic results from Late Ordovician rocks of the Yangtze Block, South China, and their paleogeographic implications. Journal of Geophysical Research: Solid Earth, 120(7), pp.4759-4772.

Hartz, E.H. and Torsvik, T.H., 2002. Baltica upside down: a new plate tectonic model for Rodinia and the Iapetus Ocean. Geology, 30(3), pp.255-258.

Hawkesworth, C., Cawood, P. and Dhuime, B., 2013. Continental growth and the crustal record. Tectonophysics, 609, pp.651-660.

Hawkesworth, C.J., Cawood, P.A. and Dhuime, B., 2016. Tectonics and crustal evolution. GSA Today.

Heron, P.J. and Lowman, J.P., 2011. The effects of supercontinent size and thermal insulation on the formation of mantle plumes. Tectonophysics, 510(1), pp.28-38.

Hill, R.I., 1991. Starting plumes and continental break-up. Earth and Planetary Science Letters, 104(2-4), pp.398-416.

Hoffman, P.F., 1991. Did the breakout of Laurentia turn Gondwanaland inside-out. Science, 252(5011), pp.1409-1412.

Hoffman, P.F., 1999. The break-up of Rodinia, birth of Gondwana, true polar wander and the snowball Earth. Journal of African Earth Sciences, 28(1), pp.17-33.

Huang, B., Yang, Z., Otofuji, Y.I. and Zhu, R., 1999. Early Paleozoic paleomagnetic poles from the western part of the North China Block and their implications. Tectonophysics, 308(3), pp.377-402.

Huang, K., Opdyke, N.D. and Zhu, R., 2000. Further paleomagnetic results from the Silurian of the Yangtze Block and their implications. Earth and Planetary Science Letters, 175(3), pp.191-202.

Jiang, G., Sohl, L.E. and Christie-Blick, N., 2003. Neoproterozoic stratigraphic comparison of the Lesser Himalaya (India) and Yangtze block (south China): Paleogeographic implications. Geology, 31(10), pp.917-920.

Johnson, S.P., Rivers, T. and De Waele, B., 2005. A review of the Mesoproterozoic to early Palaeozoic magmatic and tectonothermal history of south–central Africa: implications for Rodinia and Gondwana. Journal of the Geological Society, 162(3), pp.433-450.

Keppie, D.F., 2015. How the closure of paleo-Tethys and Tethys oceans controlled the early breakup of Pangaea. Geology, 43(4), pp.335-338.

Kröner, A., Windley, B.F., Badarch, G., Tomurtogoo, O., Hegner, E., Jahn, B.M., Gruschka, S., Khain, E.V., Demoux, A. and Wingate, M.T.D., 2007. Accretionary growth and crust formation in the Central Asian Orogenic Belt and comparison with the Arabian-Nubian shield. Geological Society of America Memoirs, 200, pp.181-209.

Li, L. and Tull, J.F., 1998. Cover stratigraphy and structure of the southernmost external basement massifs in the Appalachian Blue Ridge; evidence for two-stage late Proterozoic rifting. American Journal of Science, 298(10), pp.829-867.

Li, Y., McWilliams, M., Sharps, R., Cox, A., Li, Y., Li, Q., Gao, Z., Zhang, Z. and Zhai, Y., 1990. A Devonian paleomagnetic pole from red beds of the Tarim Block, China. Journal of Geophysical Research: Solid Earth, 95(B12), pp.19185-19198.

Li, Z.X. and Evans, D.A., 2011. Late Neoproterozoic 40 intraplate rotation within Australia allows for a tighter-fitting and longer-lasting Rodinia. Geology, 39(1), pp.39-42.

Li, Z.X., Bogdanova, S.V., Collins, A.S., Davidson, A., De Waele, B., Ernst, R.E., Fitzsimons, I.C.W., Fuck, R.A., Gladkochub, D.P., Jacobs, J. and Karlstrom, K.E., Lu, S., Natapov, L.M., Pease, V., Pisarevsky, S.A., Thrane, K. and Vernikovsky, V., 2008. Assembly, configuration, and break-up history of Rodinia: a synthesis. Precambrian research, 160(1), pp.179-210.

Li, Z.X., Evans, D.A. and Halverson, G.P., 2013. Neoproterozoic glaciations in a revised global palaeogeography from the breakup of Rodinia to the assembly of Gondwanaland. Sedimentary Geology, 294, pp.219-232.

Li, Z.X., Evans, D.A.D. and Zhang, S., 2004. A 90 spin on Rodinia:

possible causal links between the Neoproterozoic supercontinent, super-plume, true polar wander and low-latitude glaciation. Earth and Planetary Science Letters, 220(3), pp.409-421.

Li, Z.X., Li, X.H., Kinny, P.D. and Wang, J., 1999. The breakup of Rodinia: did it start with a mantle plume beneath South China?. Earth and Planetary Science Letters, 173(3), pp.171-181.

Li, Z.X., Li, X.H., Kinny, P.D., Wang, J., Zhang, S. and Zhou, H., 2003. Geochronology of Neoproterozoic syn-rift magmatism in the Yangtze Craton, South China and correlations with other continents: evidence for a mantle superplume that broke up Rodinia. Precambrian Research, 122(1), pp.85-109.

Li, Z.X., Zhang, L. and Powell, C.M., 1995. South China in Rodinia: part of the missing link between Australia–East Antarctica and Laurentia?. Geology, 23(5), pp.407-410.

Likhanov, I.I., Reverdatto, V.V., Kozlov, P.S., Zinoviev, S.V. and Khiller, V.V., 2015, May. Evidence for the Valhalla tectonic events at the western margin of the Siberian Craton. In Doklady Earth Sciences (Vol. 462, No. 1, pp. 458-462). Pleiades Publishing.

Lowman, J.P. and Jarvis, G.T., 1999. Effects of mantle heat source distribution on supercontinent stability. Journal of Geophysical Research: Solid Earth, 104(B6), pp.12733-12746.

Macdonald, F.A., Strauss, J.V., Rose, C.V., Dudás, F.Ő. and Schrag, D.P., 2010. Stratigraphy of the Port Nolloth Group of Namibia and South Africa and implications for the age of Neoproterozoic iron formations. American Journal of Science, 310(9), pp.862-888.

Mallard, C., Coltice, N., Seton, M., Müller, R.D. and Tackley, P.J., 2016. Subduction controls the distribution and fragmentation of Earth's tectonic plates. Nature, 535(7610), pp.140-143.

Martin, E.L., Collins, W.J. and Kirkland, C.L., 2017. An Australian source for Pacific-Gondwanan zircons: Implications for the assembly of northeastern Gondwana. Geology, pp.G39152-1.

Matthews, K.J., Maloney, K.T., Zahirovic, S., Williams, S.E., Seton, M. and Müller, R.D., 2016. Global plate boundary evolution and kinematics since the late Paleozoic. Global and Planetary Change, 146, pp.226-250.

McMenamin, M.A. and McMenamin, D.L.S., 1990. The emergence of animals: the Cambrian breakthrough. Columbia University Press.

Meert, J.G., 2002. Paleomagnetic evidence for a Paleo-Mesoproterozoic supercontinent Columbia. Gondwana Research, 5(1), pp.207-215.

Meert, J.G., 2012. What's in a name? The Columbia (Paleopangaea/Nuna) supercontinent. Gondwana Research, 21(4), pp.987-993.

Meert, J.G., 2014. Strange attractors, spiritual interlopers and lonely wanderers: the search for pre-Pangean supercontinents. Geoscience Frontiers, 5(2), pp.155-166.

Merdith, A.S., Collins, A.S., Williams, S.E., Pisarevsky, S., Foden, J.F., Archibald, D., Blades, M.L., Alessio, B.L., Armistead, S., Plavsa, D., Clark, C. and Müller, R.D., 2017. A full-plate global reconstruction of the Neoproterozoic. Gondwana Research.

Metcalfe, I., 2013. Gondwana dispersion and Asian accretion: tectonic and palaeogeographic evolution of eastern Tethys. Journal of Asian Earth Sciences, 66, pp.1-33.

Metelkin, D.V., Vernikovsky, V.A. and Kazansky, A.Y., 2012. Tectonic evolution of the Siberian paleocontinent from the Neoproterozoic to the Late Mesozoic: paleomagnetic record and reconstructions. Russian Geology and Geophysics, 53(7), pp.675-688.

Mitchell, R.N., Kilian, T.M. and Evans, D.A., 2012. Supercontinent cycles and the calculation of absolute palaeolongitude in deep time. Nature, 482(7384), pp.208-211.

Moores, E.M., 1991. Southwest US-East Antarctic (SWEAT) connection: a hypothesis. Geology, 19(5), pp.425-428.

Moura, C.A.V., Pinheiro, B.L.S., Nogueira, A.C.R., Gorayeb, P.S.S. and Galarza, M.A., 2008. Sedimentary provenance and palaeoenvironment of the Baixo Araguaia Supergroup: constraints on the palaeogeographical evolution of the Araguaia Belt and assembly of West Gondwana. Geological Society, London, Special Publications, 294(1), pp.173-196.

Müller, R.D., Seton, M., Zahirovic, S., Williams, S.E., Matthews, K.J., Wright, N.M., Shephard, G.E., Maloney, K.T., Barnett-Moore, N., Hosseinpour, M. and Bower, D.J., 2016. Ocean basin evolution and global-scale plate reorganization events since Pangea breakup. Annual Review of Earth and Planetary Sciences, 44, pp.107-138.

Murphy, J.B., Nance, R.D. and Cawood, P.A., 2009. Contrasting modes of supercontinent formation and the conundrum of Pangea. Gondwana Research, 15(3), pp.408-420.

Nance, R.D. and Murphy, J.B., 2013. Origins of the supercontinent cycle. Geoscience Frontiers, 4(4), pp.439-448.

Nance, R.D., Murphy, J.B. and Santosh, M., 2014. The supercontinent cycle: a retrospective essay. Gondwana Research, 25(1), pp.4-29.

Nance, R.D., Murphy, J.B., Strachan, R.A., Keppie, J.D., Gutiérrez-Alonso, G., Fernández-Suárez, J., Quesada, C., Linnemann, U., D'lemos, R. and Pisarevsky, S.A., 2008. Neoproterozoic-early Palaeozoic tectonostratigraphy and palaeogeography of the peri-Gondwanan terranes: Amazonian v. West African connections. Geological Society, London, Special Publications, 297(1), pp.345-383.

Nunn, J.A. and Aires, J.R., 1988. Gravity anomalies and flexure of the lithosphere at the Middle Amazon Basin, Brazil. Journal of Geophysical Research: Solid Earth, 93(B1), pp.415-428.

Paixão, M.A.P., Nilson, A.A. and Dantas, E.L., 2008. The Neoproterozoic Quatipuru ophiolite and the Araguaia fold belt, central-northern Brazil, compared with correlatives in NW Africa. Geological Society, London, Special Publications, 294(1), pp.297-318.

Pedrosa-Soares, A.C., Noce, C.M., Wiedemann, C.M. and Pinto, C.P., 2001. The Araçuaí-West-Congo Orogen in Brazil: an overview of a confined orogen formed during Gondwanaland assembly. Precambrian research, 110(1), pp.307-323.

Piper, J.D.A., Beckmann, G.E.J. and Badham, J.P.N., 1976. Palaeomagnetic evidence for a Proterozoic super-continent. Philosophical Transactions of the Royal Society of London A: Mathematical, Physical and Engineering Sciences, 280(1298), pp.469-490.

Pisarevsky, S.A., Gladkochub, D.P., Konstantinov, K.M., Mazukabzov, A.M., Stanevich, A.M., Murphy, J.B., Tait, J.A., Donskaya, T.V. and Konstantinov, I.K., 2013. Paleomagnetism of Cryogenian Kitoi mafic dykes in South Siberia: implications for Neoproterozoic paleogeography. Precambrian Research, 231, pp.372-382.

Pisarevsky, S.A., Gurevich, E.L. and Khramov, A.N., 1997. Palaeomagnetism of Lower Cambrian sediments from the Olenek River section (northern Siberia): palaeopoles and the problem of magnetic polarity in the Early Cambrian. Geophysical Journal International, 130(3), pp.746-756.

Pisarevsky, S.A. and Natapov, L.M., 2003. Siberia and Rodinia. Tectonophysics, 375(1), pp.221-245.

Pisarevsky, S.A., Natapov, L.M., Donskaya, T.V., Gladkochub, D.P. and Vernikovsky, V.A., 2008. Proterozoic Siberia: a promontory of Rodinia. Precambrian Research, 160(1), pp.66-76.

Pisarevsky, S.A., Wingate, M.T., Powell, C.M., Johnson, S. and Evans, D.A., 2003. Models of Rodinia assembly and fragmentation. Geological Society, London, Special Publications, 206(1), pp.35-55.

Popov, L.E., Bassett, M.G., Zhemchuzhnikov, V.G., Holmer, L.E. and Klishevich, I.A., 2009. Gondwanan faunal signatures from Early Palaeozoic terranes of Kazakhstan and Central Asia: evidence and tectonic implications. Geological Society, London, Special Publications, 325(1), pp.23-64.

Prave, A.R., 1999. Two diamictites, two cap carbonates, two δ13C excursions, two rifts: the Neoproterozoic Kingston Peak Formation, Death Valley, California. Geology, 27(4), pp.339-342.

Preiss, W.V., 2000. The Adelaide Geosyncline of South Australia and its significance in Neoproterozoic continental reconstruction. Precambrian Research, 100(1), pp.21-63.

Ramos, V.A. and Folguera, A., 2009. Andean flat-slab subduction through time. Geological Society, London, Special Publications, 327(1), pp.31-54.

Roberts, N.M., 2013. The boring billion?–Lid tectonics, continental growth and environmental change associated with the Columbia supercontinent. Geoscience Frontiers, 4(6), pp.681-691.

Rogers, J.J. and Santosh, M., 2002. Configuration of Columbia, a Mesoproterozoic supercontinent. Gondwana Research, 5(1), pp.5-22.

Rogers, J.J. and Santosh, M., 2003. Supercontinents in Earth history. Gondwana Research, 6(3), pp.357-368.

Ryu, I.C., Oh, C.W. and Kim, S.W., 2005. A middle Ordovician drowning unconformity on the northeastern flank of the Okcheon (Ogcheon) belt, south Korea. Gondwana Research, 8(4), pp.511-528.

Schellart, W.P., Stegman, D.R., Farrington, R.J., Freeman, J. and Moresi, L., 2010. Cenozoic tectonics of western North America controlled by evolving width of Farallon slab. Science, 329(5989), pp.316-319.

Schulz, K.J., Stewart, D.B., Tucker, R.D., Pollock, J.C. and Ayuso, R.A., 2008. The Ellsworth terrane, coastal Maine: Geochronology, geochemistry, and Nd-Pb isotopic composition—Implications for the rifting of Ganderia. Geological Society of America Bulletin, 120(9-10), pp.1134-1158.

Şengör, A.M.C., Natal'in, B.A., 2001. Rifts of the world. In: Ernst, R.E., Buchan, K.L. (Eds.), Mantle Plumes: Their Identification Through Time, Special Paper, vol. 352. Geological Society of America, Boulder, CO, pp. 389–482.

Sigloch, K. and Mihalynuk, M.G., 2013. Intra-oceanic subduction shaped the assembly of Cordilleran North America. Nature, 496(7443), p.50.

Su, W., Li, H., Xu, L., Jia, S.H., Geng, J.Z., Zhou, H.Y., Wang, Z.H. and Pu, H.Y., 2012. Luoyu and Ruyang Group at the south margin of the North China Craton (NCC) should belong in the Mesoproterozoic Changchengian System: Direct constraints from the LA-MC-ICPMS U-Pb age of the tuffite in the Luoyukou Formation, Ruzhou, Henan, China. Geological Survey and Research, 35(2), pp.96-108.

Sun, L.S. and Huang, B.C., 2009. New paleomagnetic result for Ordovician rocks from the Tarim Block, Northwest China and its tectonic implications. Chinese Journal of Geophysics, 52(7), pp.1836-1848.

Thomas, W.A. and Astini, R.A., 1996. The Argentine precordillera: a traveler from the Ouachita embayment of North American Laurentia. SCIENCE-NEW YORK THEN WASHINGTON-, pp.752-756.

Torsvik, T.H., Van der Voo, R., Preeden, U., Mac Niocaill, C., Steinberger, B., Doubrovine, P.V., van Hinsbergen, D.J., Domeier, M., Gaina, C., Tohver, E. and Meert, J.G., 2012. Phanerozoic polar wander, palaeogeography and dynamics. Earth-Science Reviews, 114(3), pp.325-368.

Valentine, J.W. and Moores, E.M., 1970. Plate-tectonic regulation of faunal diversity and sea level: a model. Nature, 228(5272), pp.657-659.

Valeriano, C.M., Machado, N., Simonetti, A., Valladares, C.S., Seer, H.J. and Simões, L.S.A., 2004. U–Pb geochronology of the southern Brasília belt (SE-Brazil): sedimentary provenance, Neoproterozoic orogeny and assembly of West Gondwana. Precambrian Research, 130(1), pp.27-55.

Van Der Meer, D.G., Spakman, W., Van Hinsbergen, D.J., Amaru, M.L. and Torsvik, T.H., 2010. Towards absolute plate motions constrained by lower-mantle slab remnants. Nature Geoscience, 3(1), p.36.

Van der Meer, D.G., Torsvik, T.H., Spakman, W., Van Hinsbergen, D.J.J. and Amaru, M.L., 2012. Intra-Panthalassa Ocean subduction zones revealed by fossil arcs and mantle structure. Nature Geoscience, 5(3), p.215.

Van der Voo, R., Spakman, W. and Bijwaard, H., 1999. Tethyan subducted slabs under India. Earth and Planetary Science Letters, 171(1), pp.7-20.

Villeneuve, M., 2008. Review of the orogenic belts on the western side of the West African craton: the Bassarides, Rokelides and Mauritanides. Geological Society, London, Special Publications, 297(1), pp.169-201.

Voice, P.J., Kowalewski, M. and Eriksson, K.A., 2011. Quantifying the timing and rate of crustal evolution: global compilation of radiometrically dated detrital zircon grains. The Journal of Geology, 119(2), pp.109-126.

Wang, C., Liu, L., Wang, Y.H., He, S.P., Li, R.S., Li, M., Yang, W.Q., Cao, Y.T., Collins, A.S., Shi, C. and Wu, Z.N., 2015. Recognition and tectonic implications of an extensive Neoproterozoic volcano-sedimentary rift basin along the southwestern margin of the Tarim Craton, northwestern China. Precambrian Research, 257, pp.65-82.

Wang, J. and Li, Z.X., 2003. History of Neoproterozoic rift basins in South China: implications for Rodinia break-up. Precambrian Research, 122(1), pp.141-158.

Weil, A.B., Geissman, J.W. and Ashby, J.M., 2006. A new paleomagnetic pole for the Neoproterozoic Uinta Mountain Supergroup, central Rocky Mountain states, USA. Precambrian Research, 147(3), pp.234-259.

White, R. and McKenzie, D., 1989. Magmatism at rift zones: the generation of volcanic continental margins and flood basalts. Journal of Geophysical Research: Solid Earth, 94(B6), pp.7685-7729.

Worsley, T.R., Nance, D. and Moody, J.B., 1984. Global tectonics and eustasy for the past 2 billion years. Marine Geology, 58(3-4), pp.373-400.

Xiao, W., Windley, B.F., Allen, M.B. and Han, C., 2013. Paleozoic multiple accretionary and collisional tectonics of the Chinese Tianshan orogenic collage. Gondwana Research, 23(4), pp.1316-1341.

Xu, B., Xiao, S., Zou, H., Chen, Y., Li, Z.X., Song, B., Liu, D., Zhou, C. and Yuan, X., 2009. SHRIMP zircon U–Pb age constraints on Neoproterozoic Quruqtagh diamictites in NW China. Precambrian Research, 168(3), pp.247-258.

Yan, Q., Hanson, A.D., Wang, Z., Druschke, P.A., Yan, Z., Wang, T., Liu, D., Song, B., Jian, P., Zhou, H. and Jiang, C., 2004. Neoproterozoic subduction and rifting on the northern margin of the Yangtze Plate, China: implications for Rodinia reconstruction. International Geology Review, 46(9), pp.817-832.

Yang, Z., Sun, Z., Yang, T. and Pei, J., 2004. A long connection (750–380 Ma) between South China and Australia: paleomagnetic constraints. Earth and Planetary Science Letters, 220(3), pp.423-434.

Yang, Z.Y., Sun, Z.M., Ma, X.H., Huang, B.C., Dong, J.M., Zhou, Y.X. and Zhu, H., 1996. Preliminary paleomagnetic results from the Lower Paleozoic of North China (Henan Province) and its implications. Chin. Sci. Bull, 42, pp.401-405.

Yonkee, W.A., Dehler, C.D., Link, P.K., Balgord, E.A., Keeley, J.A., Hayes, D.S., Wells, M.L., Fanning, C.M. and Johnston, S.M., 2014. Tectono-stratigraphic framework of Neoproterozoic to Cambrian strata, west-central US: Protracted rifting, glaciation, and evolution of the North American Cordilleran margin. Earth-Science Reviews, 136, pp.59-95.

Zaffos, A., Finnegan, S. and Peters, S.E., 2017. Plate tectonic regulation of global marine animal diversity. Proceedings of the National Academy of Sciences, 114(22), pp.5653-5658.

Zhao, G., 2015. Jiangnan Orogen in South China: developing from divergent double subduction. Gondwana Research, 27(3), pp.1173-1180.

Zhao, G., Sun, M., Wilde, S.A. and Li, S., 2004. A Paleo-Mesoproterozoic supercontinent: assembly, growth and breakup. Earth-Science

Reviews, 67(1), pp.91-123.

Zhao, P., Chen, Y., Zhan, S., Xu, B. and Faure, M., 2014. The Apparent Polar Wander Path of the Tarim block (NW China) since the Neoproterozoic and its implications for a long-term Tarim–Australia connection. Precambrian Research, 242, pp.39-57.

Zhao, X., Coe, R.S., Liu, C. and Zhou, Y., 1992. New Cambrian and Ordovician paleomagnetic poles for the North China Block and their paleogeographic implications. Journal of Geophysical Research: Solid Earth, 97(B2), pp.1767-1788.

Zhou, M.F., Yan, D.P., Kennedy, A.K., Li, Y. and Ding, J., 2002. SHRIMP U–Pb zircon geochronological and geochemical evidence for Neoproterozoic arc-magmatism along the western margin of the Yangtze Block, South China. Earth and Planetary Science Letters, 196(1), pp.51-67.

Supplementary Material 1 (SM1)

R1 Macaúbas Basin, Congo – São Francisco Cratons

The Macaúbas Basin formed as a response to extension and spreading between the Congo and São Francisco cratons during the early Neoproterozoic, and is preserved from north to south in the Ediacaran aged Araçuaui-Ribiera-West Congo orogens. Interestingly, there was never full separation of the cratonic crust, so spreading is inferred to be contained just to the south and only a small ocean basin formed. Rifting is poorly constrained from the geological record in the more northerly Araçuaui-Ribiera belts with a series of zircons extracted from a synrift tillite within the Macaúbas Basin have an age cluster around 980±10 Ma with a youngest age of 950 Ma (Pedrosa-Soares et al., 2000). The West Congo Belt, however, records intrusive granites and rhyolites at 999 Ma, interpreted as the onset of rifting (Tack et al., 2001). The transition to drift is better constrained, with a U-Pb age of 906±2 Ma extracted from zircons from baddelyite (Machado et al., 1989 - cited in Pedrosa-Saores et al., 1998), inferred to represent the initiation of oceanic crust (e.g. Bradley, 2008; Pedrosa-Soares et al., 1992; 2001), with a preserved metamorphic ophiolites in the Ribiera belt giving a younger Sm-Nd age of 816±72 Ma (Pedrosa-Soares et al., 1998). Some of the extension was also accommodated further north with the coeval Paramirim and Sangha aulacogens, which are preserved in the São Francisco and Congo cratons respectively (e.g. Pedrosa-Soares et al., 2001; Alkmim et al., 2006). Here we interpret 1000 Ma as the age of rift initiation, and 900 Ma as the age of rift-drift transition.

R2 Katanga Supergroup, Congo Craton

Deposition of the Katanga Supergroup constrains the initiation of rifting on the southern margin of the Congo Craton, and remnants of it are preserved in the Damara-Zambezi-Lufilian belts between the Congo and Kalahari cratons. Johnson et al. (2005) identified two key rifting-to-extensional phases which we briefly summarise below. Across the margin various Tonian ages of rift-initiation are suggested, basal 879±18 Ma extrusive rocks are preserved in the Zambezi belt (Hanson et al., 1994), the basal Roan Group (of the Katanga Supergroup) sits unconformably on 877±11 Ma Nchanga granite (Armstrong et al., 1999; 2005), and an intrusive, syntectonic granite from Lusaka is dated to 846±68 (Barr et al., 1977). We interpret the initation of rifting here to be at 880 Ma. Renewed pulses of magmatism at ca. 820 Ma coupled with a transition to dolomite within the upper Roan Group (e.g. Bull et al., 2011) are interpreted to represent a transition to drift. The second phase of rifting and extension occur during the Cryogenian and lead to the development of the Mwashia-Kundelungu Basin. This rifting is constrained by a number of measurements including a U-Pb zircon age from basal ash beds in the Ombombo Subgroup of 760±1 Ma (Halverson et al., 2005) and tuffs and mafic lava flows from the Mwashia Subgroup giving ages from 760-730 Ma (Armstrong et al., 1999; Key et al., 2001). Initial rifting of the second phase was followed by renewed and voluminous sedimentation and the deposition of the Otavi Group (Hoffman and Prave, 1996). Bradley (2008) estimated the rift-drift transition occurring between the deposition of the Gruis and Ombaatjie Formations at ca. 670 Ma, on the basis of the conformably overlaying glacial Ghuab Formation. This glacial unit is correlated with the global Marinoan Glaciation event and, on this basis, is constrained from 663-635 Ma (Halverson et al., 2005).

R3 Anti-Atlas, eastern margin of West African Craton

Two Tonian aged aulacogens, the Ougarta Aulacogen in the north (Ennih and Liégeois, 2001) and Gourma Aulacogen in the south (Ennih and Liégeois, 2001) coupled with a preserved thick passive margin on the northern and eastern margins (e.g. Thomas et al., 2002; 2004). The passive margin, preserved in the Anti-Atlas mountains in Morocco and also in the Pharuside and Dahomeyide belts, have few age constraints available. Preserved tholeiitic and flood basalts in the Tachdamt Formation (from lithostratigraphic divisions by Bouougri and Saquaque, 2004) have a Rb-Sr age of 788±10 Ma (Clauer, 1976 - cited in Ennih and Liégeois, 2001). This is overlain by turbidites and a thick carbonate platform, leading to most proposed tectonic models having an ocean basin opening by ca. 800-780 Ma (e.g. Bouougri and Saquaque, 2004; Gasquet et al., 2005; Thomas et al.,

2004). Importantly, the Tachdamt Formation is underlain by ~1000 m of fluvial and shallow water siliciclastic sedimentary rocks (e.g. Taghdout group), indicating that rifting was occurring prior to ca. 800 Ma. The only age constraint on rifting are from recently dated detrital zircons by Ganade et al. (2016). They found four zircon grains in rocks preserved in the Dahomey belt, with ages between 993-930 Ma, providing a tentative maximum age of deposition of 930 Ma. We infer a rifting time of 880 Ma based on the plate model of Meridth et al. (2017), due to the coupling of the C-SF and WAC cratons in the Tonian. The two aforementioned aulacogens are given similar times of rifting

R4 Bassaride Sea, western margin of West African Craton

A small Tonian rifted margin existed on the western margin of the WAC and is presently preserved in the Bassaride belt. Similarly to the eastern margin, age constraints are few; rhyolite dated to between 1050 and 1000 Ma are unconformably overlain by the basal sediments of the Madina-Kouta (Villeneuve, 2008, p. 187), which preserves the evolution of the ocean basin. Metamorphosed ophiolites are preserved in the Guinguan Group with a metamorphic age of ca. 660 Ma, interpreted to be the time of basin closure (Dallmeyer and Villeneuve, 1987; Villeneuve, 2008). There are no preserved HP or UHP metamorphic rocks. Villeneuve (2008) proposed a model of ca. 850 Ma rifting, followed by ca. 800-750 Ma ocean basin development, before inversion by 650 Ma, which we follow here, taking rift time at 850 Ma, and the rift-drift transition at 800 Ma.

R5 Australia-Laurentia

Both Australia and Laurentia preserve thick passive margins from the Neoproterozoic. Their broad similiarity in ages and stratigraphy was one of the original pieces of evidence for a Neoproterozoic supercontinent (e.g. Dalziel, 1991; Hoffman, 1991; Moores, 1991), though the exact configuration and rift and drift times between the two is still ambigious due to uncertainties from age controls of the stratigraphy, temporally mismatched magmatic events and lack of reliable palaeomagnetic data. On the Austra-

lia margin, the lowest age constraint comes from the Stewart dyke swarm, which intruded the basement at 1076±33 Ma (Sm-Nd) (Zhao and McCulloch, 1993). The earliest evidence of rifting is preserved here as well, with a series of magmatic events, the intrusive Gairdner Dyke Swarm, and extrusive Wooltana and Beda volcanics, dated to 827±7 Ma (Preiss, 2000; Wingate et al., 1998), followed by the extrusion of the Rook Tuff at 802±10 Ma (Fanning et al., 1986). These are overlain by the series of sandstone and carbonate formations of the Warrina Supergroup, before the ignimbritic Boucaut Volcanics were extruded at 777±7 Ma (Fanning, 1994 - cited in Preiss, 2000). This particular extrusive event is coeval with the earliest preserved magmatism on the Laurentian margin, a series of ca. 780 Ma dyke swarms and sheets from the Mackenzie Supergroup, Canadian Shield and Wyoming Province (Jefferson and Parrish, 1989; LeCheminant and Heaman, 1994; summarised by Park et al., 1995), and has been interpreted to represent a second(?) rifting event (Preiss, 2000). The Laurentian margin consists of a thick sedimentary succession with initial deposition dating from the Mesoproterozoic before its cessation in the Palaeozoic. Young et al. (1979) and Young (1981) divided the margin into three successions; A, deposited between 1.7-1.2 Ga; B, deposited between 1000 and 720 Ma and C, deposited between 720 and 540 Ma all broken by unconformities. Detrital zircon ages of 1077±4 Ma, 1081±4 Ma and 1003±4 Ma have been determined from the base formation of Succession B, providing a maximum age of deposition of ca. 1000 Ma (Rainbird et al., 1996), and U-Pb dating of the Natkusiak basalt, which lies between Succession B and C, gives a lower age constraint of 723 Ma (Rainbird et al., 1993). The aforementioned 780 Ma dyke swarms sit within Succession B and Rainbird et al. (1996) proposed that Succession B is correlated with the Warrina Supergroup of Australia, based on the broad sedimentological similarities between the two.

The younger sedimentation of Succession C, preserved on the Laurentian margin, is suggestive of a series of further rifting events (Yonkee et al., 2014) (or a single protracted rifting event?). Yonkee et al. (2014) proposed a period of intracratonic basin development from 760 to 720 Ma followed by a rifting event from 720 to 660 Ma, which was heralded by the 720 Ma Franklin Dyke swarm (Heaman et al., 1992)

and mafic volcanism preserved in clasts of younger diamictite units (Yonkee et al., 2014). This period of rifting is inferred to have failed as the mature siliciclastic rocks are conformably overlain by immature siliciclastic rocks and (more) extensive magmatism at 580 Ma in the basal layers of the Prospect Mountain formation (e.g. Crittenden and Wallace, 1973). Renewed rifting from 580 to 540 Ma is finished with the development of a thick carbonate layer from ca. 540 Ma (Yonkee et al., 2014). The earlier failed rift identified by Yonkee et al. (2014) is broadly compatible with further rift development on the Australian margin identified by Preiss (2000), which is undated, but inferred to be at ca. 700 Ma based on correlation between global glacial events, and marked by a change in the strike of graben formation. It is unknown how the younger rifting event preserved in Laurentia is reconciled to the Australian margin, though some studies to propose (extremely) late rifting between Australia and Laurentia at ca. 540 Ma.

The transition from rift-drift between these two margins is particularly difficult to pin down, especially as palaeomagnetically derived models of Rodinia tend to require breakup prior to 750 Ma (e.g. Wingate and Giddings, 2000), and kinematic constraints on having late breakup (post 700 Ma) require abnormally high rates of motions (200 mm/yr) (Merdith et al. 2017a), while the geological data favours late(?) rifting, post 700 Ma (e.g. Priess, 2000) or early Cambrian (e.g. Veevers et al, 1997; Yonkee et al., 2014). Here we attribute a series of rifting events to this margin between 825 and 540 Ma, noting two things:

1) Early rifting could have resulted in separation, meaning that the later rifting events could represent a series of micro-terranes being removed from either Laurentia or Australia.
2) Early rifting could have failed successively, resulting a long, protracted rifting event.

We identify an early phase of rifting, initiating with the magmatic events in Australia at ca. 830 Ma, with the rift phase finishing at ca. 775 Ma (this is the most poorly constrained time). This phase encompasses all the early magmatism and concludes prior to the intracratonic basin development of Yonkee et al. (2014) and the deposition of Succession C. A second phase of rifting begins at 720 Ma, marked by

the Franklin Dyke swarm and Natkusiak basalt in Laurentia, and continues until 670 Ma (Yonkee et al., 2014). A final rift phase, which preserves the passive margin on the Laurentian side, occurred from 580 to 540 Ma.

R6 Amazonia – Araguaia Belt?

A rift and passive margin is preserved in the Baixo Araguaia Supergroup of the Araguaia fold belt (Moura et al., 2008), though there are few age constraints. Alkali magmatism intruding the basement and thought to represent early rifting is dated to 1006±86 Ma using 207PB/206Pb from a single zircon grain (Arcanjo & Moura, 2000 - cited in Moura et al., 2008). Moura et al. (2008) suggested that the probable maximum age of deposition for the sediments of the Baixo Supergroup is 900 Ma based on Sm-Nd model ages. A series of grabbroic intrusions into the sediments yielded a 817±5 Ma ^{207}Pb/^{206}Pb zircon age and an ophiolitic remnant has been dated using Sm-Nd isochron to 757±49 Ma (Paixão et al., 2008), indicating that oceanic crust was produced during the Cryogenian. We opt for an initiation of rifting at 850 Ma to match the (inferred) conjugate margin of WAC, with the rift-drift transition occurring at 800 Ma, after the gabbro intrusion, but prior to the ophiolite.

R7 Amazonia – Paraguay Belt

Lying further south than the Araguaia Belt in a reconstructed Gondwana, the Paraguay belt also preserves the development of a passive margin, before its inversion and basin closure with Gondwana amalgamation. The basal unit of the Paraguay Belt, the Puga Formation, consists of a diamictite interbedded with conglomerate, siltstone and sandstone (e.g. de Alvarenga et al., 2009), and is correlated to the Marinoan glaciation based on C and Sr isotopes (de Alvarenga et al., 2004). Coeval with the Puga Formation was the deposition of the Jacadigo Group, which outcrops only towards the south of the belt. The Jacadigo Group, an iron-manganese rich siliciclastic group containing no glacially derived sediments, is considered to have been deposited synchronously with graben development in the basement (Trompette et al., 1998). Overlaying the Puga Fomration is the Araras Group, which consists of a carbonate

layer thickening towards the palaeo-margin, and is typically interpreted as the rift-drift transition and onset of the passive margin (e.g. Bradley, 2008). Age constraints are few as there are no dykes or basaltic sheets to constrain sedimentation. The youngest detrital zircon found in the Puga Formation has a U-Pb age of 706±9 Ma (Babinski et al., 2013), providing a maximum depositional age of ca. 700 Ma, which we use as the initialisation of rifting. The overlaying Araras Group, representing the passive margin, yielded a Pb-Pb isochron age of 633±25 Ma from the carbonates (Alvarenga et al., 2009), which is congruent with it overlaying the glacial Puga Formation, as the global Marinoan glaciation event ended at ca. 635 Ma (e.g. Condon et al. 2005; Halverson et al. 2005). We follow Bradley (2008) and place the rift-drift transition slightly earlier at 640 Ma.

R8 Goiás arc, western margin of São Francisco

A passive margin is preserved on the western margin of the São Francisco craton within the Bambui Group (Campos Neto, 2000). This passive margin is preserved partly in the ca. 650 Ma Brasilia belt, where the Neoarchaean Goiás Massif and Goiás arc collided with the São Francisco craton (Campos Neto and Caby, 1999; Valeriano et al., 2008). Age constraints are sparse, and small regional unconformities between basal sedimentary layers and the overlaying formations coupled with strong deformation during the amalgamation of Gondwana, make both temporal and spatial correlation difficult (e.g. Sial et al., 2009). Two basal groups, inferred to be coeval, in part because of fossilised stromatolites, the Vazante Group and the Paranoá Group, were deposited between 1100-950 Ma on the cratonic domain. The Vazante Group is constrained by Re-Os radiometric ages from shale layers in its upper units of 993±46 Ma and 1100±77 Ma (Azmy et al., 2008), with the youngest detrital zircon being dated at 998±15 Ma (Azmy et al., 2008), while the presence of the aforementioned stromatolite fossil in the Paranoá Group suggests sedimentation during a similar, late Mesoproterozoic-early Neoproterozoic time frame (Dardenne et al. 1976). This is supported by a minimum depositional age of 1042 Ma from U-Pb and Lu-Hf data from detrital zircons recovered from the Paranoá Group (Matteini et al., 2012). Further

outboard from the cratonic domain, sediments preserved in the Araxá and Andrelândia groups (preserved as a series of nappes and thrusts throughout the Brasilia Belt) have a youngest detrital zircon ages of ca. 900 Ma (Valeriano et al., 2004). Unconformably overlaying the Paranoá Group is the carbonate rich Bambui Group, typically inferred to represent the development of Neoproterozoic passive margin (Bradley, 2008). Scattered age constraints, including a maximum depositional age of ca. 900 Ma (Pb-Pb isochron dating, Buschwaldt et al,. 1999) for a basal diamictite layer. Babinski et al. (2007) extracted a Pb-Pb isochron age of 740±22 Ma from undeformed carbonates of the Bambui Group. We attach an age of initial rifting of 850 Ma, to match the tectonic activity that occurs in this vicinity in a reconstructed Rodinia and to fit the maximum age of sedimentation provided by the detrital zircons from the Araxá and Andrelândia groups. We opt for rifting after the deposition of the Paranoá and Vazante groups, instead interpreting these as a product of a Mesoproterozoic aged rifting event. The transition from rift to drift is placed at 745 Ma, after Bradley (2008), being constrained by age of the Bambio Group after Babinski et al. (2007).

R9 Laurentia-Baltica-Amazonia-Rio de la Plata

The opening of the Iapetus Ocean between Laurentia and Amazonia, Baltica and Rio de la Plata (RDLP), and the opening of the Torniquest Sea, between Amazonia and Baltica, at ca. 600 to 570 Ma is generally considered as the final breakup event of Rodinia. Evidence for earlier rifting exists in the Cryogenian, with a series of magmatic intrusions occurring south of the New York promontory dated between 760 and 700 Ma, including Mt Rogers, 758±12 Ma (Aleinikoff et al., 1991; 1995), Crossnore Pluton, 741±3 Ma (Su et al., 1994), Robertson River Formation, 732±5 Ma (Lukert and Banks, 1984) and the Adirondack Massif, ca. 700 Ma (Heizler and Harrison, 1998). Sedimentation during this time is synchronous with the formation of grabens (Li and Tull, 1998), however a hiatus in sedimentation and an angular unconformity between these lower units and the overlaying ca. 600 to 550 Ma sediments suggest that rifting was aborted.

Re-initiation of rifting occurred from 615 Ma, with the intrusion of a series of dykes in Baltica and Laurentia giving a U-Pb baddeleyite age of 616±3 Ma for the Egersund dykes of Norway (Bingen et al., 1998), and a U-Pb baddeleyite age of 615±2 Ma for the Long Range dykes of Newfoundland (Kamo and Gower, 1994). Magmatism is preserved extensively until the Cambrian, until the 550±3 Ma Skinner Cove Formation (McCausland and Hodych, 1998; Puffer, 2002), and drift related sediments are preserved from 520 to 515 Ma (based on faunal data - Bowring and Erwin, 1998; Cawood et al., 2001), marked by the transition from the siliciclastic rich Bradore Formation to the carbonate platform preserved in the Forteau Formation (Williams and Hiscott, 1987). Though, Cawood et al. (2001) pointed out that the rift-drift transition may be at the base of the Bradore Formation, not its top, as its base is associated with the cessation of magmatism and tectonic motion, proposing that the rift-drift transition is slightly older, at 525-520 Ma. This is somewhat problematic, as palaeomagnetic data require a large (~3000 km) ocean basin between Laurentia, Amazonia and Baltica by 550 Ma (e.g. Pisarevsky et al., 2008). Cawood et al. (2001) proposed a two-stage Ediacaran-Cambrian rifting model, where opening of the Iapetus margin occurred earlier, at 570 Ma, but that a micro-continent rifted off Laurentia at ca. 540 Ma, and that this rifting event led to the preserved passive margin. Rifting is inferred to have occurred slightly later between Amazonia and Laurentia (and RDLP and Laurentia) due to the slightly younger ages of magmatic events further south on the Laurentian margin, relative to the Newfoundland, Greenland area (adjacent to Baltica in a reconstructed Rodinia). The absence of any geological controls from the Amazonian margin makes determining the exact time more difficult though.

Here we interpret an earlier, failed rift event, with rifting initiation at 760 Ma and failing by 700 Ma (e.g. Aleinikoff et al., 1995; Li and Tull, 1998). This is followed by a second rifting event consisting of two stages, that eventually lead to the opening of the Iapetus Ocean. Here rifting initialised at 615 Ma between Baltica and Laurentia, and Baltica and Amazonia. Rifting propagated southwards along the Laurentian margin, to initiate between Laurentia and Amazonia and RDLP by 590 Ma. The Iapetus opened at ca. 570 Ma, but rifting continued inland

of Laurentia, with the removal of a micro-continent and the final transition to drift and development of a passive margin occurred at ca. 540 Ma, with passive margin sedimentation preserved from 535 Ma.

R10 South China

A failed, intracratonic rift is preserved in the South China craton, between the Yangtze and Cathaysia blocks. Here late Tonian-Cryogenian sediments are preserved in the Kangdian basin and the Nanhua basin along the western margin of the South China craton and between the two blocks respectively. Mafic dykes with a zircon U-Pb age of 828±7 Ma (Li et al., 1999) mark the onset of rifting, this is supported by a U-Pb age 819±7 Ma from granites that are unconformably overlain by the basins (Ma et al., 1984). Sedimentation with extensive magmatism and volcanic units continued from here until ca. 750, where the final volcanic unit yielded a U-Pb age to 748±12 (Ma et al., 1984). Sedimentary units deposited after ca. 700 Ma exhibit a distinctively different deposition pattern, suggesting an ending to rifting and a transition to a sag phase and passive margin somewhere between 750-700 Ma (Jiang et al. 2003; Wang and Li, 2003). There is, however, no evidence of oceanic crust being produced in the Nanhua basin, between the Yangtze and Cathaysia blocks, which suggests a failed rift, but given the complexity of the area and the reworking during the Palaeozoic, the extent to which the basin developed is uncertain. Here we place the initiation of the rift at 830 Ma, with a cessation of rifting at 750 Ma. Conversely, the Kangdian basin (along the western margin of South China) preserves a thick passive margin (as well) and based on comparative stratigraphy between it and the Lesser Himalaya (northern India), separation and formation of ocean basin did occur (Jiang et al., 2003). We follow Jiang et al. (2003) and have the rift-drift transition occurring at 550 Ma in the Early Cambrian, when the stratigraphy of South China and India began to diverge (which, interestingly, makes this a very long rifted margin).

R11 Kalahari-RDLP-Laurentia

The rift and passive margin between Laurentia and Kalahari-RDLP is inferred from the model, as there is no data from RDLP (covered almost entirely by Pha-

nerozoic basins) and little data from the southern-most margin of Laurentia and Kalahari. The rifting of Kalahari and RDLP, which created the Adamastor Ocean, is somewhat more constrained, and the rocks inferred to be part of the passive margin are preserved in the Gariep Belt (Frimmel et al., 2011). Granitoid intrusions preserved in the Richtersveld Suite yielded a range of ages from U-Pb dating of zircons of 837±2 Ma down to 771±6 Ma (Frimmel et al., 2001). The youngest of these granitoids is unconformably overlain by the oldest sedimentary rocks preserved in the Gariep belt, the Port Nolloth Group, providing a maximum time of deposition of ca. 770 Ma. Magmatism synchronous with sediment deposition has yielded U-Pb zircon ages of 752±5.5 Ma (Borg et al., 2003) and Pb-Pb ages 741±6 Ma (Frimmel et al., 1996), suggesting onset of rifting by 750 Ma. Transition to drift is more difficult to pin down because of large lateral variations in facies of the Port Nolloth Group and poor dating constraints. Using glacial deposits as regional stratigraphic controls, a haitus and unconformity was inferred to occur after early sediment deposition (e.g. Frimmel, 2008), but the discovery of another glacial unit with a ca. 716 Ma age (Sr isotope dating) suggests that there was no haitus and that sedimentation was constant (MacDonald et al., 2010). MacDonald et al. (2010) suggest that tectonic activity was still occurring during the deposition of the 716 Ma glacial, providing a lower age constraint on the transition. An age constraint of 635 Ma from a cap carbonate at a higher glacial unit provides an upper time constraint, indicating that the transition from rift to drift occurred between 716 and 650 Ma. We place the transition at 690 Ma, noting that this is determined on a plate tectonic model that has divergent motion between Kalahari and Laurentia from 700 Ma (Merdith et al., 2017b). The model itself expresses some uncertainty at 700 Ma motion, noting that divergent motion anytime from ca. 725-675 Ma would produce a kinematically feasible model in a global context.

The margin between Kalahari and Laurentia has no direct geological or palaeomagnetic constraints, consequently the time of rifting and rift-drift transition are modelled. We opt to mirror the geological data preserved in the Gariep belt, having rifting initiating at 750 Ma and the rift-drift transition at 690 Ma.

R12 Argentine Precordillera

The Argentine Precordillera, preserved in the Cuyania terrane, drifted from Laurentia in the Cambrian, and collided with South America along the proto-Andean margin in the Ordovician-Silurian (e.g. Domeier, 2016; Thomas and Astini, 1996). Faunal records and with similar stratigraphy indicate a shared history during the early Cambrian, with differences in stratigraphy and fossils, coupled with the development of a carbonate platform by ca. 515 Ma, and a mature platform by 505 Ma, suggest drift from Laurentia sometime between these times (Thomas and Astini, 1996; 1999), slightly before the initiation of drifting of the peri-Gondwanian terranes rifting from Gondwana and closing the Iapetus. Constraints on the initialisation of rifting are from syn-rift volcanism in the Arbuckle Mountains, yielding U-Pb zircon and baddelyite ages of 539±6 Ma and 536±5 Ma. These overlay intrusive gabbroic suites that record Ar^{40}/Ar^{39} ages between 540 and 535 Ma (Hames et al., 1998). We place initiation of rifting at 540 Ma, and the rift-drift transition at 515 Ma.

R13 Peri-Gondwanan terranes (Avalonia, Carolina and Gandoria)

The Peri-Gondwana terranes developed outboard of Baltica, Amazonia and the West African Craton during the Neoproterozoic, before colliding with the Amazonian-West African margin of Gondwana in the Ediacaran (e.g. Murphy et al., 2000; Nance et al., 2008). They rifted off the Gondwanan margin during the Cambrian, and migrated to Laurentia and Baltica, closing the Iapetus Ocean infront of them and opening the Rheic Ocean behind them (e.g. Domeier, 2016). The initiation of rifting was slightly dyssynchronous, though the transition to rift in all terranes was roughly coeval. We follow Nance et al. (2008) in assigning ages to both rifting and the transition to drift. The timing of events is subtle as rifting developed within a back-arc basin, above rocks deposited and emplaced in a continental arc setting. A series of young intrusions between 571 and 540 Ma are suggested to be related to initial rifting as they post-date the more clearly arc related gneisses and granites from 625 to 610 Ma (Barr et al., 2003). These intrusions also share geochemical characteristics of an extensional setting (e.g. Barr et al., 2003).

The transition to drift is more well constrained, between 505-503 Ma, based on rhyolites and tholeiitic basalts preserved in the Ellsworth Schist and Castine Volcanics units. These units are dated using U-Pb on zircon grains preserved in the rhyolites to 508±1 Ma and 503±2.5 Ma (Schulz et al., 2008). For Ganderia, we opt for rifting initialising at 570 Ma with the onset of volcanism, and the rift-drift transition at 505 Ma. Similarly to Ganderia, Nance et al. (2008) identifies a transition from continental arc to rift setting occurring between 590 and 550 Ma for the Avalonian terranes. However, faunal data from the Late Cambrian and Early Ordovician is still remarkably similar to Gondwanan patterns (Fortey and Cocks, 2003), suggesting a later breakup. We follow the proposal of Nance et al. (2008) that between ca. 550 and 500 Ma wrench tectonics brought about by ridge-trench subduction resulting in a transform boundary being preserved along the margin, was occurring. This created small, discrete depositional basins onshore of Avalonia and Gondwana, but did not generate ocean crust. We infer the start of these little basins at ca. 550 Ma, and, based on faunal patterns and stratigraphy, the transition from rift-drift at ca. 490 Ma. The Carlonian terrane shares similar early Ediacaran characteristics with the Avalonian terranes, though they preserve arc magmatism down to the Early Cambrian (e.g. Hibbard and Samson, 1995; Nance et al. 2008). Post arc magmatism they are unconformably overlain by siliciclastic sediments with cool water fossil assemblages, similar to Ganderia, Avalonia and Gondwana (Theokrtioff, 1979). Rifting initialisation and rift-drift transition are inferred to occur in similar time periods to Avalonia, 550 Ma for beginning of deposition and rifting with the Albemarle Group (e.g. Pollock and Hibbard, 2010), and 490 Ma for development of a siliciclastic platform representing a passive margin, though there are few constraints on the rift-drift time (the model of Domeier (2016) has a passive margin from 585 Ma, for example.)

R14 North China

A Cambrian-aged rifting in North China is preserved in a series of thick sedimentary facies, primarily located on the southern and eastern margins of the craton (e.g. Meng et al. 1997). Detrital zircon, palaeomagnetic and faunal data suggest that North China was located in proximity to the Australian-Indian margin of Gondwana, but not necessarily attached (e.g. Burret et al., 2014; Metcalfe, 2013 for a summary). Syn-rift sedimentation preserved in grabens along the eastern margin of the craton (Korean peninsula) suggest rift initialisation in the latest Cambrian-Ordovician, with graben development by mid-Ordovician (Ryu et al., 2005), however the slightly older ages of sedimentation preserved in the Cambrian basins could suggest a prolonged rift development. There are no absolute age controls on the sedimentation. Detrital zircons of ca. 560 Ma are preserved in sandstones in the North China craton (Burrett et al., 2014), giving a maximum age of deposition, and Cambrian aged fossils from ca. 520 Ma are also found in the lower limestone beds, suggesting a Cambrian age (Chough et al., 2010; Su et al., 2008). We place the initiation of rifting at 550 Ma, with the transition to drift occurring at 490 Ma.

R15 Tarim

Thick sedimentation is preserved in the southwest, northwest and northereastern margins of Tarim from the Tonian down to Cambrian (e.g. Wang et al., 2015; Xu et al., 2005). Early deposition in the southwest is preserved in the Tiekelik Belt, and constrained by a U-Pb zircon age from a mylonitic rhyolite preserved in the volcaniclastic rich basal layer at 881±6 Ma (Wang et al. 2015). A suite of rhyolites, tuffs and basalts preserved here suggest bimodal volcanism indicating some form of igneous activity related to extension. A youngest detrital zircon age of 773±6 Ma for the overlaying carbonate rich layer constrains the maximum age of deposition to the early Cryogenian, and suggests continuous sedimentation during the late Tonian. Volcanic rocks are also preserved on the northern margin in the Beiyixi volcanics (Xu et al., 2005) and dated to 755±15 Ma from U-Pb analyses on zircons, though previous geochronology dated them to ca. 810 Ma (see Xu et al., 2005 for a commentary). The stratigraphic transition (at least in the south) suggests and opening ocean basin, but uncertainties relating to the Neoproterozoic position of Tarim from palaeomagnetic data (see Merdith et al. 2017b for a summary) make it difficult to determine if Tarim rifted completely off all other continents, or was a smaller part of a larger breakaway continent.

Sedimentation continued for most of the Neoproterozoic, with some small regional hiatuses. Siliciclastics and tillites dominate the facies for most of the Cryogenian and Ediacaran (e.g. Xu et al., 2009; 2013), though there are no absolute age constraints until a volcanic bed from its northern margin that yields a SHRIMP U-Pb age of 615±6 Ma (Xu et al., 2009). Overlaying strata from this bed are predominantly carbonates (e.g. Qigebrak formation), though this is not reflected on its southern margin (e.g. Zhao et al., 2014 for regional stratigraphic columns), and an Ediacaran-Cambrian unconformity caps this sequence. This perhaps suggests that some terrane rifted off Tarim into the newly forming 'Palaeo-Asian Ocean' while Gondwana was forming, as most reconstructions place Tarim's southern margin against Australia (e.g. Wen et al., 2013; Zhao et al., 2014). We depict two rifting events, firstly, rifting initiating at 880 Ma, ceasing by 780 Ma, and constrained mostly to the southern margin. The second event initiated at 615 Ma along the northeastern-northwestern margin of Tarim, and ceased by 550 Ma.

R16 Siberia

Although Siberia is ringed by passive margins for the majority of the Neoproterozoic (e.g. Bradley, 2008; Metelkin et al., 2012; Pisarevsky et al., 2008) geological evidence of rifted margins are comparatively rare and somewhat obscured. The best evidence for rifting is preserved in the Karagas Group along the south-western margin (Sklyarov et al., 2001 - cited in Pisarevsky et al., 2008), where siliciclastics interbedded with volcanic rocks are intruded by ca. 741±4 Ma mafic dykes and sills (40Ar-39Ar dating on plagioclase) (Gladkochub et al., 2006). These are overlain by turbidites and carbonates of the upper Karagas Group (Sklyarov et al., 2001 - cited in Pisarevsky et al., 2008) and are interpreted to represent a transition from rift to drift (Gladkochub et al., 2006). On the same south-southwestern margin tholeiitic gabbro-dolerite dykes intrude into Archaean and Palaeoproterozoic basement preserve crystallisation ages of 758±4 Ma (40Ar-39Ar from plagioclase) and 743±47 Ma (Sm-Nd, whole rock-mineral) (Sklyarov et al., 2003; Pisarevsky et al., 2013 gave an age of the intrusions at 760 Ma). Finally, Ernst and Hamilton (2009) and Ariskin et al. (2013 dated the Dovyren

pluton in southwest Siberia at 725±3 Ma (similar in age to the Franklin magmatic event) suggesting a correlation between Siberia and northern Laurentia at ca. 720 Ma. We place the rift-drift transition at 720 Ma, with the implacement of the Dobyren pluton representing one of the final stages of rifting. Initiation of rifting is more difficult to determine as there are no upper age constraints from sequences on the southwest margin. Pisarevsky et al. (2013) inferred dextral motion between Siberia and Laurentia from 780 Ma as an extension of the synchronous divergent motion between Australia and Laurentia, and Merdith et al. (2017b) extended this further back to 800 Ma to match divergent motion between Australia and Laurentia on kinematic grounds (e.g. Merdith et al., 2017a). Consequently, we infer rifting initiation to occur from 800 Ma

References for Supplementary Material 1 (SM1)

Aleinikoff, J.N., Zartman, R.E., Rankin, D.W., Lyttle, P.T., Burton, W.C. and McDowell, R.C., 1991. New U-Pb zircon ages for rhyolite of the Catoctin and Mount Rogers Formations—More evidence for two pulses of Iapetan rifting in the central and southern Appalachians. In Geological Society of America Abstracts with Programs (Vol. 23, No. 1, p. 2).

Aleinikoff, J.N., Zartman, R.E., Walter, M., Rankin, D.W., Lyttle, P.T. and Burton, W.C., 1995. U-Pb ages of metarhyolites of the Catoctin and Mount Rogers Formations, central and southern Appalachians: Evidence for two pulses of Iapetan rifting. American Journal of Science, 295(4), pp.428-454.

Alkmim, F.F., Marshak, S., Pedrosa-Soares, A.C., Peres, G.G., Cruz, S.C.P. and Whittington, A., 2006. Kinematic evolution of the Araçuaí-West Congo orogen in Brazil and Africa: Nutcracker tectonics during the Neoproterozoic assembly of Gondwana. Precambrian research, 149(1), pp.43-64.

Ariskin, A.A., Kostitsyn, Y.A., Konnikov, E.G., Danyushevsky, L.V., Meffre, S., Nikolaev, G.S., McNeill, A., Kislov, E.V. and Orsoev, D.A., 2013. Geochronology of the Dovyren intrusive complex, northwestern Baikal area, Russia, in the Neoproterozoic. Geochemistry International, 51(11), pp.859-875.

Armstrong, R.A., Master, S. and Robb, L.J., 2005. Geochronology of the Nchanga Granite, and constraints on the maximum age of the Katanga Supergroup, Zambian Copperbelt. Journal of African Earth Sciences, 42(1), pp.32-40.

Armstrong, R.A., Robb, L.J., Master, S., Kruger, F.J. and Mumba, P.A.C.C., 1999. New U-Pb age constraints on the Katangan Sequence, Central African Copperbeit. Journal of African Earth Sciences, 28(4), pp.6-6.

Azmy, K., Kendall, B., Creaser, R.A., Heaman, L. and de Oliveira, T.F., 2008. Global correlation of the Vazante Group, São Francisco Basin, Brazil: Re–Os and U–Pb radiometric age constraints. Precambrian Research, 164(3), pp.160-172.

Babinski, M., Boggiani, P.C., Trindade, R.I.F. and Fanning, C.M., 2013. Detrital zircon ages and geochronological constraints on the Neoproterozoic Puga diamictites and associated BIFs in the southern Paraguay Belt, Brazil. Gondwana Research, 23(3), pp.988-997.

Babinski, M., Vieira, L.C. and Trindade, R.I., 2007. Direct dating of the Sete Lagoas cap carbonate (Bambuí Group, Brazil) and implications for the Neoproterozoic glacial events. Terra Nova, 19(6), pp.401-406.

Barr, M.W.C., Cahen, L. and Ledent, D., 1977. Geochronology of syntectonic granites from central Zambia: Lusaka Granite and granite NE of Rufunsa. Annales de la Société géologique de Belgique.

Barr, S.M., White, C.E. and Miller, B.V., 2003. Age and geochemistry of Late Neoproterozoic and Early Cambrian igneous rocks in southern New Brunswick: similarities and contrasts.

Bingen, B., Demaiffe, D. and Breemen, O.V., 1998. The 616 Ma old Egersund basaltic dike swarm, SW Norway, and late Neoproterozoic opening of the Iapetus Ocean. The Journal of Geology, 106(5), pp.565-574.

Borg, G., Kärner, K., Buxton, M., Armstrong, R. and van der Merwe, S.W., 2003. Geology of the Skorpion supergene zinc deposit, southern Namibia. Economic Geology, 98(4), pp.749-771.

Bouougri, E.H. and Saquaque, A., 2004. Lithostratigraphic framework and correlation of the Neoproterozoic northern West African Craton passive margin sequence (Siroua–Zenaga–Bouazzer Elgraara inliers, central Anti-Atlas, Morocco): an integrated approach. Journal of African Earth Sciences, 39(3), pp.227-238.

Bowring, S.A. and Erwin, D.H., 1998. A new look at evolutionary rates in deep time: uniting paleontology and high-precision geochronology. Geological Society of America.

Bradley, D.C., 2008. Passive margins through earth history. Earth-Science Reviews, 91(1), pp.1-26.

Buchwaldt, R., Toulkeridis, T., Babinski, M., Santos, R., Noce, C.M., Martins-Neto, M. and Hercos, C.M., 1999, September. Age determination and age related provenance analysis of the Proterozoic glaciation event in central eastern Brazil. In South American Symposium on Isotope Geology (Vol. 2, pp. 387-390).

Bull, S., Selley, D., Broughton, D., Hitzman, M., Cailteux, J., Large, R. and McGoldrick, P., 2011. Sequence and carbon isotopic stratigraphy of the Neoproterozoic Roan Group strata of the Zambian copperbelt. Precambrian Research, 190(1), pp.70-89.

Burrett, C., Zaw, K., Meffre, S., Lai, C.K., Khositanont, S., Chaodumrong, P., Udchachon, M., Ekins, S. and Halpin, J., 2014. The configuration of Greater Gondwana—evidence from LA ICPMS, U–Pb geochronology of detrital zircons from the Palaeozoic and Mesozoic of Southeast Asia and China. Gondwana Research, 26(1), pp.31-51.

Campos Neto, M.D.C. and Caby, R., 1999. Neoproterozoic high-pressure metamorphism and tectonic constraint from the nappe system south of the São Francisco Craton, southeast Brazil. Precambrian Research, 97(1), pp.3-26.

Campos Neto, M.D.C., 2000. Orogenic Systems from Southwestern Gondwana: an approach to Brasiliano-Pan African cycle and orogenic collage in southeastern Brazil. Tectonic Evolution of South America, 31, pp.335-365.

Cawood, P.A., McCausland, P.J. and Dunning, G.R., 2001. Opening Iapetus: constraints from the Laurentian margin in Newfoundland. Geological Society of America Bulletin, 113(4), pp.443-453.

Chough, S.K., Lee, H.S., Woo, J., Chen, J., Choi, D.K., Lee, S.B., Kang, I., Park, T.Y. and Han, Z., 2010. Cambrian stratigraphy of the North China Platform: revisiting principal sections in Shandong Province, China. Geosciences Journal, 14(3), p.235.

Condon, D., Zhu, M., Bowring, S., Wang, W., Yang, A. and Jin, Y., 2005. U-Pb ages from the neoproterozoic Doushantuo Formation, China. Science, 308(5718), pp.95-98.

Crittenden Jr, M.D. and Wallace, C.A., 1973. Possible equivalents of the Belt Supergroup in Utah. In Belt symposium (Vol. 1, pp. 116-138).

Dallmeyer, R.D. and Lecorche, J.P., 1990. 40Ar/39Ar polyorogenic mineral age record in the northern Mauritanide orogen, West Africa. Tectonophysics, 177(1-3), pp.81-107.

Dalziel, I.W., 1991. Pacific margins of Laurentia and East Antarctica-Australia as a conjugate rift pair: Evidence and implications for an Eocambrian supercontinent. Geology, 19(6), pp.598-601.

de Alvarenga, C.J., Boggiani, P.C., Babinski, M., Dardenne, M.A., Figueiredo, M., Santos, R.V. and Dantas, E.L., 2009. The amazonian palaeocontinent. Developments in Precambrian Geology, 16, pp.15-28.

de Alvarenga, C.J., Santos, R.V. and Dantas, E.L., 2004. C–O–Sr isotopic stratigraphy of cap carbonates overlying Marinoan-age glacial diamictites in the Paraguay Belt, Brazil. Precambrian Research, 131(1), pp.1-21.

Domeier, M., 2016. A plate tectonic scenario for the Iapetus and Rheic Oceans. Gondwana Research, 36, pp.275-295.

Ennih, N. and Liégeois, J.P., 2001. The Moroccan Anti-Atlas: the West African craton passive margin with limited Pan-African activity. Implications for the northern limit of the craton. Precambrian Research, 112(3), pp.289-302.

Ernst, R.E. and Hamilton, M.A., 2009, February. 725 Ma U–Pb baddeleyite age for the Dovyren mafic–ultramafic intrusion of southwestern Siberia; reconstruction with the giant 723 Ma Franklin Large Igneous Province (LIP) of northern Laurentia. In Materials from the 42nd Tectonics Conference, Moscow, Russia. GEOS.[In Russian.].

Fanning, C.M., Ludwig, K.R., Forbes, B.G. and Preiss, W.V., 1986. Single and multiple grain U–Pb zircon analyses for the early Adelaidean Rook Tuff, Willouran Ranges, South Australia. In Geological Society of Australia Abstracts (Vol. 15, pp. 71-72).

Fortey, R.A. and Cocks, L.R.M., 2003. Palaeontological evidence bearing on global Ordovician–Silurian continental reconstructions. Earth-Science Reviews, 61(3), pp.245-307.

Frimmel, H. E., 2008, The Gariep Belt, in Miller, R. M., editor, The Geology of Namibia, Handbook of the Geological Survey of Namibia: Geological Survey of Namibia, p. 1–39.

Frimmel, H.E., Basei, M.S. and Gaucher, C., 2011. Neoproterozoic geodynamic evolution of SW-Gondwana: a southern African perspective. International Journal of Earth Sciences, 100(2-3), pp.323-354.

Frimmel, H.E., Klötzli, U.S. and Siegfried, P.R., 1996. New Pb-Pb single zircon age constraints on the timing of Neoproterozoic glaciation and continental break-up in Namibia. The Journal of Geology, 104(4), pp.459-469.

Frimmel, H.E., Zartman, R.E. and Späth, A., 2001. The Richtersveld igneous complex, South Africa: U-Pb zircon and geochemical evidence for the beginning of Neoproterozoic continental breakup. The Journal of Geology, 109(4), pp.493-508.

Ganade, C.E., Cordani, U.G., Agbossoumounde, Y., Caby, R., Basei, M.A., Weinberg, R.F. and Sato, K., 2016. Tightening-up NE Brazil and NW Africa connections: New U–Pb/Lu–Hf zircon data of a complete plate tectonic cycle in the Dahomey belt of the West Gondwana Orogen in Togo and Benin. Precambrian Research, 276, pp.24-42.

Gasquet, D., Levresse, G., Cheilletz, A., Azizi-Samir, M.R. and Mouttaqi, A., 2005. Contribution to a geodynamic reconstruction of the Anti-Atlas (Morocco) during Pan-African times with the emphasis on inversion tectonics and metallogenic activity at the Precambrian–Cambrian transition. Precambrian Research, 140(3), pp.157-182.

Gladkochub, D.P., Wingate, M.T.D., Pisarevsky, S.A., Donskaya, T.V., Mazukabzov, A.M., Ponomarchuk, V.A. and Stanevich, A.M., 2006. Mafic intrusions in southwestern Siberia and implications for a Neoproterozoic connection with Laurentia. Precambrian Research, 147(3), pp.260-278.

Halverson, G.P., Hoffman, P.F., Schrag, D.P., Maloof, A.C. and Rice, A.H.N., 2005. Toward a Neoproterozoic composite carbon-isotope record. Geological Society of America Bulletin, 117(9-10), pp.1181-1207.

Hames, W.E., Hogan, J.P. and Gilbert, M.C., 1998. Revised granite-gabbro age relationships, Southern Oklahoma aulacogen USA. In Basement Tectonics 12 (pp. 247-249). Springer Netherlands.

Hanson, R.E., Wilson, T.J. and Munyanyiwa, H., 1994. Geologic evolution of the Neoproterozoic Zambezi orogenic belt in Zambia. Journal of African Earth Sciences, 18(2), pp.135-150.

Heaman, L.M., LeCheminant, A.N. and Rainbird, R.H., 1992. Nature and timing of Franklin igneous events, Canada: implications for a Late Proterozoic mantle plume and the break-up of Laurentia. Earth and Planetary Science Letters, 109(1-2), pp.117-131.

Heizler, M.T. and Harrison, T.M., 1998. The thermal history of the New York basement determined from 40Ar/39Ar K-feldspar studies. Journal of Geophysical Research: Solid Earth, 103(B12), pp.29795-29814.

Hibbard, J.P. and Samson, S.D., 1995. Orogenesis exotic to the Iapetan cycle in the southern Appalachians. Current perspectives in the Appalachian-Caledonian orogen: Geological Association of Canada Special Paper, 41, pp.191-205.

Hoffman, P.F., 1991. Did the breakout of Laurentia turn Gondwanaland inside-out. Science, 252(5011), pp.1409-1412.

Hoffmann, K.H. and Prave, A.R., 1996. A preliminary note on a revised subdivision and regional correlation of the Otavi Group based on glaciogenic diamictites and associated cap dolostones. Communications of the Geological Survey of Namibia, 11, pp.77-82.

Jefferson, C.W. and Parrish, R.R., 1989. Late Proterozoic stratigraphy, U–Pb zircon ages, and rift tectonics, Mackenzie Mountains, northwestern Canada. Canadian Journal of Earth Sciences, 26(9), pp.1784-1801.

Jiang, G., Sohl, L.E. and Christie-Blick, N., 2003. Neoproterozoic stratigraphic comparison of the Lesser Himalaya (India) and Yangtze block (south China): Paleogeographic implications. Geology, 31(10), pp.917-920.

Johnson, S.P., Rivers, T. and De Waele, B., 2005. A review of the Mesoproterozoic to early Palaeozoic magmatic and tectonothermal history of south–central Africa: implications for Rodinia and Gondwana. Journal of the Geological Society, 162(3), pp.433-450.

Kamo, S.L. and Gower, C.F., 1994. Note: U-Pb baddeleyite dating clarifies age of characteristic paleomagnetic remanence of Long Range dykes, southeastern Labrador. Atlantic Geology 30, 259–262.

Key, R.M., Liyungu, A.K., Njamu, F.M., Somwe, V., Banda, J., Mosley, P.N. and Armstrong, R.A., 2001. The western arm of the Lufilian Arc in NW Zambia and its potential for copper mineralization. Journal of African Earth Sciences, 33(3), pp.503-528.

LeCheminant, A.N. and Heaman, L.M., 1994. 779 Ma mafic magmatism in the northwestern Canadian Shield and northern Cordillera: a new regional time-marker. In Proceedings of the 8th International Conference. Geochronology, Cosmochronology and Isotope Geology, Program Abstracts, US Geological Survey Circ (Vol. 1107, p. 197).

Li, L. and Tull, J.F., 1998. Cover stratigraphy and structure of the southernmost external basement massifs in the Appalachian Blue Ridge; evidence for two-stage late Proterozoic rifting. American Journal of Science, 298(10), pp.829-867.

Li, Z.X., Li, X.H., Kinny, P.D. and Wang, J., 1999. The breakup of Rodinia: did it start with a mantle plume beneath South China?. Earth and Planetary Science Letters, 173(3), pp.171-181.

Lukert, M.T. and Banks, P.O., 1984. Geology and age of the Robertson River pluton. Geological Society of America Special Papers, 194, pp.161-166.

Ma, G., Li, H. and Zhang, Z., 1984. An investigation of the age limits of the Sinian System in South China. Bulletin of Yichang Institute of Geology and Mineral Resources, 8, pp.1-29.

Macdonald, F.A., Strauss, J.V., Rose, C.V., Dudás, F.Ő. and Schrag, D.P., 2010. Stratigraphy of the Port Nolloth Group of Namibia and South Africa and implications for the age of Neoproterozoic iron formations. American Journal of Science, 310(9), pp.862-888.

Matteini, M., Dantas, E.L., Pimentel, M.M., de Alvarenga, C.J.S. and Dardenne, M.A., 2012. U–Pb and Hf isotope study on detrital zircons from the Paranoá Group, Brasília Belt Brazil: Constraints on depositional age at Mesoproterozoic–Neoproterozoic transition and tectono-magmatic events in the São Francisco craton. Precambrian Research, 206, pp.168-181.

McCausland, P.J.A. and Hodych, J.P., 1998. Paleomagnetism of the 550 Ma Skinner Cove volcanics of western Newfoundland and the opening of the Iapetus Ocean. Earth and Planetary Science Letters, 163(1), pp.15-29.

Meng, X., Ge, M. and Tucker, M.E., 1997. Sequence Sequence stratigraphy, sea-level changes and depositional systems in the Cambro-Ordovician of the North China carbonate platform. Sedimentary Geology, 114(1-4), pp.189-222.

Merdith, A.S., Collins, A.S., Williams, S.E., Pisarevsky, S., Foden, J.F., Archibald, D., Blades, M.L., Alessio, B.L., Armistead, S., Plavsa, D. and Clark, C., 2017b. A full-plate global reconstruction of the Neoproterozoic. Gondwana Research.

Merdith, A.S., Williams, S.E., Müller, R.D. and Collins, A.S., 2017a. Kinematic constraints on the Rodinia-Gondwana transition. Precambri-

an Research.

Metcalfe, I., 2013. Gondwana dispersion and Asian accretion: tectonic and palaeogeographic evolution of eastern Tethys. Journal of Asian Earth Sciences, 66, pp.1-33.

Metelkin, D.V., Vernikovsky, V.A. and Kazansky, A.Y., 2012. Tectonic evolution of the Siberian paleocontinent from the Neoproterozoic to the Late Mesozoic: paleomagnetic record and reconstructions. Russian Geology and Geophysics, 53(7), pp.675-688.

Moores, E.M., 1991. Southwest US-East Antarctic (SWEAT) connection: a hypothesis. Geology, 19(5), pp.425-428.

Moura, C.A.V., Pinheiro, B.L.S., Nogueira, A.C.R., Gorayeb, P.S.S. and Galarza, M.A., 2008. Sedimentary provenance and palaeoenvironment of the Baixo Araguaia Supergroup: constraints on the palaeogeographical evolution of the Araguaia Belt and assembly of West Gondwana. Geological Society, London, Special Publications, 294(1), pp.173-196.

Murphy, J.B., Strachan, R.A., Nance, R.D., Parker, K.D. and Fowler, M.B., 2000. Proto-Avalonia: a 1.2–1.0 Ga tectonothermal event and constraints for the evolution of Rodinia. Geology, 28(12), pp.1071-1074.

Nance, R.D., Murphy, J.B., Strachan, R.A., Keppie, J.D., Gutiérrez-Alonso, G., Fernández-Suárez, J., Quesada, C., Linnemann, U., D'lemos, R. and Pisarevsky, S.A., 2008. Neoproterozoic-early Palaeozoic tectonostratigraphy and palaeogeography of the peri-Gondwanan terranes: Amazonian v. West African connections. Geological Society, London, Special Publications, 297(1), pp.345-383.

Paixão, M.A.P., Nilson, A.A. and Dantas, E.L., 2008. The Neoproterozoic Quatipuru ophiolite and the Araguaia fold belt, central-northern Brazil, compared with correlatives in NW Africa. Geological Society, London, Special Publications, 294(1), pp.297-318.

Park, J.K., Buchan, K.L. and Harlan, S.S., 1995. A proposed giant radiating dyke swarm fragmented by the separation of Laurentia and Australia based on paleomagnetism of ca. 780 Ma mafic intrusions in western North America. Earth and Planetary Science Letters, 132(1-4), pp.129-139.

Pedrosa-Soares, A.C. and Wiedemann-Leonardos, C.M., 2000. Evolution of the Araçuaí Belt and its connection to the Ribeira Belt, Eastern Brazil. Tectonic Evolution of South America, 31, pp.265-310.

Pedrosa-Soares, A.C., Noce, C.M., Vidal, P., Monteiro, R.L.B.P. and Leonardos, O.H., 1992. Toward a new tectonic model for the late proterozoic Araçuaí (SE Brazil)-West Congolian (SW Africa) belt. Journal of South American Earth Sciences, 6(1-2), pp.33-47.

Pedrosa-Soares, A.C., Vidal, P., Leonardos, O.H. and de Brito Neves, B.B., 1998. Neoproterozoic oceanic remnants in eastern Brazil: further evidence and refutation of an exclusively ensialic evolution for the Araçuaí–West Congo orogen. Geology, 26(6), pp.519-522.

Pisarevsky, S.A., Gladkochub, D.P., Konstantinov, K.M., Mazukabzov, A.M., Stanevich, A.M., Murphy, J.B., Tait, J.A., Donskaya, T.V. and Konstantinov, I.K., 2013. Paleomagnetism of Cryogenian Kitoi mafic dykes in South Siberia: implications for Neoproterozoic paleogeography. Precambrian Research, 231, pp.372-382.

Pisarevsky, S.A., Murphy, J.B., Cawood, P.A. and Collins, A.S., 2008. Late Neoproterozoic and Early Cambrian palaeogeography: models and problems. Geological Society, London, Special Publications, 294(1), pp.9-31.

Pisarevsky, S.A., Natapov, L.M., Donskaya, T.V., Gladkochub, D.P. and Vernikovsky, V.A., 2008. Proterozoic Siberia: a promontory of Rodinia. Precambrian Research, 160(1), pp.66-76.

Pollock, J.C. and Hibbard, J.P., 2010. Geochemistry and tectonic significance of the Stony Mountain gabbro, North Carolina: Implications for the Early Paleozoic evolution of Carolinia. Gondwana Research, 17(2), pp.500-515.

Preiss, W.V., 2000. The Adelaide Geosyncline of South Australia and its significance in Neoproterozoic continental reconstruction. Precambrian Research, 100(1), pp.21-63.

Puffer, J.H., 2002. A late Neoproterozoic eastern Laurentian superplume: Location, size, chemical composition, and environmental impact. American Journal of Science, 302(1), pp.1-27.

Rainbird, R.H., 1993. The sedimentary record of mantle plume uplift preceding eruption of the Neoproterozoic Natkusiak flood basalt. The Journal of Geology, 101(3), pp.305-318.

Rainbird, R.H., Jefferson, C.W. and Young, G.M., 1996. The early Neoproterozoic sedimentary Succession B of northwestern Laurentia: Correlations and paleogeographic significance. Geological Society of America Bulletin, 108(4), pp.454-470.

Ryu, I.C., Oh, C.W. and Kim, S.W., 2005. A middle Ordovician drowning unconformity on the northeastern flank of the Okcheon (Ogcheon) belt, south Korea. Gondwana Research, 8(4), pp.511-528.

Schulz, K.J., Stewart, D.B., Tucker, R.D., Pollock, J.C. and Ayuso, R.A., 2008. The Ellsworth terrane, coastal Maine: Geochronology, geochemistry, and Nd-Pb isotopic composition—Implications for the rifting of Ganderia. Geological Society of America Bulletin, 120(9-10), pp.1134-1158.

Sial, A.N., Dardenne, M.A., Misi, A., Pedreira, A.J., Gaucher, C., Ferreira, V.P., Silva Filho, M.A., Uhlein, A., Pedrosa-Soares, A.C., Santos, R.V. and Egydio-Silva, M., 2009. The São Francisco Palaeocontinent. Developments in Precambrian Geology, 16, pp.31-69.

Sklyarov, E.V., Gladkochub, D.P., Mazukabzov, A.M., Menshagin, Y.V., Watanabe, T. and Pisarevsky, S.A., 2003. Neoproterozoic mafic dike swarms of the Sharyzhalgai metamorphic massif, southern Siberian craton. Precambrian Research, 122(1), pp.359-376.

Su, Q., Goldberg, S.A. and Fullagar, P.D., 1994. Precise U Pb zircon ages of Neoproterozoic plutons in the southern Appalachian Blue Ridge and their implications for the initial rifting of Laurentia. Precambrian Research, 68(1-2), pp.81-95.

Su, W., Zhang, S., Huff, W.D., Li, H., Ettensohn, F.R., Chen, X., Yang, H., Han, Y., Song, B. and Santosh, M., 2008. SHRIMP U–Pb ages of K-bentonite beds in the Xiamaling Formation: implications for revised subdivision of the Meso-to Neoproterozoic history of the North China Craton. Gondwana Research, 14(3), pp.543-553.

Tack, L., Wingate, M.T.D., Liégeois, J.P., Fernandez-Alonso, M. and Deblond, A., 2001. Early Neoproterozoic magmatism (1000–910 Ma) of the Zadinian and Mayumbian Groups (Bas-Congo): onset of Rodinia rifting at the western edge of the Congo craton. Precambrian research, 110(1), pp.277-306.

Theokritoff G., 1979. Early Cambrian provincialism and biogeographic boundaries in the North Atlantic region. Lethaia, 12(4), pp.281-295.

Thomas, R.J., Chevallier, L.P., Gresse, P.G., Harmer, R.E., Eglington, B.M., Armstrong, R.A., De Beer, C.H., Martini, J.E.J., De Kock, G.S., Macey, P.H. and Ingram, B.A., 2002. Precambrian evolution of the Sirwa window, Anti-Atlas orogen, Morocco. Precambrian Research, 118(1), pp.1-57.

Thomas, R.J., Fekkak, A., Ennih, N., Errami, E., Loughlin, S.C., Gresse, P.G., Chevallier, L.P. and Liégeois, J.P., 2004. A new lithostratigraphic framework for the Anti-Atlas Orogen, Morocco. Journal of African Earth Sciences, 39(3), pp.217-226.

Thomas, W.A. and Astini, R.A., 1996. The Argentine precordillera: a traveler from the Ouachita embayment of North American Laurentia. Science, pp.752-756.

Thomas, W.A. and Astini, R.A., 1999. Simple-shear conjugate rift margins of the Argentine Precordillera and the Ouachita embayment of Laurentia. Geological Society of America Bulletin, 111(7), pp.1069-1079.

Trompette, R., De Alvarenga, C.J.S. and Walde, D., 1998. Geological evolution of the Neoproterozoic Corumbágraben system (Brazil). Depositional context of the stratified Fe and Mn ores of the Jacadigo Group.

Journal of South American Earth Sciences, 11(6), pp.587-597.

Valeriano, C.M., Machado, N., Simonetti, A., Valladares, C.S., Seer, H.J. and Simões, L.S.A., 2004. U–Pb geochronology of the southern Brasília belt (SE-Brazil): sedimentary provenance, Neoproterozoic orogeny and assembly of West Gondwana. Precambrian Research, 130(1), pp.27-55.

Valeriano, C.M., Pimentel, M.M., Heilbron, M., Almeida, J.C.H. and Trouw, R.A.J., 2008. Tectonic evolution of the Brasília Belt, Central Brazil, and early assembly of Gondwana. Geological Society, London, Special Publications, 294(1), pp.197-210.

Veevers, J.J., Walter, M.R. and Scheibner, E., 1997. Neoproterozoic tectonics of Australia-Antarctica and Laurentia and the 560 Ma birth of the Pacific Ocean reflect the 400 my Pangean supercycle. The Journal of Geology, 105(2), pp.225-242.

Villeneuve, M., 2008. Review of the orogenic belts on the western side of the West African craton: the Bassarides, Rokelides and Mauritanides. Geological Society, London, Special Publications, 297(1), pp.169-201.

Wang, C., Liu, L., Wang, Y.H., He, S.P., Li, R.S., Li, M., Yang, W.Q., Cao, Y.T., Collins, A.S., Shi, C. and Wu, Z.N., 2015. Recognition and tectonic implications of an extensive Neoproterozoic volcano-sedimentary rift basin along the southwestern margin of the Tarim Craton, northwestern China. Precambrian Research, 257, pp.65-82.

Wang, J. and Li, Z.X., 2003. History of Neoproterozoic rift basins in South China: implications for Rodinia break-up. Precambrian Research, 122(1), pp.141-158.

Wen, B., Li, Y.X. and Zhu, W., 2013. Paleomagnetism of the Neoproterozoic diamictites of the Qiaoenbrak formation in the Aksu area, NW China: Constraints on the paleogeographic position of the Tarim Block. Precambrian Research, 226, pp.75-90.

Williams, H. and Hiscott, R.N., 1987. Definition of the Iapetus rift-drift transition in western Newfoundland. Geology, 15(11), pp.1044-1047.

Wingate, M.T. and Giddings, J.W., 2000. Age and palaeomagnetism of the Mundine Well dyke swarm, Western Australia: implications for an Australia–Laurentia connection at 755 Ma. Precambrian Research, 100(1), pp.335-357.

Wingate, M.T., Campbell, I.H., Compston, W. and Gibson, G.M., 1998. Ion microprobe U–Pb ages for Neoproterozoic basaltic magmatism in south-central Australia and implications for the breakup of Rodinia. Precambrian Research, 87(3), pp.135-159.

Xu, B., Jian, P., Zheng, H., Zou, H., Zhang, L. and Liu, D., 2005. U–Pb zircon geochronology and geochemistry of Neoproterozoic volcanic rocks in the Tarim Block of northwest China: implications for the breakup of Rodinia supercontinent and Neoproterozoic glaciations. Precambrian Research, 136(2), pp.107-123.

Xu, B., Xiao, S., Zou, H., Chen, Y., Li, Z.X., Song, B., Liu, D., Zhou, C. and Yuan, X., 2009. SHRIMP zircon U–Pb age constraints on Neoproterozoic Quruqtagh diamictites in NW China. Precambrian Research, 168(3), pp.247-258.

Xu, Z.Q., He, B.Z., Zhang, C.L., Zhang, J.X., Wang, Z.M. and Cai, Z.H., 2013. Tectonic framework and crustal evolution of the Precambrian basement of the Tarim Block in NW China: new geochronological evidence from deep drilling samples. Precambrian Research, 235, pp.150-162.

Yonkee, W.A., Dehler, C.D., Link, P.K., Balgord, E.A., Keeley, J.A., Hayes, D.S., Wells, M.L., Fanning, C.M. and Johnston, S.M., 2014. Tectono-stratigraphic framework of Neoproterozoic to Cambrian strata, west-central US: Protracted rifting, glaciation, and evolution of the North American Cordilleran margin. Earth-Science Reviews, 136, pp.59-95.

Young, G.M., 1981. Upper Proterozoic supracrustal rocks of North America: a brief review. Precambrian Research, 15(3-4), pp.305-330.

Young, G.M., Jefferson, C.W., Delaney, G.D. and Yeo, G.M., 1979. Middle and late Proterozoic evolution of the northern Canadian Cordillera and Shield. Geology, 7(3), pp.125-128.

Zhao, J.X. and McCulloch, M.T., 1993. Sm Nd mineral isochron ages of Late Proterozoic dyke swarms in Australia: evidence for two distinctive events of mafic magmatism and crustal extension. Chemical geology, 109(1-4), pp.341-354.

Zhao, P., Chen, Y., Zhan, S., Xu, B. and Faure, M., 2014. The Apparent Polar Wander Path of the Tarim block (NW China) since the Neoproterozoic and its implications for a long-term Tarim–Australia connection. Precambrian Research, 242, pp.39-57.

Supplementary Material 2 (SM2)

See animation of reconstruction from 1000 to 0 Ma in 10 Ma increments.

Discussion

In this thesis I present a global, kinematic model of the Neoproterozoic based on palaeomagnetic and geological data that models the dynamic evolution of plate boundaries (and tectonic plates) from 1000 to 520 Ma. Kinematic plate models are an important way of organising first hand observable geological data to allow for both the temporal and spatial visualisation of events, and for testing of competing hypotheses. They are particularly useful because they model the motion of tectonic plates in 3D spherical coordinates and can be built using basic principles of plate tectonic theory, which do not provide information on the configuration or motion of plates, but instead can act as a control on plausibility (Chapter Two). The basic principles used are that we can infer the existence of a plate boundary based on the relative motion of two continents (i.e. where we have evidence that continents are diverging, we can infer the existence of mid-ocean ridges) and that all these plate boundaries must be connected to one another, allowing us to piece together plate boundaries to construct a fully topological plate model Further principles employed in the reconstruction presented here are that plate motion histories, particularly changes in plate direction (i.e. a reorganisation event), are likely to be linked to either regional or global changes in tectonic regimes, *evidenced* by the geological record or by a series or robust palaeomagnetic data suggesting a specific motion (e.g. Cox and Hart, 2009; Gordon et al., 1984); and that the median root-mean square velocity of plates with large portions of continental (especially cratonic) lithosphere should be less than 60 mm/a in an absolute framework, and at present day the maximum relative motion of the tectonic plates with continental lithosphere is 60 mm/a (e.g. Zahirovic et al., 2015). The validity of this final principle in deeper time is more uncertain, especially when considering other factors such as true polar wander (TPW) (e.g. Domeier and Torsvik, 2014, have plate velocities of up to 200 mm/a; see also Gurnis and Torsvik, 1994; Meert et al., 1993), implying that it could be possible to have faster plate motions. Utilising these principles in a plate model has two benefits; (i) they result in models more realistic to the observations of the present day evolution of the earth, and; (ii) they highlight areas and time periods where our understanding of 'nor-mative' tectonic or geological processes break down, suggesting other processes or phenomena may be occurring (e.g. true polar wander, greenhouse/icehouse conditions etc.).

The Neoproterozoic, the time frame of principal focus in this thesis, is a key frontier in global tectonics and geodynamics for a myriad of reasons including large variations in climate, evolution of complex multicellular life and pronounced episodes of true polar wander. This time period is also significant as it records, after Pangea, the most well known supercontinent Rodinia. Consequently, plate models of the Neoproterozoic, if they are joined to younger models of the Phanerozoic, can allow for the analysis of an entire supercontinent cycle. Furthermore, the afore-(and oft-)mentioned reasons of why the Neoproterozoic is significant are all global phenomena, necessitating the importance of global models to be able to further untangle their nature.

The discussion presented here is centred around three streams of ideas that encapsulate the work presented above. The first two streams are based on linking the themes of this thesis; integrating global models, with kinematic criteria, rifting episodes and the supercontinent cycle. The third stream discusses plate tectonics in the Neoproterozoic.

5-1 Rifted margins and allochthonous terranes in the Neoproterozoic

Chapter Three of this thesis presents a topological plate model of the Neoproterozoic that, in addition to modeling the evolution of plate boundaries, traced the motion of cratonic lithosphere through time. A criticism of the model is that there are an abundant amount of data preserved in non-cratonic lithosphere from the Neoproterozoic that contain information pertinent to untangling dispersal and accretionary events (and consequently, divergent and convergent plate boundaries). In defense of the model being presented, the tectonic evolution of these terranes and/or blocks are often considered secondary to the evolution of the larger portions of cratonic lithosphere. This is because reliable palaeomagnetic data from this time has only been preserved in cratonic lithosphere (i.e. preservation bias), meaning that any starting point for a global

Neoproterozoic model must contain the cratonic components. Nonetheless, an avenue of improving this model is through the addition of terranes to the model. Two methods of doing this are firstly, through finding terranes accreted during the Neoproterozoic and tracing their journey backwards in time. Alternatively, the second method consists of finding rifted margins (where rifting lead to breakup) in the Neoproterozoic, and tracing their journey forwards in time, as rifted margins that resulted in breakup necessitate some portion of continental lithosphere to be on a conjugate plate.

Chapter Four builds a database of rifted margins during the Neoproterozoic. For the majority of these margins the conjugate plate pair is known, even if the exact configuration between the two plates is not finalised and/or the resulting conjugate passive margins are only evident on one plate. For example, the pairing of Australia and Laurentia is reasonably well established (e.g. Dalziel, 1991; Moores, 1991), as is Laurentia with Baltica and Amazonia (for a recent model and discussion see Cawood and Pisarevsky, 2017). However, there are a number of rifting events leading to breakup preserved on cratonic crust where the conjugate plate is unknown. This is because of, in part, a lack of palaeomagnetic data of some cratons, and also poor age constraints on many ancient rifted margins (see Supplementary Material 3 of Chapter Four). Conversely, within the Gondwana forming orogens there are a series of allochthonous terranes of unknown origin, either because of strong reworking during orogenesis, ubiquitous detrital zircon signatures or poor age constraints.

A challenge of constructing full plate models (such as presented in Chapter Three) is that all portions of continental lithosphere must accounted for. Consequently, where a rifted margin (that continued to seafloor spreading) is preserved on the margin of cratonic lithosphere but the conjugate margin is unknown, we can use full plate models to trace the expected journeys of the unknown conjugate margins. Importantly, because the majority of any continental crust destroyed during subduction is from the base of the crust (e.g. Spencer et al., 2017), these conjugate margins should still be preserved somewhere at the present day. As we can account for all cratonic crust during the Neoproterozoic, it is likely that

the conjugate margins are represented by terranes or small blocks rifted off. An example of a margin that preserves Neoproterozoic rifting during this time is the West African Craton (WAC), where a passive margin is preserved in the Moroccan Anti-Atlas, and two aulacogens are preserved on its eastern margin (Ougarta and Gourma aulacogens in the north and south respectively, Ennih and Liégeois, 2001), trending into the craton, suggesting that something rifted of the eastern margin as well.

Tracing the kinematic evolution of some of these conjugate margins could be useful for future refinements of Neoproterozoic plate models. For example, Figure 1 shows the reconstruction from Chapter Four at 850 Ma, the time of rifting. Here, the conjugate margin from the WAC is trapped on two plates. In the south, it remains caught on the Rodinia plate, outboard of the (present day) northwestern margin of Amazonia), in the north, it is caught on the Congo plate. Following the reconstruction forward in time, the conjugate margin from the south should be found in the nexus between Amazonia, Parana Panema and Saõ Francisco, colliding with Saõ Francisco at ca. 660 Ma, suggesting it is preserved somewhere in the Brasilia or Araguaia belt. Conversely, the conjugate margin from the north remains as part of the Congo Plate until its deformation at ca. 550 Ma and should be preserved somewhere in the Kaoka Belt or Dom Feliciano Belt between the Congo-Kalahari margin and the Amazonian-RDLP margin (Figure 1).

Though far more rigorous geological and provincial comparisons and tests would have to be undertaken in, we can hypothesise on the present locations and identification of some of these rifted margins, which are most likely preserved as terranes. A number of terranes are preserved within the suture between Congo - Saõ Francisco - Kalahari and Amazonia - West African Craton - Rio de la Plata, such as the Archaean-Palaeoproterozoic Nico-Perez Terrane, preserved in the Dom Feliciano Belt (Basei et al., 2000; Rapela et al., 2011), the Neoproterozoic age Oriental and Coastal arc terranes, preserved in the Ribeira and Kaoka belts respectively (Heilbron and Machado, 2003; Goscombe et al., 2005; 2007), the Occidental terrane, consisting of reworked Archaean and Palaeoproterozoic basement with a Neopro-
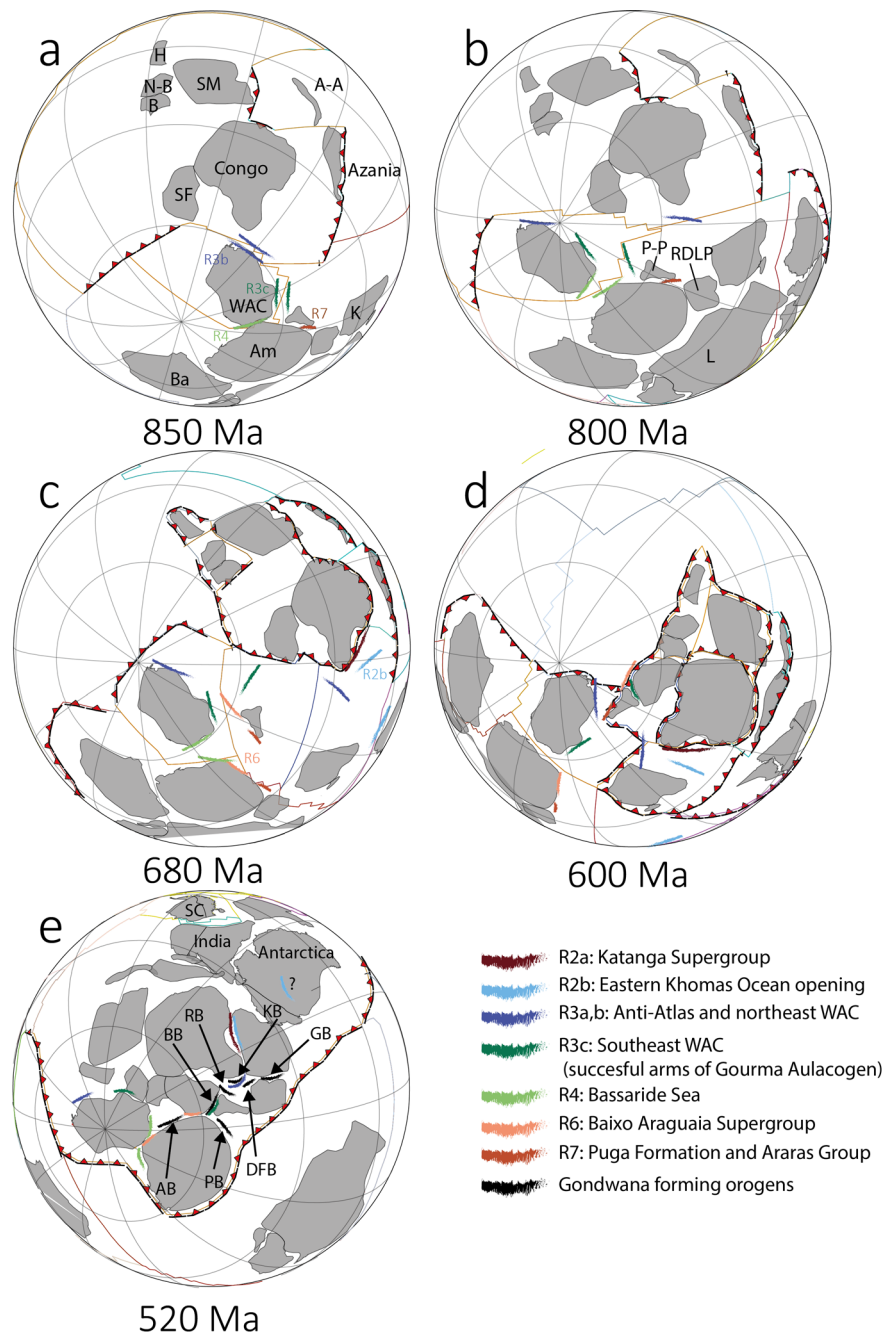
Figure 1 - Snapshots from the slightly modified plate reconstruction proposed in Chapter Three with rifts and conjugate rifts plotted (Chapter Four). (a) 850 Ma; (b) 800 Ma; (c) 680 Ma; (d) 600 Ma; and, (e) 520 Na. Rifts are labelled following Chapter Four. Continents: A-A, Afif-Abas; Am, Amazonia; Ba, Baltica; B, Borborema; H, Hoggar; K, Kalahari; L, Laurentia; N-B, Nigeria-Benin; SC, South China; SF, Saõ Francisco; SM, Sahara Metacraton; and, WAC, West African Craton. Gondwana forming orogens: AB, Araguaia Belt; BB, Brasilia Belt; DFB, Dom Feliciano Belt; GB, Gariep Belt; KB, Kaoka Belt; PB, Paraguay Belt; RB, Ribeira Belt

terozoic aged passive margin (but no Mesoproterozoic rocks?), and is interpreted as the reworked margin of SF (Heilbron et al., 2008), and the Cabo Frio, Embú and Paraíba do Sul terranes, all preserved in the Ribeira Belt and consisting of ca. 2.2 to 1.9 Ga basement (Heilbron et al., 2008). These terranes have ambiguous origins due to either reworking during the Gondwana forming orogens or being covered by Phanerozoic sedimentary basins, but

their preservation in younger fold belts between the South American and African cores of Gondwana suggest rifting during the early Neoproterozoic (Rodinia break-up) and re-aggregating during Gondwana amalgamation.

5-2 Location of subduction zones and mantle structure

Subduction is not only a key driver of plate tectonics, but also plays an important role in shaping the mantle. Mantle tomography at present day suggests that subducted slabs are not visible in the mantle for longer than 300 Ma (e.g. Van der Meer et al., 2010), and during this time play an important role in shaping the structure of, and convection of heat in, the mantle (e.g. Li and Zhong, 2009; Zhong et al., 2007). In particular, the location of subducted slabs is thought to control the position of large-low shear wave velocity provinces (LLSVPs) that are located on the core-mantle boundary (e.g. Garnero et al., 2007; Li and McNamara, 2013) by acting as 'push-brooms' (Burke et al., 2008) forcing material towards the LLSVPs. Hence, we may expect subducted slabs from either Rodinia's girdle of subduction (1000 to 750 Ma) or Gondwana's amalgamation, which peaked between 650 and 520 Ma (e.g. Chapter Four) to control the mantle structure during the Palaeozoic.

The relationship between subduction, mantle structure and positioning of continental lithosphere has been used for two proposals to constrain absolute palaeolongitude in deep time reconstructions. The first method, proposed by Burke et al. (2008) and Torsvik et al. (2008) uses the correlation that is evident for the Mesozoic and Cenzozoic that the reconstructed positions of large igneous provinces (LIPs) and kimberlites (both of which are sourced from the deep mantle) align with the margins of LLSVPs. Consequently, if we assume that LLSVP's are fixed relative to the core we can align continental blocks with deep Earth structure at times when we have evidence of LIPs or kimberlite (e.g. Domeier, 2016; Domeier and Torsvik, 2014; Torsvik et al., 2012). The second method, proposed by Mitchell et al. (2012), suggests that each subsequent supercontinent forms in the downwelling produced by the girdle of subduction of the preceding supercontinent (i.e. Pangea formed within the girdle of subduction of Rodinia, which formed within the girdle of subduction of Nuna etc.) and that these are offset by 90° (the 'orthovision model'). There are issues with both approaches, firstly, recent advancements in both modelling and seismology suggest that LLSVPs are not fully stable and can deform around their margins (e.g. Flament et al., 2017; Zhang et al., 2010; Zhong and Rudolph, 2015). Secondly, the 'orthovision model' only suggests where the centroid of the previ-

ous supercontinent should be, and does not provide information on palaeolongitude during transitional times. Therefore, it can not be used either like palaeomagnetic data is for palaeolatitude (or the fixed-LLSVP approach for palaeolongitude), where rocks in individual cratons or blocks preserve their position at a specific time.

The Neoproterozoic model presented here (Chapter Three and Four) has a palaeolongitudinal constraint inherited from Li et al. (2013), which used the 'ortho-version' model of Mitchell et al. (2012). It has been altered slightly to account for new geological and palaeomagnetic constraints, but is still controlled by the 'orthovision' concept, with Pangea forming over the the cirucm-Rodinia subduction girdle (e.g. Figure 2a-d). Even though we only have a limited control on palaeolongitude we can compare this model, and where it records subduction, to what the fixed-LLSVP model of Torsvik et al. (2008) propose, noting that while it just one possible model out of many, it is likely to be pertinent due to the aforementioned importance that subudction plays in shaping deep mantle structure. Additionally, we can also infer details of the mantle that are not dependent on the absolute position of subduction zones, such as the existence and persistence of degree-1 or degree-2 dominance in patterns of convection.

Mitchell et al. (2012) propose that Pangea formed in the girdle of subduction that surrounded Rodinia. Figure 2 shows the position of all subduction zones in from the model presented in Chapter Four between 1000 and 750 Ma (in 40 Ma increments) overlain with the positions of the continental crust elements of Domeier (2016) and Matthews et al. (2016) (which is the combination of Domeier and Torsvik, 2014 and Müller et al., 2016) and present day location of LLSVPs. There is a fit of the continental crust at 400 Ma, (after Gondwana's amalgamation prior to Pangea's amalgamation) and also Pangea at 200 Ma (Figure 2b,c) with the position of subducted slabs from Rodinia's girdle. At 400 Ma, Gondwana is located over the site of previous subduction that occurred outboard of the southern extent of Rodinia (Baltica, Amazonia and West Africa) where (it is inferred) the proto-Avalonian terranes were being developed (e.g. Murphy et al., 2000). This transitions northwards with the closure of the Rheic ocean driv-
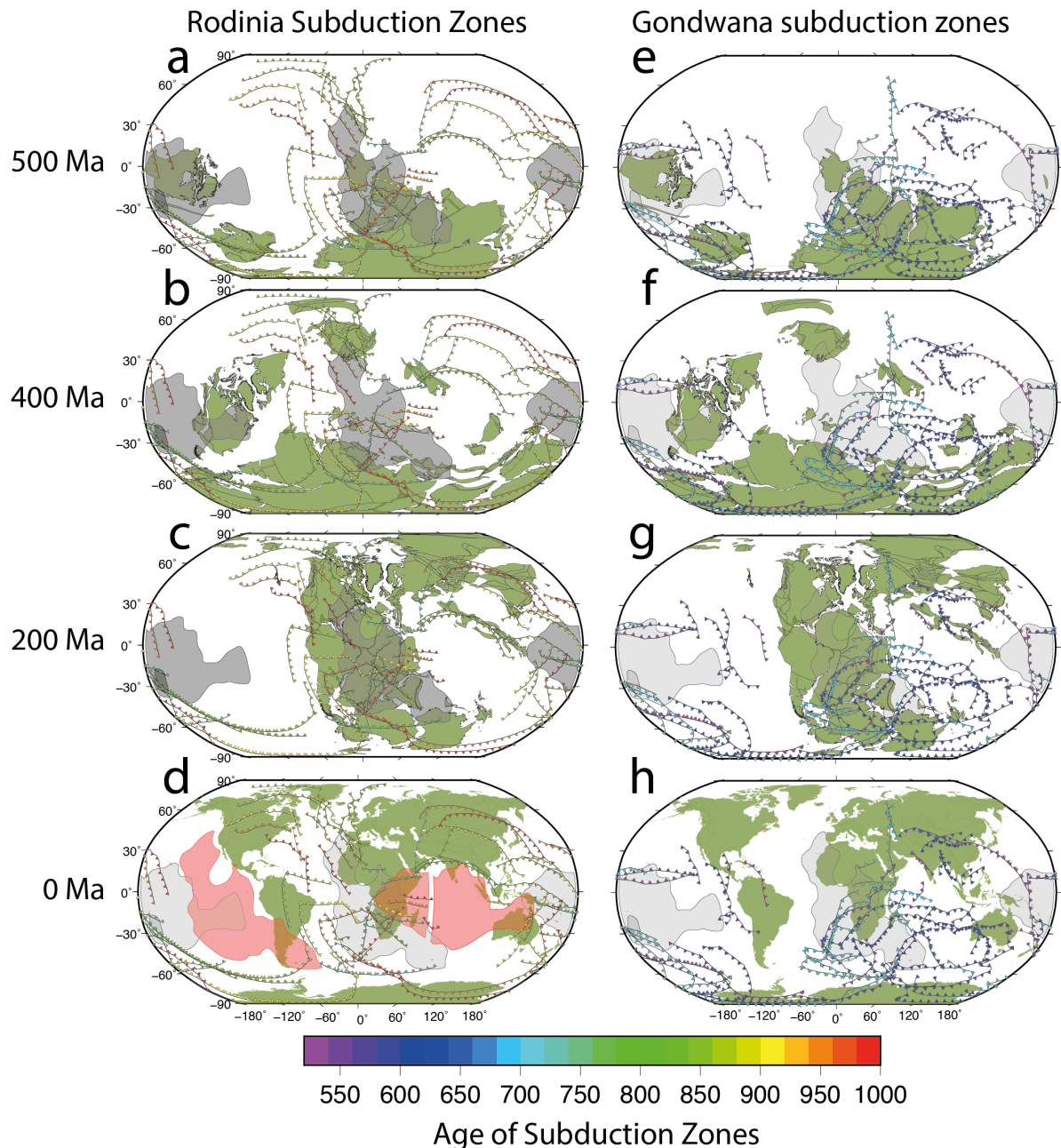
Figure 2 - Subduction zones from the modified model in Chapter Four overlain with position of continental crust during the Phanerozoic (Domeier, 2016, and Matthews et al., 2016). Each horizontal row depicts a different time of the respective reconstructions. (a)-(d), subduction zones from 1000 to 750 Ma in 40 Ma increments, (e)-(h) subduction zones from 750 to 520 Ma in 40 Ma increments. Dark grey polygons are LLSVPs in their present day location. Red polygons are LLSVPs shifted 120° longitudinally to fit the location of subduction zones around Rodinia (1000 to 750 Ma).

ing Pangea amalgamation (e.g. Murphy et al., 2009) such that the supercontinent now lies over subduction predicted from the position of India and South China between 1000 and 800 Ma, and subduction outboard of Congo and the Sahara Metacraton for the same time period. The accretion to Siberia of the central Asian orogenic belt, and closure of successive generations of Tethyan oceans at around 200 Ma occur over the subduction outboard of Siberia, North China and Australia during Rodinia (Chapters Three

and Four).

To investigate what Neoproterozoic subduction could mean for LLSVP nature during the Phanerozoic I compare both the earlier subduction girdle of Rodinia (1000 to 750 Ma) and the younger subduction leading to Gondwana's amalgamation (750 to 520 Ma) to the location of LLSVPs today. There are at least two relevant implications when considering the relationship between Neoproterozoic subduction and the position of LLSVPs at present day. Firstly,

subduction zones should occur away from LLSVPs, as they are zones of upwelling and any slabs entering the lower mantle will interact with them directly (though this could perhaps still allow short lived subduction that does not puncture the 660 km discontinuity). Secondly, as LLSVPs are typically associated with long wavelength mantle convection, their distribution in the mantle is indicative of degree-1 or degree-2 mantle convection, evidence by both the locations of subduction zones, and also the presence of antipodal or singular superplumes (e.g. Li and Zhong, 2009; Zhong et al., 2007).

The best correlation with present-day LLSVP structure comes from 1000 to 750 Ma subduction, where there is a ~120° longitudinal mismatch between the two (e.g. Figure 2e-h), but otherwise the LLSVPs have minimal overlap with subduction zones. This relationship breaks down with the Gondwana forming orogenies, where they completely cross-cut the present day LLSVP positions (e.g. Figure 2e). There is no amount of palaeolongitudinal motion that would offset these subduction zones from the positions of LLSVPs at present day. This is because the palaeolatitudinal distribution of subduction is almost completely within the southern hemisphere (e.g. Figure 17 in Chapter Three), and we know from the spatial extent of continental lithosphere that the subduction was spread across nearly an entire longitudinal hemisphere. Consequently, no matter how we may position Gondwana palaeolongitudinaly during the Ediacaran and Cambrian, the subduction marking the suturing of Gondwana will overlap and cut through the present day positions of the LLSVPs. If LLSVPs are fixed to the core (and have been since ca. 600 Ma) then the circum-Rodinia subduction girdle (e.g. Figure 2d) played an important role in shaping them, though they resisted reshaping from subduction during the Gondwana forming orogenies. This scenario requires that the reconstructions proposed here for the Neoproterozoic are shifted 120° palaeolongitudinally (e..g Figure 2d). If the LLSVPs are younger than ca. 600 Ma then it is unlikely that the subducting slabs from the Gondwana-forming orogenies shaped their structure during the Early Palaeozoic.

Finally, based on subduction from the Neoproterozoic we can explore some ideas on the nature of mantle convection, specifically whether it was dominated by degree-1 or degree-2 structure. If we assume the deep subduction of slabs during Rodinia's existence then the arrangement of subduction would suggest existence of two hemisphere-scale convection cells, one underneath Rodinia, the other under the Mirovoi Ocean, separated by a girdle of subduction reminiscent of Pangea. From ca. 750 Ma, as Gondwana began to amalgamate, the reconstructed subduction pattern suggests that the mantle shifted back into degree-1 convection, as subduction during the Cryogenian and Ediacaran was concentrated almost completely in the southern hemisphere (e.g. Figure 17, Chapter Three. Zhong et al. (2007) noted the degree-2 convection during the Neoproterozoic and suggested the existence of antipodal superplumes (one underneath Rodinia the other underneath the Mirovoi Ocean), similar to the existence of two LLSVPs at present day (see also Li and Zhong, 2009). They argued that mantle structure has alternated between degree-2 convection (during supercontinent existence) and degree-1 convection (during other times) which these results also agree with as evidenced in the change of subduction location from Rodinia to Gondwana (e.g. Figure 2).

5-3 Plate tectonics in the Neoproterozoic

The key underlying assumption to the work presented in this thesis, and also to the majority of studies conducted in the same time frame, is that plate tectonics during the Neoproterozoic operated on a similar basis to what we observe today (e.g. Chapter Two). The purpose of this section is to specifically discuss issues relating to this topic, including: what constitutes present day tectonics; how to observe these tectonic processes in the Neoproterozoic, and; what they imply for how we approach plate reconstructions.

Present day plate tectonics is typically described as the dynamic evolution of rigid, brittle bodies of rock, the lithosphere, moving coherently over a weak, plastic layer of the mantle, the asthenosphere (e.g. Condie, 2013; Frisch et al., 2010). The lithosphere is made up of two components; the crust, which is formed and preserved at the surface through differential melting and is either oceanic or continental,

and the lithospheric mantle. The lithosphere is broken into discrete bodies of oceanic and/or continental lithosphere, referred to as 'tectonic plates'. These plates deform principally around their margins, where they interact with one another along either convergent, divergent or transform boundaries - where the lithosphere is, respectively, compressed, stretched, or sheared. The fundamental driving force of this motion is attributed to heat transfer processes as the Earth cools. Specifically, the convection motion of the mantle is driven by the thermal expansion and contraction of rock. These density contrasts lead to the formation of both mantle plumes (where hot material rises from the core-mantle boundary towards the lithosphere) and subduction zones (where cold, dense material sinks into the mantle) (e.g. Gurnis, 1988; Morgan, 1972). These two processes breed much more complex dynamics, such as orogenic processes, gravitational collapse, and volcanic formations (e.g. Rey et al., 2001). While convection of heat (albeit at a higher isotherm) and gravitational potential energy are likely to be relatively ubiquitous throughout earth history, subduction as we observe it today is less so. Evidence from other non-gaseous planets, such as Mars and Venus, as well as numerical experiments (Rey et al., 2014; Sleep and Windley, 1982; Van Hunen and Moyen, 2012), show that plate tectonics can only occur in relatively specialised conditions - if the mantle is too hot, a mobile lid forms (where the shear forces from convection are too weak); if the mantle is too cold, a stagnant lid forms (where the lithosphere is too strong to be broken for rifting/subduction). Even if we consider plate tectonics operating in earth-like conditions, the assumption of present day processes may not hold for deeper times as slabs may be unable to sink as deeply within a warmer mantle, as is evident in the Archaean (e.g. Martin, 1986; Sleep and Windley, 1982; Van Hunen and Moyan, 2012; Van Hunen and Van der Berg, 2008). Consequently, our 'definition' and understanding of present-day plate tectonics must also incorporate ideas about subduction, such that present-day plate tectonics includes not only the lithospheric implications, such as rates of motions and inter-connected boundaries, but also considers the implications of the lithosphere subducting into the mantle. In addition to coherent, rigid plates, I would include in the definition of 'present day' plate tectonics that slabs are able to be subducted to the

core-mantle boundary, as is suggested by mantle tomography (e.g. Van der Hilst et al., 1997).

Applying this present day understanding to the past represents (e.g. Chapters Two and Three) the simplest choice out of the myriad of possibilities and models of how plate tectonics *could* operate under early Earth conditions. However, given the best available evidence of plate tectonics is what we observe occurring at the present day, and what is preserved in ocean basins (see Chapter Two for the application of this to an example in the Neoproterozoic), it provides a sound basis to start from. This does not discount other approaches or concepts of plate tectonics - as it is clear in the past that the mantle was warmer - and it should not necessarily be applied to the Hadean and Archaean. Rather, the key question is how far back in time are we able to use it as a constraint? This uniformitarianism assumption naturally fails periodically to explain observations from the geological and palaeomagnetic record, in which case widening our vision for alternate explanations (e.g. fast rates of motions) is necessary, and likely accurate for explaining shortfalls. Importantly, once we reach a time where the bulk of geological and palaeomagnetic data can not be accounted for by the 'present day' understanding of plate tectonics, it would then seem that we have determined the maximum age of inception of present day tectonics.

Evidence of plate boundary and lithospheric behaviour reminiscent of present day is readily preserved in the Neoproterozoic and catalogued within Chapters Three and Four of this thesis. As plate tectonics describes the motion of the lithosphere over the entire surface of the earth, it specifically includes both oceanic and continental lithospheric. This creates conceptual problems for pre-Pangea plate reconstructions, as without ocean basins as a guide it is difficult to determine direction of – and changes in – motion (e.g. Chapter Two). Additionally, it also is difficult to conceptualise oceanic lithosphere, even when it is more tangible and attached to a plate with a portion of continental lithosphere, such as during supercontinent breakup where two plates are separated by a divergent plate boundary (as opposed to plates consisting completely of oceanic lithosphere), or during the formation of a continental arc, and subduction of oceanic lithosphere leading to conti-

nent-continent collision. Arc complexes are prevalent through nearly all cratonic components and the duration of these events are similar to present day, ranging from short pulses with complex accretionary patterns to the establishment of long lived, stable voluminous subduction zones. Rifting is also ubiquitous throughout the Neoproterozoic, and is of a similar duration and cyclicity as what we observe at present day (Chapter Four). The breakup of Rodinia occurred through a series of rifting episodes between 850 and 600 Ma, rather than in one long, continuous episode - similar to Pangea which began breakup at 180 Ma. The preservation of ophiolites is also a clear indicator that ocean crust was being generated. The abundance of preserved ophiolites during the Neoproterozoic (and forward in time to the present day) also strongly imply that oceanic lithosphere during the Neoproterozoic is more similar to present day, and is distinct from Archaean and Palaeoproterozoic aged oceanic lithosphere (e.g. Moores, 2002). Consequently, despite the difficulty in modelling oceanic lithosphere, by including it within full plate models it can help better constrain plate motion.

The potential of subducted oceanic lithosphere to penetrate deeply in the mantle during the Neoproterozoic is more difficult to prove. The relevance of the sinking of slabs to plate tectonics is the role that they play in shaping deeper mantle structure (e.g. Bower et al., 2013; Zhang et al., 2010, Section 5-2), and also in initialising plate reorganisations (e.g. Pysklywec et al., 2003), which will be the focus of discussion here. Due to the length of time that sinking slabs spend in the mantle, if we can infer the occurrence of a subduction driven re-organisation event, we can infer the existence of a subduction regime similar to present day prior to the time of the re-organisation. Subsequently, characterising the nature of subduction during this time has profound implications for what we can assume about plate tectonics and mantle structure for the Phanerozoic and Proterozoic. In order to address this (since we can no longer observe these slabs in the mantle) comparisons between the surficial expression of subduction and the effects that subducting slabs are important. In particular for plate reorganisation events we can construct hypotheses as to the preserved effects of the onset of a subdcution-driven plate reorganistion in the geological and palaeomagnetic

recrod. For example, Gordon et al. (1984) describe abrupt changes in the apparent polar wander path of a continent as 'cusps' representing changes in motion. As subduction is inferred to be the driver, we would expect to record a clear onset of subduction of oceanic lithosphere, followed by the plate reorganisation event within a short time period later (rather than the other way around for example), and we would also expect to see changes in the subduction history from continental margins adjacent to the primary orogeny. Due to uncertainty in deep time it is pertinent to consider only regional re-organisation events, consequently we would require that this data comes from continents that are inferred to be adjacent to the ocean basin being closed. A possible avenue of further research would be to consider the closure of the Mozambique Ocean between Azania and India as an example of such a plate reorganisation event. Here the onset of subduction as part of the Mozambique orogeny is recorded at ca. 700 Ma (e.g. Jöns and Schenk, 2008). In a reconstructed Neoproterozoic Earth (e.g. Chapter Three), the Mozambique Ocean separates India, Azania, the Arabian Nubian Shield, Congo, Kalahari and Australia-Antarctica, therefore these locations would be appropriate for looking for futher evidence. For example In Chapter Two I suggested a possible plate reorganisation during the breakup of Rodinia with a re-orientation of the ca. 800 Ma mid-ocean ridge complex separating Australia and Laurentia to accommodate subsequent rifting of Kalahari from Laurentia at ca. 700 Ma. There is also a change in the orientation of subduction in the Arabian Nubian Shield at ca. 700 Ma, from north-south to east-west (e.g. Johnson et al., 2005; 2011; also captured in the plate model presented in Chapter Three). The palaeomagnetic record is unfortunately incomplete, however, coupling India and South China together in the Neoproterozoic permits us to use palaeomagnetic data from both continents to constrain their motion, providing us with a latitudinal record from ca. 800 to 700 Ma, with further poles at ca. 640 Ma.

How appropriate is it then to infer present-day tectonics for the Neoproterozoic? From 750 to 700 Ma there is reasonable (but perhaps not yet sufficient) evidence to accept that plate tectonics (including the behaviour of subducted slabs) is similar to what we observe to day. However, this still leaves the first 250

Ma of the Neoproterozoic unaccounted for. Though plate reorganisation events are unknown in deeper (i.e. pre Rodinia) time, similarity in rifting and voluminous subduction zones to present day (e.g. Chapter Four) could suggest that from Rodinia breakup (ca. 850 to 800 Ma) the surficial expression of plate tectonics (i.e. generation of similar oceanic crust, deformation of continental crust) was similar to present day. Consequently, we would expect that in a coupled lithosphere-mantle system, present day tectonics at the earth's surface should exist prior to any evidence of present day mantle dynamics, as crust entering the mantle must be preceded by crust being created, deformed and subducted on the surface. Therefore, if we infer slabs sinking in the mantle at ca. 750 to 700 Ma in a similar fashion to today, then the generation of oceanic crust at the surface that is conducive to deeper subduction should occur earlier than this time, which would reconcile it with a ca. 850 to 800 Ma initiation, similar to the breakup time of Rodinia. This is similar to the conclusions of Stern (2005; 2007) who suggested that evidence from ophiolites, blueschists and UHP metamorphic complexes imply a staggered initiation of plate tectonics (including subduction) starting at the surface (e.g. preservation of ophiolites), built towards high pressure shallow(er) subduction(blueschists) and finished with the deep subduction of continental crust by ca. 550 Ma (UHP metamorphic complexes). I would, therefore, suggest that present day plate tectonics was recognisable at the surface from 850 Ma with the generation of oceanic lithosphere post Rodinia breakup. By the early suturing of Gondwana (ca. 650 Ma), slabs, which were generated from ca. 850 to 800 Ma mid-ocean ridge complexes, and generally began subduction from 750 Ma, were entering the lower mantle, shaping what we observe on the surface during Gondwana's amalgamation.

Conclusions

The Neoproterozoic preserves an abundant record of plate tectonic processes, including voluminous, long lived subduction zones, pulses of arc magmatism coupled with complex accretionary histories between terranes, extensive rifting and passive margin development and the building of la6 rge scale orogens resulting from continental-continental collision. The preservation of these geological events makes it possible to trace the evolution of not just cratonic crust through the Neoproterozoic, but also the boundaries that define where each tectonic plate intersect. These boundaries are the primary locus where tectonic plates directly interact with the mantle, and consequently plate models that incorporate the dynamic evolution of them can allow for time-dependent analysis of their length and evolution and help unravel long-term cycles such as the supercontinent cycle. Kinematic data of plate motions in the Neoproterozoic is useful because it can act as a tool to assist us with ensuring that oceanic lithosphere is evolving in a way consistent with present day. In order to build a plate model that encapsulates the evolution of oceanic and continental lithosphere I designed a series of kinematic tests to evaluate four different proposed configurations of Australia and Laurentia in the supercontinent Rodinia. I also compare the impact that rifting time will have on their kinematic evolution post breakup, and evaluate these results compared to what we observe at present day where spreading rates are 40±30 mm/a. My results suggest that the AUSWUS or AUSMEX configurations are the most kinematically optimal configurations compared to present day constraints. Rifting time is a stronger constraint on producing kinematically feasible motions, with rifting at 800 Ma producing the only spreading velocities consistent at present day (~70 mm/a for AUSWUS and AUSMEX). Later rifting times, at 725 Ma, produce spreading velocities up to 200 mm/a. In this thesis I propose a new plate model of the Neoproterozoic (1000 to 520 Ma) encapsulating the breakup of Rodinia and amalgamation of Gondwana. This model diverges from earlier models by explicitly modelling the spatio-temporal evolution of plate boundaries for this time. Consequently, I directly model the evolution of tectonic plates, rather than the motion of continental crust. The model incorporates recent palaeo-

magnetic data suggesting an anti-clockwise rotation of the Congo-Saõ Francisco cratons against Rodinia between 850 and 750 Ma. I remove India and South China from Rodinia completely such that they act as lonely wanderers for the Neoproterozoic. This is on the basis of similar accretionary patterns along their northwestern and northern margins respectively, as well as palaeomagnetic data that favours a 30° latitudinal separation between India and Rodinia at 750 Ma. I extend this plate model forward by joining it to younger full plate models of the Phanerozoic to analyse how three criteria – rift length, continental arc length and continent-to-perimeter ratio – change over 1 Ga in order to help better understand the supercontinent cycle and the link between plate tectonics and the mantle. The traditional concept of the supercontinent cycle (short periods of supercontinent existence separated by longer times of dispersal and amalgamation) is not easily recognisable in each of the three criteria, rather each criteria reveal a separate component of the cycle. Supercontinent existence is evident in the perimeter-to-area ratio, the amalgamation of Gondwana is evident from changes in continental arc lengths and the breakup of Rodinia and Pangea is evident from rift lengths. The spatial and temporal relationship of subduction zones around both Rodinia and Pangea suggest that subduction (specifically continent-margin subduction) plays an important role in the breakup of a supercontinent, but once breakup has occurred do not necessarily continue to contribute to subsequent rifting.

References

Anderson, D.L., 2001. Top-down tectonics?. Science, 293(5537), pp.2016-2018.

Austermann, J., Ben-Avraham, Z., Bird, P., Heidbach, O., Schubert, G. and Stock, J.M., 2011. Quantifying the forces needed for the rapid change of Pacific plate motion at 6Ma. Earth and Planetary Science Letters, 307(3), pp.289-297.

Basei, M.A.S., Siga Jr, O., Masquelin, H., Harara, O.M., Reis Neto, J.M. and Preciozzi Porta, F., 2000. The Dom Feliciano Belt and the Rio de la Plata Craton: tectonic evolution and correlation with similar provinces of southwestern Africa. In Tectonic Evolution of South America (Vol. 31). Rio de Janeiro: SBG.

Bower, D.J., Gurnis, M. and Seton, M., 2013. Lower mantle structure from paleogeographically constrained dynamic Earth models. Geochemistry, Geophysics, Geosystems, 14(1), pp.44-63.

Burke, K., Steinberger, B., Torsvik, T.H. and Smethurst, M.A., 2008. Plume generation zones at the margins of large low shear velocity provinces on the core–mantle boundary. Earth and Planetary Science Letters, 265(1), pp.49-60.

Cawood, P.A. and Buchan, C., 2007. Linking accretionary orogenesis with supercontinent assembly. Earth-Science Reviews, 82(3), pp.217-256.

Cawood, P.A. and Pisarevsky, S.A., 2017. Laurentia-Baltica-Amazonia relations during Rodinia assembly. Precambrian Research, 292, pp.386-397.

Cawood, P.A., Strachan, R.A., Pisarevsky, S.A., Gladkochub, D.P. and Murphy, J.B., 2016. Linking collisional and accretionary orogens during Rodinia assembly and breakup: Implications for models of supercontinent cycles. Earth and Planetary Science Letters, 449, pp.118-126.

Collins, W.J., 2003. Slab pull, mantle convection, and Pangaean assembly and dispersal. Earth and Planetary Science Letters, 205(3), pp.225-237.

Condie, K.C., 2013. Plate tectonics & crustal evolution. Elsevier.

Cox, A. and Hart, R.B., 2009. Plate tectonics: how it works. John Wiley & Sons.

Dal Zilio, L., Faccenda, M. and Capitanio, F., 2017. The role of deep subduction in supercontinent breakup. Tectonophysics.

Dalziel, I.W., 1991. Pacific margins of Laurentia and East Antarctica-Australia as a conjugate rift pair: Evidence and implications for an Eocambrian supercontinent. Geology, 19(6), pp.598-601.

Dalziel, I.W., 1992. Antarctica; a tale of two supercontinents?. Annual Review of Earth and Planetary Sciences, 20(1), pp.501-526.

Dalziel, I.W., 1997. OVERVIEW: Neoproterozoic-Paleozoic geography and tectonics: Review, hypothesis, environmental speculation. Geological Society of America Bulletin, 109(1), pp.16-42.

Domeier, M. and Torsvik, T.H., 2014. Plate tectonics in the late Paleozoic. Geoscience Frontiers, 5(3), pp.303-350.

Domeier, M., 2016. A plate tectonic scenario for the Iapetus and Rheic Oceans. Gondwana Research, 36, pp.275-295.

Doubrovine, P.V., Steinberger, B. and Torsvik, T.H., 2012. Absolute plate motions in a reference frame defined by moving hot spots in the Pacific, Atlantic, and Indian oceans. Journal of Geophysical Research: Solid Earth, 117(B9).

Ennih, N. and Liégeois, J.P., 2001. The Moroccan Anti-Atlas: the West African craton passive margin with limited Pan-African activity. Implications for the northern limit of the craton. Precambrian Research, 112(3), pp.289-302.

Evans, D.A.D., 2009. The palaeomagnetically viable, long-lived and all-inclusive Rodinia supercontinent reconstruction. Geological Society, London, Special Publications, 327(1), pp.371-404.

Evans, D.A.D., 2013. Reconstructing pre-Pangean supercontinents. Geological Society of America Bulletin, 125(11-12), pp.1735-1751.

Flament, N., Williams, S., Müller, R.D., Gurnis, M. and Bower, D.J., 2017. Origin and evolution of the deep thermochemical structure beneath Eurasia. Nature communications, 8, p.14164.

Frisch, W., Meschede, M. and Blakey, R.C., 2010. Plate tectonics: continental drift and mountain building. Springer Science & Business Media.

Funiciello, F., Faccenna, C., Heuret, A., Lallemand, S., Di Giuseppe, E. and Becker, T.W., 2008. Trench migration, net rotation and slab–mantle coupling. Earth and Planetary Science Letters, 271(1), pp.233-240.

Garnero, E.J., Lay, T. and McNamara, A., 2007. Implications of lower-mantle structural heterogeneity for the existence and nature of whole-mantle plumes. Geological Society of America Special Papers, 430, pp.79-101.

Gordon, R.G. and Jurdy, D.M., 1986. Cenozoic global plate motions. Journal of Geophysical Research: Solid Earth, 91(B12), pp.12389-12406.

Gordon, R.G., Cox, A. and O'Hare, S., 1984. Paleomagnetic Euler poles and the apparent polar wander and absolute motion of North America since the Carboniferous. Tectonics, 3(5), pp.499-537.

Goscombe, B. and Gray, D.R., 2007. The Coastal Terrane of the Kaoko Belt, Namibia: outboard arc-terrane and tectonic significance. Precambrian Research, 155(1), pp.139-158.

Goscombe, B., Gray, D., Armstrong, R., Foster, D.A. and Vogl, J., 2005. Event geochronology of the Pan-African Kaoko Belt, Namibia. Precambrian Research, 140(3), pp.103-e1.

Gurnis, M. and Torsvik, T.H., 1994. Rapid drift of large continents during the late Precambrian and Paleozoic: Paleomagnetic constraints and dynamic models. Geology, 22(11), pp.1023-1026.

Gurnis, M. and Zhong, S., 1991. Generation of long wavelength heterogeneity in the mantle by the dynamic interaction between plates and convection. Geophysical Research Letters, 18(4), pp.581-584.

Gurnis, M., 1988. Large-scale mantle convection and the aggregation and dispersal of supercontinents. Nature, 332(6166), pp.695-699.

Gurnis, M., Turner, M., Zahirovic, S., DiCaprio, L., Spasojevic, S., Müller, R.D., Boyden, J., Seton, M., Manea, V.C. and Bower, D.J., 2012. Plate tectonic reconstructions with continuously closing plates. Computers & Geosciences, 38(1), pp.35-42.

Heilbron, M. and Machado, N., 2003. Timing of terrane accretion in the Neoproterozoic–Eopaleozoic Ribeira orogen (SE Brazil). Precambrian Research, 125(1), pp.87-112.

Heilbron, M., Valeriano, C.M., Tassinari, C.C.G., Almeida, J., Tupinambá, M., Siga, O. and Trouw, R., 2008. Correlation of Neoproterozoic terranes between the Ribeira Belt, SE Brazil and its African counterpart: comparative tectonic evolution and open questions. Geological Society, London, Special Publications, 294(1), pp.211-237.

Hoffman, P.F., 1991. Did the breakout of Laurentia turn Gondwanaland inside-out. Science, 252(5011), pp.1409-1412.

Johnson, P.R., Andresen, A., Collins, A.S., Fowler, A.R., Fritz, H., Ghebreab, W., Kusky, T. and Stern, R.J., 2011. Late Cryogenian–Ediacaran history of the Arabian–Nubian Shield: a review of depositional, plutonic, structural, and tectonic events in the closing stages of the northern East African Orogen. Journal of African Earth Sciences, 61(3), pp.167-232.

Johnson, S.P., Rivers, T. and De Waele, B., 2005. A review of the Mesoproterozoic to early Palaeozoic magmatic and tectonothermal history of south–central Africa: implications for Rodinia and Gondwana. Journal of the Geological Society, 162(3), pp.433-450.

Jöns, N. and Schenk, V., 2008. Relics of the Mozambique Ocean in the central East African Orogen: evidence from the Vohibory Block of southern Madagascar. Journal of Metamorphic Geology, 26(1), pp.17-28.

Lallemand, S., Heuret, A., Faccenna, C. and Funiciello, F., 2008. Subduction dynamics as revealed by trench migration. Tectonics, 27(3).

Li, M. and McNamara, A.K., 2013. The difficulty for subducted oceanic crust to accumulate at the Earth's core-mantle boundary. Journal of Geophysical Research: Solid Earth, 118(4), pp.1807-1816.

Li, Z.X. and Zhong, S., 2009. Supercontinent–superplume coupling, true polar wander and plume mobility: plate dominance in whole-mantle tectonics. Physics of the Earth and Planetary Interiors, 176(3), pp.143-156.

Li, Z.X., Bogdanova, S.V., Collins, A.S., Davidson, A., De Waele, B., Ernst, R.E., Fitzsimons, I.C.W., Fuck, R.A., Gladkochub, D.P., Jacobs, J., Karlstrom, K.E., Lu, S., Natapov, L.M., Pease, V., Pisarevsky, S.A., Thrane, K., Vernikovsky, V. 2008. Assembly, configuration, and break-up history of Rodinia: a synthesis. Precambrian research, 160(1), pp.179-210.

Li, Z.X., Evans, D.A. and Halverson, G.P., 2013. Neoproterozoic glaciations in a revised global palaeogeography from the breakup of Rodinia to the assembly of Gondwanaland. Sedimentary Geology, 294, pp.219-232.

Mallard, C., Coltice, N., Seton, M., Müller, R.D. and Tackley, P.J., 2016. Subduction controls the distribution and fragmentation of Earth's tectonic plates. Nature, 535(7610), pp.140-143.

Martin, H., 1986. Effect of steeper Archean geothermal gradient on geochemistry of subduction-zone magmas. Geology, 14(9), pp.753-756.

Matthews, K.J., Maloney, K.T., Zahirovic, S., Williams, S.E., Seton, M. and Müller, R.D., 2016. Global plate boundary evolution and kinematics since the late Paleozoic. Global and Planetary Change, 146, pp.226-250.

Matthews, K.J., Müller, R.D., Wessel, P. and Whittaker, J.M., 2011. The tectonic fabric of the ocean basins. Journal of Geophysical Research: Solid Earth, 116(B12).

McMenamin, M.A. and McMenamin, D.L.S., 1990. The emergence of animals: the Cambrian breakthrough. Columbia University Press.

Meert, J.G., Van der Voo, R., Powell, C.M., Li, Z.X., McElhinny, M.W., Chen, Z. and Symons, D.T.A., 1993. A plate-tectonic speed limit?. Nature, 363(6426), pp.216-217.

Mitchell, R.N., Kilian, T.M. and Evans, D.A., 2012. Supercontinent cycles and the calculation of absolute palaeolongitude in deep time. Nature, 482(7384), pp.208-211.

Moores, E.M., 1991. Southwest US-East Antarctic (SWEAT) connection: a hypothesis. Geology, 19(5), pp.425-428.

Moores, E.M., 2002. Pre–1 Ga (pre-Rodinian) ophiolites: Their tectonic and environmental implications. Geological Society of America Bulletin, 114(1), pp.80-95.

Morgan, W.J., 1972. Plate motions and deep mantle convection. Geological Society of America Memoirs, 132, pp.7-22.

Müller, R.D., Seton, M., Zahirovic, S., Williams, S.E., Matthews, K.J., Wright, N.M., Shephard, G.E., Maloney, K.T., Barnett-Moore, N., Hosseinpour, M. and Bower, D.J., 2016. Ocean basin evolution and global-scale plate reorganization events since Pangea breakup. Annual Review of Earth and Planetary Sciences, 44, pp.107-138.

Murphy, J.B., Nance, R.D. and Cawood, P.A., 2009. Contrasting modes of supercontinent formation and the conundrum of Pangea. Gondwana Research, 15(3), pp.408-420.

Murphy, J.B., Strachan, R.A., Nance, R.D., Parker, K.D. and Fowler, M.B., 2000. Proto-Avalonia: a 1.2–1.0 Ga tectonothermal event and constraints for the evolution of Rodinia. Geology, 28(12), pp.1071-1074.

O'Neill, C., Müller, D. and Steinberger, B., 2005. On the uncertainties in hot spot reconstructions and the significance of moving hot spot reference frames. Geochemistry, Geophysics, Geosystems, 6(4).

Patriat, P. and Achache, J., 1984. India–Eurasia collision chronology has implications for crustal shortening and driving mechanism of plates. Nature, 311(5987), pp.615-621.

Pehrsson, S.J., Eglington, B.M., Evans, D.A., Huston, D. and Reddy, S.M., 2016. Metallogeny and its link to orogenic style during the Nuna supercontinent cycle. Geological Society, London, Special Publications, 424(1), pp.83-94.

Piper, J.D., 2000. The Neoproterozoic Supercontinent: Rodinia or Palaeopangaea?. Earth and Planetary Science Letters, 176(1), pp.131-146.

Piper, J.D.A., 2007. The neoproterozoic supercontinent palaeopangaea. Gondwana Research, 12(3), pp.202-227.

Piper, J.D.A., 2010. Palaeopangaea in Meso-Neoproterozoic times: The palaeomagnetic evidence and implications to continental integrity, supercontinent form and Eocambrian break-up. Journal of geodynamics, 50(3), pp.191-223.

Piper, J.D.A., Beckmann, G.E.J. and Badham, J.P.N., 1976. Palaeomagnetic evidence for a Proterozoic super-continent. Philosophical Transactions of the Royal Society of London A: Mathematical, Physical and Engineering Sciences, 280(1298), pp.469-490.

Pisarevsky, S.A., Elming, S.Å., Pesonen, L.J. and Li, Z.X., 2014. Mesoproterozoic paleogeography: supercontinent and beyond. Precambrian Research, 244, pp.207-225.

Pisarevsky, S.A., Wingate, M.T., Powell, C.M., Johnson, S. and Evans, D.A., 2003. Models of Rodinia assembly and fragmentation. Geological Society, London, Special Publications, 206(1), pp.35-55.

Powell, C.M., Li, Z.X., McElhinny, M.W., Meert, J.G. and Park, J.K., 1993. Paleomagnetic constraints on timing of the Neoproterozoic breakup of Rodinia and the Cambrian formation of Gondwana. Geology, 21(10), pp.889-892.

Pysklywec, R.N., Mitrovica, J.X. and Ishii, M., 2003. Mantle avalanche as a driving force for tectonic reorganization in the southwest Pacific. Earth and Planetary Science Letters, 209(1), pp.29-38.

Rapela, C.W., Fanning, C.M., Casquet, C., Pankhurst, R.J., Spalletti, L., Poiré, D. and Baldo, E.G., 2011. The Rio de la Plata craton and the adjoining Pan-African/brasiliano terranes: their origins and incorporation into south-west Gondwana. Gondwana Research, 20(4), pp.673-690.

Rey, P., Vanderhaeghe, O. and Teyssier, C., 2001. Gravitational collapse of the continental crust: definition, regimes and modes. Tectonophysics, 342(3), pp.435-449.

Rey, P.F., Coltice, N. and Flament, N., 2014. Spreading continents kick-started plate tectonics. Nature, 513(7518), pp.405-408.

Rolf, T., Capitanio, F.A. and Tackley, P.J., 2017. Constraints on mantle viscosity structure from continental drift histories in spherical mantle convection models. Tectonophysics.

Seton, M., Müller, R.D., Zahirovic, S., Gaina, C., Torsvik, T., Shephard, G., Talsma, A., Gurnis, M., Turner, M., Maus, S. and Chandler, M., 2012. Global continental and ocean basin reconstructions since 200Ma. Earth-Science Reviews, 113(3), pp.212-270.

Sleep, N.H. and Windley, B.F., 1982. Archean plate tectonics: constraints and inferences. The Journal of Geology, 90(4), pp.363-379.

Stampfli, G.M. and Borel, G.D., 2002. A plate tectonic model for the Paleozoic and Mesozoic constrained by dynamic plate boundaries and restored synthetic oceanic isochrons. Earth and Planetary Science Letters, 196(1), pp.17-33.

Stern, R.J., 2005. Evidence from ophiolites, blueschists, and ultrahigh-pressure metamorphic terranes that the modern episode of subduction tectonics began in Neoproterozoic time. Geology, 33(7), pp.557-560.

Stern, R.J., 2007. When and how did plate tectonics begin? Theoretical and empirical considerations. Chinese Science Bulletin, 52(5), pp.578-591.

Stoddard, P.R. and Abbott, D., 1996. Influence of the tectosphere upon plate motion. Journal of Geophysical Research: Solid Earth, 101(B3), pp.5425-5433.

Tackley, P.J., 2000. Mantle convection and plate tectonics: toward an integrated physical and chemical theory. Science, 288(5473), pp.2002-2007.

Torsvik, T.H., 2003. The Rodinia jigsaw puzzle. Science, 300(5624), pp.1379-1381.

Torsvik, T.H., Smethurst, M.A., Meert, J.G., Van der Voo, R., McKerrow, W.S., Brasier, M.D., Sturt, B.A. and Walderhaug, H.J., 1996. Continental break-up and collision in the Neoproterozoic and Palaeozoic—a tale of Baltica and Laurentia. Earth-Science Reviews, 40(3-4), pp.229-258.

Torsvik, T.H., Steinberger, B., Cocks, L.R.M. and Burke, K., 2008. Longitude: linking Earth's ancient surface to its deep interior. Earth and Planetary Science Letters, 276(3), pp.273-282.

Valentine, J.W. and Moores, E.M., 1970. Plate-tectonic regulation of faunal diversity and sea level: a model. Nature, 228(5272), pp.657-659.

Van der Hilst, R.D., Widiyantoro, S. and Engdahl, E.R., 1997. Evidence for deep mantle circulation from global tomography. Nature, 386, pp.578-584.

Van Der Meer, D.G., Spakman, W., Van Hinsbergen, D.J., Amaru, M.L. and Torsvik, T.H., 2010. Towards absolute plate motions constrained by lower-mantle slab remnants. Nature Geoscience, 3(1), p.36.

Van Hunen, J. and Moyen, J.F., 2012. Archean subduction: fact or fiction?. Annual Review of Earth and Planetary Sciences, 40, pp.195-219.

van Hunen, J. and van den Berg, A.P., 2008. Plate tectonics on the early Earth: limitations imposed by strength and buoyancy of subducted lithosphere. Lithos, 103(1), pp.217-235.

Worsley, T.R., Nance, D. and Moody, J.B., 1984. Global tectonics and eustasy for the past 2 billion years. Marine Geology, 58(3-4), pp.373-400.

Zahirovic, S., Müller, R.D., Seton, M. and Flament, N., 2015. Tectonic speed limits from plate kinematic reconstructions. Earth and Planetary Science Letters, 418, pp.40-52.

Zhang, N., Zhong, S., Leng, W. and Li, Z.X., 2010. A model for the evolution of the Earth's mantle structure since the Early Paleozoic. Journal of Geophysical Research: Solid Earth, 115(B6).

Zhong, S. and Rudolph, M.L., 2015. On the temporal evolution of long-wavelength mantle structure of the Earth since the early Paleozoic. Geochemistry, Geophysics, Geosystems, 16(5), pp.1599-1615.

Zhong, S., Zhang, N., Li, Z.X. and Roberts, J.H., 2007. Supercontinent cycles, true polar wander, and very long-wavelength mantle convection. Earth and Planetary Science Letters, 261(3), pp.551-564.

Prospectivity of Western Australian iron ore from geophysical data using a reject option classifier

Andrew S. Merdith [a,b,*], Thomas C.W. Landgrebe [a], R. Dietmar Müller [a]

[a] EarthByte Group, School of Geosciences, The University of Sydney, Madsen Building F09, Australia
[b] National ICT Australia (NICTA), Australian Technology Park, Australia

ABSTRACT

There has recently been a rapid growth in the amount and quality of digital geological and geophysical data for the majority of the Australian continent. Coupled with an increase in computational power and the rising importance of computational methods, there are new possibilities for a large scale, low expenditure digital exploration of mineral deposits. Here we use a multivariate analysis of geophysical datasets to develop a methodology that utilises machine learning algorithms to build and train two-class classifiers for provincial-scale, greenfield mineral exploration. We use iron ore in Western Australia as a case study, and our selected classifier, a mixture of a Gaussian classifier with reject option, successfully identifies 88% of iron ore locations, and 92% of non-iron ore locations. Parameter optimisation allows the user to choose the suite of variables or parameters, such as classifier and degree of dimensionality reduction, that provide the best classification result. We use randomised hold-out to ensure the generalisation of our classifier, and test it against known ground-truth information to demonstrate its ability to detect iron ore and non-iron ore locations. Our classification strategy is based on the heterogeneous nature of the data, where a well-defined target "iron-ore" class is to be separated from a poorly defined non-target class. We apply a classifier with reject option to known data to create a discriminant function that best separates sampled data, while simultaneously "protecting" against new unseen data by "closing" the domain in feature space occupied by the target class. This shows a substantial 4% improvement in classification performance. Our predictive confidence maps successfully identify known areas of iron ore deposits through the Yilgarn Craton, an area that is not heavily sampled in training, as well as suggesting areas for further exploration throughout the Yilgarn Craton. These areas tend to be more concentrated in the north and west of the Yilgarn Craton, such as around the Twin Peaks mine (~27°S, 116°E) and a series of lineaments running east–west at ~25°S. Within the Pilbara Craton, potential areas for further expansion occur throughout the Marble Bar vicinity between the existing Spinifex Ridge and Abydos mines (21°S, 119–121°E), as well as small, isolated areas north of the Hamersley Group at ~21.5°S, ~118°E. We also test the usefulness of radiometric data for province-scale iron ore exploration, while our selected classifier makes no use of the radiometric data, we demonstrate that there is no performance penalty from including redundant data and features, suggesting that where possible all potentially pertinent data should be included within a data-driven analysis. This methodology lends itself to large scale, reconnaissance mineral explorations, and, through varying the datasets used and the commodity being targeted, predictive confidence maps for a wide range of minerals can be produced.

© 2015 Elsevier B.V. All rights reserved.

1. Introduction

The viability of an ore deposit is governed not only by its geological features, but also by economic factors such as global demand and market value. Consequently, economic geology links together frontier geological science with an economic framework; what defines an economically viable ore deposit can alter over time as a consequence of changes in the cost of exploration, extraction and production as well as demand in the global market (Pohl, 2011). As ore deposits, which are both easy to find and extract, are being depleted, there is a rising cost associated with finding new ore deposits using existing exploration techniques. The increase in computational power and in the availability of high-resolution data allows for new methodologies to be developed for the purposes of data-driven mineral exploration, in an effort to reduce exploration costs in finding large ore bodies.

The challenge in developing effective targeting aids that generalise to new geographic locations is in developing methods and models that exploit available data without over-fitting, and lend themselves to continuous improvement as more/higher-quality data become

* Corresponding author at: EarthByte, School of Geosciences, The University of Sydney, Madsen Building F09, Australia.
E-mail address: Andrew.merdith@sydney.edu.au (A.S. Merdith).

available. Of particular importance is understanding the impact that factors such as data redundancy, correlation between datasets, sample-sizes and data-dimensionality have on the effectiveness of the models and outputs generated by their amalgamation. In this paper we have used a multivariate analysis of geophysical databases to develop a methodology that utilises machine learning algorithms (MLAs) to build and train a classifier to predict the presence and absence of iron ore deposits throughout Western Australia. Importantly, our classifier is designed to be applied over large areas of land (on the order of 1000 km), as such, while generalising well for the exploration of iron ore over multiple cratons and orogenies, it is not specifically adapted for local geology and regional–local scale exploration. As such, we utilise a training and evaluation methodology, which takes into account the various aforementioned factors and attempts to make use of available data in the most effective way.

As conceptual targeting of potential sites at a province/district to regional scale is one of the largest challenges facing geoscience (Hronsky and Groves, 2008) this methodology will assist with first order, large-scale exploration. Mineral exploration consists of a number of successive but interlinked stages, starting with planning and large-scale reconnaissance exploration, before moving towards smaller scale appraisals and explorative drilling, and then finally assessment drilling and mine development (Moon and Whateley, 2006; Pohl, 2011). Generally, as the stages progress the associated economic risk decreases, but the expenditure required increases (i.e. more money is spent on stages that have a higher confidence of success) (Moon and Whateley, 2006). The methodology outlined in this paper is designed to fit in the early reconnaissance stage of mineral exploration, assisting and facilitating in the identification of potential target locations for a commodity. The nature of this methodology fits well in the exploration method, as it has a low expenditure. However, unlike existing reconnaissance exploration, we believe that there is less associated risk with this methodology. While formal mineral exploration already consists of the analysis of geophysical data, our approach differs in that we minimise human bias and use computational methods that allow for the combination and analysis of large amounts of high-dimensional data to create a prospectivity map of a target commodity. We argue that studies in the past such as Groves et al. (2000) and Nykänen et al. (2008) in which targeting "layers" are independently combined together are suboptimal. They do not take into account that many geological/geophysical statistics are not independent, resulting in under-exploited data separability (Brown et al., 2000; Porwal et al., 2003; Singer and Kouda, 1999). In this paper a multivariate approach is taken where we explicitly attempt to deal with these issues, thus combining various data sources into a single model that involves feature extraction and classification to both cope with the dependence between variables, and make trade-offs between the number of dimensions, available data and classifier complexity.

2. Background geology

Though iron ore is one of the most economically important natural commodities, there is still some uncertainty about its genesis. This is due, in part, to an absence of modern analogues with respect to both the process of formation (Bekker et al., 2010) and also the scale at which the deposits form (Morris, 1985). Additionally, ambiguities about Archean and Proterozoic geology, climatic conditions and seawater chemistry (e.g. Canfield, 2005; Lyons et al., 2009; Planavsky et al., 2011) have also caused numerous mechanisms and ideas being proposed over time for the source and transport paths of iron, the timing of deposition of iron formations and the subsequent enrichment of iron formation to iron ore. For instance, while it is generally accepted that all major iron ore deposits occurred in an oceanic setting, the source of the iron within the oceans was thought to originate from continental erosion until, an alternative hydrothermal source was proposed (Isley, 1995).

Banded iron formations (BIF) are defined after James and Trendall (1982) as a rock with thin laminations of chert alternating with iron minerals, and can be broadly classified into two categories based on their depositional environment, Algoma-type and Superior-type (Gross, 1980). Algoma-type deposits are found through Archean and Proterozoic formations, and are associated with volcanic centres and exhalative submarine processes, and typically contain some greywacke or volcanic units (Gross, 1980). They are typically found within Archean greenstone belts (Bekker et al., 2010; Goodwin, 1973; Isley and Abbott, 1999) and are usually smaller, both in terms of tonnage of ore (largest deposits around 10^7 Mt) and in spatial extent than Superior-type deposits. Comparably, Superior-type deposits are more common in Proterozoic aged formations and are associated with a near-shore continental-shelf depositional setting, usually found with carbonates, quartzite, black shales, and small amounts of volcanogenic rocks (Gross, 1980). The Superior-type tend to be larger, up to 10^{14} Mt, and also occupy a larger spatial extent (Bekker et al., 2010; Huston and Logan, 2004; Isley, 1995). Both types of iron formation are associated with oxide, silicate and carbonate facies (Gross, 1980; James, 1954), while Algoma-types may be associated with polymetallic sulphide facies if they occurred in close proximity to a volcanic centre.

2.1. Geological setting

Australia is host to both Algoma- and Superior-type deposits, though it is predominantly known for its massive Superior-type deposits occurring throughout the Hamersley Basin in the Pilbara Craton (Fig. 1). The Pilbara Craton consists of a Paleo-Neoarchean core overlain with a strong angular unconformity by Neoarchean–Paleoproterozoic volcano-sedimentary sequences (Blake and Barley, 1992; van Kranendonk et al., 2002). The core consists of a granite–greenstone terrane that outcrops towards the north, collectively called the North Pilbara terrain (Fig. 2). The North Pilbara terrain has been subdivided into three distinct granite–greenstone terranes, the East Pilbara granite–greenstone terrane (3.72–2.85 Ga), the West Pilbara granite–greenstone terrane (3.27–2.92 Ga) and the Kurunna terrane (3.3–3.2 Ga) towards the southeast of the craton, and two intracratonic sedimentary basins, the Mallina Basin (3.01–2.94 Ga) and the Mosquito Creek basin (~3.3–2.9 Ga) (van Kranendonk et al., 2002). Smaller Algoma-type deposits occur in the Eastern Pilbara granite–greenstone terrane amongst the Gorge Creek Group and Cleaverville Formation (Huston and Logan, 2004). The volcano-sedimentary sequences, collectively referred to as the Hamersley-province, overlay the southern part of the craton and are of principal interest to this study as they contain some of the largest and richest iron ore deposits in the world. The stratigraphy of the Hamersley province is divided into five key groups. The lower three, the Fortescue Group (2770–2630 Ma), the iron rich Hamersley Group (2630–2470 Ma) and the Turee Creek Group (2470–ca.2350 Ma) all conformably overlay one another and comprise the Mt. Bruce Supergroup (Taylor et al., 2001). The upper two groups, the Lower and Upper Wyloo Groups (2209–2150 Ma and 2000–1800 Ma respectively), are separated from the Mt. Bruce Supergroup by a first order regional unconformity (Taylor et al., 2001). The Fortescue Group is characterised by mafic–clastic sedimentation, while the lower and middle units of the Hamersley Group are indicative of a deep-water environment consisting of volcanoclastic sedimentary and some carbonate sedimentary units and the Turee Creek Group consists of coarser, clastic sedimentary rocks overlaying iron formation, suggesting a transition from a deep to shallow sea environment (Blake and Barley, 1992; Simonson et al., 1993). Iron ore is found extensively throughout the Hamersley Group. Deformation is more pronounced in the south of the Hamersley province where the younger units outcrop, with the older basal units in the north of the province only being gently folded (Taylor et al., 2001).

The Yilgarn Craton is a large, Archean aged section of crust within Western Australia, to the south of the Pilbara Craton. Similar to the Pilbara Craton, it is comprised predominantly of Mesoarchean low-grade metamorphosed granite–greenstone belts, though it also contains
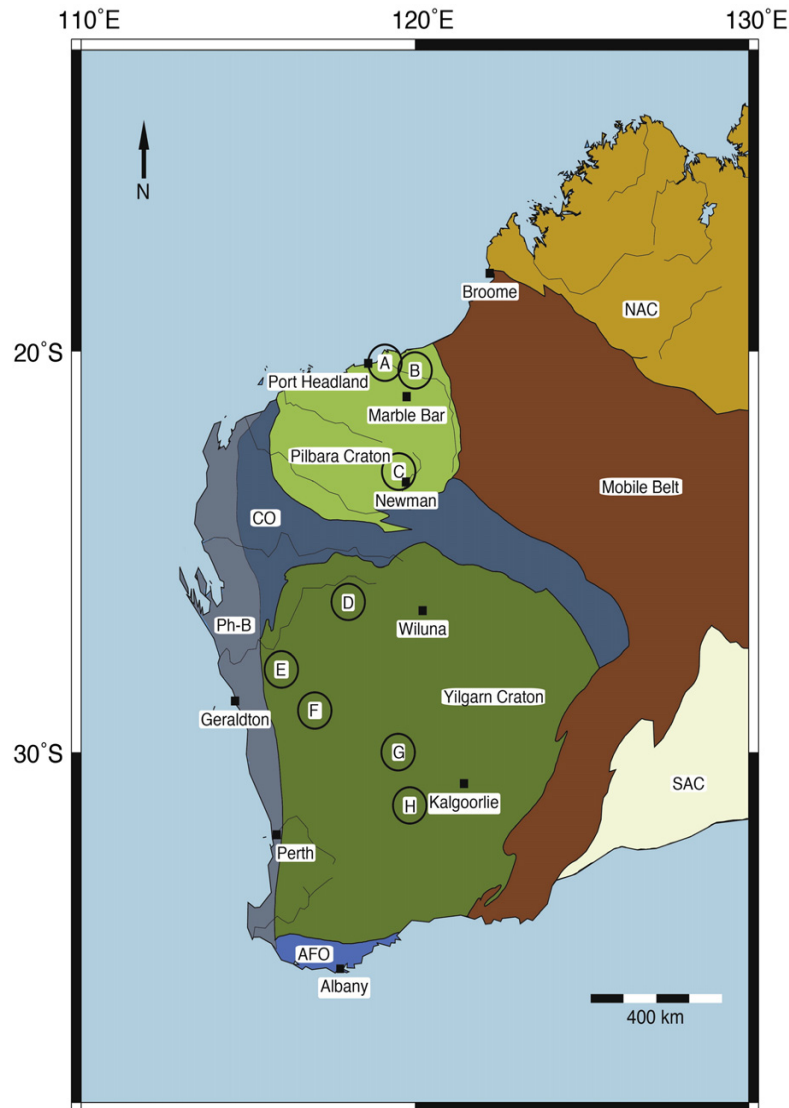
Fig. 1. Map of Western Australia showing geological provinces and major towns and cities. (AFO) Albany-Fraser Orogen; (CO) Capricorn Orogen; (NAC) North Australian Craton; (Ph-B) Phanerozoic Basin; (SAC) South Australian Craton. Black circles represent some iron deposits (A) Pardoo-Mt Goldsworthy; (B) Cattle Gorge; (C), Mt. Whaleback; (D) Madoonga; (E) Tallering Peak; (F) Karara; (G) Windarling; and (H) Koolyanobbing.

an Eo-Paleoarchean gneissetic component in the north west (Griffin et al., 2004; Myers, 1993). A number of studies aiming to subdivide the craton into discrete geological domains have been attempted using geological, geophysical and geochemical data (e.g. Gee et al., 1981; Griffin et al., 2004; Myers, 1993; Whitaker, 2001), though it is considerably more difficult than in the case of the Pilbara Craton due to the thick regolith that covers large areas of the craton (Anand and Paine, 2002; Dauth, 1997). Key terranes outlined by Myers (1993) include the West Yilgarn Superterrane (3.8–3.7 Ga core in the northwest, intruded by 3.0 Ga granitoids, and 3.0 Ga core in the west and southwest, intruded by 2.9 Ga granitoids), the West Central Yilgarn Superterrane (2.8–2.7 Ga greenstones), the East Central Yilgarn Superterrane (2.7 Ga greenstones) and the East Yilgarn Superterrane (2.8 Ga greenstones). In the Yilgarn Craton, iron ore is restricted to the greenstone belts, such as the Woongan Hill Terrane, Noganyer Formation and Koolyanobbing Greenstone Belt (Huston and Logan, 2004; Isley and Abbott, 1999) and also throughout the Yilgarn Craton within the Woongan Hill Terrane and the Noganyer Formation (both greenstone belts) (Huston and Logan, 2004; Isley and Abbott, 1999) (Fig. 3). Recent advances in iron ore exploration have acknowledged the

importance of these smaller Algoma-type deposits in the Yilgarn Craton to the Australian iron industry, and a large body of research is being built up about their deposition, geological properties, structural controls on ore genesis and exploration strategies (e.g. Angerer and Hagemann, 2010; Duuring and Hagemann, 2013; Lascelles, 2006).

2.2. Models of formation

While classification of the depositional environment for BIF is widely accepted, the process(-es) by which enrichment occurs (from ~15% to ~55% iron) is more uncertain. Broadly, methods of enrichment are divided into three main models; syngenetic, supergene and hypogene–supergene models. The syngenetic models advocate that the conversion from BIF to ore is completed during diagenesis. This can occur during an extensional event through the creation of a dilational space within the chert–iron bands, allowing for the incremental removal of silica and concentration of iron where extensional disturbances during diagenesis allowed for iron enrichment to occur (Findlay, 1994), or through breaks in the iron laminae during diagenesis allowing for the escape of gelatinous, amorphous
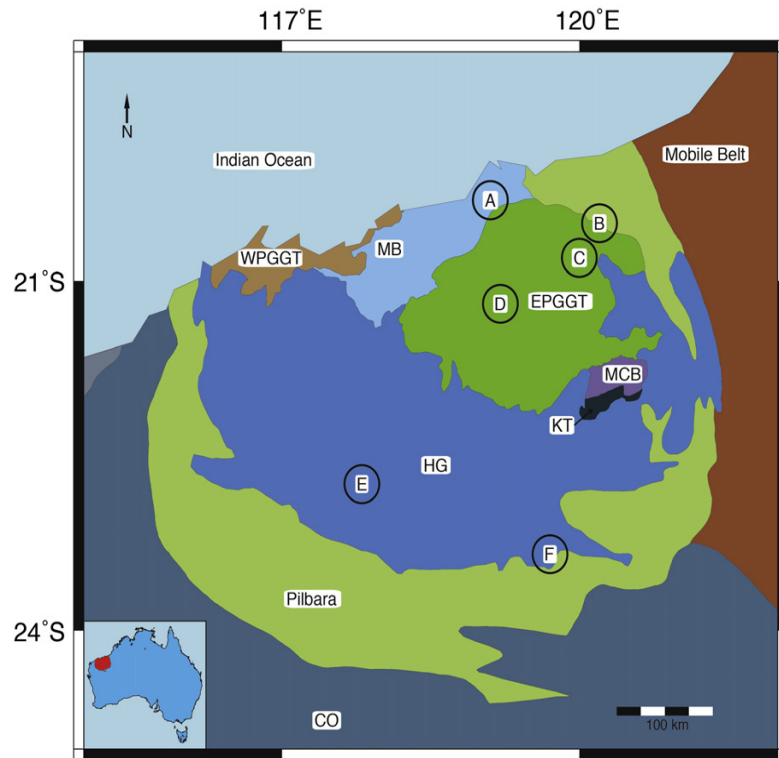
Fig. 2. Overview of key geological terranes in the Pilbara Craton based on Hickman (2004). (CO) Capricorn Orogen; (EPGGT) Eastern Pilbara Granite–Greenstone Terrane; (HG) Hamersley Province; (KT) Kurunna Terrane; (MB) Mallina Basin; (MCB) Mosquito Creek Basin; (WPGGT) Western Pilbara Granite–Greenstone Terrane. Black circles represent some iron deposits (A) Pardoo-Mt Goldsworthy; (B) Cattle Gorge; (C) Spinifex Ridge; (D) Abydos; (E) Mt. Tom Price; and (F) Mt. Whaleback.

silica leaving chert free BIF (Lascelles, 2007). As silica removal occurs prior to lithification, these models solve the recurring problem of silica removal that both supergene and hypogene–supergene models must account for.

Supergene models for iron ore formation have been proposed since the beginning of the twentieth century (e.g. Leith, 1903) and have grown in prominence and support since the midtwentieth century (e.g. Macleod, 1966; Morris, 1980), though the focus of these models
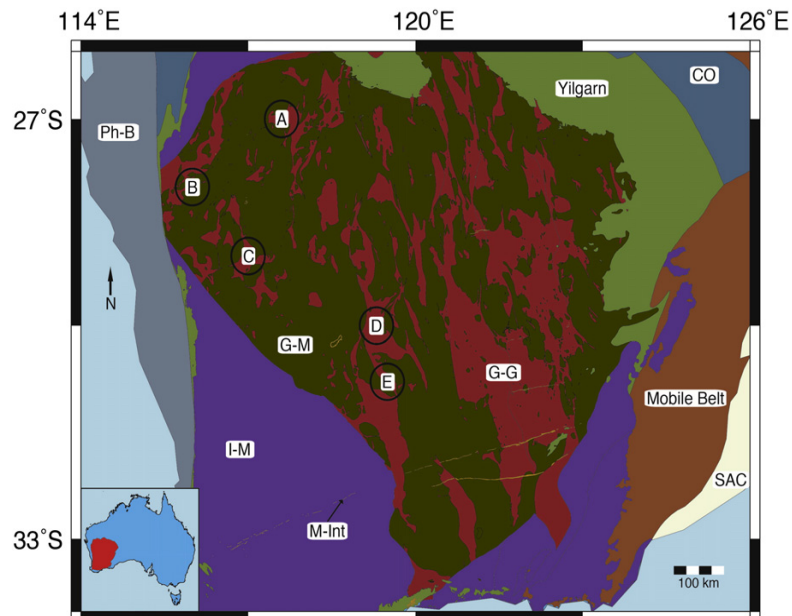
Fig. 3. Overview of key geological features in the Yilgarn Craton (excluding regolith) based on Tyler and Hocking (2007, 2008). (CO) Capricorn Orogen; (G–G) Granite–greenstone belts; (G–M) granite–mafic complexes; (I–M) igneous–metamorphic complexes; (M-Int) mafic intrusions; (Ph-B) Phanerozoic Basins; (SAC) South Australian Craton. Black circles represent some iron deposits (A) Madoonga; (B) Tallering Peak; (C) Karara; (D) Windarling; and (E) Koolyanobbing.

tends to be on Australian and North American deposits. The basis of the supergene models is that surficial processes over long periods of time have caused the enrichment of BIF through preferential leaching of silica and deposition of iron. Advancements in these models have progressed from enrichment occurring continuously over the Proterozoic and Phanerozoic (Macleod, 1966) to it exclusively occurring within shorter time intervals of weathering during the Palaeoproterozoic (Morris, 1985). These weathering events formed martite–goethite (M–G) ores, and, in small number of cases, was followed by a period of low grade metamorphism during the Proterozoic, converting the M–G to martite–microplaty hematite (M–mplH) ores with some residual goethite (Morris and Kneeshaw, 2011). Subsequent erosion during the Mesozoic and Cenozoic exposed this ore to leaching, which removed the residual goethite leaving high quality M–mplH ores (Morris and Kneeshaw, 2011).

A key problem faced by supergene models are mechanisms for removal of large amounts of silica and enrichment of iron at depths. Morris (1985) proposed the development of electrochemical cells allowing for silica at depth to be replaced with iron from the near-surface. In this case the cathode occurs within the vadose zone of the BIF, and the anode at depth, where iron is transported as the soluble Fe^{2+} but oxidised to the insoluble Fe^{3+} at the anode and then precipitated by hydrolysis. This results in an upward growing ore body, and the silica is liberated at depth and then removed via flowing aquifer systems into surface drainage (Morris and Kneeshaw, 2011). Alternatively, infiltration of high-pH, hypersaline brines have also been proposed to assist with the removal of silica, with the concentration of iron occurring through weathering and leaching of near-surface BIF and precipitation at depth (e.g. Evans et al., 2013).

Hypogene–supergene models have only recently been proposed, and have been developed based on the observation of features depictive of high temperature crystallisation as well as supergene enrichment over periods of time (e.g. Barley et al., 1999; Taylor et al., 2001). Taylor et al. (2001) outline four phases of events within the Hamersley Province, most importantly of which is an initial hydrothermal stage where large amounts of silica are stripped and removed from the BIF at depth. Later stages involve supergene processes such as oxidation of remaining iron oxides to martite and microplaty hematite, further removal of gangue material such as carbonates and finally another supergene stage concentrated the ore further with the removal of elements such as calcium and phosphorous (Taylor et al., 2001). A key, fundamental difference between these models and the supergene model are that irrespective of the ubiquity of the supergene processes, ores could only form where first they were hydrothermally altered to remove silica. Hypogene–supergene models have also been developed for deposits throughout the Yilgarn Craton, where early hypogene stages facilitate iron deposition and silica removal, and the supergene conditions occur later on and assist in enriching the ore further (e.g.Duuring and Hagemann, 2013).

The ambiguity of these models is related to a number of key points, and exacerbated by the expanse of time between the key events of formation, enrichment and present day. Primarily, a mechanism by which silica is removed from BIF in order for enrichment to occur is critical in order to explain the ore formation (Barley et al., 1999; Findlay, 1994). Secondly, the extent of deformation, weathering and metamorphism within BIF masks the primary features making it difficult to concretely determine original facies and the number of deformation or weathering events that the BIF has undergone (Klein, 2005; Lascelles, 2007). Finally, the geological controls related to iron ore genesis are important for models to encompass as they link together spatially expansive geological events with broader geological mechanisms, such as weathering, iron sources, fluid transport mechanisms and spatial and temporal constraints on iron formation (Bekker et al., 2010; Gole and Klein, 1981; James and Trendall, 1982; Klein, 2005).

3. Machine learning for mineral exploration

Machine learning is a computational method used to approach automatic classification problems involving multiple input features through learning from representative examples. Essentially, machine learning is characterised by improvement in some criteria with respect to a task over experience or exposure to examples. Its premise is that given a suitable size of data, computers should be able to determine associations and relationships, and learn from examples such that the programmer does not need to specify solutions or know the intended outcome (Alpaydin, 2010; Duda et al., 2000). This is especially important in catering for inter- and intra-class statistical variabilities that become increasingly difficult to deal with as the number of features increase. It has been used extensively in targeted marketing and the retail industry to determine buyer interests (Alpaydin, 2010), credit scoring in the bank industry to assist in risk prediction (Hand, 1998), pattern recognition for features such as facial and character (handwriting) recognition, and in the medical and biological sciences for tumour classification and biometrics.

Broadly, MLAs can be divided into two approaches, namely supervised and unsupervised learning, with both working towards a similar objective i.e. attempting to determine or exploit relationships and associations within data. Supervised learning involves data that have labels associated with it, so that the computer has a set or series of known positive and negative examples from which to learn (in the 2-class case). Unsupervised learning uses data *without* labels, and can be used to find patterns and relationships between examples within large amounts of data via methods such as clustering, density estimation (Bishop, 2006), and multivariate data projection/mapping.

Bonham-Carter (1994) has outlined two conceptual approaches to large-scale data analysis for geosciences, either empirical, data-driven approaches, or conceptual, knowledge-driven approaches. Briefly, knowledge-driven approaches are built based on human expertise, and tend to reflect established relationships between the seed points and data. Comparably, data-driven approaches tend to focus on impartially establishing objective criteria to assist in finding pertinent relationships and associations between seed points (e.g. mineral locations) and datasets. Data-driven approaches typically use MLAs such as neural networks (e.g. Brown et al., 2000; Porwal et al., 2010) or logistic regression (e.g. Chung and Agterberg, 1980) to produce target maps. The two primary concerns with data-driven methods with respect to mineral prospectivity are firstly, that the determined associations are artificial and do not actually reflect the geological relationship between the target points and the data (Carranza et al., 2008). Secondly, as mineral exploration is inherently a function of economics as well as geology, it is critical that the final result provides an acceptable trade-off between both positive and negative examples. That is, a machine learning method must achieve a high separability by reliably identifying positive targets without incurring too many false detections (i.e. areas of low prospectivity). The first concern relates to the concept of representivity, where reliance on known target examples in data is not necessarily accurate due to factors such as preservation bias. We nevertheless argue that the growth in high-resolution digital datasets and known locations is increasing the effectiveness of this approach substantially. We also argue that traditional conceptual models themselves are based on observations on known mineral formations, so the same reasoning holds for these. Manual and heuristic-based approaches are limited in their ability to cope with statistical variability, compounding further as more features/datasets are combined, and may thus be unable to discover co-associations explained therein.

We propose that the most important aspect is to utilise flexible methodologies that can be improved when new knowledge/data becomes available, and we utilise methods such as the classifier with reject option (Landgrebe et al., 2006) to cope better with problems such as poorly represented classes while at the same time capitalising on known information. The second concern is addressed via the methodology used in this

paper, where the separation of positive and negative data is the principal criterion, through training models on both target and outlier examples, and selecting a model that can encompass a complex, heterogeneous outlier class. Both concerns are also addressed, in a geoscientific framework, through ground-truthing, and by testing the classifier in regions (unseen in training) where we expect strong positive and negative responses respectively.

While MLAs have been used extensively in other fields, their application and usefulness to geoscience is lagging, with state of the art methods only recently becoming more commonplace (e.g. Cracknell and Reading, 2014). Previously, both supervised and unsupervised MLAs were used predominantly for land and vegetation classification, and mapping using Landsat and remote imaging (e.g. Huang et al., 2002; Rogan et al., 2008; Wulder et al., 2004). However, increases in available data, computational power increases, and availability of new algorithms are creating opportunities for application to more complex problems.

Groves et al. (2000) explored numerical modelling of stress mapping to predict locations of gold throughout the Yilgarn. They used a knowledge driven approach that does not require a training set of known gold locations, rather using expert knowledge on the timing of gold formation and its relationship to strain and stress regimes to determine areas of higher prospectivity. Similarly, shape analyses of geological data were used by Gardoll et al. (2000) for prediction of gold deposits in the Kalgoorlie Terrane. Their approach followed the assumption that gold deposits typically exhibit specific and identifiable geological structures, allowing for reliable detection through pattern recognition. A classification stage was also incorporated into their work by comparing geometries to a known gold deposit in order to assist with accurate prediction. Comparably, Holden et al. (2008, 2012) used a data-driven approach by developing an automated image processing technique using pattern recognition for predicting the location of gold deposits throughout the Yilgarn Craton in Western Australia and the Superior Craton in Canada. By training an algorithm on linear features present within an aeromagnetic dataset, they removed the need for knowing both the detailed geology of a target area, and a detailed model of formation, rather automatically exploiting unlabelled geophysical data. A data driven approach using support vector machines was undertaken by Abedi et al. (2012) for multiclass prediction of boreholes drilled into porphyry copper deposits on a local scale in the Kerman Province in Iran. Their approach involved a synthesis of geological, geophysical and geochemical data and was used to help identify areas for further drilling.

More recently, a number of studies have begun exploring a range of methods by which machine learning techniques can be applied to geological problems. Carranza et al. (2014) used evidential belief functions for predictive mapping of orogenic gold in the Giyani greenstone belt (GGB). Their approach determined relationships between local geological data and spatially coherent deposit occurrences to determine the percent of the GGB that is prospective for orogenic gold. Comparably, Porwal et al. (2014) used a knowledge driven approach employing fuzzy inference systems for uranium exploration in the Yeelirrie area (Western Australia). Their methodology involved establishing a series of expert fuzzy-"if" rules governing the relationship between uranium occurrence and geological and geophysical data for determining uranium prospectivity. Additionally, Andrada de Palomera et al. (2014) used a weights-of-evidence approach for gold–silver deposits in Argentina at both regional and district scales. Their approach encompassed data such as clay alteration, ASTER and lineament densities, and indicated the importance of high resolution data at smaller scales for generating more accurate prospectivity maps.

A data-mining approach to mineral exploration has become more widely used over the past few years. This approach is more useful for resources or areas of land for which little is known, as this makes it implausible to use a knowledge-driven model. For either case, large datasets are used in association with known deposits to find

commonality (Tan et al., 2006) either spatially (Merdith et al., 2013) or temporally (Landgrebe et al., 2013). The commonality is then used to define a model of exploration and typically produce a prospectivity map of a target area (e.g. Carranza, 2011; Cracknell et al., 2013; Merdith et al., 2013).

4. Data and methodology

Our method takes a holistic approach to mineral exploration and adopts a multivariate, data-driven methodology using supervised MLAs. Our analysis uses twelve features calculated from six different geophysical datasets, and is flexible such that a user can choose to add or remove features that they deem important (e.g. distance to fault, degree of weathering, filtered magnetic data, shape analysis, shear and stress mapping etc.). This is to allow for the appropriation of the methodology to a wide array of minerals, such as by using shape analysis for gold exploration, and also to other geographical locations where access to some data may not be possible. The basis of the approach is to achieve good generalisation i.e. high accuracy not only on data used in training, but also on new unseen data. As such, the approach lends itself to large-scale analysis (on the order of 1000 km) for potential mineral deposits.

An important consideration is the need to protect against unseen or unsampled (non-target) classes, as even though the classifier may be trained on data that represents a target class (i.e. mineral deposits) well, it may be difficult to sample the non-targets in a representative fashion since it is highly heterogeneous (Landgrebe et al., 2006). We argue that posing the classification problem in this fashion suits the imprecise nature of geological data, where the notion of representivity has practical limitations. Consequently, our selected MLA for this study (a mixture of Gaussians with distance-based reject option classifier preceded by principal component analysis) seeks to minimise the impact that an unseen class may have during testing and classification by utilising a dual-thresholding approach for the purposes of discrimination (against known data) and rejection (against unseen data) respectively. This strategy of using dual thresholding of both the classifier outputs, and the domain occupied by each class results in a unique feature in which examples either far from the classifier decision boundary, or outside the region enclosed by the rejection threshold are rejected (Landgrebe et al., 2006). Such a strategy was first proposed by Dubuisson and Masson (1993) by introducing a distance-based reject option, which allows for explicit classification rejection for problems wherein some data falls outside the domain in feature space occupied by training samples. This is built upon the reject option first introduced by Chow (1970), but in that case, classified samples with insufficient confidence regarding class membership were rejected. Thus a safeguard was introduced to reduce misclassifications by allowing for the rejection of ambiguous data, rather than forcing a classification decision.

McLachlan and Basford (1987) outline the usefulness of mixture models for classifying or clustering multivariate data, with particular relevance to the geophysical datasets used in this study, exhibiting substantial variability. Typically a single Gaussian is unable to fully capture and describe the distribution of 'real' datasets (Bishop, 2006), but this can be overcome by incorporating a superposition of two (or more) Gaussians, allowing more complex data distributions to be approximated. As this is a less common technique for geosciences, we compare our result with a baseline classifier, a support vector machine (Vapnik, 1995). Subsequent to establishing the base classifier, we implement the distance-based reject option, thereby highlighting the importance of closing the feature space.

Recently Cracknell and Reading (2014) applied an ensemble Random Forest classifier to tackle a high dimensional, multi-class (eight classes) scenario over a small geographical area, well suited for an ensemble classifier such as Random Forests. Conversely, our scenario is only a two-class problem and has much lower dimensionality (12 dimensions) with emphasis on recognising unseen outlier classes over a large geographical area. Our experimentation involving several

classification models were returning high results (80–90% classification accuracies) with little differences between competing classifiers, indicating that we were successfully exploiting all available discriminatory information. If we were to include other features or classes (e.g. discriminate between Algoma and Superior type deposits) that increase dimensionality, then an ensemble classifier (e.g. Random Forests) could become a more effective choice. We note that we have preferred the use of density-based classifiers rather than a discriminant classifier so that the known target data domain is preserved and rejection of unknown outlier data can be performed in a more optimal fashion.

Here we use iron ore as a case study to highlight the ease and usefulness of our chosen methodology for mineral exploration. Two key underlying assumptions of this approach are that firstly each dataset being used is independent and represents a discrete class of information about iron ore. Secondly, we assume that a geophysical characterisation of the location of iron ore deposits can be determined by a unique combination of geophysical features. Due to the predominance of iron ore being found in Western Australia, as well as computational demands, we restricted the area of study to Western Australia, though it can be easily adapted to analyse other areas. Finally, Australia presents itself as a unique and useful case study for any analysis on mineral location and prospectivity, especially considering that high quality data is made publicly available. Australia is well endowed with natural deposits, and is the only example of a country occupying the entire extent of a tectonic plate, allowing for continuous datasets that characterise the entire continental crust of a tectonic plate in high resolution.

4.1. Dataset and feature selection

As the purpose of this investigation is province-scale, greenfield reconnaissance exploration, we suggest that using as many (potentially) pertinent datasets as possible is advantageous in order to maximise discriminatory information, with the notion that each dataset may contain independent information. As such we focus on developing an algorithm that generalises well for use in large target areas, while being mindful of computational limitations. We utilise six geophysical datasets that are available with relatively high coverage and resolution, namely gravity, magnetics, topography and radiometric signal (3-band), to create an algorithm to predict iron ore occurrence that generalises well across large spatial distances and across a variety of different types of iron deposits (Table 1).

Traditionally geophysics has not been used extensively in iron ore exploration within Australia due to the ease of finding deposits, as iron ore (especially in the Pilbara) tends to be found in continuous to semi-continuous formations that can be followed from outcrops and correlated over large distances (Dentith et al., 1994). Specifically, Dentith et al. (1994) outlines that the two primary uses of geophysics in iron ore exploration are aeromagnetic surveys, which are used to confirm stratigraphic and structural controls on mineralisation, and gamma ray logging of boreholes for correlation of shale layers within the BIF. Gravity surveys have started to be used relatively recently to assist with identifying different ore types on a local-scale based on density contrasts between the ores and surrounding rock, with BHP Billiton using self organising maps to help distinguish ores in the Pilbara using an amalgamation of

magnetic and gravity data (Mahanta, 2015). There is a correlation between ridges and outcropping ore bodies (e.g. Morris, 1985) on the basis that iron ore is more weathering-resistant relative to the surrounding rock, suggesting that present day topography could be a proxy for iron ore formation. Dauth (1997) suggests that the regolith regimes of the Yilgarn Craton have typical and identifiable radiometric signatures that can be determined. Additionally, considering the well-established relationship of Yilgarn and non-Hamersley Pilbara iron ore deposits with mafic greenstone belts (Angerer and Hagemann, 2010; Huston and Logan, 2004) we suggest that there may be some relevant discriminatory information contained within the radiometric data, through the determination of a signal for non-iron ore deposits (i.e. assisting in determining where regolith is and is not). We test this by omitting radiometric data from the classification chains and comparing the results to the chains where it is included.

The features that we have extracted from the data for use in the classification chain are mean and contrast-ratio (i.e. local deviation of the data) from a predefined area (1 km and 4 km respectively) around each sample point. Both mean and contrast-ratio were chosen due to the spatial size of iron ore deposits in Western Australia, with sizes ranging between 100s and 1000s of metres in length, width and depth (Angerer and Hagemann, 2010). We expect simple features to result in the most robust representation of these deposits at a coarse resolution on a broad, provincial scale, thus avoiding over-sensitivity brought about by more complex features adapting to local geographic patterns. Importantly, both features are indicative of the present day relationship between iron ore and the geophysical datasets, rather than a reflection or recording of their depositional setting, original mineralogy or enrichment over time. This is either through enrichment (e.g. mineralogical end members reflected in magnetics and gravity) or products of recent geological history and events (e.g. surficial weathering and erosion of regolith and iron formations reflected in topography and radiometrics).

The advantage of our approach is that by using large datasets across spatially large areas we can draw more robust statistical conclusions about the commodity being investigated. A drawback of our approach is that while we generalise across large areas well (i.e. Western Australia), our algorithm is not adapted for local geology. Therefore, it is important to stress that we do not necessarily propose using the same datasets and features for finer detail exploration on regional to local-scales. We would however advocate using a similar methodology, but suggest greater differentiation in sample selection coupled with a more precise selection of data and features that are pertinent to the specific deposit types in question and the surrounding geology that is being analysed. For example, a user investigating regional-scale exploration within a greenstone belt would benefit from a sample selection of target/outlier points only occurring within greenstone belts (i.e. only Algoma-type deposits), and the prerogative to remove radiometric and topography data but include ASTER and geochemical data instead.

4.2. Model building

To ensure the robustness of our model we make use of a robust statistical methodology for training and validation (Fig. 4). Firstly, our classification chain incorporates randomised hold-out to ensure that testing data are independent from training data, while simultaneously revealing the stability of the classifiers (i.e. variance or stability). Secondly, known ground-truth data are used to ensure that our model can correctly identify cases of iron ore and also identify cases of non-iron ore. The validation was carried out by selecting two areas of Western Australia with which the algorithm could be applied, i.e. the Pilbara in the northwest of the state, known for its richness of iron ore deposits, and the Yeelirrie, an iron-poor area in central Western Australia (Fig. 5). The success of the classification model is based on its ability to satisfy these ground-truth predictions, such that the Pilbara would satisfy the model's ability to predict iron ore, and the Yeelirrie to predict the absence of iron ore. Finally, we compare the results by overlaying

Table 1
List of geophysical datasets used with their resolution and reference. All datasets were acquired freely from Geoscience Australia.

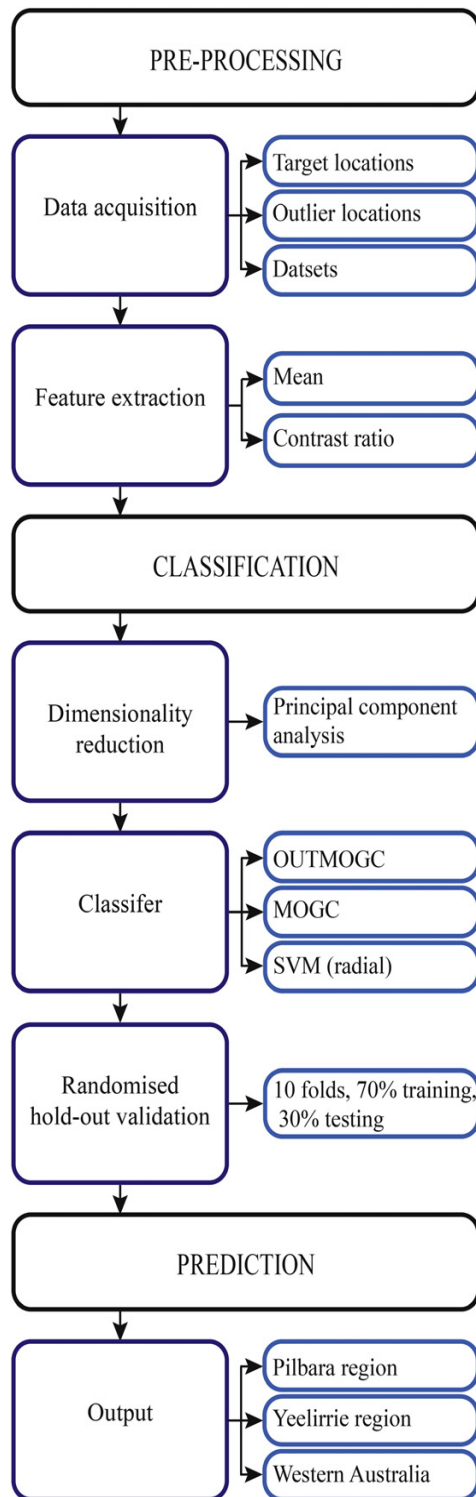| Dataset	Resolution	Reference
Bouguer gravity	800 m	Bacchin et al. (2008)
Magnetic anomaly	80 m	Milligan and Franklin (2010)
Topography	250 m	Hutchinson et al. (2006)
Radiometric — potassium	100 m	Minty et al. (2010)
Radiometric — thorium	100 m	Minty et al. (2010)
Radiometric — uranium	100 m	Minty et al. (2010)

Fig. 4. Scheme of methodology using iron ore and geophysical data in Australia. The method could be applied to any mineral deposit in association with any geological data. Additionally, different features can be extracted and other classification tools can be used depending on what commodity is being targeted. Classifiers tested include a mixture of Gaussians with reject option (OUTMOGC), a mixture of Gaussians (MOGC) and support vector machine (SVM).

an independent dataset of 42 known iron ore camps (five sites occur out of range of data) that were not used in any stage of the classification chain (Ewers et al., 2001).

4.3. Pre-processing

For this study, the OZMIN Mineral Deposits Database (Ewers et al., 2002) was used to find locations of commodities within Australia. Selecting iron ore as our case study, a training set comprising 37 iron ore locations throughout Western Australia was used for the analysis (these points are referred to as the 'target' for the classification model). The OZMIN dataset does not differentiate the type or mineralogy of the deposits; therefore we used all 37 available locations, of which 36 are found within the Pilbara Craton, and one being located in the Yilgarn Craton (Fig. 5).

The rationale for this decision and not separating them based on deposit type is firstly the scope of this experiment, which is to design a classification chain that generalises well for iron ore, rather than trying to identify unique deposits (which would be more appropriate for regional–local scale exploration). Secondly, as discussed above, the features being extracted are not necessarily characteristic of either the deposition of iron formation or early stages of its enrichment, but rather they characterise present day signatures. This is also evident by broad similarities in ore mineralogy for deposits throughout both cratons (e.g. dominance of hematite/martite as the end member of iron ore enrichment (Cooper, 2013a,b; Greentree and Lord, 2007)). The classification reject threshold was set such that the most outer 5% of target is excluded, which results in a good compromise between classification and rejection performance.

The non-target data used for classifier model training and validation involved the random selection of 1000 locations throughout Western Australia (though these were filtered down to 590 random locations due to incomplete geophysical data in some locations). These locations are referred to as 'outliers' for the classification-chain, that is they provide an indication of non-iron ore locations that are used to train the classifier to distinguish iron ore from non-iron ore. We follow two criteria outlined in Carranza et al. (2008), i.e. that outlier points are randomly generated, and they must have values for all data being used in the feature vector. A third criteria, i.e. that sampled data points must not lie in the vicinity of the target locations is not necessary to enforce where the number of outliers far exceeds targets, since the statistical classifiers aim to develop models that represent the entire population of data. Note that our approach results in a significant imbalance between the abundance of outlier and target points. Addressing the effects due to this class skew can be achieved using ROC analysis (Metz, 1978), in which the classification thresholds are shifted in accordance with desired error trade-offs (i.e. false positives and false negatives). In this way we can make use of all the target data available and ensure that non-targets are sampled very broadly without introducing artificial techniques such as super sampling or noise generation, with the emphasis of making use of available data.

Two features were extracted from the geophysical data at each sample location (both iron ore and random location); mean and contrast ratio (80th percentile pixel divided by 20th percentile pixel to give an indication of gradient in the data). To determine the mean value of a geophysical dataset at single point locations, a circle of radius of 1 km was constructed around the point and the mean of all the values within this circle was taken. This was to ensure that the extracted values were not over-sensitive to individual data spikes or noise, but rather were more representative of the area from which they were taken. For the contrast ratio, a larger circle, with a radius of 4 km, was used to ensure that any proximity to a geophysical boundary that was present would be included. Furthermore, as the locations are simple 2D points while mineral deposits occur within a spatial 3D framework, by using the radius around each point we are able to extract a more representative characterisation of an actual ore deposit. The features that were extracted from each sample location (both target and outlier) were stored in a 12-dimensional feature vector for classification.
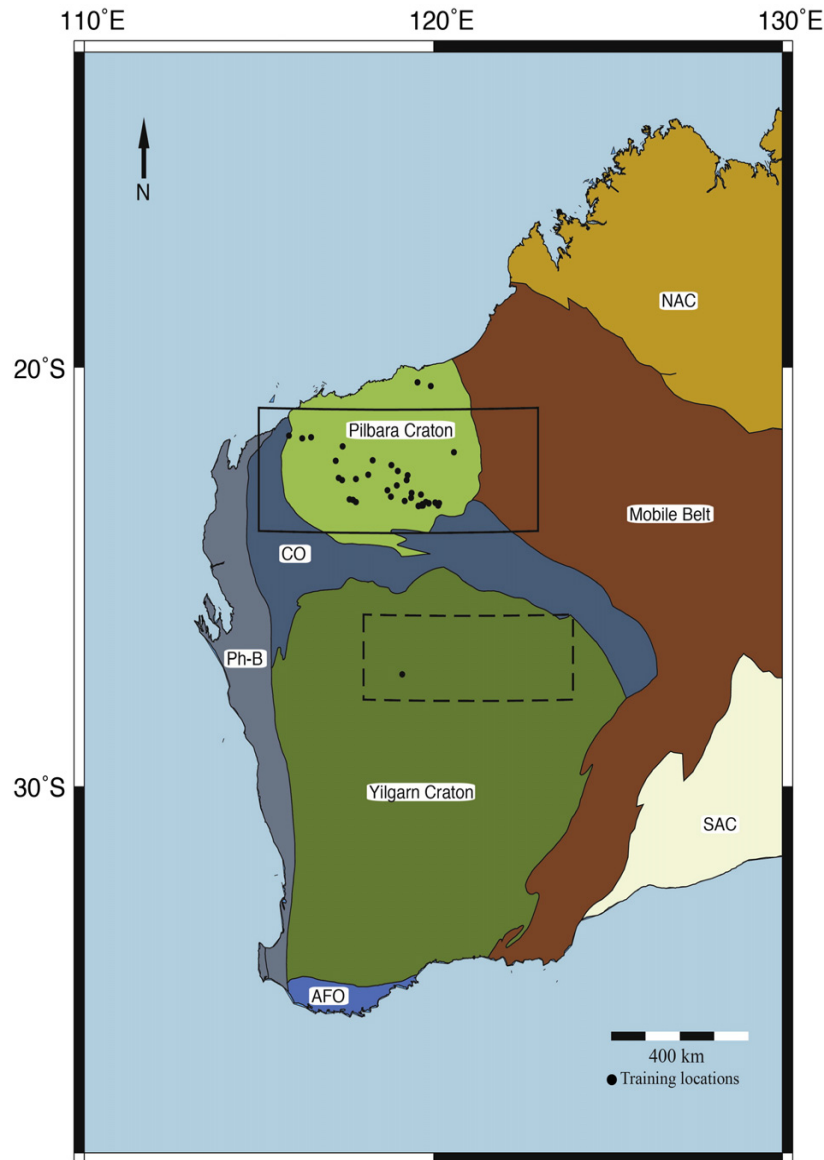
Fig. 5. Map of Western Australia showing geological provinces (see Fig. 1 for key), ground truth areas and the training locations of iron ore used for construction of the classifier. The two boxes indicate the extent of our analyses that were used for ground truth validation. The solid line box represents the Pilbara, known for its richness in iron deposits, while the dashed line box represents the Yeelirrie, an iron-poor region in the Yilgarn Craton.

4.4. Classification

There were three key stages of operation performed in the training and testing of our model. Firstly, dimensionality reduction algorithms, such as principal component analysis (PCA), were used to reduce the dimensionality to better cope with redundant correlated data while maximising variability (Jolliffe, 2002). Secondly, we tested three different classification algorithms to determine which returned the best result. All classification tools that were used are from the freely available PRTools (Duin et al., 2007) and DD_tools (Tax, 2014) libraries for Matlab. We selected a mixture of Gaussian distribution with reject option classifier (OUTMOGC) for this classification, though we compared the results with other classifiers, in particular, support vector machines (SVM) and a mixture of Gaussian classifier (MOGC). Finally, for each classification chain, the data underwent a 10-fold randomised hold-out (70% training, 30% testing) in order to assess accuracy and ensure that our classification scheme and choice of classifier was robust. We optimised each classifier by varying key parameters, such as number of Gaussians per class, and the sigmoid, 'r', for the SVM. Additionally, for each of the Gaussian classification chains we varied the degree of dimensionality reduction through PCA to between two and five dimensions (i.e. projecting down from 12D to 2–5D). Note that we also investigated other dimensionality reduction techniques such as the Fisher discrimination, with poor results. Finally, in order to investigate the value of the radiometric data, we also ran the same classification chains but omitting the radiometric features, using instead just the mean and gradient values of gravity, magnetics and topography.

Importantly, the flexibility of this methodology allows a user to optimise the various parameters to compare between the abilities of models to successfully classify a target, and then pick the most appropriate classifier and parameters for the commodity being targeted.

4.5. Prediction

Once the final classification chain has been selected, the classifier is trained using all available training data, and applied to the areas of

147

interest by computing the probability of iron ore occurring at each pixel. Instead of forcing a classification decision, the "soft" classifier outputs (these are posterior probabilities for density based classifiers) for each location are used. For effective visualisation we converted these classifier outputs into a predictive confidence map by data scaling, thus depicting the fit to the classification model as a proxy to the likelihood of iron ore occurring. For this case study the trained classifier chain was applied to the Pilbara and Yeelirrie regions to test our ground-truth predictions (Figs. 6 and 7) and determine the success of our model. Once satisfied that the model correctly identifies both target and outlier classes, it was applied to a larger area for explorative purposes. In this case, it was applied to the entirety of Western Australia. Computational time using Matlab was 24 h on a personal laptop with a 2.6 GHz Intel Core i7 processor for ~2.2 million computations. Use of computational parallelisation computers will allow for larger, continental scale analysis in shorter times.

5. Results

5.1. Classifier results

A selection of results from the classification chains of the various classifiers is in Table 2 (for a full table of results, including other classifiers, see Supplementary material). The mixture of Gaussians with reject option (two Gaussians permitted for target and two for outlier) coupled with a PCA projection to 4 dimensions (D) was the best performing classifier, successfully identifying 87.6% of target locations and 92.7% of outlier locations, with a standard deviation of 2.6% and 7.2% respectively (9.8% mean class-weighted error rate). This is an improvement of 4% (based on error rate) over the next most effective classifier (MOGC, one Gaussian, PCA to 5D), which achieved 97.8% for target locations and 74.5% for outlier locations (standard deviations of 1.3% and 8.6% respectively) with 13.8% error rate. Comparably, the highest performance of the SVM using a radial-basis kernel ($r = 9.1$) was substantially lower, with 98.6% for target and 68.2% for outlier (standard deviations of 0.8% and 7.7% respectively) with a 16.6% error rate.

5.2. Omitting the six radiometric features

The results of the best performance of each classification chain by omitting the radiometric features are highlighted in Table 2. The mixture of Gaussians with reject option (two Gaussians for target and outlier, PCA to 4D) was the once again the most successful classifier, obtaining the same results when omitting the radiometric features as when they are included (87.6% and 92.7% success for target and outlier respectively). The mixture of Gaussians performed highest when optimised with two Gaussians coupled with PCA to 3D, achieving 97.3% on target and 70.9% on outlier (standard deviation of 1.3% and 12.7% respectively). This resulted in a classification error rate of 15.9% (compared to 9.8% achieved with the radiometric features included). The SVM was optimised with $r = 9.0$ achieving 98.5% on target and 65.5% on outlier (standard deviation of 0.9% and 8.4% respectively) and 18.0% error.

5.3. Predictive confidence maps

Our classification model indicates areas of high and low prospectivity of iron ore throughout Western Australia. Figs. 6 and 7 depict the results in the Pilbara Craton and Yeelirrie region, respectively. The Pilbara Craton (Fig. 6) is dominated by a thick band (~400 km long and ~150 km wide) of elevated prospectivity that trends northwest to southeast, and is easily identifiable as corresponding to the Mount Bruce Supergroup. Within this band there are a number of thin lineaments (~10 km wide and ~40–100 km long) of extremely high prospectivity. Additionally, there are a number of smaller features that depict an elevated and extremely high probability of iron ore. These are found predominantly in the central northern area of the Pilbara region. Further east than ~121°E the area is dominated by low probability of iron ore occurring, though there are a few smaller 'islands' of higher probability (e.g. at 22.75°S, 123°E). Comparably, the Yeelirrie region (Fig. 7) is dominated by low probability for iron ore with small islands (trending north–south) of higher probability occurring throughout the entire region.

The final output of the classification model is an application of the algorithm to the entirety of Western Australia for greenfield and first order, province-scale reconnaissance exploration (Fig. 8). Outside both the Pilbara and Yeelirrie regions, the majority of Western Australia has a low probability of iron ore, though there are notable areas of higher probability. There are a number of areas throughout the Yilgarn Craton (~25–30°S, 115–120°E) that have high probability, as well further south on the southern coast (~32.5–35°S) amongst the Albany-Fraser Orogen.
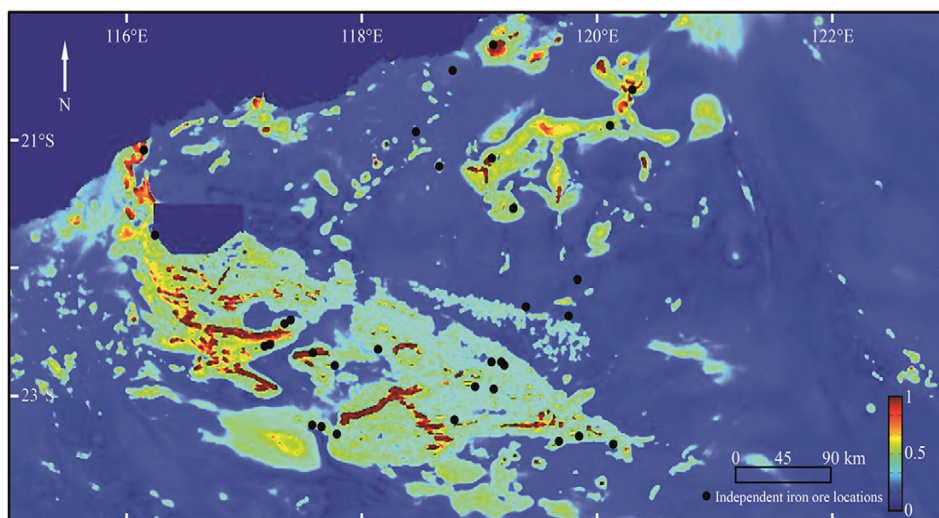

Fig. 6. The output from the trained model for the Pilbara region as a predictive confidence map depicting probability of iron ore occurrence. The independent iron ore locations (Ewers et al., 2001) have not been used in any stage of the model. As predicted by observations, large areas in the Pilbara Craton are highly probable for iron ore, indicating that our classifier can successfully distinguish positive examples.
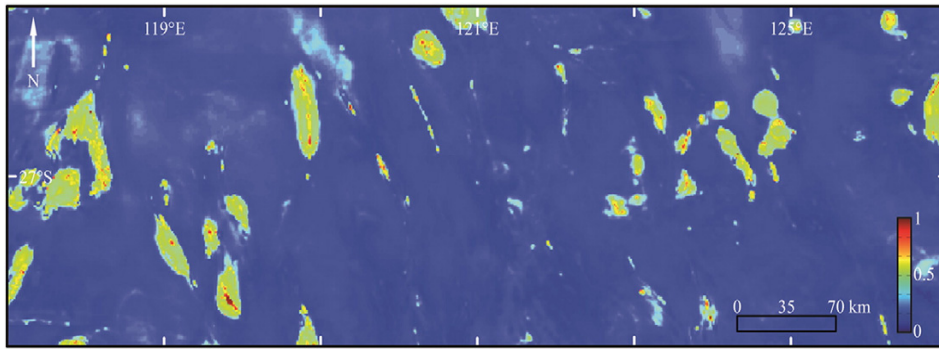
Fig. 7. The output from the trained model for the Yeelirrie region as a predictive confidence map depicting probability of iron ore occurrence. As predicted by observations, the Yeelirrie region is predominantly dull, indicating that our classifier can successfully find negative examples.

5.4. Areas of high prospectivity

In order to highlight potential areas for exploration the confidence map is bracketed into 15 intervals based on the calculated probability of iron ore occurring at each individual pixel, thus allowing for sufficiently fine resolution to identify key areas. This facilitates ranking and isolating areas of Western Australia based on their expected iron ore occurrence by depicting the areas of highest through to lowest prospectivity. Divisions 1–14 contain the same number of points (88,520 points, or ~7.04% of the total area), while the final division, division 15, contains 18,795 points, or ~1.49% of the total area and represents the areas of highest confidence as predicted by the classifier. Fig. 9 depicts the division of Western Australia into the 15 intervals, with Fig. 9a–e showing Western Australia divided into selection of three intervals and Fig. 9f showing all the divisions. The areas of lowest confidence of iron ore (Fig. 9a, intervals 1–3, and 9b, intervals 4–6) are typically concentrated around the Proterozoic mobile belts towards the east of the Pilbara Craton in the north, and large areas of the central Yilgarn Craton in the south. The areas of medium confidence (Fig. 9c, intervals 7–9) occur throughout the Capricorn and Albany-Fraser Orogeny as well towards the periphery of the Pilbara.

Finally, the areas of highest confidence (Fig. 9d, intervals 10–12, and 9e, intervals 13–15) are reserved for the bulk of the Hamersley Group in the Pilbara Craton, with a number of areas scattered throughout the central-western area of the Yilgarn Craton.

6. Discussion

6.1. Classification chains

The best performing classifier chain used the mixture of Gaussian classifier with reject option. By comparing the results of the mixture of Gaussian classifiers we can determine the usefulness of the reject option (i.e. dual thresholding and closing the 'feature space'). Overall, there is an 18% improvement between the MOGC and OUTMOGC for predicting outlier locations, indicating that by closing the feature-space around the target locations is a very effective strategy for dealing with the poorly defined non-target class. This is of paramount importance for the mineral exploration industry, helping to establish more selective prospectivity maps, thus lowering the risk associated with the early stages of an exploration project and providing confidence

Table 2

Selection of results for various classification chains using the mixture of Gaussians classifier (MOGC), outlier mixture of Gaussians with reject option classifier (OUTMOGC) and support vector machine classifier (SVM). Principal component analysis (PCA) was varied for both the MOGC and OUTMOGC and not used for the SVM. The brackets after the MOGC and OUTMOGC indicate the number of Gaussians used to describe the data; in the case of OUTMOGC they are read as number of Gaussians to describe [target outlier]. Results for all classifiers are read as [true positive, false positive] in the top row and [false negative, true negative] in the bottom row. The standard deviations (SD) of each result are indicated underneath, respectively. Best performing results are in bold type.

| PCA		2		2		3		3		4		4		5		5	
		12 features		6 features (grav/mag/topo)		12 features		6 features (grav/mag/topo)		12 features		6 features (grav/mag/topo)		12 features		6 features (grav/mag/topo)	
MOGC [1]	Results	0.987	0.013	0.9831	0.0169	0.9836	0.0164	0.9695	0.0305	0.9836	0.0164	0.9672	0.0328	**0.978**	**0.022**	0.9582	0.0418
		0.4091	0.5909	0.3818	0.6182	0.3727	0.6273	0.3455	0.6545	0.3364	0.6636	0.2909	0.7091	**0.2545**	**0.7455**	0.2727	0.7273
	SD	0.0084	0.0084	0.0096	0.0096	0.0094	0.0094	0.0205	0.0205	0.0068	0.0068	0.0213	0.0213	0.0128	0.0128	0.0241	0.0241
		0.0773	0.0773	0.0835	0.0835	0.0671	0.0671	0.0939	0.0939	0.1054	0.1054	0.1118	0.1118	0.0862	0.0862	0.1134	0.1134
MOGC [2]	Results	0.9881	0.0119	0.9763	0.0237	0.987	0.013	**0.9729**	**0.0271**	0.9864	0.0136	0.9582	0.0418	0.9802	0.0198	0.9537	0.0463
		0.4273	0.5727	0.3909	0.6091	0.4364	0.5636	**0.2909**	**0.7091**	0.3455	0.6545	0.2818	0.7182	0.3273	0.6727	0.3	0.7
	SD	0.0073	0.0073	0.0145	0.0145	0.0083	0.0083	0.0133	0.0133	0.0081	0.0081	0.0261	0.0261	0.0115	0.0115	0.0289	0.0289
		0.0748	0.0748	0.0862	0.0862	0.0717	0.0717	0.1271	0.1271	0.1342	0.1342	0.1317	0.1317	0.1926	0.1926	0.0862	0.0862
OUTMOGC [2 2]	Results	0.8503	0.1497	0.8503	0.1497	0.8746	0.1254	0.8746	0.1254	**0.8757**	**0.1243**	**0.8757**	**0.1243**	0.8559	0.1441	0.8554	0.1446
		0.1	0.9	0.1	0.9	0.0909	0.9091	0.0909	0.9091	**0.0727**	**0.9273**	**0.0727**	**0.9273**	0.0909	0.9091	0.0909	0.9091
	SD	0.0259	0.0259	0.0259	0.0259	0.0194	0.0194	0.0194	0.0194	0.0257	0.0257	0.0257	0.0257	0.0304	0.0304	0.0306	0.0306
		0.0671	0.0671	0.0671	0.0671	0.0606	0.0606	0.0606	0.0606	0.0717	0.0717	0.0717	0.0717	0.0606	0.0606	0.0606	0.0606
Radial parameter		r8.9				r9				r9.1				r9.2			
SVM (radial)	Results	0.9853	0.0147	**0.9853**	**0.0147**	0.9836	0.0164	**0.9853**	**0.0147**	**0.9864**	**0.0136**	0.9853	0.0147	0.9853	0.0147	0.9876	0.0124
		0.3273	0.6727	**0.3545**	**0.6455**	0.3182	0.6818	**0.3455**	**0.6545**	**0.3182**	**0.6818**	0.4273	0.5727	0.3273	0.6727	0.4636	0.5364
	SD	0.0076	0.0076	0.0089	0.0089	0.0094	0.0094	0.0089	0.0089	0.0085	0.0085	0.0085	0.0085	0.0089	0.0089	0.0052	0.0052
		0.0977	0.0977	0.1	0.1	0.0982	0.0982	0.0835	0.0835	0.0773	0.0773	0.1821	0.1821	0.0977	0.0977	0.145	0.145
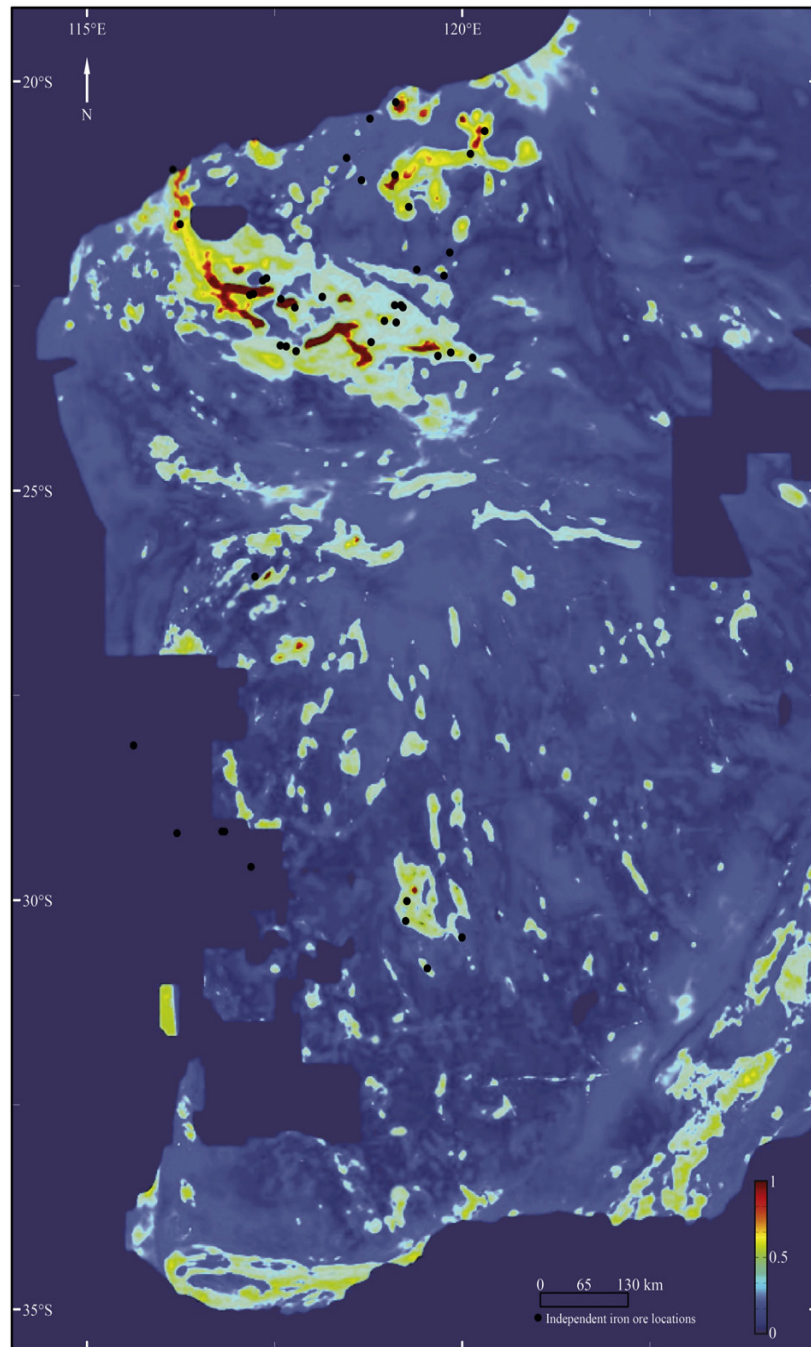
Fig. 8. The output from the trained model for Western Australia. The independent iron ore locations (Ewers et al., 2001) have not been used in any stage of the model. Due to some of the geophysical datasets being incomplete, some areas have not been computed.

that the final map accurately portrays areas of both high and low prospectivity for the targeted mineral. The mixture of Gaussian classifier also substantially outperforms SVM for this application, attributed to the large degree of variability and class overlap exhibited by the chosen features. These are clearly modelled well using the mixture model algorithm, which is a density-based approach (i.e. places more emphasis on regions in feature space with more abundant data), as opposed to SVM which is discriminative (focusing on data on the overlap region only). We note that increasing the dimensionality by selecting more features such as through including geochemical or geological data could improve the performance of the SVM relative to both the MOGC and OUTMOGC.

6.2. Value of radiometric data

The comparison between the 12 feature classification chains (where radiometric data was included) and six feature chains (where it was omitted) shows no improvement in our best performing classifier, OUTMOGC, and a 4–5% improvement in performance for the 12 feature classification chains using both the MOGC and SVM classifier. This suggests that there is no benefit in including radiometric data for provincial-scale iron ore exploration, though some lesser overall performance classifiers may see some improvement and demonstrates that redundant features can be incorporated within the workflow without loss of classification performance. This indicates that, assuming
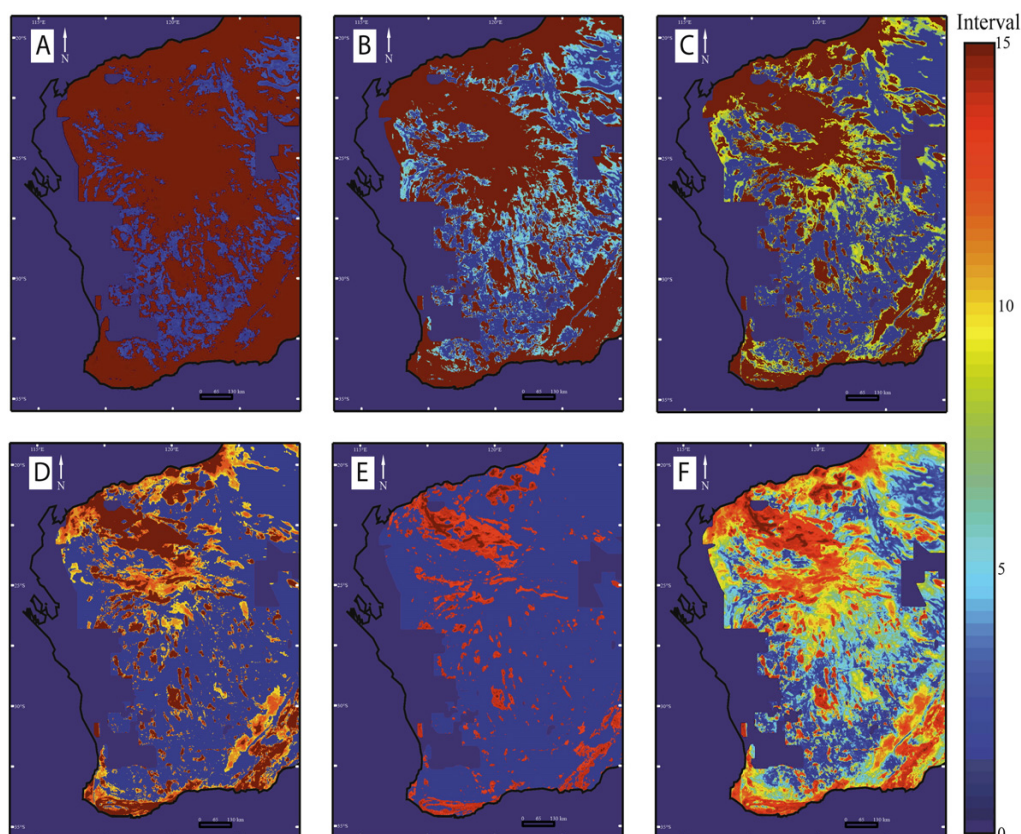
Fig. 9. Predictive confidence map for Western Australia using bracketed intervals based on the probability of a pixel to contain iron ore; (A) intervals 1–3 (lowest probability, 0–21.1%); (B) intervals 4–6 (low probability, 21.1–42.2%); (C) intervals 7–9 (medium probability, 42.2–63.3%); (D) intervals 10–12 (high probability, 63.3–84.4%); (E) intervals 13–15 (highest probability, 84.4–100%), and; (F) all intervals. The dull blue colour (interval 0) represents areas where there is no geophysical data.

computational cost is minimal, a user faced with a decision of whether or not to include a dataset in an analysis (i.e. unsure on whether a dataset contains useful discriminatory information) can include the data to maximise potentially useful discriminatory information without risking a decrease in the classification ability.

6.3. Exploration for iron ore

It is apparent from our results that our classifier has successfully distinguished a number of known iron ore deposits throughout Western Australia. Within a mineral exploration framework, the focus of our results is on their predictive success i.e. their generalisation performance, how confident we are that what we predict as iron ore is actually iron ore, such that we can trust it to accurately predict potential areas for further exploration. The success of our methodology is based on its ability to satisfy two criteria. Firstly, the satisfaction of our ground-truth hypotheses that the Pilbara is iron rich and Yeelirrie iron poor; and, secondly, that it can accurately predict the locations of existing deposits that it wasn't explicitly trained on. The first criteria establishes the veracity of our classifier's ability to recognise both iron ore and non-iron ore cases and should give an indication as to whether the algorithm is using artefacts or meaningful associations, while the second criteria builds confidence in its ability to predict in unseen areas.

The predictive confidence maps of the Pilbara and Yeelirrie regions (Figs. 6 and 7) demonstrate that our classifier is capable of distinguishing both iron ore and non-iron ore, satisfying the first criteria. The Pilbara Craton (Fig. 6) is relatively bright, showing large areas of elevated probability of iron ore. Comparably, the Yeelirrie region (Fig. 7) is relatively dull, with a few small islands of higher probability.

The results for the entire of Western Australia (Fig. 8) show an abundance of highly prospective areas throughout the Yilgarn Craton. Comparisons of our map to published maps of both areas (Cooper, 2013a, 2013b) indicate a notable similarity between areas of high probability of iron ore and already established iron ore mines, satisfying the second criteria. In the Yilgarn Craton our map correctly identifies most key iron ore localities (Fig. 10), though it misses the Tallering Peak, Karara and Extension Hill Hematite mines due to incomplete geophysical data, causing them to be omitted from the analysis. The map also suggests some new areas for greenfield exploration such as a series of narrow E–W ridges at 25°S, an area near the Twin Peaks mine, around 27°S, 116.4°E, and a few small areas around the Steeple Hill mine in the southeast of the Yilgarn Craton.

Outside the Hamersley Basin in the Pilbara region, the Marble Bar area stands outs as an area of high prospectivity, specifically a thin ridge between the current mines of Abydos and Spinifex Ridge, located between 119 and 120°E and at about 21°S. Additionally, further north along the coastline there is a distinct area of higher probability of iron ore (~20°S, 119–121°E) as well as a number of small, scattered areas just north of the Hamersley Basin (21–21.5°S, 118°E).

Our classifier is trained predominantly on iron ore deposits from the Pilbara region, which are typically volcano-sedimentary rocks, yet it successfully detects iron ore found throughout the Yilgarn Craton, which tends to host iron ore in mafic-greenstone belts. Additionally, our classifier successfully picks up all styles of mineralisation, including: supergene enriched hematite and hematite–goethite; primary banded-iron formation deposits (magnetite); stratabound clastic-hosted deposits (both supergene enriched and magnetite); and, orthomagnetic layered mafic intrusives (Fe and V–Ti). The near universality of iron ore (determined both by present mineralogy and depositional setting)
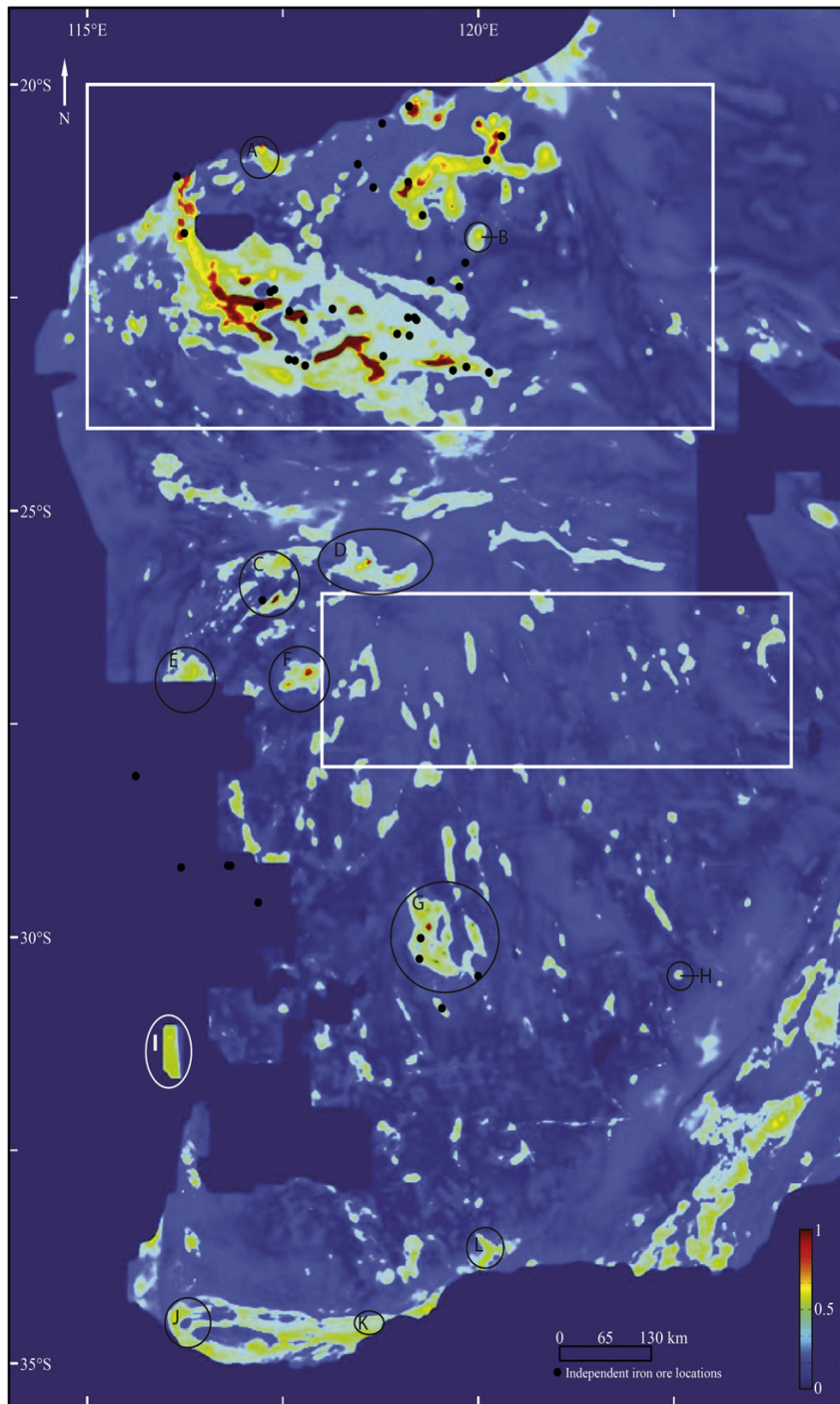
Fig. 10. Predictive confidence map for Western Australia overlayed with independent iron ore locations (Ewers et al., 2001). Open circles are mining areas throughout the Yilgarn Craton A, Cape Lambert; B, Nullagine GID; C, Dead Goat Hill, Taylor Range, Mt Gould; D, Mt Fraser, Jabiru, Valley Bore; E, Twin Peaks; F, Weld Range–Madoonga; G, Deception, Windarling, Mt Jackson; H, Steeple Hill; I, Coates (Fe and V–Ti), Crows Nest Hill, Wongamine North; J, Western Southdown; K, Southdown; and L, Ravensthorpe.

detected within Australia suggests that this methodology could be used globally for iron ore exploration.

6.4. Relationship of predictive map with regional geology

Comparing the predictive confidence map with the broad geological features of the Yilgarn Craton (Raymond and Retter, 2010), there is a notable similarity between the high prospective locations and the greenstone belts within the craton, especially towards the northwest where they follow the extent of the greenstone belts closely. Towards the southeast of the Yilgarn Craton, the areas of higher prospectivity still occur within greenstone belts though they occupy a considerably smaller extent of the belts than in the northwest. At a finer scale, comparing the predictive map with the geology of Western Australia, there is a correlation in the southwest Yilgarn Craton and in the Marble Bar area (e.g. between Abydos and Spinifex Ridge) of the Pilbara Craton between the higher areas of prospectivity and outcropping bands of mafic and ultramafic extrusive and intrusive rocks, and sedimentary–volcanic units.

This is likely a reflection of their mode of formation being associated with submarine volcanic processes akin to Algoma type deposits, rather than sedimentary derived Superior type deposits. It is important to note that while the areas of high prospectivity occur overlapping these units, not all mafic and ultramafic units are correlated with the higher probability of iron ore. Furthermore, this correlation is consistent with the associated geology of already established Yilgarn deposits such as the Koolyanobbing deposit (Angerer and Hagemann, 2010) and Madoonga deposit (Duuring and Hagemann, 2013).

6.5. Application to economic geology

The primary focus of this paper is to present a new methodology for low expenditure, greenfield exploration. For iron ore in Australia, we have used simple and easily extractable features to demonstrate how machine learning techniques can be coupled to exploration problems in order to arrive at innovative solutions. The key to our methodology is the three-step process; pre-processing, feature extraction and classification, coupled with rigorous validation to ensure its generalisation. The preliminary data and feature selection phase is critical as it allows for a human to provide expert, knowledge-based input into the process by identifying features and parameters that are associated with different deposit types (e.g. edge and texture analysis for gold exploration). It also ensures the separation of organising the data to be analysed with the classification training, cutting down on computational cost and time, allowing for the user to easily switch between or compare different classification models and parameters. The second phase, classification, is general, allowing for the user to test and compare alternative classification models and parameters. It is expected that in exploring for other mineral types in other geographical areas, different algorithms for both dimensionality reduction and classification should be used in order to best determine the location of mineral deposits. Importantly, our method lends itself to continuous improvement over time, as more datasets are generated (e.g. ASTER multispectral data), other datasets improve in coverage and quality, and new machine learning algorithms are developed.

7. Conclusions

We present a versatile, low cost, generic methodology for greenfield mineral exploration using iron ore as a case study. Our selected classifier, a mixture of Gaussians with reject option preceded by principal component reduction, identified 88% of iron ore locations and eliminated 92% of non-iron ore locations during randomised hold-out validation and successfully fulfilled our ground-truthing hypotheses. The nature of our methodology is such that it lends itself to continual improvement over time as data increases in coverage and resolution, computational power increases and techniques develop further. It is also highly adaptable, allowing for users to target different commodities at different scales, with data and features that they believe are pertinent or have access to. The use of the reject option in the classifier (i.e. enclosing the domain in feature space around the target class) resulted in an overall ~4% increase in classification ability and a reduction in the misclassification rate for the outlier class, while suffering only a small loss in the performance for the target class. The use of reject option classifiers for greenfield mineral prospectivity is promising for protecting a small target class against a large heterogeneous outlier class. We test the value of radiometric data for iron ore exploration and show that it is of minimal use for exploration, though our results demonstrate that, with effective processing of data and algorithm choice, potentially useful data can be included without risk of penalising classification ability. The near universality of iron deposits detected throughout both the Pilbara and Yilgarn Craton by our classifier indicates that the algorithm could be easily applied for iron ore exploration in other regions that are well covered by geophysical data (e.g. Canada).

Conflict of interest

There is no conflict of interest in the work completed in this study or its submission to *Ore Geology Reviews* that the authors are aware of.

Acknowledgements

References

Abedi, M., Norouzi, G.H., Bahroudi, A., 2012. Support vector machine for multi-classification of mineral prospectivity areas. Comput. Geosci. 46, 272–283.

Alpaydin, E., 2010. Introduction to machine learning. 2nd ed. Methods in Molecular Biology vol. 1107. Massachusetts Institute of Technology, Cambridge.

Anand, R.R., Paine, M., 2002. Regolith geology of the Yilgarn Craton, Western Australia: implications for exploration. Aust. J. Earth Sci. 49 (1), 3–162.

Andrada de Palomera, P., van Ruitenbeek, F.J., Carranza, E.J.M., 2014. Prospectivity for epithermal gold–silver deposits in the Deseado Massif, Argentina. Ore Geol. Rev. http://dx.doi.org/10.1016/j.oregeorev.2014.12.007.

Angerer, T., Hagemann, S.G., 2010. The BIF-hosted high-grade iron ore deposits in the Archean Koolyanobbing Greenstone Belt, Western Australia: structural control on synorogenic- and weathering-related magnetite-, hematite-, and goethite-rich iron ore. Econ. Geol. 105, 917–945.

Bacchin, M., Milligan, P.R., Wynne, P., Tracey, R., 2008. Gravity Anomaly Grid of the Australian Region. Geoscience Australia, Canberra.

Barley, M.E., Pickard, a.L., Hagemann, S.G., Folkert, S.L., 1999. Hydrothermal origin for the 2 billion year old Mount Tom Price giant iron ore deposit, Hamersley Province, Western Australia. Mineral. Deposita 34, 784–789.

Bekker, A., Slack, J.F., Planavsky, N.J., Krapež, B., Hofmann, A., Konhauser, K.O., Rouxel, O.J., 2010. Iron formation: the sedimentary product of a complex interplay among mantle, tectonic, oceanic, and biospheric processes. Econ. Geol. 105, 467–508.

Bishop, C.M., 2006. In: Jordan, M., Kleinberg, J., Schölkopf, B. (Eds.), Pattern Recognition and Machine Learning. Springer Science, Singapore.

Blake, T.S., Barley, M.E., 1992. Tectonic evolution of the Late Archaean to Early Proterozoic Mount Bruce Megasequence set, Western Australia. Tectonics 11 (6), 1415–1425.

Bonham-Carter, G.F., 1994. Geographic Information Systems for Geoscientists. Pergamon, New York.

Brown, W.M., Gedeon, T.D., Groves, D.I., Barnes, R.G., 2000. Artificial neural networks: a new method for mineral prospectivity mapping. Aust. J. Earth Sci. 47 (4), 37–41.

Canfield, D.E., 2005. The early history of atmospheric oxygen: homage to Robert M. Garrels. Annu. Rev. Earth Planet. Sci. 33, 1–36.

Carranza, E.J.M., 2011. From predictive mapping of mineral prospectivity to quantitative estimation of number of undiscovered prospects. Resour. Geol. 61 (1), 30–51.

Carranza, E.J.M., Hale, M., Faassen, C., 2008. Selection of coherent deposit-type locations and their application in data-driven mineral prospectivity mapping. Ore Geol. Rev. 33 (3–4), 536–558.

Carranza, E.J.M., Sadeghi, M., Billay, A., 2014. Predictive mapping of prospectivity for orogenic gold, Giyani greenstone belt (South Africa). Ore Geol. Rev. http://dx.doi.org/10.1016/j.oregeorev.2014.10.030.

Chow, C.K., 1970. On optimum recognition error and reject tradeoff. IEEE Trans. Inf. Theory 16 (1), 41–46.

Chung, C.F., Agterberg, F.P., 1980. Regression models for estimating mineral resources from geological map data. Math. Geol. 12 (5), 473–488.

Cooper, R. 2013a. Iron deposits of the Pilbara Region — 2013 (1:750000 scale). Geological Survey of Western Australia.

Cooper, R. 2013b. Iron ore deposits of the Yilgarn Craton — 2013 (1:1500000 scale). Geological Survey of Western Australia.

Cracknell, M.J., Reading, A.M., 2014. Geological mapping using remote sensing data: a comparison of five machine learning algorithms, their response to variations in the spatial distribution of training data and the use of explicit spatial information. Comput. Geosci. 63, 22–33.

Cracknell, M.J., Reading, A.M., McNeill, A.W., 2013. Mapping geology and volcanic-hosted massive sulfide alteration in the Hellyer–Mt Charter region, Tasmania, using Random Forests™ and self-organising maps. Aust. J. Earth Sci. 61 (2), 287–304.

Dauth, C., 1997. Airborne magnetic radiometric and sat imagery for regolith mapping in the Yilgarn Craton of Western Australia. Explor. Geophys. 28 (2), 199–203.

Dentith, M.C., Frankcombe, K.F., Trench, A., 1994. Geophysical signatures of Western Australian mineral deposits: an overview. Explor. Geophys. 25, 103–160.

Dubuisson, B., Masson, M., 1993. A statistical decision rule with incomplete knowledge about classes. Pattern Recogn. 26 (1), 155–165.

Duda, R., Hart, P., Stork, D., 2000. Pattern Classification. 2nd ed. Wiley, New York.

Duin, R.P.W., Juszczak, P., Paclik, P., Pekalska, E., de Ridder, D., Tax, D.M.J., Verzakov, S., 2007. PRTools4.1, A Matlab Toolbox for Pattern Recognition. Delft University of Technology.

Duuring, P., Hagemann, S., 2013. Genesis of superimposed hypogene and supergene Fe orebodies in BIF at the Madoonga deposit, Yilgarn Craton, Western Australia. Mineral. Deposita 48, 371–395.

Evans, K.A., McCuaig, T.C., Leach, D., Angerer, T., Hagemann, S.G., 2013. Banded iron formation to iron ore: a record of the evolution of Earth environments. Geology 41 (2), 99–102.

Ewers, G.R., Evans, N., Kilgour, B., 2001. MINLOC Mineral Localities Database. Geoscience Australia, Canberra.

Ewers, G.R., Evans, N., Hazell, M., Kilgour, B., 2002. OZMIN Mineral Deposits Database. Geoscience Australia, Canberra.

Findlay, D., 1994. Diagenetic boudinage, an analogue model for the control on hematite enrichment iron ores of the Hamersley Iron Province of Western Australia, and a comparison with Krivoi Rog of Ukraine, and Nimba Range, Liberia. Ore Geol. Rev. 9, 311–324.

Gardoll, S.J., Groves, D.I., Knox-Robinson, C.M., Yun, G.Y., Elliott, N., 2000. Developing the tools for geological shape analysis, with regional- to local-scale examples from the Kalgoorlie Terrane of Western Australia. Aust. J. Earth Sci. 47 (5), 943–953.

Gee, R.E., Baxter, J.L., Wilde, S.A., Williams, I.R., 1981. Crustal development in the Archaean Yilgarn Block, Western Australia. In: Glover, J.E., Groves, D.I. (Eds.), Archaean Geology. Geological Society of Australia Special Publication, pp. 43–57.

Gole, M.J., Klein, C., 1981. Banded iron-formations through much of Precambrian time. J. Geol. 89 (2), 169–183.

Goodwin, A.M., 1973. Archean iron-formations and tectonic basins of the Canadian Shield. Econ. Geol. 68, 915–933.

Greentree, M.R., Lord, D., 2007. Iron Mineralisation in the Yilgarn Craton and Future Potential. Geoconferences (WA) Inc., Kalgoorlie, pp. 70–73.

Griffin, W.L., Belousova, E.A., Shee, S.R., Pearson, N.J., Reilly, S.Y., 2004. Archean crustal evolution in the northern Yilgarn Craton: U–Pb and Hf-isotope evidence from detrital zircons. Precambrian Res. 131, 231–282.

Gross, G.A., 1980. On classification of iron formations based on depositional environments. Can. Mineral. 18, 215–222.

Groves, D.I., Goldfarb, R.J., Knox-Robinson, C.M., Ojala, J., Gardoll, S., Yun, G.Y., Holyland, P., 2000. Late-kinematic timing of orogenic gold deposits and significance for computer-based exploration techniques with emphasis on the Yilgarn Block, Western Australia. Ore Geol. Rev. 17, 1–38.

Hand, D., 1998. Consumer credit and statistics. In: Hand, D., Jacka, S. (Eds.), Statistics in Finance. Arnold, London, pp. 69–81.

Hickman, A.H., 2004. Two contrasting granite–greenstone terranes in the Pilbara Craton, Australia: evidence for vertical and horizontal tectonic regimes prior to 2900 Ma. Precambrian Res. 131, 153–172.

Holden, E.-J., Dentith, M., Kovesi, P., 2008. Towards the automated analysis of regional aeromagnetic data to identify regions prospective for gold deposits. Comput. Geosci. 34, 1505–1513.

Holden, E.-J., Wong, J.C., Kovesi, P., Wedge, D., Dentith, M., Bagas, L., 2012. Identifying structural complexity in aeromagnetic data: an image analysis approach to greenfields gold exploration. Ore Geol. Rev. 46, 47–59.

Hronsky, J.M.A., Groves, D.I., 2008. Science of targeting: definition, strategies, targeting and performance measurement. Aust. J. Earth Sci. 55 (1), 3–12.

Huang, C., Davis, L.S., Townshend, J.R.G., 2002. An assessment of support vector machines for land cover classification. Int. J. Remote Sens. 23 (4), 725–749.

Huston, D.L., Logan, G.A., 2004. Barite, BIFs and bugs: evidence for the evolution of the Earth's early hydrosphere. Earth Planet. Sci. Lett. 220, 41–55.

Hutchinson, M.F., Stein, J.A., Stein, J.L., 2006. GEODATA 9 second digital elevation model (DEM-9S) version 3. Geoscience Australia, Canberra.

Isley, A.E., 1995. Hydrothermal plumes and the delivery of iron to banded iron formation. J. Geol. 103 (2), 169–185.

Isley, A.E., Abbott, D.H., 1999. Plume-related mafic volcanism and the deposition of banded iron formation. J. Geophys. Res. 104, 15461.

James, H.L., 1954. Sedimentary facies of iron-formation. Econ. Geol. 49 (3), 235–293.

James, H.L., Trendall, A., 1982. Banded iron formation: distribution in time and paleoenvironment significance. In: Holland, H., Schidlowski, M. (Eds.), Mineral Deposits and the Evolution of the Biosphere. Springer-Verlag, New York, pp. 199–218.

Jolliffe, I., 2002. Principal component analysis. Springer Series in Statistics, 2nd ed. Springer-Verlag, New York.

Klein, C., 2005. Some Precambrian banded iron-formations (BIFs) from around the world: their age, geologic setting, mineralogy, metamorphism, geochemistry, and origins. Am. Mineral. 90 (10), 1473–1499.

Landgrebe, T.C.W., Tax, D., Duin, R.P.W., 2006. The interaction between classification and reject performance for distance-based reject-option classifiers. Pattern Recogn. Lett. 27 (8), 908–917.

Landgrebe, T.C.W., Merdith, A., Dutkiewicz, A., Müller, R.D., 2013. Relationships between palaeogeography and opal occurrence in Australia: a data-mining approach. Comput. Geosci. 56, 76–82.

Lascelles, D.F., 2006. The Mount Gibson banded iron formation-hosted magnetite deposit: two distinct processes for the origin of high-grade iron ore. Econ. Geol. 101, 651–666.

Lascelles, D.F., 2007. Black smokers and density currents: a uniformitarian model for genesis of banded iron-formations. Ore Geol. Rev. 32, 381–411.

Leith, C.K., 1903. The Mesabi iron-bearing district of Minnesota. Monogr. U. S. Geol. Surv. 43, 316.

Lyons, T.W., Anbar, A.D., Severmann, S., Scott, C.T., Gill, B.C., 2009. Tracking Euxinia in the Ancient Ocean: a multiproxy perspective and Proterozoic case study. Annu. Rev. Earth Planet. Sci. 37, 507–534.

Macleod, W.N., 1966. The geology and iron deposits of the Hamersley Range area, Western Australia. West. Aust. Geol. Surv. Bull. 117, 170.

Mahanta, A.M., 2015. +40 years of geophysics in Pilbara and beyond. International Geophysical Conference and Exhibition. ASEG-PESA, Perth.

McLachlan, G.J., Basford, K.E., 1987. Mixture Models. Marcel Dekker, New York.

Merdith, A.S., Landgrebe, T.C.W., Dutkiewicz, A., Müller, R.D., 2013. Towards a predictive model for opal exploration using a spatio-temporal data mining approach. Aust. J. Earth Sci. 60 (2), 217–229.

Metz, C.E., 1978. Basic principles of ROC analysis. Semin. Nucl. Med. 8 (4), 283–298.

Milligan, P.R., Franklin, R., 2010. Magnetic Anomaly Map of Australia. 5th ed. Geoscience Australia, Canberra.

Minty, B.R.S., Franklin, R., Milligan, P.R., Richardson, L.M., Wilford, J., 2010. Radiometric Map of Australia. 2nd ed. Geoscience Australia, Canberra.

Moon, C.J., Whateley, M.K.G., 2006. Reconnaissance exploration. In: Moon, C.J., Whateley, M.K.G., Evans, A.M. (Eds.), Introduction to Mineral Exploration, 2nd ed. Blackwell Publishing, Oxford, p. 482.

Morris, R.C., 1980. A textural and mineralogical study of the relationship of iron ore to banded iron-formation in the Hamersley Iron Province of Western Australia. Econ. Geol. 75, 184–209.

Morris, R.C., 1985. Genesis of iron ore in banded iron-formation by supergene and supergene-metamorphic processes — a conceptual model. In: Wolf, K.H. (Ed.), Handbook of Strata-bound and Stratiform Ore Deposits. Elsevier, Oxford.

Morris, R.C., Kneeshaw, M., 2011. Genesis modelling for the Hamersley BIF-hosted iron ores of Western Australia: a critical review. Aust. J. Earth Sci. 58 (5), 417–451.

Myers, J.S., 1993. Precambrian history of the West Australian Craton and adjacent orogens. Annu. Rev. Earth Planet. Sci. 21, 453–481.

Nykänen, V., Groves, D.I., Ojala, V.J., Eilu, P., Gardoll, S.J., 2008. Reconnaissance-scale conceptual fuzzy-logic prospectivity modelling for iron oxide copper–gold deposits in the northern Fennoscandian Shield, Finland. Aust. J. Earth Sci. 55 (1), 25–38.

Planavsky, N.J., McGoldrick, P., Scott, C.T., Li, C., Reinhard, C.T., Kelly, A.E., Lyons, T.W., 2011. Widespread iron-rich conditions in the mid-Proterozoic ocean. Nature 477 (7365), 448–451.

Pohl, W.L., 2011. Economic Geology Principles and Practice: Metals, Minerals, Coal and Hydrocarbons — Introduction to Formation and Sustainable Exploitation of Mineral Deposits. Wiley-Blackwell, West Sussex.

Porwal, A., Carranza, E.J.M., Hale, M., 2003. Artificial neural networks for mineral-potential mapping: a case study from Aravalli Province, Western India. Nat. Resour. Res. 12 (3).

Porwal, A., González-Álvarez, I., Markwitz, V., McCuaig, T.C., Mamuse, A., 2010. Weights-of-evidence and logistic regression modeling of magmatic nickel sulfide prospectivity in the Yilgarn Craton, Western Australia. Ore Geol. Rev. 38 (3), 184–196.

Porwal, A., Das, R.D., Chaudhary, B., González-Álvarez, I., Kreuzer, O., 2014. Fuzzy inference systems for prospectivity modeling of mineral systems and a case-study for prospectivity mapping of surficial Uranium in Yeelirrie Area, Western Australia. Ore Geol. Rev. http://dx.doi.org/10.1016/j.oregeorev.2014.10.016.

Raymond, O. L., and Retter, A. J. 2010. Surface geology of Australia 1:1 000 000 scale. Canberra: Geoscience Australia.

Rogan, J., Franklin, J., Stow, D., Miller, J., Woodcock, C., Roberts, D., 2008. Mapping landcover modifications over large areas: a comparison of machine learning algorithms. Remote Sens. Environ. 112, 2272–2283.

Simonson, B.M., Schubel, K.A., Hassler, S.W., 1993. Carbonate sedimentology of the early Precambrian Hamersley Group of Western Australia. Precambrian Res. 60, 287–335.

Singer, D.A., Kouda, R., 1999. A comparison of the weights-of-evidence method and probabilistic neural networks. Nat. Resour. Res. 8 (4), 287–298.

Tan, P., Steinbach, M., Kumar, V., 2006. Introduction to Data Mining. Addison-Wesley, Boston.

Tax, D., 2014. DDTools, the Data Description Toolbox for Matlab.

Taylor, D., Dalstra, H.J., Harding, A.E., Broadbent, G.C., Barley, M.E., 2001. Genesis of highgrade hematite orebodies of the Hamersley Province, Western Australia. Econ. Geol. 96, 837–873.

Tyler, I. M., and Hocking, R. M. 2007. Tectonic units of Western Australia, 1:500 000. Geological survey of Western Australia.

Tyler, I. M., and Hocking, R. M. 2008. Interpreted bedrock geology of Western Australia, 1:500 000. Geological survey of Western Australia.

Van Kranendonk, M.J., Hickman, A.H., Smithies, R.H., Nelson, D.R., Pike, G., 2002. Geology and tectonic evolution of the Archean North Pilbara Terrain, Pilbara Craton, Western Australia. Econ. Geol. 97 (4), 695–732.

Vapnik, V.N., 1995. The Nature of Statistical Learning Theory. Springer, New York.

Whitaker, A.J., 2001. Components and structure of the Yilgarn Craton, as interpreted from aeromagnetic data. Proceedings of Fourth International Archaean Symposium Ext. Abstracts. AGSO-Geoscience Australia Record vol. 37, pp. 536–538 (Perth).

Wulder, M.A., Kurz, W.A., Gillis, M., 2004. National level forest monitoring and modeling in Canada. Prog. Plan. 61 (4), 365–381.